frontiers | Research Topics

Regulated biology via aberrant signaling pathways in liver cancer

Edited by
Xiaodong Li, Liangrong Shi, Adam Yongxin Ye,
Ioana Berindan Neagoe and Flavio Rizzolio

Published in
Frontiers in Oncology
Frontiers in Cell and Developmental Biology

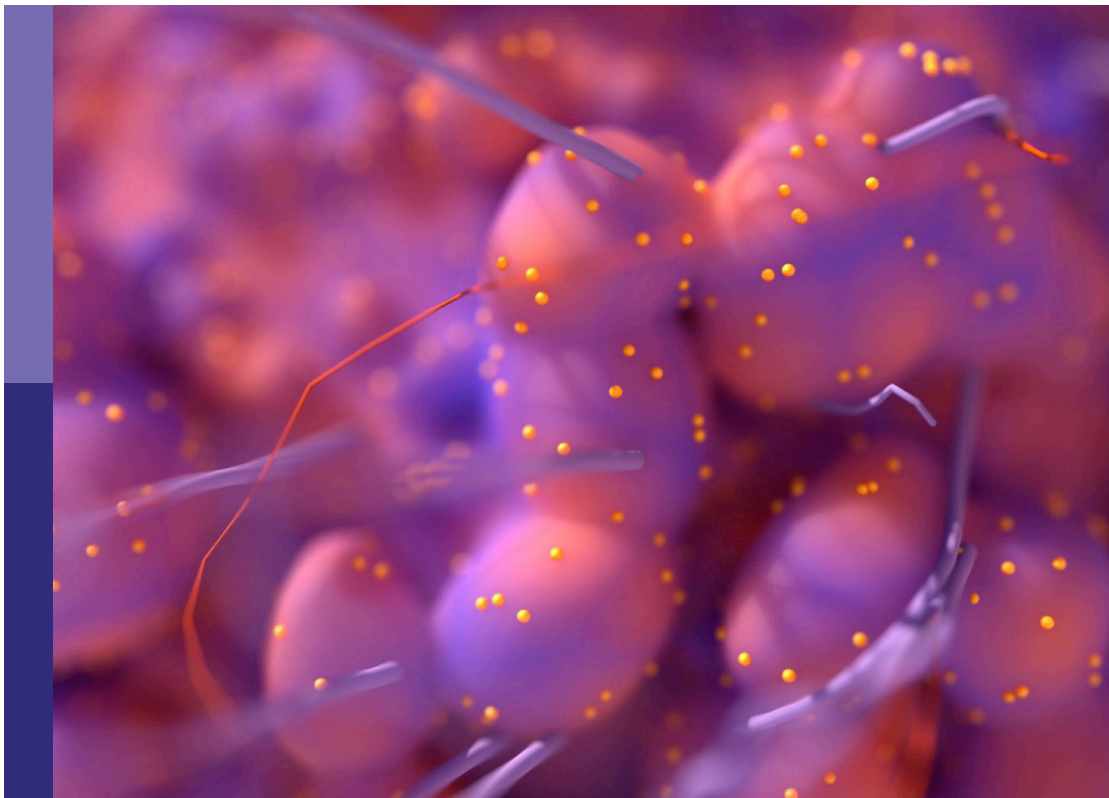

ISSN 1664-8714
ISBN 978-2-8325-1632-4
DOI 10.3389/978-2-8325-1632-4

About Frontiers

Frontiers is more than just an open access publisher of scholarly articles: it is a pioneering approach to the world of academia, radically improving the way scholarly research is managed. The grand vision of Frontiers is a world where all people have an equal opportunity to seek, share and generate knowledge. Frontiers provides immediate and permanent online open access to all its publications, but this alone is not enough to realize our grand goals.

Frontiers journal series

The Frontiers journal series is a multi-tier and interdisciplinary set of open-access, online journals, promising a paradigm shift from the current review, selection and dissemination processes in academic publishing. All Frontiers journals are driven by researchers for researchers; therefore, they constitute a service to the scholarly community. At the same time, the *Frontiers journal series* operates on a revolutionary invention, the tiered publishing system, initially addressing specific communities of scholars, and gradually climbing up to broader public understanding, thus serving the interests of the lay society, too.

Dedication to quality

Each Frontiers article is a landmark of the highest quality, thanks to genuinely collaborative interactions between authors and review editors, who include some of the world's best academicians. Research must be certified by peers before entering a stream of knowledge that may eventually reach the public - and shape society; therefore, Frontiers only applies the most rigorous and unbiased reviews. Frontiers revolutionizes research publishing by freely delivering the most outstanding research, evaluated with no bias from both the academic and social point of view. By applying the most advanced information technologies, Frontiers is catapulting scholarly publishing into a new generation.

What are Frontiers Research Topics?

Frontiers Research Topics are very popular trademarks of the *Frontiers journals series*: they are collections of at least ten articles, all centered on a particular subject. With their unique mix of varied contributions from Original Research to Review Articles, Frontiers Research Topics unify the most influential researchers, the latest key findings and historical advances in a hot research area.

Find out more on how to host your own Frontiers Research Topic or contribute to one as an author by contacting the Frontiers editorial office: frontiersin.org/about/contact

Regulated biology via aberrant signaling pathways in liver cancer

Topic editors

Xiaodong Li — First People's Hospital of Changzhou, China
Liangrong Shi — Central South University, China
Adam Yongxin Ye — Boston Children's Hospital, Harvard Medical School, United States
Ioana Berindan Neagoe — University of Medicine and Pharmacy Iuliu Hatieganu, Romania
Flavio Rizzolio — Ca' Foscari University of Venice, Italy

Citation

Li, X., Shi, L., Ye, A. Y., Neagoe, I. B., Rizzolio, F., eds. (2023). *Regulated biology via aberrant signaling pathways in liver cancer*. Lausanne: Frontiers Media SA.
doi: 10.3389/978-2-8325-1632-4

Table of contents

frontiers in Cell and Developmental Biology

ORIGINAL RESEARCH
published: 12 November 2021
doi: 10.3389/fcell.2021.796686

CircCRIM1 Promotes Hepatocellular Carcinoma Proliferation and Angiogenesis by Sponging miR-378a-3p and Regulating SKP2 Expression

Yang Ji[1†], Shikun Yang[1†], Xueqi Yan[2†], Li Zhu[3†], Wenjie Yang[1], Xinchen Yang[1], Fei Yu[1], Longqing Shi[3], Xi Zhu[4], Yunjie Lu[3], Chuanyong Zhang[1]*, Hao Lu[1]* and Feng Zhang[1]**

[1]Key Laboratory of Liver Transplantation, Hepatobiliary/Liver Transplantation Center, Chinese Academy of Medical Sciences, The First Affiliated Hospital of Nanjing Medical University, Nanjing, China, [2]Department of Oncology, The First Affiliated Hospital of Nanjing Medical University, Nanjing, China, [3]Department of Hepatobiliary Surgery, The Third Hospital Affiliated to Soochow University, Changzhou, China, [4]Department of Infectious Disease, The First People's Hospital of Kunshan Affliated with Jiangsu University, Zhenjiang, China

Mounting evidence has demonstrated that circular RNAs have an important function in tumorigenesis and cancer evolvement. CircCRIM1 has been shown to be a poor prognostic element in multiple human malignancies. However, the clinical significance and mechanism of circCRIM1 in hepatocellular carcinoma (HCC) is still unclear. The present study confirmed the expression level of circCRIM1 using quantitative real-time PCR. In addition, circCRIM1 siRNA and overexpression vectors were used for transfection into LM3 or Huh7 cells to down- or up-regulate the expression of circCRIM1. *In vitro* and *in vivo* experiments were performed to explore the function of circCRIM1 in HCC. RNA pull-down, RNA immunoprecipitation, fluorescent *in situ* hybridization, and luciferase reporter assays were conducted to confirm the relationship between miR-378a-3p and circCRIM1 or S-phase kinase-associated protein 2 (SKP2) in HCC. Then, circCRIM1 was up-regulated in HCC and its expression level was significantly associated with poor prognosis and clinicopathologic characteristics. CircCRIM1 enhanced the proliferation and angiogenesis of HCC cells *in vitro* and promoted xenograft growth *in vivo*. Moreover, circCRIM1 upregulated the expression of SKP2 by functioning as a sponge for miR-378a-3p. These findings suggest that circCRIM1 boosts the HCC progression via the miR-378-3p/SKP2 axis and may act as a crucial epigenetic therapeutic molecule target in HCC.

Keywords: circCRIM1, HCC, MiR-378a-3p, Skp2, proliferation, angiogenesis

OPEN ACCESS

Edited by:
Xiaodong Li,
First People's Hospital of Changzhou, China

Reviewed by:
Bogang Wu,
George Washington University, United States
Mingxiao Feng,
Johns Hopkins University, United States

****Correspondence:***
Feng Zhang
zhangfeng1958@hotmail.com
Hao Lu
luhao_jsph@qq.com
Chuanyong Zhang
zcy2732@163.com
Yunjie Lu
yjresearch@qq.com

[†]These authors have contributed equally to this work

Specialty section:
This article was submitted to Molecular and Cellular Oncology, a section of the journal Frontiers in Cell and Developmental Biology

Received: *17 October 2021*
Accepted: *28 October 2021*
Published: *12 November 2021*

Citation:
Ji Y, Yang S, Yan X, Zhu L, Yang W, Yang X, Yu F, Shi L, Zhu X, Lu Y, Zhang C, Lu H and Zhang F (2021) CircCRIM1 Promotes Hepatocellular Carcinoma Proliferation and Angiogenesis by Sponging miR-378a-3p and Regulating SKP2 Expression. Front. Cell Dev. Biol. 9:796686. doi: 10.3389/fcell.2021.796686

INTRODUCTION

Primary hepatocellular carcinoma (HCC) is one of the most common cancers and its mortality ranks third (Sung et al., 2021). Even though both hepatectomy and liver transplantation are the most beneficial treatments for HCC, the overall survival (OS) in HCC patients is still low because of neoplasm recurrence and metastasis with the blood after surgery (Cao et al., 2020). Moreover, the molecular pathogenesis of HCC remains largely unknown and requires further investigation. Therefore, efforts are being made to identify new molecular targets that can be used to improve HCC treatments (Allemani et al., 2018).

Circular RNA (circRNA) is a single-stranded closed loop without the 5′ caps and 3′ poly (A) tails (Kristensen et al., 2019), which is also a part of non-coding RNAs. This structure results in high stability in tissues. CircRNAs are expressed in tissues of many cancers, such as colorectal, liver, and lung cancer. They also adjust gene expression in the human body (Wu et al., 2019; Li Z. et al., 2020; Hu et al., 2020; Zuo et al., 2021). In addition, circRNAs can sponge miRNAs during post-transcriptional regulation (Poliseno et al., 2010; Gu et al., 2021). These findings indicate that circRNAs may serve as potential therapeutic target for cancer.

CircCRIM1 has been identified as a relative factor in multiple human cancer prognoses. In nasopharyngeal carcinoma, circCRIM1 promotes the proliferation, invasion, metastasis, and chemoresistance by sponging miR-422a (Hong et al., 2020). Another study has reported that circCRIM1 is a tumor-positive factor that accelerates the progression and facilitates osteosarcoma autophagy by targeting miR-432-5p (Liu J. et al., 2020). In addition, circCRIM1 has also been reported to be a suppressive factor that inhibits the progression of lung adenocarcinoma by interacting with miR-182 and miR-93 (Wang et al., 2019). However, not many research studies have investigated circCRIM1 in HCC.

S-phase kinase-associated protein 2 (SKP2) is a RING-finger type ubiquitin ligase, a member of cullin-RING ubiquitin ligases (CRLs), and a functional component of ligase complex Skpl-Cullin-F-box (SCF). SKP2 functions as a direct regulator of cyclin-dependent kinases (CDKs) (Lin et al., 2019). In colorectal carcinoma, CDKs interacting with SKP2 contributed to the loss of tumor differentiation and decreased the OS (Shapira et al., 2005). SKP2 also plays an oncogenic role in other human cancers. SKP2 induces tumorigenesis via Hippo signaling (Zhang et al., 2017) in HCC, and promotes tumor progression in breast cancer via PDCD4 ubiquitination (Li et al., 2019). Previous studies have reported that SKP2 induces the proliferation of vascular smooth muscle cells by decreasing P27/P21 expression (Song et al., 2011).

We have previously determined the expression of circCRIM1 in HCC cells, tissues, and adjacent tissues. The data indicated that circCRIM1 has a high expression in HCC cells and tissues, which obviously correlated with poor prognosis and clinicopathological characteristics of patients with HCC, containing tumor size, TNM stage, and Edmondson grade. Moreover, circCRIM1 significantly promoted the progression of HCC via sponging miR-378a-3p and targeting SKP2.Therefore, circCRIM1 can be regarded as a prognostic biomarker and a possible therapeutic target for some patients with HCC.

MATERIALS AND METHODS

Tissues and Cell Lines

A total of 76 pairs of HCC tissues and corresponding adjacent normal liver tissues were obtained from the First Affiliated Hospital in Nanjing Medical University. All samples were retrieved from patients during the operation. Patients receiving anti-tumor therapy were excluded. This research was authorized by the ethics committee of our hospital. HCC cell lines were purchased from the Cell Bank of Type Culture Collection (Shanghai, China). All cell lines were cultured in Dulbecco's modified Eagle's medium with 10% fetal bovine serum (Gibco, NY, United States) at 37°C with 5% CO_2.

QRT-PCR

TRIzol reagent (Invitrogen, United States) was employed to extract RNA from HCC tissues and cell lines described above. Then, RNA from each specimen was used for reverse transcription of cDNA. The cDNA acting as a template was used for RT-qPCR. The expression of human GAPDH genes was used for normalizing the expression of circRNA or mRNA, while U6 was used for miRNA. Gene expression level was calculated using the $2^{-\Delta\Delta Ct}$ method. The primer sequences used in this study are listed in **Supplementary Table S1**.

Nuclear Cytoplasmic Fractionation, RNase R, and Actinomycin D Treatment

Nuclear and cytoplasmic fractions were separated using the PARIS™ kit (Invitrogen, United States). Total RNA (2 μg) and 3 U/μg RNase R (Li S. et al., 2020) (Epicentre Technologies, Madison, United States) were incubated together for 15 min at 37°C. Then, 5 μg/ml actinomycin D (Chen et al., 2020)was introduced to detect the expression of endogenous circRNA and mRNA. CircCRIM1 and linear CRIM1 expression was analyzed by qRT-PCR.

RNA FISH

To determine the circCRIM1 and miR-378a-3p locations in HCC cells and tissues, FAM-labelled circCRIM1 probes and cy3-labelled miR-378a-3p probes were designed and constructed by Sevicebio (Wuhan, China). Samples were analyzed using a Nikon inverted fluorescence microscope. The respective circCRIM1 and miR-378a-3p probe sequences used in the FISH assay were as follows: 5′-AGTCCAGTT CTCATCTTGTTG GCAAAGTAC-3′ and 5′-CCTTCTGAC TCCAAGTCCAGT-3'.

Transfection Experiment

Specific circCRIM1 siRNA, miR-378a-3p inhibitors, mimics, and their corresponding NCs were constructed by TSINGKE Biological Technology (Beijing, China). Full-length circCRIM1 was added into the pEX-3 (TSINGKE Biological Technology, Beijing, China) overexpression vector. LM3 and Huh7 cells were transfected with circCRIM1 siRNAs, miRNA-378a-3p mimics, or inhibitors using Lipofectamine 3000 (Invitrogen), while circCRIM1 overexpression plasmids were prepared using jetPRIME (Polyplus-transfection, France). Cells were harvested after a 48-h transfection. SKP2-overexpressing lentivirus and SKP2 shRNAs were constructed by GenePharma (Shanghai, China) and transfected. All of the sequences used in the present study are listed in **Supplementary Table S1**.

CCK-8 Assay

For detecting cell proliferation, we used CCK-8 assay kit (Dojindo, Japan). Briefly, a 96-well plate were seeded in (1.0×10^3 cells/well) and were cultured 24, 48, 96, 120 and 148 h. At the certain point. 10μL of CCK-8 assay solution spread in each well was incubated for 120min in the dark. An enzyme immunoassay analyzer (Thermo Fisher Scientific, Inc. Waltham, MA, United States) was used to evaluate the absorbance of each well at OD450 nm.

Clone Formation Assay

The stably transfected Huh7 and LM3 cells were plated in six-well plates (800 cells/well). The plates cultured in DMEM with 10% fetal bovine serum (FBS) were harvested after 2 weeks. Then, the colonies were fixed with 1 ml of 4% paraformaldehyde (Sevicebio, Wuhan, China) for 25 min and stained with 0.1% crystal violet (Beyotime). The colonies were photographed and counted after washing with phosphate-buffered saline (PBS).

EdU Assay

After seeded evenly in 24-well plates, HCC cells were cultured with DMEM. Subsequently, Edu solution (Beyotime) was added in each wells and incubated for 2 h. The rest of steps were following the manufacturer's instruction. The specimens were imaged and measured by a microscope (Olympus, Tokyo, Japan).

Western Blot Analysis

Protease and phosphorylation inhibitor cocktail (New cell & Molecular Biotech Suzhou, China) in the RIPA buffer was used to lyse Huh7 and LM3 cells. Then, the total protein was separated via SDS-PAGE and transferred onto a PVDF membrane (Millipore, United States). Next, the membranes were blocked using Quick Block™ Blocking Buffer for Western Blot (Beyotime, Shanghai, China) within 15 min. After washing with TBST, the membranes were incubated with the appropriate primary antibodies. After an incubation with the corresponding HRP-labelled secondary antibodies on the next day, an enhanced chemiluminescence detection system was used for antigen-antibody complex visualization. All antibodies used in the study are listed in **Supplementary Table S2**.

Flow Cytometry Assay

For flow cytometry assay, 1×10^6 cells were suspended in 1 ml of PBS at room temperature. Then, 3 ml of precooled absolute ethyl alcohol were added and the mixture was kept overnight at −20°C. On the next day, the fixed cells were centrifuged and hydrated using PBS for 15 min, centrifuged again, then stained with 1 ml of the DNA staining solution (MultiSciences Biotech Co., Ltd., Hangzhou, China) away from light for at least 30 min. Finally, flow cytometry (LSR, BD Biosciences) was used to analyze the cell cycle.

HUVEC Tube Formation Assays

The conditioned medium was obtained from the DMEM cultured with LM3 or Huh7 cells transfected with circCRIM1-overexpressing lentivirus or si-RNA for 48 h. Subsequently, 50 μL of precooled Matrigel (BD Biosciences, San Jose, CA, United States) were carefully added into precooled 96-well plates for 30 min at 37°C. Then, HUVECs were seeded and cultured with the conditioned medium for 6 h at 37°C. An inverted microscope (Olympus) was used to observe and photograph tube formation.

HUVEC Recruitment Assays

First, HUVECs were harvested and suspended in DMEM without FBS. Next, 400 μL of cell suspension containing ten thousand cells were seeded into the upper chambers (Millicell, United States). A total of 600 μL of TCM were added into the lower chambers. After 36 h, the Transwell chambers were fixed with 4% formalin (Sevicebio, Wuhan, China). Then, 0.1% crystal violet was added dye for cell visible for 30 min. After washing twice with PBS, the cells migrated through the membrane were counted and photographed using a microscope (Olympus).

Biotin-Labelled RNA Pull-Down

The biotinylated circCRIM1 probes were designed by RiboBio (Guangzhou, China). First, 1×10^7 cells were lysed. Next, 50 μL of beads were incubated with 50 μL of circCRIM1 probe for 2 h. After washing twice with 50 μL of Tris, the cell lysates obtained from LM3 cells with probe-coated beads were incubated overnight at 4°C. At last, we eluted and extracted the RNA complexes for qRT-PCR.

RIP Assay

RNA immunoprecipitation assay (Zhang et al., 2021) was conducted using a Magna RIP RNA-Binding Protein Immunoprecipitation Kit (Millipore, United States) following the manufacturer's protocol. Purified RNA extracted from cells was used for qRT-PCR.

Dual-Luciferase Assay

WT and MUT circCRIM1 (pLuc-Firefly-Renilla with circCRIM1 WT or MUT sequence) were constructed by GeneChem Co. (Shanghai, China), while WT and MUT SKP2 were constructed. Lipofectamine 3000 was used to transfect Huh7 and LM3 cells with the corresponding reporter plasmids and microRNA mimics or the negative control. Finally, their activity was detected using the Dual-Luciferase Reporter System Kit (E1910, Promega, United States). Each experiment was repeated three times.

Animal Experiments

For tumor growth *in vivo*, four-week-old nude female mice were purchased from the institution: Animal Core Facility of Nanjing Medical University (Nanjing, China). Then, those mice were randomly divided into four groups ($n = 5$ for each group). After, 2×10^6 Huh7 cells were suspended in 100uL PBS for each mouse and subcutaneously injected into the dorsal flank, which were stably down-regulated the expression of circCRIM1 or NC. The rest of the mice were injected with LM3 cells containing circCRIM1-overexpressing plasmids or NC. Subsequently, tumor volumes and weights were measured at several time points. All samples were fixed in 4% paraformaldehyde and stained using IHC.

Immunohistochemistry

For IHC, the xenografts and HCC tissues were dewaxed and rehydrated with a gradient of ethanol. After an incubation in citrate buffer (10 mM, pH 6.0) for 20 min at 95°C, the samples were first incubated with polyclonal antibodies against SKP2 (Proteintech) and CD34 (Cell Signaling Technology) overnight

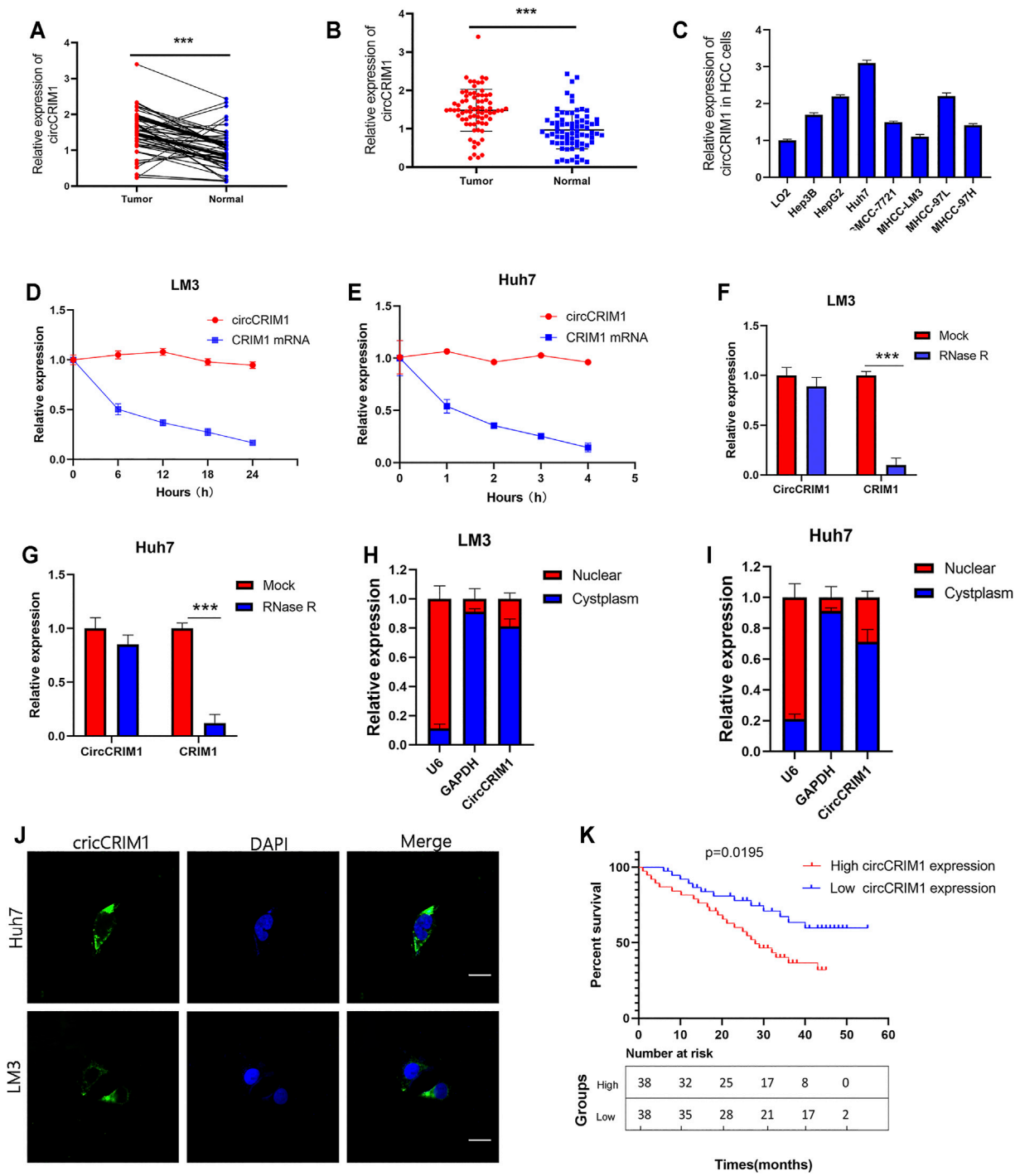

FIGURE 1 | CircCRIM1 is upregulated in HCC cell lines and tissues. **(A,B)** Relative circCRIM1 expression in HCC tissues (tumor) and adjacent non-tumor tissues (adjacent) was detected by qRT-PCR (n = 76). **(C)** Relative circCRIM1 expression in HCC cell lines was determined by qRT-PCR. **(D,E)** Actinomycin D treatment was used to evaluate the stability of circCRIM1 and CRIM1 mRNA in HCC cells. **(F,G)** CircCRIM1 and linear CRIM1 expression in HCC cells was detected after RNase R treatment and compared with mock treatment. **(H,I)** Nuclear-cytoplasmic fractionation assay results indicated that cirCRIM1 is primarily localized in the cytoplasm of HCC cells. GADPH and U6 genes were used as cytoplasmic and nuclear controls, respectively. **(J)** FISH results showed cellular localization of circCRIM1. The circCRIM1 probe was labeled with FAM (green), while nuclei were stained with DAPI (blue).Scale bar = 10 μm. **(K)** Kaplan-Meier survival analysis showed that HCC patients with high circCRIM1 expression had a lower OS (p = 0.0195) than those with low circCRIM1 expression. All data are presented as the means ± SD of three independent experiments. $^{*}p < 0.05$, $^{**}p < 0.01$, and $^{***}p < 0.001$.

TABLE 1 | Correlation between circCRIM1 expression and clinicopathological features in HCC tissues (n = 76, χ^2-test).

	CircCRIM1 expression		
	High	Low	
Variable	**38**	**38**	***p*-value**
Age (year)	—	—	0.2119
<60	29	24	—
≥60	9	14	—
Gender	—	—	0.4721
Male	23	26	—
Female	15	12	—
Tumor size	—	—	0.0116*
<5 cm	14	25	—
≥5 cm	24	13	—
TNM stage	—	—	0.0216*
I–II	25	15	—
III–IV	13	23	—
Liver cirrhosis	—	—	0.2432
Yes	25	20	—
No	13	18	—
AFP (ng/ml)	—	—	0.6445
≤200	18	16	—
>200	20	22	—
HBsAg	—	—	0.9999
Positive	28	28	—
Negative	10	10	—
Edmondson grade	—	—	0.0280*
I–II	30	21	—
III–IV	8	17	—
$p < 0.05$	—	—	—

at 4°C and then with secondary antibodies for 1 h. The staining was scored in terms of the rate of positive cells. Intensity of each sample was measured using four grades: 0, negative; 1, weak; 2, moderate; and 3, strong.

Statistical Analysis

All data were analyzed using SPSS 24.0 (SPSS, Chicago, IL, United States) and Prism 8 (GraphPad Software, La Jolla, CA, United States). Differences between the means were analyzed using Student's t-test. The correlations between cricCRIM1 and miR-378a-3p or miR-378a-3p and SKP2 expression levels were analyzed using Pearson's test (r, P). The χ2 test was used to evaluate the association between circCRIM1, miR378a-3p, SKP2 expression, and clinicopathological parameters. The OS rate was calculated using the Kaplan-Meier method and compared with a log-rank test. $^*p < 0.05$, $^{**}p < 0.01$, and $^{***}p < 0.001$ were considered as statistically significant.

RESULTS

Upregulation of circCRIM1 in Both HCC Cell Lines and Tissues Is Associated With Poor Prognosis

The expression of circCRIM1 in HCC and adjacent normal tissue samples from 76 patients was detected by qRT-PCR. CircCRIM1 expression in HCC tissues was higher than that in corresponding adjacent normal samples (**Figures 1A,B**). In addition, circCRIM1 was upregulated in human HepG2, Hep3B, SMMC-7721, MHCC-LM3, MHCC-97L, MHCC-97H, and Huh-7 cell lines (HCC cell lines) compared with normal hepatic cells L02 (**Figure 1C**), indicating that circCRIM1 expression levels may becorrelated with HCC progression. Based on the circBase annotation (http://www.circbase.org/), hsa_circ_0002346 (chr2: 36623756–36,669,878) (also named circCRIM1) originated from the 2, 3, and 4 exons in the CRIM1 gene. In order to determine the circular and linear forms of CRIM1, we designed divergent and convergent primers, respectively. Actinomycin D (Chen et al., 2020) assays and RNase R (Li S. et al., 2020) assays showed that circCRIM1 was more stable than linear CRIM1 (**Figures 1D–G**). In addition, the results of FISH assay were identified that circCRIM1 was mainly located in the cytoplasm (**Figure 1H**). Nuclear cytoplasmic fractionation had similar results (**Figures 1I,J**). The samples were split into two groups to investigate the connection between circCRIM1 and to investigate the clinical significance of HCC. The high circCRIM1 expression group was associated with tumor size ($p = 0.0049$), TNM stage ($p = 0.0216$), as well as Edmondson grade ($p = 0.0280$), rather than gender, age, liver cirrhosis, AFP, or HBsAg ($p > 0.05$; **Table 1**). In addition, HCC patients with higher circCRIM1 expression had a conspicuously worse OS in our center (**Figure 1K**). Taken together, circCRIM1 is a stable existing circRNA located in the cytoplasm that has the potential to be a biomarker for the diagnosis and prognosis of HCC.

CircCRIM1 Accelerates Proliferation of HCC Cells and Promotes Transition From G1 to S Phase

To evaluate the biological function of circCRIM1 in the progression of HCC, a short interfering RNA (siRNA) targeting the back splice region of circCRIM1 was transfected into HCC cells to knock down circCRIM1. In addition, circCRIM1 plasmids were transfected into Huh7 and LM3 cell lines to overexpress circCRIM1 without changing the expression of CRIM1 mRNA. Then, qRT-PCR was conducted to verify the efficiency and specificity of knocked down and overexpressed circCRIM1 in Huh7 and LM3 cells (**Figures 2A,B**). Cell Counting Kit-8 (CCK-8) assays were also conducted. Their results suggested that circCRIM1 silencing notably inhibits the proliferation of Huh7 cells, while circCRIM1 overexpression increases the growth of LM3 cells (**Figures 2C,D**). Concordant with these results, colony formation assays showed that downregulating circCRIM1 expression curbed cell growth. Conversely, overexpressing circCRIM1 increased the colony forming ability of LM3 cells (**Figures 2E,F**). In addition, 5-ethynyl-2-deoxyuridine (EdU) assays showed that the growth in siRNA-transfected cells was inhibited at first and subsequently promoted by circCRIM1 overexpression (**Figures 2G–I**). Then, the cell cycle assay revealed that silencing circCRIM1 arrested cells in the G0/G1 phase. Conversely, circCRIM1 overexpression induced the transition to the S phase (**Figures 2J,K**). Therefore, circCRIM1 exerts oncogenic effects on HCC cells.

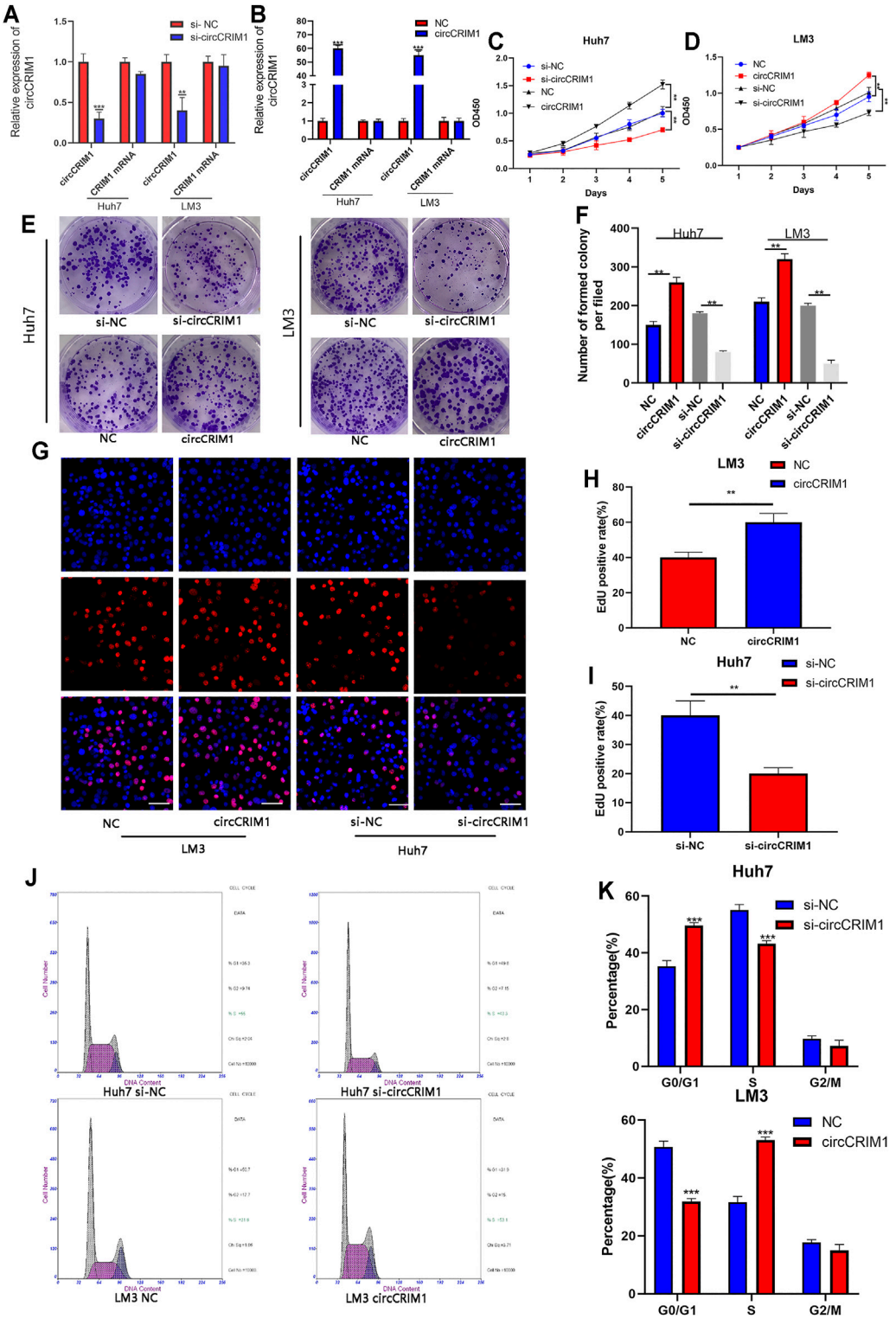

FIGURE 2 | CircCRIM1 promotes the proliferation of HCC cells and accelerates the transition from G1 to S phase. **(A,B)** QRT-PCR analysis of circCRIM1 and CRIM1 mRNA expression in LM3 and Huh7 cells transfected with si-NC, si-circCRIM1, circCRIM1, and NC. **(C,D)** Cellular growth curves were evaluated by CCK-8 assays after knocking down or overexpressing circCRIM1 in LM3 or Huh7 cells. **(E,F)** Colony formation assays were performed to evaluate cell proliferation. **(G–I)** EdU assays were performed on HCC cells to evaluate cell proliferation. Scale bar, 50 μm. **(J,K)** Flow cytometry assays show that circCRIM1 can accelerate the G1 to S phase cell cycle transition, while circCRIM1 knockdown increases the percentage of G1 phase cells. All data are presented as the means ± SD of three independent experiments. $^{*}p < 0.05$, $^{**}p < 0.01$, and $^{***}p < 0.001$.

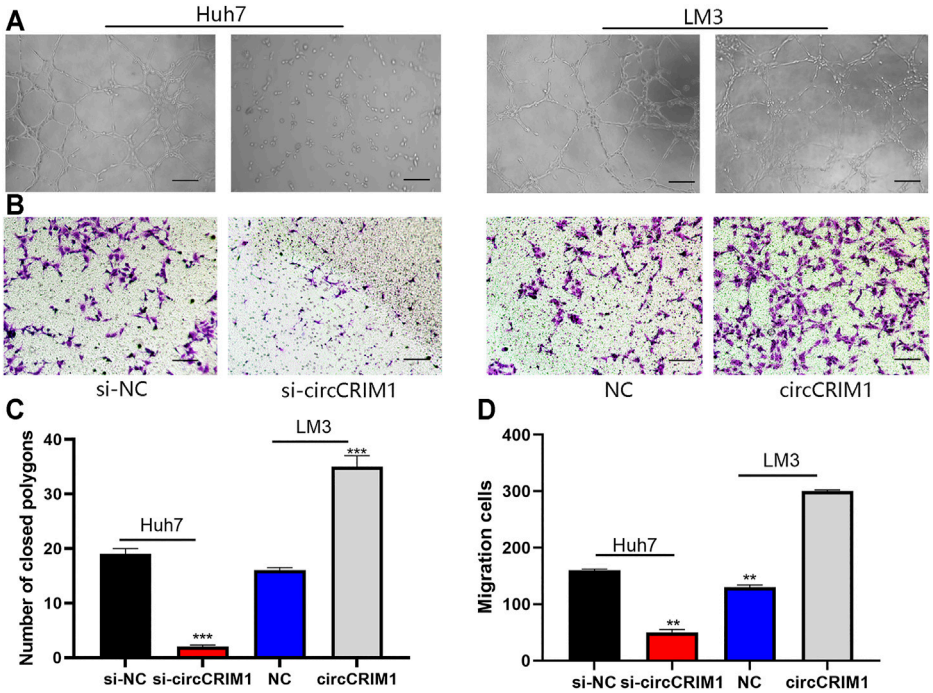

FIGURE 3 | CircCRIM1 enhances the angiogenic capability of HCC cells. **(A,C)** Tube formation assays with HUVECs in indicated conditioned media. Numbers of branches were calculated using Image Pro Plus 6. Scale bar, 50 μm. **(B,D)** Endothelial recruitment assays with HUVECs performed for each group. Scale bar, 50 μm Cell migration was quantified using cell numbers. All experiments were performed three times. Data are mean ± SD. *$p < 0.05$, **$p < 0.01$, and ***$p < 0.001$.

CircCRIM1 Enhances Angiogenic Capability of HCC Cells

Angiogenesis is essential for tumor cell proliferation. In order to study the functions of circCRIM1 in HCC angiogenesis, different tumor-conditioned media (TCM) were used to perform endothelial recruitment and tube formation assays *in vitro*. Compared with the control group, human umbilical cord endothelial cell (HUVEC) tube formation was decreased in the si-cricCRIM1 group (**Figures 3A,C**). The capability of LM3 cells to accelerate HUVEC tube formation was boosted in the circCRIM1 overexpression group (**Figures 3A,C**). Next, the function of cricCRIM1 in HUVEC migration was investigated using endothelial recruitment assays. Compared with the control group, the extent of HUVEC migration was enhanced by TCM, which was collected from LM3 cells transfected with circCRIM1-overexpressing plasmids (**Figures 3B,D**). On the contrary, TCM originating from si-circCRIM1 Huh7 cells significantly decreased HUVEC migration (**Figures 3B,D**). Taken together, these data demonstrate that circCRIM1 enhances the capacity of cancer cells to accelerate HUVEC migration and tube formation.

CircCRIM1 Functions as miR-378a-3p Sponge in HCC

Researchers have suggested that circRNAs have the ability to sponge miRNA to regulate gene expression (Wu et al., 2019). Therefore, we analyzed the circCRIM1 sequence using miRanda, circbank, and RNAhybrid (Xia et al., 2009; Krol et al., 2010). Eight candidate miRNAs that may bind to circCRIM1 were identified for further study (**Figure 4A**). Next, the biotinylated circCRIM1 probe was used for the pull-down assay to indirectly capture binding miRNAs. The fold changes in miR-378a-3p pulled down by the circCRIM1-specific probe were observed in both HCC cell types (**Figures 4B,C**). Silencing or overexpressing circCRIM1 resulted in fold changes in the microRNA expression in LM3 or Huh7 cells, respectively (**Figures 4D,E**). To identify the relationship between circCRIM1 and miR-378a-3p, a dual-luciferase reporter assay was carried out. Special luciferase plasmids with cloned full-length circCRIM1 were constructed and transfected into cells with the microRNA mimics or inhibitor. Luciferase reporter genes contained the primary wild-type (WT) or mutant (MUT) circCRIM1 sequence based on the binding site (**Figure 4F**). When circCRIM1-WT reporter genes and the microRNA mimics were co-transfected into LM3 cells, the result was obviously decreased, while the inhibitor enhanced the luciferase activity of Huh7 cells that were transfected with WT plasmids. However, miR-378a-3p mimics, inhibitor, or corresponding negative control (NC) did not alter the results of luciferase activity after co-transfection with mutant reporters, indicating that circCRIM1 expression has an opposite effect on miR-378a-3p expression (**Figures 4G,H**). In general, miRNAs bind to Argonaute-2 (AGO2), which has a key role in RISC components (Xia et al., 2009). Thus, an anti-AGO2 RIP assay (Zhang et al., 2021) was carried out. At the same time, the data suggested that both circCRIM1 and miR-378a-3p from LM3

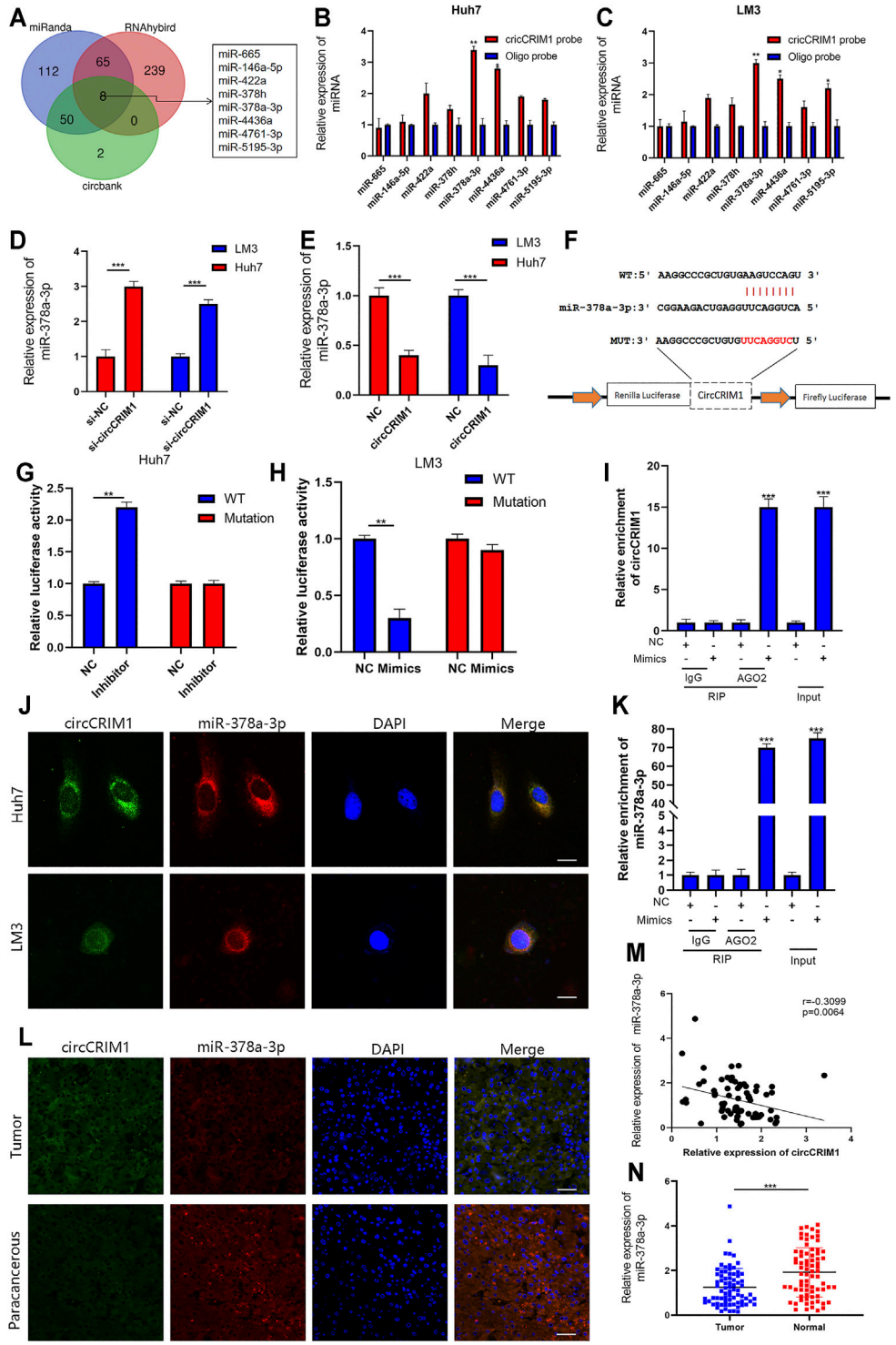

FIGURE 4 | CircCRIM1 functions as miR-378a-3p sponge in HCC **(A)** Venn diagram showing the overlap of target miRNAs for circCRIM1 predicted by miRanda, circbank, and RNAhybrid. **(B,C)** Relative abundance of eight miRNA candidates in Huh7 and LM3 lysates with circCRIM1 or oligo probe was examined by qRT-PCR. **(D,E)** Relative levels of miR-378a-3p in Huh7 and LM3 cell lines transfected with si-circCRIM1, si-NC, circCRIM1, or NC were detected by qRT-PCR **(F)** Schematic of wild-type (WT) and mutant (MUT) circCRIM1 luciferase reporter vectors **(G,H)** Effects of miR-378a-3p mimics, inhibitor, and NC on luciferase activity were detected in HCC cells transfected with luciferase reporter vectors expressing WT, MUT, or NC. **(I,J)** RIP assay for circCRIM1 was performed with anti-AGO2 antibody in HCC cells transfected with mimics or NC, and expression of circCRIM1 and miR-378a-3p was detected by qRT-PCR. **(K)** Co-localization of circCRIM1 and miR-378a-3p in HCC cells was detected using a FISH assay. Scale bar,10 μm **(L)** FISH results showing co-localization of circCRIM1 and miR-378a-3p in HCC and para-cancerous tissues from patients. Scale bar, 25 μm **(M)** Obviously negative correlation between levels of circCRIM1 and miR-378a-3p in 76 pairs of freshly-frozen HCC tissues and matched normal liver tissues was analyzed by Pearson correlation analysis. **(N)** Relative miR-378a-3p expression in 76 pairs of freshly-frozen HCC tissues and matched normal liver tissues. All data are presented as the means ± SD of three independent experiments. *$p < 0.05$, **$p < 0.01$, and ***$p < 0.001$.

TABLE 2 | Correlation between miR-378a-3p expression and clinicopathological features in HCC tissues (n = 76, χ^2-test).

	miR-378a-3p expression		
	High	Low	—
Variable	38	38	*p*-value
Age (year)	—	—	0.8028
<60	27	26	—
≥60	11	12	—
Gender	—	—	0.0816
Male	25	24	—
Female	13	14	—
Tumor size	—	—	0.0029*
<5 cm	26	13	—
≥5 cm	12	25	—
TNM stage	—	—	0.0058*
I–II	26	14	—
III–IV	12	24	—
Liver cirrhosis	—	—	0.8154
Yes	22	23	—
No	16	15	—
AFP (ng/ml)	—	—	0.3561
≤200	15	19	—
>200	23	19	—
HBsAg	—	—	0.1181
Positive	25	31	—
Negative	13	7	—
Edmondson grade	—	—	0.0280*
I–II	30	21	—
III–IV	8	17	—
$p < 0.05$	—	—	—

cell lysates were combined via anti-AGO2 antibody, rather than IgG (**Figures 4I,J**). FISH assays revealed that both of them were more co-localized in the cytoplasm than in the cell nuclei of Huh7 and LM3 cells (**Figure 4K**). In addition, FISH suggested that circCRIM1 was significantly expressed in the HCC samples, while the miRNA was mostly located in the para-cancerous tissues (**Figure 4L**). Contrary to circCRIM1, miR-378a-3p had a lower expression in HCC tissues than in liver para-cancerous tissues (**Figures 4M,N**). The miRNA in HCC tissues had a clinical significance with tumor size (p = 0.0029), TNM stage (p = 0.0058), and as well as Edmondson grade (p = 0.028; **Table 2**). Moreover, patients with high expression of miR-378a-3p had better OS (**Supplementary Figure S1**). These data reveal that circCRIM1 functions as a sponge for miR-378a-3p in HCC.

MiR-378a-3p Attenuates Oncogenic Effects of circCRIM1 in HCC Cells

Rescue experiments were implemented with co-transfection of the miRNA mimics or their inhibitors with si-circCRIM1 or circCRIM1 plasmids. QRT-PCR was employed to verify the effects of its mimics and inhibitors in LM3 and Huh7 cells (**Figures 5A,B**). The results showed that the inhibitors significantly promoted the growth of Huh7 cells, while the inhibitory effect on Huh7 cell proliferation caused by circCRIM1 downregulation was reversed by the introduction of the mentioned inhibitors in CCK-8 assays, colony formation, and EdU assays (**Figures 5C–G**). Data were also obtained after transfection with mimics and circCRIM1 plasmids in LM3 cells (**Supplementary Figure S1**). In conclusion, miR-378a-3p plays an anti-oncogenic function in HCC cells and acts as a critical downstream target of circCRIM1.

SKP2 Is a Direct Target of miR-378a-3p and Indirectly Regulated by circCRIM1

To investigate the regulatory molecule mechanism of miR-378a-3p in HCC, four online databases (TargetScan, miRDB, Starbase, and miRWalk) were used to search for its candidate target genes (Xia et al., 2009; Li J.-H. et al., 2014; Wong and Wang, 2015; Sticht et al., 2018). A total of 21 genes were filtered out from the four databases by overlapping the prediction results for miR-378a-3p (**Figure 6A**). QRT-PCR experiments were conducted to detect the expression of these genes in Huh7 and LM3 cells with the miRNA mimics or inhibitors. The results suggested that SKP2 was the most likely target (**Figure 6B**). In addition, miR-378a-3p silencing up-regulated the expression of SKP2 in HCC cells, while its mimics transfected into HCC cells obviously decreased the mRNA and protein levels of SKP2 (**Figures 6C,D**). Moreover, SKP2 expression was up-regulated with circCRIM1 overexpression, while co-transfection with miR-378a-3p mimics recovered SKP2 expression in LM3 cells. At the same time, Huh7 cells were co-transfected with si-circCRIM1 and the microRNA inhibitors. The depletion of miR-378a-3p rescued the abundance of SKP2, which was down-regulated by si-circCRIM1 (**Figures 6E–G**). A luciferase reporter gene assay was then performed to further evaluate the connection between SKP2 mRNA and miR-378a-3p. In addition, luciferase reporter plasmids containing WT SKP2 3′-UTRs and MUT SKP2 3′-UTRs were constructed (**Figure 6H**). The WT plasmids' luciferase activity was significantly inhibited by the miRNA mimics and increased by the inhibitors. Conversely, the MUT plasmid co-transfection with miR-378a-3p mimics or inhibitors exhibited no evident differences (**Figures 6I,J**). The SKP2 expression levels of HCC tissues were negatively connected with miR-378a-3p (**Figure 6M**). In addition, immunohistochemistry (IHC) and qRT-PCR assays further confirmed that SKP2 was higher in HCC samples than in adjacent normal samples (**Figure 6K,L**). Meanwhile, HCC patients in the high SKP2 expression group had a worse OS (Figure. S2F). These results suggest that circCRIM1 up-regulates SKP2 by interacting with miR-378a-3p in HCC.

CircCRIM1 Enhances HCC Proliferation and Angiogenesis via miR-378a-3p/SKP2 Axis

To further evaluate the influence of the circCRIM1/miR-378a-3p/SKP2 axis on HCC cell growth, a short hairpin RNA and lentivirus were constructed to regulate the expression of SKP2. SKP2 was silenced or overexpressed in HCC cells, and the SKP2 expression was measured via qRT-PCR and western blotting (**Figures 7A–C**). Subsequently, colony formation, EdU, and CCK-8 assay results suggested that SKP2 overexpression accelerated the growth of Huh7 cells (**Figures 7D–H**). On the

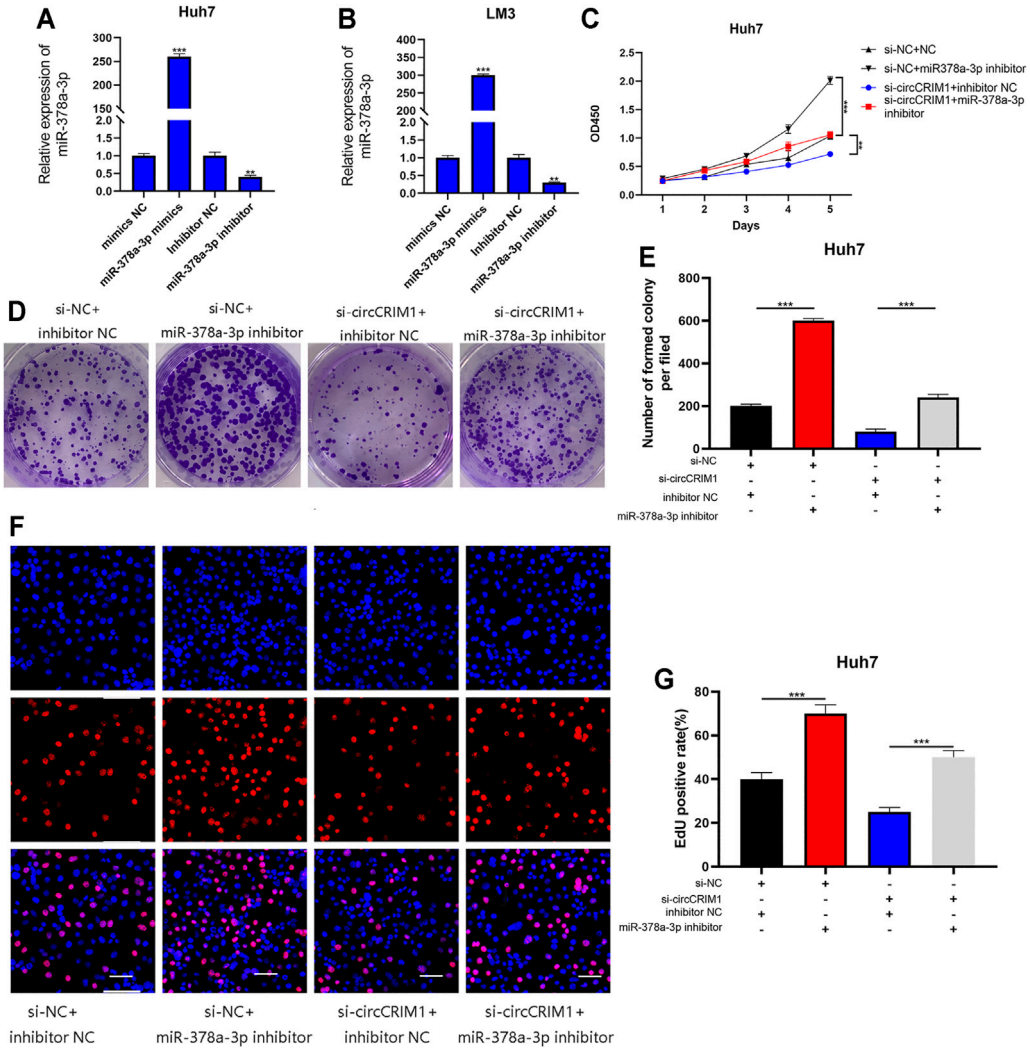

FIGURE 5 | MiR-378a-3p attenuates the oncogenic effects of circCRIM1 in HCC cells. **(A,B)** Expression of miR-378a-3p in LM3 and Huh7 cells transfected with miR-378a-3p mimics, inhibitor, and corresponding NC was detected by qRT-PCR. **(C)** Cellular growth curves were evaluated by CCK-8 assays after transfection with miR-378a-3p inhibitor and NC in Huh7 cells. **(D,E)** Colony formation assays were performed to evaluate cell proliferation. **(F,G)** EdU assays for HCC cells were performed to evaluate cell proliferation. Scale bar, 50 μm. All data are presented as the means ± SD of three independent experiments. $^{*}p < 0.05$, $^{**}p < 0.01$, $^{***}p < 0.001$, and $^{****}p < 0.0001$.

contrary, SKP2 silencing had an opposite effect on LM3 cells (**Supplementary Figure S2**). Furthermore, Skp2 overexpression largely reversed the inhibition of malignant biological behavior following disruption of circCRIM1 expression (**Figures 7D–H**), while the proliferation of HCC cells enhanced by circCRIM1 overexpression was inhibited by SKP2 knockdown (**Supplementary Figure S2**). In summary, circCRIM1 promotes HCC proliferation and relies on the miR-378a-3p/SKP2 axis.

As mentioned, circCRIM1 promotes cell proliferation by accelerating the transition from G1 to S phase. The SKP2 plasmid and si-circCRIM1 were transfected into HCC cells. The resulting data indicated that the G0/G1 phase arrest was reversed (**Supplementary Figure S3A**). Western blot assays were then used to detect key molecules involved in the G1/S transition. The related protein levels of CDK4, CDK6, cyclin D1, and cyclin E1 were significantly decreased, while P27 was upregulated in Huh7 cells after circCRIM1 silencing, which was consistent with the G0/G1 phase arrest (**Supplementary Figure S3B**). Previous research has reported that SKP2 is required for induction of vascular smooth muscle cell proliferation (Wang et al., 2017). We further examined whether circCRIM1 induces angiogenesis via SKP2 by performing rescue experiments. The results showed that culture with si-circCRIM1 CM, significantly inhibited HUVEC tube formation and endothelial recruitment compared with si-NC CM, which could be fully reversed by SKP2 overexpression

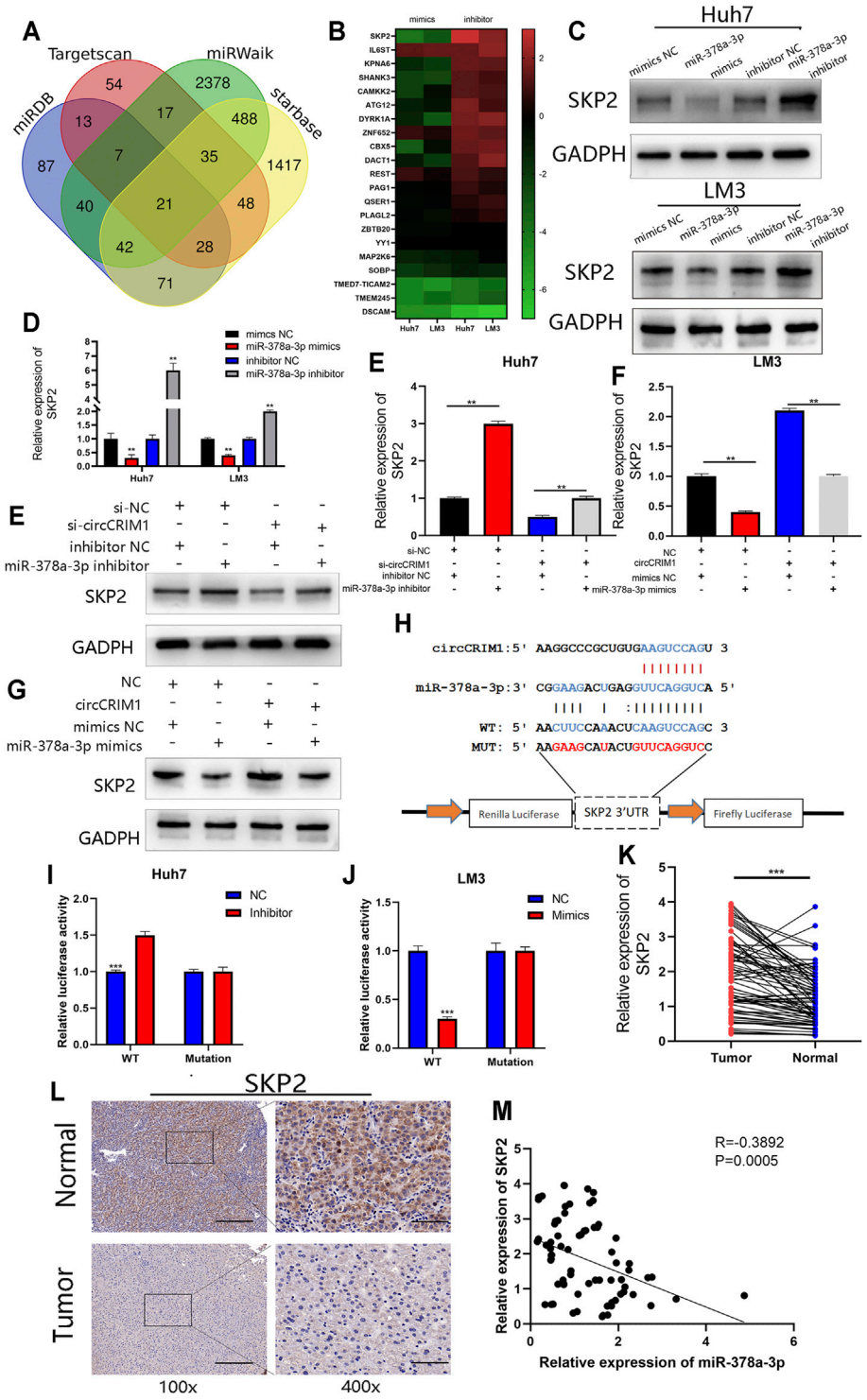

FIGURE 6 | SKP2 is a direct target of miR-378a-3p and is indirectly regulated by circCRIM1. **(A)** Venn diagram showing 21 genes that are putative miR-378a-3p targets predicted by four algorithms (TargetScan, miRDB, starbase, and miRWalk). **(B)** Heat map was used to visualize the expression of predicted target genes in LM3 and Huh7 cells transfected with miR-378a-3p mimics, inhibitor, and corresponding NC. **(C,D)** SKP2 expression in Huh7 and LM3 cells was analyzed by RT-qPCR and western blotting after transfection with miR-378a-3p mimics, inhibitor, and corresponding NC. **(E–G)** SKP2 expression was analyzed by RT-qPCR and western blotting. LM3 cells were transfected with miR-378a-3p mimic or co-transfected with corresponding indicated circCRIM1 vectors and Huh7. **(H)** Schematic of SKP2 3′UTR WT and MUT luciferase reporter vectors. **(I,J)** Effects of miR-378a-3p mimics and inhibitor on luciferase activities of SKP2 3′UTR WT and MUT. **(K)** RT-qPCR analysis of SKP2 expression in HCC tissues (n = 76) paired with adjacent normal tissues (n = 76). **(L)** IHC staining of SKP2 in HCC and adjacent normal tissues from patients. Samples were imaged at 100× and 400× magnification. Scale bar, 100 and 25 μm **(M)** Negative relationship between levels of miR-378a-3p and SKP2 was identified in 76 paired HCC and normal liver tissues by Pearson correlation analysis. All data are presented as the means ± SD of three independent experiments. *p < 0.05, **p < 0.01, ***p < 0.001, and ****p < 0.0001.

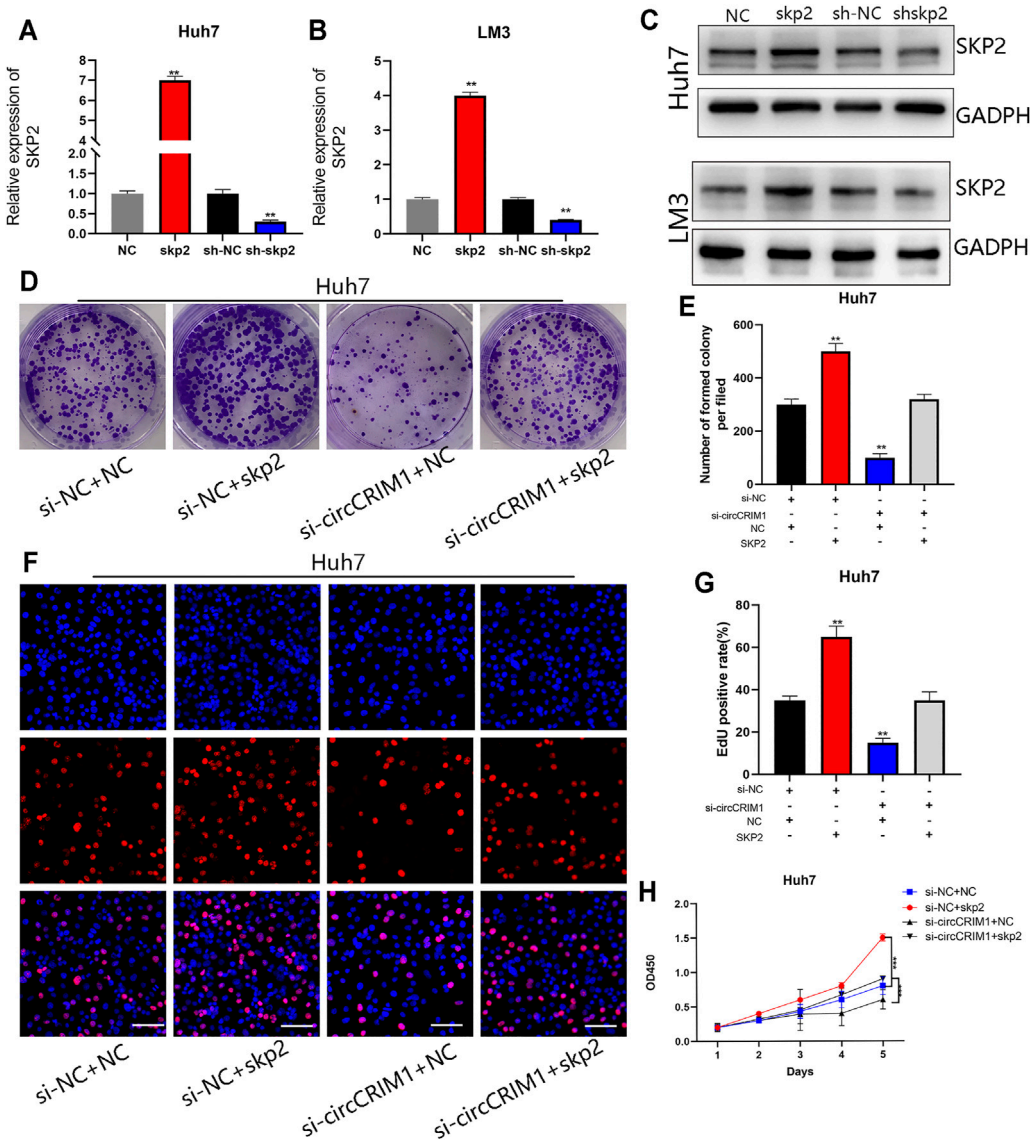

FIGURE 7 | CircCRIM1 promotes HCC proliferation and angiogenesis via miR-378a-3p/SKP2 axis. **(A–C)** Transfection efficiency of shSKP2, shNC, SKP2, and NC in LM3 and Huh7 cells was verified by RT-qPCR and western blotting. **(D,E)** Colony formation assays were performed to evaluate cell proliferation. **(F,G)** EdU assays for HCC cells were performed to evaluate cell proliferation. Scale bar, 50 μm. **(H)** Cellular growth curves were evaluated by CCK-8 assays in Huh7 cells. All data are presented as the means ± SD of three independent experiments. $^{*}p < 0.05$, $^{**}p < 0.01$, $^{***}p < 0.001$, and $^{****}p < 0.0001$.

(**Supplementary Figures S3D,E**). In summary, circCRIM1 promotes the angiogenesis of HUVECs and cell cycle transition of HCC cells via SKP2.

CircCRIM1 Promotes HCC Xenograft Growth *in vivo*

To further investigate whether circCRIM1 contributes to the growth of tumor cells, an *in vivo* xenograft tumor model was established using LM3 and Huh7 cells. LM3 cells were effectively transfected with stably overexpressed circCRIM1 or NC and Huh7 cells were silenced by si-circCRIM1 or si-NC. Afterwards, the mice were evaluated every 3 days and sacrificed after 5 weeks. The results showed that tumors derived from si-circCRIM1 Huh7 cells grew more slowly than those derived from si-circCRIM1 NC cells (**Figure 8A**). Compared with the NC group, the si-circCRIM1 group developed tumors with lower weights and volumes (**Figures 8B,C**). In contrast, mice inoculated with LM3 circCRIM1-overexpressing cells had a larger mean tumor volume and weight than the control group during the fifth week (**Figures 8A–C**). Additionally, circCRIM1 expression was observed in the

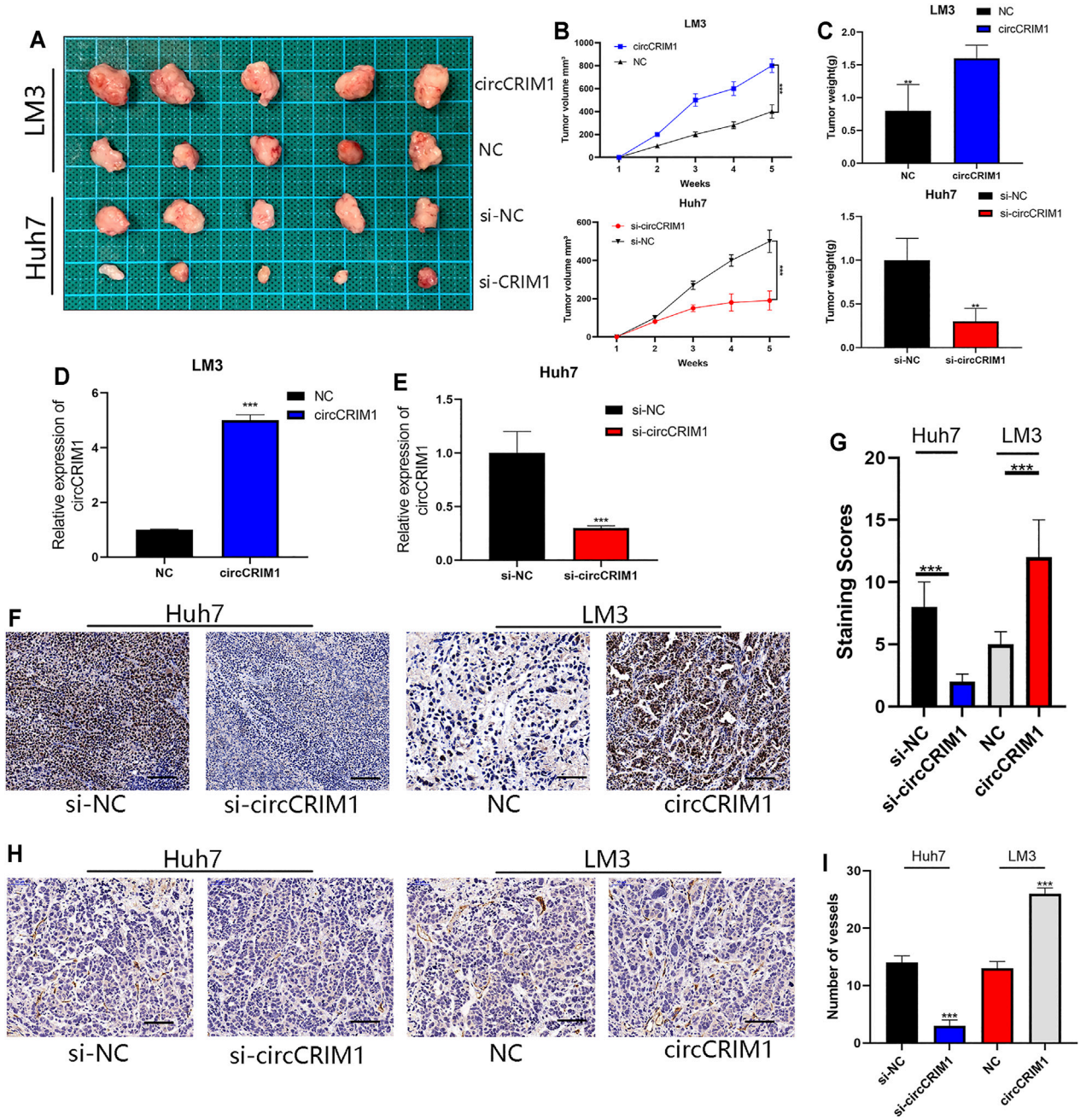

FIGURE 8 | CircCRIM1 promotes HCC xenograft growth *in vivo*. **(A)** Representative images of subcutaneous xenograft tumors ($n = 5$ for each group). **(B)** Growth curves for tumor volumes, which were measured every week. **(C)** Tumor weight analysis. **(D,E)** Expression of circCRIM1 was observed in mouse tumors from each group. **(F,G)** IHC staining of xenograft tumors. SKP2 protein levels were analyzed based on IHC staining. Scale bar, 25 μm **(H,I)** Blood vessels were stained using anti-CD34 and positively stained vessels were counted in five areas per slide to determine maximum number of micro-vessels, ten slides per experiment. Scale bar, 25 μm. All data are presented as the means ± SD of three independent experiments. $^{*}p < 0.05$, $^{**}p < 0.01$, $^{***}p < 0.001$, and $^{****}p < 0.0001$.

tumors of mice from each group (**Figures 8D,E**). IHC was also used to investigate Skp2 level and CD34 expressions in xenografts. Lower expression of SKP2 in the si-circCRIM1 group and higher SKP2 expression in the circCRIM1 group were detected (**Figures 8F,G**). Compared with the si-NC tumors, the tumor-containing si-circCRIM1 Huh7 cells had smaller and fewer vessels. The CD34-marked tumor vessels in circCRIM1-overexpressing tumors were larger and more abundant, while SKP2 expression was obviously higher (**Figures 8H,I**). Overall, circCRIM1 promoted the proliferation and angiogenesis of HCC *in vivo*, confirming our *in vitro* findings.

DISCUSSION

Statistical analysis shows that although diagnosis and treatment methods have greatly improved during the past decades, the five-year OS rate in HCC patients remained at a disappointing level (Allemani et al., 2018). Currently, chemotherapy, targeted therapy, and immunotherapy are the primary treatment choices for advanced HCC patients (Greten et al., 2019; Mahipal et al., 2019). However, surgery is still the most efficient tool that prolongs patient survival (Bai et al., 2021). Therefore, it is necessary to investigate new molecular HCC targets for early diagnosis and treatment.

Recently, circRNAs have been demonstrated to play critical roles in the progression of cancers, such as migration, invasion, metastasis (Hu et al., 2020), and chemotherapy resistance (Weng et al., 2021). CircRNAs regulate target gene expression by sponging miRNAs, directly binding to specific proteins, or encoding functional oligopeptides (Wu et al., 2020; Zhou et al., 2021). For example, circZNF566 sponged miR-4738-3p to accelerate the progression of HCC(Li S. et al., 2020). CircBACH1 promoted the growth of HCC by interacting with p27 (Liu B. et al., 2020). In colon cancer, circFNDC3B encoded a novel oligopeptide to regulate cancer progression. CircCRIM1 has been identified as a tumor-associated factor in human cancers. For example, in nasopharyngeal carcinoma, circCRIM1 has been shown to promote the proliferation, invasion, metastasis, and chemoresistance by sponging miR-422a (Hong et al., 2020), while circCRIM1 accelerated the progression and facilitated the autophagy of osteosarcoma by targeting miR-432-5p (Liu J. et al., 2020). However, circCRIM1 has also been identified as a tumor-suppressive factor that inhibits metastasis in lung adenocarcinoma by interacting with miR-182 and miR-93 (Hong et al., 2020). The present study determined that circCRIM1 has a high expression in HCC samples and is closely related to malignant HCC progression, making it a promising prognostic biomarker. Tumor growth slows down when tumor volume exceeds 2–3 mm^3 (Harper and Moses, 2006) due to the lack of a vascular system. In this case, the angiogenic switch is activated to facilitate cancer growth and metastasis. Importantly, it has been discovered that circCRIM1 silencing significantly inhibits both HCC cell proliferation and angiogenesis, indicating that circCRIM1 has a strong tumor-promoting effect. Emerging evidence suggests that circRNAs can function as a sponge to silence miRNA and regulate expression of the targeted gene (Han et al., 2017; Wu et al., 2021).

Using bioinformatics analysis with miRanda, circbank, and RNAhybrid, miR-378a-3p was determined to be a target of circCRIM1 in HCC cells and identified as a tumor-suppressive factor. Cai et al. have reported that it promotes the sorafenib sensitivity in HCC cells (Lin et al., 2020). Moreover, Cheng et al. have suggested that the microRNA inhibition accelerates the metastasis of oral squamous cell carcinoma (Wang et al., 2018). In addition, Han et al. have observed that it inhibits the growth of colorectal cancer and induces apoptosis (Li H. et al., 2014). The present RNA pull-down assay results revealed that it is the most abundant miRNA in the complex. In addition, dual-luciferase reporter assay, FISH, and anti-AGO2 RNA immunoprecipitation (RIP) assays collectively suggested HCC cell cytoplasm might be the location of circCRIM1 and miR-378a-3p, where circCRIM1 interaction occurs and decreases its expression. Furthermore, rescue experiments revealed that circCRIM1 knockdown effects can be reversed by the inhibitors. The present experimental data demonstrated that circCRIM1 sponge this miRNA during the progression of HCC, which is consistent with the results mentioned above, indicating that circCRIM1 plays a critical role in HCC progression.

SKP2 is a RING-finger type ubiquitin ligase, a well-characterized member of CRLs, and a functional component of ligase complex SCF. Several statistical analyses showed that SKP2 promotes the progression and induces tumorigenesis of nasopharyngeal carcinoma (Yu et al., 2019) and accelerates the growth of renal cell carcinoma (Chen et al., 2021). The present experimental results verified SKP2 as the most likely target of miR-378a-3p. Furthermore, the microRNA reversed the effect of circCRIM1 by promoting SKP2 expression and HCC proliferation, while SKP2 silencing attenuated the tumor-promoting capability of circCRIM1. This result revealed that circCRIM1 can sponge it to increase the expression of target gene SKP2, thus promoting the progression of HCC. Subsequently, circCRIM1 was shown to promote HCC angiogenesis *in vivo* and *in vitro* via the circCRIM1/miR-378a-3p/SKP2 axis. All of these results provided a promising direction for circCRM1-based biotherapeutics. Several studies have suggested that circRNAs exist in the serum or some tumor tissues (Tian and Wang, 2016), suggesting that they have the potential to be biomarkers for specific diseases or targets for carcinoma treatment. Thus, more studies are needed to verify its presence in the serum of HCC patients. In addition, the function and mechanism of circCRIM1 in HCC need to be determined and its potential to be a prognosis target explored.

In summary, the present study revealed that circCRIM1 is highly upregulated in HCC tissues and acts as a promoter in tumorigenesis and angiogenesis via the circCRIM1/miR-378a-3p/SKP2 axis (**Supplementary Figure S3C**). The performance of circCRIM1 *in vivo* indicates that it can function as a possible prognosis prediction factor and used for future targeted therapy in HCC patients.

DATA AVAILABILITY STATEMENT

The raw data supporting the conclusion of this article will be made available by the authors, without undue reservation.

ETHICS STATEMENT

The studies involving human participants were reviewed and approved by the Ethics Committee of the First Affiliated Hospital of Nanjing Medical University. The patients/participants provided their written informed consent to participate in this study.

AUTHOR CONTRIBUTIONS

FZ, HL, XL, and CZ designed the study. YJ, SY, XuY, LZ, and FY performed the experiments. YJ, SY, and YL wrote the manuscript. WY, XiY, LS, XZ, ML, and JX collected the samples. All authors contributed to the writing and reviewing of the manuscript and approved the final manuscript for submission.

FUNDING

This work was supported by the National Natural Science Foundation of China (81971504), Post-Doctoral Special Foundation of China (2020M670065ZX), Post-Doctoral Foundation of Jiangsu Province (2020Z021), Postgraduate Research and Practice Innovation Program of Jiangsu Province (SJCX20_0474), and Changzhou Society Development Funding (CE20205038), The lifting Project of Young Scientific and Technological Talents in Changzhou (2021).

SUPPLEMENTARY MATERIAL

The Supplementary Material for this article can be found online at: https://www.frontiersin.org/articles/10.3389/fcell.2021.796686/full#supplementary-material

Supplementary Figure S1 | MiR-378a-3p attenuates the oncogenic effects of circCRIM1 in LM3 cells.

Supplementary Figure S2 | CircCRIM1 promotes LM3 cell proliferation via the miR-378a-3p/SKP2 axis.

Supplementary Figure S3 | CircCRIM1 promotes HCC proliferation and angiogenesis *via* the miR-378a- 3p/SKP2 axis.

Supplementary Table S1 | Primers for qRT-PCR used in this study.

Supplementary Table S2 | Antibodies used in this study.

Supplementary Table S3 | Eight candidate miRNAs binding to circCRIM1 predicted by cross-analyzing three miRNA target prediction databases.

Supplementary Table S4 | Twenty-one candidate miRNAs binding to miR-378a-3p predicted by cross-analyzing four mRNA target prediction databases.

REFERENCES

Allemani, C., Matsuda, T., Di Carlo, V., Harewood, R., Matz, M., Nikšić, M., et al. (2018). Global Surveillance of Trends in Cancer Survival 2000-14 (CONCORD-3): Analysis of Individual Records for 37 513 025 Patients Diagnosed with One of 18 Cancers from 322 Population-Based Registries in 71 Countries. *Lancet* 391 (10125), 1023–1075. doi:10.1016/S0140-6736(17)33326-3

Bai, Y., Lian, Y. e., Wu, J., Chen, S., Lai, J., Zheng, Y., et al. (2021). A Prognostic Scoring System for Predicting Overall Survival of Patients with the TNM 8th Edition Stage I and II Hepatocellular Carcinoma after Surgery: A Population-Based Study. *Cmar* 13, 2131–2142. doi:10.2147/CMAR.S289826

Cao, M., Li, H., Sun, D., and Chen, W. (2020). Cancer burden of Major Cancers in China: A Need for Sustainable Actions. *Cancer Commun.* 40 (5), 205–210. doi:10.1002/cac2.12025

Chen, L.-Y., Wang, L., Ren, Y.-X., Pang, Z., Liu, Y., Sun, X.-D., et al. (2020). The Circular RNA Circ-ERBIN Promotes Growth and Metastasis of Colorectal Cancer by miR-125a-5p and miR-138-5p/4EBP-1 Mediated Cap-independent HIF-1α Translation. *Mol. Cancer* 19 (1), 164. doi:10.1186/s12943-020-01272-9

Chen, T., Liu, L., Zou, Y., Hu, X., Zhang, W., Zhou, T., et al. (2021). Nobiletin Downregulates the SKP2-P21/p27-CDK2 axis to Inhibit Tumor Progression and Shows Synergistic Effects with Palbociclib on Renal Cell Carcinoma. *Cancer Biol. Med.* 18 (1), 227–244. doi:10.20892/j.issn.2095-3941.2020.0186

Greten, T. F., Lai, C. W., Li, G., and Staveley-O'Carroll, K. F. (2019). Targeted and Immune-Based Therapies for Hepatocellular Carcinoma. *Gastroenterology* 156 (2), 510–524. doi:10.1053/j.gastro.2018.09.051

Gu, X., Zhang, J., Ran, Y., Pan, H., Jia, J., Zhao, Y., et al. (2021). Circular RNA Hsa_circ_101555 Promotes Hepatocellular Carcinoma Cell Proliferation and Migration by Sponging miR-145-5p and Regulating CDCA3 Expression. *Cell Death Dis* 12 (4), 356. doi:10.1038/s41419-021-03626-7

Han, D., Li, J., Wang, H., Su, X., Hou, J., Gu, Y., et al. (2017). Circular RNA circMTO1 Acts as the Sponge of microRNA-9 to Suppress Hepatocellular Carcinoma Progression. *Hepatology* 66 (4), 1151–1164. doi:10.1002/hep.29270

Harper, J., and Moses, M. A. (2006). Molecular Regulation of Tumor Angiogenesis: Mechanisms and Therapeutic Implications. *EXS* (96), 223–268. doi:10.1007/3-7643-7378-4_10

Hong, X., Liu, N., Liang, Y., He, Q., Yang, X., Lei, Y., et al. (2020). Circular RNA CRIM1 Functions as a ceRNA to Promote Nasopharyngeal Carcinoma Metastasis and Docetaxel Chemoresistance through Upregulating FOXQ1. *Mol. Cancer* 19 (1), 33. doi:10.1186/s12943-020-01149-x

Hu, Z. Q., Zhou, S. L., Li, J., Zhou, Z. J., Wang, P. C., Xin, H. Y., et al. (2020). Circular RNA Sequencing Identifies CircASAP1 as a Key Regulator in Hepatocellular Carcinoma Metastasis. *Hepatology* 72 (3), 906–922. doi:10.1002/hep.31068

Kristensen, L. S., Andersen, M. S., Stagsted, L. V. W., Ebbesen, K. K., Hansen, T. B., and Kjems, J. (2019). The Biogenesis, Biology and Characterization of Circular RNAs. *Nat. Rev. Genet.* 20 (11), 675–691. doi:10.1038/s41576-019-0158-7

Krol, J., Loedige, I., and Filipowicz, W. (2010). The Widespread Regulation of microRNA Biogenesis, Function and Decay. *Nat. Rev. Genet.* 11 (9), 597–610. doi:10.1038/nrg2843

Li, C., Du, L., Ren, Y., Liu, X., Jiao, Q., Cui, D., et al. (2019). SKP2 Promotes Breast Cancer Tumorigenesis and Radiation Tolerance through PDCD4 Ubiquitination. *J. Exp. Clin. Cancer Res.* 38 (1), 76. doi:10.1186/s13046-019-1069-3

Li, H., Dai, S., Zhen, T., Shi, H., Zhang, F., Yang, Y., et al. (2014a). Clinical and Biological Significance of miR-378a-3p and miR-378a-5p in Colorectal Cancer. *Eur. J. Cancer* 50 (6), 1207–1221. doi:10.1016/j.ejca.2013.12.010

Li, J.-H., Liu, S., Zhou, H., Qu, L.-H., and Yang, J.-H. (2014b). starBase v2.0: Decoding miRNA-ceRNA, miRNA-ncRNA and Protein-RNA Interaction Networks from Large-Scale CLIP-Seq Data. *Nucl. Acids Res.* 42, D92–D97. doi:10.1093/nar/gkt1248

Li, S., Weng, J., Song, F., Li, L., Xiao, C., Yang, W., et al. (2020a). Circular RNA circZNF566 Promotes Hepatocellular Carcinoma Progression by Sponging miR-4738-3p and Regulating TDO2 Expression. *Cell Death Dis* 11 (6), 452. doi:10.1038/s41419-020-2616-8

Li, Z., Yao, H., Wang, S., Li, G., and Gu, X. (2020b). CircTADA2A Suppresses the Progression of Colorectal Cancer via miR-374a-3p/KLF14 axis. *J. Exp. Clin. Cancer Res.* 39 (1), 160. doi:10.1186/s13046-020-01642-7

Lin, H., Ruan, G. Y., Sun, X. Q., Chen, X. Y., Zheng, X., and Sun, P. M. (2019). Effects of RNAi-induced Skp2 I-nhibition on C-ell C-ycle, A-poptosis and P-roliferation of E-ndometrial C-arcinoma C-ells. *Exp. Ther. Med.* 17 (5), 3441–3450. doi:10.3892/etm.2019.7392

Lin, Z., Xia, S., Liang, Y., Ji, L., Pan, Y., Jiang, S., et al. (2020). LXR Activation Potentiates Sorafenib Sensitivity in HCC by Activating microRNA-378a Transcription. *Theranostics* 10 (19), 8834–8850. doi:10.7150/thno.45158

Liu, B., Yang, G., Wang, X., Liu, J., Lu, Z., Wang, Q., et al. (2020a). CircBACH1 (Hsa_circ_0061395) Promotes Hepatocellular Carcinoma Growth by Regulating P27 Repression via HuR. *J. Cell Physiol* 235 (10), 6929–6941. doi:10.1002/jcp.29589

Liu, J., Feng, G., Li, Z., Li, R., and Xia, P. (2020b). Knockdown of CircCRIM1 Inhibits HDAC4 to Impede Osteosarcoma Proliferation, Migration, and Invasion and Facilitate Autophagy by Targeting miR-432-5p. *Cmar* 12, 10199–10210. doi:10.2147/CMAR.S253130

Mahipal, A., Kommalapati, A., Mehta, R., and Kim, R. D. (2019). "Molecular-Targeted Therapies in Hepatocellular Carcinoma," in *Hepatocellular Carcinoma: Translational Precision Medicine Approaches*. Editor Y. Hoshida (Cham: Humana Press), 225–238. doi:10.1007/978-3-030-21540-8_11

Poliseno, L., Salmena, L., Zhang, J., Carver, B., Haveman, W. J., and Pandolfi, P. P. (2010). A Coding-independent Function of Gene and Pseudogene mRNAs Regulates Tumour Biology. *Nature* 465 (7301), 1033–1038. doi:10.1038/nature09144

Shapira, M. a., Ben-Izhak, O., Linn, S., Futerman, B., Minkov, I., and Hershko, D. D. (2005). The Prognostic Impact of the Ubiquitin Ligase Subunits Skp2 and Cks1 in Colorectal Carcinoma. *Cancer* 103 (7), 1336–1346. doi:10.1002/cncr.20917

Song, P., Wang, S., He, C., Wang, S., Liang, B., Viollet, B., et al. (2011). AMPKα2 Deletion Exacerbates Neointima Formation by Upregulating Skp2 in Vascular Smooth Muscle Cells. *Circ. Res.* 109 (11), 1230–1239. doi:10.1161/CIRCRESAHA.111.250423

Sticht, C., De La Torre, C., Parveen, A., and Gretz, N. (2018). miRWalk: An Online Resource for Prediction of microRNA Binding Sites. *PLoS One* 13 (10), e0206239. doi:10.1371/journal.pone.0206239

Sung, H., Ferlay, J., Siegel, R. L., Laversanne, M., Soerjomataram, I., Jemal, A., et al. (2021). Global Cancer Statistics 2020: GLOBOCAN Estimates of Incidence and Mortality Worldwide for 36 Cancers in 185 Countries. *CA A. Cancer J. Clin.* 71 (3), 209–249. doi:10.3322/caac.21660

Tian, H., and Wang, Q. (2016). Quantitative Analysis of Microcirculation Blood Perfusion in Patients with Hepatocellular Carcinoma before and after Transcatheter Arterial Chemoembolisation Using Contrast-Enhanced Ultrasound. *Eur. J. Cancer* 68, 82–89. doi:10.1016/j.ejca.2016.08.016

Wang, L., Liang, Y., Mao, Q., Xia, W., Chen, B., Shen, H., et al. (2019). Circular RNA Circ CRIM 1 Inhibits Invasion and Metastasis in Lung Adenocarcinoma through the microRNA (miR)-182/miR-93-leukemia Inhibitory Factor Receptor Pathway. *Cancer Sci.* 110 (9), 2960–2972. doi:10.1111/cas.14131

Wang, S.-T., Ho, H. J., Lin, J.-T., Shieh, J.-J., and Wu, C.-Y. (2017). Simvastatin-induced Cell Cycle Arrest through Inhibition of STAT3/SKP2 axis and Activation of AMPK to Promote P27 and P21 Accumulation in Hepatocellular Carcinoma Cells. *Cell Death Dis* 8 (2)–e2626. doi:10.1038/cddis.2016.472

Wang, Y., Zhang, X., Wang, Z., Hu, Q., Wu, J., Li, Y., et al. (2018). LncRNA-p23154 Promotes the Invasion-Metastasis Potential of Oral Squamous Cell Carcinoma by Regulating Glut1-Mediated Glycolysis. *Cancer Lett.* 434, 172–183. doi:10.1016/j.canlet.2018.07.016

Weng, H., Zeng, L., Cao, L., Chen, T., Li, Y., Xu, Y., et al. (2021). circFOXM1 Contributes to Sorafenib Resistance of Hepatocellular Carcinoma Cells by Regulating MECP2 via miR-1324. *Mol. Ther. - Nucleic Acids* 23, 811–820. doi:10.1016/j.omtn.2020.12.019

Wong, N., and Wang, X. (2015). miRDB: an Online Resource for microRNA Target Prediction and Functional Annotations. *Nucleic Acids Res.* 43, D146–D152. doi:10.1093/nar/gku1104

Wu, D., Xia, A., Fan, T., and Li, G. (2021). circRASGRF2 Functions as an Oncogenic Gene in Hepatocellular Carcinoma by Acting as a miR-1224 Sponge. *Mol. Ther. - Nucleic Acids* 23, 13–26. doi:10.1016/j.omtn.2020.10.035

Wu, N., Yuan, Z., Du, K. Y., Fang, L., Lyu, J., Zhang, C., et al. (2019). Translation of Yes-Associated Protein (YAP) Was Antagonized by its Circular RNA via Suppressing the Assembly of the Translation Initiation Machinery. *Cell Death Differ* 26 (12), 2758–2773. doi:10.1038/s41418-019-0337-2

Wu, P., Mo, Y., Peng, M., Tang, T., Zhong, Y., Deng, X., et al. (2020). Emerging Role of Tumor-Related Functional Peptides Encoded by lncRNA and circRNA. *Mol. Cancer* 19 (1), 22. doi:10.1186/s12943-020-1147-3

Xia, W., Cao, G., and Shao, N. (2009). Progress in miRNA Target Prediction and Identification. *Sci. China Ser. C* 52 (12), 1123–1130. doi:10.1007/s11427-009-0159-4

Yu, X., Wang, R., Zhang, Y., Zhou, L., Wang, W., Liu, H., et al. (2019). Skp2-mediated Ubiquitination and Mitochondrial Localization of Akt Drive Tumor Growth and Chemoresistance to Cisplatin. *Oncogene* 38 (50), 7457–7472. doi:10.1038/s41388-019-0955-7

Zhang, D., Ni, N., Wang, Y., Tang, Z., Gao, H., Ju, Y., et al. (2021). CircRNA-vgll3 Promotes Osteogenic Differentiation of Adipose-Derived Mesenchymal Stem Cells via Modulating miRNA-dependent Integrin α5 Expression. *Cell Death Differ* 28 (1), 283–302. doi:10.1038/s41418-020-0600-6

Zhang, S., Chen, Q., Liu, Q., Li, Y., Sun, X., Hong, L., et al. (2017). Hippo Signaling Suppresses Cell Ploidy and Tumorigenesis through Skp2. *Cancer Cell* 31 (5), 669–684. doi:10.1016/j.ccell.2017.04.004

Zhou, B., Yang, H., Yang, C., Bao, Y.-l., Yang, S.-m., Liu, J., et al. (2021). Translation of Noncoding RNAs and Cancer. *Cancer Lett.* 497, 89–99. doi:10.1016/j.canlet.2020.10.002

Zuo, H., Li, X., Zheng, X., Sun, Q., Yang, Q., and Xin, Y. (2021). A Novel circRNA-miRNA-mRNA Hub Regulatory Network in Lung Adenocarcinoma. *Front. Genet.* 12, 673501. doi:10.3389/fgene.2021.673501

Conflict of Interest: The authors declare that the research was conducted in the absence of any commercial or financial relationships that could be construed as a potential conflict of interest.

Publisher's Note: All claims expressed in this article are solely those of the authors and do not necessarily represent those of their affiliated organizations, or those of the publisher, the editors and the reviewers. Any product that may be evaluated in this article, or claim that may be made by its manufacturer, is not guaranteed or endorsed by the publisher.

frontiers in Oncology

ORIGINAL RESEARCH
published: 28 January 2022
doi: 10.3389/fonc.2021.823054

Preoperative Prognostic Nutritional Index and Neutrophil-to-Lymphocyte Ratio Predict Survival Outcomes of Patients With Hepatocellular Carcinoma After Curative Resection

Zhen Qu[1†], Yun-jie Lu[1†], Jia-Wei Feng[1†], Yu-xiang Chen[1], Long-qing Shi[1], Jing Chen[1], Navin Rambaran[2], Yun-Fei Duan[1] and Xiao-zhou He[1*]*

[1] The Third Affiliated Hospital of Soochow University, Changzhou First People's Hospital, Changzhou, China, [2] Department of General Surgery, Georgetown Hospital Complex, Georgetown, Guyana

Increasing evidence indicates that preoperative prognostic indices can serve as independent predictors of survival in patients with cancer. However, the applicability of these indices in patients with hepatocellular carcinoma (HCC) is controversial. This study aims to investigate the prognostic value of these indices in patients with HCC after curative hepatectomy. We retrospectively analyzed the data of 215 patients who underwent curative resection for HCC. Prognostic indices including prognostic nutritional index (PNI) and neutrophil-to-lymphocyte ratio (NLR) were evaluated by comparing by the area under the curve (AUC). Univariate analysis and multivariate analysis were performed to identify independent prognostic factors. Additionally, risk factors were combined to predict the survival of patients. We found that serum albumin concentration, tumor diameter, tumor stage, degree of differentiation, PNI, and NLR were independent prognostic factors for overall survival (OS). Vascular invasion, tumor stage, degree of differentiation, and PNI were independent prognostic factors for recurrence-free survival (RFS). The cutoff value of the PNI and NLR was 43.75 and 3.29, respectively. Patients with low NLR and high PNI had the best outcomes, potentially indicative of the intensive antitumor effects of the immune system. Moreover, patients with at least three risk factors had a significantly lower OS and RFS compared with those with two or fewer risk factors. This new nomogram based on PNI and NLR may provide an accessible and individualized prediction of survival and recurrence for HCC patients.

Keywords: hepatocellular carcinoma, prognostic nutrition index, neutrophil-to-lymphocyte ratio, survival, prognostic factors

OPEN ACCESS

Edited by:
Liangrong Shi,
Central South University, China

Reviewed by:
Jie Pan,
Stanford University, United States
Kurt Sartorius,
University of the Witwatersrand, South Africa

***Correspondence:**
Yun-Fei Duan
duanyunfei1980@suda.edu.cn
Xiao-zhou He
605035098@qq.com

[†]These authors have contributed equally to this work

Specialty section:
This article was submitted to Molecular and Cellular Oncology, a section of the journal Frontiers in Oncology

Received: *26 November 2021*
Accepted: *29 December 2021*
Published: *28 January 2022*

Citation:
Qu Z, Lu Y-j, Feng J-W, Chen Y-x, Shi L-q, Chen J, Rambaran N, Duan Y-F and He X-z (2022) Preoperative Prognostic Nutritional Index and Neutrophil-to-Lymphocyte Ratio Predict Survival Outcomes of Patients With Hepatocellular Carcinoma After Curative Resection. Front. Oncol. 11:823054. doi: 10.3389/fonc.2021.823054

INTRODUCTION

Hepatocellular carcinoma (HCC) is one of the most common cancers with the mortality rate ranking fifth among men and eighth among women (1). Removal of HCC is one of the most effective treatments; however, the high incidence of recurrence remains the leading cause of death after curative resection. As the survival of patients who received potentially curative treatment remains poor, risk factors for postoperative survival should be determined to personalize therapies and improve clinical outcomes.

Increasing evidence shows that the occurrence of systemic inflammation and nutritional disorders promote carcinogenesis by inhibiting apoptosis, promoting angiogenesis, and damaging DNA (2, 3). For example, elevated C-reactive protein (CRP) concentration is associated with lower survival in patients with various malignancies, including HCC (4). Furthermore, it is reported that the presence of an inflammatory response is pathogenic in the development of cancer-associated malnutrition, especially in patients with cirrhosis (5). The prognostic nutritional index (PNI), an overall measure of a patient's immunonutritional condition, has been demonstrated to be an independent prognostic factor in various types of cancer, such as gastric carcinoma (6), colon cancer (7), pancreatic cancer (8), and HCC (9, 10). The previous studies have been reported that the PNI was a prognostic factor for evaluating short- and long-term outcomes after liver resection in HCC patients (9) and preoperative PNI predicts prognosis after curative hepatectomy in early Barcelona clinic liver cancer (BCLC) stage HCC (11). However, in the present study, we further explore the correlation between PNI and other series of prognostic indicators and clinical features; in addition, we aimed to combine two or more risk factors to better predict the prognosis of HCC patients after hepatectomy.

A previous study suggested that the platelet–lymphocyte ratio (PLR) may provide a reliable and individualized prediction of tumor recurrence in HCC patients after radiofrequency ablation (RFA) (12). Other inflammatory-based prognostic indices, notably neutrophil-to-lymphocyte ratio (NLR), γ-glutamyl transferase/alanine aminotransferase ratio (GGT/ALT), and the aspartate aminotransferase/platelet count ratio index (APRI), have been studied for their prognostic roles for various cancers (13–15). A previous study found that high NLR is associated with poor survival in patients with unresectable and recurrent gastric cancer (14), and a high preoperative NLR stood for poor prognostic factor in HCC patients after curative resection while some were in doubt. Preoperative NLR could predict survival better than the conventional alpha-fetoprotein (AFP) in HCC patients after curative resection (16, 17), and NLR was an accurate prognostic marker for OS and PFS of unresectable intermediate and advanced HCC patients on apatinib treatment (18). However, Chan found that NLR had no prognostic significance on OS and disease-free survival in early-stage HCC (11). This may be related to the fact that the author only selected early-stage HCC patients as the research object. Lastly, different methods are used to obtain the cutoff value in previous studies; all of this may lead to the controversial prognostic value of these indices. Therefore, the novelty of the present study compared with previous studies was that the prognostic values of PNI, NLR, APRI, GGT/ALT, and PLR were analyzed in both OS and RFS after curative hepatectomy, that the analysis included all stages of HCC, and we also verified that the combination of PNI, NLR, and other risk factors improved the prognostic value.

MATERIALS AND METHODS

Patients and Methods

This retrospective study was approved by the Institutional Review Board of Changzhou First People's Hospital. All study participants gave written informed consent for the use of their clinical records. A total of 243 patients who received curative surgery for HCC from January 2010 to August 2018 at the Changzhou First People's Hospital were retrospectively reviewed from our department's prospective surgical database. Twenty-eight patients were lost to follow-up and excluded. Exclusion criteria for this study included the following: patients with recurrent or metastatic HCC (n = 10), patients deceased from causes other than HCC (n = 4), patients with preoperative fever (n = 2), infection or systemic inflammatory diseases (n = 2), patients with Child–Pugh C grade (n = 5), patients with hematologic disorders (n = 2), and lack of an entire set of laboratory data (n = 3). In total, 215 patients were ultimately included and evaluated.

Blood samples were collected from patients within 7 days before surgery and analyzed in the same laboratory. The white blood cell, neutrophil, lymphocyte, and platelet counts were measured with the automated hematology analyzer Sysmex XT-4000i (Sysmex, Kobe, Japan). The alanine aminotransferase (ALT), aspartate aminotransferase (AST), γ-glutamyl transferase (γ-GT), and albumin (ALB) were measured with immunochemistry analyzer cobas 8000 (Roche, Rotkreuz, Switzerland). Routine assessments were also performed within 7 days before surgery, including a complete physical examination, chest X-ray, abdominal ultrasound, and computed tomography (CT) or magnetic resonance imaging (MRI). Other additional examinations, such as positron emission tomography-computed tomography (PET-CT), were carried out when necessary. The tumor staging was classified using the TNM staging system for HCC, and the TNM system was assessed using the seventh edition of the Union Internationale Contre le Cancer classification (UICC) (19). The NLR was calculated by dividing neutrophil count by lymphocyte count; the PNI was calculated using the following formula: serum albumin (g/L) + 5 × lymphocyte count (10^9/L) (20).

Treatment and Follow-up

The extent of hepatic resection was determined based on age, preoperative risk factors, the plasma retention rate of indocyanine green at 15 min, size, number and location of tumors, and Child–Pugh grade. Curative hepatectomy was defined as radical resection when no distant metastasis was detected, and tumor clearance was macroscopically and histologically complete. Anatomical hepatectomy included left or right hepatectomy, and left lateral sectionectomy, with sectionectomy defined as any type of complete excision of at least one segment based on Couinaud's classification.

In the sectionectomy surgeries, the resection line was made along the demarcation on the liver surface after ligation of the sectional pedicle, and the trunk of the hepatic vein was exposed on the resected surface. Non-anatomical hepatectomy was defined as tumor resection with a surgical margin of 5–10 mm unless the tumor was close to the main hepatic vein or the Glissonian pedicle. Postoperative activity time was defined as the time interval after surgery when the patient gets out of bed to perform any activity. Postoperative eating time was defined as the time interval after surgery when the patient was fed fluids. Postoperative drainage tube removal time was defined as the time interval after surgery in which the drainage tube was removed as determined by slowed drainage speed before stopping. All patients were followed carefully through outpatient examinations or telephone visits after the initial treatment. The serum alpha-fetoprotein (AFP) and liver function test were measured every 3 months, and contrast-enhanced CT or MRI was performed every 6 months. Percutaneous biopsy or selective hepatic arterial angiography was performed in patients with suspected tumor recurrence. Repeated hepatectomy, RFA, and transcatheter arterial chemoembolization (TACE) were performed for patients diagnosed with HCC recurrence. Disease-specific overall survival (OS) was defined as the interval between the time of surgery to the time of HCC-related death or the date of the last follow-up if death had not occurred. Disease-free survival (DFS) was the time interval defined as the time from surgery to radiological evidence of tumor recurrence. The start date of follow-up was the initial diagnostic date for HCC, and the end of the follow-up was the last follow-up (August 2018) or the time of death.

Statistical Analyses

All statistical analyses were carried out using the SPSS 25.0 software (Chicago, IL, USA). A receiver operating characteristic (ROC) curve was generated to evaluate the sensitivity and specificity of the scoring systems for predicting OS. Based on the ROC curves, the cutoff values were determined by seeking the maximal sum of sensitivity and specificity. The measurement data were expressed as the mean ± standard deviation. The c^2 test or Fisher's exact test was used, as appropriate, for categorical data. Kaplan–Meier analysis was used to analyze the survival for different groups. Differences of survival were performed using the log-rank test. The Cox proportional hazard model was employed for univariate and multivariate analyses. p values less than 0.05 (two-tailed) was considered statistically significant.

RESULTS

Determine the Best Cutoff Point of PNI and NLR

We determined the best cutoff values for indices by the ROC curve analysis for predicting the 5-year OS. A PNI of 43.75 with a sensitivity of 74.5% and a specificity of 78.2% was chosen as the best cutoff point for 5-year OS, and the area under the curve (AUC) was 0.592. Similarly, the optimal cutoff value was set as 3.29 for NLR with a sensitivity of 59.5% and a specificity of 73.0%, and the AUC was 0.602. Determined in the same manner as the cutoff values of PNI and NLR, APRI, GGT/ALT and PLR did not show any discriminative value for 5-year OS ($p > 0.05$) (**Table 1**).

HCC Patient Characteristics and Correlation With PNI and NLR

The clinicopathologic characteristics of HCC patients with different PNI and NLR are summarized in **Table 2**. Correlation analysis of our study proved that a low PNI was significantly associated with older age, higher Child–Pugh grade, more intraoperative blood loss, worse degree of tumor differentiation, and higher recurrence rate ($p < 0.05$). Likewise, a high NLR was positively associated with a higher Child–Pugh grade and a higher recurrence rate ($p < 0.01$).

Univariate and Multivariate Analyses of Prognostic Factors for OS and RFS

The median duration of follow-up was 31 (range 3–96) months. In all, 92 patients (42.8%) developed recurrence, and 88 (40.9%) died during follow-up. The 1-, 3-, and 5-year OS were 87.7% (95% CI: 83.2%–92.2%), 62.1% (95% CI: 54.7%–69.5%), and 45.3% (95% CI: 36.7%–53.9%), respectively (**Figure 1A**). The 1-, 3-, and 5-year RFS were 81.3% (95% CI: 76.0%–86.6%), 52.9% (95% CI: 45.5%–60.3%), and 40.8% (95% CI: 32.8%–48.8%), respectively (**Figure 1B**).

The results of the Cox regression hazard model for predictors of overall survival are shown in **Table 3**. In univariate analysis, CRP, Child–Pugh grade, tumor diameter, vascular invasion, tumor stage, degree of differentiation, intraoperative transfusion, PNI, and NLR were significant predictors of OS ($p < 0.05$). A multivariate analysis of significant variables showed that tumor diameter (HR: 1.100, 95% CI: 1.011–1.197, $p = 0.026$), tumor stage (HR: 0.149, 95% CI: 0.061–0.365, $p < 0.001$), degree of differentiation (HR: 3.684, 95% CI: 1.978–6.861, $p < 0.001$), PNI (HR: 5.081, 95% CI: 2.209–11.688, $p < 0.001$), and NLR (HR: 0.510, 95% CI: 0.272–0.957, $p = 0.036$) were independently associated with OS. The outcomes of the Cox regression hazard model for predictors of OS are shown in **Table 3**.

Likewise, the univariate analysis indicated that CRP, Child–Pugh grade, vascular invasion, tumor stage, degree of differentiation, PNI, and NLR were significant predictors of RFS ($p < 0.001$). A multivariate analysis of significant variables showed that vascular invasion (HR: 0.513, 95% CI: 0.277–0.952, $p = 0.034$), tumor stage (HR: 0.184, 95% CI: 0.059–0.569, $p = 0.003$), degree of differentiation (HR: 2.836, 95% CI: 1.593–5.050, $p < 0.001$), and PNI (HR: 6.530, 95% CI: 3.456–12.338, $p < 0.001$) were independently associated with RFS. The outcomes of the Cox regression hazard model for predictors of RFS are shown in **Table 4**.

Overall and Recurrence-Free Survival Curve According to NLR and PNI

The OS in the PNI-high group were significantly higher than those in the PNI-low group ($p < 0.001$). The 1-, 3-, and 5-year OS were 94.6% (95% CI: 90.5%–98.7%), 77.8% (95% CI: 68.9%–86.6%), and 62.6% (95% CI: 50.6%–74.6%) in the PNI-high group; 79.1% (95% CI: 70.7%–87.5%), 44.8% (95% CI: 33.8%–55.8%), and 22.1% (95% CI: 10.9%–33.3%) in the PNI-low group (**Figure 2A**). The OS in the NLR-low group were significantly higher than those in the NLR-high group ($p < 0.001$). The 1-, 3-,

TABLE 1 | Comparison of the AUC between inflammation-based prognostic scores.

	AUC	95% CI	*p*-value	Cutoff value
PNI	0.592	0.512–0.672	0.024	43.75
NLR	0.602	0.566–0.725	<0.001	3.29
APRI	0.448	0.367–0.528	0.198	0.14
GGT/ALT	0.466	0.386–0.547	0.409	0.62
PLR	0.475	0.395–0.555	0.538	69.17

PNI, prognostic nutritional index; NLR, neutrophil to lymphocyte ratio; APRI, aspartate aminotransferase/platelet count ratio index; GGT/ALT, gamma glutamyl transferase/alanine aminotransferase ratio; PLR, platelet–lymphocyte ratio.

and 5-year OS were 94.4% (95% CI: 90.3%–98.5%), 75.5% (95% CI: 67.1%–83.9%), and 58.4% (95% CI: 47.6%–69.2%) in the NLR-low group; 77.0% (95% CI: 67.6%–86.4%), 40.6% (95% CI: 28.3%–52.9%), and 26.3% (95% CI: 12.4%–40.2%) in the NLR-high group (**Figure 2B**). Expected tumor number ($p = 0.059$), other prognostic factors, such as Child–Pugh A grade ($p < 0.001$); without vascular invasion ($p < 0.001$), moderate or good differentiation ($p = 0.006$); and tumor stage I or II ($p < 0.001$) were associated with an increased OS (**Figures 2C–F**).

Homoplastically, the RFS in PNI-high were significantly higher than those in the PNI-low group ($p < 0.001$). The 1-, 3-, and 5-year RFS were 87.9% (95% CI: 82.0%–93.8%), 68.9% (95% CI: 59.5%–78.3%), and 56.3% (95% CI: 45.1%–67.5%) in the PNI-high group; 73.0% (95% CI: 64.0%–82.0%), 34.6% (95% CI: 24.2%–45.0%), and 19.3% (95% CI: 8.7%–29.9%) in the PNI-low group (**Figure 3A**), respectively. The RFS in the NLR-low group were significantly higher than those in the NLR-high group ($p < 0.001$). The 1-, 3-, and 5-year RFS were 86.7% (95% CI: 80.8%–92.6%), 62.5% (95% CI: 53.5%–71.5%), and 49.2% (95% CI: 39.2%–59.2%) in the NLR-low group; 72.8% (95% CI: 63.0%–82.6%), 36.7% (95% CI: 24.5%–48.9%), and 23.5% (95% CI: 8.6%–38.4%) in the NLR-high group (**Figure 3B**), respectively. Other prognostic factors, such as Child–Pugh A grade ($p < 0.001$), without vascular invasion ($p < 0.001$), moderate or good differentiation ($p < 0.001$), and tumor stage I or II ($p < 0.001$), were associated with an increased RFS (**Figures 3C–F**).

The Prognostic Value Ground on the Combination of NLR and PNI

Patients were divided into four groups to analyze the prognostic value of NLR combined with PNI: Group 1, the both low NLR and PNI group (n = 42, 19.5%); Group 2, the low NLR and high PNI group (n = 91, 42.3%); Group 3, the high NLR and low PNI group (n = 54, 25.1%); and Group 4, the both high NLR and PNI group (n = 28, 13%). Group 2 which stood for the intensive antitumor effects of the immune system had the best outcome while group 3 which represented the depression and malnutrition of the immune system had the worst outcome ($p < 0.001$). The 1-, 3-, and 5-year OS were 86.7% (95% CI: 75.7%–97.7%), 54.4% (95% CI: 37.5%–71.3%), and 29.3% (95% CI: 11.9%–46.7%) in group 1; 97.7% (95% CI: 94.6%–100%), 85.5% (95% CI: 77.1%–93.9%), and 72.2% (95% CI: 60.1%–84.4%) in group 2; 73.8% (95% CI: 62.0%–85.6%), 37.8% (95% CI: 23.7%–51.9%), and 15.1% (95% CI: 0.1%–30.4%) in group 3; 83.4% (95% CI: 68.5%–98.3%), 47.8% (95% CI: 23.7%–71.9%), and 31.9% (95% CI: 1.7%–62.1%) in group 4, respectively (**Figure 4A**). Accordingly, the 1-, 3-, and 5-year RFS were 79.3% (95% CI: 66.6%–92.0%), 40.5% (95% CI: 24.4%–56.6%), and 17.8% (95% CI: 3.5%–32.1%) in group 1; 91.0% (95% CI: 84.9%–97.1%), 72.8% (95% CI: 62.6%–83.0%), and 62.0% (95% CI: 50.2%–73.8%) in group 2; 70.2% (95% CI: 58%–82.4%), 30.0% (95% CI: 16.5%–43.5%), and 12.0% (95% CI: 1.3%–27%) in group 3; and 73.6% (95% CI: 56.5%–90.7%), 45.8% (95% CI: 20.9%–70.7%), and 22.9% (95% CI: 3.3%–49.2%) in group 4, respectively (**Figure 4B**).

Combinations of Risk Factors Better Predict OS and RFS

We then try to find out if the combination of independent prognostic factors could provide a better diagnostic value for OS and RFS. ROC analysis showed that for predicting OS, when the number of combined risk factors was set to >2.5, the model had the best predictive value with an AUC = 0.694 ($p < 0.001$, **Figure 5A**). The sensitivity and specificity were 56.9% and

TABLE 2 | Clinicopathological characteristics of the patients and clinicopathological correlations of inflammatory indices.

Characteristics	Overall (N = 215)	High PNI (N = 119)	Low PNI (N = 96)	*p*	Low NLR (N = 133)	High NLR (N = 82)	*p*
Age (years)	59.10 ± 10.49	57.54 ± 9.96	60.95 ± 10.86	**0.017**	58.69 ± 10.27	59.65 ± 10.87	0.521
Sex (male/female)	178/37	100/19	78/18	0.591	111/22	67/15	0.741
HBsAg positive (%)	160 (74.4%)	86(72.3%)	74(77.1%)	0.421	99(74.4%)	61(74.1%)	0.994
Child–Pugh grade (A/B)	188/27	117/2	71/25	**<0.001**	125/8	63/19	**<0.001**
Intraoperative blood loss	637.07 ± 1001.64	440.44 ± 737.65	888.33 ± 1220.20	**0.003**	613.41 ± 1019.38	677.24 ± 976.17	0.661
Tumor diameter (cm)	5.94 ± 8.60	5.23 ± 3.21	6.82 ± 12.35	0.178	5.30 ± 3.19	6.96 ± 13.31	0.169
Vascular invasion	170/45	98/23	72/22	0.432	110/23	60/22	0.095
Tumor stage (I/II/III)	149/52/14	84/27/8	65/25/6	0.421	95/31/7	54/21/7	0.765
Degree of differentiation	49/139/27	29/73/17	20/66/10	**<0.001**	25/87/21	24/52/6	0.068
Postoperative death	211/4	118/1	93/3	0.469	130/3	81/1	0.979
Recurrence	119/92	89/29	30/63	**<0.001**	82/47	3745	**0.007**

The bold values meaning statistically significant.

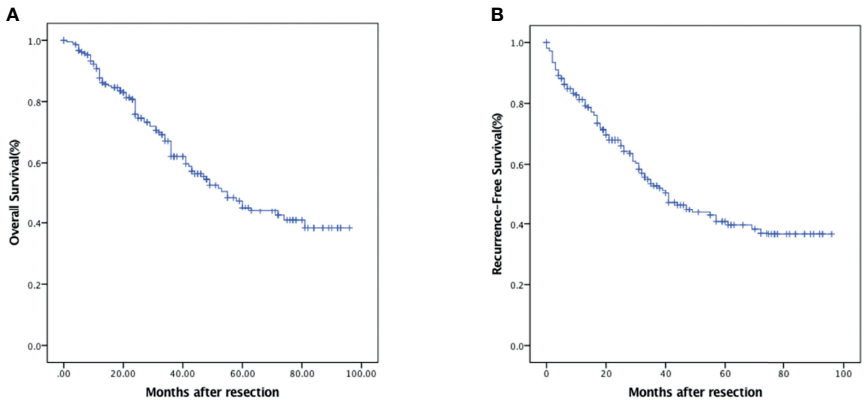

FIGURE 1 | Kaplan–Meier survival analysis of HCC patients. **(A)** OS in HCC patients who underwent curative hepatectomy. **(B)** RFS in HCC patients who underwent curative hepatectomy.

78.2%, respectively. The OS in patients with at least three risk factors were significantly lower than those with two or fewer risk factors ($p < 0.001$, **Figure 5C**). The 1-, 3-, and 5-year OS were 83.4% (95% CI: 76.5%–90.3%), 54.7% (95% CI: 44.7%–64.7%), and 32.9% (95% CI: 21.7%–44.1%) in patients with at least three risk factors, and 93.2% (95% CI: 87.9%–98.5%), 72.2% (95% CI: 61.6%–82.8%), and 58.3% (95% CI: 45.2%–71.4%) in patients with two or less risk factors, respectively. Likewise, for RFS, the optimal cutoff value for the number of combined risk factors was >2.5. The sensitivity and specificity of this model were 90.6% and 46.0%, respectively (AUC = 0.732, p < 0.001, **Figure 5B**). The RFS in patients with at least three risk factors were significantly lower than those with two or fewer risk factors ($p = 0.001$, **Figure 5D**). The 1-, 3-, and 5-year RFS were 65.6% (95% CI: 52.5%–78.7%), 35.6% (95% CI: 21.5%–49.7%), and 22.4% (95% CI: 9.3%–35.5%) in patients with at least three risk factors, and 86.1% (95% CI: 80.8%–91.4%), 58.1% (95% CI: 49.5%–66.7%), and 45.1% (95% CI: 35.7%–54.5%) in patients with two or less risk factors, respectively.

DISCUSSION

Surgical resection is the primary method for the curative treatment of HCC, but the major complication of this procedure is tumor recurrence. Factors such as AFP, TNM staging, and liver reserve function can be used to predict the survival of HCC patients after the operation and the risk of tumor recurrence. However, these traditional predictive indices have practical limitations in predicting the prognosis of HCC, such as the high negative detection rate (over 30%) of serum AFP and the hysteresis of TNM (21). Therefore, the identification of reliable and simple prognostic biomarkers is essential for identifying patients with potentially poor prognosis prognoses.

The importance of host inflammatory responses points to the utility of inflammatory indices for predicting clinical outcomes in patients with cancers. The most common causes of HCC patients, especially in China, are related to chronic viral hepatitis infections (B and C). Several inflammatory-based prognostic indices (NLR, PNI, PLR, and GGT/ALT) and liver fibrosis

TABLE 3 | Univariate and multivariate analyses of prognostic factors for overall survival of patients.

Variable	Univariate		Multivariate	
	OS HR (95% CI)	*p*	OS HR (95% CI)	*p*
Age (years)	1.013 (0.991–1.035)	0.250		
Sex (male/female)	0.972 (0.5340–1.770)	0.926		
HBsAg positive	0.697 (0.425–1.141)	0.151		
Cirrhosis	1.205 (0.763–1.902)	0.425		
CRP (mg/L)	1.018 (1.005–1.032)	**0.007**	0.994 (0.975–1.014)	0.561
AFP (ng/mL)	1.159 (0.675–1.992)	0.592		
Child–Pugh grade (A/B)	2.587 (1.511–4.428)	**0.001**	0.700 (0.237–2.069)	0.519
Tumor diameter (cm)	1.025 (1.003–1.046)	**0.023**	1.100 (1.011–1.197)	**0.026**
Vascular invasion	0.302 (0.188–0.486)	**<0.001**	0.828 (0.395–1.737)	0.617
Tumor stage (I and II/III)	0.388 (0.199–0.757)	**0.005**	0.149 (0.061–0.365)	**<0.001**
Degree of differentiation	2.105 (1.277–3.468)	**0.004**	3.684 (1.978–6.861)	**<0.001**
Intraoperative blood loss (mL)	1.000 (1.000–1.001)	0.050		
PNI (≥43.75/<43.75)	6.176 (3.523–10.862)	**<0.001**	5.081 (2.209–11.688)	**<0.001**
NLR (≥3.29/<3.29)	0.283 (0.176–0.455)	**<0.001**	0.510 (0.272–0.957)	**0.036**

TABLE 4 | Univariate and multivariate analyses of prognostic factors for recurrence-free survival of patients.

Variable	Univariate		Multivariate	
	HR (95% CI)	*p*	HR (95% CI)	*p*
Age (years)	1.003 (0.984–1.023)	0.738		
Sex (male/female)	0.883 (0.507–1.535)	0.658		
HBsAg positive	1.287 (0.817–2.028)	0.276		
Cirrhosis	1.171 (0.778–1.764)	0.450		
CRP (mg/L)	1.015 (1.002–1.029)	**0.027**	0.988 (0.968–1.007)	0.218
AFP (ng/mL)	0.784 (0.483–1.272)	0.324		
Child–Pugh grade (A/B)	0.314 (0.190–0.517)	**<0.001**	0.775 (0.290–2.071)	0.611
Tumor diameter (cm)	1.015 (0.997–1.033)	0.096		
Vascular invasion	0.379 (0.244–0.589)	**<0.001**	0.513 (0.277–0.952)	**0.034**
Tumor stage (I and II/III)	0.136 (0.073–0.256)	**<0.001**	0.184 (0.059–0.569)	**0.003**
Degree of differentiation	1.404 (0.932–1.886)	**<0.001**	2.836 (1.593–5.050)	**<0.001**
Intraoperative blood loss (mL)	1.000 (1.000–1.001)	0.279		
PNI (≥43.75/<43.75)	3.846 (2.451–6.035)	**<0.001**	6.530 (3.456–12.338)	**<0.001**
NLR (≥3.29/<3.29)	0.448 (0.296–0.679)	**<0.001**	0.972 (0.435–2.170)	0.944

predictor (APRI) were examined in this study. The PNI was initially designed to assess the risk of surgical complications and mortality in patients undergoing gastrointestinal tract surgery (22). Increasing studies suggested that preoperative PNI could predict the overall survival of HCC patients undergoing surgery or targeted therapy (9, 10, 23). Our study is somewhat different from previous studies. Firstly, instead of only selecting BCLC stage 0/A primary HCC patients as the research object, all patients including some HCC patients with clinically middle to advanced stage who received curative surgery were retrospectively reviewed in the present study. It is well known that HCC progression could lead to liver function damage, biliary tract infection, and nutritional deficiency; these may better confirm the prognostic values of PNI and NLR. Secondly, different methods are used to obtain the cutoff value in the previous study; Chan used the mean or median of PNI (45) and NLR (5) as the cutoff value, and they found that NLR had no prognostic significance on OS and disease-free survival (11). The best cutoff value in each institute can be established by the receiver operating characteristic curve, and the best cutoff value for balancing sensitivity and specificity was determined by Youden index = (sensitivity + specificity-1) (16). We use this

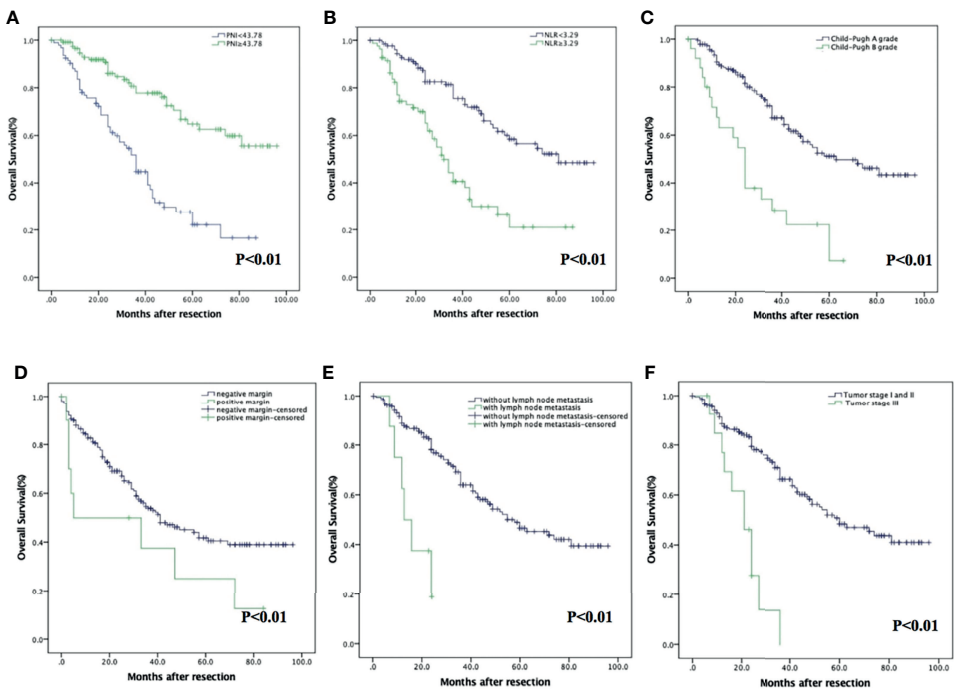

FIGURE 2 | Kaplan–Meier analysis of HCC patients showing OS curves stratified according to PNI **(A)**, NLR **(B)**, Child–Pugh grade **(C)**, vascular invasion **(D)**, tumor stage **(E)**, and degree of differentiation **(F)**.

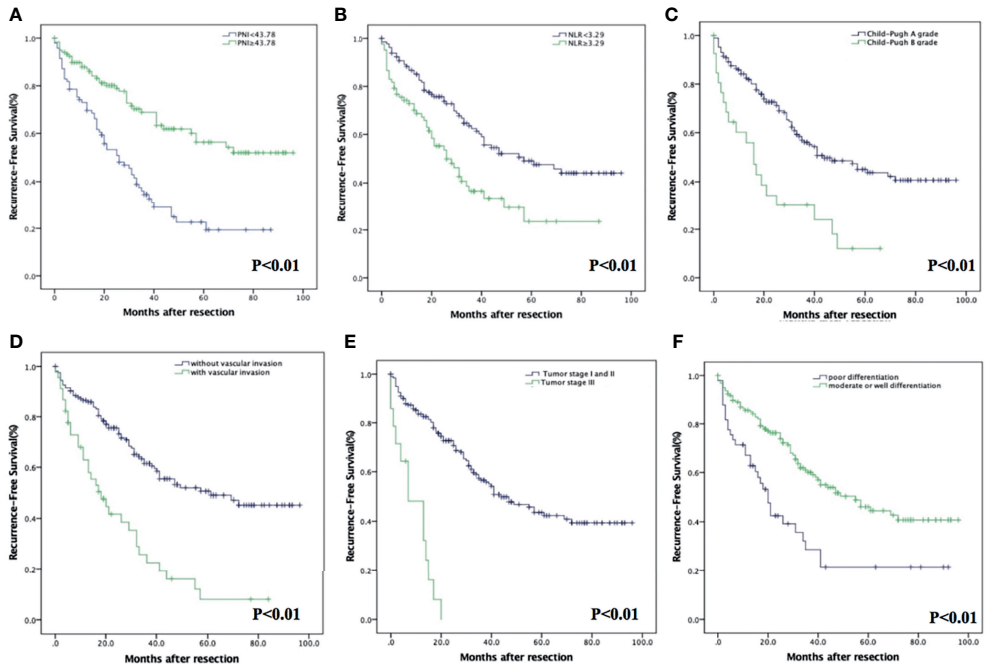

FIGURE 3 | Kaplan–Meier analysis of HCC patients showing RFS curves stratified according to PNI **(A)**, NLR **(B)**, Child–Pugh grade **(C)**, vascular invasion **(D)**, tumor stage **(E)**, and degree of differentiation **(F)**.

method in the present study, and the best cutoff value of PNI was 43.75 and presented a sensitivity of 74.5% and a specificity of 78.2%; similarly, the optimal cutoff value was set as 3.29 for NLR with a sensitivity of 59.5% and a specificity of 73.0%.

In the present study, we collected and analyzed the data of HCC patients at our institution seeking to identify more definitive correlations. After excluding 28 patients with preoperative underlying diseases or postoperative complications, our study determined that a preoperative PNI greater than 43.78 was an independent prognostic factor for favorable OS and RFS. Lymphopenia and/or hypoalbuminemia result in low survival, and we speculate that several immunological factors are involved and lymphocytes play an important role in the eradication of the formation and development of tumors (24, 25). CD8+ and CD4+ lymphocytes can induce antitumor immunity, and therefore, HCC characterized by inflammatory cell infiltration would have a better prognosis (26). Previous studies have demonstrated that age is inversely correlated with liver regeneration in humans (27). In our study, the PNI-low group, composed of older patients, had worse survival than the PNI-high group after surgery. Therefore, good

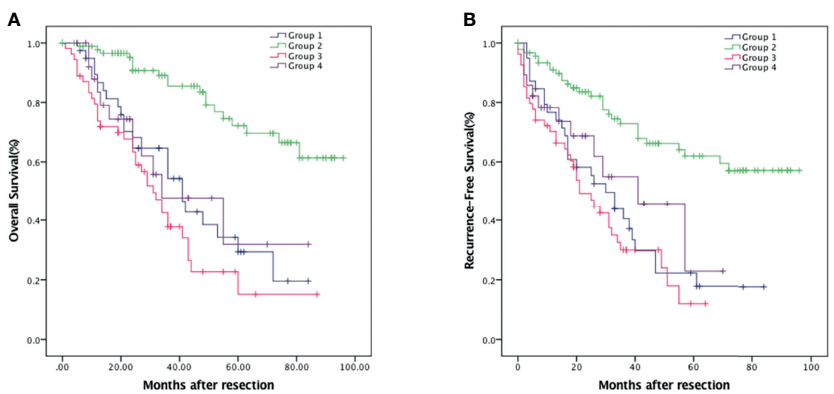

FIGURE 4 | Kaplan–Meier survival analysis of HCC patients showing survival curves stratified according to the combination of NLR and PNI. OS **(A)** and RFS **(B)** curve comparing different groups. Group 1, NLR <3.29 and PNI <43.75 (n = 42); Group 2, NLR <3.29 and PNI ≥43.75 (n = 91); Group 3, NLR ≥3.29 and PNI <43.75 (n = 54); Group 4, NLR ≥3.29 and PNI ≥43.75 (n = 28).

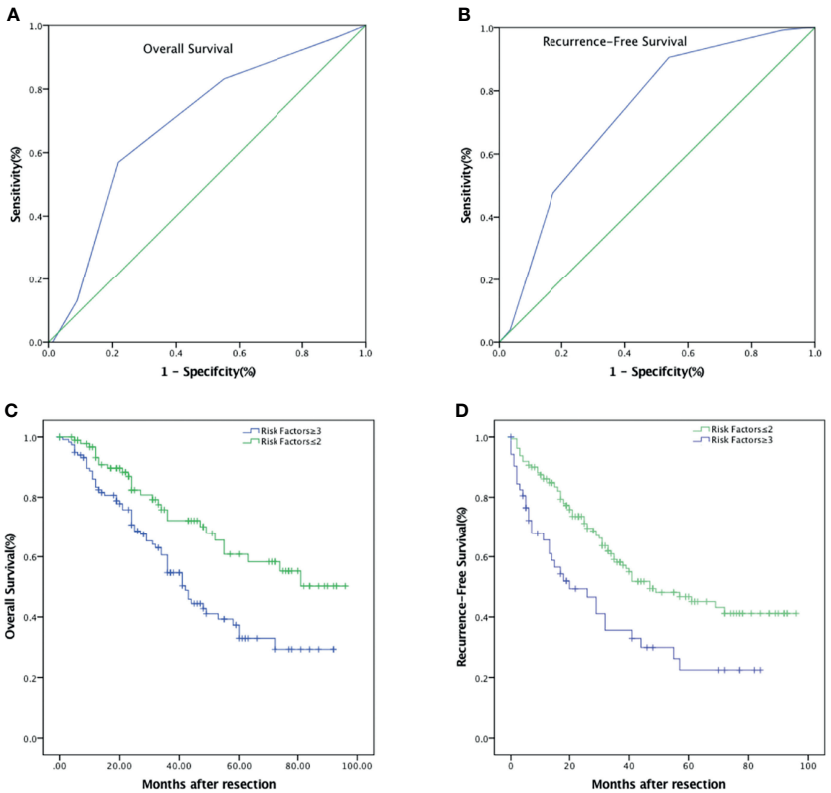

FIGURE 5 | Combinations of independent risk factors better predict survival of patients with HCC after hepatic resection. **(A)** ROC of combined risk factors for the prediction of OS. **(B)** ROC of combined risk factors for the prediction of RFS. **(C)** OS curve comparing risk factors ≥3 and risk factors ≤2. **(D)** RFS curve comparing risk factors ≥3 and risk factors ≤2.

nutrition and immune status before surgery are important factors for the improvement of postoperative survival, particularly in elderly patients.

Several studies have shown that high preoperative NLR is a predictor of negative prognosis for patients receiving liver transplantation or surgical treatment (28). However, some researchers doubt the utility of preoperative NLR as an independent prognostic factor in HCC patients, supposing that it is only an indicator of the patient's overall inflammation status (11). In the present study, the proportion of hepatitis B-positive patients (74.4%) was higher than in previous studies; these may lead to poor Child–Pugh grade and poor OS. In addition, NLR was associated with inflammatory activity, and it also upregulated in HCC patients with HBV infection (16). Our results suggested that high NLR (≥3.29), indicating a relative increase in neutrophils or decrease in lymphocytes, is an independent adverse prognostic factor for OS. Although the present study could not demonstrate any association between the NLR and RFS, this may be related to our limited number of patients. Intriguingly, the PNI and NLR combination can enhance the accuracy of PNI in predicting RFS.

In the present study, we also verified that the combination of PNI, NLR, and other risk factors improved the prognostic value. Risk factors for OS include serum albumin concentration, tumor diameter, tumor stage III, and poor differentiation, and risk factors for RFS include vascular invasion, tumor stage III, and poor differentiation. We found that after combining risk factors, the model had a better predictive value with a higher AUC when the number of risk factors was greater than 2. Appropriate plans can be put in place to prevent recurrence and achieve long time survival (29). Also, survival in patients with a low PNI and high NLR may be improved by nutritional and anti-infection therapy (30). In addition, intensive postoperative follow-up or postoperative adjuvant therapy could be applied for patients with more than two risk factors.

In conclusion, our study has demonstrated that PNI and NLR are independent prognostic factors for the OS of all clinical stages of HCC patients undergoing hepatectomy. Moreover, PNI is a reliable predictor of RFS in postoperative HCC patients. Importantly, monitoring combined risk factors can increase accuracy for predicting the OS and RFS in HCC patients.

DATA AVAILABILITY STATEMENT

The original contributions presented in the study are included in the article/**Supplementary Material**. Further inquiries can be directed to the corresponding authors.

ETHICS STATEMENT

Written informed consent was obtained from the individual(s) for the publication of any potentially identifiable images or data included in this article.

AUTHOR CONTRIBUTIONS

Conception and design: ZQ, Y-FD, and J-WF. Data collection: ZQ and J-WF. Writing of the article: ZQ, Y-FD, J-WF, Y-xC, JC, L-qS, NR, and Y-jL. Critical revision of the article: Y-jL, NR, and X-zH. Final approval of the article: ZQ, Y-jL, J-WF, Y-xC, JC, L-qS, NR, Y-FD, and X-zH. Statistical analysis: ZQ, Y-FD, J-WF, and Y-jL. Obtained funding: ZQ and Y-jL. Overall responsibility: Y-FD. All authors contributed to the article and approved the submitted version.

FUNDING

The research was supported by the National Natural Science Foundation of China (no. 81971504) and Scientific and Technological Projects for Young Talents, Changzhou Health and Family Planning Commission (QN201809). Changzhou Society Development Funding (CE20205038), The lifting Project of Young Scientific and technological talents in Changzhou (2021).

SUPPLEMENTARY MATERIAL

The Supplementary Material for this article can be found online at: https://www.frontiersin.org/articles/10.3389/fonc.2021.823054/full#supplementary-material

REFERENCES

1. Siegel RL, Miller KD, Fuchs HE, Jemal A. Cancer Statistics, 2021. *CA Cancer J Clin* (2021) 71(1):7–33. doi: 10.3322/caac.21654
2. Grivennikov SI, Greten FR, Karin M. Immunity, Inflammation, and Cancer. *Cell* (2010) 140(6):883–99. doi: 10.1016/j.cell.2010.01.025
3. Mayne ST, Playdon MC, Rock CL. Diet, Nutrition, and Cancer: Past, Present and Future. *Nat Rev Clin Oncol* (2016) 13(8):504–15. doi: 10.1038/nrclinonc.2016.24
4. Kinoshita A, Onoda H, Takano K, Imai N, Saeki C, Fushiya N, et al. Pretreatment Serum C-Reactive Protein Level Predicts Poor Prognosis in Patients With Hepatocellular Carcinoma. *Med Oncol* (2012) 29(4):2800–8. doi: 10.1007/s12032-012-0220-1
5. Meng QH, Yu HW, Li J, Wang JH, Ni MM, Feng YM, et al. Inadequate Nutritional Intake and Protein-Energy Malnutrition Involved in Acute and Chronic Viral Hepatitis Chinese Patients Especially in Cirrhosis Patients. *Hepatogastroenterology* (2010) 57(101):845–51. doi: 10.1136/gut.2008.155226corr1
6. Liu JY, Dong HM, Wang WL, Wang G, Pan H, Chen WW, et al. The Effect of the Prognostic Nutritional Index on the Toxic Side Effects of Radiochemotherapy and Prognosis After Radical Surgery for Gastric Cancer. *Cancer Manag Res* (2021) 13:3385–92. doi: 10.2147/CMAR.S301140
7. Wen J, Bedford M, Begum R, Mitchell H, Hodson J, Whiting J, et al. The Value of Inflammation Based Prognostic Scores in Patients Undergoing Surgical Resection for Oesophageal and Gastric Carcinoma. *J Surg Oncol* (2018) 117(8):1697–707. doi: 10.1002/jso.25057
8. Smith RA, Bosonnet L, Raraty M, Sutton R, Neoptolemos JP, Campbell F, et al. Preoperative Platelet-Lymphocyte Ratio Is an Independent Significant Prognostic Marker in Resected Pancreatic Ductal Adenocarcinoma. *Am J Surg* (2009) 197(4):466–72. doi: 10.1016/j.amjsurg.2007.12.057
9. Saito Y, Imura S, Morine Y, Ikemoto T, Yamada S, Shimada M. Preoperative Prognostic Nutritional Index Predicts Short- and Long-Term Outcomes After Liver Resection in Patients With Hepatocellular Carcinoma. *Oncol Lett* (2021) 21(2):153. doi: 10.3892/ol.2020.12414
10. Fan X, Chen G, Li Y, Shi Z, He L, Zhou D, et al. The Preoperative Prognostic Nutritional Index in Hepatocellular Carcinoma After Curative Hepatectomy: A Retrospective Cohort Study and Meta-Analysis. *J Invest Surg* (2021) 34 (8):826–33. doi: 10.1080/08941939.2019.1698679
11. Chan AW, Chan SL, Wong GL, Wong VW, Chong CC, Lai PB, et al. Prognostic Nutritional Index (PNI) Predicts Tumor Recurrence of Very Early/Early Stage Hepatocellular Carcinoma After Surgical Resection. *Ann Surg Oncol* (2015) 22(13):4138–48. doi: 10.1245/s10434-015-4516-1
12. Chen Y, Yang Y, Zhang XY, Fan QS, Li X, Xin YJ, et al. Nomogram Based on Neutrophil-To-Lymphocyte Ratio and Platelet-To-Lymphocyte Ratio to Predict Recurrence in Patients With Hepatocellular Carcinoma After Radiofrequency Ablation. *Cardiovasc Intervent Radiol* (2021) 44(10):1551–60. doi: 10.1007/s00270-021-02872-8
13. Shusterman M, Jou E, Kaubisch A, Chuy JW, Rajdev L, Aparo S, et al. The Neutrophil-To-Lymphocyte Ratio Is a Prognostic Biomarker in An Ethnically Diverse Patient Population With Advanced Pancreatic Cancer. *J Gastrointest Cancer* (2020) 51(3):868–76. doi: 10.1007/s12029-019-00316-8
14. Namikawa T, Shimizu S, Yokota K, Tanioka N, Munekage M, Uemura S, et al. Neutrophil-To-Lymphocyte Ratio and C-Reactive Protein-to-Albumin Ratio as Prognostic Factors for Unresectable Advanced or Recurrent Gastric Cancer. *Langenbecks Arch Surg* (2021) 10:1–13. doi: 10.1007/s00423-021-02356-w
15. Ji F, Liang Y, Fu SJ, Guo ZY, Shu M, Shen SL, et al. A Novel and Accurate Predictor of Survival for Patients With Hepatocellular Carcinoma After Surgical Resection: The Neutrophil to Lymphocyte Ratio (NLR) Combined With the Aspartate Aminotransferase/Platelet Count Ratio Index (APRI). *BMC Cancer* (2016) 16:137. doi: 10.1186/s12885-016-2189-1
16. Hung HC, Lee JC, Cheng CH, Wu TH, Wang YC, Lee CF, et al. Impact of Neutrophil to Lymphocyte Ratio on Survival for Hepatocellular Carcinoma After Curative Resection. *J Hepatobiliary Pancreat Sci* (2017) 24(10):559–69. doi: 10.1002/jhbp.498
17. Bannaga A, Arasaradnam RP. Neutrophil to Lymphocyte Ratio and Albumin Bilirubin Grade in Hepatocellular Carcinoma: A Systematic Review. *World J Gastroenterol* (2020) 26(33):5022–49. doi: 10.3748/wjg.v26.i33.5022
18. Wang H, Wang Z, Hou Z, Yang X, Zhu K, Cao M, et al. The Neutrophil-To-Lymphocyte Ratio (NLR) Predicts the Prognosis of Unresectable Intermediate and Advanced Hepatocellular Carcinoma Treated With Apatinib. *Cancer Manag Res* (2021) 13:6989–98. doi: 10.2147/CMAR.S311526
19. Tokunaga H, Shimada M, Ishikawa M, Yaegashi N. TNM Classification of Gynaecological Malignant Tumours, Eighth Edition: Changes Between the Seventh and Eighth Editions. *Jpn J Clin Oncol* (2019) 49(4):311–20. doi: 10.1093/jjco/hyy206
20. Akgul O, Cetinkaya E, Yalaza M, Ozden S, Tez M. Prognostic Efficacy of Inflammation-Based Markers in Patients With Curative Colorectal Cancer Resection. *World J Gastrointest Oncol* (2017) 9(7):300–7. doi: 10.4251/wjgo.v9.i7.300
21. Tateishi R, Yoshida H, Matsuyama Y, Mine N, Kondo Y, Omata M. Diagnostic Accuracy of Tumor Markers for Hepatocellular Carcinoma: A Systematic Review. *Hepatol Int* (2008) 2(1):17–30. doi: 10.1007/s12072-007-9038-x
22. Onodera T, Goseki N, Kosaki G. Prognostic Nutritional Index in Gastrointestinal Surgery of Malnourished Cancer Patients. *Nihon Geka Gakkai Zasshi* (1984) 85(9):1001–5.
23. Ji F, Liang Y, Fu S, Chen D, Cai X, Li S, et al. Prognostic Value of Combined Preoperative Prognostic Nutritional Index and Body Mass Index in HCC After Hepatectomy. *HPB (Oxford)* (2017) 19(8):695–705. doi: 10.1016/j.hpb.2017.04.008
24. Goh BK, Tan DM, Chan CY, Lee SY, Lee VT, Thng CH, et al. Are Preoperative Blood Neutrophil-to-Lymphocyte and Platelet-to-Lymphocyte Ratios Useful in Predicting Malignancy in Surgically-Treated Mucin-Producing Pancreatic Cystic Neoplasms? *J Surg Oncol* (2015) 112(4):366–71. doi: 10.1002/jso.23997

25. Stotz M, Pichler M, Absenger G, Szkandera J, Arminger F, Schaberl-Moser R, et al. The Preoperative Lymphocyte to Monocyte Ratio Predicts Clinical Outcome in Patients With Stage III Colon Cancer. *Br J Cancer* (2014) 110 (2):435–40. doi: 10.1038/bjc.2013.785
26. Dunn GP, Old LJ, Schreiber RD. The Immunobiology of Cancer Immunosurveillance and Immunoediting. *Immunity* (2004) 21(2):137–48. doi: 10.1016/j.immuni.2004.07.017
27. Shirabe K, Motomura T, Takeishi K, Morita K, Kayashima H, Taketomi A, et al. Human Early Liver Regeneration After Hepatectomy in Patients With Hepatocellular Carcinoma: Special Reference to Age. *Scand J Surg* (2013) 102 (2):101–5. doi: 10.1177/1457496913482250
28. Tanemura A, Mizuno S, Hayasaki A, Gyoten K, Fujii T, Iizawa Y, et al. Onodera's Prognostic Nutritional Index Is a Strong Prognostic Indicator for Patients With Hepatocellular Carcinoma After Initial Hepatectomy, Especially Patients With Preserved Liver Function. *BMC Surg* (2020) 20 (1):261. doi: 10.1186/s12893-020-00917-2
29. Dan J, Zhang Y, Peng Z, Huang J, Gao H, Xu L, et al. Postoperative Neutrophil-to-Lymphocyte Ratio Change Predicts Survival of Patients With Small Hepatocellular Carcinoma Undergoing Radiofrequency Ablation. *PloS One* (2013) 8(3):e58184. doi: 10.1371/journal.pone.0058184
30. Okabayashi T, Nishimori I, Sugimoto T, Maeda H, Dabanaka K, Onishi S, et al. Effects of Branched-Chain Amino Acids-Enriched Nutrient Support for Patients Undergoing Liver Resection for Hepatocellular Carcinoma. *J Gastroenterol Hepatol* (2008) 23(12):1869–73. doi: 10.1111/j.1440-1746.2008.05504.x

Conflict of Interest: The authors declare that the research was conducted in the absence of any commercial or financial relationships that could be construed as a potential conflict of interest.

Publisher's Note: All claims expressed in this article are solely those of the authors and do not necessarily represent those of their affiliated organizations, or those of the publisher, the editors and the reviewers. Any product that may be evaluated in this article, or claim that may be made by its manufacturer, is not guaranteed or endorsed by the publisher.

frontiers | Frontiers in Oncology

ORIGINAL RESEARCH
published: 21 April 2022
doi: 10.3389/fonc.2022.878513

Circular RNA ERBIN Promotes Proliferation of Hepatocellular Carcinoma *via* the miR-1263/CDK6 Axis

Shikun Yang[1†], Fei Yu[1†], Yang Ji[1†], Yanjun Shen[1], Hao Lu[1], Yuan Gao[2], Feng Zhang[1*], Xuehao Wang[1*] and Chuanyong Zhang[1*]*

[1] Hepatobiliary Center, The First Affiliated Hospital of Nanjing Medical University, Key Laboratory of Liver Transplantation, Chinese Academy of Medical Sciences, Nanjing, China, [2] Department of Hepato–Biliary–Pancreatic Surgery, The Affiliated Changzhou No. 2 People's Hospital of Nanjing Medical University, Changzhou, China

Objectives: Hepatocellular carcinoma (HCC) is the most common primary liver cancer and characterized by high aggressiveness and extremely poor prognosis. Increasing evidence has suggested that circular RNAs (circRNAs), which are highly stable, play crucial roles in the progression of multiple malignancies. However, the roles of circRNAs in HCC remain elusive.

Materials and Methods: The expression patterns of circRNAs in HCC were identified by qRT-PCR. A series of functional experiments both *in vivo* and *in vitro* were used to determine the role of circERBIN in HCC proliferation. Bioinformatics and an RNA pulldown assay were used to identify potential downstream targets of circERBIN.

Results: The expression of circERBIN was upregulated in HCC cell lines and tissues, which was predictive of a poor prognosis in HCC patients. Elevated circERBIN promoted G1/S transition of HCC cells, thus facilitating the proliferation and tumorigenesis of HCC cells. Mechanistic investigations revealed that circERBIN regulated HCC proliferation by acting as a sponge of miR-1263, which subsequently targeted cyclin dependent kinase 6 and controlled G1/S transition.

Conclusion: Taken together, these results determined that circERBIN functions as an important epigenetic regulator in HCC development, highlighting that circERBIN is a promising target for treatment of HCC.

Keywords: HCC, circERBIN, proliferation, miRNA sponge, miR-1263, CDK6

OPEN ACCESS

Edited by:
Xiaodong Li,
First People's Hospital of Changzhou, China

Reviewed by:
Xiaofei Zhang,
Shanghai JiaoTong University, China
Yanqing Liu,
Columbia University, United States

***Correspondence:**
Chuanyong Zhang
zcy2732@163.com
Xuehao Wang
wangxh@njmu.edu.cn
Feng Zhang
zhangfeng1958@hotmail.com
Yuan Gao
drgaoyuan@njmu.edu.cn

[†]*These authors have contributed equally to this work*

Specialty section:
This article was submitted to Molecular and Cellular Oncology, a section of the journal Frontiers in Oncology

Received: *18 February 2022*
Accepted: *22 March 2022*
Published: *21 April 2022*

Citation:
Yang S, Yu F, Ji Y, Shen Y, Lu H, Gao Y, Zhang F, Wang X and Zhang C (2022) Circular RNA ERBIN Promotes Proliferation of Hepatocellular Carcinoma via the miR-1263/CDK6 Axis. Front. Oncol. 12:878513. doi: 10.3389/fonc.2022.878513

INTRODUCTION

Hepatocellular carcinoma (HCC) is the sixth most common malignant cancer and the third leading cause of cancer-related death worldwide (1). The overall survival of HCC patients remains extremely poor due to high disease aggressiveness and malignant biological behavior. Although significant progress has been made in the treatment of HCC, the effects of current strategies, such as targeted molecular therapy, surgical treatment, and immunotherapy, remain largely unsatisfactory (2, 3). Hence, further efforts are needed to elucidate the molecular mechanisms underlying the development and progression of HCC to improve the therapeutic outcomes of HCC patients.

Circular RNAs (circRNAs) are a series of widespread and conserved non-coding RNA that are mostly generated by direct back-splicing of precursor mRNA (4, 5). Accumulating evidence has demonstrated that aberrantly expressed circRNAs are involved in diseases progression, particularly malignant cancers.

With the development of next-generation sequencing of noncoding RNAs, a growing number of circRNAs have been found play important roles in cancer cell proliferation, metastasis, and treatment resistance by functioning as microRNA (miRNA) sponges and RNA-binding proteins (6–8). For instance, our group previously reported that circ_0011385 promoted HCC cell proliferation and was associated with poor clinicopathologic features (9). A recent study showed that hsa_circ_0001492 (circERBIN), originating from exons 2, 3, and 4 of the Erbin gene (ERBB2 inter-acting protein), promoted the proliferation and metastasis of colorectal cancer cells *via* targeting miR-125a-5p-5p/miR-138-5p to subsequently increase the expression of eukaryotic translation initiation factor 4E binding protein 1 and translation of hypoxia induced factor-1 (10). Nevertheless, little is known about the expression patterns and role of circERIN in the carcinogenesis and progression of HCC.

The results of this study showed that upregulation of circERIN was correlated with poor clinicopathologic outcomes of HCC. In addition, CircERIN facilitated proliferation of HCC cells both *in vivo* and *in vitro*. Mechanistically, circERIN regulates the cell cycle by sponging miR-1263 and regulating the expression of cyclin dependent kinase 6 (CDK6). Therefore, circERBIN may be considered as a promising therapeutic target for HCC patients.

MATERIALS AND METHODS

Cell Culture and Tissue Samples

Forty-four samples of HCC and paired adjacent liver tissues were obtained from patients who underwent surgery at the First Affiliated Hospital of Nanjing Medical University (Nanjing, China). All procedures were approved by Ethics Committee of the First Affiliated Hospital of Nanjing Medical University. HCC cell lines and normal hepatic cells were purchased from the Cell Bank of the Chinese Academy of Sciences (Shanghai, China) and cultured in Dulbecco's modified Eagle's medium (HyClone Laboratories, Inc., South Logan, UT, USA) supplemented with 10% fetal bovine serum (Gibco, Carlsbad, CA, USA) and 1% penicillin-streptomycin solution (HyClone Laboratories, Inc.).

Transfection Experiments

Short interfering RNA (si-circERBIN), miR-1263 inhibitors, mimics, and appropriate negative controls (NCs) were designed by TSINGKE Biotechnology Co., Ltd. (Beijing, China). Lipofectamine 3000 transfection reagent (Invitrogen Corporation, Carlsbad, CA, USA) was used for transient transfection. Lentiviruses coding for circERBIN, CDK6, and shCDK6 were constructed by GenePharma Co., Ltd. (Shanghai, China).

Western Blot Analysis

Proteins were extracted from cells using radioimmunoprecipitation assay buffer containing phenylmethylsulfonyl fluoride. The quality of the protein samples was evaluated using a NanoDrop ND-2000 spectrophotometer (Thermo Fisher Scientific, Waltham, MA, USA). Equal amounts of protein were separated by sodium dodecyl sulfate-polyacrylamide gel electrophoresis and then transferred onto polyvinylidene fluoride membranes (Merck Millipore, Billerica, MA, USA), which were blocked with Quick Block™ Blocking Buffer for Western Blot (Beyotime Institute of Biotechnology, Haimen, China) and incubated with primary antibodies against CDK6 (13331S; Cell Signaling Technology, Inc., Danvers, MA, USA) and glyceraldehyde-3-phosphate dehydrogenase (GAPDH; 5174T; Cell Signaling Technology, Inc.) overnight at 4°C. The next day, the membranes were incubated with corresponding horseradish peroxidase-labelled secondary antibodies at room temperature for 2 h. Afterward, the membranes were visualized using an enhanced chemiluminescence detection system.

Quantitative Real-Time Polymerase Chain Reaction (qRT-PCR)

Total RNA was extracted and reverse transcribed into complementary DNA with forward and reverse primers targeting circERBIN (TAC CAG CAT CCA TTG CAA AC/TCC TCT TCC CCT CGT AGA CA), miR-1263 (AAC AAG ATG GTA CCC TGG CAT AC/CAG TGC AGG GTC CGA GGT), CDK6 (CAG CAG CGG ACA AAT AAA/CTG GGA GTC CAA TCA CGT), and GAPDH (AAG GTG AAG GTC GGA GTC A/GGA AGA TGG TGA TGG GAT TT). The qRT-PCR cycling conditions included an initial denaturation step at 95°C for 5 min, followed by 95°C for 10 s and 60°C for 30 s, and 40 cycles at 95°C for 15 s, 60°C for 1 min, and 95°C for 15 s.

Fluorescence *In Situ* Hybridization (FISH)

The FISH assay was conducted using a Ribo FISH kit (Guangzhou RiboBio Co., Ltd., Guangzhou, China) with probes targeting circERBIN, which were designed and synthesized by Guangzhou RiboBio Co., Ltd. All FISH procedures were conducted in accordance with the manufacturer's protocols.

Flow Cytometry

Transfected cells (1×10^6) were harvested and stored in 75% ethanol at −20°C overnight. After centrifugation, the cells were stained with DNA staining solution [Multisciences (Lianke)

Biotech Co., Ltd, Hangzhou, China]. Analysis was conducted using a BD™ LSR II flow cytometer (BD Biosciences, San Jose, CA, USA).

Cell Counting Kit-8 (CCK-8), EdU Cell Proliferation, and Colony Formation Assays

The CCK-8, EdU cell proliferation, and colony formation assays were performed as previously reported.

RNA Pulldown Assay

MiRNAs bound to circERBIN were detected using the Pierce Magnetic RNA-Protein Pull-Down Kit (Thermo Fisher Scientific) in accordance with the manufacturer's instructions with biotin-labeled probes designed and synthesized by Guangzhou RiboBio Co., Ltd.

In Vivo Tumor Models

Four-week-old nude male mice were purchased from the Animal Core Facility of Nanjing Medical University and assigned to one of two groups. Then, each mouse was subcutaneously injected with 2×10^6 cells. After two weeks, mice with palpable tumors were injected intratumorally with 50 nmol cholesterol-conjugated si-NC or si-circERBIN 3 times a week for 2 weeks. Tumor volumes were measured weekly. After 5 weeks, all mice were sacrificed and the tumor tissues were harvested and weighed.

Luciferase Reporter Assay

Luciferase reporter plasmids coding for mutant (MUT) and wild-type (WT) circERBIN and CDK6 were constructed by Shanghai GeneChem Co., Ltd. (Shanghai, China). Cells were transfected with the plasmids using Lipofectamine 3000 transfection reagent

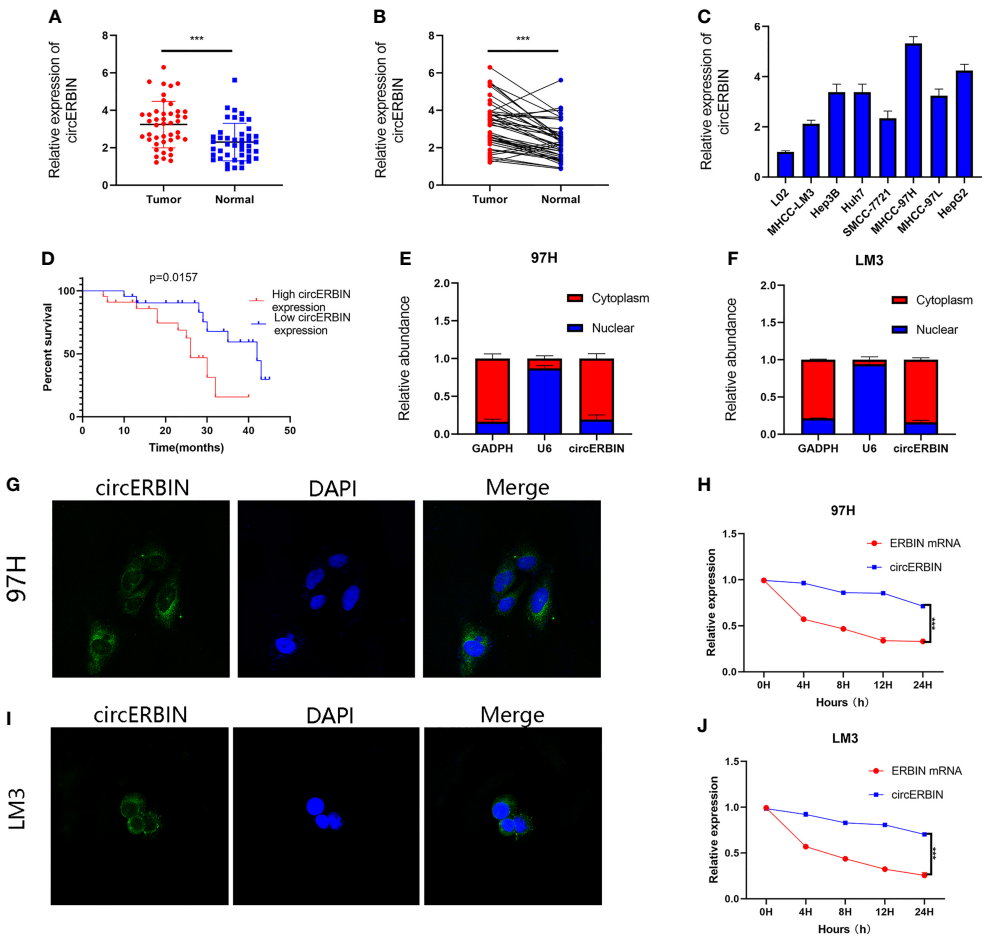

FIGURE 1 | CircERBIN is upregulated in HCC cells and tissues. **(A, B)** The relative expression of circERBIN was determined in 44 pairs of HCC and para-cancer tissues by qRT-PCR. **(C)** The relative expression of circERBIN was examined in HCC cell lines by qRT-PCR. **(D)** Kaplan–Meier survival curve analysis showed that high expression of circERBIN was associated with shorter overall survival of HCC patients. **(E, F)** qRT-PCR analysis of circERBIN abundance in the cytoplasmic and nuclear fractions of 97H and LM3 cells. GAPDH and U6 were used as positive controls in the cytoplasm and nucleus, respectively. **(G, H)** FISH was used to determine the localization of circERBIN in HCC cells. **(I, J)** Time-course qRT-PCR analyses of the relative abundance of circERBIN and linear ERBIN in LM3 and 97H cells treated with actinomycin D (10 μg/mL). (***$p < 0.001$).

and activity was measured with the Dual-Luciferase Reporter System Kit (E1910; Promega Corporation, Madison, WI, USA).

Statistical Analysis

Statistical analyses were performed using GraphPad Prism 9.0 software (GraphPad Software, Inc., San Diego, CA, USA) and IBM SPSS Statistics for Windows, version 24.0. (IBM Corporation, Armonk, NY, USA). Data are expressed as the mean ± standard deviation. The Student's *t*-test was used to identify differences between the control and experimental groups. The log-rank test was used to assess the survival data, which are presented as Kaplan–Meier survival curves. Correlations between groups were analyzed using Pearson's test. The chi-squared test was performed to analyze the association between the expression levels of target genes and clinicopathological parameters.

RESULTS

circERBIN Is Upregulated in HCC Cells and Tissues

The qRT-PCR results revealed that circERBIN was significantly upregulated in HCC tissues as compared with para-cancerous normal tissues (**Figures 1A, B**). Among seven HCC cell lines and one normal cell line, circERBIN expression was highest in 97H cells and lowest in LM3 cells (**Figure 1C**). Furthermore, upregulation of circERBIN was associated with lower overall survival of HCC patients (**Figure 1D**). As shown in **Table 1**, circERBIN was significantly correlated with tumor size, Edmondson grade, and TNM stage, but not age, sex, hepatitis B virus infection, and liver cirrhosis. Next, the localization of circERBIN in HCC cells was investigated. The nuclear-cytoplasmic fractionation experiments (**Figures 1E, F**) and FISH assays (**Figures 1G, H**) demonstrated that circERBIN was mainly localized in the cytoplasm. To further evaluate the circular structure of circERBIN, the actinomycin D assay (**Figures 1I, J**) was performed. The results showed that circERBIN was more stable than linear ERBIN.

TABLE 1 | Correlation between circERBIN expression and clinicopathological features in HCC tissues (n = 44, $\chi 2$ -test).

Variable	circERBIN expression		P-value
	high 22	low 22	
Age (year)			0.7609
<60	13	12	
≥60	9	10	
Gender			0.7569
Male	8	13	
Female	14	9	
Tumor size			0.0346*
<5 cm	10	14	
≥5 cm	12	8	
TNM stage			0.0142*
I–II	9	17	
III–IV	13	5	
Liver cirrhosis			0.7628
Yes	12	11	
No	10	11	
AFP (ng/mL)			0.0658
≤200	6	12	
>200	16	10	
HBsAg			0.7505
positive	15	14	
negative	7	8	
Edmondson grade			0.0053**
I–II	4	13	
III–IV	18	9	

*$p < 0.05$, **$p < 0.001$.

circERBIN Promotes the Proliferation and G1/S Transition of HCC Cells

To investigate the biological role of circERBIN in HCC, LM3 cells were transfected with plasmids overexpressing circERBIN (**Figure 1A**). In addition, circERBIN expression was silenced in 97H cells by transfection with short interfering (si) RNA (**Figure 2A**). Knockdown of circERBIN significantly impaired the proliferation of 97H cells as compared with the si-NC, as demonstrated by the CCK-8 assay (**Figure 2B**), while overexpression of circERBIN accelerated the proliferation of LM3 cells (**Figure 2C**). The results of the colony formation assay showed that 97H cells transfected with si-circERBIN produced fewer colonies as compared with the control cells (**Figures 2D, E**). In addition, the colony formation rate was higher in LM3 cells overexpressing circERBIN (**Figures 2D, E**). The results of the EdU cell proliferation assay (**Figures 2F, G**) were consistent with those of the colony formation and CCK-8 assays. Besides, flow cytometry was performed to assess the proportions of cells in each stage of the cell cycle. The results revealed that silencing of circERBIN increased the proportion of 97H cells in the G0/G1 phase, while overexpression of circERBIN had an opposite effect in LM3 cells (**Figure 2H**). These results demonstrated that circERBIN was a tumor promotor and accelerated the proliferation of HCC cells *in vitro*.

circERBIN Promotes the Proliferation of HCC Cells *In Vivo*

To determine whether circERBIN functions as a tumor promotor *in vivo*, nude mice were subcutaneously injected with HCC cells (**Figure 3A**). Tumor volumes were measured and recorded weekly (**Figure 3C**). After 5 weeks, all mice were sacrificed and tumor tissues were harvested and weighed (**Figure 3B**). Additionally, IHC staining showed a reduction Ki-67 levels in tumor cells after circERBIN knockdown (**Figures 3D, F**). The results revealed that downregulation of circERBIN significantly suppressed tumor growth, thereby further verifying the role of circERBIN in HCC tumorigenesis *in vivo*.

miR-1263 Is Sponged by circERBIN

Considering that circRNAs have been reported as sponges of miRNAs and regulate mRNA expression, we hypothesized that circERBIN functions *via* a mechanism dependent on competing endogenous RNA. To determine whether circERBIN can bind to miRNA, possible targets of circERBIN were predicted

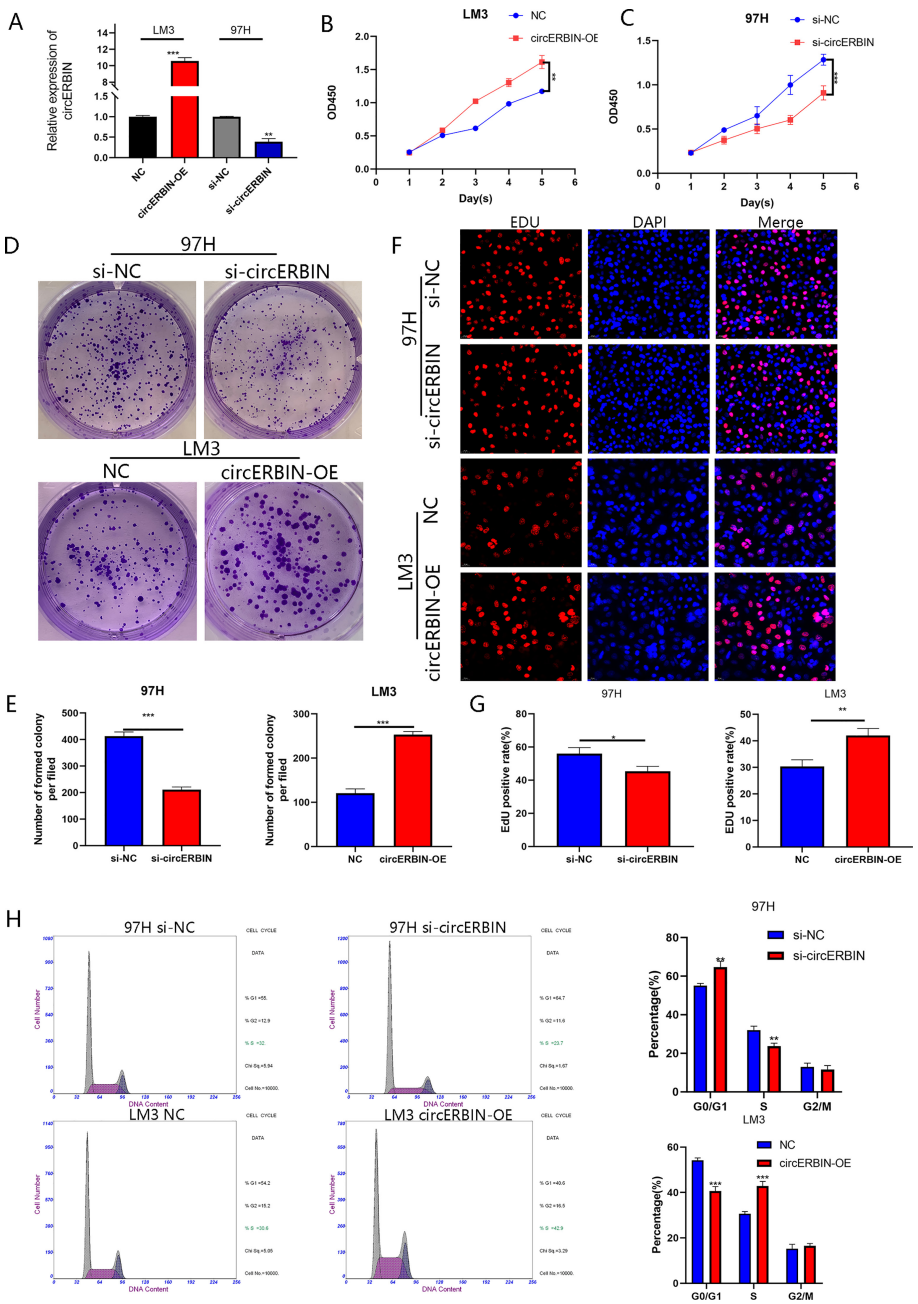

FIGURE 2 | CircERBIN promotes the proliferation and G1/S transition of HCC cells. **(A)** Expression of circERBIN was confirmed by qRT-PCR in HCC cells transfected with NC, circERBIN, si-NC, or si-circERBIN. **(B)** CCK-8 assay of 97H cells after circ-ERBIN knockdown. **(C)** CCK-8 assay of LM3 cells overexpressing circERBIN. **(D, E)** Effects of si-ERBIN and circERBIN-OE on proliferation of HCC cell lines by a colony formation assay. **(F, G)** EdU assays of LM3 and 97H cells treated with circERBIN or si-circERBIN. **(H)** Flow cytometry assays showing that circERBIN can accelerate G1 to S phase transition, while circERBIN knockdown increased the proportion of cells in the G1 phase. (*$p < 0.05$, **$p < 0.01$, ***$p < 0.001$).

with the online databases circBank (http://www.circbank.cn/) and CircInteractome (http://circinteractome.nia.nih.gov/) (**Figure 4A**). Two candidate miRNAs (miR1263 and miR-548c-3p) with potential binding sites for circERBIN were identified. The results of a pull-down assay using biotin-labeled probes showed significant fold changes of miR-1263 as compared with a NC (**Figures 4B, C**). To further verify the interaction between circERBIN and miR-1263, luciferase reporter plasmids were constructed containing the full length WT or MUT sequence of circERBIN within the binding sites of miR-1263 (**Figure 4D**). Then, HCC cells were co-transfected with the luciferase plasmids and miR-1263 mimics or inhibitors.

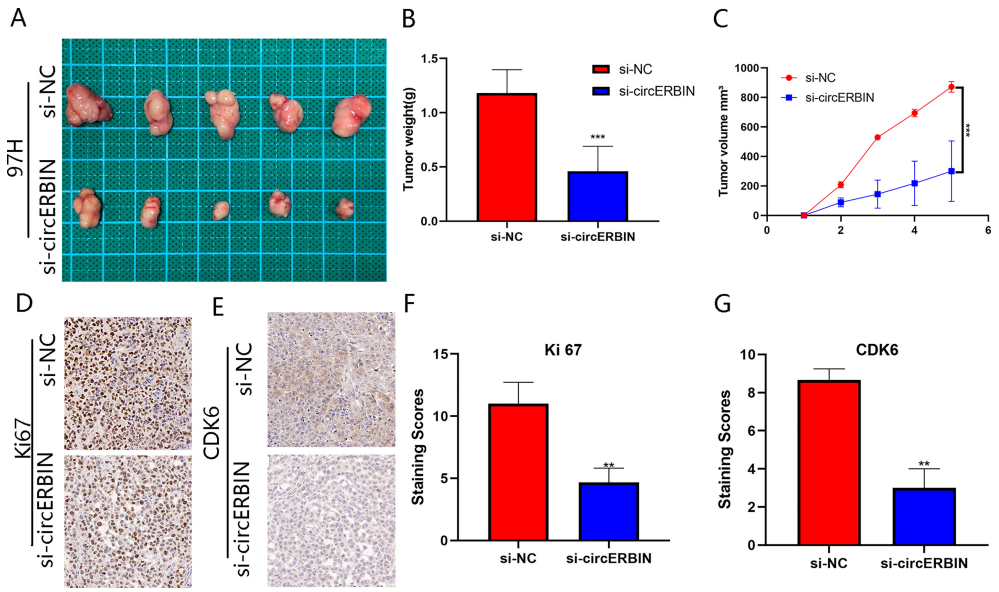

FIGURE 3 | CircERBIN promotes the proliferation of HCC cells *in vivo*. **(A–C)** 97H cells transfected with si-circ-ERBIN were injected into BALB/C nude mice (n = 5/group). Tumor volumes and weights were monitored. **(D, F)** IHC staining of xenograft tumors. The protein levels of Ki67 were analyzed based on IHC staining. **(E, G)** IHC staining of xenograft tumors. The protein levels of CDK6 were analyzed based on IHC staining. The samples were imaged at 400× magnification. (**$p < 0.01$, ***$p < 0.001$).

The results showed that the miR-1263 mimics significantly decreased the luciferase activity of the WT (**Figure 4E**), but not the MUT, while the miR-1263 inhibitor had an opposite effect (**Figure 4F**). These findings indicate that there could be a direct interaction between circERBIN and miR-1263. Moreover, miR-1263 expression was notably downregulated in HCC tissues (**Figure 4G**), while circERBIN was negatively correlated with miR-1263 (**Figure 4H**). The FISH results indicated that circERBIN and miR-1263 co-localized in the cytoplasm of HCC cells and tissues (**Figures 4K, L**). In contrast to miR-1263, circERBIN levels were increased in tumor tissues. In addition, overexpression of circERBIN inhibited the expression of miR-1263, whereas silencing of circERBIN had a significant opposite effect (**Figures 4I, J**). Taken together, these results suggest that circERBIN may function as a sponge for miR-1263.

miR-1263 Inhibits the Proliferation of HCC Cells

To further elucidate the effects of miR-1263-mediated regulation of HCC cells, LM3 and 97H cells were transfected with miR-1263 mimics or inhibitors. The transfection efficiency was verified by qRT-PCR (**Figures 4M, N**). The results of the CCK-8 (**Figure 5A**), colony formation (**Figures 5B–D**), and EdU cell proliferation (**Figures 5E–G**) assays confirmed that overexpression of miR-1263 inhibited the proliferation of 97H cells, while silencing miR-1263 remarkably decreased these cellular behaviors.

CDK6 Is a Direct Target of miR-1263

The DIANA (http://diana.imis.athena-innovation.gr/DianaTools/index.php), miRmap (https://mirmap.ezlab.org/), miRwalk (http://mirwalk.umm.uni-heidelberg.de/), and Targetscan (https://www.targetscan.org/vert_80/) bioinformatic tools were used to predict the downstream targets of miR-1263 (**Figure 6A**). The results revealed three putative genes: CDK6, GTPBR10, and ZFHX4. It is well known that miRNA binds to the 3′-untranslated region of target genes to regulate expression. The expression of potential target genes were detected by qRT-PCR analysis of cells transfected with the miR-1263 mimics or inhibitor (**Figures 6B, C**). The results showed that CDK6 was the most probable target gene. To further confirm the interaction between miR-1263 and CDK6, luciferase reporter plasmids containing the WT or MUT CDK6 sequence were constructed (**Figure 6D**). The activity of the luciferase reporter was decreased when co-transfected with miR-1263 mimics as compared with the NC (**Figures 6E, F**). Moreover, the western blot results showed that inhibition of miR-1263 actually elevated CDK6 protein levels in 97H cells, while overexpression had an opposite effect (**Figure 6G**). These findings confirmed that miR-1263 directly targeted CDK6. Moreover, the results of the rescue experiments indicated that CDK6 expression was indirectly regulated by circERBIN *via* the circERBIN/miR-1263/CDK6 regulatory axis at the RNA and protein levels (**Figures 6H–K**). To explore the roles of CDK6 on HCC phenotypes, further analysis found that CDK6 mRNA expression was obviously upregulated in HCC tissues (**Figure 6L**). In addition, CDK6 expression was negatively correlated with miR-1263 in HCC tissues (**Figure 6M**).

circERBIN Promotes HCC Progression *via* the miR-1263/CDK6 Axis

The efficiency of shCDK6 transfection was verified by qRT-PCR (**Figures 7A, B**) and western blot (**Figure 7C**) analyses.

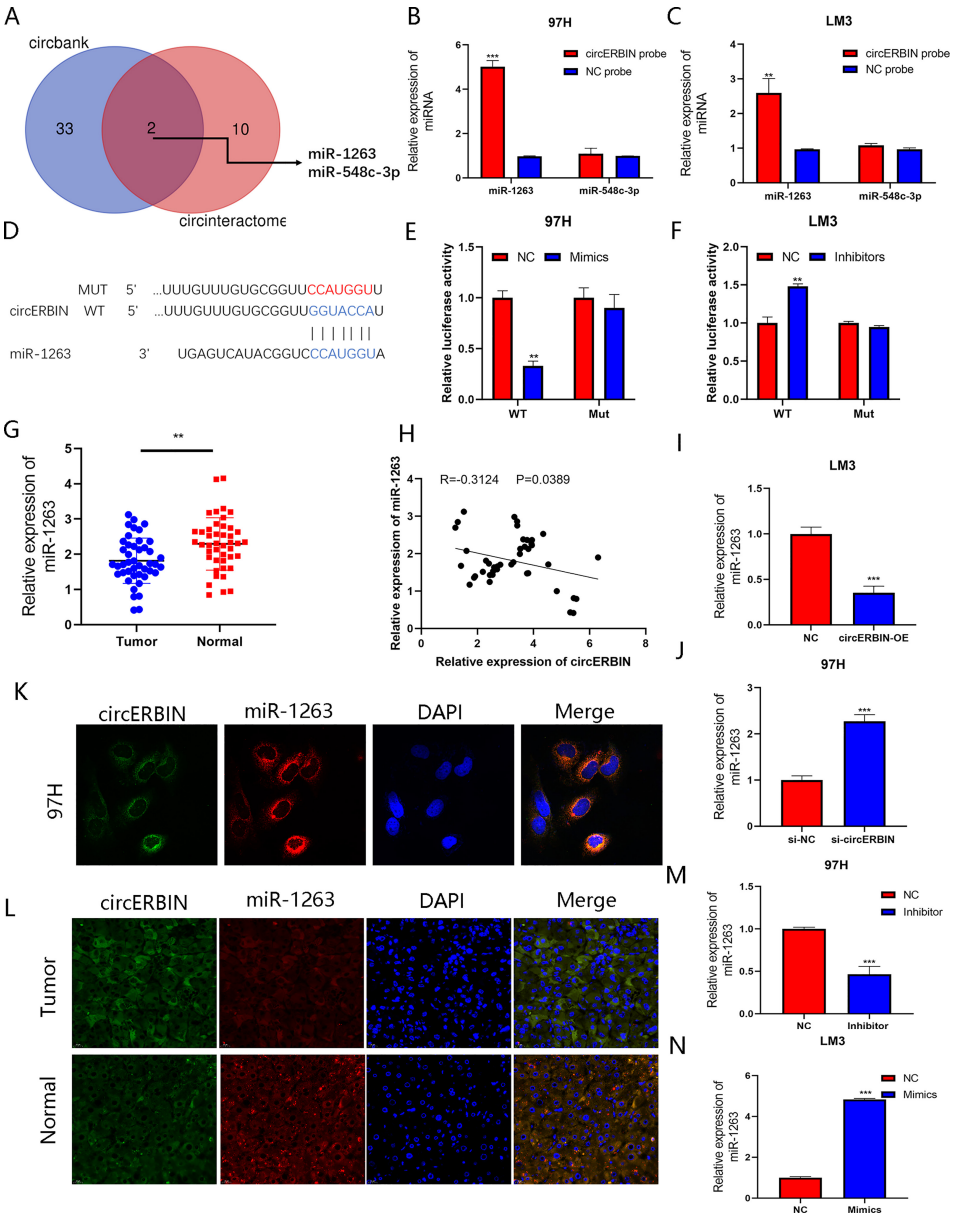

FIGURE 4 | miR-1263 is sponged by circERBIN. **(A)** Schematic illustration exhibiting overlapping of the target miRNAs of circERBIN as predicted by the circBank and CircInteractome database. **(B, C)** The relative abundances of two miRNA candidates in 97H and LM3 lysates with circERBIN or oligonucleotide probes were examined by qRT-PCR. **(D)** Schematic illustration of the sequence of WT and MUT circERBIN at the miR-1263 binding site. **(E, F)** The effects of miR-1263 mimics, an inhibitor, and NC on luciferase activity were detected in HCC cells transfected with luciferase reporter plasmids. **(G)** Relative miR-1263 expression in 44 pairs of fresh frozen HCC tissues and matched normal liver tissues. **(H)** An obvious negative correlation between the levels of circERBIN and miR-1263 in 44 pairs of fresh frozen HCC tissues and matched normal liver tissues as determined by Pearson correlation analysis. **(I, J)** The relative levels of miR-1263 in 97H and LM3 cell lines transfected with si-circERBIN, circERBIN, or NC as detected by qRT-PCR. **(K)** Co-localization of circERBIIN and miR-1263 in HCC cells as detected with the FISH assay. Scale bar, 10 μm. **(L)** FISH results showing co-localization of circERBIIN and miR-1263 in HCC and para-cancerous tissues from patients. Scale bar, 25 μm. **(M, N)** Relative miR-1263 expression in transfected 97H and LM3 cells. (**$p < 0.01$, ***$p < 0.001$).

Transfection with shCDK6 significantly decreased CDK6 expression as compared with the shNC. Silencing of circERBIN downregulated the proliferation of 97H cells, while the addition of CDK6 reversed the inhibiting effects on cell growth as determined by the CCK-8 (**Figure 7I**), colony formation (**Figures 7D, E**), and EdU cell proliferation (**Figures 7F–H**) assays. In contrast, circERBIN-mediated growth was counteracted by transfection with shCDK6. Moreover, the addition of CDK6 reversed G1 arrest induced by silencing of circERBIN (**Figure 7J**). ShCDK6 also inhibited G1 to S

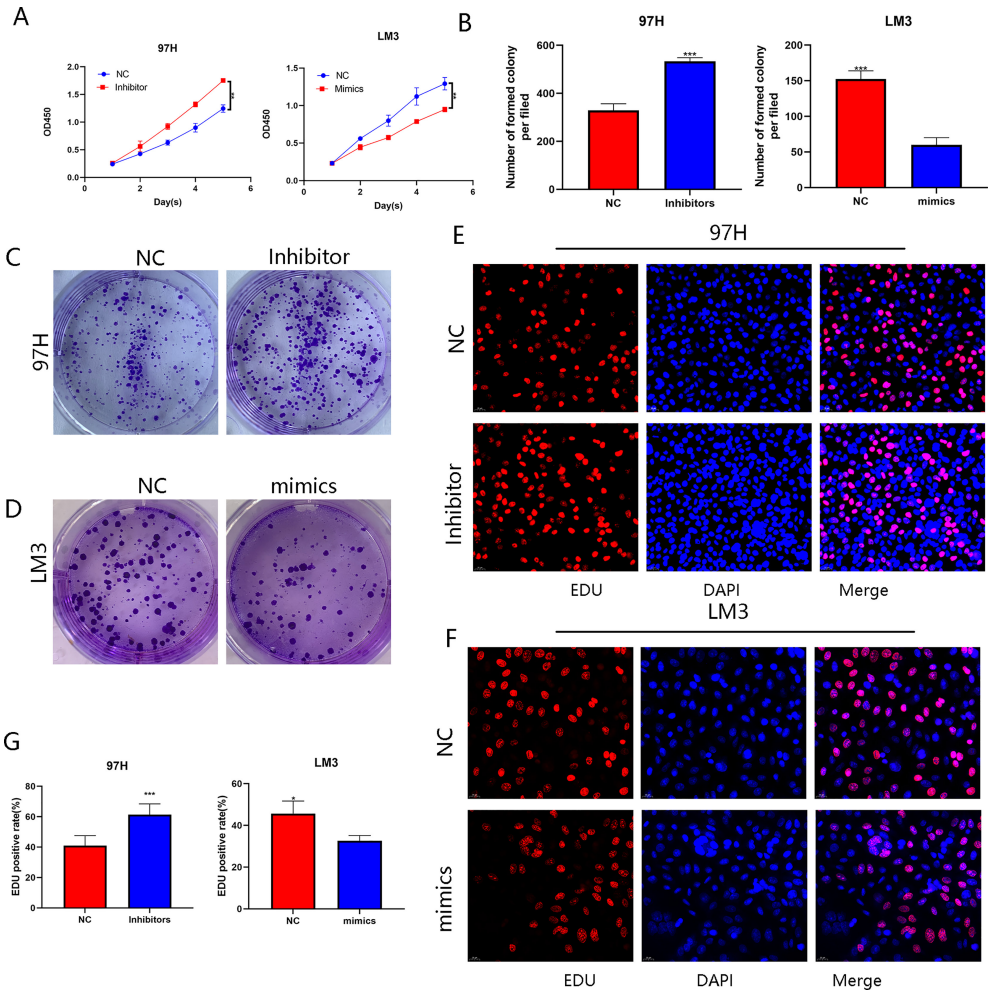

FIGURE 5 | miR-1263 inhibits the proliferation of HCC cells. **(A)** CCK-8 assay of LM3 and 97H cells transfected with mimics or an inhibitor. **(B–D)** Effect of mimics or an inhibitor on the proliferation in HCC cell lines as determined by the colony formation assay. **(E–G)** EDU assay of LM3 and 97H cells treated with mimics or an inhibitor. (*$p < 0.05$, **$p < 0.01$, ***$p < 0.001$).

phase transition accelerated by circERBIN overexpression (**Figure 7K**). IHC staining results for CDK6 in subcutaneous tumors in a previously described *in vivo* model confirmed the correlation between circERBIN and CDK6 (**Figures 3E, G**). In short, circERBIN promoted the progression of HCC *via* CDK6.

DISCUSSION

Mounting evidence has demonstrated that dysregulation of circRNAs plays critical roles in HCC tumorigenesis and progression through regulating key tumor regulatory genes. In view of the great importance of circRNAs in HCC, we previously revealed that circ_0011385 enhances HCC cell proliferation and tumor activity *via* regulation through the miR-361-3p/STC2 axis and that circCRIM1 facilitates HCC progression and angiogenesis by sponging miR-378a-3p (9, 11). Owning to the circular structures, circRNAs are more stable than the corresponding linear forms and are expected to be exciting targets for tumor drug discovery (12). Importantly, dysregulation of circRNAs has been extensively profiled, although the exact functions and molecular mechanisms of specific circRNAs in HCC progression remain to be fully elucidated.

The results of this study clarified that circERBIN originates from exons 2, 3, and 4 of the Erbin gene which plays critical roles in multiple malignancies, including lung adenocarcinoma, colorectal cancer, kidney renal papillary cell carcinoma, and particularly HCC (13–15). Erbin is reportedly elevated in HCC and promotes tumorigenesis by enhancing the ubiquitination and degradation of estrogen receptor-alpha (16). A recent study reported that circERBIN is a potential biomarker of the progression of colorectal cancer (10). Nevertheless, the expression pattern and function of circERBIN in HCC

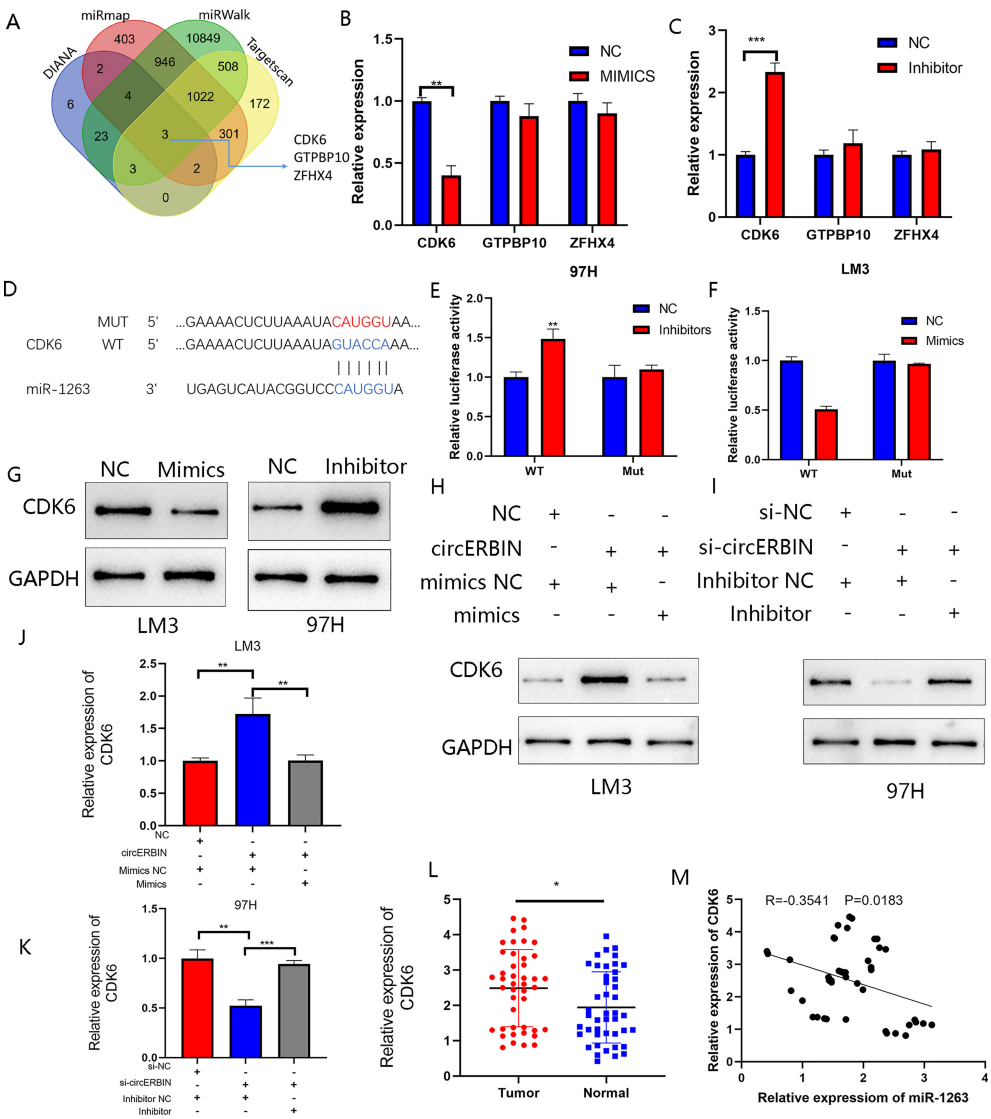

FIGURE 6 | CDK6 is a direct target of miR-1263. **(A)** Schematic illustration exhibiting overlapping of the target mRNAs of miR-1263 predicted by the DIANA, miRmap, miRwalk, and Targetscan databases. **(B, C)** Expression of predicted target genes in LM3 and97H cells transfected with miR-1263 mimics, an inhibitor, and corresponding NC. **(D)** Schematic illustration of the WT and MUT CDK6 sequences at the miR-1263 binding site. **(E, F)** The effects of miR-1263 mimics and inhibitor on the luciferase activities of the WT and MUT CDK6 mRNA 3'-untranslated regions as detected by qRT-PCR. **(G)** The effects of miR-1263 on the protein expression of TDO2 were detected by western blot analysis. **(H, I)** Western blotting showing CDK6 protein expression in transfected 97H and LM3 cells. **(J, K)** QRT-PCR showing CDK6 mRNA expression in transfected 97H and LM3 cells. **(L)** Relative CDK6 expression in 44 pairs of fresh frozen HCC tissues and matched normal liver tissues. **(M)** An obvious negative correlation between the levels of miR-1263 and CDK6 in 44 pairs of fresh frozen HCC tissues and matched normal liver tissues as determined by Pearson correlation analysis. (*$p < 0.05$, **$p < 0.01$, ***$p < 0.001$).

progression have yet to be determined. Hence, the present investigation focused on the role and potential mechanism of circERBIN in HCC.

The results of the present study showed that circERBIN is upregulated in HCC, which was consistent with the expression pattern of the linear form of Erbin. Additionally, higher circERBIN expression was associated with poorer clinicopathological features and prognosis. Furthermore, circERBIN facilitated the proliferation of HCC cells both *in vitro* and *in vivo via* regulation of the cell cycle. Based on the competing endogenous RNA mechanisms, we further assumed that circERBIN worked as a miRNA sponge in the cytoplasm. Bioinformatics, the RNA pull-down assay, and luciferase reporter gene assay were employed to predict and confirm that circERBIN directly targeted miR-1263. Then, we illustrated the tumor suppressive role of miR-1263 in HCC. Our data showed that miR-1263 was downregulated in the cytoplasm and inhibited the growth of HCC cells by targeting CDK6, which is

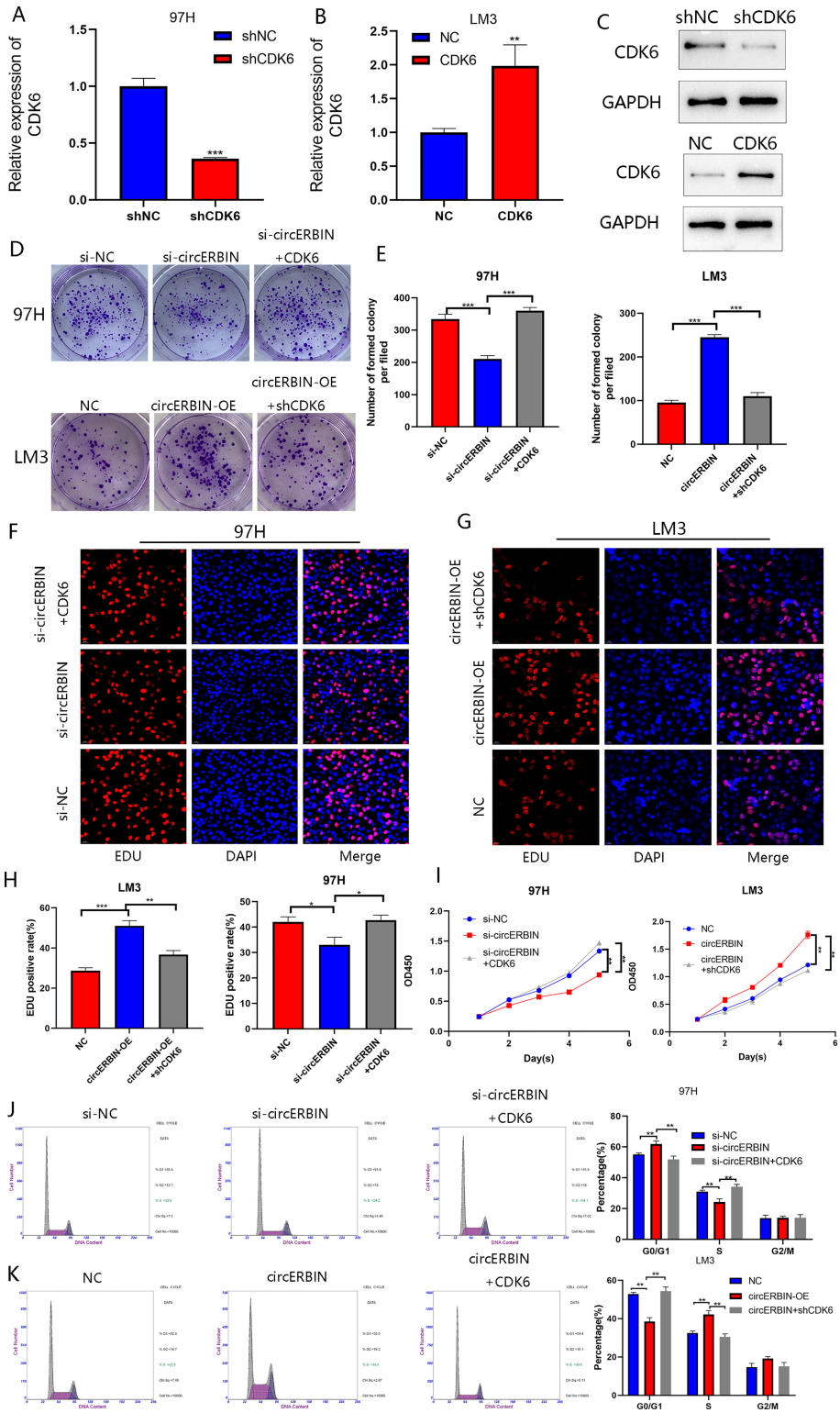

FIGURE 7 | CircERBIN promotes the progression of HCC *via* the miR-1263/CDK6 axis. **(A–C)** Relative expression of CDK6 in 97H and LM3 cells transfected with shCDK6, CDK6, or NC as detected by qRT-PCR and western blot analyses. **(D–I)** The effects of circERBIN and CDK6 on HCC cells proliferation in HCC cell lines were evaluated by colony formation, EdU cell proliferation, and CCK-8 assays. **(J, K)** Flow cytometry showing that circERBIN and CDK6 affect G1 to S phase transition. (*$p < 0.05$, **$p < 0.01$, ***$p < 0.001$).

indispensable for cell cycle progression to the G1 phase and G1/S transition (17). However, further investigations are needed to determine whether the effects of circ-ERBIN are dependent on the host Erbin gene.

Dysregulation of cell cycle proteins is a common characteristic of cancer cells, thus targeting cell cycle pathways has attracted considerable interest as a promising strategy for cancer therapy (18). As the key driver of cell division and G1/S transition, expression of CDK6 is tightly controlled in cancer cells. CDK6 expression is reportedly regulated by transcription factors, miRNAs, and long non-coding RNAs (19–21). Recent studies have reported that CDK6 is regulated by circRNAs and participates in circRNAs-mediated G1/S transition (22, 23). In this study, circERBIN upregulated CDK6 expression by sponging miR-1263. Furthermore, circERBIN-induced growth of HCC cells and cell cycle transition were abolished by CDK6 knockdown. To date, the United States Food and Drug Administration has approved several CDK6 inhibitors for the treatment of breast cancer and other malignancies (17, 24). The results of the present study outline a promising strategy for the use of CDK6 for treatment of HCC patients with positive circERBIN expression.

In conclusion, circERIN was upregulated in HCC tissues and cells and strongly associated with unfavorable clinicopathological features and prognosis. Furthermore, circERBIN can modulate the cell cycle to facilitate HCC progression *via* the miR-1263/CDK6 axis. Hence, blocking circ-ERBIN presents a potential therapeutic target to halt the progression of HCC.

DATA AVAILABILITY STATEMENT

The raw data supporting the conclusion of this article will be made available by the authors without undue reservation.

ETHICS STATEMENT

The study protocols involving human participants were reviewed and approved by the Ethics Committee of the First Affiliated Hospital of Nanjing Medical University. The patients/participants provided written informed consent to participate in this study.

AUTHOR CONTRIBUTIONS

SY and YJ conducted the experiments and wrote this manuscript. FY, YS, and HL conducted parts of the experiments. SY, YJ, and YG analyzed the data. FZ, XW, and CZ conceived and supervised this study. All authors contributed to the article and approved the submitted version.

FUNDING

This work was financially supported by the National Natural Science Foundation of China (grant nos. 81870488, 81530048, and 31930020).

REFERENCES

1. Sung H, Ferlay J, Siegel RL, Laversanne M, Soerjomataram I, Jemal A, et al. Global Cancer Statistics 2020: Globocan Estimates of Incidence and Mortality Worldwide for 36 Cancers in 185 Countries. *CA Cancer J Clin* (2021) 71 (3):209–49. doi: 10.3322/caac.21660
2. Yang S, Jiang W, Yang W, Yang C, Yang X, Chen K, et al. Epigenetically Modulated Mir-1224 Suppresses the Proliferation of Hcc Through Creb-Mediated Activation of Yap Signaling Pathway. *Mol Ther Nucleic Acids* (2021) 23:944–58. doi: 10.1016/j.omtn.2021.01.008
3. Marrero JA, Kulik LM, Sirlin CB, Zhu AX, Finn RS, Abecassis MM, et al. Diagnosis, Staging, and Management of Hepatocellular Carcinoma: 2018 Practice Guidance by the American Association for the Study of Liver Diseases. *Hepatology* (2018) 68(2):723–50. doi: 10.1002/hep.29913
4. Chen LL. The Biogenesis and Emerging Roles of Circular Rnas. *Nat Rev Mol Cell Biol* (2016) 17(4):205–11. doi: 10.1038/nrm.2015.32
5. Jeck WR, Sharpless NE. Detecting and Characterizing Circular Rnas. *Nat Biotechnol* (2014) 32(5):453–61. doi: 10.1038/nbt.2890
6. Lei M, Zheng G, Ning Q, Zheng J, Dong D. Translation and Functional Roles of Circular Rnas in Human Cancer. *Mol Cancer* (2020) 19(1):30. doi: 10.1186/s12943-020-1135-7
7. Rong D, Wu F, Lu C, Sun G, Shi X, Chen X, et al. M6a Modification of Circhps5 and Hepatocellular Carcinoma Progression Through Hmga2 Expression. *Mol Ther Nucleic Acids* (2021) 26:637–48. doi: 10.1016/j.omtn.2021.09.001
8. Chen Q, Wang H, Li Z, Li F, Liang L, Zou Y, et al. Circular Rna Actn4 Promotes Intrahepatic Cholangiocarcinoma Progression by Recruiting Ybx1 to Initiate Fzd7 Transcription. *J Hepatol* (2022) 76(1):135–47. doi: 10.1016/j.jhep.2021.08.027
9. Ni C, Yang S, Ji Y, Duan Y, Yang W, Yang X, et al. Hsa_Circ_0011385 Knockdown Represses Cell Proliferation in Hepatocellular Carcinoma. *Cell Death Discov* (2021) 7(1):270. doi: 10.1038/s41420-021-00664-0
10. Chen LY, Wang L, Ren YX, Pang Z, Liu Y, Sun XD, et al. The Circular Rna Circ-Erbin Promotes Growth and Metastasis of Colorectal Cancer by Mir-125a-5p and Mir-138-5p/4ebp-1 Mediated Cap-Independent Hif-1alpha Translation. *Mol Cancer* (2020) 19(1):164. doi: 10.1186/s12943-020-01272-9
11. Ji Y, Yang S, Yan X, Zhu L, Yang W, Yang X, et al. Circcrim1 Promotes Hepatocellular Carcinoma Proliferation and Angiogenesis by Sponging Mir-378a-3p and Regulating Skp2 Expression. *Front Cell Dev Biol* (2021) 9:796686. doi: 10.3389/fcell.2021.796686
12. Zhou X, Zhan L, Huang K, Wang X. The Functions and Clinical Significance of Circrnas in Hematological Malignancies. *J Hematol Oncol* (2020) 13(1):138. doi: 10.1186/s13045-020-00976-1
13. Shen T, Liu JL, Wang CY, Rixiati Y, Li S, Cai LD, et al. Targeting Erbin in B Cells for Therapy of Lung Metastasis of Colorectal Cancer. *Signal Transduct Target Ther* (2021) 6(1):115. doi: 10.1038/s41392-021-00501-x
14. Zhang L, Wang L, Wang Y, Chen T, Liu R, Yang W, et al. Lncrna Ktn1-As1 Promotes Tumor Growth of Hepatocellular Carcinoma by Targeting Mir-23c/Erbb2ip Axis. *BioMed Pharmacother* (2019) 109:1140–7. doi: 10.1016/j.biopha.2018.10.105
15. Zhou Q, Li D, Zheng H, He Z, Qian F, Wu X, et al. A Novel Lncrna-Mirna-Mrna Competing Endogenous Rna Regulatory Network in Lung Adenocarcinoma and Kidney Renal Papillary Cell Carcinoma. *Thorac Cancer* (2021) 12(19):2526–36. doi: 10.1111/1759-7714.14129
16. Wu H, Yao S, Zhang S, Wang JR, Guo PD, Li XM, et al. Elevated Expression of Erbin Destabilizes Eralpha Protein and Promotes Tumorigenesis in Hepatocellular Carcinoma. *J Hepatol* (2017) 66(6):1193–204. doi: 10.1016/j.jhep.2017.01.030
17. Petroni G, Formenti SC, Chen-Kiang S, Galluzzi L. Immunomodulation by Anticancer Cell Cycle Inhibitors. *Nat Rev Immunol* (2020) 20(11):669–79. doi: 10.1038/s41577-020-0300-y
18. Otto T, Sicinski P. Cell Cycle Proteins as Promising Targets in Cancer Therapy. *Nat Rev Cancer* (2017) 17(2):93–115. doi: 10.1038/nrc.2016.138
19. Wang YL, Liu JY, Yang JE, Yu XM, Chen ZL, Chen YJ, et al. Lnc-Ucid Promotes G1/S Transition and Hepatoma Growth by Preventing Dhx9-

Mediated Cdk6 Down-Regulation. *Hepatology* (2019) 70(1):259–75. doi: 10.1002/hep.30613
20. Nebenfuehr S, Kollmann K, Sexl V. The Role of Cdk6 in Cancer. *Int J Cancer* (2020) 147(11):2988–95. doi: 10.1002/ijc.33054
21. Dai M, Boudreault J, Wang N, Poulet S, Daliah G, Yan G, et al. Differential Regulation of Cancer Progression by Cdk4/6 Plays a Central Role in DNA Replication and Repair Pathways. *Cancer Res* (2021) 81(5):1332–46. doi: 10.1158/0008-5472.CAN-20-2121
22. Chen L, Zhang S, Wu J, Cui J, Zhong L, Zeng L, et al. Circrna_100290 Plays a Role in Oral Cancer by Functioning as a Sponge of the Mir-29 Family. *Oncogene* (2017) 36(32):4551–61. doi: 10.1038/onc.2017.89
23. Ishola AA, Chien CS, Yang YP, Chien Y, Yarmishyn AA, Tsai PH, et al. Oncogenic Circrna C190 Promotes Non-Small Cell Lung Cancer *Via* Modulation of the Egfr/Erk Pathway. *Cancer Res* (2022) 82(1):75–89. doi: 10.1158/0008-5472.CAN-21-1473
24. Fassl A, Geng Y, Sicinski P. Cdk4 and Cdk6 Kinases: From Basic Science to Cancer Therapy. *Science* (2022) 375(6577):eabc1495. doi: 10.1126/science.abc1495

Conflict of Interest: The authors declare that the research was conducted in the absence of any commercial or financial relationships that could be construed as a potential conflict of interest.

Publisher's Note: All claims expressed in this article are solely those of the authors and do not necessarily represent those of their affiliated organizations, or those of the publisher, the editors and the reviewers. Any product that may be evaluated in this article, or claim that may be made by its manufacturer, is not guaranteed or endorsed by the publisher.

frontiers | Frontiers in Oncology

REVIEW
published: 04 May 2022
doi: 10.3389/fonc.2022.891812

RNA Therapeutic Options to Manage Aberrant Signaling Pathways in Hepatocellular Carcinoma: Dream or Reality?

Kurt Sartorius[1,2,3]*, *Samuel O. Antwi*[2,4], *Anil Chuturgoon*[5], *Lewis R. Roberts*[2,6] *and Anna Kramvis*[1]

[1] Hepatitis Virus Diversity Research Unit, School of Internal Medicine, University of the Witwatersrand, Johannesburg, South Africa, [2] The Africa Hepatopancreatobiliary Cancer Consortium (AHPBCC), Mayo Clinic, Jacksonville, FL, United States, [3] Department of Surgery, KZN Kwazulu-Natal (UKZN) Gastrointestinal Cancer Research Centre, Durban, South Africa, [4] Division of Epidemiology, Department of Quantitative Health Sciences, Mayo Clinic, Jacksonville, FL, United States, [5] Discipline of Medical Biochemistry, School of Laboratory Medicine and Medical Sciences, College of Health Science, University of KwaZulu-Natal, Durban, South Africa, [6] Division of Gastroenterology and Hepatology, Mayo Clinic, Rochester, MN, United States

OPEN ACCESS

Edited by:
Liangrong Shi,
Central South University, China

Reviewed by:
Xiaojin Wu,
First People's Hospital of Xuzhou, China
Hao Lu,
Nanjing Medical University, China

***Correspondence:**
Kurt Sartorius
Kurt.Sartorius@wits.ac.za

Specialty section:
This article was submitted to Molecular and Cellular Oncology, a section of the journal Frontiers in Oncology

Received: *08 March 2022*
Accepted: *04 April 2022*
Published: *04 May 2022*

Citation:
Sartorius K, Antwi SO, Chuturgoon A, Roberts LR and Kramvis A (2022) RNA Therapeutic Options to Manage Aberrant Signaling Pathways in Hepatocellular Carcinoma: Dream or Reality? Front. Oncol. 12:891812. doi: 10.3389/fonc.2022.891812

Despite the early promise of RNA therapeutics as a magic bullet to modulate aberrant signaling in cancer, this field remains a work-in-progress. Nevertheless, RNA therapeutics is now a reality for the treatment of viral diseases (COVID-19) and offers great promise for cancer. This review paper specifically investigates RNAi as a therapeutic option for HCC and discusses a range of RNAi technology including anti-sense oligonucleotides (ASOs), Aptamers, small interfering RNA (siRNA), ribozymes, riboswitches and CRISPR/Cas9 technology. The use of these RNAi based interventions is specifically outlined in three primary strategies, namely, repressing angiogenesis, the suppression of cell proliferation and the promotion of apoptosis. We also discuss some of the inherent chemical and delivery problems, as well as targeting issues and immunogenic reaction to RNAi interventions.

Keywords: small interfering RNA (siRNA), antisense oligonucleotide (ASO), aptamer, ribozyme, riboswitch, CRISPR/Cas9, RNAi strategies

INTRODUCTION

Hepatocellular carcinoma (HCC) therapeutics remain an intractable global problem against a background of rising incidence and changing etiology (1). A wide range of novel HCC therapeutics have been developed and tested over the last two decades, including molecular targeted therapy, protein antibodies, targeted radionucleotide therapy, and epigenetic therapy. Other HCC therapies include immunotherapy, immune-cell therapy, differentiation strategy and RNA interference (RNAi) (2). Despite these advances a cure is yet to be developed and to date survival time has only been modestly extended (3). Central to the problem of HCC management is that this cancer remains (largely) asymptomatic until it is very advanced (4).

This review paper specifically investigates RNAi as a therapeutic option for HCC. RNAi therapeutics involves the deployment of RNA molecules in sequence-specific modulation to

repress gene specific expression (5). In this paper we review the deployment of a range of RNAi technology including anti-sense oligonucleotides (ASO), Aptamers, small interfering RNA (siRNA), ribozymes, riboswitches and CRISPR/Cas9 technology for the management of HCC. The use of these RNA based interventions is specifically outlined in three primary strategies, namely, repressing angiogenesis, the suppression of cell proliferation and the promotion of apoptosis.

RNAi BASED THERAPEUTIC OPTIONS IN HCC

Small Interfering RNA

Small interfering RNA (siRNA) are double stranded RNA (dsRNA) that load a guide strand into some form of Argonaut (AGO) based RNA-induced silencing complex (RISC) after separation from its passenger strand (see **Figure 1**). A RISC with its encapsulated RNA attach to a complementary strip of mRNA and cause repression or cleavage. In effect, the silencing process adopted by siRNA is identical to that of microRNA (miRNA) in nature which are endogenously synthesized by endonucleases (DICER) and the guide strand packaged in a specific AGO based RISC in the cytoplasm. In humans, naturally occurring siRNA have a specific target and their origin seems to be the result of responding to a pathogen encountered in the past. For therapeutic purposes, siRNA can be chemically produced and modified and delivered in a wide range of nanoparticles (NPs). To increase their efficacy, siRNA vectors have been developed to achieve longer term application including modifications like a cassette that includes RNA Pol 11 that can perpetuate the transcription of siRNA. Transcriptional gene silencing (TGS) can also be influenced by siRNA where the complementary bases create a complex that binds to DNA (6).

Exogenous siRNAs are dsRNA characterized by a 2nt overhang on the 3' end of both strands that are delivered to an AGO based RISC that especially represses translation in the critical 2-8 position on the 5' end of its target mRNA. Although siRNA therapeutics mostly deploys manufactured siRNA, endogenous siRNA can also be harnessed and deployed for RNAi by using a viral vector to express short hairpin RNA (shRNA). Alternatively, manufactured siRNA that are miRNA mimics can be utilized for RNAi. Manufactured siRNA-based therapeutics use siRNAs that have been chemically stabilized to increase their potency and reduce RNase degradation *in vivo* but challenges remain due to off-target effects, as well as unintended immunogenic reaction (7). The stabilization and delivery of siRNA is, therefore, a critical issue (8).

Clustered Regularly Interspaced Palindromic Repeats/Caspase-9 (CRISPR/Cas9)

CRISPR/Cas9 uses CRISPR to guide Cas9 cleavage of targeted DNA sequences. This therapeutic application has been developed as a guide RNA/enzyme complex that can delete targeted RNA or DNA, as well as conduct precise DNA edits or inserts. CRISPR/Cas9 technology uses gRNA to guide and bind Cas9 cleavage to a its target DNA, however, CRISPR/Cas9 can also be used to re-engineer mutations, as well as ex vivo therapy to edit and then re-introduce edited cells *in vivo* (9). Cleavage of targeted DNA occurs by RNase 111. The CRISPR/Cas9 DNA gene replacement technology is developed in three steps: (i) insertion of the short sequence of the foreign DNA as a spacer in CRISPR array; (ii) transcription of the precursor cRNA (pre-cRNA) followed by its processing to generate individual cRNAs that comprise of a repeat and a spacer; and (iii) recognition of the target sequence by cRNAs and cleavage of the foreign nucleic acid by Caspase DNA nucleases at sites complementary to the cRNA spacer sequence. Repair of DNA

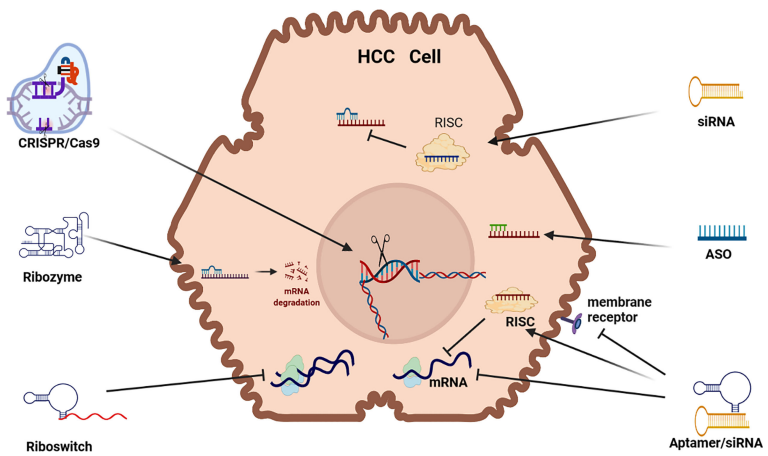

FIGURE 1 | RNAi Therapeutic options for HCC. siRNA (small interfering RNA), ASO (antisense oligonucleotides, Aptamer, Riboswitch, Ribozyme, CRISPR/Cas9 (clustered regularly interspaced short palindromic repeats/Caspase-9) mRNA (messenger RNA) (mRNA) RISC (RNA-induced silencing complex).

following cleavage is activated by CRISPR-Cas9 gene editing that introduces a donor repair template with homology identical to the area of the dsDNA cleaved DNA. The CRISPR/Cas systems (1, 10, 11) can activate or repress gene expression (7).

Antisense Oligonucleotides

Antisense oligonucleotides (ASOs) are short single stranded (ss) DNA/RNA that exist in nature as small RNA molecules. RNA based ASOs bind to a complementary nucleotide sequence site in mRNA causing splicing, degradation (R Nase H) or the repression of mRNA translation (6, 12) and DNA based ASOs form a DNA-RNA heteroduplex to precipitate RNases. Most ASO based drugs precipitate RNases but they can also repress translation, as well as be deployed to splice target DNA/RNA (7, 10). The chemistry and target sequence of ASOs determine their mechanism of action and the fate of the targeted RNA (13).

RNA Aptamers

Aptamers are short, single-stranded DNA or RNA (ssDNA or ssRNA) molecules that can selectively bind to a specific target. Aptamers can fold into a multi-functional state to bind to a target DNA/RNA in a similar fashion to an antibody to suppress protein expression. Aptamers, often labeled as chemical antibodies, can bind to a wide range of molecules including toxins, viruses, proteins and peptides and its binding facility is not based on complementarity but rather its ability to fold into a 3-dimensional structure to enfold a target molecule in the same way as an antibody (2, 6). RNA aptamers can be used as a delivery vehicle for a wide range of chemical agents and are less expensive and illicit low immunogenicity response compared to antibodies. Aptamers, which have a unique niche in RNAi therapeutics, can be developed to bind to an intracellular or extracellular target, and they can be used to activate or repress target expression (14). RNA aptamers can also bind to cell surface proteins to block their function, for example they can bind to VEGFR to inhibit VEGF signaling (15). Alternatively, they can be used to deliver RNAi based cargo (siRNA, shRNA, miRNA) to the intracellular space where they are encapsulated by RISC and delivered to target mRNA (16).

Ribozymes

Ribozymes are ribonucleic acid enzymes that play a catalytic silencing role to promote the cleaving of target mRNA by hybridizing with. This is a process where two ssRNA molecules combine into a single dsRNA molecule. There are three predominant forms of ribozyme, namely, hammerhead (HH), hepatitis delta virus (HDV) and hairpin (HP) ribozymes (7) but the most common ribozymes used in a therapeutic capacity take a "hammerhead" or "hairpin/paperclip" format (2). Ribozyme RNA molecules can catalyze specific biochemical reactions, as well as RNA splicing (trans-splicing ribozyme), and can be classified as genetic material (like DNA) or a catalyst. The most common activity of ribozymes includes cleavage/degradation of RNA/DNA but they can also play a role in linking peptide sequences (e.g. protein construction) within ribosomes.

Ribozymes can be directed to target the 5' end of RNA to induce RNaseP and cleavage in a sequence specific manner. Liposome mediated ribozymes can be delivered exogenously or transcribed endogenously to cleave target mRNA and they can be used repeatedly because they are not consumed in the cleavage process. Ribozyme therapy can be used to target most non-coding RNA (ncRNA) including siRNA, microRNA (miRNA), long noncoding (lncRNA), piwi-interacting RNA (piRNA) and small nucleolar RNA (snoRNA) that all play a regulatory role in carcinogenesis (17, 18). Trans-cleaving ribozymes can target specific mRNA segments in the same way as a dedicated siRNA (19). Due to poor stability of fully-RNA based ribozymes, they are chemically stabilized for therapeutic deployment using some of the following modifications: 5′-PS backbone linkage, 2′-*O*-Me, 2′-deoxy-2′-*C*-allyl uridine, and terminal inverted 3′-3′ deoxyabasic nucleotides (20).

Riboswitches

Riboswitches are a group of dynamic ncRNA motifs found upstream, in the 5′ untranslated region of mRNAs, where they regulate translation through binding of their cognate ligand to their aptamer domain (21). A riboswitch can be in an "on"/"off" state depending on the presence of a ligand. For example, in the absence of a ligand, the riboswitch folds to an "on" state and binds to the ribosome binding site (RBS) triggering translation initiation (RNA Polymerase). Conversely, in the presence of a ligand, the riboswitch folds to an "off" state to bar RBS binding and translation is blocked (7).

RNAi CHALLENGES AND DELIVERY OPTIONS

RNA Delivery Challenges

RNA can be delivered in their 'naked' state but they have a short circulation life *in vivo* due to speedy degradation *via* nuclease activity (22). Some of the problems of RNA-based therapeutics, therefore, include maintaining their stability and efficacy in sustained systemic delivery, as well as avoiding off-target effects. Other problems of RNA delivery include avoiding renal clearance, adverse immunogenic response, such as cytoplasmic RNA triggering IFN expression (2, 22, 23), and avoiding endosomal escape that can trigger unwanted TLR signaling (23). Additional problems arise because of the need to counter the negatively charged phosphate backbone of RNA, as well as its high molecular weight that reduce its stability and act as a barrier to cell entry and repress targeting ability (24). RNA based drugs are easily modified and their long term efficacy can be increased by the inclusion of replicative ability in the RNA based vesicle (6).

Stabilization of RNA

To overcome delivery challenges, a range of chemical modifications can prolong RNA half-life without jeopardizing their biological activity. RNA can be stabilized by chemical modifications to both sense strands, as well as the 3' and 5' caps, as well as ribose modifications. Ribose modifications to the 2'-OH site are a common modification to stabilize RNA to be

stabilized, including the following options, namely, 2'-Me, 2'-F and 2'-H. RNA molecules can also be stabilized by intramolecular linkages of 2'-Oxygen to 4'-carbon to create bridged nucleic acid (locked nucleic acid-LNA) molecules. Modifications to the RNA backbone can also increase nuclease resistance and involve substituting non bridging phosphate oxygen for sulfur, as well as boranophosphate substituted with the BH3 group (22). These modifications reduce off-target interference (25) and reduce immunogenicity response, mediated by TLR or PKR activation (26).

Nanoparticle Delivery of RNA

A wide variety of nanoparticles (NPs) have been developed and tested over 40 years. Delivery of RNAi based drugs can utilize lipid-based (cholesterol and α-tocopherol) NPs, polymer-based (polyethylene-PEG) NPs, inorganic NPs and a range of exosome-mimetic nanovesicles (27, 28).

Lipid-based NPs (LNPs) include liposomes, micelles, emulsions and solid lipid nanoparticles (SLNPs). LNPs also include stable nucleic acid lipid particles (SNALPs) (29), lipidoid nanoparticles (LNs), and SLNPs (30). LNPs have a biochemical structure (phosphate/sugar group) that mimics a cell membrane thus allowing fusion with a target cell membrane and its transport RNA into a target cell (24). LNPs, for example, are extensively used to deliver siRNA and small activating ds RNA (saRNA) that target gene promoters (7).

Polymer-based NPs like Polyethylene (PEG) can be complexed with Polyvinylimine (PEI) to form a PEG-PEI based RNA conjugate that increases stability *in vivo*, as well as enhances the targeting of its RNA based cargo (31). PEG can also be complexed with Poly Lysine (PLL) and Poly Amidoamine (PAMAM) that consist of macromolecules designed to carry RNA. Natural polymers conjugated with RNA include chitosan, atelocollagen and Hyaluronic acid (HA) which, for example, readily binds to CD44 expressing cancer cells (32). Upon delivery in the cytoplasm, the RNAi cargo is released from the polymer-based NP by the cleavage of its di-sulfide linkages (22).

NPs can use a ligand to target delivery where these conjugates promote improved binding and reduced immunogenicity. Upon cell entry the NPs can be separated (cleaved) to facilitate RNA loading into an AGO based RISC. For example, a Ga1NAc-siRNA conjugate readily binds to ASGPR thus providing siRNA entry access to hepatocytes (8, 33). Antibodies are also efficient delivery vehicles for cell specific delivery because they are stable *in vivo* and also specific to a chosen target (34). The delivery of RNA can incorporate nano-emulsions (35) including cationic nano-emulsions which are highly potent, versatile delivery vehicles for siRNA to target pathogens or induce antibodies (31).

Inorganic-based RNA NPs consist of mesoporous silica nanoparticles, superparamagnetic nanoparticles, carbon nanotubes and gold nanoparticles and exosome-mimetic nanovesicles can also be used to transport RNAi cargo (28, 31). Viral vectors are highly effective delivery systems using genetically modified viruses to deliver genetic materials to the cells. Virus-based vectors have been proven to have several advantages in delivering the payload into cells *in vitro* and *in vivo*, including high efficacy by natural cell transduction, sustained gene expression, and long-term gene silencing. The use of an adenovirus vector encoding a siRNA, for example, can deliver RNA (36). Finally, aptamers can be modified for delivery of RNA and can be compared to antibodies with respect to their binding specificity. They are also stable, very small and easy to manufacture and can be combined with siRNA/CRISPR technology to target specific cell types (7, 31).

RNAi STRATEGIES

HBV-HCC pathways typically include aberrant expression in the retinoblastoma-tumor protein 53 (RB1-TP53) suppressor networks, the Wingless-related integration site/beta-catenin (WNT/β-Catenin) pathway, and the phosphoinositide 3-kinase/mitogen-activated protein kinase (PI3K/MAPK) and Janus kinase/signal transducer (JAK/STAT) pathways and transforming growth factor-beta (TGF-β) signaling (37). Typically, a range of growth factor receptors including VEGFR/IGFR/EGFR/PDGFR/FGFR and C-Met activate receptor tyrosine kinases in the P13/MAPK and RAS/RAF/MEK/ERK pathways (38). TGF-β signaling activates members of the Smad family of signal transducers (39) and activation of the WNT/B-Catenin pathway occurs *via* the binding of a WNT protein ligand to a Frizzled receptor (40). In addition, the binding of extracellular ligand (IL-6) leads to pathway activation of the JAK/STAT pathway (41).

Three primary strategies are interrogated in this section, namely, anti-angiogenesis, anti-cell proliferation and pro-apoptosis. In each therapeutic strategy, aberrantly expressed mRNA in HCC pathogenesis have been identified and targeted by RNAi therapy (see **Figure 2**). For example, VEGF mRNA is often targeted in RNAi anti-angiogenesis therapy, MYC mRNA to repress cell proliferation and BIRC5/Survivin mRNA to induce a pro-apoptotic effect (see **Tables 1**–**3**).

Anti-Angiogenesis RNAi Strategies

HCC pathogenesis including hypervascularity and marked vascular abnormalities are common feature of disease progression in HCC (115). Vascular abnormalities encompass the arterialization of tumor blood supply, as well as sinusoid capillarization that is promoted in the presence of hypoxia expressed HIF-1α (116). At a molecular level, the drivers of angiogenesis override their inhibitors (117). The drivers of angiogenesis include a range of growth factors (GFs) that include the vascular endothelial growth factor and its receptors (VEGF/VEGF-R), fibroblast growth factors and their receptors (FGF/FGF-R) and platelet derived growth factors and their receptors (PDGF/PDGF-R) (see **Figure 3**). FGFs, in particular, play an important role in angiogenesis and cross-signaling between FGF-2 and VEGF-A occurs early in HCC pathogenesis inducing neovascularization, increased capillarization of sinusoids and tumor growth. FGF expression also promotes angiogenesis by modulating integrin related regulation of endothelial cells in the microenvironment (117, 118). The FGF1, FGF2, FGF4, and FGF8 subfamilies are the most frequently studied FGFs in the angiogenic processes of HCC and FGF2 (in particular) is a characteristic

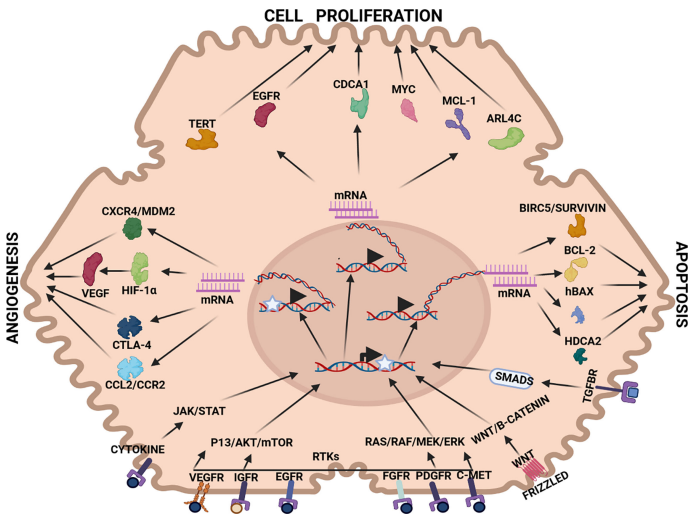

FIGURE 2 | Therapeutic targets in HCC pathways: *Angiogenesis:* CXCR4/MDM2(chemokine receptor/murine double minute 2 protein), CTLA-4 (constitutively expressed in regulatory T cells), HIF-1α (hypoxia-inducible factor 1-alpha, a subunit of a heterodimeric transcription factor hypoxia-inducible factor 1 that is encoded by the HIF1A gene), VEGF (vascular endothelial growth factor, stimulates the formation of blood vessels), *Cell proliferation:* TERT (telomerase reverse transcriptase, a catalytic subunit of telomerase, EGFR (epidermal growth factor receptor), CDCA1 (Cell division cycle associated 1, an oncoantigen), MYC (transcription factor, proto-oncogene), MCL-1 (induced myeloid leukaemia cell differentiation protein), ARL4C (ADP-ribosylation factor-like 4C). *Apoptosis:* BIRC5/Survivin (baculoviral inhibitor of apoptosis repeat-containing 5 or survivin), BCL-2 (B-cell lymphoma 2, regulatory protein inducing or inhibiting apoptosis), hBAX (human Bcl-2-associated X protein, apoptosis regulator), HDCA2 (histone deacetylase 2, removed acetyl groups from lysine at the N' terminal of core histones). *Receptors:* VEGFR (vascular endothelial growth factor receptor), IGFR (insulin-like growth factor receptor), EGFR (epithelial growth factor receptor), FGFR (fibroblast growth factor receptor), PDGFR (platelet-derived growth factor receptor), C-MET (tyrosine-protein kinase *Met* or hepatocyte growth factor receptor (HGFR)), WNT (Wingless and Int-1). *Pathways:* JAK/STAT (Janus kinase (*JAK*)-signal transducer and activator of transcription (*STAT*)), P13/AKT/mTOR (phosphatidylinositol-3-kinase (*PI3K*)/*Akt* and the mammalian target of rapamycin (*mTOR*) signalling pathway), RTKs (receptor tyrosine kinases), RAS/RAF/MEK/ERK (extracellular signal-regulated kinases), WNT/B-CATENIN (highly conserved pathway).

factor in angiogenesis. FGF2 mainly targets FGFR1 as its receptor to mediate angiogenic multiple angiogenic stages (117, 119).

Other growth factors driving angiogenesis are hepatocyte growth factor (HGF) and its receptor c-Met, angiopoietins (ANG1/2 and Tie2) and endoglin (CD105) (117, 120–123). Endoglin (CD105) is a type-1 integral transmembrane glycoprotein and coreceptor for transforming growth factor-β (TGF-β) ligands that promotes angiogenesis in HCC by participating in the neovascularization process (124). Typically, the drivers of angiogenesis induce endothelial cell tyrosine kinases in the P13/Akt/mTOR cancer pathway. Conversely, angiogenesis inhibitors include angiostatin, endostatin and thrombospondin-1 (125).

The development of RNAi drugs to repress angiogenesis in HCC has been promoted by the moderate efficacy of the Sorafenib family of drugs. RNAi therapeutics to repress angiogenesis include the deployment of siRNA, aptamers, riboswitches, ribozymes, ASOs and CRISPR/Cas9 (See **Table 1** and **Figure 2**).

Small interfering RNA: This branch of therapeutics has largely focused on siRNA repression of the drivers of angiogenesis in HCC including VEGF, FGF, PDGF, HGF, angiopoietins (ANG1/2), endoglin (CD105) and their respective receptors. A preponderance of siRNA therapeutic models targeting angiogenesis in HCC have targeted vascular endothelial growth factor (VEGF) expression (117) possibly because Sorafenib and its descendants, FDA approved antiangiogenic agents targeting VEGF, have had modest efficacy (126). RNAi based VEGF siRNAs, delivered by a range of organic and inorganic nanoparticles (NPs), have proved effective to repress VEGF mRNA translation to demonstrate an anti-angiogenic effect on HCC pathogenesis both *in vitro* and *in vivo* (see **Table 1**).

Innovative examples of VEGF delivery using lipid based NPs include a VEGF-siRNA-sorafenib co-loaded pH sensitive liposomes that exhibited enhanced VEGF downregulation and anti-angiogenic effect, as well as induced apoptosis (45). In another model, AMD3100, a CXCR4 antagonist associated with HCC progression (43), as well as VEGF siRNA was delivered by an LNP demonstrated the ability to repress angiogenesis and tumor growth in HCC (44). AMD3100 is a molecule that can block the SDF1α/CXCR4 axis and sensitizes HCC to sorafenib treatment (127). Some lipid-based NPs (LNPs) have used the ASGP-R to gain cell entry and guide siRNA or shRNA delivery to repress VEGF expression. This form of cell entry that is facilitated by the recognition of galactose receptors, also demonstrated effective endosome escape (42, 50, 52). Another innovative LNP included both siRNA and a drug (Tremelimumab) to repress angiogenesis *via* the PD-L1/CTLA-4 pathway (56) while LNP-siRNA modulation of PD-L1/PD-1 acted as an immunoinhibitory receptor to express T/B cells to overcome the tolerance to angiogenic activity in the liver (128).

VEGF delivery using an inorganic gold NP containing VEGF siRNA repressed tumor revascularization in HCC *in vitro* and

TABLE 1 | RNAi anti-angiogenesis therapeutics.

RNAi NP delivery method	Target mRNA	Outcome	Source
siRNA			
LCP-NP (siRNA)	ASGP-R/VEGF	Anti-angiogenic effect	(42)
LNP (siRNA and AMD3100)	CXCR4/SFF1α	Repressed angiogenesis	(43, 44)
LNP pH sensitive (siRNA + sorafenib)	VEGF	Reduced VEGF and induced apoptosis	(45)
Stabilized (siRNA)	VEGF	Repressed angiogenesis	(46, 47)
Gold NP (siRNA)	VEGF/P13K/AKT	Repress vascularization	(48)
PEG-SS-PLL NP (siRNA)	VEGF	Anti-angiogenic effect	(49)
LNP (shRNA)	ASGP-R/VEGF	Repressed angiogenesis	(50)
LNP (siRNA + sorafenib)	Survivin	Repressed growth/angiogenesis	(51)
UA-GT/PAH-Cit NP (siRNA)	ASGP-R/VEGF	Reduced vascularization	(52)
Stabilized siRNA transfection	FGF	Reduced hepatic endothelial cells	(53, 54)
Stabilized siRNA transfection	MDM2/PDGF-B	Reduced tumor growth	(55)
LNP (siRNA + Tremelimumab)	PD-L1/CTLA-4	Promote T/B cell response	(56, 57)
NP (siRNA)	C-Met/AKT	Reduced angiogenesis	(58, 59)
CRISPR/Cas9			
Crisp/Cas9 NP (HIF-1 α knockout)	HIF-1α DNA	Repressed angiogenesis and invasion	(60)
Crispr/Cas9 NP (gene-chemo-silica NP)	EGFR-p13K-Akt	Repress angiogenesis	(61)
ASO			
PS-LNA ASO NP	HIF-1α/VEGF	Reduced endothelial expression	(12)
Isoform-specific ASO	HIF-1α/HIF-2α	Repressed tumorigenesis	(62)
Aptamer			
RNA aptamer	CCL2/CCR2	Inhibited angiogenesis	(63, 64)
NP (peptide-mod-miR-195 + fasudil)	VEGF/ROCK2	Repress vasculogenic activity	(15)
Ribozyme			
Hairpin ribozyme	VEGF	Inhibit VEGF expression/tumor growth	(65)
Hammerhead ribozyme	VEGF/MMP-1	Target VEGF/MMP-1 angiogenesis	(66, 67)
Riboswitch			
AFP sensing Riboswitch	YAP/14-3-3σ	Repress angiogenesis	(68)

lipid-based nanoparticle (LNP), lipid/calcium/phosphate NP (LCP-NP), polyethylene glycol-poly(ε-benzyloxycarbonyl-l-lysine) NP (PEG-SS-PLL NP), urocanic acid-modified galactosylated trimethyl chitosan (UA-GT), poly(allylamine hydrochloride)-citraconic anhydride NP (UA-GT/PAH-Cit NP), phosphorothioate antisense oligonucleotides-locked nucleic acid NP (PS-LNA NP).

in vivo (48). In another case, a polymer NP complex was used to transport VEGF siRNA and demonstrated a marked anti-angiogenic effect *in vitro* and *in vivo* (49). An alternate siRNA design involved methylation of VEGF siRNA ends to stabilize them *in vivo* and this therapy reduced HCC induced angiogenesis through inactivation of VEGF/PI3K/AKT signaling pathway (46). In another example, stabilized VEGF siRNA significantly reduced VEGF expression and resulted in the knockdown of endothelial cell production *in vitro* and reduced tumor size *in vivo* (47).

FGF targeted siRNA models have been largely anchored in a series of *in vitro* studies and there is little evidence yet that siRNA-based therapeutics have progressed to *in vivo* applications. For example, transfections of FGF8, FGF19, FGFR4 with siRNA in a range of HCC cell-lines significantly repressed the proliferation and tube formation of hepatic endothelial cells (53, 54). The HGF/c-Met axis is involved in cell proliferation, movement, differentiation, invasion, angiogenesis, and apoptosis by activating multiple downstream signaling pathways (129). Additionally, C-Met (HGF-R) may induce VEGF-A expression to enhance angiogenesis (130). A wide range of siRNA experiments have also targeted the HGFR induced tyrosine kinases *in vitro* and *in vivo* (58, 59, 129, 131, 132).

Similarly, PDGFs are secreted growth factors closely related to VEGF and are important in HCC-induced angiogenesis because they activate tyrosine kinases contributing to the upregulation of VEGF and recruitment of perivascular cells (133). Stabilized Mdm2 siRNA or PDGF-B siRNA, transfected into an Hep3B cell line plasmid, demonstrated angiogenic effects *in vivo*, as well suppressed tumor growth (55). Stabilized siRNA also reported good efficacy in a murine mammary adenocarcinoma experiment to target endoglin which as a receptor for TGF-β signaling (134). Finally a polymer NP complex transporting shRNA and sorafenib and surviving shRNA inhibited tumor growth and angiogenesis for resistant HCC (51).

CRISPR/Cas9: The use of CRISPR/Cas9 therapy in HCC offers an exciting new option to manage pathogenesis. To date examples of this therapy in HCC include an HIF-1α knockout in a xenograft model to repress angiogenesis and invasion (60). HIF-1α is a key transcription factor involved in the hypoxic response of cancer cells. It activates transcription of genes responsible for angiogenesis, glucose metabolism, proliferation, invasion and metastasis in HCC (135). In another *in vivo* HCC study, a CRISPR/Cas9 system was deployed for gene–chemo-combination therapy that used a silica nanoparticle to initiate CRISPR/Cas9 editing of EGFR, as well as the co-delivery of sorafenib to modulate EGFR-p13K-Akt expression and repress angiogenesis (61).

ASOs: There has been a limited application of ASO-based RNAi for this strategy. One example of an anti-angiogenic ASO repressed HIF-1α led VEGF expression (12).

Aptamers: Although the use of aptamers in RNAi is less evident than other anti-angiogenic strategies in HCC, there are some examples. Aptamers targeting of CCL2/CCR2 and CCR2

TABLE 2 | RNAi anti-proliferation therapeutics.

RNAi NP delivery method	Target mRNA	Outcome	Source
siRNA			
Fa-PEG-g-PEI-SPION NP (siRNA)	TBLR1/SIK1	Inhibits growth/angiogenesis	(69, 70)
Lipid-polyplex NP (siRNA)	TERT/EGFR	Repressed cell proliferation	(71, 72)
LNP (siRNA)	b1 and av integrin	Repressed cell proliferation	(73)
Liposome-based NP (siRNA +AD3100)	RRM2	Inhibited growth	(74)
SNALP (siRNA)	CDCA1*	Reduced cell proliferation	(75, 76)
Stabilized siRNA transfection	CENP-A*	Inhibits HCC growth	(77)
LNP (siRNA)	MYC*	Inhibited tumor metabolism	(78)
LNP (siRNA)	PLK1*	Inhibits tumor growth	(79)
Stabilized siRNA	AQP3/HIPK3	Repressed proliferation	(11)
Stabilized siRNA	DLGAP5	inhibited cell proliferation	(80)
Stabilized siRNA	FoxM1/MMP-2/uPA	repressed proliferation	(81)
Stabilized siRNA	VEGF/KSP	anti-proliferation/pro-apoptosis	(82)
Stabilized siRNA	NET-1/EMS1/VEGF	anti-proliferation/pro-apoptotic	(83)
CRISPR/Cas9			
Crisp/Cas9 NP (NSD1 knockout)	NSD1	Repressed H3/WNT signaling	(84)
Crisp/Cas9 NP (TET knockout)	TET (1-3), SRY/UTY	Reduces cell proliferation	(85)
CRISPR/Cas9 NP (gene-chemo-silica)	PD-1	Enhanced T cell response	(86)
CRISPR/CAS9 (gene disruption)	PTEN/P53	Demonstrates TS role	(87)
ASO			
Stabilized ASO	MCL-1	Repressed MCL-1 expression	(88)
2-O-methyl modified ASO	STAT3	Inhibits HCC growth	(89)
Lipid ASO (PTO backbone)	MYC	Impedes tumorigenesis	(90)
Isoform-specific ASO	HIF-1α/HIF-2α	Repressed tumorigenesis	(62)
PTO backbone ASO	ARL4C	Inhibited proliferation	(91)
Aptamer			
RNA aptamer (guided by AFP)	C-jun/C-fos/nucleolin	Reduced	(92)
ssDNA aptamer	GAL-14	expression/proliferation	(93)
Ribozyme			
Trans-splicing ribozyme	hTERT	GAL-14 increase/reduced	(6)
Trans-splicing ribozyme	AFP	growth	(94)
Riboswitch			
RBP/Riboswitch	MS2	Inhibits tumorigenesis	(95)

*folate- polyethylene glycol-grafted polyethylenimine and superparamagnetic iron oxide NP (Fa-PEG-g-PEI-SPION NP), Stable nucleic acid lipo-particle (SNALP), Lipid-based NP (LNP), RNA-Binding protein (RBP) phosphorothioate modified backbone (PTO) *clinical trial stage.*

expression using small-molecule antagonists, neutralizing antibodies, or RNA aptamer-based inhibitors have demonstrated efficacy to repress angiogenesis in subcutaneous HCC xenografts and endogenous liver tumors (63, 64). In another study, an aptamer-functionalized peptide (H3CR5C) was deployed to co deliver fasudil and miRNA-195 in a nanoparticle to inhibit VEGF expression and suppress vasculogenic activity by repressing ROCK2 (15).

Ribozymes: Ribozyme therapeutics in HCC used an anti-VEGF hairpin ribozyme to effectively inhibit VEGF expression and the tumor growth *in vitro* and *in vivo* (65). In another *in vivo* study, an anti-VEGF-A hammerhead type ribozymes suppressed not only VEGF mRNA but also VEGF protein (66, 67).

Riboswitch: In one HCC study a riboswitch that could sense AFP triggered the promotion of YAP induced 14-3-3σ expression to repress angiogenesis and promote degradation (68).

Anti-Cell Proliferation RNAi Strategies

Cell Proliferation Pathways in HCC: Several signaling pathways in HCC influence cell proliferation in HCC pathogenesis including the TGF-β, Wnt/B-catenin, Hedgehog (Hh), Notch, JAK/STAT and Hippo pathways (see **Figure 4**). TGF-β upregulates the expression of Snail, downregulates E-cadherin to promote epithelial to mesenchymal transition (EMT) and metastasis. The TGF-β signaling pathway also influences the preservation of the cancer stem cell (CSC) subpopulation and cell proliferation (136). In HCC pathogenesis, aberrant Wnt/β-catenin signaling is often induced by *CTNNB1* mutations leading to the accumulation of β-catenin in the nucleus and cytoplasm to promote vascular invasion, cell proliferation, and poorly differentiated tumors (40, 137), as well as cross-talk with hypoxia signaling pathways (138).

The Hedgehog (Hh) pathway also plays an important role in cell proliferation and invasion (139), as well as in EMT (140) while there is growing evidence that supports the critical role of Notch signaling in HCC in the regulation of the tumor microenvironment, tumorigenesis, progression, angiogenesis, invasion and metastasis (141). Furthermore there is evidence that a Notch1-Snail1-E-cadherin type association affects invasion and metastasis in HCC pathogenesis (142). The JAK/STAT signaling pathway plays important roles in many cellular functions, including cell proliferation activated by the transcription CCND1, BIRC5 and Mcl-1 (143) and the repression of Hippo signaling in HCC pathogenesis *via* Hippo kinase (Mst1 and Mst2) also plays a role in the promotion of proliferation (144). Finally, the MAPK/ERK signaling pathway is activated in more than 50% of human HCC cases (145) by a range of growth factor receptors in HCC including

TABLE 3 | RNAi pro-apoptotic therapeutics.

RNAi NP delivery method	Target mRNA	Outcome	Source
siRNA			
PEI NP (shRNA+ sorafenib)	Survivin	Inhibited growth, angiogenesis	(51)
RGD-PEG-*g*-PEI-SPION NP (siRNA)	Survivin	Promotes apoptosis	(96)
NP (siRNA-miR-122)	PKM2/HDAC-8	Induces apoptosis	(97–99)
SNALP (siRNA)	HDCA2*	p27/p53-led apoptosis/BCL-2	
NP (siRNA +cisplatin)	hTERT	down	(100, 101)
NP (siRNA)	CYCLIN-E	G2/M/S control -led apoptosis	(102)
NP (siRNA)	CXCL1	Induces apoptosis	(103)
NP (siRNA)	PDGFR-ß	Induces apoptosis and cell	(104)
Polymeric NP	VEGF/survivin*	growth	(105)
Polymeric NP	VEGF	Represses cell survival	(106)
			(107)
CRISPR/Cas9			
Crisp/Cas9 NP (insert HSV1)	HSV1 DNA	Induce apoptosis	(108)
Crisp/Cas9 NP (targeted PD-1)	PD-1	Induce apoptosis	(86)
ASO			
Chemically stabilized ASO	TERT	Promoted T-cell response	(109)
Aptamer			
ssDNA aptamer (GT repetition)	eEF1A	Targets cell survival/apoptosis	(110)
Ribozyme			
Trans-splicing ribozyme/cleave/replace	Mutant TP53	Replace TP53 promote apoptosis	(111)
Trans-splicing ribozyme	hTERT	Replacement of TERT RNA	(112–114)
Trans-splicing ribozyme	AFP	Promotes cell suicide	(94)
Trans-splicing ribozyme	VEGF/MMP-1	Promotes autophagy	(67)
Riboswitch			
RBP/Riboswitch	cNOT7/BCl-2/hBAX	BCL-2 up/hBAX down/apoptosis	(95)
(RBP)/riboswitch	YAP/14-3-3σ	Induces cell degradation	(68)

*Polyethylenimine NP (PEI NP), tripeptide arginine glycine aspartic acid (RGD)-modified non-viral vector, polyethylene glycol-grafted polyethylenimine functionalized with superparamagnetic iron oxide NP (RGD-PEG-g-PEI-SPION NP), Stable nucleic acid lipo-particle (SNALP). RNA-binding protein (RBP) *clinical trial stage.*

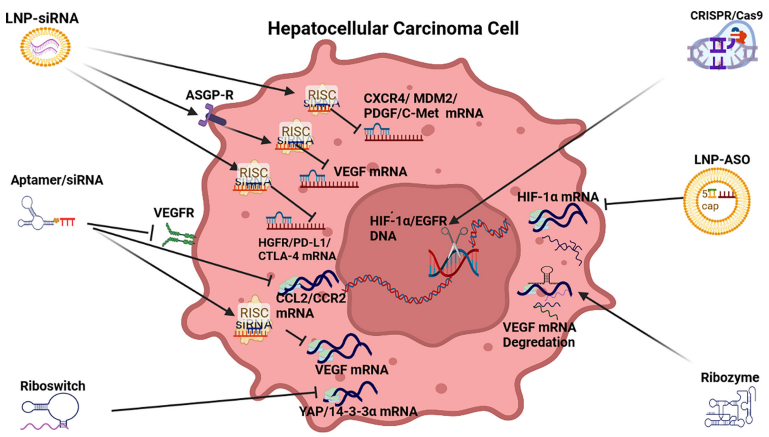

FIGURE 3 | RNAi anti-angiogenic strategies. LNP-siRNA (Lipid nanoparticles for targeted small interfering RNA delivery), CRISPR/Cas9 V (clustered regularly interspaced short palindromic repeats/CRISPR-associated protein 9), LNP-ASO (lipid nanoparticle associated antisense oligonucleotide), siRNA (small interfering RNA). VEGFR (vascular endothelial growth factor receptor), ASGPR (asialoglycoprotein receptor), RISC (RNA-induced silencing complex), HIF-1α (hypoxia-inducible factor 1-alpha, a subunit of a heterodimeric transcription factor hypoxia-inducible factor 1 that is encoded by the HIF1A gene), CCL2/CCR2 (chemokine *CCL2* and its main receptor *CCR2*), HGFR/PD-L1/CTLA-4 (human growth factor receptor/programmed death-ligand 1/constitutively expressed in regulatory T cells), CXCR4/ MDM2/PDGF/C-Met [chemokine receptor/murine double minute 2 protein/platelet-derived growth factor/tyrosine-protein kinase *Met* or hepatocyte growth factor receptor (HGFR)].

VEGF-R, EGF-R, FGF-R, PDGF-R and C-MET that interlink with angiogenic expression (146).

siRNA: RNAi based therapeutics to modulate cell proliferation in HCC pathogenesis has deployed a range of polymer and lipid-based NPs, Stable nucleic acid lipo-particles (SNALPs), and chemically stabilized siRNA (see **Table 2**). For example, a polymer-based NP delivering TBLR1 siRNA inhibited growth and angiogenesis in HCC in both *in vitro* and *in vivo*

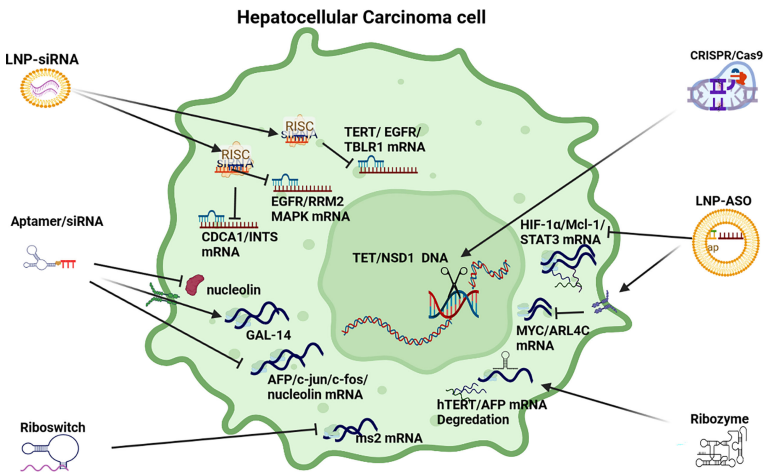

FIGURE 4 | RNAi anti-cell proliferation strategies. LNP-siRNA (Lipid nanoparticles for targeted small interfering RNA delivery), CRISPR/Cas9 V (clustered regularly interspaced short palindromic repeats/CRISPR-associated protein 9), LNP-ASO (lipid nanoparticle associated antisense oligonucleotide), siRNA (small interfering RNA). HIF-1α/Mcl-1/STAT3 (hypoxia-inducible factor 1-alpha, a subunit of a heterodimeric transcription factor hypoxia-inducible factor 1 that is encoded by the HIF1A gene/induced myeloid leukaemia cell differentiation protein gene/signal transducer and activator of transcription 3), MYC/ARL4C (transcription factor, proto-oncogene/ADP-ribosylation factor-like 4C), hTERT/AFP (human telomerase reverse transcriptase/alpha fetoprotein), AFP/c-Jun/c-fos/nucleolin (transcription factors), GAL-14 (galectin 14), CDCA1/INTS (Cell division cycle associated 1, an oncoantigen), EGFR/RRM2/MAPK (epidermal growth factor receptor/ribonucleoside-diphosphate reductase subunit M2/mitogen-activated protein kinase), TERT/EGFR/TBLR1 [telomerase reverse transcriptase, a catalytic subunit of telomerase/transducin (beta)-like 1 X-linked receptor 1].

applications. TBLR1 acts as a key oncogene in HCC to promote cell proliferation and angiogenesis in the WNT/B-Catenin pathway (69). In another example, a lipid-polyplex based NP delivering TERT and EGFR shRNA effectively repressed cell proliferation (71). EGFR is (often) highly expressed in HCC and is associated with cell proliferation and an aggressive phenotype that is prone to metastasis (147) Upregulated TERT as a result of mutations in the promoter region are also a frequent event in HCC and are significantly linked to disease progression (72). Another anti-cell proliferation started used LNPs injected into HCC mouse models to target integrin and CDCA1 expression (73). In support of this approach, integrins are found in HCC tissue but not in normal liver tissue and are associated with proliferation and invasion (148). Another SNALP based NP targeting CDCA1 also demonstrated reduced cell proliferation and pro-apoptotic activation as well as linkages with immune response (75, 76).

In another study a liposome complex NP model delivering a siRNA cargo plus Adriamycin inhibited growth by repressing RRM2 in EGFR expressing HCC (74). Interestingly, the elevated expression of RRM2 signifies a poor prognosis in HCC (149). Overexpression of CENP-A is frequently observed in HCC and a stabilized siRNA plasmid model targeting CENP-A reduced proliferation *via* repression of gene expression promoting cell cycle and inhibiting apoptosis (77). In a phase 1 trial, a Dicer-substrate small interfering RNA (DsiRNA) targeting MYC, exhibited some potential to repress cell proliferation (78). In HCC PLK1 expression, which is associated with cell cycle, is often elevated and a phase 2 trial using an LNP siRNA model is currently in progress to determine its use as an HCC drug to modulate proliferation/apoptosis (79).

Other *In vivo* based studies deploying stabilized siRNA have yielded positive results to illustrate the potential of RNAi. For example, stabilized siRNA targeting HIPK3 mRNA regulated tumorigenesis *via* the miR-124-AQP3 axis (11) while another stabilized siRNA model repressed DLGAP5 repression to suppress cell growth, migration and colony formation *in vitro* (80). Down-regulation of FoxM1 by stabilized siRNA also reduced the expression of matrix metalloproteinase-2 (MMP-2) and urokinase plasminogen activator (uPA) resulting in reduced cell proliferation in HCC cell lines (81). Silencing of VEGF and KSP mRNA by siRNA inhibited cell proliferation, migration, invasion and induced apoptosis in Hep3B cell-line experiments and it was hypothesized that this could be explained by the significant downregulation of Cyclin D1, Bcl-2 and Survivin (82). In a more recent study, a multi-target siRNA model inhibited NET-1, EMS1 and VEGF mRNA in HCC cells resulting in a significant reduction in proliferation, migration, invasion, angiogenesis and induced apoptosis in HCC cells (83).

CRISPR/Cas9: In a novel *in vivo* application of this therapy in HCC, CRISPR/Cas9 was used to test the hypothesis that deactivated PTEN/p53 genes in HCC promote carcinogenesis (87). In another application of CRISPR/Cas9 technology the expression of five oncogenes (*Tet1*, *2*, *3*, *Sry*, *Uty* - 8 alleles) was disrupted to reduce cell proliferation and highlight the key role of methylation of DNA in HCC (85). In addition, CRISPR/Cas9 therapy has been used to promote immunotherapy by modifying PD-1 in immune cells to promote T-cell response (86). In another example, a NSD1 knockout cell line was constructed by a CRISPR/Cas9 editing system to demonstrate its potential

therapeutic application to HCC cell proliferation, migration and invasion as a result of NSD1 positive role in the expression of histone H3, Wnt10b and Wnt/β-catenin signaling (84).

ASOs: ASOs have been widely deployed in HCC to suppress oncogene expression that results in promoting cell proliferation. Oncogenes suppressed by a range of stabilized ASOs include *Mcl-1, HIF-1α, MYC* and *STAT3* (62, 88–90). MYC mRNA expression in HCC has also been silenced by siRNA based on a combination of 13 miRNA to suppress aberrant signaling promoting cell proliferation (2) and an MYC ASO model suppressed cell proliferation in mouse and human transgenic models (90). HCC cell proliferation was also repressed in another *in vitro* ASO based study which targeted ARL4C expression which is often highly expressed in HCC (91).

Aptamer: In 2012, a first report demonstrated that an RNA aptamer was able to detect cancer cells and inhibit proliferation in an alpha-fetoprotein (AFP) expressing HCC cell-line *via* the suppression of oncogene expression in *c-jun* and *c-fos*. This aptamer can also targeted nucleolin (92). In a later study a modified aptamer reduced cell proliferation by the upregulation of GAL-14 expression which is linked to immune response (93).

Ribozyme: In one study it was demonstrated that a trans-splicing ribozyme-mediated replacement of HCC-associated specific RNAs could target and replace AFP mRNA, which becomes increasingly expressed in HCC pathogenesis (94). In another study, a trans-splicing ribozyme was deployed to target hTERT expression which is elevated in HCC pathogenesis and promotes cell proliferation and survival (6).

Riboswitch: In one study deploying this therapy, a chimeric RNA-binding protein-based killing switch targeting MS2 to reduce cell priliferation in HCC (95).

Pro-Apoptotic RNAi Strategies

Apoptosis pathways become increasingly dysregulated in HCC pathogenesis. Mutation od the p53 tumor suppressor gene is a common feature, as well as the disruption of the TGF-β family of cytokines that play a prominent role in apoptosis (150, 151). Other alterations include mutations in the Hedgehog pathway to promote anti-apoptotic resistance (152), as well as dysregulation of the death receptor pathways which include Fas-mediated caspase induced apoptosis (153). The upregulation of many anti-apoptotic proteins is also a common feature including NF-κB, Bcl-2 and Bcl-X_L, as well as the downregulation of pro-apoptotic expression by *BID, BAX* and *BCL-Xs* (154). Tumor necrosis factor (TNF) common feature in HCC (155) alongside upregulated IGF and IGF-1 signaling pathways which can activate STAT signaling (156). Finally, the repression of many tumor suppressors like *SOCS-1/3* can also promote JAK/STAT signaling (157) while *PTEN* dysregulation promotes P13/MAPK/Akt signaling (158).

siRNA: Multiple RNAi pro-apoptotic siRNA strategies have been developed and tested, especially those targeting BIRC5/survivin. BIRC5/Survivin is often highly expressed in HCC and has been linked to cell proliferation, inhibiting apoptosis and promoting stromal angiogenesis (159) (see **Figure 5**). A co-polymer complex based NP has been operationalized with superparamagnetic oxide to deliver Survivin siRNA to successfully induce apoptosis (96). In another study targeting Survivin, a polymer based NP was used to deliver survivin shRNA and sorafenib to repress tumor growth and inhibit angiogenesis (51). Survivin is a recently described inhibitor of apoptosis and its overexpression translates into a decrease in the G_0/G_1 phase and an increase in the S phase in cell cycle controls resulting in the activation of cell cycle network (160–162).

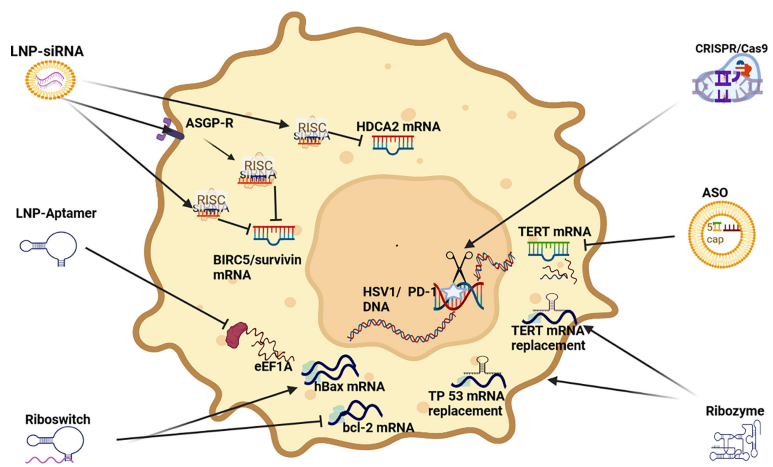

FIGURE 5 | RNAi apoptosis strategies LNP-siRNA (Lipid nanoparticles for targeted small interfering RNA delivery), CRISPR/Cas9 V (clustered regularly interspaced short palindromic repeats/CRISPR-associated protein 9), LNP-ASO (lipid nanoparticle associated antisense oligonucleotide), siRNA (small interfering RNA); HIF-1α (hypoxia-inducible factor 1-alpha, a subunit of a heterodimeric transcription factor hypoxia-inducible factor 1 that is encoded by the HIF1A gene), TERT (telomerase reverse transcriptase), hBAX (human Bcl-2-associated X protein, apoptosis regulator), eEF1A (Eukaryotic translation elongation factors 1 alpha), BIRC5/Survivin (baculoviral inhibitor of apoptosis repeat-containing 5 or survivin), RISC (RNA-induced silencing complex), ASGP-R (asialoglycoprotein receptor), HDCA2 (histone deacetylase 2, deacetylates lysine of N' terminal of core histones).

A stabilized siRNA (based on miR-122) model targeting PKM2, induced apoptosis and growth arrest by downregulating PKM2 in HCC *in vitro* and *in vivo* (97). In another stabilized siRNA model both HDAC8 and PKM2 mRNA expression was reduced to promote pro-apoptotic effects. Interestingly, HDAC8 caused PKM2 to translocate to the nucleus and synergize with *β-catenin* transcription to upregulate the expression of cyclin D1 (98). SNALP based NPs have also been used to transport both HDAC1 and HDAC2 siRNA to induce apoptosis by upregulating p57/p27 expression, as well as downregulating bcl-2 expression (100, 101) which is associated with a pro-survival effect in HCC (163). Another stabilized siRNA model demonstrated the synergistic effect between hTERT siRNA and Cisplatin in the suppression of HCC progression and indicated that the combination of hTERT-specific siRNA and cisplatin could be an effective therapy for HCC to promote cell cycle controls *via* G2/M and S phases thus inducing apoptosis (102). In another study, stabilized siRNA were tested *in vivo* to demonstrate that the depletion of cyclin E expression in this manner promotes apoptosis in HCC cells and blocks cell proliferation (103). Cyclin E (cyclins E1 and E2) are components of the core cell cycle machinery and are usually co-expressed in proliferating cells (164). Another study using a stabilized siRNA transfection to target CXCL1 induced apoptosis *in vitro* and *in vivo* (104). CXCL1 expression promotes fibrogenesis and angiogenesis HCC (165). In another experiment, the knockdown of PDGFR-ß mRNA by siRNA led to the upregulation of LC3-II and downregulation of p62, indicating that knockdown of PDGFR-ß could activate autophagy and indicating that PDGFR-ß plays a role in the Akt/mTOR and Mek/Erk pathways (105).

A multifunctional polymeric NP, that has progressed to clinical trial stage, has been developed to transport shRNA survivin and VEGF siRNA to trigger apoptosis and inhibit angiogenesis in HCC patients (106). This work was largely based on an earlier study by the same researchers where the polymeric NP was deployed in a mouse to transport VEGF siRNA that demonstrated a pro-apoptotic effect as a result of RNAi silenced VEGF mRNA (107). This demonstrates that VEGF and survivin repression can also influence pro-apoptotic activity, as well anti-angiogenic potential in HCC.

CRISPR/Cas9: In one study using a mouse xenograft model, a CRISPR/Cas9 model used Cas9-based genome editing to introduce the prodrug-converting enzyme herpes simplex virus type 1 thymidine kinase (HSV1-tk) into the genomes of HCC cells resulting in the precipitation of apoptosis (108). In another study, CRISPR/Cas9 gene editing was deployed to disrupt the expression of the the programmed death 1 receptor (PD-1) to enhance the activity of CAR T cells. Disruption of PD-1, therefore, enhanced the anti-tumor activity of CAR T cells against HCC (86).

ASO: A chemically stabilized ASO was successfully deployed to repress aberrant TERT expression in HCC models to induce apoptosis *in vitro* and *in vivo* (109).

Aptamer: A 75 nucleotide long aptamer (GT75) was tested in three HCC cell lines, HepG2, HuH7 and JHH6. When delivered by liposomes. GT75 was able to effectively reduce HCC cell viability and promote apoptosis. No effects on cell cycle were observed and the effect of this aptamer was likely due to the interference with eEF1A activity (110).

Ribozyme: A number of *trans*-splicing ribozymes have been tested for RNAi therapeutic applications in HCC, many of which have targeted the elevated expression of telomerase reverse transcriptase (TERT) because of its role in promoting cell survival (112). Examples include an *in vivo* HCC experiment an intra-tumoral injection of an adenovirus encoding for the hTERT-targeting *trans*-splicing ribozyme demonstrated marked regression of tumors that had been subcutaneously inoculated with hTERT-positive liver cancer cells in mice (112). Another RNAi experiment using an hTERT-targeting ribozyme with an miR-122 target site added to its 3' end effectively promoted cell death because miR-122 is upregulated in HCC and is the most predominant microRNA(miRNA) expressed in liver tissue. Effectively repressing hTERT and miR-122 levels also improved the selectivity of this therapy, as well as reduced hepatotoxicity (113, 114). Other ribozyme targets in HCC targeted (cleaved) mutant TP 53 mRNA and replaced it with normal TP 53 mRNA to promote TP53 expression and induce apoptosis (111), as well as a trans-splicing ribozyme-mediated replacement of HCC-associated specific AFP to promote cell suicide (94). Ribozyme mediated suppression of VEGF expression enhanced matrix metalloproteinase 1 (MMP-1) nexpression in annHCC cell line to underline that repressing one oncoprotein can result in stimulating another (67).

Riboswitch: In one HCC study a riboswitch that could sense AFP triggered the promotion of YAP induced 14-3-3σ expression to promote degradation (68). A chimeric RNA-binding protein-based killing switch targeting HCC cells deployed a synthetic circuit for cNOT7 that is a deadenylase that can inhibit mRNA translation and promote their degradation. It was demonstrated in this study that the result of this deadenylase triggered apoptosis by switching on bcl-2 and repressing hBAX respectively (95).

CONCLUSION

RNA are key molecules involved in all biological pathways. Their history of therapeutic deployment begins with the first antisense oligonucleotide (ASO) drug in 1998, first aptamer drug in 2004, the first RNAi clinical trial in 2010 and the first siRNA drug in 2018. These RNAi drugs were based on the synthetic development of complementary RNA sequences that can bind to mRNA or a protein to repress (silence) expression. Six FDA approved RNA based drugs have been approved from 1998 to 2019 with the majority developed for muscular dystrophy/atrophy (6).

To date, a few clinical trials have been registered for siRNA RNAi based therapy in HCC. These trials include an LNP to target MYC mRNA to repress proliferation, a SNALP to target PLK1 mRNA (79) to retard cell cycle and an LNP to target EPHA2 mRNA to repress angiogenesis. Other trials include a polymer based NP to target PKN3 mRNA to repress vascularization, an LNP to target STMN1 mRNA to repress cell cycle, an LNP to target miR-34, and a polymer based NP to

target RRM2 mRNA to repress cell proliferation (31). Another trial deployed a siRNA (miR-34) tumor suppressor to target 20 HCC associated genes, as well as to sensitize the tumor microenvironment to cytotoxic therapy (166). Bearing in mind the first siRNA-based drug was only approved in 2018 the indications are it will be some time before their true potential can be evaluated (6).

Despite the early promise of RNA therapeutics as a magic bullet to modulate aberrant signaling in cancer, this field remains a work-in-progress largely due to the inherent instability of RNA *in vivo*, as well as delivery and host immunogenic issues. RNAi targeting is often problematic because of the cross-talk between genes and some RNAi studies have demonstrated that repressing one oncoprotein can result in stimulating another (67). Nevertheless, RNA therapeutics is now a reality for the prevention of viral diseases (COVID-19) and offers great promise for cancer. Currently, most HCC drugs are based on recombinant proteins or antibodies that target pathologic proteins which are often difficult to reach because of their location in the cell. In addition, these drugs often struggle to differentiate between target protein sub-types, whereas RNA can more easily target specific mRNA or other ncRNA (31). A wide range of novel HCC therapeutics, including RNAi have been developed over the last two decades, however, a cure is not a reality at present (3).

AUTHOR CONTRIBUTIONS

KS conceptualized, developed first draft and responded to reviewer edits and comments to develop final draft. SA reviewed and revised drafts, AC reviewed and revised drafts, AK reviewed and revised drafts. All authors contributed to the article and approved the submitted version.

REFERENCES

1. Akinyemiju T, Abera S, Ahmed M, Alam N, Alemayohu MA, Allen C, et al. The Burden of Primary Liver Cancer and Underlying Etiologies From 1990 to 2015 at the Global, Regional, and National Level: Results From the Global Burden of Disease Study 2015. *JAMA Oncol* (2017) 3(12):1683–91. doi: 10.1001/jamaoncol.2017.3055
2. Feng R, Patil S, Zhao X, Miao Z, Qian A. RNA Therapeutics-Research and Clinical Advancements. *Front Mol Biosci* (2021) 913. doi: 10.3389/fmolb.2021.710738
3. Shokoohian B, Negahdari B, Aboulkheyr Es H, Abedi-Valugerdi M, Baghaei K, Agarwal T, et al. Advanced Therapeutic Modalities in Hepatocellular Carcinoma: Novel Insights. *J Cell Mol Med* (2021) 25(18):8602–14. doi: 10.1111/jcmm.16875
4. Samant H, Amiri HS, Zibari GB. Addressing the Worldwide Hepatocellular Carcinoma: Epidemiology, Prevention and Management. *J Gastrointest Oncol* (2021) 12(Suppl 2):S361. doi: 10.21037/jgo.2020.02.08
5. Hannon GJ. RNA Interference. *Nature* (2002) 418(6894):244–51. doi: 10.1038/418244a
6. Kim Y-K. RNA Therapy: Current Status and Future Potential. *Chonnam Med J* (2020) 56(2):87. doi: 10.4068/cmj.2020.56.2.87
7. Pandey M, Ojha D, Bansal S, Rode AB, Chawla G. From Bench Side to Clinic: Potential and Challenges of RNA Vaccines and Therapeutics in Infectious Diseases. *Mol Aspects Med* (2021) 81:101003. doi: 10.1016/j.mam.2021.101003
8. Thangamani L, Balasubramanian B, Easwaran M, Natarajan J, Pushparaj K, Meyyazhagan A, et al. GalNAc-siRNA Conjugates: Prospective Tools on the Frontier of Anti-Viral Therapeutics. *Pharmacol Res* (2021) 173:105864. doi: 10.1016/j.phrs.2021.105864
9. Li H, Yang Y, Hong W, Huang M, Wu M, Zhao X. Applications of Genome Editing Technology in the Targeted Therapy of Human Diseases: Mechanisms, Advances and Prospects. *Signal Transduct Target Ther* (2020) 5(1):1–23. doi: 10.1038/s41392-019-0089-y
10. Abdulrahman GO, Rahman GA. Epidemiology of Breast Cancer in Europe and Africa. *J Cancer Epidemiol* (2012) 2012:1–5. doi: 10.1155/2012/915610
11. Chen G, Shi Y, Liu M, Sun J. Circhipk3 Regulates Cell Proliferation and Migration by Sponging miR-124 and Regulating AQP3 Expression in Hepatocellular Carcinoma. *Cell Death Dis* (2018) 9(2):175. doi: 10.1038/s41419-017-0204-3
12. Wu J, Contratto M, Shanbhogue KP, Manji GA, O'Neil BH, Noonan A, et al. Evaluation of a Locked Nucleic Acid Form of Antisense Oligo Targeting HIF-1α in Advanced Hepatocellular Carcinoma. *World J Clin Oncol* (2019) 10(3):149. doi: 10.5306/wjco.v10.i3.149
13. Gagliardi M, Ashizawa AT. The Challenges and Strategies of Antisense Oligonucleotide Drug Delivery. *Biomedicines* (2021) 9(4):433. doi: 10.3390/biomedicines9040433
14. Ladju RB, Pascut D, Massi MN, Tiribelli C, Sukowati CH. Aptamer: A Potential Oligonucleotide Nanomedicine in the Diagnosis and Treatment of Hepatocellular Carcinoma. *Oncotarget* (2018) 9(2):2951. doi: 10.18632/oncotarget.23359
15. Liu Y, Wu X, Gao Y, Zhang J, Zhang D, Gu S, et al. Aptamer-Functionalized Peptide H3CR5C as a Novel Nanovehicle for Codelivery of Fasudil and miRNA-195 Targeting Hepatocellular Carcinoma. *Int J Nanomedicine* (2016) 11:3891. doi: 10.2147/IJN.S108128
16. Germer K, Leonard M, Zhang X. RNA Aptamers and Their Therapeutic and Diagnostic Applications. *Int J Biochem Mol Biol* (2013) 4(1):27. doi: 2152-4114/IJBMB1212003
17. Klingenberg M, Matsuda A, Diederichs S, Patel T. Non-Coding RNA in Hepatocellular Carcinoma: Mechanisms, Biomarkers and Therapeutic Targets. *J Hepatol* (2017) 67(3):603–18. doi: 10.1016/j.jhep.2017.04.009
18. Xiao Z, Shen J, Zhang L, Li M, Hu W, Cho C. Therapeutic Targeting of Noncoding RNAs in Hepatocellular Carcinoma: Recent Progress and Future Prospects. *Oncol Lett* (2018) 15(3):3395–402. doi: 10.3892/ol.2018.7758
19. Balke D, Müller S. Therapeutic Potential of Ribozymes. In: S Agrawal and MJ Gait, editors. *Advances in Nucleic Acid Therapeutics, 1st ed* (2019) Cambridge, United Kingdom: Royal Society of Chemistry. p. 434. doi: 10.1039/9781788015714-00434
20. Burnett JC, Rossi JJ. RNA-Based Therapeutics: Current Progress and Future Prospects. *Chem Biol* (2012) 19(1):60–71. doi: 10.1016/j.chembiol.2011.12.008
21. Scull CE, Dandpat SS, Romero RA, Walter NG. Transcriptional Riboswitches Integrate Timescales for Bacterial Gene Expression Control. *Front Mol Biosci* (2021) 480. doi: 10.3389/fmolb.2020.607158
22. Ku SH, Jo SD, Lee YK, Kim K, Kim SH. Chemical and Structural Modifications of RNAi Therapeutics. *Adv Drug Deliv Rev* (2016) 104:16–28. doi: 10.1016/j.addr.2015.10.015
23. Reynolds A, Anderson EM, Vermeulen A, Fedorov Y, Robinson K, Leake D, et al. Induction of the Interferon Response by siRNA is Cell Type–and Duplex Length–Dependent. *RNA* (2006) 12(6):988–93. doi: 10.1261/rna.2340906
24. Whitehead KA, Langer R, Anderson DG. Knocking Down Barriers: Advances in siRNA Delivery. *Nat Rev Drug Discov* (2009) 8(2):129–38. doi: 10.1038/nrd2742
25. Jackson AL, Burchard J, Leake D, Reynolds A, Schelter J, Guo J, et al. Position-Specific Chemical Modification of siRNAs Reduces "Off-Target" Transcript Silencing. *RNA* (2006) 12(7):1197–205. doi: 10.1261/rna.30706
26. Eberle F, Gießler K, Deck C, Heeg K, Peter M, Richert C, et al. Modifications in Small Interfering RNA That Separate Immunostimulation From RNA Interference. *J Immunol* (2008) 180(5):3229–37. doi: 10.4049/jimmunol.180.5.3229

27. Xin Y, Huang M, Guo WW, Huang Q, zhen Zhang L, Jiang G. Nano-Based Delivery of RNAi in Cancer Therapy. *Mol Cancer* (2017) 16(1):1–9. doi: 10.1186/s12943-017-0683-y
28. Dong Y, Siegwart DJ, Anderson DG. Strategies, Design, and Chemistry in siRNA Delivery Systems. *Adv Drug Deliv Rev* (2019) 144:133–47. doi: 10.1016/j.addr.2019.05.004
29. Angela Barba A, Lamberti G, Sardo C, Dapas B, Abrami M, Grassi M, et al. Novel Lipid and Polymeric Materials as Delivery Systems for Nucleic Acid Based Drugs. *Curr Drug Metab* (2015) 16(6):427–52. doi: 10.2174/1389200216666150812142557
30. Bochicchio S, Dalmoro A, Angela Barba A, Grassi G, Lamberti G. Liposomes as siRNA Delivery Vectors. *Curr Drug Metab* (2014) 15(9):882–92. doi: 10.2174/1389200216666150206124913
31. Scarabel L, Perrone F, Garziera M, Farra R, Grassi M, Musiani F, et al. Strategies to Optimize siRNA Delivery to Hepatocellular Carcinoma Cells. *Expert Opin Drug Deliv* (2017) 14(6):797–810. doi: 10.1080/17425247.2017.1292247
32. Park K, Yang J-A, Lee M-Y, Lee H, Hahn SK. Reducible Hyaluronic Acid–siRNA Conjugate for Target Specific Gene Silencing. *Bioconjug Chem* (2013) 24(7):1201–9. doi: 10.1021/bc4001257
33. Prakash TP, Graham MJ, Yu J, Carty R, Low A, Chappell A, et al. Targeted Delivery of Antisense Oligonucleotides to Hepatocytes Using Triantennary N-Acetyl Galactosamine Improves Potency 10-Fold in Mice. *Nucleic Acids Res* (2014) 42(13):8796–807. doi: 10.1093/nar/gku531
34. Dammes N, Peer D. Monoclonal Antibody-Based Molecular Imaging Strategies and Theranostic Opportunities. *Theranostics* (2020) 10(2):938. doi: 10.7150/thno.37443
35. Mukherjee S, Ray S, Thakur R. Solid Lipid Nanoparticles: A Modern Formulation Approach in Drug Delivery System. *Indian J Pharm Sci* (2009) 71(4):349. doi: 10.4103/0250-474X.57282
36. Kara G, Calin GA, Ozpolat B. RNAi-Based Therapeutics and Tumor Targeted Delivery in Cancer. *Adv Drug Deliv Rev* (2022) 182:114113. doi: 10.1016/j.addr.2022.114113
37. Schulz W. *Molecular Biology of Human Cancers: An Advanced Student's Textbook*. Switzerland: Springer Science & Business Media (2005).
38. Chen H, Yu J. Crosstalk of Molecular Signaling in Hepatocellular Carcinoma. In: *Liver Diseases*. Switzerland: Springer (2020). p. 85–94. doi: 10.1007/978-3-030-24432-3_8
39. Giannelli G, Villa E, Lahn M. Transforming Growth Factor-β as a Therapeutic Target in Hepatocellular Carcinoma. *Cancer Res* (2014) 74 (7):1890–4. doi: 10.1158/0008-5472.CAN-14-0243
40. Khalaf AM, Fuentes D, Morshid AI, Burke MR, Kaseb AO, Hassan M, et al. Role of Wnt/β-Catenin Signaling in Hepatocellular Carcinoma, Pathogenesis, and Clinical Significance. *J Hepatocell Carcinoma* (2018) 5:61. doi: 10.2147/JHC.S156701
41. Harrison DA. The Jak/Stat Pathway. *Cold Spring Harb Perspect Biol* (2012) 4 (3):a011205. doi: 10.1101/cshperspect.a011205
42. Huang K-W, Lai Y-T, Chern G-J, Huang S-F, Tsai C-L, Sung Y-C, et al. Galactose Derivative-Modified Nanoparticles for Efficient siRNA Delivery to Hepatocellular Carcinoma. *Biomacromolecules* (2018) 19(6):2330–9. doi: 10.1021/acs.biomac.8b00358
43. Hu F, Miao L, Zhao Y, Xiao Y-Y, Xu Q. A Meta-Analysis for CXC Chemokine Receptor Type 4 as a Prognostic Marker and Potential Drug Target in Hepatocellular Carcinoma. *Drug Des Dev Ther* (2015) 9:3625. doi: 10.2147/DDDT.S86032
44. Liu J-Y, Chiang T, Liu C-H, Chern G-G, Lin T-T, Gao D-Y, et al. Delivery of siRNA Using CXCR4-Targeted Nanoparticles Modulates Tumor Microenvironment and Achieves a Potent Antitumor Response in Liver Cancer. *Mol Ther* (2015) 23(11):1772–82. doi: 10.1038/mt.2015.147
45. Yao Y, Wang T, Liu Y, Zhang N. Co-Delivery of Sorafenib and VEGF-siRNA *via* pH-Sensitive Liposomes for the Synergistic Treatment of Hepatocellular Carcinoma. *Artif Cells Nanomed Biotechnol* (2019) 47(1):1374–83. doi: 10.1080/21691401.2019.1596943
46. Zou Y, Guo C, Zhang M. Inhibition of Human Hepatocellular Carcinoma Tumor Angiogenesis by siRNA Silencing of VEGF *via* Hepatic Artery Perfusion. *Eur Rev Med Pharmacol Sci* (2015) 19(24):4751–61.
47. Raskopf E, Vogt A, Sauerbruch T, Schmitz V. siRNA Targeting VEGF Inhibits Hepatocellular Carcinoma Growth and Tumor Angiogenesis *In Vivo*. *J Hepatol* (2008) 49(6):977–84. doi: 10.1016/j.jhep.2008.07.022
48. Li X, Li J, Li C, Guo Q, Wu M, Su L, et al. Aminopeptidase N-Targeting Nanomolecule-Assisted Delivery of VEGF siRNA to Potentiate Antitumour Therapy by Suppressing Tumour Revascularization and Enhancing Radiation Response. *J Mater Chem B* (2021) 9(36):7530–43. doi: 10.1039/D1TB00990G
49. Wang G, Gao X, Gu G, Shao Z, Li M, Wang P, et al. Polyethylene Glycol–Poly (ϵ-Benzyloxycarbonyl-L-Lysine)-Conjugated VEGF siRNA for Antiangiogenic Gene Therapy in Hepatocellular Carcinoma. *Int J Nanomedicine* (2017) 12:3591. doi: 10.2147/IJN.S131078
50. Huang Z, Dong L, Chen J, Gao F, Zhang Z, Chen J, et al. Low-Molecular Weight Chitosan/Vascular Endothelial Growth Factor Short Hairpin RNA for the Treatment of Hepatocellular Carcinoma. *Life Sci* (2012) 91(23-24):1207–15. doi: 10.1016/j.lfs.2012.09.015
51. Shen J, Sun H, Meng Q, Yin Q, Zhang Z, Yu H, et al. Simultaneous Inhibition of Tumor Growth and Angiogenesis for Resistant Hepatocellular Carcinoma by Co-Delivery of Sorafenib and Survivin Small Hairpin RNA. *Mol Pharm* (2014) 11(10):3342–51. doi: 10.1021/mp4006408
52. Cao G, Li X, Qin C, Li J. Prognostic Value of VEGF in Hepatocellular Carcinoma Patients Treated With Sorafenib: A Meta-Analysis. *Med Sci Monit* (2015) 21:3144. doi: 10.12659/MSM.894617
53. Miura S, Mitsuhashi N, Shimizu H, Kimura F, Yoshidome H, Otsuka M, et al. Fibroblast Growth Factor 19 Expression Correlates With Tumor Progression and Poorer Prognosis of Hepatocellular Carcinoma. *BMC Cancer* (2012) 12(1):1–15. doi: 10.1186/1471-2407-12-56
54. Gauglhofer C, Sagmeister S, Schrottmaier W, Fischer C, Rodgarkia-Dara C, Mohr T, et al. Up-Regulation of the Fibroblast Growth Factor 8 Subfamily in Human Hepatocellular Carcinoma for Cell Survival and Neoangiogenesis. *Hepatology* (2011) 53(3):854–64. doi: 10.1002/hep.24099
55. Xiao Z, Wang Y, Ding H. XPD Suppresses Cell Proliferation and Migration *via* miR-29a-3p-Mdm2/PDGF-B Axis in HCC. *Cell Biosci* (2019) 9(1):6. doi: 10.1186/s13578-018-0269-4
56. Sangro B, Gomez-Martin C, de la Mata M, Iñarrairaegui M, Garralda E, Barrera P, et al. A Clinical Trial of CTLA-4 Blockade With Tremelimumab in Patients With Hepatocellular Carcinoma and Chronic Hepatitis C. *J Hepatol* (2013) 59(1):81–8. doi: 10.1016/j.jhep.2013.02.022
57. Pardee AD, Butterfield LH. Immunotherapy of Hepatocellular Carcinoma: Unique Challenges and Clinical Opportunities. *Oncoimmunology* (2012) 1 (1):48–55. doi: 10.4161/onci.1.1.18344
58. Fu R, Jiang S, Li J, Chen H, Zhang X. Activation of the HGF/c-MET Axis Promotes Lenvatinib Resistance in Hepatocellular Carcinoma Cells With High C-MET Expression. *Med Oncol* (2020) 37(4):1–7. doi: 10.1007/s12032-020-01350-4
59. Han P, Li H, Jiang X, Zhai B, Tan G, Zhao D, et al. Dual Inhibition of Akt and C-Met as a Second-Line Therapy Following Acquired Resistance to Sorafenib in Hepatocellular Carcinoma Cells. *Mol Oncol* (2017) 11(3):320–34. doi: 10.1002/1878-0261.12039
60. Liu Q, Fan D, Adah D, Wu Z, Liu R, Yan QT, et al. CRISPR/Cas9–mediated Hypoxia Inducible Factor–1α Knockout Enhances the Antitumor Effect of Transarterial Embolization in Hepatocellular Carcinoma. *Oncol Rep* (2018) 40(5):2547–57. doi: 10.3892/or.2018.6667
61. Zhang B-C, Luo B-Y, Zou J-J, Wu P-Y, Jiang J-L, Le J-Q, et al. Co-Delivery of Sorafenib and CRISPR/Cas9 Based on Targeted Core–Shell Hollow Mesoporous Organosilica Nanoparticles for Synergistic HCC Therapy. *ACS Appl Mater Interfaces* (2020) 12(51):57362–72. doi: 10.1021/acsami.0c17660
62. Vanderborght B, De Muynck K, Lefere S, Geerts A, Degroote H, Verhelst X, et al. Effect of Isoform-Specific HIF-1α and HIF-2α Antisense Oligonucleotides on Tumorigenesis, Inflammation and Fibrosis in a Hepatocellular Carcinoma Mouse Model. *Oncotarget* (2020) 11(48):4504. doi: 10.18632/oncotarget.27830
63. Avila MA, Berasain C. Targeting CCL2/CCR2 in Tumor-Infiltrating Macrophages: A Tool Emerging Out of the Box Against Hepatocellular Carcinoma. *Cell Mol Gastroenterol Hepatol* (2019) 7(2):293–4. doi: 10.1016/j.jcmgh.2018.11.002
64. Bartneck M, Schrammen PL, Möckel D, Govaere O, Liepelt A, Krenkel O, et al. The CCR2+ Macrophage Subset Promotes Pathogenic Angiogenesis for Tumor Vascularization in Fibrotic Livers. *Cell Mol Gastroenterol Hepatol* (2019) 7(2):371–90. doi: 10.1016/j.jcmgh.2018.10.007

65. Li L-H, Guo Z-J, Yan L-L, Yang J-C, Xie Y-F, Sheng W-H, et al. Antitumor and Antiangiogenic Activities of Anti-Vascular Endothelial Growth Factor Hairpin Ribozyme in Human Hepatocellular Carcinoma Cell Cultures and Xenografts. *World J Gastroenterol* (2007) 13(47):6425. doi: 10.3748/wjg.v13.i47.6425
66. Morino F, Tokunaga T, Tsuchida T, Handa A, Nagata J, Tomii Y, et al. Hammerhead Ribozyme Specifically Inhibits Vascular Endothelial Growth Factor Gene Expression in a Human Hepatocellular Carcinoma Cell Line. *Int J Oncol* (2000) 17(3):495–504. doi: 10.3892/ijo.17.3.495
67. Kamochi J, Tokunaga T, Morino F, Nagata J, Tomii Y, Abe Y, et al. Ribozyme Mediated Suppression of Vascular Endothelial Growth Factor Gene Expression Enhances Matrix Metalloproteinase 1 Expression in a Human Hepatocellular Carcinoma Cell Line. *Int J Oncol* (2002) 21(1):81–4. doi: 10.3892/ijo.21.1.81
68. Han X, Yang J, Zeng F, Weng J, Zhang Y, Peng Q, et al. Programmable Synthetic Protein Circuits for the Identification and Suppression of Hepatocellular Carcinoma. *Mol Ther Oncolytics* (2020) 17:70–82. doi: 10.1016/j.omto.2020.03.008
69. Guo Y, Wang J, Zhang L, Shen S, Guo R, Yang Y, et al. Theranostical Nanosystem-Mediated Identification of an Oncogene and Highly Effective Therapy in Hepatocellular Carcinoma. *Hepatology* (2016) 63(4):1240–55. doi: 10.1002/hep.28409
70. Qu C, He D, Lu X, Dong L, Zhu Y, Zhao Q, et al. Salt-Inducible Kinase (SIK1) Regulates HCC Progression and WNT/β-Catenin Activation. *J Hepatol* (2016) 64(5):1076–89. doi: 10.1016/j.jhep.2016.01.005
71. Hu Y, Shen Y, Ji B, Wang L, Zhang Z, Zhang Y. Combinational RNAi Gene Therapy of Hepatocellular Carcinoma by Targeting Human EGFR and TERT. *Eur J Pharm Sci* (2011) 42(4):387–91. doi: 10.1016/j.ejps.2011.01.004
72. Ma Z-X, Yang C-M, Li M-G, Tu H. Telomerase Reverse Transcriptase Promoter Mutations in Hepatocellular Carcinogenesis. *Hepatoma Res* (2019) 5. doi: 10.20517/2394-5079.2018.104
73. Bogorad RL, Yin H, Zeigerer A, Nonaka H, Ruda VM, Zerial M, et al. Nanoparticle-Formulated siRNA Targeting Integrins Inhibits Hepatocellular Carcinoma Progression in Mice. *Nat Commun* (2014) 5 (1):1–14. doi: 10.1038/ncomms4869
74. Gao J, Chen H, Yu Y, Song J, Song H, Su X, et al. Inhibition of Hepatocellular Carcinoma Growth Using Immunoliposomes for Co-Delivery of Adriamycin and Ribonucleotide Reductase M2 siRNA. *Biomaterials* (2013) 34(38):10084–98. doi: 10.1016/j.biomaterials.2013.08.088
75. Wang Y, Yang Y, Gao H, Ouyang T, Zhang L, Hu J, et al. Comprehensive Analysis of CDCAs Methylation and Immune Infiltrates in Hepatocellular Carcinoma. *Front Oncol* (2021) 10:3199. doi: 10.3389/fonc.2020.566183
76. Li L, Wang R, Wilcox D, Sarthy A, Lin X, Huang X, et al. Developing Lipid Nanoparticle-Based siRNA Therapeutics for Hepatocellular Carcinoma Using an Integrated Approach. *Mol Cancer Ther* (2013) 12(11):2308–18. doi: 10.1158/1535-7163.MCT-12-0983-T
77. Li Y, Zhu Z, Zhang S, Yu D, Yu H, Liu L, et al. ShRNA-Targeted Centromere Protein A Inhibits Hepatocellular Carcinoma Growth. *PloS One* (2011) 6(3): e17794. doi: 10.1371/journal.pone.0017794
78. Tolcher AW, Papadopoulos KP, Patnaik A, Rasco DW, Martinez D, Wood DL, et al. Safety and Activity of DCR-MYC, a First-in-Class Dicer-Substrate Small Interfering RNA (DsiRNA) Targeting MYC, in a Phase I Study in Patients With Advanced Solid Tumors. *Am Soc Clin Oncol* (2015). doi: 10.1200/jco.2015.33.15_suppl.11006
79. El Dika I, Lim HY, Yong WP, Lin CC, Yoon JH, Modiano M, et al. An Open-Label, Multicenter, Phase I, Dose Escalation Study With Phase II Expansion Cohort to Determine the Safety, Pharmacokinetics, and Preliminary Antitumor Activity of Intravenous TKM-080301 in Subjects With Advanced Hepatocellular Carcinoma. *Oncologist* (2019) 24(6):747–e218. doi: 10.1634/theoncologist.2018-0838
80. Liao W, Liu W, Yuan Q, Liu X, Ou Y, He S, et al. Silencing of DLGAP5 by siRNA Significantly Inhibits the Proliferation and Invasion of Hepatocellular Carcinoma Cells. *PloS One* (2013) 8(12):e80789. doi: 10.1371/journal.pone.0080789
81. Wu Q-f, Liu C, Tai M-h, Liu D, Lei L, Wang R-t, et al. Knockdown of FoxM1 by siRNA Interference Decreases Cell Proliferation, Induces Cell Cycle Arrest and Inhibits Cell Invasion in MHCC-97H Cells *In Vitro*. *Acta Pharmacol Sin* (2010) 31(3):361–6. doi: 10.1038/aps.2010.4
82. Doan CC, Le LT, Hoang SN, Do SM, Van Le D. Simultaneous Silencing of VEGF and KSP by siRNA Cocktail Inhibits Proliferation and Induces Apoptosis of Hepatocellular Carcinoma Hep3B Cells. *Biol Res* (2014) 47 (1):1–15. doi: 10.1186/0717-6287-47-70
83. Li T, Xue Y, Wang G, Gu T, Li Y, Zhu YY, et al. Multi-Target siRNA: Therapeutic Strategy for Hepatocellular Carcinoma. *J Cancer* (2016) 7 (10):1317. doi: 10.7150/jca.15157
84. Zhang S, Zhang F, Chen Q, Wan C, Xiong J, Xu J. CRISPR/Cas9-Mediated Knockout of NSD1 Suppresses the Hepatocellular Carcinoma Development *via* the NSD1/H3/Wnt10b Signaling Pathway. *J Exp Clin Cancer Res* (2019) 38(1):1–14. doi: 10.1186/s13046-019-1462-y
85. Wang H, Yang H, Shivalila CS, Dawlaty MM, Cheng AW, Zhang F, et al. One-Step Generation of Mice Carrying Mutations in Multiple Genes by CRISPR/Cas-Mediated Genome Engineering. *Cell* (2013) 153(4):910–8. doi: 10.1016/j.cell.2013.04.025
86. Guo X, Jiang H, Shi B, Zhou M, Zhang H, Shi Z, et al. Disruption of PD-1 Enhanced the Anti-Tumor Activity of Chimeric Antigen Receptor T Cells Against Hepatocellular Carcinoma. *Front Pharmacol* (2018) 9:1118. doi: 10.3389/fphar.2018.01118
87. Xue W, Chen S, Yin H, Tammela T, Papagiannakopoulos T, Joshi NS, et al. CRISPR-Mediated Direct Mutation of Cancer Genes in the Mouse Liver. *Nature* (2014) 514(7522):380–4. doi: 10.1038/nature13589
88. Sieghart W, Losert D, Strommer S, Cejka D, Schmid K, Rasoul-Rockenschaub S, et al. Mcl-1 Overexpression in Hepatocellular Carcinoma: A Potential Target for Antisense Therapy. *J Hepatol* (2006) 44 (1):151–7. doi: 10.1016/j.jhep.2005.09.010
89. Li W-C, Ye S-L, Sun R-X, Liu Y-K, Tang Z-Y, Kim Y, et al. Inhibition of Growth and Metastasis of Human Hepatocellular Carcinoma by Antisense Oligonucleotide Targeting Signal Transducer and Activator of Transcription 3. *Clin Cancer Res* (2006) 12(23):7140–8. doi: 10.1158/1078-0432.CCR-06-0484
90. Dhanasekaran R, Park J, Yevtodiyenko A, Bellovin DI, Adam SJ, Kd AR, et al. MYC ASO Impedes Tumorigenesis and Elicits Oncogene Addiction in Autochthonous Transgenic Mouse Models of HCC and RCC. *Mol Ther Nucleic Acids* (2020) 21:850–9. doi: 10.1016/j.omtn.2020.07.008
91. Harada T, Matsumoto S, Hirota S, Kimura H, Fujii S, Kasahara Y, et al. Chemically Modified Antisense Oligonucleotide Against ARL4C Inhibits Primary and Metastatic Liver Tumor Growth. *Mol Cancer Ther* (2019) 18 (3):602–12. doi: 10.1158/1535-7163.MCT-18-0824
92. Lee YJ, Lee S-W. Regression of Hepatocarcinoma Cells Using RNA Aptamer Specific to Alpha-Fetoprotein. *Biochem Biophys Res Commun* (2012) 417 (1):521–7. doi: 10.1016/j.bbrc.2011.11.153
93. Cho Y, Lee YB, Lee J-H, Lee DH, Cho EJ, Yu SJ, et al. Modified AS1411 Aptamer Suppresses Hepatocellular Carcinoma by Up-Regulating Galectin-14. *PloS One* (2016) 11(8):e0160822. doi: 10.1371/journal.pone.0160822
94. Won Y-S, Lee S-W. Targeted Retardation of Hepatocarcinoma Cells by Specific Replacement of Alpha-Fetoprotein RNA. *J Biotechnol* (2007) 129 (4):614–9. doi: 10.1016/j.jbiotec.2007.02.004
95. Yang J, Ding S. Chimeric RNA-Binding Protein-Based Killing Switch Targeting Hepatocellular Carcinoma Cells. *Mol Ther Nucleic Acids* (2021) 25:683–95. doi: 10.1016/j.omtn.2021.08.012
96. Wu C, Gong F, Pang P, Shen M, Zhu K, Cheng D, et al. An RGD-Modified MRI-Visible Polymeric Vector for Targeted siRNA Delivery to Hepatocellular Carcinoma in Nude Mice. *PloS One* (2013) 8(6):e66416. doi: 10.1371/journal.pone.0066416
97. Xu Q, Zhang M, Tu J, Pang L, Cai W, Liu X. MicroRNA-122 Affects Cell Aggressiveness and Apoptosis by Targeting PKM2 in Human Hepatocellular Carcinoma. *Oncol Rep* (2015) 34(4):2054–64. doi: 10.3892/or.2015.4175
98. Zhang R, Shen M, Wu C, Chen Y, Lu J, Li J, et al. HDAC8-Dependent Deacetylation of PKM2 Directs Nuclear Localization and Glycolysis to Promote Proliferation in Hepatocellular Carcinoma. *Cell Death Dis* (2020) 11(12):1–15. doi: 10.1038/s41419-020-03212-3
99. Xu J, Zhu X, Wu L, Yang R, Yang Z, Wang Q, et al. MicroRNA-122 Suppresses Cell Proliferation and Induces Cell Apoptosis in Hepatocellular Carcinoma by Directly Targeting Wnt/β-Catenin Pathway. *Liver Int* (2012) 32(5):752–60. doi: 10.1111/j.1478-3231.2011.02750.x
100. Lee Y-H, Seo D, Choi K-J, Andersen JB, Won M-A, Kitade M, et al. Antitumor Effects in Hepatocarcinoma of Isoform-Selective Inhibition of

HDAC2. *Cancer Res* (2014) 74(17):4752–61. doi: 10.1158/0008-5472.CAN-13-3531
101. Yin T, Wang P, Li J, Wang Y, Zheng B, Zheng R, et al. Tumor-Penetrating Codelivery of siRNA and Paclitaxel With Ultrasound-Responsive Nanobubbles Hetero-Assembled From Polymeric Micelles and Liposomes. *Biomaterials* (2014) 35(22):5932–43. doi: 10.1016/j.biomaterials.2014.03.072
102. Guo X, Wang W, Zhou F, Lu Z, Fang R, Jia F, et al. siRNA-Mediated Inhibition of hTERT Enhances Chemosensitivity of Hepatocellular Carcinoma. *Cancer Biol Ther* (2008) 7(10):1555–60. doi: 10.4161/cbt.7.10.6539
103. Li K, Lin S-Y, Brunicardi FC, Seu P. Use of RNA Interference to Target Cyclin E-Overexpressing Hepatocellular Carcinoma. *Cancer Res* (2003) 63 (13):3593–7.
104. Han K-Q, He X-Q, Ma M-Y, Guo X-D, Zhang X-M, Chen J, et al. Targeted Silencing of CXCL1 by siRNA Inhibits Tumor Growth and Apoptosis in Hepatocellular Carcinoma. *Int J Oncol* (2015) 47(6):2131–40. doi: 10.3892/ijo.2015.3203
105. Pan H, Wang Z, Jiang L, Sui X, You L, Shou J, et al. Autophagy Inhibition Sensitizes Hepatocellular Carcinoma to the Multikinase Inhibitor Linifanib. *Sci Rep* (2014) 4(1):1–10. doi: 10.1038/srep06683
106. Han L, Tang C, Yin C. Oral Delivery of shRNA and siRNA *via* Multifunctional Polymeric Nanoparticles for Synergistic Cancer Therapy. *Biomaterials* (2014) 35(15):4589–600. doi: 10.1016/j.biomaterials.2014.02.027
107. Han L, Tang C, Yin C. Effect of Binding Affinity for siRNA on the *In Vivo* Antitumor Efficacy of Polyplexes. *Biomaterials* (2013) 34(21):5317–27. doi: 10.1016/j.biomaterials.2013.03.060
108. Chen Z-H, Yan PY, Zuo Z-H, Nelson JB, Michalopoulos GK, Monga S, et al. Targeting Genomic Rearrangements in Tumor Cells Through Cas9-Mediated Insertion of a Suicide Gene. *Nat Biotechnol* (2017) 35(6):543–50. doi: 10.1038/nbt.3843
109. Ningarhari M, Caruso S, Hirsch TZ, Bayard Q, Franconi A, Védie A-L, et al. Telomere Length is Key to Hepatocellular Carcinoma Diversity and Telomerase Addiction is an Actionable Therapeutic Target. *J Hepatol* (2021) 74(5):1155–66. doi: 10.1016/j.jhep.2020.11.052
110. Scaggiante B, Farra R, Dapas B, Baj G, Pozzato G, Grassi M, et al. Aptamer Targeting of the Elongation Factor 1A Impairs Hepatocarcinoma Cells Viability and Potentiates Bortezomib and Idarubicin Effects. *Int J Pharm* (2016) 506(1-2):268–79. doi: 10.1016/j.ijpharm.2016.04.031
111. Shin K-S, Sullenger BA, Lee S-W. Ribozyme-Mediated Induction of Apoptosis in Human Cancer Cells by Targeted Repair of Mutant P53 RNA. *Mol Ther* (2004) 10(2):365–72. doi: 10.1016/j.ymthe.2004.05.007
112. Song M, Jeong J, Ban G, Lee J, Won Y, Cho K, et al. Validation of Tissue-Specific Promoter-Driven Tumor-Targeting Trans-Splicing Ribozyme System as a Multifunctional Cancer Gene Therapy Device *In Vivo*. *Cancer Gene Ther* (2009) 16(2):113–25. doi: 10.1038/cgt.2008.64
113. Han SR, Lee CH, Im JY, Kim JH, Kim JH, Kim SJ, et al. Targeted Suicide Gene Therapy for Liver Cancer Based on Ribozyme-Mediated RNA Replacement Through Post-Transcriptional Regulation. *Mol Ther Nucleic Acids* (2021) 23:154–68. doi: 10.1016/j.omtn.2020.10.036
114. Kim J, Won R, Ban G, Ju MH, Cho KS, Han SY, et al. Targeted Regression of Hepatocellular Carcinoma by Cancer-Specific RNA Replacement Through microRNA Regulation. *Sci Rep* (2015) 5(1):1–13. doi: 10.1038/srep12315
115. Cazejust J, Bessoud B, Colignon N, Garcia-Alba C, Planché O, Menu Y. Hepatocellular Carcinoma Vascularization: From the Most Common to the Lesser Known Arteries. *Diagn Interv Imaging* (2014) 95(1):27–36. doi: 10.1016/j.diii.2013.04.015
116. Xiong XX, Qiu XY, Hu DX, Chen XQ. Advances in Hypoxia-Mediated Mechanisms in Hepatocellular Carcinoma. *Mol Pharmacol* (2017) 92 (3):246–55. doi: 10.1124/mol.116.107706
117. Morse MA, Sun W, Kim R, He AR, Abada PB, Mynderse M, et al. The Role of Angiogenesis in Hepatocellular Carcinoma. *Clin Cancer Res* (2019) 25 (3):912–20. doi: 10.1158/1078-0432.CCR-18-1254
118. Zheng N, Wei W, Wang Z. Emerging Roles of FGF Signaling in Hepatocellular Carcinoma. *Trans Cancer Res* (2016) 5(1):1.
119. Sawey ET, Chanrion M, Cai C, Wu G, Zhang J, Zender L, et al. Identification of a Therapeutic Strategy Targeting Amplified FGF19 in Liver Cancer by Oncogenomic Screening. *Cancer Cell* (2011) 19(3):347–58. doi: 10.1016/j.ccr.2011.01.040
120. Heldin C-H. Targeting the PDGF Signaling Pathway in Tumor Treatment. *Cell Commun Signal* (2013) 11(1):1–18. doi: 10.1186/1478-811X-11-97
121. Chae YK, Ranganath K, Hammerman PS, Vaklavas C, Mohindra N, Kalyan A, et al. Inhibition of the Fibroblast Growth Factor Receptor (FGFR) Pathway: The Current Landscape and Barriers to Clinical Application. *Oncotarget* (2017) 8(9):16052. doi: 10.18632/oncotarget.14109
122. Bupathi M, Kaseb A, Janku F. Angiopoietin 2 as a Therapeutic Target in Hepatocellular Carcinoma Treatment: Current Perspectives. *Onco Targets Ther* (2014) 7:1927. doi: 10.2147/OTT.S46457
123. Li Y, Zhai Z, Liu D, Zhong X, Meng X, Yang Q, et al. CD105 Promotes Hepatocarcinoma Cell Invasion and Metastasis Through VEGF. *Tumor Biol* (2015) 36(2):737–45. doi: 10.1007/s13277-014-2686-2
124. Jeng K-S, Sheen I, Lin S-S, Leu C-M, Chang C-F. The Role of Endoglin in Hepatocellular Carcinoma. *Int J Mol Sci* (2021) 22(6):3208. doi: 10.3390/ijms22063208
125. Sharma BK, Srinivasan R, Kapil S, Singla B, Chawla YK, Chakraborti A, et al. Angiogenic and Anti-Angiogenic Factor Gene Transcript Level Quantitation by Quantitative Real Time PCR in Patients With Hepatocellular Carcinoma. *Mol Biol Rep* (2013) 40(10):5843–52. doi: 10.1007/s11033-013-2690-4
126. Wang Y, Liu D, Zhang T, Xia L. FGF/FGFR Signaling in Hepatocellular Carcinoma: From Carcinogenesis to Recent Therapeutic Intervention. *Cancers* (2021) 13(6):1360. doi: 10.3390/cancers13061360
127. Gao D-Y, Lin T-T, Sung Y-C, Liu YC, Chiang W-H, Chang C-C, et al. CXCR4-Targeted Lipid-Coated PLGA Nanoparticles Deliver Sorafenib and Overcome Acquired Drug Resistance in Liver Cancer. *Biomaterials* (2015) 67:194–203. doi: 10.1016/j.biomaterials.2015.07.035
128. Umemoto Y, Okano S, Matsumoto Y, Nakagawara H, Matono R, Yoshiya S, et al. Prognostic Impact of Programmed Cell Death 1 Ligand 1 Expression in Human Leukocyte Antigen Class I-Positive Hepatocellular Carcinoma After Curative Hepatectomy. *J Gastroenterol* (2015) 50(1):65–75. doi: 10.1007/s00535-014-0933-3
129. Wang H, Rao B, Lou J, Li J, Liu Z, Li A, et al. The Function of the HGF/c-Met Axis in Hepatocellular Carcinoma. *Front Cell Dev Biol* (2020) 8:55. doi: 10.3389/fcell.2020.00055
130. Zhang Y, Gao X, Zhu Y, Kadel D, Sun H, Chen J, et al. The Dual Blockade of MET and VEGFR2 Signaling Demonstrates Pronounced Inhibition on Tumor Growth and Metastasis of Hepatocellular Carcinoma. *J Exp Clin Cancer Res* (2018) 37(1):1–15. doi: 10.1186/s13046-018-0750-2
131. Tan S, Li R, Ding K, Lobie PE, Zhu T. miR-198 Inhibits Migration and Invasion of Hepatocellular Carcinoma Cells by Targeting the HGF/c-MET Pathway. *FEBS Lett* (2011) 585(14):2229–34. doi: 10.1016/j.febslet.2011.05.042
132. Hu C-T, Wu J-R, Cheng C-C, Wu W-S. The Therapeutic Targeting of HGF/c-Met Signaling in Hepatocellular Carcinoma: Alternative Approaches. *Cancers* (2017) 9(6):58. doi: 10.3390/cancers9060058
133. Moawad AW, Szklaruk J, Lall C, Blair KJ, Kaseb AO, Kamath A, et al. Angiogenesis in Hepatocellular Carcinoma; Pathophysiology, Targeted Therapy, and Role of Imaging. *J Hepatocell Carcinoma* (2020) 7:77. doi: 10.2147/JHC.S224471
134. Dolinsek T, Markelc B, Sersa G, Coer A, Stimac M, Lavrencak J, et al. Multiple Delivery of siRNA Against Endoglin Into Murine Mammary Adenocarcinoma Prevents Angiogenesis and Delays Tumor Growth. *PloS One* (2013) 8(3):e58723. doi: 10.1371/journal.pone.0058723
135. Lin D, Wu J. Hypoxia Inducible Factor in Hepatocellular Carcinoma: A Therapeutic Target. *World J Gastroenterol* (2015) 21(42):12171. doi: 10.3748/wjg.v21.i42.12171
136. Farzaneh Z, Vosough M, Agarwal T, Farzaneh M. Critical Signaling Pathways Governing Hepatocellular Carcinoma Behavior; Small Molecule-Based Approaches. *Cancer Cell Int* (2021) 21(1):1–15. doi: 10.1186/s12935-021-01924-w
137. Zhang X, Luo X, Liu W, Shen A. Identification of Hub Genes Associated With Hepatocellular Carcinoma Prognosis by Bioinformatics Analysis. *J Cancer Ther* (2021) 12(04):186. doi: 10.4236/jct.2021.124019
138. Bogaerts E, Heindryckx F, Vandewynckel Y-P, Van Grunsven LA, Van Vlierberghe H. The Roles of Transforming Growth Factor-β, Wnt, Notch and Hypoxia on Liver Progenitor Cells in Primary Liver Tumours. *Int J Oncol* (2014) 44(4):1015–22. doi: 10.3892/ijo.2014.2286
139. Cheng W-T, Xu K, Tian D-Y, Zhang Z-G, Liu L-J, Chen Y. Role of Hedgehog Signaling Pathway in Proliferation and Invasiveness of Hepatocellular Carcinoma Cells. *Int J Oncol* (2009) 34(3):829–36. doi: 10.3892/ijo_00000209

140. Della Corte CM, Viscardi G, Papaccio F, Esposito G, Martini G, Ciardiello D, et al. Implication of the Hedgehog Pathway in Hepatocellular Carcinoma. *World J Gastroenterol* (2017) 23(24):4330. doi: 10.3748/wjg.v23.i24.4330
141. Huang Q, Li J, Zheng J, Wei A. The Carcinogenic Role of the Notch Signaling Pathway in the Development of Hepatocellular Carcinoma. *J Cancer* (2019) 10(6):1570. doi: 10.7150/jca.26847
142. Wang XQ, Zhang W, Lui EL, Zhu Y, Lu P, Yu X, et al. Notch1-Snail1-E-Cadherin Pathway in Metastatic Hepatocellular Carcinoma. *Int J Cancer* (2012) 131(3):E163–E72. doi: 10.1002/ijc.27336
143. Hin Tang JJ, Hao Thng DK, Lim JJ, Toh TB. JAK/STAT Signaling in Hepatocellular Carcinoma. *Hepat Oncol* (2020) 7(1):HEP18. doi: 10.2217/hep-2020-0001
144. Kim W, Khan SK, Liu Y, Xu R, Park O, He Y, et al. Hepatic Hippo Signaling Inhibits Protumoural Microenvironment to Suppress Hepatocellular Carcinoma. *Gut* (2018) 67(9):1692–703. doi: 10.1136/gutjnl-2017-314061
145. Moon H, Ro SW. MAPK/ERK Signaling Pathway in Hepatocellular Carcinoma. *Cancers* (2021) 13(12):3026. doi: 10.3390/cancers13123026
146. Dimri M, Satyanarayana A. Molecular Signaling Pathways and Therapeutic Targets in Hepatocellular Carcinoma. *Cancers* (2020) 12(2):491. doi: 10.3390/cancers12020491
147. Liu Z, Chen D, Ning F, Du J, Wang H. EGF is Highly Expressed in Hepatocellular Carcinoma (HCC) and Promotes Motility of HCC Cells *via* Fibronectin. *J Cell Biochem* (2018) 119(5):4170–83. doi: 10.1002/jcb.26625
148. Giannelli G, Astigiano S, Antonaci S, Morini M, Barbieri O, Noonan DM, et al. Role of the α3β1 and α6β4 Integrins in Tumor Invasion. *Clin Exp Metastasis* (2002) 19(3):217–23. doi: 10.1023/A:1015579204607
149. Lee B, Ha SY, Song DH, Lee HW, Cho SY, Park C-K. High Expression of Ribonucleotide Reductase Subunit M2 Correlates With Poor Prognosis of Hepatocellular Carcinoma. *Gut Liver* (2014) 8(6):662. doi: 10.5009/gnl13392
150. Hussain S, Schwank J, Staib F, Wang X, Harris C. TP53 Mutations and Hepatocellular Carcinoma: Insights Into the Etiology and Pathogenesis of Liver Cancer. *Oncogene* (2007) 26(15):2166–76. doi: 10.1038/sj.onc.1210279
151. Massagué J. TGFβ in Cancer. *Cell* (2008) 134(2):215–30. doi: 10.1016/j.cell.2008.07.001
152. Wang Y, Han C, Lu L, Magliato S, Wu T. Hedgehog Signaling Pathway Regulates Autophagy in Human Hepatocellular Carcinoma Cells. *Hepatology* (2013) 58(3):995–1010. doi: 10.1002/hep.26394
153. Lee SH, Shin MS, Lee HS, Bae JH, Lee HK, Kim HS, et al. Expression of Fas and Fas-Related Molecules in Human Hepatocellular Carcinoma. *Hum Pathol* (2001) 32(3):250–6. doi: 10.1053/hupa.2001.22769
154. Fabregat I. Dysregulation of Apoptosis in Hepatocellular Carcinoma Cells. *World J Gastroenterol* (2009) 15(5):513. doi: 10.3748/wjg.15.513
155. Johnstone RW, Frew AJ, Smyth MJ. The TRAIL Apoptotic Pathway in Cancer Onset, Progression and Therapy. *Nat Rev Cancer* (2008) 8(10):782–98. doi: 10.1038/nrc2465
156. Breuhahn K, Longerich T, Schirmacher P. Dysregulation of Growth Factor Signaling in Human Hepatocellular Carcinoma. *Oncogene* (2006) 25 (27):3787–800. doi: 10.1038/sj.onc.1209556
157. Yoshikawa H, Matsubara K, Geng-Sun Q, Jackson P, Groopman JD, Manning JE, et al. SOCS-1, a Negative Regulator of the JAK/STAT Pathway, is Silenced by Methylation in Human Hepatocellular Carcinoma and Shows Growth-Suppression Activity. *Nat Genet* (2001) 28(1):29. doi: 10.1038/ng0501-29
158. Horie Y, Suzuki A, Kataoka E, Sasaki T, Hamada K, Sasaki J, et al. Hepatocyte-Specific Pten Deficiency Results in Steatohepatitis and Hepatocellular Carcinomas. *J Clin Invest* (2004) 113(12):1774–83. doi: 10.1172/JCI20513
159. Su C. Survivin in Survival of Hepatocellular Carcinoma. *Cancer Lett* (2016) 379(2):184–90. doi: 10.1016/j.canlet.2015.06.016
160. Wang D, Liu J, Liu S, Li W. Identification of Crucial Genes Associated With Immune Cell Infiltration in Hepatocellular Carcinoma by Weighted Gene Co-Expression Network Analysis. *Front Genet* (2020) 11:342. doi: 10.3389/fgene.2020.00342
161. Wang Q, Wu PC, Roberson RS, Luk BV, Ivanova I, Chu E, et al. Survivin and Escaping in Therapy-Induced Cellular Senescence. *Int J Cancer* (2011) 128 (7):1546–58. doi: 10.1002/ijc.25482
162. Ito T, Shiraki K, Sugimoto K, Yamanaka T, Fujikawa K, Ito M, et al. Survivin Promotes Cell Proliferation in Human Hepatocellular Carcinoma. *Hepatology* (2000) 31(5):1080–5. doi: 10.1053/he.2000.6496
163. Garmpis N, Damaskos C, Garmpi A, Georgakopoulou VE, Sarantis P, Antoniou EA, et al. Histone Deacetylase Inhibitors in the Treatment of Hepatocellular Carcinoma: Current Evidence and Future Opportunities. *J Pers Med* (2021) 11(3):223. doi: 10.3390/jpm11030223
164. Geng Y, Michowski W, Chick JM, Wang YE, Jecrois ME, Sweeney KE, et al. Kinase-Independent Function of E-Type Cyclins in Liver Cancer. *Proc Natl Acad Sci* (2018) 115(5):1015–20. doi: 10.1073/pnas.1711477115
165. Ghanem I, Riveiro ME, Paradis V, Faivre S, de Parga PMV, Raymond E. Insights on the CXCL12-CXCR4 Axis in Hepatocellular Carcinoma Carcinogenesis. *Am J Trans Res* (2014) 6(4):340.
166. Beg MS, Borad M, Sachdev J, Hong DS, Smith S, Bader A, et al. Abstract CT327: Multicenter Phase I Study of MRX34, a First-in-Class microRNA miR-34 Mimic Liposomal Injection. *Cancer Research* (2014) 74. doi: 10.1158/1538-7445.AM2014-CT327

Conflict of Interest: The authors declare that the research was conducted in the absence of any commercial or financial relationships that could be construed as a potential conflict of interest.

frontiers | Frontiers in Oncology

ORIGINAL RESEARCH
published: 16 May 2022
doi: 10.3389/fonc.2022.892192

Myosteatosis can Predict Unfavorable Outcomes in Advanced Hepatocellular Carcinoma Patients Treated With Hepatic Artery Infusion Chemotherapy and Anti-PD-1 Immunotherapy

Xiaoping Yi[1,2,3,4,5†], Yan Fu[1,2†], Qianyan Long[1,2†], Yazhuo Zhao[1,2], Sai Li[1,2], Chunhui Zhou[1,2], Huashan Lin[6], Xiaolian Liu[1], Chang Liu[1], Changyong Chen[1] and Liangrong Shi[1,2]*

[1] Department of Radiology, Xiangya Hospital, Central South University, Changsha, China, [2] National Clinical Research Center for Geriatric Disorders (Xiangya Hospital), Central South University, Changsha, China, [3] Hunan Key Laboratory of Skin Cancer and Psoriasis, Xiangya Hospital, Changsha, China, [4] Hunan Engineering Research Center of Skin Health and Disease, Xiangya Hospital, Changsha, China, [5] Department of Dermatology, Xiangya Hospital, Central South University, Changsha, China, [6] Department of Pharmaceuticals Diagnosis, GE Healthcare, Changsha, China

Aim : To evaluate the feasibility of computed tomography (CT) - derived measurements of body composition parameters to predict the risk factor of non-objective response (non-OR) in patients with hepatocellular carcinoma (HCC) undergoing anti-PD-1 immunotherapy and hepatic artery infusion chemotherapy (immune-HAIC).

Methods: Patients with histologically confirmed HCC and treated with the immune-HAIC were retrospectively recruited between June 30, 2019, and July 31, 2021. CT-based estimations of body composition parameters were acquired from the baseline unenhanced abdominal CT images at the level of the third lumbar vertebra (L3) and were applied to develop models predicting the probability of OR. A myosteatosis nomogram was built using the multivariate logistic regression incorporating both myosteatosis measurements and clinical variables. Receiver operating characteristic (ROC) curves assessed the performance of prediction models, including the area under the curve (AUC). The nomogram's performance was assessed by the calibration, discrimination, and decision curve analyses. Associations among predictors and gene mutations were also examined by correlation matrix analysis.

Results: Fifty-two patients were recruited to this study cohort, with 30 patients having a OR status after immune-HAIC treatment. Estimations of myosteatosis parameters, like SM-RA (skeletal muscle radiation attenuation), were significantly associated with the probability of predicting OR (P=0.007). The SM-RA combined nomogram model, including serum red blood cell, hemoglobin, creatinine, and the mean CT value of visceral fat (VFmean) improved the prediction probability for OR disease with an AUC of

OPEN ACCESS

Edited by:
Zexian Liu,
Sun Yat-sen University Cancer Center (SYSUCC), China

Reviewed by:
Xuefeng Wang,
Soochow University, China
Junjie Kong,
Shandong Provincial Hospital, China
Bin Liang,
Huazhong University of Science and Technology, China

***Correspondence:**
Liangrong Shi
shiliangrong@csu.edu.cn

†These authors have contributed equally to this work and share first authorship

Specialty section:
This article was submitted to Molecular and Cellular Oncology, a section of the journal Frontiers in Oncology

Received: 08 March 2022
Accepted: 19 April 2022
Published: 16 May 2022

Citation:
Yi X, Fu Y, Long Q, Zhao Y, Li S, Zhou C, Lin H, Liu X, Liu C, Chen C and Shi L (2022) Myosteatosis can Predict Unfavorable Outcomes in Advanced Hepatocellular Carcinoma Patients Treated With Hepatic Artery Infusion Chemotherapy and Anti-PD-1 Immunotherapy. Front. Oncol. 12:892192. doi: 10.3389/fonc.2022.892192

0.713 (95% CI, 0.75 to 0.95) than the clinical model nomogram with AUC of 0.62 using a 5-fold cross-validation methodology. Favorable clinical potentials were observed in the decision curve analysis.

Conclusions: The CT-based estimations of myosteatosis could be used as an indicator to predict a higher risk of transition to the Non-OR disease state in HCC patients treated with immune-HAIC therapy. This study demonstrated the therapeutic relevance of skeletal muscle composition assessments in the overall prediction of treatment response and prognosis in HCC patients.

Keywords: myosteatosis, predictor, treatment response, hepatocellular carcinoma, hepatic artery infusion chemotherapy, anti-PD-1 immunotherapy

INTRODUCTION

Hepatocellular carcinoma (HCC) is considered the third leading cause of cancer-related mortalities worldwide (1). In the case of unresectable HCCs, transcatheter arterial chemoembolization (TACE) is considered the first-line treatment to combat the tumor outgrowth by restricting the blood and nutrient supply to the tumor. Despite the minimally invasive nature of TACE and satisfactory success rate, patients may show the disease progression after TACE, and most importantly, patients who cannot tolerate the TACE procedure due to the portal vein thrombosis often exhibit extremely poor prognostic outcomes. For these patients, administration of FOLFOX (fluorouracil, leucovorin, and oxaliplatin) through hepatic artery infusion chemotherapy (HAIC) has been commonly practiced owing to its higher response rates and improved survival outcomes compared with the sorafenib-based standard systemic treatment (2). However, outcomes of patients treated with HAIC alone or in combination with sorafenib were unsatisfactory (median overall survival: 10.8 - 14.5 months) (3–5).

Recently, HAIC combined with checkpoint blockade immunotherapy (CBI) is proposed to benefit patients with advanced HCC, since HAIC can reduce the tumor burden and induce immunogenic cell death to activate the host anti-tumor immunogenicity (6, 7). The modality of immune-HAIC has shown promising anti-tumor activities in advanced-stage HCC patients (8–10). However, about 40-60% of HCC patients ultimately progress to the non-objective response (Non-OR) disease after immune modulation-HAIC treatment. With the lack of effective treatment and growing demand for alternative aggressive cancer therapy for patients with Non-OR disease, early identification and diagnosis would be essential for formulating an efficient HCC management with a satisfactory prognosis.

To date, a huge gap between the knowledge of predictive biomarkers and the treatment response in HCC patients receiving immuno-HAIC therapy remains the major limitation. Several risk factors associated with poor response rates in HCC patients undergoing HAIC have been identified, including liver cirrhosis and hepatitis B virus (HBV) infection (11). However, due to occurrences of overlapping clinical factors among HCC patients with varying responses at baseline, effective prediction of individualized immune-HCC success rate in HCC patients has not been possible. Preliminary screening of HCC patients at high risk of progressing to the Non-OR status is an unmet need to predict the chance of aggressive treatment failure in this subset of patients.

Myosteatosis refers to abnormal distributions of adipose tissues between and within muscle cells, leading to excessive fat deposition in the muscle, a pathological situation associated with decreased muscle quality, limb function, and physical fitness. Myosteatosis is evaluated on the conventional computed tomography (CT) images, using the radiological characterization of skeletal muscle radiation attenuation (SMRA) (12–14). A growing body of evidence suggests myosteatosis as the negative indicator of poor treatment response and prognosis in several cancers, including HCC (15). However, there is limited understanding of the clinical impact of assessing the baseline body composition, for example, CT-derived myosteatosis, in HCC patients undergoing immune-HAIC therapy.

Therefore, this study evaluated the clinico-pathological implication of myosteatosis to abdominal CT images collected to determine treatment responses in HCC patients. We hypothesized that the CT-based evaluation of myosteatosis might be effective in predicting the probability of objective response (OR) to immune-HAIC in HCC patients prior to the treatment initiation. Early screening of HCC patients to determine the risk of Non-OR development and the urgent necessity of alternative aggressive therapy could be beneficial in reducing the HCC mortality rate.

PATIENTS AND METHODS

Study Design and Patients

Patients with histologically confirmed HCC between June 30, 2019, and July 30, 2021, were retrospectively identified from our hospital. Patient inclusion criteria were as follows: 1) age ≥18 years; 2) had portal vein invasion; 3) had disease progression or were intolerant to one or more systemic treatments with antiangiogenic tyrosine kinase inhibitors (TKIs); 4) an Eastern Cooperative Oncology Group (ECOG) performance score of 0-1; 5) belonged to Child Pugh Class A or B (score =7).While patients

having coexisting non-HCC malignancies, missing or suboptimal CT images, or missing complete clinical data were excluded from this study.

SM-RA measurements for myosteatosis were acquired from the baseline pre-enhanced abnormal CT images at the L3 vertebra level to build the predictive model of the risk of treatment failure. Descriptions of patient selection/recruitment and applied exclusion criteria are shown in **Figure 1**. This single-centered retrospective study protocol was approved by the Medical Ethics Committee of the Xiangya Hospital.

Data Collection

Information on the abdominal CT images, demographics, laboratory test results, clinical records, outcome data were retrieved from our hospital medical record archives. Only the available baseline data were included for analysis. All data were thoroughly reviewed by two independent, experienced clinicians (SL and YZ) who were blind to the clinical and pathological information of study subjects. A third reviewer (LS) was introduced to adjudicate any differences in interpretations between the two primary reviewers.

Treatment, Tumor Response Assessments, and Follow-Up

HAIC was conducted as reported previously (2). The femoral artery puncture following TACE was performed in every treatment cycle. FOLFOX was administered *via* a 2.7 French microcatheter connected to the feeding arteries of the tumor and associated thrombus at the following doses: on day 1, oxaliplatin at 85 mg/m^2 from 0 - 2 h; leucovorin at 400 mg/m^2 from 2 - 3 h, and 5-fluorouracil at 400 mg/m^2 bolus at 3 h, then at 2400 mg/m^2 over 46 h. PD-1 inhibitors, including pembrolizumab, camrelizumab, and toripalimab, were administrated intravenously within 3 days after HAIC. Decisions on the dose adjustment of FOLFOX, disruption or discontinuation of HAIC and/or PD-1 therapy were made at the discretion of the investigator based on the patient's clinical status.

Patients' radiological responses were assessed per hepatocellular carcinoma-specific modified RECIST guidelines (16) such as at the interval of every 6 to 8 weeks. Two experienced radiologists (XY, and LS with 11 and 20 years' experience, respectively), determined the tumor responses by consensus. In case of any discrepancy in the opinion between the two primary radiologists, a third radiologist (CC, with more than 30 years of experience in abdominal radiology) was introduced to determine the final tumor response by consensus.

The objective response (ORR) and disease control (DCR) rates were recorded. Progression-free survival (PFS) was defined as the time period between the treatment initiation and disease advancement or death. Overall survival (OS) was defined by the time period between the treatment initiation and cancer-related death.

Analysis of Abdominal CT Images and the Measurement of Body Composition

Patients' baseline abdominal CT scans taken prior to the initial treatment were retrieved from the PACS (Picture Archiving and Communication Systems, Carestream, Canada) of our hospital. The time length between the baseline abdominal CT imaging and treatment was 1 to 14 days. Reconstruction of all axial CT images was made to a uniform thickness of 1 mm.

One axially unenhanced image from the set of each abdominal CT scan at the L3 level was included. Back and abdominal wall muscles including the paraspinal, transversus abdominis, psoas, rectus abdominis, external and internal oblique muscles were segmented (manually) for each scan on the specific axial image. Then body compositions were measured on each of the segmented images using the ImageJ software (National Institutes of Health).

Multiple body composition measurement parameters such as the skeletal muscle area (SMA) (-29 to -150Hu), visceral fat area (VFA) (-150 to -50Hu), subcutaneous fat area (SFA) (-150 to -50Hu), skeletal muscle fat area (SMFA) (-150 to -30Hu), SM-RA, as well as the mean CT values of SMA (SM-Mean), VFA (VF-Mean), SFA (SF-Mean), SMFA (SMF-Mean) were calculated following the previously reported method (17). Subsequently, the skeletal muscle fat index (SMFI) and skeletal

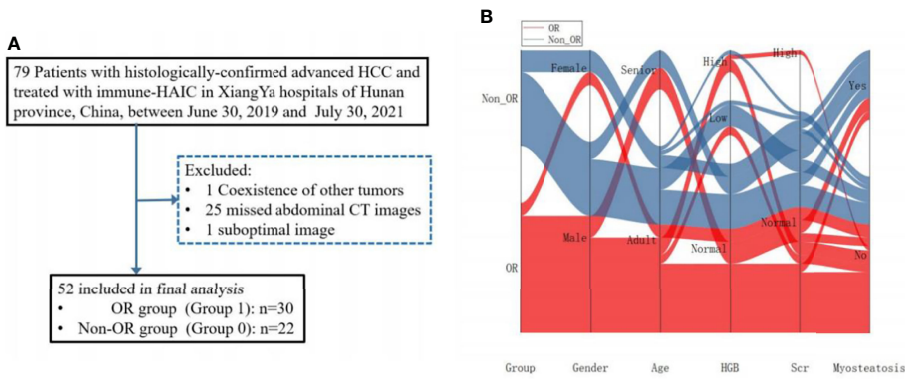

FIGURE 1 | **(A)** The flow-chart illustrating the recruiting procedure for hepatocellular carcinoma (HCC) patients. **(B)** Sankey diagram exhibiting projections of outcomes between the groups, gender, age, HGB, Scr, as well as Myosteatosis.

muscle index (SMI) were estimated with the normalization of the measured muscle area to the square height (cm^2/m^2). The CT imaging analysis and corresponding prediction modeling are illustrated in **Figure 2**.

Sarcopenia referred to the sex-specific cut-off points (Men: 52.4 cm^2/m^2; Women: 38.5 cm^2/m^2) for L3 SMI (18). Because of the unavailability of any established cutoff value for myosteatosis diagnosis, we determined the cut-off value of myosteatosis for the L3 SMI based on the gender stratified tertiles, which were adjusted to the lowest SM-RA tertile for the myosteatosis diagnosis.

Testing the Reproducibility of CT Body Composition Estimations

Thirty randomly picked abdominal CT images were independently segmented by two expert radiologists. The intra-observer (reader 1 two times) and inter-observer (reader 1 vs. reader 2) correlation coefficients (ICC) were calculated. The final consistency was assessed following the criteria applied to the ICC value, such as poor reproducibility at <0.20, fair reproducibility at 0.21–0.40, moderate reproducibility at 0.40–0.60, good reproducibility at 0.61–0.80, and excellent reproducibility at 0.81–1.00 values. The CT body composition measurement ICC (Inter-) values were ranged between 0.977 and 1.000, while that for the intra-observer ICC was ranged from 0.983 to 1.000. Hence, reader 1's body composition measurements were included in the subsequent analyses.

Risk Factors Associated With Treatment Response to Immunotherapy

Univariate and multivariable logistic regressions were executed to explore associations between risk factors and treatment responses. For survival analysis, Cox proportional hazard modeling was applied to reveal the connection between myosteatosis and PFS/OS in HCC patients. Adjusted odd ratio (OR) and hazard ratio (aHR) with 95% confidence interval (CI) were calculated to assess the effect size. Survival differences between patients with or without myosteatosis were compared using the log-rank test. Additionally, the correlation analyses between SM-RA and other clinical parameters were also performed.

An Individualized Prediction Model Development

The univariate logistic regression was conducted to evaluate the association between clinical/laboratory variables and myosteatosis, and risks of unfavorable outcomes. The univariate analysis (P<0.05) identified the predictor candidates, then the multivariate logistic regression analysis, including the likelihood ratio test, with Akaike's information criterion (AIC) as the stopping rule was applied to select the correlated factors. The optimal combination of factors was well-correlated with AIC minimums.

The numbers of predictors were set to <1/10-1/3 of the dependent group's number to control the overfitting. The number of potential features was restricted to not more than 6 for treatment-response predictions (20 Non-ORs). A model for predicting the probability of OR based on clinical data excluding myosteatosis parameters was developed. Subsequently, another model including myosteatosis parameters combined with the clinical model was constructed. A nomogram was created to support clinicians with an efficient quantitative tool in predicting the individual probability of response risk. Comparisons of performance data for these two models were carried out.

The Nomogram Validation and Model Performance Test

The nomogram was calibrated by evaluating calibration curves (Hosmer-Lemeshow H test), and the receiver operating characteristic (ROC) curve was plotted to assess the diagnostic efficiency. The final predictive performances of the two models

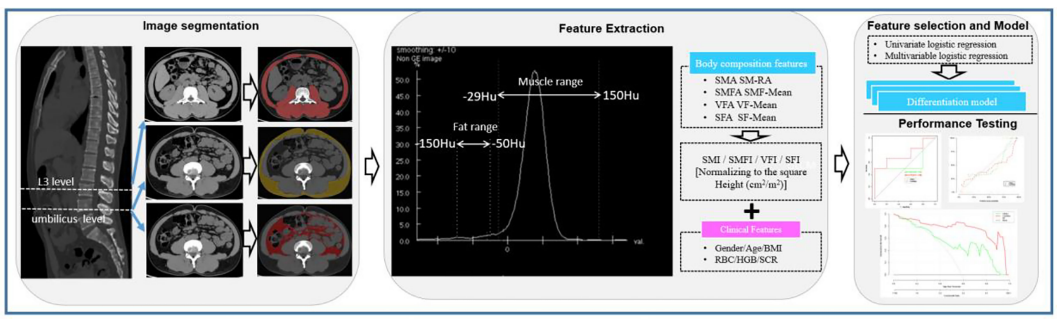

FIGURE 2 | Workflow for unenhanced abdominal CT images segmentation, feature extraction, selection, modeling, and performance testing for this study. (I) Segmentation of CT images. The third lumbar vertebra (L3) and umbilical level were selected for the body composition feature extractions. (II) Strategy for extracting body composition features from selected CT images. (III) Feature selection and prediction model construction with the univariate and multivariate logistic regressions based on the body composition and clinical features. Receiver operating characteristic (ROC) and calibration curves were applied to assess the model performance. Decision curve analysis was carried out to evaluate the clinical values of prediction models. L3 level, the third lumbar vertebra; SMA, skeletal muscle area; SM-RA, skeletal muscle radiation attenuation; SMFA, skeletal muscle fat area; SMF-Mean, skeletal muscle fat mean; VFA, visceral fat area; VF-Mean, visceral fat mean; SFA, subcutaneous fat area; SF-Mean, subcutaneous fat mean; SMI, skeletal muscle index; SMFI, skeletal muscle fat index; VFI, visceral fat index; SFI, subcutaneous fat index; RBC, red blood cell; HGB, hemoglobin; Scr, serum creatinine.

were examined using the 4-fold cross-validation strategy, and the average performance of the model was presented as the cross-validated performance. A 1000-iteration bootstrap analysis was performed for the proposed model to estimate the prediction error. A random subset of 70% of patients from either the validation or training cohort was selected for each repetition, and the respective AUC values were determined. The clinical applications of the nomogram were evaluated using the decision curve analysis in the validation cohort.

Next-Generation Sequencing

The mutation status of targeted genes was determined by next-generation sequencing using tumor sample (Foundation Medicine, Cambridge, Massachusetts, USA). The targeted DNA library comprising 425 genes for panel sequencing was constructed by blood-based circulating tumor DNA next-generation sequencing (Nanjing Shihe Jiyin Biotechnology Inc. Nanjing, China). In brief, extracted tumor genomic DNA was fragmented into 300~350bp using Covaris M220 instrument (Covaris). Sequencing libraries were prepared with KAPA Hyper Prep kit (KAPA Biosystems) with optimized protocols.

Analyses of Interrelationships Between Body Composition, Clinical and Genetic Features

The association between the identified significant body composition features and clinical features or genetic features was also examined using the correlation matrix analysis (Pearson or Spearman analysis). The scanter plot and heat-map plot were drawn, respectively.

Statistical Analysis

Statistical analyses were conducted using the R software (v3.5.2; http://www.Rproject.org) or SPSS v22.0 (IBM, United States). Univariate analysis for clinical features was executed by the chi-squared (χ^2) test for categorical variables or the Mann-Whitney U test for continuous variables, as appropriate to compare differences between the patients with non-severe and severe illnesses. The calibration plotting and nomogram construction were conducted using the "rms" package (R software). Two-sided statistical significance analyses were performed with the cut-off P=0.05.

RESULTS

Patient Characteristics

Fifty-two patients receiving HAIC combining anti-PD-1 immunotherapy were included in this study. Amongst them, 30 patients had the OR disease, including one complete response (CR) and 29 partial responses (PR). The ORR was 57.7%. The remaining 22 patients exhibited the Non-OR status, including 10 with stable disease (SD) and 12 with progressive disease (PD).

Significant differences between the OR and Non-OR groups were detected for several laboratory biomarkers, including hemoglobin (HGB), red blood cells (RBC), serum, and creatinine (Scr) level (**Table 1**). There were no statistically significant differences between the effective and invalid groups in terms of other clinical variables.

Myosteatosis Measurements in Patients With OR and Non-OR Disease

Body composition features of all patients are shown in **Table 1**. In comparison to the Non-OR group, the OR patients exhibited a significantly higher skeletal muscle density (median SM-RA: 46.05 Hu vs. 41.47 Hu), and lower incidences of myosteatosis (16.7% vs. 50.0%) with P=0.007 (**Table 1**). The above differences were also reflected in the following two specific cases (**Figure 3**). Moreover, OR patients demonstrated a lower VF density (mean: -95.07 Hu vs. -89.61 Hu). There were no significant differences between the two groups in the remaining body composition parameters, such as SMI and the incidence of sarcopenia.

Patient characteristics for the comparison between patients with or without myosteatosis status are described in **Table 1**.

Association of SM-RA With OR, OS and PFS in HCC

To further access the association of SM-RA with the treatment response and prognosis in HCC patients receiving HAIC combined with PD-1 immunotherapy, binary logistic regression and Cox proportional hazard models were constructed. Our results (**Tables 2**–**4**) demonstrated that a lower SM-RA was an independent risk predictor for treatment failure, shorter PFS and OS, in this cohort of HCC patients, after adjusting all other risk factors, including gender, age, HGB, Scr, and VFmean (AOR=1.21, 95% CI: 1.02-1.44, P=0.033; AHR for PFS=0.92, 95%CI: 0.85-0.99, P=0.023; AHR for OS=0.91, 95%CI: 0.84-0.98, P=0.012). We also found that a higher VFmean value at baseline was an independent indicator for OS in this cohort.

Impact of Myosteatosis on the Performance of Prediction Models

The clinical model developed, including RBC, HGB, Scr, and VFmean achieved a mild efficiency with an average AUC of only 0.62 (95% CI: 0.25-0.94). After the addition of SM-RA to this model, we observed a significant improvement in the performance of the combined prediction model, with an average AUC of 0.711 (95%CI: 0.75-0.95) (**Figures 4A–C**).

The calibration curve of the nomogram revealed significant agreement between predicted and observed values (Hosmer-Lemeshow H test, P =0.680, **Figure 4D**). Decision curve analysis demonstrated that if the threshold probability of a doctor or a patient was >5%, application of the nomogram to predict the OR status in HCC patients could add extra benefits than either the diagnose-none or diagnose-all-patients scheme (**Figure 4E**). Importantly, the combined model offered more clinical utilitilizations than the clinical model alone beyond the threshold of~10%.

Survival Analysis

The median follow-up period was 10.0 months (IQR: 6.0-13.8, range: 2.0–21.0 months) for all patients. The median PFS and OS

TABLE 1 | Demographic, clinical, laboratory, pathologic and body composition characteristics of 52 HCC patients.

Characteristic	Total (n=52)	Objective remission (n=30)	Non-objective remission (n=22)	*P* Value	Myosteatosis (n=16)	Non-myosteatosis (n=36)	*P* Value
Demographics and clinical characteristics							
Gender (n, %)				0.209			0.701
Male	44 (84.6)	27 (90)	17 (77.3)		14 (87.5)	30 (83.3)	
Female	8 (15.4)	3 (10)	5 (22.7)		2 (12.5)	6 (16.7)	
Age (y)#	50 (42-58)	50 (45-57)	49 (39-58)	0.824	58 (51-68)	47 (39-54)	0.001
BMI#	24.1 (22.5-26.6)	23.6 (22.5-26.9)	24.3 (21.8-26.7)	0.817	24.9 (23.1-28.1)	23.5 (22.4-26.3)	0.378
HBV Infection (n, %)				0.584			0.412
Yes	41 (80.8)	25 (83.3)	17 (77.3)		14 (87.5)	28 (77.8)	
No	10 (19.2)	5 (16.7)	5 (22.7)		2 (12.5)	8 (22.2)	
Child-Pugh (n, %)				0725			0.412
A	42 (80.8)	25 (83.3)	17 (77.3)		14 (87.5)	28 (77.8)	
B	10 (19.2)	5 (16.6)	5 (22.7)		2 (12.5)	8 (22.2)	
Port vein invasion (n, %)				0.971			0.842
Vp1-2	5 (9.6)	3 (10.0)	2 (9.1)		2 (12.5)	3 (8.3)	
Vp3	25 (48.1)	14 (46.7)	11 (50.0)		8 (50.0)	17 (47.2)	
Vp4	22 (42.3)	13 (43.3)	9 (40.9)		6 (37.5)	16 (44.4)	
Extrahepatic site (n, %)				0.526			1.000
Absent	40 (76.9)	22 (76.7)	18 (77.3)		12 (75.0)	28 (77.8)	
Present	12 (23.1)	8 (23.3)	4 (22.7)		4 (25.0)	8 (22.2)	
Laboratory findings							
Blood routine test							
WBC (10^9/L)#	4.7 (3.2 -5.9)	4.5 (3.5-6.3)	4.7 (2.9-5.6)	0.863	4.6 (3.1-5.5)	4.7 (3.3-6.3)	0.736
RBC (10^9/L)#	4.2 (4.0 -4.7)	4.3 (4.1-4.8)	4.1 (3.9-4.37)	0.044	4.1 (3.9-4.4)	4.2 (4.16-4.8)	0.177
HGB (g/L)#	130.0 (118.8-144.3)	131.5 (127.0-148.8)	128.0 (112.3-133.0)	0.014	128.5 (117.0-134.8)	131.0 (121.5-150.3)	0.201
PLT (10^9/L)#	122.5 (78.3-206.0)	124.0 (64.5-198.0)	119.0 (88.5-225.8)	0.560	119.0 (76.3-184.3)	124.0 (78.3-232.5)	0.781
Liver function test							
TP (g/L)#	68.0 (63.4-72.9)	68.0 (63.6-71.8)	67.0 (63.1-74.9)	0.889	65.2 (65.8-71.0)	69.5 (65.3-74.9)	0.113
Albumin (g/L)#	37.6 (34.1-40.8)	37.6 (34.6-41.8)	37.4 (31.3-39.3)	0.274	35.6 (31.7-38.9)	38.0 (34.5-41.9)	0.129
Globulin (g/L)#	30.1 (27.0-34.3)	29.2 (27.4-32.7)	33.1 (25.9-41.4)	0.295	29.2 (25.5-34.1)	30.8 5(27.0-34.7)	0.804
ALT (U/L)#	42.3 (28.4-62.2)	45.6 (29.6-72.7)	33.7 (25.8-52.6)	0.082	46.6 (29.9-61.6)	39.0 (27.3-62.2)	0.378
AST (U/L)#	65.8 (37.9-89.8)	61.6 (38.2-84.6)	74.3 (36.4-100.1)	0.493	78.2 (52.6-146.2)	61.2 (5.1-79.4)	0.052
Tbile (μmol/L)#	15.7 (10.5-23.7)	15.9 (10.0-24.1)	15.0 (11.3-23.8)	0.817	19.6 (13.3-27.9)	14.2 (10.0-21.9)	0.132
Scr (mg/dl)#	75.5 (65.0-90.6)	82.5 (66.0-93.3)	70.9 (57.9-81.9)	0.022	68.5 (58.2-82.6)	77.4 (66.0-91.0)	0.102
AFP							
<400 ng/mL	21 (40.4)	13 (43.3)	8 (36.4)		6 (37.5)	15 (41.7)	
≥400 ng/mL	31 (59.6)	17 (56.7)	14 (63.6)		10 (62.5)	21 (58.3)	
CT-based body composition							
SMFmean#	-56.8 (-59.5-54.3)	-56.3 (-58.8-54.6)	-58.2 (-61.5-53.4)	0.259	-56.8 (-59.1-54.3)	-56.9 (-59.9-54.7)	0.968
Myomean#	12.3 (9.8-13.9)	12.5 (9.8-13.4)	12.2 (9.7-14.5)	0.970	11.0 (9.8-12.7)	12.8 (9.8-14.5)	0.104
VFmean#	-92.3 (-96.4-85.2)	-95.1 (-97.8-87.9)	-89.6 (-95.2-82.6)	0.036	-89.8 (-95.8-83.6)	-97.3 (-101.4-91.7)	0.648
SFmean#	-97.4 (-101.6-91.3)	-98.2 (-102.1-93.4)	-94.8 (-101.4-88.6)	0.236	-97.7 (-104.0-89.8)	-97.3 (-101.4-91.7)	0.706

(Continued)

TABLE 1 | Continued

Characteristic	Total (n=52)	Objective remission (n=30)	Non-objective remission (n=22)	*P* Value	Myosteatosis (n=16)	Non-myosteatosis (n=36)	*P* Value
SMFI#	1.4 (0.7-2.5)	1.1 (0.6-1.9)	1.5 (0.8-3.2)	0.115	2.5 (1.5-3.1)	0.9 (0.6-1.6)	0.0005
SMI#	42.4 (39.1-47.5)	45.1 (40.5-48.2)	40.8 (31.6-45.2)	0.078	41.1 (33.1-52.5)	42.7 (39.2-47.2)	0.565
VFI#	40.1 (28.7-53.1)	41.6 (27.9-57.2)	39.7 (31.4-50.4)	0.767	41.0 (33.1-52.5)	39.3 (27.3-53.2)	0.341
SFI#	51.3 (35.4-69.2)	50.6 (30.6-63.2)	51.3 (35.8-80.2)	0.517	51.33 (39.0-69.2)	49.3 (31.7-69.0)	0.89
SVR#	1.2 (1.0-1.6)	1.1 (0.9-1.5)	1.3 (1.0-2.0)	0.159	1.1 (1.0-1.4)	1.3 (0.9-2.0)	0.394
SM-RA#	44.3 (40.2-48.6)	46.1 (43.1-50.1)	41.5 (37.2-45.9)	0.007	37.6 (36.2-40.2)	46.7 (44.0-50.6)	0.000
Sarcopenia, n (%)				0.393			
Yes	45 (86.5)	27 (90)	18 (81.8)		14 (87.5)	31 (86.1)	
No	7 (13.5)	3 (10)	4 (18.2)		2 (12.5)	5 (13.9)	
Myosteatosis, n (%)				0.010			
Yes	16 (30.8)	5 (16.7)	11(50.0)				
No	36 (69.2)	25 (83.3)	11 (50.0)				

Unless otherwise indicated, data are numbers of patients, and data in parentheses are percentages. #represents data was presented as media (IQR, inter-quartile range). BMI, Body Mass Index; SBP, Systolic Blood Pressure; DBP, Diastolic Blood Pressure; HBV, Hepatitis B Virus; WBC, white blood cell; RBC, Red Blood Cell; HGB, Hemoglobin; PLT, Platelet count; TP, Total, Protein; ALT, Alanine aminotransferase; AST, Aspartate aminotransferase; Tbile, Total Bilirubin; Scr, Serum creatinine; AFP, A-fetoprotein; SMFmean, skeletal muscle fat mean; Myomean, Myosteatosis mean; VFmean, visceral fat mean; SFmean, subcutaneous fat mean; SMFI, skeletal muscle fat index; SMI, skeletal muscle index; VFI, visceral fat index; SFI, subcutaneous fat index; SVR, Surface-Volume Ratio; SM-RA, skeletal muscle radiation attenuation.

were 7.1 and 15.6 months, respectively. Patients with OR demonstrated significantly better PFS (median ± SD, 8.0 ± 0.6 months) and OS (20.0 ± 1.4 months) time when compared to that of Non-OR patents (PFS, 3.0 ± 0.5; OS, 6.0 ± 1.8, months) (**Figures 5A, B**) (*P*<0.001).

For patients without myosteatosis, there were significantly higher PFS (8.0 ± 0.4 months) (*P*<0.001) and OS (19.0 ± 2.8 months) (*P*=0.003) time when compared to patients with myosteatosis (PFS, 4.0 ± 0.5; OS, 9.0 ± 3.4, months) (**Figures 5C, D**).

Correlation Analysis

The correlation analysis results indicated that the SM-RA was positively correlated with the serum HGB (r=0.518, *P*<0.001),

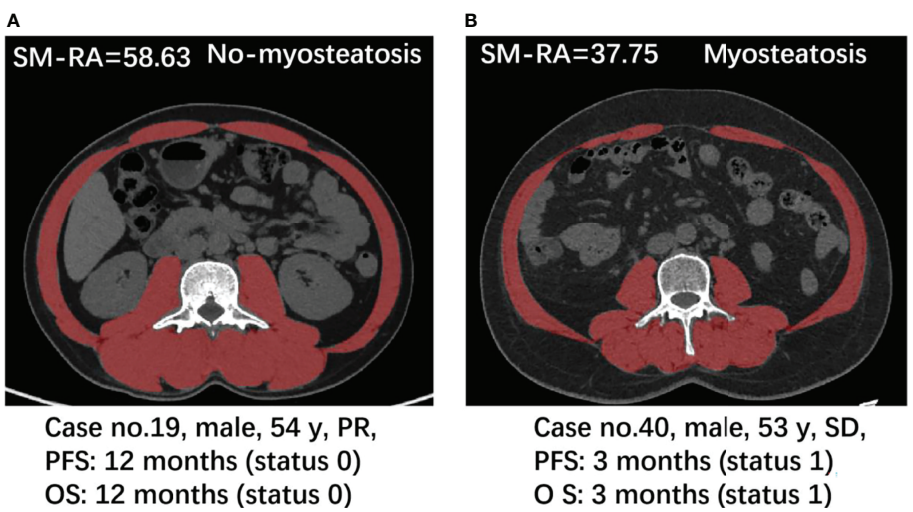

FIGURE 3 | Case presentation. Axial CT images at the L3 level used for the measurement of multiple parameters for body composition, respectively in a 54-year-old man with PR **(A)** and a 53-year-old man with SD **(B)**.

TABLE 2 | Associations of lower SM-RA with treatment response of HAIC combined with immunotherapy in 52 patients with advanced HCC.

Vaiable	Model Ia		Model IIb		Model IIIc	
	AOR (95%CI)	*P*	AOR (95%CI)	*P*	AOR (95%CI)	*P*
SM-RA	1.258 (1.081, 1.463)	0.003	1.203 (1.019 1.420)	0.029	1.209 (1.016, 1.438)	0.033

SM-RA, Skeletal muscle radiation attenuation; HAIC, hepatic artery infusion chemotherapy; AOR, adjusted odd ratio; CI, confidence interval; VFmean, Mean CT value of visceral fat.
a Adjusted for gender and age.
b Additionally adjusted for hemoglobin and Serum creatinine.
c Additionally adjusted for VFmean.

TABLE 3 | Associations of lower SM-RA with progression free survival (PFS) of HAIC combined with immunotherapy in 52 patients with advanced HCC.

Vaiable	Model Ia		Model IIb		Model IIIc	
	AHR (95%CI)	*P*	AHR (95%CI)	*P*	AHR (95%CI)	*P*
SM-RA	0.896 (0.841, 0.954)	0.001	0.902 (0.839, 0.970)	0.005	0.915 (0.848, 0.988)	0.023

SM-RA, Skeletal muscle radiation attenuation; HAIC, hepatic artery infusion chemotherapy; AHR, adjusted hazard ratio; CI, confidence interval.
a Adjusted for gender and age.
b Additionally adjusted for hemoglobin.
c Additionally adjusted for Serum creatinine.

TABLE 4 | Associations of lower SM-RA with overall survival (OS) of HAIC combined with immunotherapy in 52 patients with advanced HCC.

Vaiable	Model Ia		Model IIb		Model IIIc	
	AHR (95%CI)	*P*	AHR (95%CI)	*P*	AHR (95%CI)	*P*
SM-RA	0.933 (0.879, 0.990)	0.023	0.896 (0.835, 0.962)	0.002	0.905 (0.837, 0.978)	0.012
VFmean	1.063 (1.007, 1.121)	0.026	1.076 (1.013, 1.142)	0.017	1.072 (1.009, 1.138)	0.017

SM-RA, Skeletal muscle radiation attenuation; HAIC, hepatic artery infusion chemotherapy; AHR, adjusted hazard ratio; CI, confidence interval; VFmean, Mean CT value of visceral fat.
a Before adjusted for other variables.
b Adjusted for gender and age.
c Additionally adjusted for hemoglobin.

albumin (r=0.402, *P*=0.003), Scr (r=0.368, *P*=0.007) levels, and negatively correlated with aspartate aminotransferase (AST) (r=-0.398, *P*=0.003) (**Figure 6**). In addition, there is no significant relationship between SM-RA and common tumor-related factors, such as AFP (P=0.121), metastasis (P=0.731) and portal vein invasion (P=0.306). Furthermore, there were significant associations between VFmean and KRAS mutations (r=-0.590, *P*=0.021), RBC count, FAT1 mutation (r=-0.521, *P*=0.046), Scr level, and ROS1 mutation (r=-0.545, *P*=0.036) (**Figure 7**).

From the pathway analysis of gene mutations, the following pathways might be associated with these meaningful radiological and clinical features, including cell_morphogenesis, epithelial _cell_development, Sphingolipid_metabolism, chromatin_or ganization, and Integrated_breast_cancer_pathway (**Figure 8**).

DISCUSSION

Here, we detected the CT-derived myosteatosis measurement as the independent predictor for OR and prognosis in HCC patients undergoing immune-HAIC therapy. Our combined prediction model and the pre-treatment clinical and laboratory data showed a modest performance level in differentiating patients with a higher probability of OR disease risks from those with lower risks. In summary, this study showed the promising prognostic value of myosteatosis for assessing HCC patients undergoing immune-HAIC treatment in the clinical setting.

Our findings of the importance of abdominal myosteatosis in predicting the OR of HCC patients receiving the immune-HAIC treatment were in line with prior studies reporting adverse effects of myosteatosis in various cancers, including HCC. Myosteatosis is positively associated with accelerated disease severity, higher level of complications, longer hospital stays, worse prognosis, and earlier postoperative recurrence. Recently myosteatosis has been linked to the weak physical state of patients (12), a higher risk of developing severe symptoms (19), and shorter survival (20). Thus, we speculated that patients with myosteatosis of this cohort might have implicated relatively poor physical fitness, resulting in a higher susceptibility to treatment failure.

Moreover, patients in the Non-OR group not only showed significantly higher rates of myosteatosis (54.5% vs. 13.3%) and VF-Mean but also exhibited a higher SMFI and lower SMI values, but not at a statistically significant level, owing to the smaller cohort size. A higher SMFI value indicated enhanced subcutaneous adipose tissue depositions in abdominal muscles, which could lead to obesity, an important underlying etiological factor of myosteatosis. Metabolically active visceral adipose tissue secretes and/or synthesizes many proteins that can lead to the onset of liver carcinoma (21). An increased fat density may represent inflammatory changes in the body. It is reported that the serum

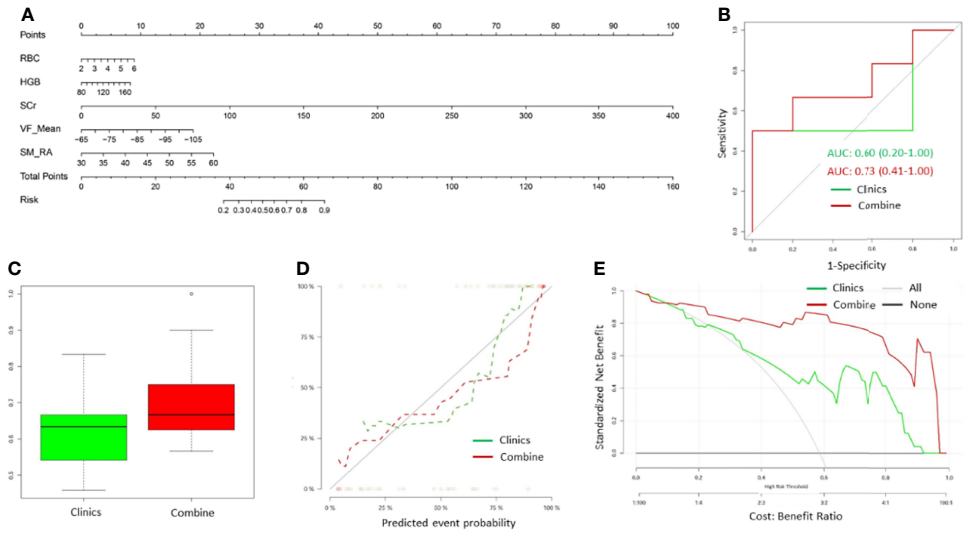

FIGURE 4 | The myosteatosis nomogram, ROC curve, calibration curve, and decision curve for predicting unfavorable outcomes in advanced-stager HCC patients treated with hepatic artery infusion chemotherapy (HAIC) combined with PD-1 immunotherapy. **(A)** Myosteatosis nomogram was constructed in the training cohort, including SM-RA, VFMean, Scr, HGB, and RBC. Risk represents the probability that the patient may obtain ORR after treatment. **(B)** An example of ROC curves for the independent training cohort for both clinical and combined models. **(C)** Box plots showing the AUCs for the clinical and combined models in multiple modeling processes. The green label indicates the clinical model, and the red indicates the combined model. **(D)** Calibration curves of the myosteatosis nomogram for clinical and combined models. **(E)** Decision curve analysis of the myosteatosis nomograms for the combined and clinical model alone. The Y-axis measures the net benefit. The green line represents the decision curve for the clinical model. The red line represents the decision curve for the combined model with the addition of CT myosteatosis features to the clinical model. The black line represents the assumption that no patients had the risk of transitioning to unfavorable outcomes, and the grey line represents all patients who would transition to unfavorable outcomes.

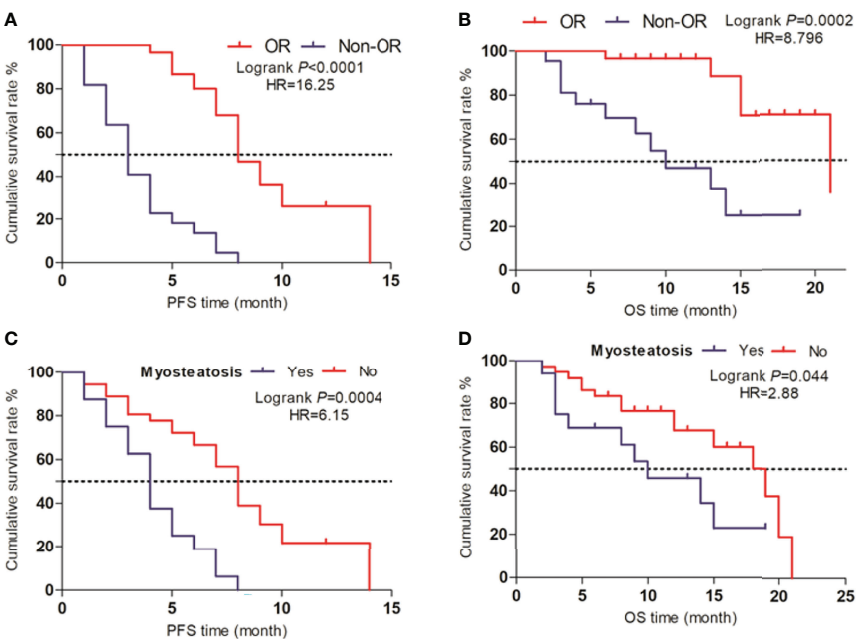

FIGURE 5 | Survival analysis **(A, B)** Life curves showing the PFS and OS time periods between the OR and Non-OR groups. **(C, D)** Life curves showing the PFS and OS time periods between patients with myosteatosis and non-myosteatosis.

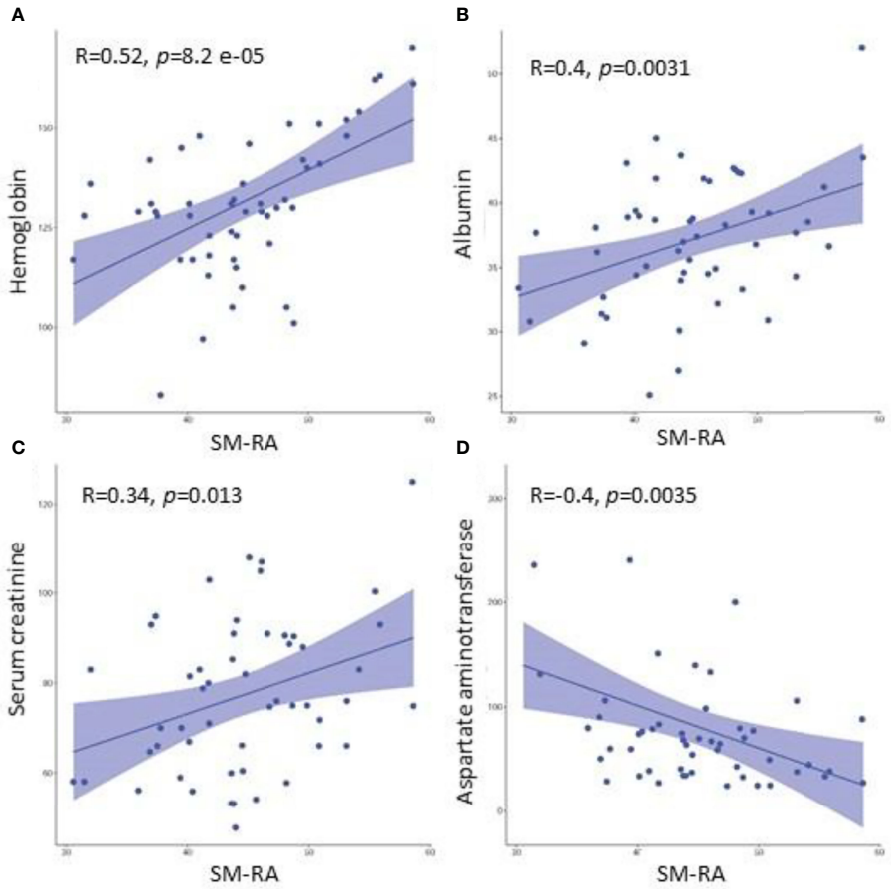

FIGURE 6 | Associations between the SM-RA and clinical parameters (HGB, albumin, Scr, AST). Scatter plots demonstrate that SM-RA is positively associated with HGB **(A)**, albumin **(B)**, and Scr **(C)**, while negatively correlated with AST **(D)**. HGB, hemoglobin; A, albumin; Scr, Serum creatinine; AST, Aspartate aminotransferase.

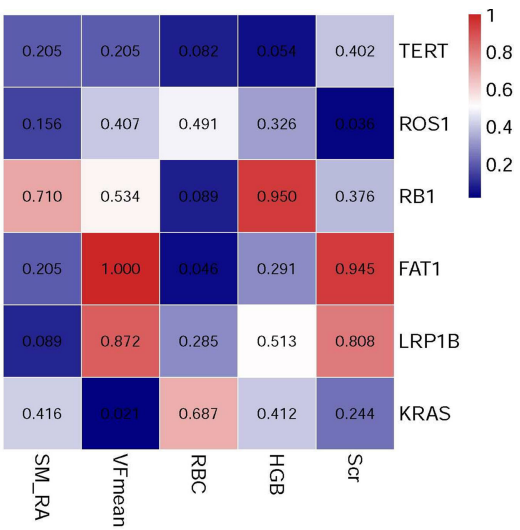

FIGURE 7 | The heat map illustrates associations between the genetic mutation and selected body composition features and clinical variables.

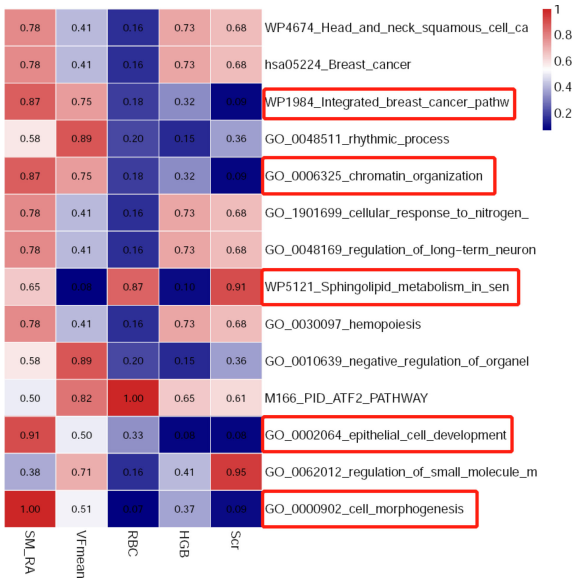

FIGURE 8 | The heat map indicating associations between related biological pathways and selected body composition features and clinical variables.

inflammatory cytokines' levels are correlated with survival and OR to various cancer therapies (22). There is a shortage of relevant knowledge about the possible reasons for the association between visceral fat inflammation, immunotherapeutic responses, and poor prognosis of liver cancer, and further explorations need to be continued. Furthermore, the independent association between a lower SMI (sarcopenia) and worse survival in cancer patients has been widely reported, including HCC. We, therefore, hypothesized that patients with myosteatosis might have simultaneously undergone muscular atrophy and obesity as reflected by their higher SMFI values, substantially predisposing them to a higher HCC risk.

The underlying pathophysiological association between the myosteatosis and worse response to immune-HAIC therapy and prognosis in HCC patients has not been explored. In this study, we found a positive correlation between the SM-RA and serological indicators (HGB, albumin, Scr, and AST) in HCC patients, which indicated the nutritional status, organ function, and metabolic status of the body. Recent reports have also shown that skeletal muscle quality (myosteatosis), rather than quantity (sarcopenia), is an independent prognostic marker for a variety of tumorigenesis (15, 23). Therefore, myosteatosis may be useful for quantitatively assessing a common clinical phenotype for the overall status of the body, such as metabolic status, gene status, obesity, inflammation and so on, which is thought to underlie variability in responses to immune-HAIC therapy and prognosis in HCC. On the one hand, this pathological linkage might have played a role in the induced effectiveness of immune-HAIC treatment in HCC. Several studies have suggested that patients' metabolic state is a critical modulator of the effectiveness of immune checkpoint inhibitors (24). Turner et al. revealed a strong association between pembrolizumab (a kind of ICI) clearance and prognosis. Patients with high pembrolizumab clearance rates showed significantly lower survival rates compared to that in patients with low clearance rates, suggesting that the major catabolic pathway of pembrolizumab could be influenced by factors that might also be involved in the development of cancerous cachexia, including myosteatosis. Therefore, myosteatosis patients with muscle weakening/wasting in our cohort might have resulted in a high nivolumab clearance status, which could partly be responsible for a worse therapeutic response and prognosis. Hence, myosteatosis with poor muscle quality in this cohort of patients could be due to metabolic disturbances, which are further associated with an increased risk of worse treatment response and survival time. Since many patients may have simultaneous muscle mass loss (sarcopenia), relative measurements of the body composition changes may facilitate or guide the effectiveness of ICI treatment. On the other hand, we believe the potential for improving interpretability of body composition features, such as myotsteatosis for prediction of treatment response may be assessed in several ways. First, correlation matrix evaluation may be performed between myosteatosis and clinical parameters which may be associated with treatment response in HCC, such as serum creatinine level, albumin (25), etc. This approach may help to understand how body composition features may be associated with the routine clinical features that are commonly used in clinical practice. Second, body composition features may reflect the biological behavior of the tumor such as tumor aggressiveness status, which should help to predict response to treatment.

The performance of our prediction models also reflected the role of myosteatosis as a predictor for treatment response and prognosis. Upon the addition of SM-RA, the efficacy of our

combined prediction model was significantly improved for predicting therapeutic efficacies in HCC patients. In addition, the modest differentiation efficiency of our model was also attributed to the introduction of several clinical and radiological parameters, including RBC, HGB, Scr, and VFmean, whose potential prognostic roles were investigated in previous studies. For example, RBC (26) and HGB (27) have been shown to be critical risk factors for poor prognosis in HCC patients. Relatively reduced Scr level in the Non-OR group when compared to that in the OR group suggested a significant loss of skeleton muscle mass (sarcopenia), which was clearly visible in our cohort and was reported to be associated with the poor prognosis in HCC. As a potential marker for visceral fat inflammatory response, increased VFmean could be associated with a higher risk of treatment failure and poor prognosis in HCC patients. A recent study has reported that elevated visceral fat inflammation is frequently observed in HCC patients indicating the possibility of an unfavorable prognosis. Therefore, it was not surprising to notice that the model performance was significantly improved after incorporating these known etiological factors associated with unfavorable outcomes.

RAS mutation is the second most important oncogenic driver in liver carcinoma (28, 29). KRAS mutations are pathologically linked to the increased expression of PD-L1 (30), a known predictor of treatment response to ICIs. However, some of the recent studies have suggested that patients with activating mutations in the *KRAS* gene may benefit from PD-1 blockade (31, 32). Interestingly, we revealed a negative correlation between the VFmean and *KRAS* mutations in this study. However, it is still uncertain whether there is a causal relationship between these two factors. Further investigations are warranted to determine the association between the VFmean and *KRAS* mutation.

There are a few limitations to this study. First, it was a single-centered retrospective study that might involve the case selection bias. Second, despite the inclusion of a relatively large number of OR patients, the number of cases with Non-OR was relatively small, which could have affected the performance of the predictive models as well as the generalizability of our study results. Third, our research lacks external validation, which may potentially affect the generalization ability of our results. Large-scale multicenter prospective studies with a standardized imaging protocol and the standard body composition measurement tool should be important to validate our results.

CONCLUSIONS

Measurements of CT-derived myosteatosis could be associated with a higher risk of treatment failure and poor prognosis in HCC patients undergoing immune-HAIC therapy. The myosteatosis nomogram constructed in this study could potentially support an individualized prediction of treatment response and prognosis, thus assisting in making treatment decisions for HCC patients before the initiation of immune-HAIC. This study revealed potential clinical uses of the body composition analysis in the overall assessment of disease outcomes in HCC patients.

DATA AVAILABILITY STATEMENT

The original contributions presented in the study are included in the article/supplementary material. Further inquiries can be directed to the corresponding author.

ETHICS STATEMENT

The studies involving human participants were reviewed and approved by the Medical Ethics Committee of the Xiangya Hospital. The patients/participants provided their written informed consent to participate in this study. Written informed consent was obtained from the individual(s) for the publication of any potentially identifiable images or data included in this article.

AUTHOR CONTRIBUTIONS

All authors listed have made a substantial, direct and intellectual contribution to the work, and approved it for publication.

FUNDING

This work was supported by grants from the National Natural Science Foundation of China (No. 81773234) and Scientific Research Project of Hunan Health and Health Commission (No. C2019189).

ACKNOWLEDGMENTS

We thank all referring hospital staff from Department of Radiology for their efforts in assisting data collection and analysis.

REFERENCES

1. Sung H, Ferlay J, Siegel RL, Laversanne M, Soerjomataram I, Jemal A, et al. Global Cancer Statistics 2020: GLOBOCAN Estimates of Incidence and Mortality Worldwide for 36 Cancers in 185 Countries. *CA Cancer J Clin* (2021) 71(3):209–49. doi: 10.3322/caac.21660
2. Vejdani-Noghreiyan A, Ebrahimi-Khankook A. An Age-Dependent Series of Eye Models for Radiation Dosimetry. *Phys Med Biol* (2019) 64(13):135004. doi: 10.1088/1361-6560/ab2059
3. He M, Li Q, Zou R, Shen J, Fang W, Tan G, et al. Sorafenib Plus Hepatic Arterial Infusion of Oxaliplatin, Fluorouracil, and Leucovorin vs Sorafenib Alone for Hepatocellular Carcinoma With Portal Vein Invasion: A

Randomized Clinical Trial. *JAMA Oncol* (2019) 5(7):953–60. doi: 10.1001/jamaoncol.2019.0250
4. Lyu N, Wang X, Li JB, Lai JF, Chen QF, Li SL, et al. Arterial Chemotherapy of Oxaliplatin Plus Fluorouracil Versus Sorafenib in Advanced Hepatocellular Carcinoma: A Biomolecular Exploratory, Randomized, Phase III Trial (FOHAIC-1). *J Clin Oncol* (2022) 40 (5):468–80. doi: 10.1200/JCO.21.01963
5. Lyu N, Kong Y, Mu L, Lin Y, Li J, Liu Y, et al. Hepatic Arterial Infusion of Oxaliplatin Plus Fluorouracil/Leucovorin vs. Sorafenib for Advanced Hepatocellular Carcinoma. *J Hepatol* (2018) 69(1):60–9. doi: 10.1016/j.jhep.2018.02.008
6. Llovet JM, De Baere T, Kulik L, Haber PK, Greten TF, Meyer T, et al. Locoregional Therapies in the Era of Molecular and Immune Treatments for Hepatocellular Carcinoma. *Nat Rev Gastroenterol Hepatol* (2021) 18(5):293–313. doi: 10.1038/s41575-020-00395-0
7. Kepp O, Marabelle A, Zitvogel L, Kroemer G. Oncolysis Without Viruses - Inducing Systemic Anticancer Immune Responses With Local Therapies. *Nat Rev Clin Oncol* (2020) 17(1):49–64. doi: 10.1038/s41571-019-0272-7
8. Mei J, Li SH, Li QJ, Sun XQ, Lu LH, Lin WP, et al. Anti-PD-1 Immunotherapy Improves the Efficacy of Hepatic Artery Infusion Chemotherapy in Advanced Hepatocellular Carcinoma. *J Hepatocell Carcinoma* (2021) 8:167–76. doi: 10.2147/JHC.S298538
9. Liu BJ, Gao S, Zhu X, Guo JH, Kou FX, Liu SX, et al. Real-World Study of Hepatic Artery Infusion Chemotherapy Combined With Anti-PD-1 Immunotherapy and Tyrosine Kinase Inhibitors for Advanced Hepatocellular Carcinoma. *Immunotherapy* (2021) 13(17):1395–405. doi: 10.2217/imt-2021-0192
10. Xu YJ, Lai ZC, He MK, Bu XY, Chen HW, Zhou YM, et al. Toripalimab Combined With Hepatic Arterial Infusion Chemotherapy Versus Lenvatinib for Advanced Hepatocellular Carcinoma. *Technol Cancer Res Treat* (2021) 20:15330338211063848. doi: 10.1177/15330338211063848
11. Hepatocellular Carcinoma. *Nat Rev Dis Primers* (2021) 7(1):7. doi: 10.1038/s41572-021-00245-6
12. Hamaguchi Y, Kaido T, Okumura S, Kobayashi A, Hammad A, Tamai Y, et al. Proposal for New Diagnostic Criteria for Low Skeletal Muscle Mass Based on Computed Tomography Imaging in Asian Adults. *Nutrition* (2016) 32(11-12):1200–5. doi: 10.1016/j.nut.2016.04.003
13. Nemec U, Heidinger B, Sokas C, Chu L, Eisenberg RL. Diagnosing Sarcopenia on Thoracic Computed Tomography: Quantitative Assessment of Skeletal Muscle Mass in Patients Undergoing Transcatheter Aortic Valve Replacement. *Acad Radiol* (2017) 24(9):1154–61. doi: 10.1016/j.acra.2017.02.008
14. Chindapasirt J. Sarcopenia in Cancer Patients. *Asian Pac J Cancer Prev* (2015) 16(18):8075–7. doi: 10.7314/APJCP.2015.16.18.8075
15. Meister FA, Lurje G, Verhoeven S, Wiltberger G, Heij L, Liu WJ, et al. The Role of Sarcopenia and Myosteatosis in Short- and Long-Term Outcomes Following Curative-Intent Surgery for Hepatocellular Carcinoma in a European Cohort. *Cancers (Basel)* (2022) 14(3). doi: 10.3390/cancers14030720
16. Lencioni R, Llovet JM. Modified RECIST (mRECIST) Assessment for Hepatocellular Carcinoma. *Semin Liver Dis* (2010) 30(1):52–60. doi: 10.1055/s-0030-1247132
17. van derKroft G, van Dijk DPJ, Rensen SS, Van Tiel FH, de Greef B, West M, et al. Low Thoracic Muscle Radiation Attenuation is Associated With Postoperative Pneumonia Following Partial Hepatectomy for Colorectal Metastasis. *HPB (Oxford).* (2020) 22(7):1011–9. doi: 10.1016/j.hpb.2019.10.1532
18. Choi MH, Oh SN, Lee IK, Oh ST, Won DD. Sarcopenia is Negatively Associated With Long-Term Outcomes in Locally Advanced Rectal Cancer. *J Cachexia Sarcopenia Muscle* (2018) 9(1):53–9. doi: 10.1002/jcsm.12234
19. Ali LK, Saver JL, Liebeskind DS, Pineda S, Ovbiagele B. Influence of Height on the Clinical Characteristics and Prognosis of Patients With Ischemic Stroke. *Neurologist* (2011) 17(1):21–3. doi: 10.1097/NRL.0b013e3181de48f2
20. Tsekoura M, Kastrinis A, Katsoulaki M, Billis E, Gliatis J. Sarcopenia and Its Impact on Quality of Life. *Adv Exp Med Biol* (2017) 987:213–8. doi: 10.1007/978-3-319-57379-3_19
21. Zheng X, Cao F, Qian L, Dong J. Body Composition Changes in Hepatocellular Carcinoma: Prediction of Survival to Transcatheter Arterial Chemoembolization in Combination With Clinical Prognostic Factors. *Cancer Control* (2021) 28:10732748211038445. doi: 10.1177/10732748211038445
22. Sanmamed MF, Carranza-Rua O, Alfaro C, Oñate C, Martín-Algarra S, Perez G, et al. Serum Interleukin-8 Reflects Tumor Burden and Treatment Response Across Malignancies of Multiple Tissue Origins. *Clin Cancer Res* (2014) 20 (22):5697–707. doi: 10.1158/1078-0432.CCR-13-3203
23. Hsieh YC, Joo SK, Koo BK, Lin HC, Lee DH, Chang MS, et al. Myosteatosis, But Not Sarcopenia, Predisposes NAFLD Subjects to Early Steatohepatitis and Fibrosis Progression. *Clin Gastroenterol Hepatol* (2022). doi: 10.1016/j.cgh.2022.01.020
24. JHRJ D, Dingemans AC, ACH W, Gietema HA, Hurkmans DP, Aerts JG, et al. The Prognostic Value of Weight and Body Composition Changes in Patients With non-Small-Cell Lung Cancer Treated With Nivolumab. *J Cachexia Sarcopenia Muscle* (2021) 12(3):657–64. doi: 10.1002/jcsm.12698
25. Sun J, Zhou G, Xie X, Gu W, Huang J, Zhu D, et al. Efficacy and Safety of Drug-Eluting Beads Transarterial Chemoembolization by CalliSpheres® in 275 Hepatocellular Carcinoma Patients: Results From the Chinese CalliSpheres® Transarterial Chemoembolization in Liver Cancer (CTILC) Study. *Oncol Res* (2020) 28(1):75–94. doi: 10.3727/096504019X15662966719585
26. Qiu Y, Wang T, Yang X, Shen S, Yang Y, Wang W. Development and Validation of Artificial Neural Networks for Survival Prediction Model for Patients With Spontaneous Hepatocellular Carcinoma Rupture After Transcatheter Arterial Embolization. *Cancer Manag Res* (2021) 13:7463–77. doi: 10.2147/CMAR.S328307
27. Marasco G, Poggioli F, Colecchia A, Cabibbo G, Pelizzaro F, Giannini EG, et al. A Nomogram-Based Prognostic Model for Advanced Hepatocellular Carcinoma Patients Treated With Sorafenib: A Multicenter Study. *Cancers (Basel)* (2021) 13(11). doi: 10.3390/cancers13112677
28. Fujimoto A, Furuta M, Shiraishi Y, Gotoh K, Kawakami Y, Arihiro K, et al. Whole-Genome Mutational Landscape of Liver Cancers Displaying Biliary Phenotype Reveals Hepatitis Impact and Molecular Diversity. *Nat Commun* (2015) 6:6120.
29. Ye H, Zhang C, Wang BJ, Tan XH, Zhang WP, Teng Y, et al. Synergistic Function of Kras Mutation and HBx in Initiation and Progression of Hepatocellular Carcinoma in Mice. *Oncogene.* (2014) 33(43):5133–8. doi: 10.1038/onc.2013.468
30. Chen N, Fang W, Lin Z, Peng P, Wang J, Zhan J, et al. KRAS Mutation-Induced Upregulation of PD-L1 Mediates Immune Escape in Human Lung Adenocarcinoma. *Cancer Immunol Immunother* (2017) 66(9):1175–87. doi: 10.1007/s00262-017-2005-z
31. Dong ZY, Zhong WZ, Zhang XC, Su J, Xie Z, Liu SY, et al. Potential Predictive Value of TP53 and KRAS Mutation Status for Response to PD-1 Blockade Immunotherapy in Lung Adenocarcinoma. *Clin Cancer Res* (2017) 23 (12):3012–24. doi: 10.1158/1078-0432.CCR-16-2554
32. Lauko A, Kotecha R, Barnett A, Li H, Tatineni V, Ali A, et al. Impact of KRAS Mutation Status on the Efficacy of Immunotherapy in Lung Cancer Brain Metastases. *Sci Rep* (2021) 11(1):18174. doi: 10.1038/s41598-021-97566-z

Conflict of Interest: Author HL was employed by GE Healthcare.

The remaining authors declare that the research was conducted in the absence of any commercial or financial relationships that could be construed as a potential conflict of interest.

Publisher's Note: All claims expressed in this article are solely those of the authors and do not necessarily represent those of their affiliated organizations, or those of the publisher, the editors and the reviewers. Any product that may be evaluated in this article, or claim that may be made by its manufacturer, is not guaranteed or endorsed by the publisher.

frontiers | Frontiers in Oncology

ORIGINAL RESEARCH
published: 20 June 2022
doi: 10.3389/fonc.2022.911715

CircASPH Promotes Hepatocellular Carcinoma Progression Through Methylation and Expression of HAO2

Han Zhuo[1†], Jinguo Xia[1†], Jin Zhang[2], Junwei Tang[3], Sheng Han[1], Qitong Zheng[1], Deming Zhu[1], Feihong Zhang[1], Zhenggang Xu[1], Dongwei Sun[1], Zhongming Tan[1] and Chen Wu[1*]*

[1] Hepatobiliary Center, The First Affiliated Hospital of Nanjing Medical University, Nanjing, China, [2] School of Medicine, Jiangsu University, Zhenjiang, China, [3] General Surgery, The First Affiliated Hospital of Nanjing Medical University, Nanjing, China

CircRNAs have been reported to be related to hepatocellular carcinoma (HCC) development. Limited studies have revealed the expression profile of circRNAs in tumor and para-tumor normal samples in HCC patients. We found that circASPH was significantly increased in HCC tumor samples and that the level of circASPH was closely related to the overall survival of HCC patients. Mechanistically, circASPH could regulate the methylation of the promoter and expression of hydrocyanic oxidase 2 (HAO2) to promote HCC progression by acting as a sponge for miR-370-3p, and miR-370-3p could target DNMT3b and increase the 5mC level. In summary, our study determined that circASPH could regulate the methylation and expression of HAO2 and it could be considered an important epigenetic regulator in HCC progression.

Keywords: HCC, circASPH, miR-370-3p, DNMT3b, methylation

OPEN ACCESS

Edited by:
Xiaodong Li,
First People's Hospital of Changzhou, China

Reviewed by:
Yanqing Liu,
Columbia University, United States
Xin Wang,
National Institutes of Health (NIH), United States

****Correspondence:***
Chen Wu
mcwuchen@foxmail.com
Zhongming Tan
seektzm@hotmail.com

[†]These authors have contributed equally to this work

Specialty section:
This article was submitted to Molecular and Cellular Oncology, a section of the journal Frontiers in Oncology

Received: *03 April 2022*
Accepted: *16 May 2022*
Published: *20 June 2022*

Citation:
Zhuo H, Xia J, Zhang J, Tang J, Han S, Zheng Q, Zhu D, Zhang F, Xu Z, Sun D, Tan Z and Wu C (2022) CircASPH Promotes Hepatocellular Carcinoma Progression Through Methylation and Expression of HAO2. Front. Oncol. 12:911715. doi: 10.3389/fonc.2022.911715

INTRODUCTION

Hepatocellular carcinoma (HCC) is becoming one of the most common malignancies, with a high rate of cancer-related death worldwide, increasing the burden worldwide (1). Hepatitis C virus (HCV) and hepatitis B virus (HBV) infections and non-alcoholic fatty liver are risk factors that result in HCC (2–4), as well as excessive drinking, genetic factors, smoking, excess body weight, and type 2 diabetes (5–7). HCC possesses its unique characteristics because the prognosis depends on the tumor stage and severity of the liver disease. The interventions include liver transplantation and surgical resection, which are only effective in the early stages (8). Therefore, the mechanism of HCC development should be uncovered to improve patient prognosis and treatment effects.

Circular RNAs (circRNAs) have been identified as a new type of non-coding RNAs. CircRNAs have a covalently closed loop structure without a 5' cap and a 3' tail, which is different from traditional linear RNA (9). Because of their special structure, circRNAs could be resistant to ribonuclease cleavage, making them more stable (10–12). At the same time, circRNAs have developmental stage–related patterns, tissue specificity, and a high species conservation (13–15). Thereby, circRNAs have been used as biomarkers in disease diagnosis, prognosis evaluation, and progress monitoring. CircRNAs are divided into exon circular RNAs (EcircRNAs), exon–intron circular RNAs (EIciRNAs), and intron circular RNAs (ciRNAs), depending on sequences spliced from mRNA (9). More and more circRNAs are identified and verified to play a crucial role in cancers, especially in HCC. For instance, hepatocyte nuclear factor 4 alpha can activate circ_104075

transcription by binding to its promoter, sponging miR-582-3p to upregulate Yes-associated protein (YAP) to advance the process of HCC (16). CircTMEM45A could interact with miR-665 to inhibit the expression of insulin-like growth factor 2 to promote HCC tumorigenesis (17). However, the role of circASPH remains unclear in HCC.

DNA methylation is catalyzed by two types of enzymes. In the first type, after DNA replication, DNA methyltransferase 1 (DNMT1) and its cofactor could recognize hemimethylated DNA (18). In the second type, DNMT3A and DNMT3B, together with their coactivator DNMT3L, catalyze new methyl groups to unmethylated cytosines (19). However, the mechanism of the DNMT3b/5mC axis in the regulation of HCC remains unresolved. HAO2, hydroxy acid oxidase 2, is a member of the flavoenzyme family that is responsible for the oxidation of l-2-hydroxy acids to ketoacids at the expense of molecular oxygen. HAO2 is downregulated in HCC and can be used to predict metastasis and poor survival (20). HAO2 is demonstrated to inhibit the malignancy of clear cell renal cell carcinoma (21). The methylation of HAO2 in HCC remains unclear.

Here, two circRNA-seq databases were used to identify whether circASPH was significantly upregulated in tumor tissues in HCC patients. The expression of circASPH levels in tumor tissues was closely related to the prognosis of HCC patients. Mechanistically, circASPH could regulate the methylation process and expression of HAO2 by acting as a sponge for miR-370-3p, and miR-370-3p targeted DNMT3b to increase the 5mC level. Therefore, circASPH could be considered an important epigenetic regulator in HCC progression.

MATERIALS AND METHODS

Clinical Data

In total, 181 samples were collected from consecutive patients with HCC who underwent curative resection in the Hepatobiliary Center, The First Affiliated Hospital of Nanjing Medical University. Fresh human HCC and adjacent nontumor liver tissue samples were blindly collected from the cohort. Informed consent was obtained from each patient, and ethical approval was granted by the Ethics Committee of The First Affiliated Hospital of Nanjing Medical University. The information is summarized in **Table 1**.

Cell Culture, RNA Extraction, and Transfection

The human HCC cell lines Huh-7, SMMC-7721, HepG2, MHCC97H, and HCCLM3 were routinely maintained in our laboratory. The normal liver cell line was THLE-2. Transfection was carried out by using Lipofectamine 3000 (Invitrogen, Invitrogen, Carlsbad City, CA, USA), and total RNA was obtained according to the manufacturer's instructions. Si-circASPH (5'-GCAAAAGGACUUUAAAGAGAUU-3') and miR-370-3p mimics were purchased from GenePharma (GenePharma, Shanghai, China).

TABLE 1 | Clinicopathological features of HCC patients (n = 20).

Patients	n (%)
Age (years)	
<60	12 (60.0)
≥60	8 (40.0)
Gender	
Male	14 (70.0)
Female	6 (30.0)
T stage	
T1–T2	9 (45.0)
T3–T4	11 (55.0)
Regional lymph node metastasis	
Yes	16 (80.0)
No	4 (20.0)
Distance metastasis	
Yes	3 (15.0)
No	17 (85.0)
Tumor size	
< 5 cm	11 (55.0)
≥ 5 cm	9 (45.0)

Plasmid Construction

The lentiviral vectors pGMLV-SC5-shmiR-370-3p and pGMLV-SC5-shRNA-circASPH and negative sequences were purchased from GenePharma (China). The lentiviral cDNA templates of circASPH and DNMT3b were cloned into the pPB-CAG vector according to the manufacturer's instructions. Cells were then transduced with the appropriate lentivirus.

RT-qPCR

MiRNAs were extracted with the mirVana™ miRNA Isolation Kit (Life Technologies, Carlsbad City, CA, USA) (Genewiz, Shanghai, China). Real-time PCR was performed in triplicate with the SYBR Green PCR method. All miRNA levels were normalized to the U6 small nuclear RNA level; other RNA levels were adjusted using 18S as the reference. Relative expression was analyzed by the comparative cycle threshold (Ct) method. Primer sequences are listed below (Genewiz, China): circASPH, forward: 5'- ACTGCTCCCCCTGAGGAT-3, reverse: 5'- GGGACTGCTGGCTCTGAA-3'; miR-370-3p, forward: 5'-AGACCCCGCTATGGCTCTATT-3', reverse: 5'-TTTTGGCATAACTAAGGCCGAA -3'; U6, forward: 5'- TGT AACCAGAGAGCGGGATGT-3', reverse: 5'-AACGCTTCAC GAATTTGCGT-3'. 18SrRNA, forward: 5'-CAGCCACCCGA GATTGAGCA-3', reverse: 5'-TAGTAGCGACGGGCGGTG TG-3'; DNMT3b, forward: 5'-AGGGAAGACTCGATCCTCGT C-3', reverse: 5'- GTGTGTAGCTTAGCAGACTGG-3'; HAO2, forward: 5'-GCATCACGCGGGATGACAA-3', reverse: 5'- GCG ATACAAATAGGGGCACTGA-3'.

Western Blotting Analysis

The protein was extracted by using Radio-Immunoprecipitation Assay (RIPA) lysis buffer. After being centrifuged, the concentration of protein was checked by a BCA kit. Proteins were separated by Sodium Dodecyl Sulfate Polyacrylamide Gel electropheresis (SDS-PAGE) and transferred to Polyvinylidenefluoride (PVDF) membranes (Millipore, Boston,

MA, USA). DNMT3b (#57868, CST, Danvers, MA, USA), HAO2 (ab229817, abcam, UK), and β-actin (#3700, CST, USA) antibodies were incubated overnight. After the incubation of the secondary antibodies, the bands were used in Image Lab after adding a chemiluminescent substrate (Millipore, USA) to visualize. Image Lab software was used to analyze the results.

Immunofluorescence and Immunocytochemistry Assay

For 5mC (ab10805, abcam, United Kingdom) and 5hmC (ab106918, abcam, United Kingdom) staining, the treated cells or tissues were fixed with 4% PFA and washed with PBS, then permeabilized with 0.3% Triton X-100 (Beyotime, China). For immunofluorescence, after blocking, the cells or tissues were incubated with the primary antibody (Abcam, UK) overnight at 4°C. Cells or tissues were incubated with secondary antibodies and DAPI. Images were taken under the microscope. For immunocytochemistry, 3% hydrogen peroxide was used to block the endogenous peroxidase. After being washed with PBS, the tissues were incubated with 10% goat serum and the primary antibody was added for 4°C overnight. After incubating with the secondary antibody, a DAB solution was added for color staining.

Luciferase Assay

The wild-type (WT) and mutant (MUT) 3′-UTR fragment sequences of circASPH and human DNMT3b were constructed into pmirGLO vectors (Genewiz, China). Each cell was seeded with a proper density in 12-well plates. Alternatively, the cells were co-transfected with plasmids and mimics. After transfection, the cells were harvested and lysed. Luciferase activity was recorded using the dual-luciferase reporter assay kit (Promega, USA).

FISH Assay

A FISH kit was used for the FISH assay. Specific probes for circASPH and miR-370-3p were synthesized by GenePharma (China). Briefly, cells were fixed with 4% paraformaldehyde, treated with 0.5% Triton X-100 (Beyotime, Shanghai, China), and incubated with circASPH and miR-370-3p probes overnight. Then, cell nuclei were stained with DAPI (Yeasen, Shanghai, China). Images were obtained with a fluorescence microscope. The sequences of probes were: circASPH probe 5′-TCTCTCTTTAAGTCCTTTTGCTTTTTGTTC-3′ and miR-370 probe 5′-ACCAGGTTCCACCCCAGCAGGC-3′.

CCK8 Assay

Transfected BC cells at a density of 2,000 were seeded in 96-well plates. A CCK8 assay kit (Sigma, Carlsbad City, CA, USA) was added and incubated with cells. Then, the absorbance was measured by a microplate reader at five time periods.

Wound-Healing Assay

Transfected HCC cells were seeded in six-well plates. A 200 μl pipette tip was used to generate a linear gap. After 24 h, we used the microscope to take pictures and measured the width (W) of the scratch wound. The rate of close distance of the wounds was calculated. All measurements were carried out three times.

Transwell Assay

The cell suspension was added into Transwell chamber inserts (Millipore, USA) with Matrigel. Approximately 24 h later, cells were stained and pictures taken were used to measure invasion assays under a microscope.

Biotin-Coupled RNA Capture

SMMC-7721 cells were transfected with biotinylated circASPH or miRNA-370-3p (GenePharma, China) according to the standard protocol of Lipofectamine™ 3000 (Invitrogen, Carlsbad City, CA, USA). After transfection, cells were harvested and lysed. Streptavidin-conjugated magnetic beads were activated and blocked with a blocking buffer for 2 h. Then, the beads were incubated with cell lysates at 4°C for 8 h to pull down the biotin-coupled RNA complex. The level of RNA was evaluated by PCR.

MeDIP Assay

Methylation was detected by the MeDIP kit (Abcam, London, United Kingdom) by applying a non-cross-reactive 5mC antibody. In the assay of the kit, DNA is sheared and then added into a microplate well and an antibody specific to methylcytosine is then used to capture methylated DNA in the wells. Then, the specificity of enriched methylated DNA was evaluated by quantitative PCR.

Migration and Invasion Assays and *In Vivo* Metastasis Assays

The HCC cell lines were transfected with shRNA-circASPH and negative control (NC). Next, HCC cell lines were collected for subcutaneous injection. BALB/c nude mice were randomly divided into two groups. Mice in the control groups received subcutaneous injection with control cells, and experimental groups received a subcutaneous administration of treated HCC cells. After 5 weeks, the imaging of mice was performed and the tumor volume and weight were examined. The tumor volume was measured and calculated as follows: $V = (\text{length} \times \text{width}^2)/2$. All animal experiments were approved by the Committee on the Ethics of Animal Experiments of Nanjing Medical University.

Target Prediction and Bioinformatics

The TargetScan (http://www.targetscan.org), miRBase (http://www.mirbase.org), and miRanda (www.microrna.org) algorithms were used to screen for the targets of miRNAs. Circbase (http://circbase.org/) was used to predict the interaction between circRNAs and miRNAs. Previously published RNA-Seq and BS-Seq datasets (GSE55752) were re-analyzed. RNA-Seq reads were trimmed using Trim Galore and mapped to the GRCh38 human genome using HISAT2. Read count quantification was performed with HTSeq-count. Differential gene expression analysis was conducted with DESeq2. BS-Seq data were mapped with Bismark, and differential methylation regions were identified by Diffbind. The distribution of DMRs was analyzed by ChiPseeker and deepTools.

Statistical Analysis

Statistical analysis was performed with SPSS 19.0 software (SPSS). All tests were two tailed, and $p<0.05$ was considered statistically significant.

RESULTS

CircASPH Expression Is Significantly Upregulated in HCC Tissues and Related to Patient Prognosis

To identify the differentially expressed circRNAs between normal tissues and HCC tumor tissues, we used two GEO databases (GSE28274 and GSE125469) for investigation (**Figures 1A, B**). The circRNAs with significant differential expression (fold change ≥2.0 and $P < 0.05$) between the groups were identified. From the results of two GEO databases, one circRNA was preliminarily identified to be upregulated, while two circRNAs were downregulated in the HCC tissue samples compared to the para-tumor normal samples (**Figure 1C**). In this study, we chose circASPH for further investigation.

To determine whether circASPH was associated with HCC, firstly, RT-qPCR was used to indicate that the expression of circASPH was higher in HCC tissues (**Figure 1D**). Then, we used the FISH assay to identify the expression of circASPH in HCC tumor tissues. It showed that the level of circASPH expression was higher in tumor tissues (**Figure 1E**). We also investigated the level of circASPH in several HCC cell lines. The level of circASPH was higher in HCC cell lines (HepG2, SMMC-7721, Huh7, and HCCLM3) (**Figure 1F**). Then, we analyzed the relationship between the circASPH level and HCC patient prognosis. Multivariate Cox analysis revealed that the circASPH level in HCC tissue was an independent prognostic factor in HCC patients (**Figure 1G**). These data suggest that circASPH plays an important role in HCC tumorigenesis and progression.

CircASPH Promotes Cell Proliferation, Migration, and Invasion in HCC Cells

To investigate the biological function of circASPH in HCC progression, circASPH was stably overexpressed and knocked down in SMMC-7721 cell lines (**Figure 2A**). The CCK8 assay and EDU staining assay were carried out to verify the proliferation of HCC cells. The results indicated that the cell proliferation was enhanced by circASPH overexpression, whereas it was reduced by circASPH knockdown (**Figures 2B, C**). Meanwhile, wound-healing assays were performed to evaluate the cell migration ability and Transwell assays were used to examine the cell invasion. The results showed that the migration and invasion capacities were significantly increased after circASPH overexpression. However, the ability of cell migration and invasion capacities were reduced when the circASPH level was decreased *in vitro* (**Figures 2D, E**). To further determine whether circASPH induced the tumor growth *in vivo*, we injected control or shRNA-circASPH-transfected cells into nude mice. Our results revealed that the tumors composed of shRNA-circASPH-transfected cells were significantly smaller than those in control cells (**Figures 2F–H**). Therefore, we verified that circASPH functioned as a tumor promoter to enhance the proliferation, invasion, and metastasis of HCC *in vitro* and *in vivo*.

CircASPH Regulates the Level of the DNMT3b/5mC Axis by Sponging miR-370-3p in HCC Cells

CircRNAs have been reported to function as sponges for miRNAs. Therefore, we investigated the role of circASPH to function as a sponge for miRNAs. Candidate targets were determined using target prediction. According to the predicted results, miR-370-3p gained the highest score (**Figure 3A**). Then, we used molecular biological methods to investigate the direct interaction between circASPH and miR-370-3p. The 3′-UTR fragment of circASPH containing the putative binding site [wild type (WT)] of miR-370-3p or a mutant sequence was cloned into pmirGlo vectors. The results showed that, when co-transfected with WT and NC or mimic, the mimic miR-370-3p significantly decreased the luciferase activity (**Figures 3B, C**). We also designed a linear biotinylated circASPH probe. Our RT-qPCR results showed that miR-370-3p was abundantly pulled down by the circASPH probe in HCC cells (**Figure 3D**). We also used the FISH assay to detect the interaction between the circASPH and miR-370-3p. The result showed that circASPH and miR-370-3p could be co-localized (**Figure 3E**). At the same time, overexpressing circASPH could decrease the miR-370-3p expression level, while the reduction of miR-370-3p was induced by circASPH knockdown (**Figure 3F**).

To further elucidate the molecular mechanism in which circASPH promoted HCC progression, we attempted to identify the target genes of miR-370-3p. We used the bioinformatic analysis to indicate the function of the target gene. It showed that the molecular function was enriched in chromatin binding (**Figure 4A**). In addition, the biological process was enriched in the regulation of transcription, especially in the apoptotic process (**Figure 4B**). The KEGG pathway showed that target genes mainly functioned in pathways in cancer and transcription misregulation in cancer (**Figure 4C**). Previous studies revealed that DNMT3b played a key role in establishing *de novo* DNA methylation and was upregulated in cancers. So, we used GEO databases (GSE124535) to analyze the expression of the family of DNMT. It showed that the family of DNMT was enhanced in HCC tissues (**Figure 4D**). Based on online target prediction algorithms, we found that DNMT3b was a potential candidate target gene for miR-370-3p (**Figure 4E**). The dual luciferase assay was performed, and it indicated that miR-370-3p could interact with DNMT3b (**Figure 4F**). The overexpressed miR-370-3p could decrease the DNMT3b expression level, while the upregulation of DNMT3b was induced by miR-370-3p knockdown (**Figures 4G, H**). Then, we detected changes in 5hmC and 5mC levels to assess whether miR-370-3p could remodel the epigenetic landscape by targeting DNMT3b genes and regulating 5mC levels in the genome. As expected, miR-370-3p knockdown exhibited lower levels of 5hmC and enhanced the level of 5mC (**Figure 4I**). Next, we verified the expression of DNMT3b and level of 5mC under the circASPH changed

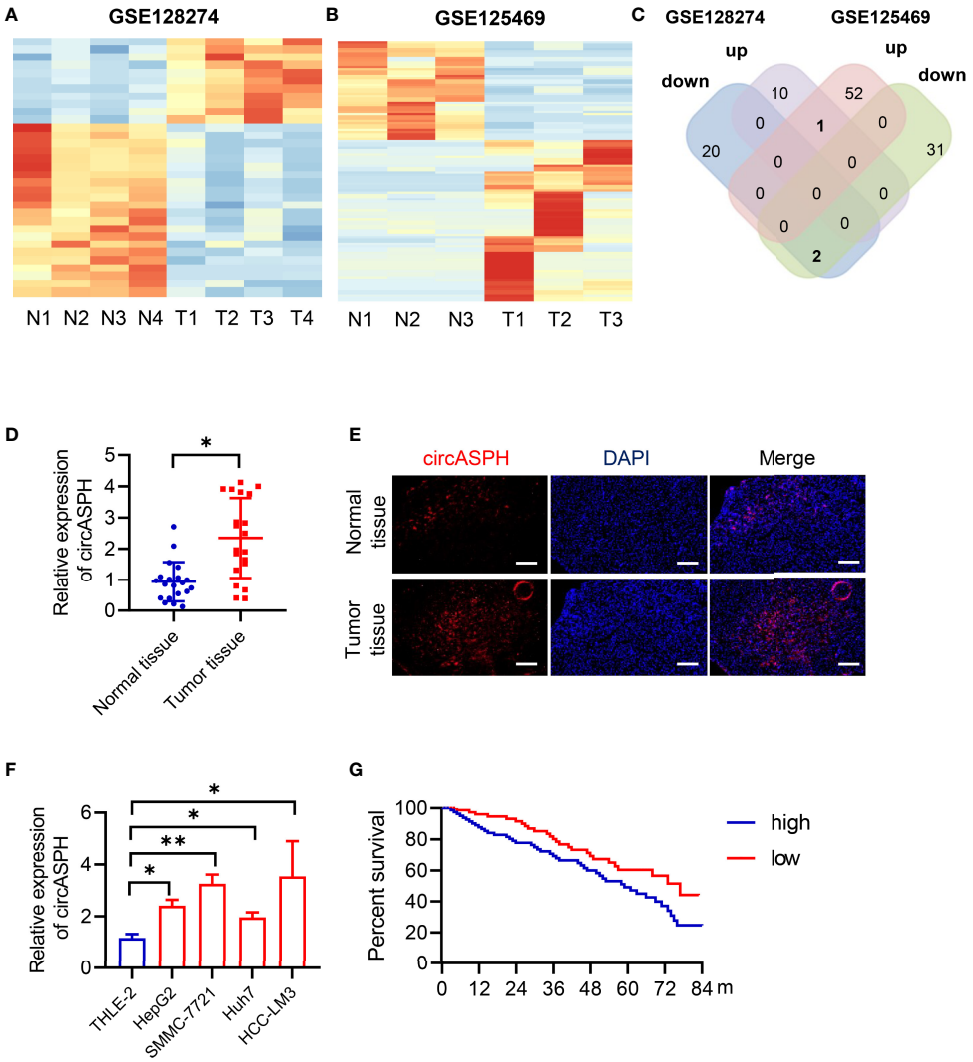

FIGURE 1 | CircASPH expression was identified to be significantly upregulated in HCC tissues and related to patient prognosis. **(A, B)** Heat maps of differentially expressed circRNAs in HCC tissues and non-tumor tissues obtained from GSE128274 and GSE125469. **(C)** The numbers of overlapping differentially expressed circRNAs from two GEO databases are shown in the Venn diagram. **(D)** The level of circASPH expression was evaluated by RT-qPCR in 20 paired HCC tissues and normal tissues. **(E)** FISH analysis of the expression of circASPH in HCC tissues and normal tissues. **(F)** CircASPH expression in HCC cell lines compared with THLE-2 cells. **(G)** Kaplan–Meier analysis showed that the level of circASPH was predictive of overall survival. *p < 0.05, **p < 0.01.

condition. The result showed that circASPH knockdown could decrease the DNMT3b expression level and decrease the level of 5mC (**Figures 4J–L**). These data indicated that circASPH could sponge miR-370-3p and regulate the DNMT3b/5mc axis in HCC cells.

CircASPH Promotes the HCC Process *via* the miR-370-3p/DNMT3b/5mC Axis

First, we used RT-qPCR to indicate that the level of DNMT3b was higher in HCC tumor tissues (**Figure 5A**). The Pearson analysis also showed that the expression of the DNMT3b level was positively related to the level of circASPH (**Figure 5B**). The IHC assay also showed that the 5mC level was enhanced in HCC tumor tissues (**Figure 5C**). These results prompted us to hypothesize that circASPH may promote HCC progression *via* the miR-370-3p/DNMT3b/5mC axis. DNMT3b was knocked down in HCC cell lines with circASPH overexpression or miR-370-3p knockdown, and the proliferation ability of these cells was evaluated by CCK8 assays and EDU staining assays. We found that DNMT3b knockdown significantly reduced the cell proliferation, which was enhanced by circASPH overexpression or miR-370-3p knockdown (**Figures 5D, E**). In addition, the wound-healing assays and Transwell assays also indicated that DNMT3b knockdown significantly reduced the enhanced cell migration and invasion mediated by circASPH overexpression or miR-370-3p knockdown (**Figures 5F, G**). These results suggest

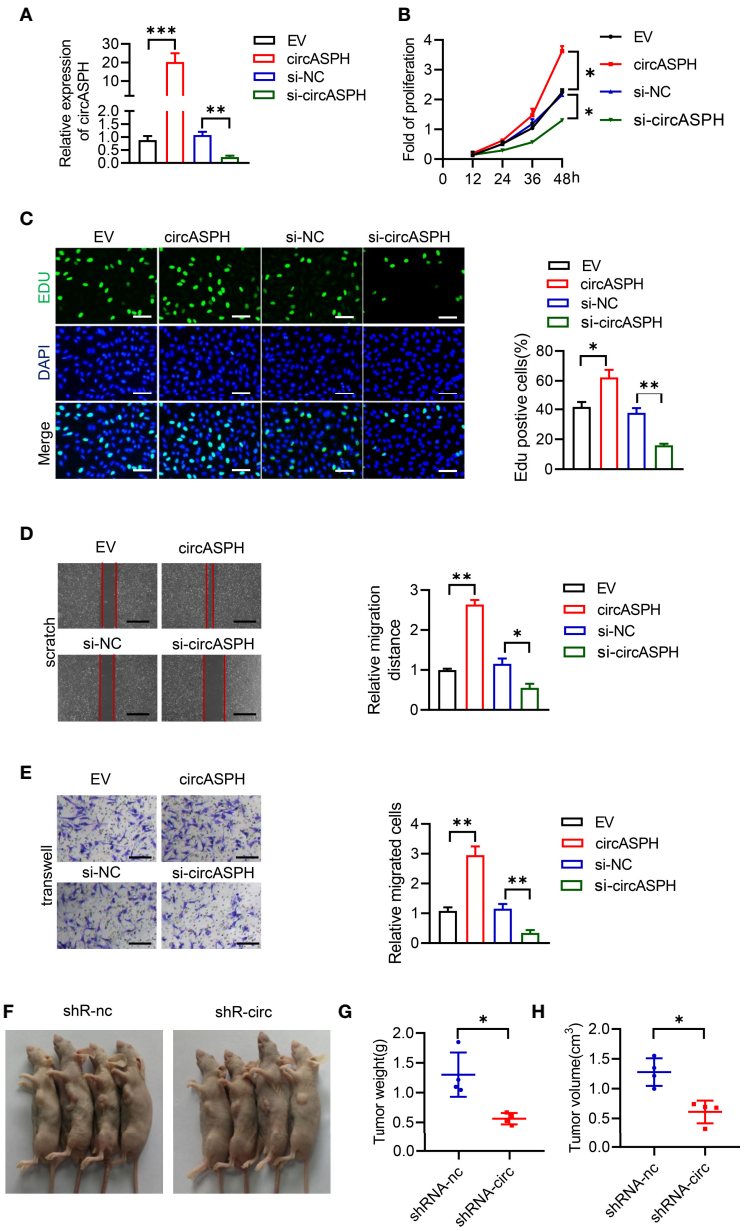

FIGURE 2 | CircASPH promoted HCC cell proliferation, migration, and invasion. **(A)** The expression of the circASPH level was detected by circASPH overexpressed and knocked down in HCC cells. **(B, C)** Cell Counting Kit-8 (CCK-8) assays and EDU staining assays were used to indicate the function of circASPH in the proliferation of HCC cells. **(D)** Wound-healing assays showed the role of circASPH in the migration of HCC cells. **(E)** Transwell assays showed the function of circASPH in the invasion of HCC cells. **(F–H)** Xenograft tumors composed of shRNA-circASPH-transfected HCC cells were significantly smaller than those composed of shRNA-NC-transfected HCC cells. *p < 0.05, **p < 0.01, ***p < 0.001.

that the DNMT3b/5mC axis plays an important role in the function of miR-370-3p and circASPH in HCC cells.

CircASPH Promotes HCC Progression by Regulating the DNA Methylation and Expression of HAO2

DNMT3b enzymes catalyzed 5hmC to 5mC, leading to DNA methylation and gene expression regulation. Then, we used the methylation GEO database (GSE55752) in the HCC tumor. It indicated that the DNA methylation was enhanced in HCC tumors and was enriched in the promoter area (**Figures 6A–D**). GSEA also showed that methylated genes also take part in the negative regulation of growth. In addition, HAO2 was one of the highly methylated genes in HCC tumors (**Figure 6E**). CHIP seq also showed that the methylation of HAO2 occurred in the promoter region (**Figure 6F**). Then, we examined the effect of circASPH and miR-370-3p on the

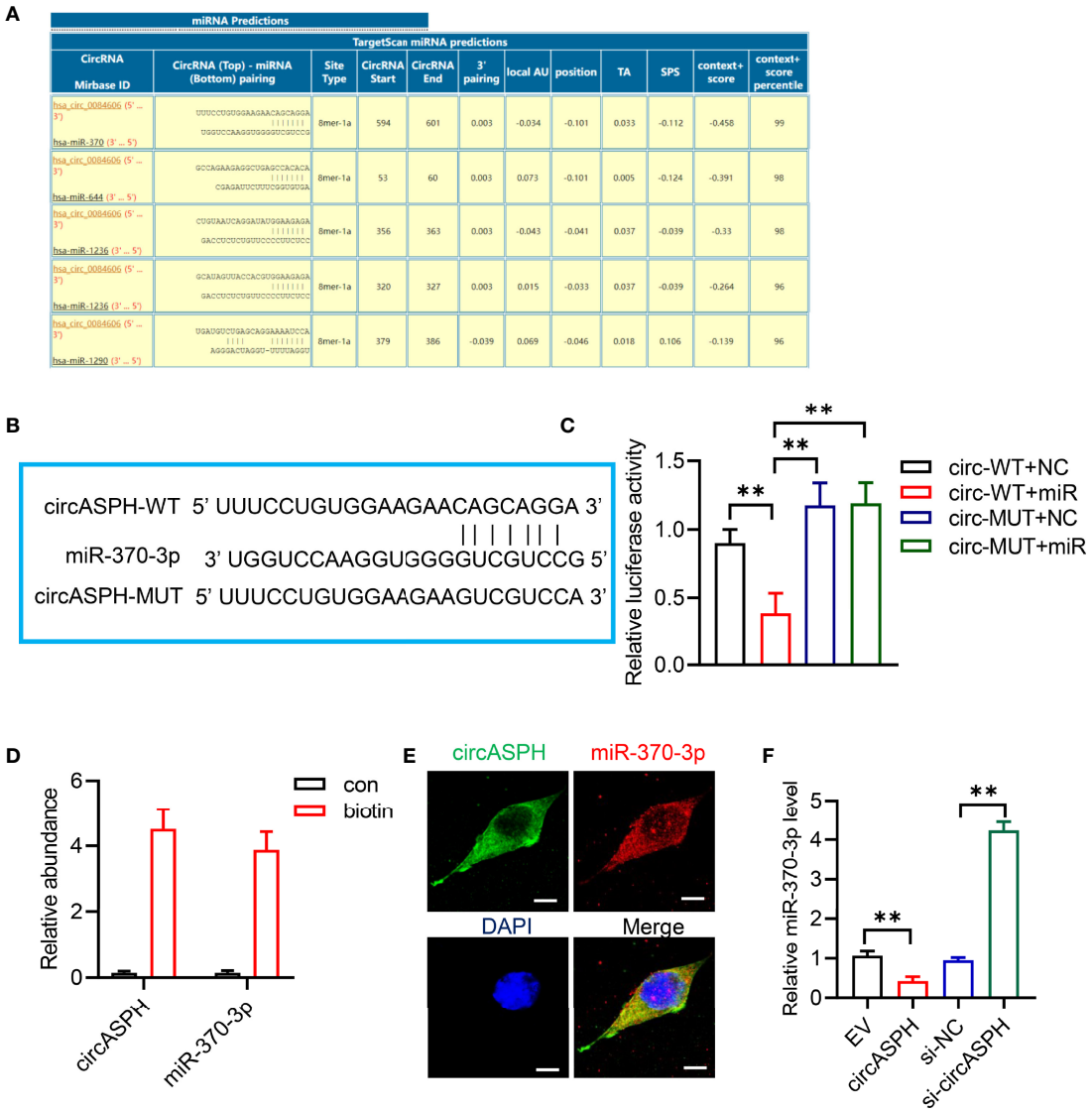

FIGURE 3 | CircASPH sponged miR-370-3p. **(A)** Score list for the circInteractome of predicting miRNAs sponged by circASPH. **(B)** Predicted binding sites between circASPH and miR-370-3p. **(C)** Dual-luciferase reporter assay showed that the co-transfection of WT and mimic miR-370-3p markedly decreased the luciferase activity. **(D)** MiR-370-3p was abundantly pulled down by a circASPH probe. **(E, F)** Images of circASPH and miR-370-3p co-localized in the cytoplasm; scale bar, 20 μm. *p < 0.05, **p < 0.01, ***p < 0.001.

HAO2 expression. Overexpressed miR-370-3p could increase the HAO2 expression level (**Figures 6G, H**). However, overexpressed circASPH could decrease the HAO2 expression level, while the upregulation of HAO2 was induced by circASPH knockdown (**Figures 6I, J**). Meanwhile, we also verified the 5mC enrichment in the HAO2 promoter region (**Figure 6K**). It indicated that circASPH overexpression could enhance the 5mC enrichment on the HAO2 promoter region and regulated the expression of HAO2.

Then, we detected the expression of HAO2 in the HCC tumor. RT-qPCR indicated that the level of HAO2 was decreased in HCC tumor tissues (**Figure 7A**). The Pearson analysis also showed that the expression of the HAO2 level was negatively related to the level of circASPH (**Figure 7B**). HAO2 was overexpressed in HCC cell lines with circASPH overexpression or miR-370-3p knockdown, and the proliferation ability of these cells was evaluated by EDU staining assays. We found that HAO2 overexpression significantly reduced cell proliferation, which was enhanced by circASPH overexpression or miR-370-3p knockdown (**Figure 7C**). In addition, the wound-healing assays and Transwell assays also indicated that HAO2 overexpression significantly reduced the increased cell migration and invasion mediated by circASPH overexpression or miR-370-3p knockdown (**Figures 7D, E**). These results demonstrated that circASPH promoted HCC progression by regulating the DNA promoter methylation and expression of HAO2.

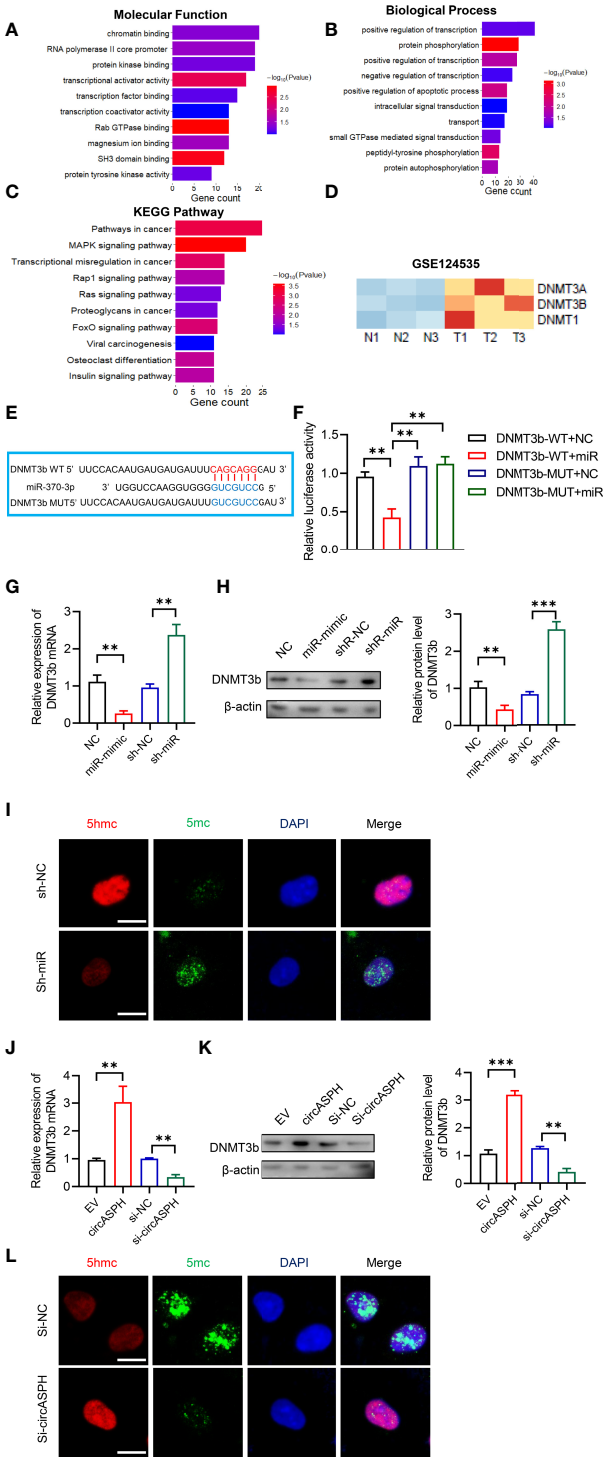

FIGURE 4 | CircASPH regulated the level of the DNMT3b/5mC Axis by sponging miR-370-3p in HCC cells. **(A, B)** Molecular function and biological process of miR-370-3p target genes in gene ontology analysis. **(C)** KEGG analysis of miR-370-3p target genes. **(D)** Heatmap of the expression of the DNMT gene family level in GSE124535. **(E)** Predicted binding sites between DNMT3b and miR-370-3p. **(F)** Dual-luciferase reporter assay showed that miR-370-3p could interact with the 3'UTR of DNMT3b mRNA. **(G, H)** The expression of the DNMT3b level with miR-370-3p overexpression and knockdown was detected by RT-qPCR and Western blot. **(I)** Images of 5hmC-, 5mC-, and DAPI-stained HCC cells with different levels of miR-370-3p; scale bar = 20 μm. **(J, K)** The expression of DNMT3b level with circASPH overexpression and knockdown was detected by RT-qPCR and Western blot. **(L)** Images of 5hmC-, 5mC-, and DAPI-stained HCC cells with different levels of circASPH; scale bar = 20 μm. $^{**}p < 0.01$, $^{***}p < 0.001$.

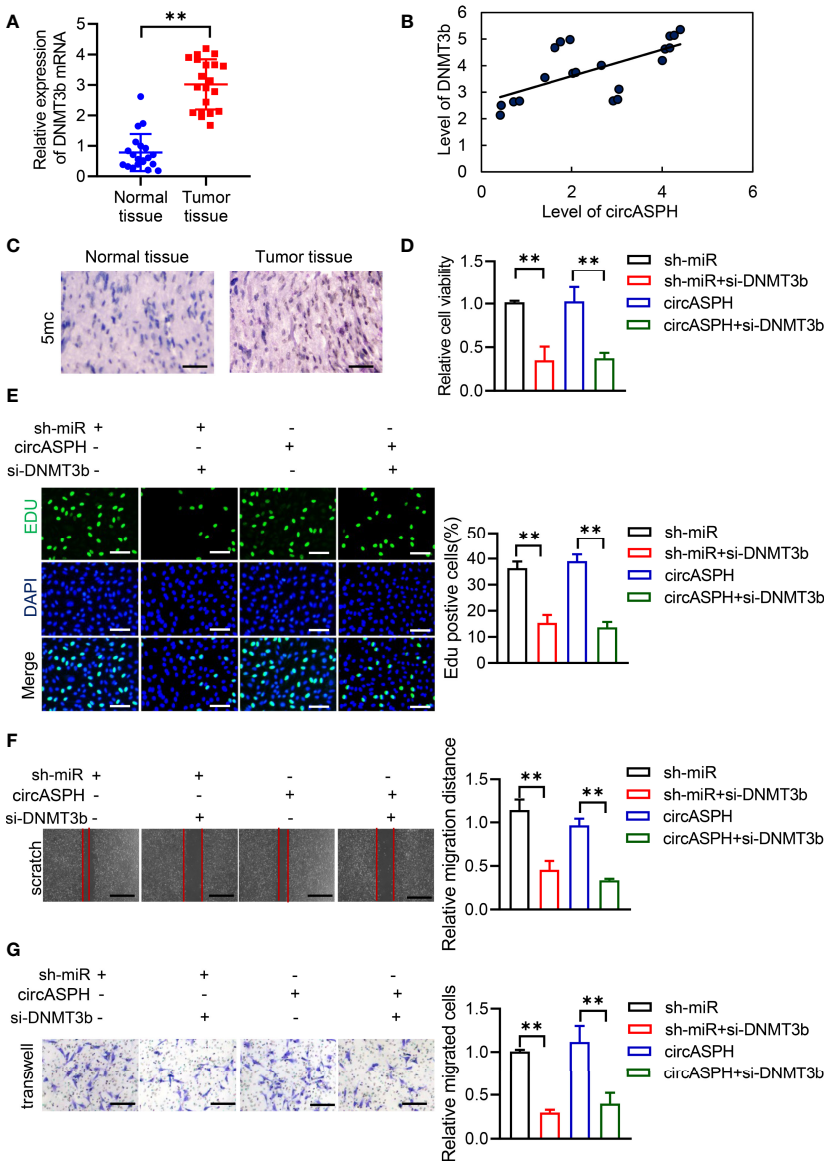

FIGURE 5 | CircASPH promoted the HCC process via miR-370-3p/DNMT3b/5mC. **(A)** The level of DNMT3b expression was evaluated by RT-qPCR in 20 paired HCC tumor tissues and normal tissues. **(B)** Pearson analysis indicated the relationship between circASPH and DNMT3b. **(C)** Immunohistochemical staining for 5mC in HCC tumor tissues; scale bar = 100 μm. **(D, E)** Cell Counting Kit-8 (CCK-8) assays and EDU staining assays indicated the proliferation of cells expressing a combination of circASPH, sh-miR-370-3p, and si-DNMT3b. **(F, G)** Wound-healing assays and Transwell assays indicated the ability of migration and invasion of cells expressing a combination of circASPH, sh-miR-370-3p, and si-DNMT3b. **p < 0.01.

DISCUSSION

Here, we indicated that circASPH could regulate the promoter methylation and expression of HAO2 to promote HCC progression *via* the miR-370-3p/DNMT3b/5mC axis. First, two databases were used to identify that circASPH was the only upregulated circRNA in tumor tissues in HCC patients and that the expression of circASPH level was closely related to the OS of HCC patients. The overexpression of circASPH could increase cell proliferation, migration, and invasion in HCC cells. It showed that circASPH could regulate the methylation process of the HAO2 promoter, by acting as a sponge for miR-370-3p, and miR-370-3p targeted DNMT3b and increased the 5mC level. Therefore, circASPH could promote the methylation process and regulate the expression of HAO2 in the HCC process.

CircRNAs are verified to play an important role in many diseases, especially in different types of cancer. CircASPH has been reported in other diseases. For instance, upregulated circASPH contributed to glioma cell proliferation and aggressiveness by the miR-599/AR/SOCS2-AS1 signaling

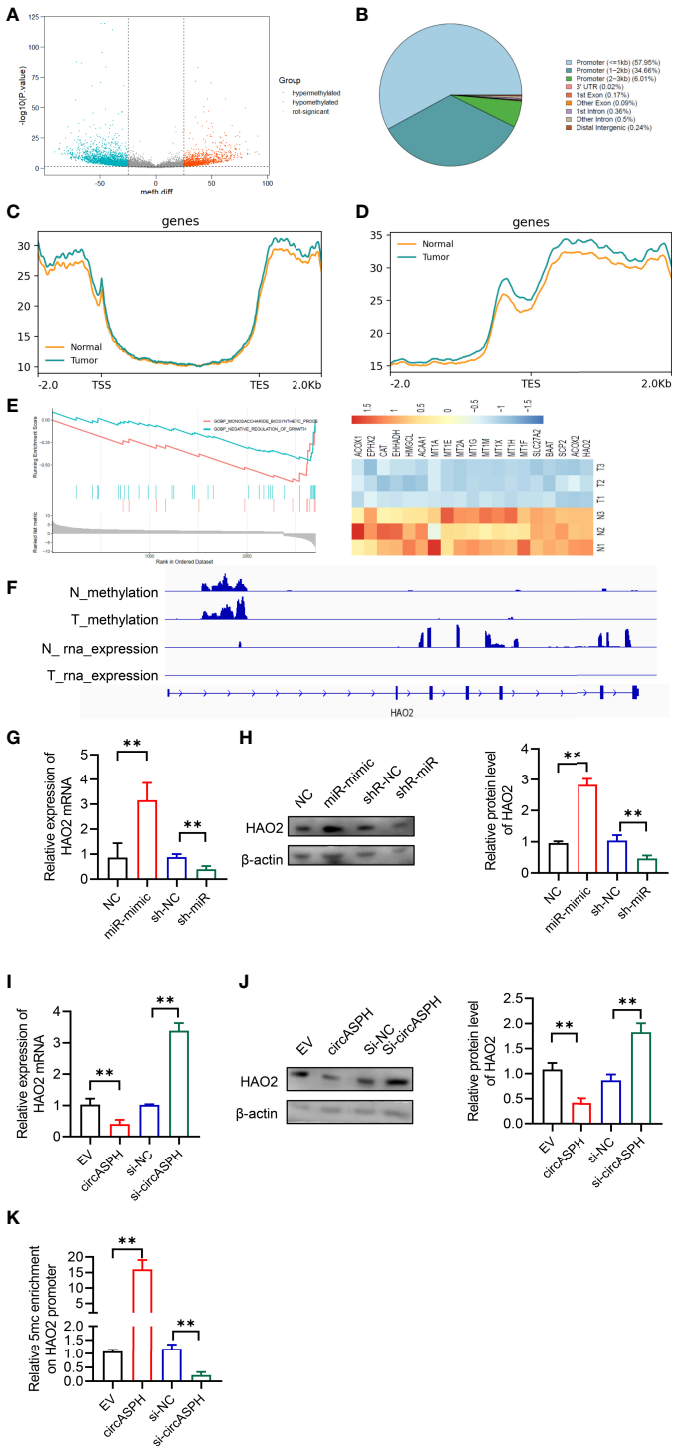

FIGURE 6 | CircASPH promoted HCC progression by regulating the DNA methylation and expression of HAO2. **(A)** Volcano plot of the methylation difference between HCC tumor tissues and normal tissues. **(B)** CpG island distribution of promoter differential methylated CpG sites. **(C, D)** Average profiles of 5mC and input DNA coverage across the binding-site motif identified on 5mCp enhancers. **(E)** GSEA analysis of the gene enriched in the negative regulation of the growth pathway. **(F)** IGV profile of 5mC-enriched regions and RNA-seq profiles in HCC tumor tissues. **(G, H)** The expression of the HAO2 level with miR-370-3p overexpression and knockdown was detected by RT-qPCR and Western blot. **(I, J)** The expression of the HAO2 level with circASPH overexpression and knockdown was detected by RT-qPCR and Western blot. **(K)** MeDIP-qPCR assays showed 5mC in HAO2 genes with different circASPH levels. **p < 0.01.

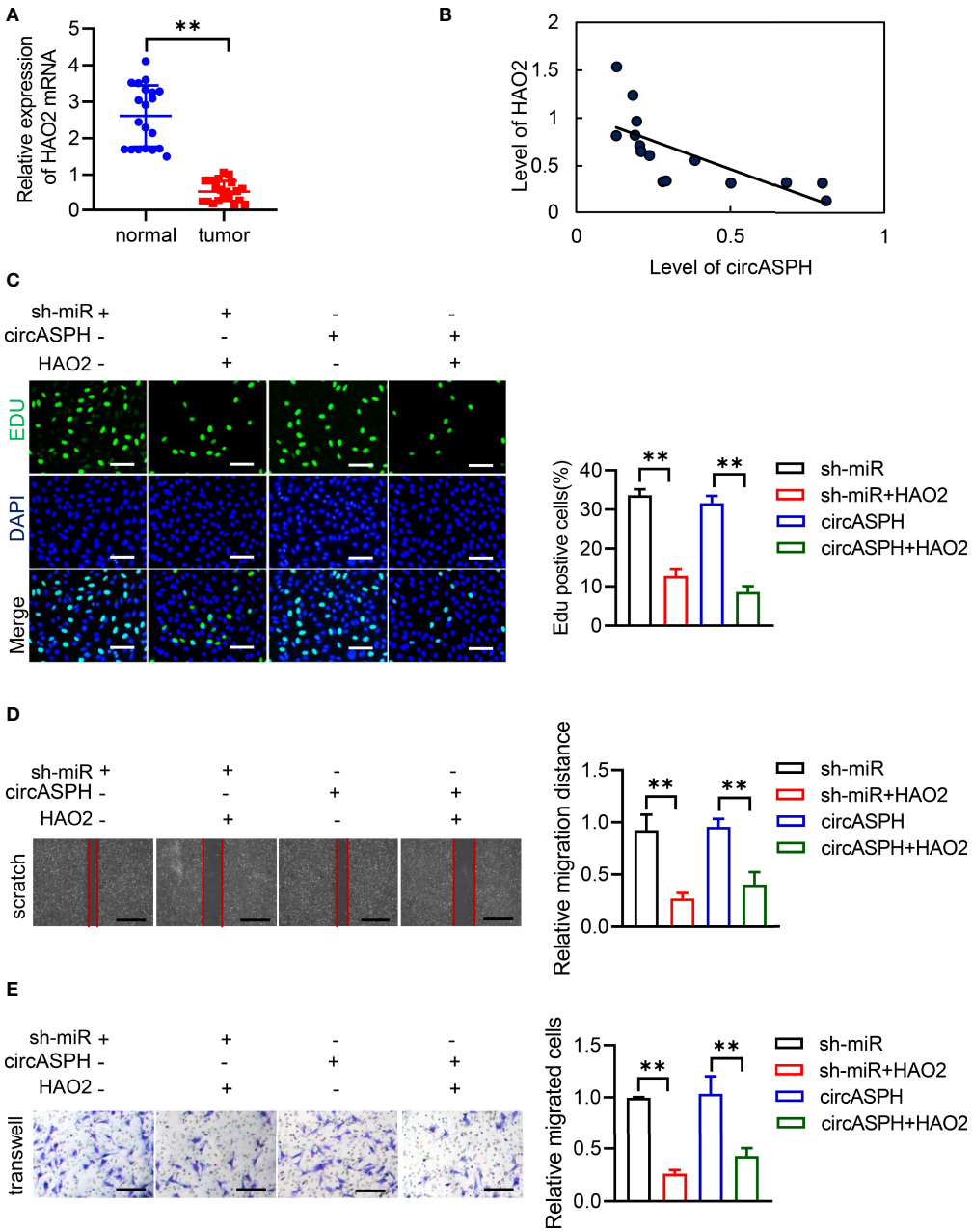

FIGURE 7 | CircASPH promoted the HCC process *via* the miR-370-3p/DNMT3b/5mC/HAO2 axis. **(A)** The level of HAO2 expression was evaluated by RT-qPCR in 20 paired HCC tumor tissues and normal tissues. **(B)** Pearson analysis indicated the relationship between circASPH and HAO2. **(C)** EDU staining assays indicated the proliferation of cells expressing a combination of circASPH, sh-miR-370-3p, and HAO2. **(D, E)** Wound-healing assays and Transwell assays indicated the ability of migration and invasion of cells by expressing a combination of circASPH, sh-miR-370-3p, and HAO2. **p < 0.01.

pathway (22). CircASPH also promoted KGN cell proliferation through the miR-375/MAP2K6 axis in polycystic ovary syndrome (23). In lung adenocarcinoma, circASPH could be regulated by HMGA2 to promote tumor growth (24). However, the function of circASPH in HCC is still uncovered. Here, we indicated that circASPH led to increased cell proliferation, migration, and invasion in HCC cells, which could be a diagnostic and treatment biomarker for HCC treatment. The other two circRNAs that were identified in databases were circLIFR and circSOX5. It showed that an enforced expression of circLIFR enhanced HUASMC proliferation and impeded apoptosis (25). CircSOX5 promotes proliferation and inhibits

the apoptosis of the HCC (26). Hence, we chose circASPH for the investigation.

DNA methylation is definite by the addition of a methyl group to the 5′ position of a CpG dinucleotide cytosine pyrimidine ring. Active demethylation could be regulated by the ten–eleven translocation (TET) enzyme family, including Tet 1, Tet 2, and Tet 3. 5mC and 5hmC could also also changed to thymine or 5-hydroxymethyluracil (5-hmU), depending on an alternative pathway (27). In HCC, TET1 and TET2 have been reported to be downregulated in tumor tissues and regulate DNA methylation (28–30). The DNMT1-mediated methylation of BEX1 regulates stemness and tumorigenicity in liver cancer (31). However, the mechanism of DNMT3b/5mC activation and whether the DNMT3b/5mC axis is involved in the regulation of HCC remain unresolved. Here, we identified circASPH as an important noncoding RNA that regulated the expression of DNMT3b and the 5mC level in HCC progression. Mechanistically, circASPH acted as the sponge of miR-370-3p, and miR-370-3p could bind to the 3′-UTR of DNMT3b mRNAs in HCC cells and upregulate 5mC levels. In HCC samples, there was a positive correlation between circASPH and DNMT3b expression. These data supported the conclusion that circASPH could regulate the level of the DNMT3B/5mC axis and act as a key epigenetic modifier in HCC. There are also multiple targets that can be methylated. According to GEO databases, it also showed that SIRT5 downregulation is associated with increased succinylation and activity of ACOX1 and oxidative DNA damage response in HCC (32). We will investigate the function of other genes in a future study.

In conclusion, we identified that circASPH could act like an oncogene in HCC to promote cell proliferation, migration, and invasion *via* the miR-370-3p/DNMT3b/5mC/HAO2 axis. CircASPH could be considered an important epigenetic regulator in HCC progression.

DATA AVAILABILITY STATEMENT

The datasets presented in this study can be found in online repositories. The names of the repository/repositories and accession number(s) can be found in the article/**Supplementary Material**.

ETHICS STATEMENT

The animal study was reviewed and approved by the ethics committee of the First Affiliate Hospital of Nanjing Medical University Ethics Review Board.

AUTHOR CONTRIBUTIONS

CW and ZT designed the research. HZ and JX wrote the paper. JZ, JT, SH, QZ, and FZ performed the *in vitro* experiments. HZ, JX, ZX, and DS analyzed data. All authors contributed to the article and approved the submitted version.

FUNDING

The study was supported by grants from the National Natural Science Foundation of China (Grant no. 81972675). The work was also supported in part by the Program for Development of Innovative Research Teams in the First Affiliated Hospital of NJMU, the Priority Academic Program of Jiangsu Higher Education Institutions.

SUPPLEMENTARY MATERIAL

The Supplementary Material for this article can be found online at: https://www.frontiersin.org/articles/10.3389/fonc.2022.911715/full#supplementary-material

REFERENCES

1. Akinyemiju T, Abera S, Ahmed M, Alam N, Alemayohu MA, Allen C, et al. The Burden of Primary Liver Cancer and Underlying Etiologies From 1990 to 2015 at the Global, Regional, and National Level: Results From the Global Burden of Disease Study 2015. *JAMA Oncol* (2017) 3:1683–91. doi: 10.1001/jamaoncol.2017.3055
2. Yang HI, Sherman M, Su J, Chen PJ, Liaw YF, Iloeje UH, et al. Nomograms for Risk of Hepatocellular Carcinoma in Patients With Chronic Hepatitis B Virus Infection. *J Clin Oncol* (2010) 28:2437–44. doi: 10.1200/JCO.2009.27.4456
3. Singal AG, Rich NE, Mehta N, Branch AD, Pillai A, Hoteit M, et al. Direct-Acting Antiviral Therapy for Hepatitis C Virus Infection is Associated With Increased Survival in Patients With a History of Hepatocellular Carcinoma. *Gastroenterology* (2019) 157:1253–63.e1252. doi: 10.1053/j.gastro.2019.07.040
4. Degasperi E, Colombo M. Distinctive Features of Hepatocellular Carcinoma in non-Alcoholic Fatty Liver Disease. *Lancet Gastroenterol Hepatol* (2016) 1:156–64. doi: 10.1016/S2468-1253(16)30018-8
5. Donato F, Tagger A, Gelatti U, Parrinello G, Boffetta P, Albertini A, et al. Alcohol and Hepatocellular Carcinoma: The Effect of Lifetime Intake and Hepatitis Virus Infections in Men and Women. *Am J Epidemiol* (2002) 155:323–31. doi: 10.1093/aje/155.4.323
6. Wu J, Wang Y, Jiang R, Xue R, Yin X, Wu M, et al. Ferroptosis in Liver Disease: New Insights Into Disease Mechanisms. *Cell Death Discovery* (2021) 7:276. doi: 10.1038/s41420-021-00660-4
7. Lange NF, Radu P, Dufour JF. Prevention of Nafld-Associated Hcc: Role of Lifestyle and Chemoprevention. *J Hepatol* (2021) 75(5):1217–27. doi: 10.1016/j.jhep.2021.07.025
8. Samant H, Amiri HS, Zibari GB. Addressing the Worldwide Hepatocellular Carcinoma: Epidemiology, Prevention and Management. *J Gastrointest Oncol* (2021) 12:S361–73. doi: 10.21037/jgo.2020.02.08
9. Huang Z, Xia H, Liu S, Zhao X, He R, Wang Z, et al. The Mechanism and Clinical Significance of Circular Rnas in Hepatocellular Carcinoma. *Front Oncol* (2021) 11:714665. doi: 10.3389/fonc.2021.714665
10. Santer L, Bar C, Thum T. Circular Rnas: A Novel Class of Functional Rna Molecules With a Therapeutic Perspective. *Mol Ther* (2019) 27:1350–63. doi: 10.1016/j.ymthe.2019.07.001
11. Li Y, Ge YZ, Xu L, Jia R. Circular Rna Itch: A Novel Tumor Suppressor in Multiple Cancers. *Life Sci* (2020) 254:117176. doi: 10.1016/j.lfs.2019.117176
12. Suzuki H, Tsukahara T. A View of Pre-Mrna Splicing From Rnase R Resistant Rnas. *Int J Mol Sci* (2014) 15:9331–42. doi: 10.3390/ijms15069331
13. Kristensen LS, Andersen MS, Stagsted LVW, Ebbesen KK, Hansen TB, Kjems J. The Biogenesis, Biology and Characterization of Circular Rnas. *Nat Rev Genet* (2019) 20:675–91. doi: 10.1038/s41576-019-0158-7
14. Jeck WR, Sorrentino JA, Wang K, Slevin MK, Burd CE, Liu J, et al. Circular Rnas are Abundant, Conserved, and Associated With Alu Repeats. *RNA* (2013) 19:141–57. doi: 10.1261/rna.035667.112
15. Lu Q, Liu T, Feng H, Yang R, Zhao X, Chen W, et al. Circular Rna Circslc8a1 Acts as a Sponge of Mir-130b/Mir-494 in Suppressing Bladder Cancer

Progression *via* Regulating Pten. *Mol Cancer* (2019) 18:111. doi: 10.1186/s12943-019-1040-0
16. Zhang X, Xu Y, Qian Z, Zheng W, Wu Q, Chen Y, et al. Circrna_104075 Stimulates Yap-Dependent Tumorigenesis Through the Regulation of Hnf4a and May Serve as a Diagnostic Marker in Hepatocellular Carcinoma. *Cell Death Dis* (2018) 9:1091. doi: 10.1038/s41419-018-1132-6
17. Zhang T, Jing B, Bai Y, Zhang Y, Yu H. Circular Rna Circtmem45a Acts as the Sponge of Microrna-665 to Promote Hepatocellular Carcinoma Progression. *Mol Ther Nucleic Acids* (2020) 22:285–97. doi: 10.1016/j.omtn.2020.08.011
18. Bronner C, Alhosin M, Hamiche A, Mousli M. Coordinated Dialogue Between Uhrf1 and Dnmt1 to Ensure Faithful Inheritance of Methylated DNA Patterns. *Genes (Basel)* (2019) 10(1):65. doi: 10.3390/genes10010065
19. Gujar H, Weisenberger DJ, Liang G. The Roles of Human DNA Methyltransferases and Their Isoforms in Shaping the Epigenome. *Genes (Basel)* (2019) 10(2):172. doi: 10.3390/genes10020172
20. Mattu S, Fornari F, Quagliata L, Perra A, Angioni MM, Petrelli A, et al. The Metabolic Gene Hao2 is Downregulated in Hepatocellular Carcinoma and Predicts Metastasis and Poor Survival. *J Hepatol* (2016) 64:891–8. doi: 10.1016/j.jhep.2015.11.029
21. Xiao W, Wang X, Wang T, Chen B, Xing J. Hao2 Inhibits Malignancy of Clear Cell Renal Cell Carcinoma by Promoting Lipid Catabolic Process. *J Cell Physiol* (2019) 234:23005–16. doi: 10.1002/jcp.28861
22. Qu Y, Qi L, Hao L, Zhu J. Upregulation of Circ-Asph Contributes to Glioma Cell Proliferation and Aggressiveness by Targeting the Mir-599/Ar/Socs2-As1 Signaling Pathway. *Oncol Lett* (2021) 21:388. doi: 10.3892/ol.2021.12649
23. Wu G, Xia J, Yang Z, Chen Y, Jiang W, Yin T, et al. Circasph Promotes Kgn Cells Proliferation Through Mir-375/Map2k6 Axis in Polycystic Ovary Syndrome. *J Cell Mol Med* (2020) 26(6):1817–25. doi: 10.1111/jcmm.16231
24. Xu L, Ma Y, Zhang H, Lu QJ, Yang L, Jiang GN, et al. Hmga2 Regulates Circular Rna Asph to Promote Tumor Growth in Lung Adenocarcinoma. *Cell Death Dis* (2020) 11:593. doi: 10.1038/s41419-020-2726-3
25. Zhang H, Zhang B, Chen C, Chen J. Circular Rna Circlifr Regulates the Proliferation, Migration, Invasion and Apoptosis of Human Vascular Smooth Muscle Cells *via* the Mir-1299/Kdr Axis. *Metab Brain Dis* (2022) 37:253–63. doi: 10.1007/s11011-021-00853-x
26. Cai Y, Jia Y. Circular Rna Sox5 Promotes the Proliferation and Inhibits the Apoptosis of the Hepatocellular Carcinoma Cells by Targeting Mir-502-5p/Synoviolin 1 Axis. *Bioengineered* (2022) 13:3362–70. doi: 10.1080/21655979.2022.2029110
27. Wu X, Zhang Y. Tet-Mediated Active DNA Demethylation: Mechanism, Function and Beyond. *Nat Rev Genet* (2017) 18:517–34. doi: 10.1038/nrg.2017.33
28. Dong ZR, Ke AW, Li T, Cai JB, Yang YF, Zhou W, et al. Circmemo1 Modulates the Promoter Methylation and Expression of Tcf21 to Regulate Hepatocellular Carcinoma Progression and Sorafenib Treatment Sensitivity. *Mol Cancer* (2021) 20:75. doi: 10.1186/s12943-021-01361-3
29. Cao LQ, Yang XW, Chen YB, Zhang DW, Jiang XF, Xue P. Exosomal Mir-21 Regulates the Tets/Ptenp1/Pten Pathway to Promote Hepatocellular Carcinoma Growth. *Mol Cancer* (2019) 18:148. doi: 10.1186/s12943-019-1075-2
30. Liu J, Jiang J, Mo J, Liu D, Cao D, Wang H, et al. Global DNA 5-Hydroxymethylcytosine and 5-Formylcytosine Contents are Decreased in the Early Stage of Hepatocellular Carcinoma. *Hepatology* (2019) 69:196–208. doi: 10.1002/hep.30146
31. Wang Q, Liang N, Yang T, Li Y, Li J, Huang Q, et al. Dnmt1-Mediated Methylation of Bex1 Regulates Stemness and Tumorigenicity in Liver Cancer. *J Hepatol* (2021) 75(5):1142–53. doi: 10.1016/j.jhep.2021.06.025
32. Chen XF, Tian MX, Sun RQ, Zhang ML, Zhou LS, Jin L, et al. Sirt5 inhibits peroxisomal acox1 to prevent oxidative damage and is downregulated in liver cancer. *EMBO Rep* (2018) 19(5):e45124. doi: 10.15252/embr.201745124

Conflict of Interest: The authors declare that the research was conducted in the absence of any commercial or financial relationships that could be construed as a potential conflict of interest.

Publisher's Note: All claims expressed in this article are solely those of the authors and do not necessarily represent those of their affiliated organizations, or those of the publisher, the editors and the reviewers. Any product that may be evaluated in this article, or claim that may be made by its manufacturer, is not guaranteed or endorsed by the publisher.

frontiers | Frontiers in Oncology

SYSTEMATIC REVIEW
published: 29 June 2022
doi: 10.3389/fonc.2022.943866

Emerging Perspectives of Bone Metastasis in Hepatocellular Carcinoma

Xiaofeng Yuan[1†], Ming Zhuang[1†], Xi Zhu[1,2†], Dong Cheng[1], Jie Liu[1], Donglin Sun[1], Xubin Qiu[1], Yunjie Lu[1*] and Kurt Sartorius[3,4,5*]*

[1] The Third Affiliated Hospital of Soochow University, Changzhou, China, [2] Department of Infectious Diseases, The First Peoples' Hospital of Kunshan, Kunshan, China, [3] Hepatitis Diversity Research Unit, School of Internal Medicine, University of the Witwatersrand, Johannesburg, South Africa, [4] Africa Hepatopancreatobiliary Cancer Consortium (AHPBCC), Mayo Clinic, Jacksonville, FL, United States, [5] School of Laboratory Medicine and Molecular Sciences, College of Health Science, University of KwaZulu-Natal, Durban, South Africa

OPEN ACCESS

Edited by:
Liangrong Shi,
Central South University, China

Reviewed by:
Qizhao Huang,
Southern Medical University, China
Xiaosheng Ma,
Fudan University, China

***Correspondence:**
Xubin Qiu
qiuxubinyiyi@sina.com
Yunjie Lu
lyj0001@suda.edu.cn
Kurt Sartorius
kurt.sartorius@wits.ac.za

[†]These authors have contributed equally to this work

Specialty section:
This article was submitted to Molecular and Cellular Oncology, a section of the journal Frontiers in Oncology

Received: *14 May 2022*
Accepted: *30 May 2022*
Published: *29 June 2022*

Citation:
Yuan X, Zhuang M, Zhu X, Cheng D, Liu J, Sun D, Qiu X, Lu Y and Sartorius K (2022) Emerging Perspectives of Bone Metastasis in Hepatocellular Carcinoma. Front. Oncol. 12:943866. doi: 10.3389/fonc.2022.943866

Recent evidence suggests the global incidence and mortality of hepatocellular carcinoma (HCC) are increasing. Although the highest incidence of HCC remains entrenched in WHO regions with high levels of HBV-HCV infection, the etiology of this disease is rapidly changing to include other lifestyle risk factors. Extrahepatic metastasis is a frequent feature of advanced HCC and most commonly locates in the lungs and bone. Bone metastasis in HCC (HCC-BM) signals a more aggressive stage of disease and a poorer prognosis, simultaneously HCC-BM compromises the function and integrity of bone tissue. HCC induced osteolysis is a prominent feature of metastasis that complicates treatment needed for pathologic fractures, bone pain and other skeletal events like hypercalcemia and nerve compression. Early detection of bone metastases facilitates the treatment strategy for avoiding and relieving complications. Although recent therapeutic advances in HCC like targeting agents and immunotherapy have improved survival, the prognosis for patients with HCC-BM remains problematic. The identification of critical HCC-BM pathways in the bone microenvironment could provide important insights to guide future detection and therapy. This review presents an overview of the clinical development of bone metastases in HCC, identifying key clinical features and identifying potential molecular targets that can be deployed as diagnostic tools or therapeutic agents.

Keywords: hepatocellular carcinoma (HCC), bone metastasis, biomarkers, osteolysis, bone remodeling

BACKGROUND OF BONE METASTASIS IN HCC

A recent analysis of the Globocan 2020 results indicates that the highest incidence of liver cancer persists in East Asia (17.8), North Africa (15.2), Micronesia (14.6), South East Asia (13.6) and Micronesia (11.4) against a global ASR of 9.5 (1). Hepatocellular carcinoma makes up > 75% of all primary liver cancer incidence (2, 3) and accounts for the fourth highest number of cancer-related death in the entire world (4). The incidence and etiology of HCC differ markedly across the WHO regions. In regions like Eastern Asia and Sub-Saharan Africa, for example, where HBV infection is

endemic, the etiology of disease is significantly different from risk factors like NASH and NAFLD that predominate in Western countries. Early detection of HCC is also more likely in developed countries and patients in developing countries often only present at advanced stage disease (5, 6). Early diagnosis or screening for HCC is crucial and eliminating risk factors like viral infection (HBV/HCV), alcohol, dietary toxins, tobacco, aflatoxins and aristolochic acid is likely to reduce incidence more than current clinical treatment options. Due to progress in diagnostics of HCC such as CT/MRI, PET-CT and bone scintigraphy (BS), during the past 20 years, overall survival rates for HCC patients have improved (7–9). Nevertheless, extrahepatic metastases have become more common in recent years and most HCC patients are only diagnosed at an advanced stage. About 16.1% to 38.5% of HCC patients exhibit bone metastasis (BM) at first diagnosis, and 11.7% develop BM following curative resections (10). Patients with HCC who have developed bone metastasis (HCC-BM) have a poor prognosis and a median survival time of only 4.6 months. Risk factors contributing to poor survival among HCC-BM patients include Child-Pugh class A group, alpha-fetoprotein (AFP) levels (> 30 ng/mL), and tumor size (> 5 cm) (11). Moreover, the majority of HCC-BM patients suffer from skeletal-related events (SREs), including fractures and spinal cord compression caused by pathological conditions. Symptoms of these SREs include severe pain and neurological deficits that drastically deteriorate the patients' quality of life. Sadly, there is no definitive therapeutic strategy for the management of HCC-BM. There are contrasting findings about the extent of HCC-BM and some studies indicate it is an infrequent form of presentation (10, 12) whereas others suggest it is relatively common and occurs in ~33.3% of patients with HCC (13). HCC cases reported with bone metastasis tend to have multiple metastatic spreads elsewhere as well (14).

In most cases, bone metastases from HCC are irreversible and incurable, as well as associated with pathological fractures, severe pain, decrease quality of life and poor prognosis (15). Bone metastases increase the burden on healthcare providers and individuals due to switching the medical paradigm from cure to palliation. As a result of advancements in the treatment of HCC-BM patients, it has become possible to identify which patients benefit the most from the treatments available (16). On a more encouraging note, the combined strategies of locoregional therapies and/or systemic therapy are constantly being evaluated. This review paper specially describes HCC-BM pathogenesis and identifies key biomarkers and potential therapeutic agents that could potentially be employed for the early diagnosis and/or treatment.

METASTATIC DISSEMINATION IN HCC

HCC pathogenesis occurs in a setting of chronic inflammation, fibrogenesis and liver damage against a background of frequent immune reactions, uncontrolled hepatocyte proliferation and the frequent mutations of proto-oncogenes and tumor suppressor genes (2). Typically, a key step in HCC metastasis is the loss of regulatory controls in cellular replication and metastasis occurs in conditions of chromosomal instability that can cause a leakage of tumor cell DNA that spread to distant organs (17). When primary HCC proliferates locally, epithelial-mesenchymal transformation (EMT) is activated by widespread epigenetic reprogramming of gene expression, and epithelial cells lose their cell polarity and adhesion properties, becoming more migratory and invasive (18). Once cell polarity transition occurs, polarized epithelial cells lose intercellular crosslinking and acquire a spindle-like morphology thus facilitating migration to distant organs (19). Simultaneously neo-angiogenesis is stimulated to deliver oxygen, nutrients, and growth factors to facilitate tumor growth and enable invasion (20). Vascular endothelial growth factor (VEGF), known as a crucial factor driving angiogenesis in the primary HCC lesion and its metastasis to bone, plays a critical role in stimulating bone resorption and facilitating tumor growth in bone (21).

Macro-and Microinvasion in HCC-BM

A small proportion of cancer cells in a primary HCC tumor have the metastatic potential to disseminate and distribute from the blood and/or lymphatic systems to distant tissues or organs (22) (See **Figure 1**). Various studies have demonstrated that both macro-and microvascular invasion are universally recognized as a predictor of distant metastasis for HCC (23, 24). The presence of tumor cells in the hepatic portal vein can contribute to intrahepatic metastasis, while they can also appear in the hepatic vein to induce the occurrence of distant metastasis of HCC and recurrence after liver transplantation. Clinicopathological features of HCC with portal hypertension account for the predilection of metastases to the spine throughout the valve-less venous plexus (25).

In recent years, the rapid development of radionics and artificial intelligence has made it easy to detect micro-vascular invasion (MVI) by analyzing the peritumoral area. This technology has unique diagnostic advantages and can guide HCC treatment selection and prognosis evaluation (24). Currently, the use of this technology for MVI detection is limited by the radiologists' subjective judgment and lack of uniform guidelines. This method, however, is a promising way to determine the degree of HCC progression using simple imaging data before surgery. Cancer cells can also be found in neuronal spaces as well as the vascular and lymphatic systems, and the process of migration along nerves is termed perineural invasion (PNI) (26). After vascular invasion, metastatic cancer cells in the blood or lymph nodes are called circulating tumor cells (CTCs) and the presence of positive CTCs or ctDNA in HCC indicates a more aggressive phenotype and poorer prognosis (27, 28). Detection of CTCs and circulating tumor DNA (ctDNA) using the new emerging methodologies of liquid biopsy or lymph node biopsy is currently an important method for the diagnosis of metastatic cancers (29, 30).

Preconditions for HCC-BM Establishment

The transport of cancer cells *via* blood vessels and lymph nodes, disseminates them from the primary tumor to bone marrow for further progression to bone metastasis (31). The CTCs enter the

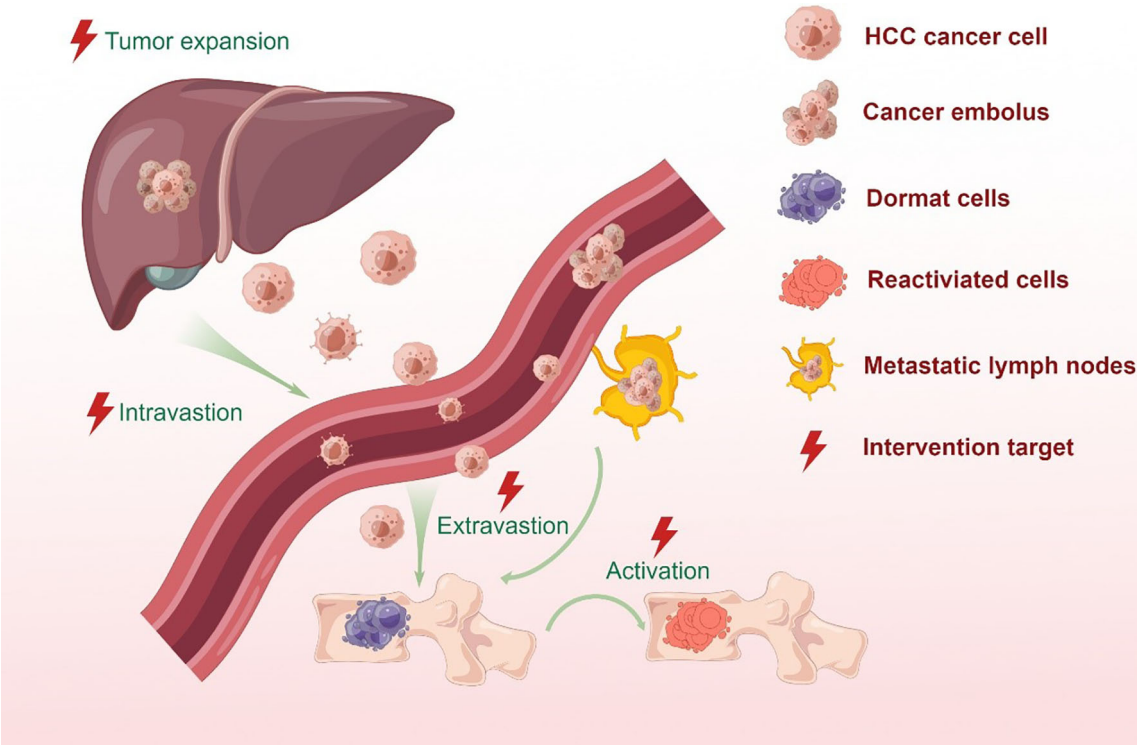

FIGURE 1 | Bone metastatic steps of HCC cells. In situ hepatocellular carcinoma results from the mutation of protooncogenes or suppressor genes in normal cells as a combined result of physical, chemical or biological factors. Cancer cells stimulate angiogenesis to fulfill its nutritional needs. During tumor growth, the extracellular matrix is dissolved, which causes the invasion of the lymphatic and circulatory systems. But only a small proportion of cancer cells can survive and form a tumor thrombus in the circulatory system due to immune surveillance. Meanwhile, CTCs and ctDNA can be detected by the liquid biopsy for monitoring tumor in real time. At the proper time, the surviving cells migrate from the circulatory system to the target organ or tissue and colonize the area. Metastatic tumor cells in distant locations are inactive for a period of time in order to adapt to stress stimuli and survive a hostile environment. When stimulated by an appropriate signal, dormant tumor cells become active and continue to behave in a malignant fashion.

bone marrow compartment by crossing the endothelial cell barrier as well as the basement membrane of blood vessels, and engage in specialized microenvironments or 'bone niche'. A few of these disseminated tumor cells (DTCs) survive to grow in the bone marrow after extravasating into the metastatic site (32). They can either exist as individual cells in a quiescent state or form small masses that do not expand. Besides the invasive qualities, they need to have the ability to adapt to the microenvironment in ways that encourage colonization (32). Often, DTCs that colonize bone and evade the immune system typically remain dormant for long periods. Cellular dormancy, moreover, is a profound mechanism that helps tumor cells evade immune surveillance and evolve to develop chemoresistance (33, 34).

The molecular mechanisms including extracellular matrix (ECM) development, metabolic and epigenetic changes, stemness, dysregulated non-coding RNAs, as well as the activation of the p38 stress-induced pathway, can mobilize dormant cancer cells to progress to form a micro-metastasis (35). As the metastasis progresses, the reactivated dormant cells proliferate uncontrollably and eventually begin to modify bone structure. Clinical speculation also indicates that these tumor cells are at their most vulnerable state in this transition stage for therapeutic targeting (36). Fortunately, technology has made it possible to study rare cells in bone, including dormant cells to complement our understanding of these early steps in BM development (36). Although the general progress of bone metastasis from different soft cancers is similar, however, the thorough and exact pathophysiology underlying the crucial early events of HCC-BM is not yet fully understood. Further research is necessary to elucidate the precise mechanism of DTCs in the bone and determine the optimum conditions for dormancy-break, or - eradication.

HCC-BM BIOMARKERS

According to various studies, HCC metastases and prognosis can be determined by reproducible gene expression patterns in the liver microenvironment (37, 38). Gene-expression profiles that strongly predict metastasis and poor outcome may already be present in primary tumors (see **Figure 2**). Potential biomarkers in serum, urine, and tumor tissue, that have been identified in a

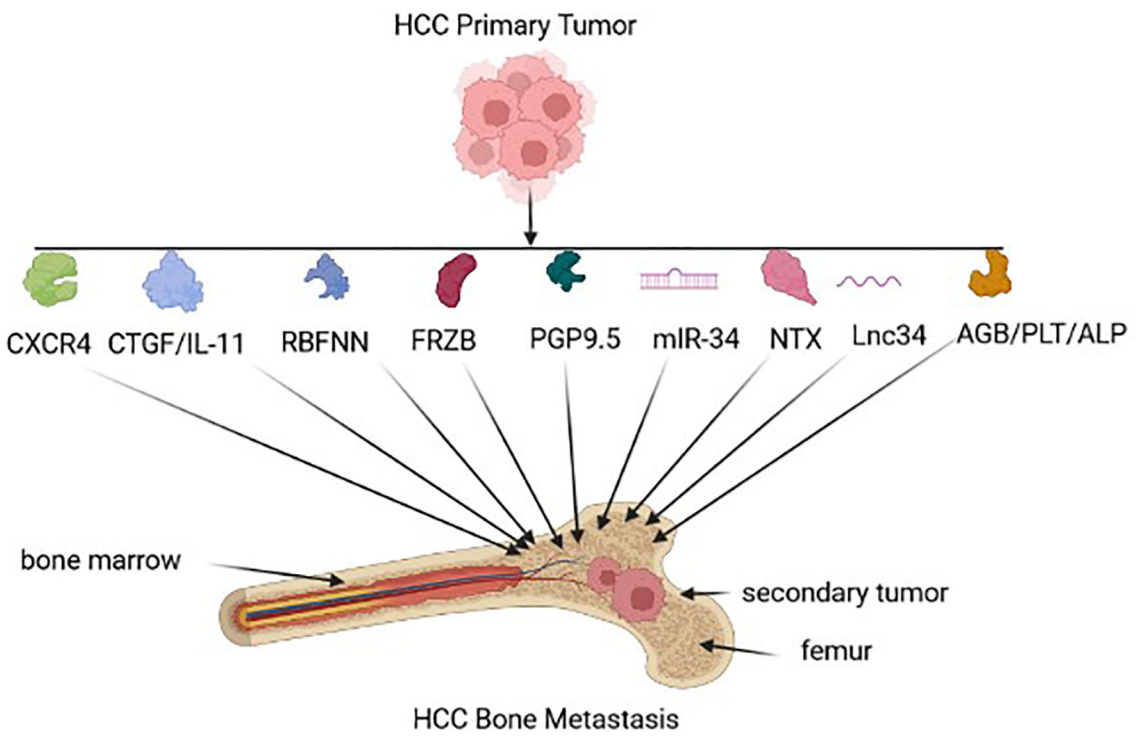

FIGURE 2 | HCC biomarkers for Bone metastasis. Early HCC-BM biomarkers expressed by the tumor-environment include chemokine receptor type 4 (CXCR4), connective tissue growth factor (CTGF)/interleuken 11(Il-11), radial basis function neural network (RBFNN) algorithm containing six peptides, Secreted Frizzled Related Protein 3 (FRZB), neuron cytoplasmic protein 9.5 (PGP 9.5), microRNA-34a (miR-34a), N-terminal telopeptide (NTx), long non-coding RNA 34 (Lnc34), hemoglobin (HGB)/ platelet count (PLT), alkaline phosphatase (ALP).

range of clinical studies to predict HCC-BM, as well as determine prognosis in HCC patients (see **Table 1**).

In HCC, the molecular pathogenesis is extremely complex and heterogeneous, and the process of metastatic dissemination from HCC can be generally separated into the sequential steps: primary tumor growth, cell polarity transition, seed, dormancy, and secondary outgrowth (47, 48). Each step cannot be missed, which means that the process of metastasis is time-consuming and complicated. Given the vulnerability of the metastatic process discussed above, a number of target-oriented HCC-BM biomarkers have been identified (see **Figure 1**/**Table 1**).

In primary HCCs, CXC chemokine receptor 4 (CXCR4) expression may be a biomarker for BM that is associated with poor clinical outcome (39). Stromal cell-derived factor-1 (SDF-1), also known as chemokine ligand 12 (CXCL12), can induce metastases through interacting with CXCR4. Interestingly, an elevated CXCR4 level alone does not necessarily result in HCC-BM due to the loss of SDF-1 expression (49). In another study, the expression of seven serum peptides sourced from AFP, prothrombin, fibrinogen beta chains, serglycin, transthyretin, isoform 2 of inter-alpha-trypsin inhibitor heavy chain H4 (ITIH4), and isoform 1 of autophagy-related protein 16-2 (ATG-16.2) were used as a collective predictive tool for HCC-BM detection (41). FRZB expression was also up-regulated in HCC-BM suggesting that FRZB might play a key predictor of HCC-BM (42). Neuronal cell bodies and axons of peripheral and central nervous systems express PGP9.5, which is a ubiquitin-protein hydrolase could also be considered as a BM biomarker. Interestingly, one study revealed that PGP 9.5 had a higher nerve density in bone metastases tissues compared with HCC tissues (26). The dysregulated expression of miR-34a as a serum and intra-tumoral tissue biomarker was also found to be a useful predictor for the risk of BM in HCC patients (43), as well as the elevated expression of lnc34a expression (45). In another serum based test, low baseline NTX levels could be correlated with a better outcome in HCC-BM patients with Child–Pugh grade A (44) and finally, serum HGB, ALP and PLT could also be useful predictors of BM-HCC versus HCC (46).

BONE REMODELING AND BONE DESTRUCTION

There is a balance between the resorption of mineralized bone by bone-resorbing cells (osteoclasts, OCs) and the formation of new bone by bone-forming cells (osteoblasts, OBs), which is essential for maintaining bone mass in humans (50). The process of bone remodeling is closely influenced by both systemic and local factors to maintain this physiological balance. Once bone metastasis initiation is activated by homotypic and heterotypic

TABLE 1 | Clinical studies about molecular markers in HCC-BM.

Year	Patient	Type of specimens	Biomarker	Status in HCC-BM	Clinical value	Refs
2009	HCC patients with/without BM (n = 43/138)	TMA	CXCR4 expression	Increase	An independent risk factor may be associated with poor clinical outcomes.	(39)
2011	HCC patients with/without BM (n = 24/24) and an independent cohort of 350 HCC patients which was conducted to evaluate the clinical significance of the candidate genes	FFPE, TMA	Intratumoral CTGF combined with IL-11 expression	Increase	An independent risk factor for HCC-BM	(40)
2014	HCC patients with/without BM (n = 66/72)	Serum	RBFNN model based on six significant peptides (m/z for these six peptides were 1535.4, 1780.7, 1866.5, 2131.6, 2880.4, and 2901.9)	Increase	A serological diagnosis tool for HCC-BM	(41)
2015	HCC patients with synchronous or metachronous BM received surgery (n=13)	FFPE	FRZB expression	Increase	A novel predictor for poor prognosis of HCC-BM after surgical resection	(42)
2015	HCC patients with sBM or mBM who received surgery (n=13)	FFPE	PGP9.5 expression	Increase	A potential role of the PNI in HCC-BM	(26)
2016	HCC patients with/without BM (n = 10/10) and an independent cohort of 106 HCC patients for evaluating candidate miRNAs and 296 HCC patients for evaluating the clinical significance of miRNA-34a	Serum, TMA	miRNA-34a expression levels in serum and intratumoral tissue	Decrease	An independent risk factor for HCC-BM	(43)
2017	HCC patients with BM who had been treated with ZOL (n=99)	Serum	The baseline serum NTX	Decrease	Reflecting longer progression-free survival	(44)
2021	HCC patients who underwent curative hepatectomy (n=157)	Serum	Circulating lnc34a expression	Increase	An independent risk factor for HCC-BM	(45)
2022	HCC patients with sBM or mBM (n=77/51)	Serum	Serum HGB, PLT and ALP level	Decrease/ Decrease/ Increase	Risk factors for HCC-BM.	(46)

IHC, immunohistochemistry; TMA, the tissue microarray; MALDI-TOF-MS, Matrix-assisted laser desorption ionization-time of flight mass spectrometry; LC-MS, liquid chromatography-mass spectrometry; m/z, Mass to charge ratio; RBFNN, radial basis function neural network; sBM, synchronous bone metastasis; mBM, metachronous bone metastasis; FRZB, frizzled-related protein; PGP9.5, protein gene product 9.5; PNI, perineural invasion; qRT-PCR, real-time quantitative polymerase chain reaction; ISH, in situ hybridization; ZOL, zoledronic acid; NTX, N-telopeptide of type I collagen; HGB, hemoglobin; PLT, platelet; ALP, alkaline phosphatase.

cellular interactions between cancer cells, OBs and OCs, normal bone homeostasis is easily broken and can lead to a negative chain reaction. Usually, osteolytic and osteogenic metastasis are two opposite types of cancer-related bone metastases (51). The classification is decided by which cell type exerts a dominant effect and represents two extremes of the dysregulation of bone homeostasis, which are bone lysis or sclerosis. Bone metastases in HCC are predominantly osteolytic in nature, and osteoblastic or mixed osteoblastic-osteolytic lesions are possible (21, 52). The main manifestations of osteolytic metastasis are an increased likelihood of systematic severe osteolytic bone lesions and SREs, resulting in fracture, nerve compression syndromes, and even paralysis (53–55). It is worth mentioning that, besides OBs and OCs, the bone microenvironment also consists of stromal cells, hematopoietic cells, and others. However, there is limited recent research reported on these important cells in the evolution of HCC-BM.

MOLECULAR PATHWAYS OF BONE REMODELING

As a key regulator of bone homeostasis, receptor activator of nuclear factor-kB (NF-κB) ligand (RANKL) is also referred to as osteoprotegerin ligand (OPGL), osteoclast differentiation factor (ODF), and TNF-related activation-induced cytokine (TRANCE). Various studies indicate that multinucleated osteoclasts originate from monocyte-/macrophage-lineage cells and resorb mineralized bone matrix by creating a microenvironment. Osteoclast precursors overexpress RANK when exposed to macrophage colony-stimulating factor (M-CSF), which binds to RANKL expressed by osteoblasts (56). Through the PI3K/Akt/mTOR and NF-κB pathway, the complex of RANK/RANKL recruits TNF receptor-associated factors (TRAF6), and finally induces osteoclast maturation (57, 58). In contrast, OPG, a soluble RANKL decoy receptor, could block its interaction with RANK by binding RANKL (59). The relative expression levels of RANKL and OPG determine the activation of osteoclasts and bone metabolism.

The normal bone microenvironment consists of osteoblasts, osteoclasts, stromal cells, mineralized bone matrix, hematopoietic cells, and others. But in the presence of metastatic HCC cells, its molecular interactions with the bone microenvironment disrupt the balance of bone metabolism and further drive skeletal metastases. Previous studies (60) have shown that metastatic tumor cells in many cancers including those of the breast, prostate and lung, could directly secret

RANKL or induce osteoblasts to produce RANKL, thereby causing bone destruction and bone formation which is characterized by matrix degradation and release of numerous cytokines and growth factors. Sasaki et al. (61) firstly studied RANKL produced by HCC cells and showed that RANKL activated and differentiated osteoclast precursors, which resulted in osteolysis and bone metastasis. Parathyroid hormone-related protein (PTHrP), an important prognostic factor of malignancy-associated hypercalcemia (MAH), was known to increase the RANKL expression and repress the OPG expression, indicating that PTHrP could promote bone metastasis in breast cancer (62–64). Previous studies have shown that a similar expression trend of PTHrP is undetectable in HCC cells by immunohistochemistry (65). On the other hand, recent clinical studies addressing PTHrP-mediated hypercalcemia have demonstrated that PTHrP can be detected in HCC patients from Australia and Korea (66, 67). Despite the important role of PTHrP in calcium/phosphorus metabolism and bone resorption, there has been no previous evidence of a link between PTHrP expression and bone metastasis in HCC, unlike in other cancers.

POSSIBLE HCC-BM THERAPEUTIC PATHWAYS

Due to the absence of obvious symptoms in the early onset of bone metastases, the diagnosis of bone metastases is difficult, and an effective treatment has not yet been established. The presence of multiple levels of intratumor heterogeneity is recognized as a distinct characteristic of human tumors that modulates the efficacy of targeted therapy in HCC-BM (see **Table 2**). Based on next-generation sequencing (NGS), however, important driver of mutations in HCC cells have been determined including EGFR, ALK, KRAS, and PI3KCA (72).

The secreted multifunctional glycoprotein LGALS3 (Lectin galactoside-binding soluble 3) is generally upregulated in tumors through various intracellular and extracellular mechanisms (73). LGALS3 produced by HCC is located on the outer surface of osteoclast progenitor cells (OPs) and promotes CD98- and integrin ?α/?β complex–mediated fusion and podosome formation of osteoclasts. This is explained by increased the formation of $TRAP^+$-multinuclear OCs and TRAP activity, but no alteration of ALP^+-OBs along with the interface of bone-tumor (68). Furthermore, E3 ligase RNF219-mediated α-catenin degradation promotes the overexpression of LGALS3 through YAP1/β-catenin-dependent epigenetic modifications, resulting in HCC-BM and following SREs. A potential therapeutic option, namely, Verteporfin (VP), a YAP specific inhibitor, can block RNF219/α-catenin/LGALS3 axis to effectively inhibit HCC-BM (74). Other studies have focused on the role of long non-coding transcripts in HCC-BM. Long noncoding RNAs (lncRNAs) are RNAs with limited or no coding potential that are longer than two hundred nucleotides in size (75). Emerging evidences indicated that dysregulated lncRNAs lead significantly to the initiation and progression of tumorigenesis (76). Targeting dysregulated lncRNA in HCC-BM pathways, thus, offers another therapeutic option. It has been suggested that the expression of lncZEB1-AS1, an oncogenic lncRNA, is evident in HCC patients with lung (77) and bone metastasis (70). Zinc finger E-box binding homeobox 1 (ZEB1) is also a pivotal regulator that induces EMT and metastasis. LncZEB1-AS1, however, also influences matrix metalloproteinases (MMPs) without EMT-related markers including Vimentin, N-cadherin, or E-cadherin (70). Furthermore, lncZEB1-AS1 serves as a ceRNA for miR-302b and thereby promotes tumor progression *via* EGFR-PI3K-AKT signaling although no clear evidence about the effect of lncZEB1-AS1 on HCC-BM has been directly demonstrated (70). Lnc34a expression in serum is a potential predictive biomarker for HCC-BM patients (45). Previous series studies indicated that lnc34a epigenetically inhibits miR-34a expression through recruiting DNMT3a *via* PHB2 to methylate miR-34a promoter, as well as HDAC1 to promote histones deacetylation. Alternatively, miR-34a also targets Smad4 through the TGF-β pathway and then alters transcription of downstream genes related with BM, for instance, CTGF and IL-11 (71).

SUMMARY

HCC metastasizes into bone tissue after a cascade of short-term responses. Genetic factors, the tumor microenvironment (TME),

TABLE 2 | Recent advances in molecular mechanisms and oncogenes in HCC-BM.

Target	Clinical association	Location	Main mechanism	Blocking method	Refs
LGALS3	LGALS3- overexpression promotes HCC bone metastasis	The outermost covering of OP cells	Promoting differentiation and Activation of Osteoclasts by activating CD98- and integrin αv/β3 complex-mediated fusion and podosome formation	LGALS3 neutralizing antibody or YAP inhibitor verteporfin	(68)
H19	H19-overexpression promotes HCC bone metastasis	Chromosome 11p15.5	Reducing OPG expression *via* PPP1CA-induced P38 dephosphorylation process and promoting ZEB1-dependent EMT by downregulating miR-200b-3p	P38 inhibitor	(69)
LncZEB1-AS1	LncZEB1-AS1-overexpression promotes HCC bone metastasis	Chromosome 10p11.22 region contiguous with ZEB1	Inducing MMP2, MMP7 and MMP9 upregulation *via* inhibiting miR-302b, resulting in enhanced EGFR/PI3K-AKT signaling	Compounds targeting the lncZEB1-AS1-miR-302b-EGFR axis	(70)
Lnc34a	Lnc34a-overexpression promotes HCC bone metastasis	Enriching in colon cancer stem cells (CCSCs)	Recruiting Dnmt3a *via* PHB2 and HDAC1 to methylate and deacetylate the miR-34a promoter and thereby targeting Smad4 *via* the TGF-β pathway	Increasing miR-34a or decreasing Smad4	(71)

and other factors all work in concert to promote HCC-BM. Developments in diagnostic technologies, however, allow us to detect HCC-BM in earlier stages using multiple novel technologies, including medical image analysis which is based on artificial intelligence (AI), as well as the use of liquid biopsies and next-generation sequencing (NGS). The accurate detection of HCC-BM stage and its molecular features also promote a clearer picture for patient treatment and prognosis. Currently, traditional treatments such as surgery, radiotherapy and chemotherapy, as well as targeted therapy including sorafenib and bisphosphonate, remain complicated by the complex nature of HCC-BM. However, future research that promotes a better understanding of the intra-tumoral heterogeneity of HCC-BM can improve the development of improved therapy. Understanding the key to heterogeneity will help us develop individualized approaches for HCC patients and new generation drugs can be adjusted accordingly. Alternatively, this understanding can promote the better deployment of current drug alternatives at different stages of HCC-BM pathogenesis. However, our understanding of the molecular etiology of the HCC-BM tumor microenvironment needs to be improved by further studies covering energy metabolism and differential immune responses. In summary, we have offered some novel perspectives in HCC-BM showing that it is a complex and multistep process that currently leads to mortality. Understanding the TME and HCC-BM mechanisms will help drive future potential therapeutic interventions as a way to improve the quality of life and extend the lives of HCC-BM patients.

DATA AVAILABILITY STATEMENT

The original contributions presented in the study are included in the article/supplementary material. Further inquiries can be directed to the corresponding authors.

AUTHOR CONTRIBUTIONS

XY, MZ, and XZ reviewed the literature and wrote the manuscript. DC, JL, and DS revised the manuscript. XQ, YL, and KS reviewed, revised the manuscript and performed figures and tables of the manuscript. All authors contributed to read and approved the submitted version.

FUNDING

This work was supported by the National Natural Science Foundation of China (81971504), Post-Doctoral Special Foundation of China (2020M670065ZX), Post-Doctoral Foundation of Jiangsu Province (2020Z021), Changzhou Society Development Funding (CE20205038), The lifting Project of 2021 Young Scientific and technological talents in Changzhou, Youth Science and Technology Talent Program of Changzhou Health and Family Planning Commission (QN202106 and QN202007), Changzhou Sci&Tech Program (CJ20210085), and Youth Talent Development Plan of Changzhou Health Commission (CZQM2020047).

REFERENCES

1. Sung H, Ferlay J, Siegel RL, Laversanne M, Soerjomataram I, Jemal A, et al. Global Cancer Statistics 2020: GLOBOCAN Estimates of Incidence and Mortality Worldwide for 36 Cancers in 185 Countries. *CA: Cancer J Clin* (2021) 71(3):209–49. doi: 10.3322/caac.21660
2. El-Serag HB, Rudolph KL. Hepatocellular Carcinoma: Epidemiology and Molecular Carcinogenesis. *Gastroenterology* (2007) 132(7):2557–76. doi: 10.1053/j.gastro.2007.04.061
3. Petrick JL, Florio AA, Znaor A, Ruggieri D, Laversanne M, Alvarez CS, et al. International Trends in Hepatocellular Carcinoma Incidence, 1978–2012. *Int J Cancer.* (2020) 147(2):317–30. doi: 10.1002/ijc.32723
4. Bray F, Ferlay J, Soerjomataram I, Siegel RL, Torre LA, Jemal A. Global Cancer Statistics 2018: GLOBOCAN Estimates of Incidence and Mortality Worldwide for 36 Cancers in 185 Countries. *CA Cancer J Clin* (2018) 68 (6):394–424. doi: 10.3322/caac.21492
5. Zeng H, Chen W, Zheng R, Zhang S, Ji JS, Zou X, et al. Changing Cancer Survival in China During 2003-15: A Pooled Analysis of 17 Population-Based Cancer Registries. *Lancet Glob Health* (2018) 6(5):e555–e67. doi: 10.1016/S2214-109X(18)30127-X
6. El-Serag HB. Epidemiology of Viral Hepatitis and Hepatocellular Carcinoma. *Gastroenterology* (2012) 142(6):1264–73.e1. doi: 10.1053/j.gastro.2011.12.061
7. Seo HJ, Kim GM, Kim JH, Kang WJ, Choi HJ. (1)(8)F-FDG PET/CT in Hepatocellular Carcinoma: Detection of Bone Metastasis and Prediction of Prognosis. *Nucl Med Commun* (2015) 36(3):226–33. doi: 10.1097/MNM.0000000000000246
8. Kim S, Chun M, Wang H, Cho S, Oh YT, Kang SH, et al. Bone Metastasis From Primary Hepatocellular Carcinoma: Characteristics of Soft Tissue Formation. *Cancer Res Treat* (2007) 39(3):104–8. doi: 10.4143/crt.2007.39.3.104
9. Kutaiba N, Ardalan Z, Patwala K, Lau E, Goodwin M, Gow P. Value of Bone Scans in Work-Up of Patients With Hepatocellular Carcinoma for Liver Transplant. *Transplant Direct.* (2018) 4(12):e408. doi: 10.1097/TXD.0000000000000846
10. Natsuizaka M, Omura T, Akaike T, Kuwata Y, Yamazaki K, Sato T, et al. Clinical Features of Hepatocellular Carcinoma With Extrahepatic Metastases. *J Gastroenterol Hepatol* (2005) 20(11):1781–7. doi: 10.1111/j.1440-1746.2005.03919.x
11. Kim S, Choi Y, Kwak DW, Lee HS, Hur WJ, Baek YH, et al. Prognostic Factors in Hepatocellular Carcinoma Patients With Bone Metastases. *Radiat Oncol J* (2019) 37(3):207–14. doi: 10.3857/roj.2019.00136
12. Fukutomi M, Yokota M, Chuman H, Harada H, Zaitsu Y, Funakoshi A, et al. Increased Incidence of Bone Metastases in Hepatocellular Carcinoma. *Eur J Gastroenterol Hepatol* (2001) 13(9):1083–8. doi: 10.1097/00042737-200109000-00015
13. Harding JJ, Abu-Zeinah G, Chou JF, Owen DH, Ly M, Lowery MA, et al. Frequency, Morbidity, and Mortality of Bone Metastases in Advanced Hepatocellular Carcinoma. *J Natl Compr Canc Netw* (2018) 16(1):50–8. doi: 10.6004/jnccn.2017.7024
14. Bukhari S, Ward K, Styler M. Hepatocellular Carcinoma: First Manifestation as Solitary Humeral Bone Metastasis. *Case Rep Oncol Med* (2020) 2020:8254236. doi: 10.1155/2020/8254236
15. Longo V, Brunetti O, D'Oronzo S, Ostuni C, Gatti P, Silvestris F. Bone Metastases in Hepatocellular Carcinoma: An Emerging Issue. *Cancer Metastasis Rev* (2014) 33(1):333–42. doi: 10.1007/s10555-013-9454-4
16. Chen C, Wang G. Mechanisms of Hepatocellular Carcinoma and Challenges and Opportunities for Molecular Targeted Therapy. *World J Hepatol* (2015) 7 (15):1964–70. doi: 10.4254/wjh.v7.i15.1964
17. Bakhoum SF, Ngo B, Laughney AM, Cavallo J-A, Murphy CJ, Ly P, et al. Chromosomal Instability Drives Metastasis Through a Cytosolic

DNA Response. *Nature* (2018) 553(7689):467–72. doi: 10.1038/nature25432
18. Lin J, Lin W, Ye Y, Wang L, Chen X, Zang S, et al. Kindlin-2 Promotes Hepatocellular Carcinoma Invasion and Metastasis by Increasing Wnt/beta-Catenin Signaling. *J Exp Clin Cancer Res* (2017) 36(1):134. doi: 10.1186/s13046-017-0603-4
19. Dongre A, Weinberg RA. New Insights Into the Mechanisms of Epithelial-Mesenchymal Transition and Implications for Cancer. *Nat Rev Mol Cell Biol* (2019) 20(2):69–84. doi: 10.1038/s41580-018-0080-4
20. Bergers G, Hanahan D. Modes of Resistance to Anti-Angiogenic Therapy. *Nat Rev Cancer.* (2008) 8(8):592–603. doi: 10.1038/nrc2442
21. Iguchi H, Yokota M, Fukutomi M, Uchimura K, Yonemasu H, Hachitanda Y, et al. A Possible Role of VEGF in Osteolytic Bone Metastasis of Hepatocellular Carcinoma. *J Exp Clin Cancer Res* (2002) 21(3):309–13.
22. Luzzi KJ, MacDonald IC, Schmidt EE, Kerkvliet N, Morris VL, Chambers AF, et al. Multistep Nature of Metastatic Inefficiency: Dormancy of Solitary Cells After Successful Extravasation and Limited Survival of Early Micrometastases. *Am J Pathol* (1998) 153(3):865–73. doi: 10.1016/S0002-9440(10)65628-3
23. Rodriguez-Peralvarez M, Luong TV, Andreana L, Meyer T, Dhillon AP, Burroughs AK. A Systematic Review of Microvascular Invasion in Hepatocellular Carcinoma: Diagnostic and Prognostic Variability. *Ann Surg Oncol* (2013) 20(1):325–39. doi: 10.1245/s10434-012-2513-1
24. Renzulli M, Mottola M, Coppola F, Cocozza MA, Malavasi S, Cattabriga A, et al. Automatically Extracted Machine Learning Features From Preoperative CT to Early Predict Microvascular Invasion in HCC: The Role of the Zone of Transition (ZOT). *Cancers (Basel)* (2022) 14(7):1816. doi: 10.3390/cancers14071816
25. Batson OV. The Function of the Vertebral Veins and Their Role in the Spread of Metastases. *Ann Surg* (1940) 112(1):138–49. doi: 10.1097/00000658-194007000-00016
26. Wang X, Lan H, Shen T, Gu P, Guo F, Lin X, et al. Perineural Invasion: A Potential Reason of Hepatocellular Carcinoma Bone Metastasis. *Int J Clin Exp Med* (2015) 8(4):5839–46.
27. Amado V, Gonzalez-Rubio S, Zamora J, Alejandre R, Espejo-Cruz ML, Linares C, et al. Clearance of Circulating Tumor Cells in Patients With Hepatocellular Carcinoma Undergoing Surgical Resection or Liver Transplantation. *Cancers (Basel)* (2021) 13(10):2476. doi: 10.3390/cancers13102476
28. Yu JJ, Xiao W, Dong SL, Liang HF, Zhang ZW, Zhang BX, et al. Effect of Surgical Liver Resection on Circulating Tumor Cells in Patients With Hepatocellular Carcinoma. *BMC Cancer.* (2018) 18(1):835. doi: 10.1186/s12885-018-4744-4
29. Ye Q, Ling S, Zheng S, Xu X. Liquid Biopsy in Hepatocellular Carcinoma: Circulating Tumor Cells and Circulating Tumor DNA. *Mol Cancer.* (2019) 18(1):114. doi: 10.1186/s12943-019-1043-x
30. Sun C, Liao W, Deng Z, Li E, Feng Q, Lei J, et al. The Diagnostic Value of Assays for Circulating Tumor Cells in Hepatocellular Carcinoma: A Meta-Analysis. *Med (Baltimore).* (2017) 96(29):e7513. doi: 10.1097/MD.0000000000007513
31. Kingsley LA, Fournier PG, Chirgwin JM, Guise TA. Molecular Biology of Bone Metastasis. *Mol Cancer Ther* (2007) 6(10):2609–17. doi: 10.1158/1535-7163.MCT-07-0234
32. Clezardin P, Coleman R, Puppo M, Ottewell P, Bonnelye E, Paycha F, et al. Bone Metastasis: Mechanisms, Therapies, and Biomarkers. *Physiol Rev* (2021) 101(3):797–855. doi: 10.1152/physrev.00012.2019
33. Talukdar S, Bhoopathi P, Emdad L, Das S, Sarkar D, Fisher PB. Dormancy and Cancer Stem Cells: An Enigma for Cancer Therapeutic Targeting. *Adv Cancer Res* (2019) 141:43–84. doi: 10.1016/bs.acr.2018.12.002
34. Yang X, Liang X, Zheng M, Tang Y. Cellular Phenotype Plasticity in Cancer Dormancy and Metastasis. *Front Oncol* (2018) 8:505. doi: 10.3389/fonc.2018.00505
35. Jahanban-Esfahlan R, Seidi K, Manjili MH, Jahanban-Esfahlan A, Javaheri T, Zare P. Tumor Cell Dormancy: Threat or Opportunity in the Fight Against Cancer. *Cancers (Basel).* (2019) 11(8):1207. doi: 10.3390/cancers11081207
36. Manjili MH. Tumor Dormancy and Relapse: From a Natural Byproduct of Evolution to a Disease State. *Cancer Res* (2017) 77(10):2564–9. doi: 10.1158/0008-5472.CAN-17-0068
37. Hoshida Y, Villanueva A, Kobayashi M, Peix J, Chiang DY, Camargo A, et al. Gene Expression in Fixed Tissues and Outcome in Hepatocellular Carcinoma. *N Engl J Med* (2008) 359(19):1995–2004. doi: 10.1056/NEJMoa0804525
38. Budhu A, Forgues M, Ye QH, Jia HL, He P, Zanetti KA, et al. Prediction of Venous Metastases, Recurrence, and Prognosis in Hepatocellular Carcinoma Based on a Unique Immune Response Signature of the Liver Microenvironment. *Cancer Cell* (2006) 10(2):99–111. doi: 10.1016/j.ccr.2006.06.016
39. Xiang ZL, Zeng ZC, Tang ZY, Fan J, Zhuang PY, Liang Y, et al. Chemokine Receptor CXCR4 Expression in Hepatocellular Carcinoma Patients Increases the Risk of Bone Metastases and Poor Survival. *BMC Cancer.* (2009) 9:176. doi: 10.1186/1471-2407-9-176
40. Xiang ZL, Zeng ZC, Tang ZY, Fan J, He J, Zeng HY, et al. Potential Prognostic Biomarkers for Bone Metastasis From Hepatocellular Carcinoma. *Oncologist* (2011) 16(7):1028–39. doi: 10.1634/theoncologist.2010-0358
41. He J, Zeng ZC, Xiang ZL, Yang P. Mass Spectrometry-Based Serum Peptide Profiling in Hepatocellular Carcinoma With Bone Metastasis. *World J Gastroenterol* (2014) 20(11):3025–32. doi: 10.3748/wjg.v20.i11.3025
42. Huang J, Hu W, Lin X, Wang X, Jin K. FRZB Up-Regulated in Hepatocellular Carcinoma Bone Metastasis. *Int J Clin Exp Pathol* (2015) 8(10):13353–9.
43. Xiang ZL, Zhao XM, Zhang L, Yang P, Fan J, Tang ZY, et al. MicroRNA-34a Expression Levels in Serum and Intratumoral Tissue can Predict Bone Metastasis in Patients With Hepatocellular Carcinoma. *Oncotarget* (2016) 7(52):87246–56. doi: 10.18632/oncotarget.13531
44. Honda Y, Aikata H, Honda F, Nakano N, Nakamura Y, Hatooka M, et al. Clinical Outcome and Prognostic Factors in Hepatocellular Carcinoma Patients With Bone Metastases Medicated With Zoledronic Acid. *Hepatol Res* (2017) 47(10):1053–60. doi: 10.1111/hepr.12844
45. Zhang L, Niu H, Yang P, Ma J, Yuan BY, Zeng ZC, et al. Serum Lnc34a is a Potential Prediction Biomarker for Bone Metastasis in Hepatocellular Carcinoma Patients. *BMC Cancer.* (2021) 21(1):161. doi: 10.1186/s12885-021-07808-6
46. Zhang Y, Xu Y, Ma W, Wu H, Xu G, Chekhonin VP, et al. The Homogeneity and Heterogeneity of Occurrence, Characteristics, and Prognosis in Hepatocellular Carcinoma Patients With Synchronous and Metachronous Bone Metastasis. *J Cancer.* (2022) 13(2):393–400. doi: 10.7150/jca.65308
47. Krakhmal NV, Zavyalova MV, Denisov EV, Vtorushin SV, Perelmuter VM. Cancer Invasion: Patterns and Mechanisms. *Acta Naturae.* (2015) 7(2):17–28. doi: 10.32607/20758251-2015-7-2-17-28
48. Zheng Y, Zhou H, Dunstan CR, Sutherland RL, Seibel MJ. The Role of the Bone Microenvironment in Skeletal Metastasis. *J Bone Oncol* (2013) 2(1):47–57. doi: 10.1016/j.jbo.2012.11.002
49. Liu H, Pan Z, Li A, Fu S, Lei Y, Sun H, et al. Roles of Chemokine Receptor 4 (CXCR4) and Chemokine Ligand 12 (CXCL12) in Metastasis of Hepatocellular Carcinoma Cells. *Cell Mol Immunol* (2008) 5(5):373–8. doi: 10.1038/cmi.2008.46
50. Roodman GD. Mechanisms of Bone Metastasis. *N Engl J Med* (2004) 350(16):1655–64. doi: 10.1056/NEJMra030831
51. Mundy GR. Metastasis to Bone: Causes, Consequences and Therapeutic Opportunities. *Nat Rev Cancer.* (2002) 2(8):584–93. doi: 10.1038/nrc867
52. Santini D, Pantano F, Riccardi F, Di Costanzo GG, Addeo R, Guida FM, et al. Natural History of Malignant Bone Disease in Hepatocellular Carcinoma: Final Results of a Multicenter Bone Metastasis Survey. *PLoS One* (2014) 9(8):e105268. doi: 10.1371/journal.pone.0105268
53. Taki Y, Yamaoka Y, Takayasu T, Ino K, Shimahara Y, Mori K, et al. Bone Metastases of Hepatocellular Carcinoma After Liver Resection. *J Surg Oncol* (1992) 50(1):12–8. doi: 10.1002/jso.2930500104
54. Hirai T, Shinoda Y, Tateishi R, Asaoka Y, Uchino K, Wake T, et al. Early Detection of Bone Metastases of Hepatocellular Carcinoma Reduces Bone Fracture and Paralysis. *Jpn J Clin Oncol* (2019) 49(6):529–36. doi: 10.1093/jjco/hyz028
55. Lu Y, Hu JG, Lin XJ, Li XG. Bone Metastases From Hepatocellular Carcinoma: Clinical Features and Prognostic Factors. *Hepatobiliary Pancreat Dis Int* (2017) 16(5):499–505. doi: 10.1016/S1499-3872(16)60173-X
56. Boyle WJ, Simonet WS, Lacey DL. Osteoclast Differentiation and Activation. *Nature* (2003) 423(6937):337–42. doi: 10.1038/nature01658
57. Udagawa N, Koide M, Nakamura M, Nakamichi Y, Yamashita T, Uehara S, et al. Osteoclast Differentiation by RANKL and OPG Signaling

Pathways. *J Bone Miner Metab* (2021) 39(1):19–26. doi: 10.1007/s00774-020-01162-6
58. Soysa NS, Alles N. NF-kappaB Functions in Osteoclasts. *Biochem Biophys Res Commun* (2009) 378(1):1–5. doi: 10.1016/j.bbrc.2008.10.146
59. Hofbauer LC, Schoppet M. Clinical Implications of the Osteoprotegerin/RANKL/RANK System for Bone and Vascular Diseases. *JAMA* (2004) 292 (4):490–5. doi: 10.1001/jama.292.4.490
60. Huang L, Cheng YY, Chow LT, Zheng MH, Kumta SM. Tumour Cells Produce Receptor Activator of NF-kappaB Ligand (RANKL) in Skeletal Metastases. *J Clin Pathol* (2002) 55(11):877–8. doi: 10.1136/jcp.55.11.877
61. Sasaki A, Ishikawa K, Haraguchi N, Inoue H, Ishio T, Shibata K, et al. Receptor Activator of Nuclear factor-kappaB Ligand (RANKL) Expression in Hepatocellular Carcinoma With Bone Metastasis. *Ann Surg Oncol* (2007) 14 (3):1191–9. doi: 10.1245/s10434-006-9277-4
62. Bhatia P, Sanders MM, Hansen MF. Expression of Receptor Activator of Nuclear factor-kappaB is Inversely Correlated With Metastatic Phenotype in Breast Carcinoma. *Clin Cancer Res* (2005) 11(1):162–5.
63. Bouizar Z, Spyratos F, Deytieux S, de Vernejoul MC, Jullienne A. Polymerase Chain Reaction Analysis of Parathyroid Hormone-Related Protein Gene Expression in Breast Cancer Patients and Occurrence of Bone Metastases. *Cancer Res* (1993) 53(21):5076–8.
64. Truong NU, de BEMD, Papavasiliou V, Goltzman D, Kremer R. Parathyroid Hormone-Related Peptide and Survival of Patients With Cancer and Hypercalcemia. *Am J Med* (2003) 115(2):115–21. doi: 10.1016/S0002-9343(03)00310-3
65. Roskams T, Willems M, Campos RV, Drucker DJ, Yap SH, Desmet VJ. Parathyroid Hormone-Related Peptide Expression in Primary and Metastatic Liver Tumours. *Histopathology* (1993) 23(6):519–25. doi: 10.1111/j.1365-2559.1993.tb01237.x
66. Donovan PJ, Achong N, Griffin K, Galligan J, Pretorius CJ, McLeod DS. PTHrP-Mediated Hypercalcemia: Causes and Survival in 138 Patients. *J Clin Endocrinol Metab* (2015) 100(5):2024–9. doi: 10.1210/jc.2014-4250
67. Jin J, Chung JO, Chung MY, Cho DH, Chung DJ. Clinical Characteristics, Causes and Survival in 115 Cancer Patients With Parathyroid Hormone Related Protein-Mediated Hypercalcemia. *J Bone Metab* (2017) 24(4):249–55. doi: 10.11005/jbm.2017.24.4.249
68. Zhang S, Xu Y, Xie C, Ren L, Wu G, Yang M, et al. RNF219/alpha-Catenin/LGALS3 Axis Promotes Hepatocellular Carcinoma Bone Metastasis and Associated Skeletal Complications. *Adv Sci (Weinh).* (2021) 8(4):2001961. doi: 10.1002/advs.202001961
69. Huang Z, Chu L, Liang J, Tan X, Wang Y, Wen J, et al. H19 Promotes HCC Bone Metastasis Through Reducing Osteoprotegerin Expression in a Protein Phosphatase 1 Catalytic Subunit Alpha/p38 Mitogen-Activated Protein Kinase-Dependent Manner and Sponging microRNA 200b-3p. *Hepatology* (2021) 74(1):214–32. doi: 10.1002/hep.31673
70. Ma ZJ, Wang Y, Li HF, Liu MH, Bi FR, Ma L, et al. LncZEB1-AS1 Regulates Hepatocellular Carcinoma Bone Metastasis *via* Regulation of the miR-302b-EGFR-PI3K-AKT Axis. *J Cancer.* (2020) 11(17):5118–28. doi: 10.7150/jca.45995
71. Zhang L, Niu H, Ma J, Yuan BY, Chen YH, Zhuang Y, et al. The Molecular Mechanism of LncRNA34a-Mediated Regulation of Bone Metastasis in Hepatocellular Carcinoma. *Mol Cancer.* (2019) 18(1):120. doi: 10.1186/s12943-019-1044-9
72. Jin K, Lan H, Wang X, Lv J. Genetic Heterogeneity in Hepatocellular Carcinoma and Paired Bone Metastasis Revealed by Next-Generation Sequencing. *Int J Clin Exp Pathol* (2017) 10(10):10495–504.
73. Capone E, Iacobelli S, Sala G. Role of Galectin 3 Binding Protein in Cancer Progression: A Potential Novel Therapeutic Target. *J Transl Med* (2021) 19 (1):405. doi: 10.1186/s12967-021-03085-w
74. Dong L, Lin F, Wu W, Liu Y, Huang W. Verteporfin Inhibits YAP-Induced Bladder Cancer Cell Growth and Invasion *via* Hippo Signaling Pathway. *Int J Med Sci* (2018) 15(6):645–52. doi: 10.7150/ijms.23460
75. Peng WX, Koirala P, Mo YY. LncRNA-Mediated Regulation of Cell Signaling in Cancer. *Oncogene* (2017) 36(41):5661–7. doi: 10.1038/onc.2017.184
76. Liu SJ, Dang HX, Lim DA, Feng FY, Maher CA. Long Noncoding RNAs in Cancer Metastasis. *Nat Rev Cancer.* (2021) 21(7):446–60. doi: 10.1038/s41568-021-00353-1
77. Li T, Xie J, Shen C, Cheng D, Shi Y, Wu Z, et al. Upregulation of Long Noncoding RNA ZEB1-AS1 Promotes Tumor Metastasis and Predicts Poor Prognosis in Hepatocellular Carcinoma. *Oncogene* (2016) 35(12):1575–84. doi: 10.1038/onc.2015.223

Conflict of Interest: The authors declare that the research was conducted in the absence of any commercial or financial relationships that could be construed as a potential conflict of interest.

frontiers | Frontiers in Oncology

REVIEW
published: 08 July 2022
doi: 10.3389/fonc.2022.956225

Polo-Like Kinase 2: From Principle to Practice

Chuanyong Zhang[1,2†], *Chuangye Ni*[1,2†] *and Hao Lu*[1,2*]

[1] Hepatobiliary Center, The First Affiliated Hospital of Nanjing Medical University, Nanjing, China, [2] Key Laboratory of Liver Transplantation, Chinese Academy of Medical Sciences, Nanjing, China

Polo-like kinase (PLK) 2 is an evolutionarily conserved serine/threonine kinase that shares the n-terminal kinase catalytic domain and the C-terminal Polo Box Domain (PBD) with other members of the PLKs family. In the last two decades, mounting studies have focused on this and tried to clarify its role in many aspects. PLK2 is essential for mitotic centriole replication and meiotic chromatin pairing, synapsis, and crossing-over in the cell cycle; Loss of PLK2 function results in cell cycle disorders and developmental retardation. PLK2 is also involved in regulating cell differentiation and maintaining neural homeostasis. In the process of various stimuli-induced stress, including oxidative and endoplasmic reticulum, PLK2 may promote survival or apoptosis depending on the intensity of stimulation and the degree of cell damage. However, the role of PLK2 in immunity to viral infection has been studied far less than that of other family members. Because PLK2 is extensively and deeply involved in normal physiological functions and pathophysiological mechanisms of cells, its role in diseases is increasingly being paid attention to. The effect of PLK2 in inhibiting hematological tumors and fibrotic diseases, as well as participating in neurodegenerative diseases, has been gradually recognized. However, the research results in solid organ tumors show contradictory results. In addition, preliminary studies using PLK2 as a disease predictor and therapeutic target have yielded some exciting and promising results. More research will help people better understand PLK2 from principle to practice.

Keywords: polo-like kinase 2, cell cycle, stress, tumor, neurodegenerative disease

OPEN ACCESS

Edited by:
Xiaodong Li,
First People's Hospital of Changzhou, China

Reviewed by:
Hao Liu,
University of Pittsburgh Medical Center, United States
Xiao Zheng,
Soochow University Medical College (SUMC), China

***Correspondence:**
Hao Lu
luhao@njmu.edu.cn

[†]*These authors have contributed equally to this work*

Specialty section:
This article was submitted to Molecular and Cellular Oncology, a section of the journal Frontiers in Oncology

Received: *30 May 2022*
Accepted: *14 June 2022*
Published: *08 July 2022*

Citation:
Zhang C, Ni C and Lu H (2022) Polo-Like Kinase 2: From Principle to Practice. Front. Oncol. 12:956225. doi: 10.3389/fonc.2022.956225

INTRODUCTION

Polo-like kinase (PLK) 2 is one of PLKs, a family of serine/threonine kinases. PLK2 shares the conserved N-terminal kinase catalytic domain and one or two C-terminal Polo box domains (PBD) with its siblings (PLK1,3-5) (1, 2). The PBD of PLK2 consists of 218 amino acid residues, including two 12-chain β sandwich conserved domains formed by β6α structures consisting of 30 amino acid residues (3–5). PLK2 plays an important role in many aspects, e.g., cell cycle (6–8), cell differentiation (9–11), ontogenesis (12), stress response (13), tumorigenesis (14), neurodegenerative diseases (15–17), inflammation and injury (18).

The function of PLK2 is regulated by many mechanisms. Histone deacetylase inhibitor trichostatin A (TSA) could induce upregulated PLK2 expression in human osteosarcoma cell line (MG-63), which may be resulted from TSA-induced GATA-1 acetylation enhancing its DNA-

binding ability and initiating the PLK2 promoter, indicating acetylation promoting PLK2 expression (19). Acetylation of PLK2 prohibits the degradation by ubiquitination and participates in centriole replication at the appropriate time (20). Promoter methylation induced by hypoxia and tumor downregulates the PLK2 expression, involved in development and progression of diseases (21–26). Both E3 ubiquitin ligase RNF180 (ring finger protein 180) (27) and miR-101-3p target gene SKP1 (S-phase kinase-associated protein 1) (28) might interact with PLK2 and induce its ubiquitination and degradation. Downregulation of miR-27b in oral lichen planus reduces its inhibition to PLK2 3'untranslated region, leading to proliferation of human oral keratinocytes (29). Nuclear factor erythroid 2-related factor 2 (Nrf2) activated lncRNA (Nrf2-lncRNA) is a competing endogenous RNA of PLK2 and cyclin-dependent kinase inhibitor 1 ($p21^{cip1}$), which induces PLK2/Nrf2/$p21^{cip1}$ to complexate and activate Nrf2 during p53 activation by binding to miR-128 and miR-224, facilitating translation of PLK2 and $p21^{cip1}$ (30). Starvation results in the elevated androgen production and depresses PLK2 expression, while relationship between PLK2 and steroid metabolism remains unclear (31). Transcription factor Sp1 plays an important role in the upregulation of PLK2 stimulated by hCG in cultured rat granulosa cells (32). Chemical carcinogens (33) and γ radiation (34) could also increase the PLK2 expression.

However, there are still many deficiencies in the current understanding of PLK2. For example, studies on PLK2 in microbial infection and immunity, and fibrotic diseases are still insufficient. Its role in hematological neoplasma, solid organ tumor and neurodegenerative diseases is also controversial. Here, we summarize the roles of PLK2 in mammalian cell cycle and non-cell cycle signaling pathways, hoping to provide help for further study of PLK2.

ROLE OF PLK2 IN NORMAL PHYSIOLOGICAL PROCESSES

Mitosis

Mitosis is the process by which eukaryotic cells divide to produce their progeny. The entire process from the completion of one division to the end of the next is called the cell cycle, which consists of interphase and mitotic (M) phase. The interphase could be divided into G1 phase, S phase and G2 phase, in which DNA replication and protein synthesis finishes. During the M phase, the genetic material in the nucleus and organelles are split in a specific way to form progeny cells. Some of these cells continue to enter G1 phase and start the next round of mitosis. Others enter the G0 phase, where the cell cycle stagnates, but can re-enter the G1 phase to replicate after appropriate stimulation. PLK2 expresses in G1 phase; silencing of PLK2 results in the growth retardation and delays S phase transition in embryonic fibroblasts and placental dysplasia in mice, revealing that PLK2 if not essential, but plays a critical role at least in mammalian growth and development (35). Significantly up-regulated PLK2 expression stimulates centriole replication in human, pig, and sheep parthenogenetic cell lines (36). As a target, PLK2 could be induced by wild-type p53; inhibition with siRNA causes mitotic catastrophe in paclitaxel-exposed cells (37). High expressed PLK2 in breast tissue regulates the orientation of mitotic spindle and maintains the polarity of ductal epithelial cells (6). When breast cancer cell line MCF-7 is exposed to zinc, expression of PLK2 is dramatically reduced, leading to cell cycle arrest and cancer cell adaption (38). In rats, PLK2 is highly induced in ovarian granulosa cells; overexpressed PLK2 blocks the cell cycle in the G0/G1 phase, while downregulation of it decreases the number of G0/G1 phase cells but increases the cell vitality (32). So, effects of PLK2 on G0/G1 phase transition depends on cell type.

In mammalian cells, centrosome replication is a hallmark of mitosis, starting from G1/S transition and finishing till S/G2 (39). Activation of PLK2 in G1/S transition is essential to centriole replication and centrosome correlation, which is important for cell replication (7, 8). Mutation of PBD prohibits centriole localization and hampers centriole replication (8). PLK2 is acetylated in the process of promoting centrosome replication, which protects PLK2 from ubiquitination degradation. The deacetylase Sirtuin 1 (SIRT1) acting as a temporal regulator, is phosphorylated and activated in early and middle G1 phase promoting deacetylation and degradation and dephosphorylated itself in late G1 phase leading to a reduced PLK2 affinity and rapid PLK2 accumulation, which contributes to the timely initiation of centriole replication (20). PLK2 catalyzes the phosphorylation of S589 and S595 residues in centrosomal P4.1-associated protein (CPAP), which is crucial for the formation of procentriole; CPAP is phosphorylated in a cell cycle stage-specific manner, increasing during the G1/S transition and decreasing at the end of mitosis. Phosphorylated CPAP is preferentially located in the procentriole. Overexpression of an anti-phosphorylated CPAP mutant fails to form elongated centrioles (40).

Cell cycle regulation by PLK2 is co-regulated by CDK2/Cyclin E, CDK2/Cyclin A complex and PLK4 (7, 41). Expression of PLK2 in rat ovary is induced by hCG; prostaglandin and EGF signaling pathways are involved in regulating PLK2 expression; and the transcription factor Sp1 plays an important role in the upregulation of PLK2 (32). PLK2 regulates centrosome replication through polo-box-dependent binding of NPM (nucleophosmin)/B23 and phosphorylation of Ser4 at the S phase (42). Mis-regulation resulted from PLK2 dysfunction is the most likely cause of changes in chromosome segregation, presence of multiple polymeric functional centrosomes, and mass cell death in embryonic stem cells with beta-catenin deletion (43). Centrosome amplification is considered a main cause of chromosome instability in cancer cells. One of the mechanisms is overreplication of centrosomes within a single cell cycle. Rho-associated kinases (ROCK2), PLK2 and PLK4 are essential for centrosome duplication in cells blocked by DNA synthesis inhibitors; In the centrosome amplification rescue assay, PLK2 indirectly activates ROCK2 by phosphorylation of NPM, while PLK4 acts downstream of ROCK2 to drive and block centrosome amplification in cells (44).

Meiosis

Meiosis is needed for sexual reproduction. Within this process, the DNA replicates once but the cell divides twice, resulting in four progenies with half the number of chromosomes. In C. elegans, pairing and synapsis of homologous chromosome rely on pairing centers (PCs), which locates in special regions at the end of chromosomes and interacts with the nuclear membrane and cytoplasmic microtubules; at the onset of meiosis, PCs recruits PLK2 in response to ZIM/Him-8, a zinc finger protein, to induce nuclear membrane remodeling, chromosome pairing and synapsis (45–47). PLK2 is involved in the establishment of meiotic specific SUN-1 phosphorylation and SUN/KASH dynamic regulation (47). During meiosis, the conserved SUN/KASH nuclear membrane bridge establishes a transient link between chromosome ends and the cytoskeleton, which ensures homologous chromosome aggregation and avoids non-homologous pairing. During pairing and recombination, chromosomal movement begins and SUN-1 aggregates at the chromosomal ends associated with the nuclear membrane and is phosphorylated in a CHK2 - and PLK2-dependent manner. While meiosis is incomplete, PLK-2 continues to be recruited to the chromosome ends in a sun-1-phosphorylation-dependent manner that is required to characterize continuous chromosome movement and zygotic line stop. Chromosomal pairing (synapsis) requires SUN-1 phosphorylation (48). In addition, PLK2 and phosphorylated SYP-1 ensure the generation of short-arm subdomains and facilitates chromosome segregation in meiosis I (49). PLK2 also mediates cell cycle delay and the apoptosis with unsuccessful synapsis of nuclear chromosomes. Functional defects caused by PLK2 knockout (KO) or mutation can lead to meiosis chromosome pairing and synapsis failure (45, 47). PLK2 plays an indispensable role in the successful completion of meiosis.

Cell Differentiation

PLK2 also plays a vital role in cell differentiation in addition to cell cycle. According to zebrafish model and human umbilical vein endothelial cell (HUVEC) culture, loss of PLK2 function results in a reduction in cell sprouting and migration, while overexpression promotes angiogenesis; PLK2 controls angiogenesis by binding PDZ-GEF and regulating RAP1 activity during endothelial cell lamellipodia formation and extracellular matrix attachment; Constitutively activated RAP1 could reverse endothelial growth defects in PLK2 KO zebrafish and HUVEC (9). Lineage negative bone marrow cells (lin-BMCs) are enriched in endothelial progenitor cells and mediate vascular repair, whose number and function decrease in an age-dependent manner. PLK2 in lin-BMCs is negatively regulated by miR-146a, that is, overexpression of miR-146a in young lin-BMCs inhibits PLK2 expression, resulting in increased aging, apoptosis and impaired angiogenesis through p16Ink4a/p19Arf and p53, respectively. Inhibition of miR-146a in aged lin-BMCs increases PLK2 expression and rejuvenates lin-BMCs, leading to reduced senescence and apoptosis, thereby promoting angiogenesis (10). As a new identified target of miR-126-3p, PLK2 also plays a regulating role in perivascular cells (PVC) and perivascular matrix.

miR-126-3p inhibits the expression of target genes PLK2 and SPRED1 and induces the phosphorylation of extracellular signal-regulated kinase (ERK) 1/2 to stimulate the expression of TLR3, thus regulating the cell-cell and cell matrix contact of PVC, promoting the conversion of immature blood vessels into mature and less permeable blood vessels. Inhibition of PLK2 and SPRED1 expression could mimic the effect of miR-126-3p in PVC but has no effect on the phosphorylation of ERK1/2, suggesting that PLK2 inhibits perivascular matrix formation in an ERK-independent manner (11). Laminin (LN) slows the proliferation of cardiac progenitor cells (CPC), induces the expression of cardiac lineage-specific genes, and promotes the endothelioid differentiation of CPC. After CPC is cultured on LN, YAP (Yes-associated protein) phosphorylation (Ser127) increases, which is confined to the cytoplasm and rapidly degraded by proteasome, thereby inhibiting cell proliferation. As a possible downstream effector, the mRNA level of PLK2 depends on the stability of YAP. Downregulation of PLK2 expression might simulate CPC performance observed in LN, while overexpression of PLK2 leads to increased proliferation and decreased differentiation of CPC (50). PLK2 may also play a key role in dynamic compression enhanced chondrogenesis (51). In fibrotic diseases, the loss of PLK2 function leads to the transformation of fibroblasts into myofibroblasts, thus promoting the occurrence and development of the disease, the specific mechanism of which will be discussed later (22, 23, 52, 53).

Neural Development

A large number of studies have focused on the role of PLK2 in the development and function of the nervous system. In the fourteenth day of rat embryonic development, PLK2 expresses in cortical plate, rather than the ventricular/subventricular zones (VZ/SVZ); In immature cortical neurons, PLK2 locates in the cell body and dendrites, and is upregulated by brain-derived neurotrophic factor (BDNF) and downstream ERK signaling pathway, which is necessary for BDNF to promote dendritic growth. Deletion of PLK2 affects dendrite development in a dose-dependent manner (54). PLK2 and poliovirus receptors (PVR) are essential for neuronal differentiation driven by nerve growth factor (NGF) and are negatively regulated by alphaB-crystallin (Cryab); Silencing PLK2 or PVR could block neuronal differentiation induced by NGF (55).

Homeostatic synaptic depression (HSD) is the homeostasis compensation mechanism for increased neural network activity, including loss of some excitatory synapses to reduce excitability and subsequent downscaling of the remaining synapses to further enhance homeostasis (56). Mounting studies have shown that excessive activation of hippocampal neurons induces the expression of PLK2, leading to the degradation of the spine associated RapGAP (SPAR), and feedback reduction of neuronal excitability (57–60). CDK5 activates phosphorylation of PLK2 binding sites in SPAR (a kind of Rap suppressor), then leads to PLK2 recruitment and accumulation (57). Activated PLK2 is highly phosphorylated, and its phosphorylation sites could regulate PLK2 kinase activity, in which S299 and S588 are involved. Mutations at sites above of PLK2 (S299E, S588A, and S588E) in neurons result in extreme activation of their anti-SPAR ability and impairment of the dendritic spines stability of primary hippocampal cells (61). A multi-subunit E3 ubiquitin

ligase (Skp1/Cul1/F-box protein complex, SCF) is involved in ubiquitination degradation of SPAR, and blocking SCF might block PLK2-dependent SPAR degradation (62). In addition, over-activity induced PLK2 also directly eliminates Ras agonist RasGRF1 through phosphorylation mediated ubiquitination degradation, and PLK2 phosphorylation stimulates Ras inhibitor SynGAP and Raf agonist PDZ-GEF1. PLK2 comprehensively regulates these factors, contributing to maintain the homeostatic plasticity (60).

PLK2 directly binds to n-ethylmaleimide-sensitive fusion protein (NSF) in an ATP-dependent manner, disrupting its interaction with AMPA receptor GluA2 subunit, promoting extensive loss of GluA2 on the surface of rat hippocampal neurons and reducing AMPAR current and surface stability of synapses (59). SynGAP, a postsynaptic GTPase activating protein (GAP), is abundant in the postsynaptic density (PSD) scaffold, of which PSD-95 is the most prominent. Phosphorylation of synGAP-α1 by PLK2 and $Ca2^{+}$/calmodulin-dependent protein kinase II (CaMKII) significantly reduces its binding to PDZ domain in PSD-95. These PDZ domains are occupied by other proteins, which changes the composition of PSD. This change may be as important as the reduction of synaptic Ras/Rap GAP activity in the pathological process of autism or epilepsy (63). PLK2 co-regulates synGAP kinase activity with CDK5 and CaMKII. After $Ca2^{+}$/CaM is added to synGAP's PLK2 phosphorylation system, the combination of $Ca2^{+}$/CaM with synGAP causes conformational changes, increasing the availability of CDK5 and PLK2, accelerating kinase reaction, and phosphorylating additional residues. PLK2 phosphorylated synGAP is more likely to inactivate Ras, resulting in a relative increase in Rap and promoting the endocytosis of synaptic membrane AMPAR. PLK2 and CDK5 work together to activate the Rap pathway by triggering SPAR removal and increase GAP activity of r-synGAP on HRas, driving synaptic AMPAR elimination (64). In enhanced hippocampal activity induced by GABA receptor antagonists, upregulated PLK2 also acts as a downstream molecule of miR-134-Pum2 to maintain synaptic homeostasis (56). On the other hand, PLK2 interacts strongly and directly with the actively-induced amyloid precursor protein (APP), promoting APP phosphorylation (T668/S675) and amyloidopathy. It affects neurohomeostasis and is involved in the pathological process of Alzheimer's disease (AD) (65). Fear Condition has further confirmed that PLK2 plays an important role in maintaining synaptic plasticity (66).

Ras promotes long-term potentiation (LTP), whereas Rap mediates long-term depression (LTD) (67, 68). PLK2 regulates Ras and Rap by regulating RasGRF1/SynGAP and SPAR/PDZ-GEF1 and has significant effect on memory formation (60). Interference with PLK2 function disrupts the homeostasis adaptation of synapses to enhanced activity and impaired behavior adaptation during various learning tasks (69). The activity dependent transcription factor Npas4 aims directly on the promoter and enhancer regions of PLK2, and conditional knockout of Npas4 in hippocampal neurons results in a significant decrease in PLK2 expression, preventing the formation of context memory and the learning-induced synaptic modification. Overexpression of PLK2 can restore memory formation and normal behavior in experimental animals (70). In a rodent model of hypoxia-induced neonatal seizures, after initial upregulation, AMPA receptor function of hippocampal CA1 pyramidal neurons shows transient attenuation, which is consistent with the transient increase in PLK2 expression and function. One week later, the function of AMPA receptor is up-regulated again, while the expression and function of PLK2 are negatively regulated by increased mTOR (71). Prenatal stress decreases the density of dendritic spines and impairs the LTP in the hippocampus of young rats. The number of NR2B and NR2A subunits decreases, while the postsynaptic scaffold proteins PSD-95 and SPAR also decrease, and PLK2 and SCF ubiquitin ligases increase, promoting ubiquitination and degradation of SPAR (72).

ROLE OF PLK2 IN BASIC PATHOPHYSIOLOGICAL PROCESSES

Oxidative Stress and Endoplasmic Reticulum Stress

PLK2 is an important molecule in response to various stresses. PLK2 induced by oxidative stress in cells with abnormal mitochondrial function, mediates glycogen synthase kinase (GSK) 3β phosphorylation and promotes NRF2 nuclear translocation, preventing p53 induced cell death and promoting cell survival (73). In oxidative stress-induced glaucoma, up-regulated PLK2 provides protection to retinal ganglion cells also through this mechanism (74). Loss of synthesis of cytochrome c oxidase 2 (SCO2) impairs mitochondrial respiration, while expression of PLK2 elevates to make cell survive (75). In the treatment of protocatechuic aldehyde (PCA) to Parkinson's disease (PD) induced by 1-methyl-4-phenyl-1,2,3,6-tetrahydropyridine (MPTP), PLK2 inhibition or knockdown eliminates the protection of PCA to improve mitochondrial membrane potential (MMP), mitochondrial complex I activity and reactive oxygen species (ROS) level, while overexpression of PLK2 enhances the protection of PCA in PD model (76). However, the alternative view is that PLK2 is involved in ROS-induced cell death. Celastrol induced ROS promotes p53 phosphorylation and p53-dependent PLK2 expression and inhibits tumor survival (77). In diabetic nephropathy patients, PLK2 is upregulated, which mediates G1 phase arrest and induces apoptosis of podocyte cultured with high D-glucose (HDG). Both PLK2 knockdown and antioxidant N-acetylcysteine (NAC) inhibit ROS production and MMP reduction and promote cell survival. Cytotoxic effects of PLK2-mediated HDG are associated with increased p53 expression and caspase-3 activation, relying on inflammatory cytokines such as TNF-α, IL-6, IL-1β, COX-2 and CXCL1 (78). At the same time, PLK2 expression is upregulated during cell stress induced by ischemia-reperfusion injury, leading to cell death through nuclear factor (NF) -κB signaling (21, 79).

Effect of PLK2 on endoplasmic reticulum (ER) stress is also controversial. It is reported that ER stress could induce PLK2

expression and lead to cell death (80). But more studies have suggested that PLK2 inhibits apoptosis and promotes survival by interacting with ER stress signals. For example, interference with PLK2 might lead to the loss of interaction with miR-101-3p target gene SKP1, and the accumulation of cotransfected overexpressed α-Syn protein due to decreased ubiquitination degradation, leading to ER stress of neurons, suggesting that PLK2 could prevent ER stress (28). PLK2 is hyper-expressed in multiple myeloma (MM) patients; PLK2 further inhibits C/EBP homologous protein (CHOP) and enhances inositol-requiring enzyme 1α (IRE1α) by inhibiting KIRA8 (kinase-inhibiting RNase attenuator 8), which in turn affects ER stress and facilitates cell survival; Meanwhile, KIRA8/IRE1α could reversely regulate PLK2 expression; KIRA8 and PLK2 inhibitors exert anti-MM effects by inducing apoptosis and regulating cell proliferation (81). In ER stress induced by Brefeldin A (BFA), increased binding of CHOP to the PLK2 promoter C/EBPα response element results in downregulation of PLK2 expression; Overexpression of exogenous PLK2 could inhibit cell apoptosis and promote cell proliferation (82). However, according to the limited results available, PLK2 plays an important role in coping with stress induced by exogenous cellular stimuli; Survival or apoptosis should depend on the intensity of exogenous stimulation and the degree of cell damage. When mild stimulation induces mild damage, PLK2 participates in the correction of adverse effects caused by stress; On the contrary, when severe stimulation induces severe damage difficult to correct, PLK2 directly leads to cell apoptosis/death.

Viral Infection and Immune

PLK2 is upregulated in phytohemagluttinin (PHA) activated canine T cells, indicating PLK2 takes part in immune cell activation (83). In lipopolysaccharide (LPS) induced inflammation, expression of PLK2 is elevated, phosphorating a disintegrin and metalloprotease 17 (ADAM 17) and leading to release of tumor necrosis factor (TNF) receptor and pro-TNFα on cell membrane; Inhibition of PLK2 results in reduction of LPS-induced ADAM17-mediated pro-TNFα release from primary macrophages and dendritic cells (DCs) (84). In antiviral innate immunity, retinoic acid-inducible gene I (RIG-I)-like receptors (RLRs), RIG-I, and melanoma differentiation-associated gene 5 (MDA5) regulate transcription of type I interferon (IFN) and inflammatory cytokines by activating IFN regulatory factor (IRF) 3 and NF-κB; Knockout of the RNA-binding protein HuR, which could enhance IFN-β promoter activity and bind to the 3' untranslated region of PLK2 mRNA to increase its stability, results in a significant decrease in PLK2 expression and IFNB1 expression after RLR stimulation. PLK2 deficient cells also shows reduced IRF3 nuclear translocation and IFNB mRNA expression during RLR signal transduction. These results suggest that HuR might promote RLR mediated IRF3 nuclear translocation and subsequent antiviral innate immune mechanism by maintaining PLK2 mRNA stability (85). Pan-PLK inhibitor BI 2536 treatment results in significant inhibition of antiviral genes (e.g., Cxcl 10 and IFNB1) expression and IRF3 nuclear translocation (86). Functional redundancy exists between PLK2 and its family member PLK4 (8, 40, 87). Therefore, antiviral gene expression decreases dramatically after simultaneous knockout of PLK2 and PLK4; And PLK2 is essential for viral sensing of DCs (86). Thus, it appears that PLK2 plays an active role in host antiviral immunity. Nevertheless, PLK2 could work adversely by promoting viral integration and replication. For example, in the infection of foamy virus (FV) with retroviruses and hepadnaviruses in its replication strategy, PLK2 interacts with prototype FV (PFV) to promote efficient integration of the PFV genome into the host chromatin, ensuring successful viral replication and transmission in cell cultures (88). Besides, avian metapneumovirus subtype C (aMPV/C) infection leads to upregulation of PLK2 in mammalian cells. Inhibition of PLK2 could reduce ROS production and p53-dependant apoptosis induced by aMPV/C, and decrease the virus release, suggesting that the high expression of PLK2 is associated with aMPV/C-induced apoptosis and viral replication (89). Contrasting to its family members, PLK2 is poorly studied in viral infection, and the exact role and mechanism remain unclear.

ROLE OF PLK2 IN DISEASES

Hematological Neoplasma

Like its compatriots, the role of PLK2 in tumor has attracted considerable attention. Although it is reported that PLK2 is highly expressed in MM and facilitates tumor cell vitality by inhibiting KIRA8 induced CHOP mediated apoptosis (81), more studies have showed PLK2 acts as a tumor suppressor in hematological neoplasma. In B-cell lymphoma (26), acute myelogenous leukemia (AML) and myelodysplastic syndromes (MDS) (90), remarkable reduction of PLK2 expression might be related to abnormal methylation. As in B-cell lymphoma, abnormal methylation occurs in the CpG island of the PLK2 gene; The PLK2 expression of DG75 (EBV-) and Rael (EBV+) cell lines increase after demethylation with 5-AZA and is further upregulated by combined administration of histone deacetylase inhibitor TSA. Methylation and expression silencing occur in both p53 wild-type and mutant cell lines, suggesting that the methylation of PLK2 in B cell derived tumors is independent of p53. In contrast, B cell mitogens is able to induce PLK2 expression and re-expression of PLK2 could lead to apoptosis (26). While in AML and MDS, PLK2 is similarly methylated, although the PLK2 methylation status has no significant effect on clinical indicators and long-term prognosis (90); Additionally, in myeloproliferative neoplasm (MPN) like MDS, the disordered co-expression and disrupted signal transduction of PLK2 with myeloid tumor suppressor Egr1 and JunB may be a pathogenesis (91). Even in recent MM studies, PLK2 was identified a methylation gene independent of CpG island (92). It also suggests that there is a complex relationship between various pathogenic mechanisms. As an example, in B-cell tumor, there is functional redundancy between PLK2 and PLK3, and the decline of PLK2 expression is always accompanied by the overexpression of PLK3 (93).

In B cell chronic lymphocytic leukemia (B-CLL), the expression of PLK2 is correlated with the efficacy of purine

nucleoside therapy. PLK2 hyper-expressed patients shows higher cytotoxicity, revealing that PLK2 might inhibit B-CLL (94). MiR-126 is involved in inflammation, angiopoiesis, and thus tumorigenesis (95). The cross-talk between miR-126 and PLK2 in hematological neoplasma is also receiving increasing attention. MiR-126 could inhibit apoptosis of AML cells and enhance cell viability and PLK2 exerts anti-tumor effects through negatively regulating of miR-126 (96). PLK2 expression is downregulated in AML, while expression of p-ERK, p-MYC and total MYC, which are critical for the survival of inv(16) leukemia-initiating cells and AML cells, is increased. These effects are reversed after miR-126 knockdown (97).

Solid Organ Tumor

PLK2 is reported to be a tumor suppressor in solid organ tumor as well. Its repressed expression is associated with overall survival in non-small cell lung cancer (NSCLC) patients (98). The measured tumor diameter of human PLK2 deficient NSCLC cell xenograft is larger in mice; Interestingly, *in vitro* cell culture suggests that anti-tumor effect of PLK2 might result from a response to hypoxic tumor microenvironment (TME) (99). Compared to normal tissues and polyps, PLK2 expression is absent in colorectal cancer (CRC) (100). Also, in hepatocellular carcinoma (HCC), promotor methylation might be the reason of decreased PLK2 expression, and inhibition with siRNA could accelerate human HCC cell line growth (101). PLK2 is directly inhibited by significantly upregulated miR-27a in throat tumor, resulting in enhanced cell viability, promoted colony formation, and inhibited cell apoptosis (102). Circ_0102049 could heighten PLK2 expression by depressing miR-520g-3p, and inhibit proliferation, invasion, migration and cell cycle of osteosarcoma (OS) cell line MG63; PLK2 inhibiting leads to a significant elevation in tumor volume and weight in the MG63 cell xenograft mouse model (14). In glioblastoma multiforme (GBM), reduced PLK2 expression indicates treatment resistance and poor prognosis; overexpression of PLK2 could repress the tumor characteristics of GBM cell and lower the incidence of acquired TMZ resistance (103). And in epithelial ovarian cancer (EOC), CpG island methylation caused PLK2 downregulation was related to paclitaxel and platinum tolerance and postoperative recurrence, being confirmed by knockdown and overexpression experiments and indicating the relevance to G2-M arrest (104, 105). Besides, PLK2 collaborates with other tumor suppressor genes (TSG) (TGFBI, PTEN, LZTS1, ING4, CDKN1A, ING1, hEx, and FBW7 etc.) in the generation of paclitaxel resistance (106). p53 dependent PLK2 expression, resulting from celastrol induced ROS production, might increase the apoptosis of G1 subgroup and suppress breast cancer MCF-7 cell viability *via* pro-apoptotic poly(ADP-ribose) polymerase-2 (PARP-2) (77). The tumor-inhibiting effect of PLK2 might also be related to the mammalian target of rapamycin (mTOR) signaling pathway. p53 dependent PLK2 interacts with TSC1/2 to amplify their suppressive effect on mTOR; Loss of PLK2 function promotes CRC and NSCLC progression (99, 100); and MSI-H specific frameshift mutation may be the internal cause of PLK2 dysfunction (107).

For all this, the role of PLK2 in solid organ tumor is still elusive and more reports indicate PLK2 could exacerbate tumor progression. DNA damage and S-phase checkpoint defects in PLK2-deficient human tumor cells caused by replication stress eventually leads to increased cell death, suggesting that PLK2 plays an important role in maintaining stable replication and cell survival of human tumor cells (108). Different from EOC, PLK2 protein level elevates markedly as a result of low promotor methylation (25). Its expression is positively related to the malignancy of gliomas while high expression indicates a poor prognosis (27, 103, 109). In $PLK2^{-/-}$ triple-negative breast cancer patient-derived xenograft (PDX) mice model, re-expression of PLK2 significantly reduces the therapeutic effect of PLK1 inhibitor Volasertib (110).

PLK2 promotes tumor through complex regulatory mechanisms. Hyper-expressed PLK2 in CRC binds to Fbxw7 and leads to its degradation, stabilizing Cyclin E and facilitating cell vitality (111); And this regulation targeting to Fbxw7/Cyclin E is negatively controlled by tazarotene-induced gene 1 (TIG1) (112). Higher expression of PLK2 in proximal CRC is associated with mismatch repair defects, B-raf serine/threonine kinase proto-oncogene and Kirsten rat sarcoma virus oncogene homologous mutations, suggesting more chemotherapy resistance and worse prognosis for patients receiving chemotherapy (113). Elevation of PLK2 is also positively related to FOXD1; PLK2 knockdown causes restrained proliferation and increases apoptosis in FOXD1 overexpressed HT29 cells (114). PLK2 is also regulated by Hedgehog (Hh) signal. Inhibition of Hh signal leads to reduction of PLK2, degradation of anti-apoptotic myeloid cell leukemia 1 and cell apoptosis in cholangiocarcinoma cells (115). Additionally, PLK2 is negatively correlative to Notch signal (103, 109), and could be ubiquitin-dependently degraded in the presence of E3 ubiquitin ligase RNF180 (27).

There are feedback regulations between PLK2 and p53. Mutation of TP53 in CRC lowers PLK2 expression (113). Meanwhile, PLK2 binds and phosphorates mutated p53, enhancing its carcinogenic activity; Regulation of PLK2 by wild-type or mutated p53 results in tumor cell growth inhibition or cell proliferation enhancement and chemotherapy resistance respectively; siRNA of mutated p53 or PLK2 improves treatment outcome (116). Phosphorylation of p53 family member TAp73 at Ser48 restricts its nuclear translocation and anti-tumor effects, which could be reactivated by dephosphorylation; Contrasting to cisplatin alone, combination therapy with PLK2 inhibitor (ELN582646) upregulates p21 and puma expression in head and neck squamous cell carcinoma and OS cell line (117, 118); Inhibiting PLK2 in TAp73-rich OS cell line Saos2 leads to reduced cell proliferation, increased apoptosis, and decreased invasion; However, these changes are not observed in TAp73 KO Saos2 (119, 120). Osteoblastic OS expresses higher TAp73 and PLK2 than chondroblastic OS, indicating poor differentiation and prognosis; Abundant TAp73 in Saos2 and OS PDX mice promotes PLK2 expression, affecting osteopontin (OPN) and osteocalcin (OCN) and calcium deposit; PLK2 silencing prevents PDX-OS cell colony formation,

facilitates cisplatin sensitivity, and improves curative effects (121). Thus, p53 family is deeply involved in the tumor promotion of PLK2.

Reportedly, PLK2 expression was positively correlated to paclitaxel resistance resulting from its anti-proliferative effects during mitosis in ovarian cancer cell line A2780 and promoting tumor cell viability (122). Different from Syed et al. (104), the difference in chemotherapeutic drug resistance pattern may be responsible for the difference in the influence of PLK2. TP53 deletion or mutation has similar effects on promoting tumor cell apoptosis induced by paclitaxel and enhancing drug sensitivity as PLK2 silencing with siRNA (37). The contradiction between expression and function was also observed in gastric cancer; PLK2 was overexpressed in SGC-7901 cell line, while silencing of PLK2 could further promote the growth of SGC-7901 cell by inhibiting apoptosis (apoptosis-related genes Bax and caspase 3 were down-regulated at the protein level) (123). And, in SGC-7901, PLK2 might be inhibited by anti-tumor miR-126; But PLK2 was still identified tumor suppressive in SGC-7901, because the tumor inhibition of miR-126 might be a symphonic regulation of PLK2, PI3KR2 and Crk; The limitation of this study was the lack of direct intervention on these effectors in SGC-7901 cell line to clarify their exact role (124). However, as a potential therapeutic target, the role of PLK2 in tumors and its relationship with chemotherapy sensitivity need further exploration

Parkinson's Disease

In PD, the number, distribution and phosphorylation state of α-Synuclein (α-Syn) affect the progression of the disease. α-Syn is a soluble presynaptic protein that is low expressed under normal physiological conditions and is associated with dopamine uptake, synaptic plasticity, and vesicle maintenance (125). In and ex vivo study revealed that α-Syn significantly inhibited tyrosine hydroxylase (TH), and its overexpression could activate protein phosphatase 2A (PP2A) (126). α-Syn accumulation is related to inflammation and cell death, enhancing PLK2 and GSK3β activities, and increasing phosphorylated α-Syn and Tau levels (127). In estrogen-related receptor gamma (ERRγ) overexpressed SHSY5Y cells, PLK2 is upregulated, participating GSK3β phosphorylation, inducing synapse upscaling, and improving dopaminergic neuron characteristics (upregulation of tyrosine hydroxylase, dopamine transporter and vesicle monoamine transporter 2) (128). Endogenous GSK3β activity might affect PLK2-mediated regulation of α-Syn (129). The expression of Tau protein is also correlated with the significant increase of PLK2 level, which could activate different kinases, leading to the phosphorylation of Tau and other proteins (including α-Syn), and result in the development of PD (130). PLK2 is regulated by ubiquitination degradation (28, 127). Overexpression of the conserved E3 ubiquitin ligase Parkin (synergistic with E1 activase and E2 binding enzyme) activates the ubiquitination, reducing PLK2, PARP, caspase-3 and CD3δ levels, and promoting α-Syn degradation (131–133). α-Syn-PLk2-ROS signaling pathway is involved in PD with insulin resistance (134).

In cell line and primary culture, inhibiting PLK2 increases α-Syn in presence of GSK3β (129). Kinase activity of PLK2 could suppress α-Syn toxicity and eliminate it through autophage, protect TH+ neurons, and inhibit Neurodegeneration as well as hemiparkinsonian motor symptoms; The PLK2/α-Syn co-overexpression by Stereotaxic injection results in symmetrical rats' forelimbs, while loss of PLK2 kinase activity leads to impaired opposite forelimb activities (135). Phosphorylation at Ser129 is not necessary for PLK2 reducing α-Syn but macroautophagy (136). PLK2 interacts with N-terminal of α-Syn, forming a protein complex degraded through macroautophagy; inhibition of autophagy leads to α-Syn accumulation and PLK2 elevation; PLK2 overexpression decreases α-Syn in HEK-293T and multi-ubiquitination also plays its role (137). So, it is considered PLK2 possesses dual kinase/chaperone activity (138). On the contrary, presynaptic total and phosphorylated α-Syn decreases after BI 2536 inhibition, while aggregation of α-Syn does not change; But both phosphorylation and aggregation decrease after PLK2 KO, preventing neuropathy (139). Under iron overload, α-Syn expression and phosphorylation (Ser129) are increased, and PLK2 and Casein kinase 2 (CK2) are upregulated (140). In MPTP induced PD models, the expression of PLK2 is significantly upregulated, accompanied by increased levels of total, phosphorylated and oligomized α-Syn, and decreased levels of PP2A, TH, and dopamine transporter (DAT) (reflecting the function/number of dopaminergic neurons) (141). Therefore, PLK2 exerts different effects on α-Syn under different research settings.

Although the regulation of total α-Syn by PLK2 is controversial, it could significantly alter the phosphorylation status of α-Syn and cause neurotoxicity (15, 16). Lewy bodies (LBs) resulted from α-Syn phosphorylation and polyaggregation is the major feature of PD, dementia with LBs and other neurological diseases (17). α-Syn overexpression is associated with reduced immune proteasome function, which in turn limits PLK2 degradation, exacerbates α-Syn phosphorylation and aggregation, and ultimately leads to neurodegeneration (142). PLK2 is a major kinase that catalyzes the phosphorylation of α-Syn at Ser129 in central nerve system (143, 144), and the conversion is efficient (>95% conversion) (145); But the membrane binding and internalization abilities of different α-Syn mutants and phosphorylated proteins are different (146). More than 80% of p-Ser129 α-Syn is co-located with PLK2. In addition, the number of double-positive cells in the substantia nigra cells of older monkeys is more than 3 times higher than that of adult monkeys, suggesting PLK2 might be closely related to the accumulation of p-Ser129 α-Syn induced by aging (147). Moreover, PD patients' hippocampus with dementia contains more p-Ser129 α-Syn dramatically than without, revealing phosphorylated α-Syn exhibits strong neurotoxicity and plays a significant role in the development of PD (148). More phosphorylated and oligomerized α-Syn appears in sera or brain of PD patients and older monkeys, due to increased PLK2 and decreased PP2A expression. Phosphorylated α-Syn enters neuron, exacerbates PP2A activity decline, and promotes α-Syn phosphorylation and oligomerization (149, 150). Phosphorylation at Ser129 also regulates the inhibition of TH

by α-Syn; PLK2 reduces its ability to inhibit TH or activate PP2A by phosphorylation of α-Syn (126). PLK2 mainly phosphorylates soluble α-Syn (151); Inhibition of PLK2 triggers autophagic elimination of α-Syn (152). Oxidative stress might play a key role in PLK2 phosphorylation of α-Syn, and antioxidant NAC could completely block iron-induced up-regulation of PLK2, CK2 and p-Ser129 α-Syn (140); However, as PLK2 induces elevation of α-Syn in copper-treated SHSY5Y neuroblastoma cells, both PP2A level and oxidative status remains unchanged (153). Glutamate-mediated excitotoxicity is often considered as the mechanism of cell death in PD (154); Group II metabotropic glutamate receptors (mGLU2/3) are highly expressed in the preterminal region of subthalamic synapses, and activation of them could inhibit glutamate release from the presynaptic membrane (155, 156). In MPTP-induced PD, both expression and function of PLK2 are inhibited by mGLU2/3 (157).

Nevertheless, PLK2-induced α-Syn phosphorylation is not the only mechanism of neurodegeneration (158, 159); Transfection of PLK2 into the substantia nigra induced p-Ser129 α-Syn elevation does not lead to dopaminergic cell death neither (160). In PD, PLK2 could affect the expression, phosphorylation and aggregation of α-Syn, leading to neurotoxicity, impaired function and even death of dopaminergic neurons, and ultimately PD is still a widely held view. The use of PLK2 inhibitors to treat neurodegenerative diseases such as PD has become a possible option and will be reviewed below.

Fibrotic Diseases

The essence of fibrosis is that under the action of various pathogenic factors (smoking and dust in lung, drinking in liver, hepatitis virus infection, ischemia in heart, etc.), relying on distinct trigger mechanism and subsequent activated signal pathways (mainly transforming growth factor-β, platelet-derived growth factor, WNT, and Hh), fibrous connective tissue is excessively deposited in target organs, causing organ remodeling, malfunction, or even failure (161). In this decade, the role of PLK2 in fibrotic diseases has attracted growing attention. A recent study suggested that PLK2 KO fibroblasts exhibited higher spontaneous myofibroblast differentiation, reduced proliferation rate, and overexpression of pro-fibrotic OPN (53). PLK2 expression decreases in patients with pulmonary fibrosis; Primary fibroblasts with PLK2 KO shows myofibroblast phenotype; The expressions of OPN, IL-18, ACTA2, COL1A1 and COL3A1 in the lung tissues of PLK2 KO mice are significantly increased; And drug inhibition of PLK2 in human lung fibroblasts leads to a fibrotic phenotype (52). PLK2 is upregulated as a node gene 7 days after acute myocardial infarction, and interacts with Rasl11b, Atxn10, Myl12B-Rock2 etc. to participate myocardial remodeling (162). Promoter methylation induced by hypoxia results in a 50% decrease in PLK2 expression in atrial fibrillation (AF) patients; In canine tachycardia, PLK2 expression is decreased in tissues of atria, but not ventricles; Drug inhibition or KO of PLK2 leads to cardiac fibroblasts displaying myofibroblast phenotype; PLK2 KO mouse heart fibroblasts secretes inflammatory OPN; The concentration of OPN in peripheral blood of AF patients with myocardial fibrosis is significantly higher than that of patients with sinus rhythm and AF patients without fibrosis. PLK2 KO mice might serve as a model of diastolic heart failure, showing left ventricular diastolic dysfunction, tachycardia, and typical fibrotic surface electrocardiogram abnormalities (PQ and QRS prolonged) (22, 23). In terms of mechanism, ERK1/2 signaling pathway is the molecular association between the decrease of PLK2 expression and the upregulation of OPN (22, 23, 53).

PROSPECT OF PLK2 APPLICATION IN DISEASE DIAGNOSIS AND TREATMENT

Since PLK2 is extensively and deeply involved in the basic life activities of cells and the occurrence and development of diseases, its expression level may have predictive significance in the diagnosis and prognosis of diseases. The expression of PLK2 increases in people with high formaldehyde exposure, which can be used as an indicator of formaldehyde exposure (163). PLK2 is overexpressed in bladder cancer, and quantitative analysis of urine has showed that it is also associated with transitional cell carcinoma, which is predictive with a sensitivity of 80% and a specificity of 64% (164). Additionally, a low level of PLK2 expression indicates a poor prognosis for patients treated with radiation therapy after breast-conserving surgery (165).

In the therapeutic field, 5-ASA may be a valuable new drug target for the prevention and treatment of AF fibrosis and diastolic heart failure by restoring physiological PLK2 expression and blocking OPN release (22, 23). Cell internalization could be realized by the preparation of nanoparticle encapsulated PLK2 using the total recirculating one machine system (TROMS). In addition, the phosphorylation activity of PLK2 at α-Syn Ser129 is maintained. And a drug delivery system (DDS) has been constructed for continuous delivery of PLK2 into cells, which is conducive to further study of the biological effects of PLK2 on dopaminergic neurons (166).

Inhibition of PLK2 is also a potential treatment option for many diseases. PLK2 inhibitors at therapeutic doses are not genotoxic and are safe and effective (118). The PLK2 specific inhibitors C2 and C21 constructed based on tetrahydropteridin effectively inhibit the growth of various human tumor cell lines *in vitro* (167). PLK2 specific inhibitor 7AO (ON1231320) blocks tumor cell cycle during mitosis, leading to cell apoptosis; Synergistic action with paclitaxel effectively suppressed tumor growth *in vivo* (168). In neurodegenerative diseases, oral administration of potent selective inhibitors of PLK2 that could cross the blood-brain barrier significantly reduces the phosphorylation of α-Syn in rat brain, providing a direction for the treatment of PD (117). Isorhamnetin-3-O-β-D-glucoside (IR3G) could bind and inhibit PLK2 with high affinity and may inhibit macrophage function and exert strong anti-inflammatory activity, as well as combat neurotoxicity and motor loss induced by 6-OHDA in SHSY5Y cells (169). Oral administration of PLK2 inhibitor based on dihydropteridinone reduces p-Ser129 α-Syn in the cerebral cortex of rats by about 41-45% (170). PLK2 also plays a pathologic role in the pathogenesis of AD, promoting the

production of Aβ *in vivo*; Drug inhibition of PLK2 prevents the formation of Aβ, synaptic loss and memory decline in AD mouse models (171). In addition, calcipotriol inhibits the proliferation of keratin forming cells by inhibiting PLK2 in the treatment of psoriasis (172). Inhibition of PLK2 promotes synovial cell apoptosis, alleviates synovial injury, and prevents cartilage injury and chondrocyte apoptosis to treat knee osteoarthritis (18).

CONCLUSION

As mentioned above, PLK2, a member of the evolutionarily conserved PLK family, is extensively and deeply involved in the normal physiological activities, the stress response to external stimuli and the development and progression of diseases. In some aspects, the role of PLK2 is relatively clear. For example, normal PLK2 expression and function are necessary for the normal operation of cell cycle, and PLK2 is also involved in regulating cell differentiation and maintaining the stability of nervous system function. In addition, in hematological neoplasma, most of the current studies believe that PLK2 acts as a tumor suppressor, and the kinase activity of PLK2 is also involved in the pathological mechanism of neurodegenerative diseases such as PD. Meanwhile, there seems to be a negative relationship between PLK2 and the development of fibrotic diseases. However, the role and regulatory mechanism of PLK2 in the stress response to external stimuli and solid organ tumors development and progression are far from consensus. The essence behind many seemingly contradictory phenomena is the complexity of its function and interaction regulatory network and may also be due to the differences in experimental models and designs adopted by different studies. Nevertheless, some preliminary attempts to use PLK2 as a predictor and therapeutic target for disease have brought encouraging results and showed promising prospects. There will definitely be more studies focusing on PLK2, which will help us better understand PLK2 and make better use from principle to practice.

AUTHOR CONTRIBUTIONS

HL, CZ, and CN designed the research. CZ and CN drafted the manuscript. HL improved the structure of this manuscript. HL, CZ, and CN discussed and revised the manuscript. All authors contributed to the article and approved the submitted version.

REFERENCES

1. de Carcer G, Manning G, Malumbres M. From Plk1 to Plk5: Functional Evolution of Polo-Like Kinases. *Cell Cycle* (2011) 10(14):2255–62. doi: 10.4161/cc.10.14.16494
2. Archambault V, Glover DM. Polo-Like Kinases: Conservation and Divergence in Their Functions and Regulation. *Nat Rev Mol Cell Biol* (2009) 10(4):265–75. doi: 10.1038/nrm2653
3. Shan HM, Wang T, Quan JM. Crystal Structure of the Polo-Box Domain of Polo-Like Kinase 2. *Biochem Biophys Res Commun* (2015) 456(3):780–4. doi: 10.1016/j.bbrc.2014.11.125
4. Kim JH, Ku B, Lee KS, Kim SJ. Structural Analysis of the Polo-Box Domain of Human Polo-Like Kinase 2. *Proteins* (2015) 83(7):1201–8. doi: 10.1002/prot.24804
5. Lowery DM, Lim D, Yaffe MB. Structure and Function of Polo-Like Kinases. *Oncogene* (2005) 24(2):248–59. doi: 10.1038/sj.onc.1208280
6. Villegas E, Kabotyanski EB, Shore AN, Creighton CJ, Westbrook TF, Rosen JM. Plk2 Regulates Mitotic Spindle Orientation and Mammary Gland Development. *Development* (2014) 141(7):1562–71. doi: 10.1242/dev.108258
7. Warnke S, Kemmler S, Hames RS, Tsai HL, Hoffmann-Rohrer U, Fry AM, et al. Polo-Like Kinase-2 is Required for Centriole Duplication in Mammalian Cells. *Curr Biol* (2004) 14(13):1200–7. doi: 10.1016/j.cub.2004.06.059
8. Cizmecioglu O, Warnke S, Arnold M, Duensing S, Hoffmann I. Plk2 Regulated Centriole Duplication is Dependent on its Localization to the Centrioles and a Functional Polo-Box Domain. *Cell Cycle* (2008) 7(22):3548–55. doi: 10.4161/cc.7.22.7071
9. Yang H, Fang L, Zhan R, Hegarty JM, Ren J, Hsiai TK, et al. Polo-Like Kinase 2 Regulates Angiogenic Sprouting and Blood Vessel Development. *Dev Biol* (2015) 404(2):49–60. doi: 10.1016/j.ydbio.2015.05.011
10. Deng S, Wang H, Jia C, Zhu S, Chu X, Ma Q, et al. MicroRNA-146a Induces Lineage-Negative Bone Marrow Cell Apoptosis and Senescence by Targeting Polo-Like Kinase 2 Expression. *Arterioscler Thromb Vasc Biol* (2017) 37(2):280–90. doi: 10.1161/ATVBAHA.116.308378
11. Pitzler L, Auler M, Probst K, Frie C, Bergmeier V, Holzer T, et al. miR-126-3p Promotes Matrix-Dependent Perivascular Cell Attachment, Migration and Intercellular Interaction. *Stem Cells* (2016) 34(5):1297–309. doi: 10.1002/stem.2308
12. Galetzka D, Weis E, Rittner G, Schindler D, Haaf T. Microarray mRNA Expression Analysis of Fanconi Anemia Fibroblasts. *Cytogenet Genome Res* (2008) 121(1):10–3. doi: 10.1159/000124375
13. Schweikl H, Hiller KA, Eckhardt A, Bolay C, Spagnuolo G, Stempfl T, et al. Differential Gene Expression Involved in Oxidative Stress Response Caused by Triethylene Glycol Dimethacrylate. *Biomaterials* (2008) 29(10):1377–87. doi: 10.1016/j.biomaterials.2007.11.049
14. Zhang X, Hu Z, Li W, Liu Z, Li J, Wang Z, et al. Circular RNA 0102049 Suppresses the Progression of Osteosarcoma Through Modulating miR-520g-3p/PLK2 Axis. *Bioengineered* (2021) 12(1):2022–32. doi: 10.1080/21655979.2021.1923259
15. Basso E, Antas P, Marijanovic Z, Goncalves S, Tenreiro S, Outeiro TF. PLK2 Modulates Alpha-Synuclein Aggregation in Yeast and Mammalian Cells. *Mol Neurobiol* (2013) 48(3):854–62. doi: 10.1007/s12035-013-8473-z
16. Vancraenenbroeck R, Lobbestael E, Maeyer MD, Baekelandt V, Taymans JM. Kinases as Targets for Parkinson's Disease: From Genetics to Therapy. *CNS Neurol Disord Drug Targets* (2011) 10(6):724–40. doi: 10.2174/187152711797247858
17. Oueslati A. Implication of Alpha-Synuclein Phosphorylation at S129 in Synucleinopathies: What Have We Learned in the Last Decade? *J Parkinsons Dis* (2016) 6(1):39–51. doi: 10.3233/JPD-160779
18. Liu W, Zha Z, Wang H. Upregulation of microRNA-27a Inhibits Synovial Angiogenesis and Chondrocyte Apoptosis in Knee Osteoarthritis Rats Through the Inhibition of PLK2. *J Cell Physiol* (2019) 234(12):22972–84. doi: 10.1002/jcp.28858
19. Shen T, Li Y, Yang L, Xu X, Liang F, Liang S, et al. Upregulation of Polo-Like Kinase 2 Gene Expression by GATA-1 Acetylation in Human Osteosarcoma MG-63 Cells. *Int J Biochem Cell Biol* (2012) 44(2):423–9. doi: 10.1016/j.biocel.2011.11.018
20. Ling H, Peng L, Wang J, Rahhal R, Seto E. Histone Deacetylase SIRT1 Targets Plk2 to Regulate Centriole Duplication. *Cell Rep* (2018) 25(10):2851–2865.e3. doi: 10.1016/j.celrep.2018.11.025
21. Zhao D, Shun E, Ling F, Liu Q, Warsi A, Wang B, et al. Plk2 Regulated by miR-128 Induces Ischemia-Reperfusion Injury in Cardiac Cells. *Mol Ther Nucleic Acids* (2020) 19:458–67. doi: 10.1016/j.omtn.2019.11.029

22. Kuenzel S, Klapproth E, Kuenzel K, Piorkowski C, Mayr M, Wagner M, et al. PLK2 is a Novel Regulator of Osteopontin-Driven Fibrosis and Diastolic Dysfunction in Permanent Atrial Fibrillation, in ESC Congress. *Eur Heart J* (2020) 41:3671. doi: 10.1093/ehjci/ehaa946.3671
23. Kunzel SR, Hoffmann M, Weber S, Kunzel K, Kammerer S, Gunscht M, et al. Diminished PLK2 Induces Cardiac Fibrosis and Promotes Atrial Fibrillation. *Circ Res* (2021) 129(8):804–20. doi: 10.1161/CIRCRESAHA.121.319425
24. Xia X, Cao F, Yuan X, Zhang Q, Chen W, Yu Y, et al. Low Expression or Hypermethylation of PLK2 Might Predict Favorable Prognosis for Patients With Glioblastoma Multiforme. *PeerJ* (2019) 7:e7974. doi: 10.7717/peerj.7974
25. Deng S, Lu X, Zhang Z, Meng R, Li M, Xia S. Identification and Assessment of PLK1/2/3/4 in Lung Adenocarcinoma and Lung Squamous Cell Carcinoma: Evidence From Methylation Profile. *J Cell Mol Med* (2021) 25 (14):6652–63. doi: 10.1111/jcmm.16668
26. Syed N, Smith P, Sullivan A, Spender LC, Dyer M, Karran L, et al. Transcriptional Silencing of Polo-Like Kinase 2 (SNK/PLK2) is a Frequent Event in B-Cell Malignancies. *Blood* (2006) 107(1):250–6. doi: 10.1182/blood-2005-03-1194
27. Cao F, Xia X, Fan Y, Liu Q, Song J, Zhang Q, et al. Knocking Down of Polo-Like Kinase 2 Inhibits Cell Proliferation and Induced Cell Apoptosis in Human Glioma Cells. *Life Sci* (2021) 270:119084. doi: 10.1016/j.lfs.2021.119084
28. Zhang M, Liu W, Zhang Q, Hu H. miR-101-3p Contributes to Alpha-Synuclein Aggregation in Neural Cells Through the miR-101-3p/SKP1/PLK2 Pathway. *J Healthc Eng 2021* (2021) 6147434. doi: 10.1155/2021/6147434
29. Chen J, Du G, Chang Y, Wang Y, Shi L, Mi J, et al. Downregulated miR-27b Promotes Keratinocyte Proliferation by Targeting PLK2 in Oral Lichen Planus. *J Oral Pathol Med* (2019) 48(4):326–34. doi: 10.1111/jop.12826
30. Joo MS, Shin SB, Kim EJ, Koo JH, Yim H, Kim SG. Nrf2-lncRNA Controls Cell Fate by Modulating P53-Dependent Nrf2 Activation as an miRNA Sponge for Plk2 and P21(Cip1). *FASEB J* (2019) 33(7):7953–69. doi: 10.1096/fj.201802744R
31. Udhane SS, Pandey AV, Hofer G, Mullis PE, Fluck CE. Retinoic Acid Receptor Beta and Angiopoietin-Like Protein 1 are Involved in the Regulation of Human Androgen Biosynthesis. *Sci Rep* (2015) 5:10132. doi: 10.1038/srep10132
32. Li F, Jo M, Curry TE Jr, Liu J. Hormonal Induction of Polo-Like Kinases (Plks) and Impact of Plk2 on Cell Cycle Progression in the Rat Ovary. *PloS One* (2012) 7(8):e41844. doi: 10.1371/journal.pone.0041844
33. Okada E, Fujiishi Y, Yasutake N, Ohyama W. Detection of Micronucleated Cells and Gene Expression Changes in Glandular Stomach of Mice Treated With Stomach-Targeted Carcinogens. *Mutat Res* (2008) 657(1):39–42. doi: 10.1016/j.mrgentox.2008.08.018
34. Turtoi A, Brown I, Oskamp D, Schneeweiss FH. Early Gene Expression in Human Lymphocytes After Gamma-Irradiation-a Genetic Pattern With Potential for Biodosimetry. *Int J Radiat Biol* (2008) 84(5):375–87. doi: 10.1080/09553000802029886
35. Ma S, Charron J, Erikson RL. Role of Plk2 (Snk) in Mouse Development and Cell Proliferation. *Mol Cell Biol* (2003) 23(19):6936–43. doi: 10.1128/MCB.23.19.6936-6943.2003
36. Brevini TA, Pennarossa G, Maffei S, Tettamanti G, Vanelli A, Isaac S, et al. Centrosome Amplification and Chromosomal Instability in Human and Animal Parthenogenetic Cell Lines. *Stem Cell Rev Rep* (2012) 8(4):1076–87. doi: 10.1007/s12015-012-9379-2
37. Burns TF, Fei P, Scata KA, Dicker DT, El-Deiry WS. Silencing of the Novel P53 Target Gene Snk/Plk2 Leads to Mitotic Catastrophe in Paclitaxel (Taxol)-Exposed Cells. *Mol Cell Biol* (2003) 23(16):5556–71. doi: 10.1128/MCB.23.16.5556-5571.2003
38. Zaman MS, Barman SK, Corley SM, Wilkins MR, Malladi CS, Wu MJ. Transcriptomic Insights Into the Zinc Homeostasis of MCF-7 Breast Cancer Cells via Next-Generation RNA Sequencing. *Metallomics* (2021) 13(6): mfab026. doi: 10.1093/mtomcs/mfab026
39. Hoffmann I. Playing Polo in G1: A Novel Function of Polo-Like Kinase-2 in Centriole Duplication. *Cell Cycle* (2004) 3(10):1230–1. doi: 10.4161/cc.3.10.1192
40. Chang J, Cizmecioglu O, Hoffmann I, Rhee K. PLK2 Phosphorylation is Critical for CPAP Function in Procentriole Formation During the Centrosome Cycle. *EMBO J* (2010) 29(14):2395–406. doi: 10.1038/emboj.2010.118
41. Cizmecioglu O, Krause A, Bahtz R, Ehret L, Malek N, Hoffmann I. Plk2 Regulates Centriole Duplication Through Phosphorylation-Mediated Degradation of Fbxw7 (Human Cdc4). *J Cell Sci* (2012) 125(Pt 4):981–92. doi: 10.1242/jcs.095075
42. Krause A, Hoffmann I. Polo-Like Kinase 2-Dependent Phosphorylation of NPM/B23 on Serine 4 Triggers Centriole Duplication. *PloS One* (2010) 5(3): e9849. doi: 10.1371/journal.pone.0009849
43. Raggioli A, Junghans D, Rudloff S, Kemler R. Beta-Catenin is Vital for the Integrity of Mouse Embryonic Stem Cells. *PloS One* (2014) 9(1):e86691. doi: 10.1371/journal.pone.0086691
44. Ling H, Hanashiro K, Luong TH, Benavides L, Fukasawa K. Functional Relationship Among PLK2, PLK4 and ROCK2 to Induce Centrosome Amplification. *Cell Cycle* (2015) 14(4):544–53. doi: 10.4161/15384101.2014.989121
45. Harper NC, Rillo R, Jover-Gil S, Assaf ZJ, Bhalla N, Dernburg AF. Pairing Centers Recruit a Polo-Like Kinase to Orchestrate Meiotic Chromosome Dynamics in C. Elegans. *Dev Cell* (2011) 21(5):934–47. doi: 10.1016/j.devcel.2011.09.001
46. Labrador L, Barroso C, Lightfoot J, Muller-Reichert T, Flibotte S, Taylor J, et al. Chromosome Movements Promoted by the Mitochondrial Protein SPD-3 are Required for Homology Search During Caenorhabditis Elegans Meiosis. *PloS Genet* (2013) 9(5):e1003497. doi: 10.1371/journal.pgen.1003497
47. Labella S, Woglar A, Jantsch V, Zetka M. Polo Kinases Establish Links Between Meiotic Chromosomes and Cytoskeletal Forces Essential for Homolog Pairing. *Dev Cell* (2011) 21(5):948–58. doi: 10.1016/j.devcel.2011.07.011
48. Woglar A, Daryabeigi A, Adamo A, Habacher C, Machacek T, La Volpe A, et al. Matefin/SUN-1 Phosphorylation is Part of a Surveillance Mechanism to Coordinate Chromosome Synapsis and Recombination With Meiotic Progression and Chromosome Movement. *PloS Genet* (2013) 9(3):e1003335. doi: 10.1371/journal.pgen.1003335
49. Sato-Carlton A, Nakamura-Tabuchi C, Chartrand SK, Uchino T, Carlton PM. Phosphorylation of the Synaptonemal Complex Protein SYP-1 Promotes Meiotic Chromosome Segregation. *J Cell Biol* (2018) 217 (2):555–70. doi: 10.1083/jcb.201707161
50. Mochizuki M, Lorenz V, Ivanek R, Della Verde G, Gaudiello E, Marsano A, et al. Polo-Like Kinase 2 is Dynamically Regulated to Coordinate Proliferation and Early Lineage Specification Downstream of Yes-Associated Protein 1 in Cardiac Progenitor Cells. *J Am Heart Assoc* (2017) 6(10):e005920. doi: 10.1161/JAHA.117.005920
51. Chen J, Chen L, Hua J, Song W. Long-Term Dynamic Compression Enhancement TGF-Beta3-Induced Chondrogenesis in Bovine Stem Cells: A Gene Expression Analysis. *BMC Genom Data* (2021) 22(1):13. doi: 10.1186/s12863-021-00967-2
52. Kant TA, Newe M, Winter L, Hoffmann M, Kammerer S, Klapproth E, et al. Genetic Deletion of Polo-Like Kinase 2 Induces a Pro-Fibrotic Pulmonary Phenotype. *Cells* (2021) 10(3):617. doi: 10.3390/cells10030617
53. Newe M, Kant TA, Hoffmann M, Rausch JSE, Winter L, Kunzel K, et al. Systemic Mesalazine Treatment Prevents Spontaneous Skin Fibrosis in PLK2-Deficient Mice. *Naunyn Schmiedebergs Arch Pharmacol* (2021) 394 (11):2233–44. doi: 10.1007/s00210-021-02135-w
54. Guo SL, Tan GH, Li S, Cheng XW, Zhou Y, Jia YF, et al. Serum Inducible Kinase is a Positive Regulator of Cortical Dendrite Development and is Required for BDNF-Promoted Dendritic Arborization. *Cell Res* (2012) 22 (2):387–98. doi: 10.1038/cr.2011.100
55. Draghetti C, Salvat C, Zanoguera F, Curchod ML, Vignaud C, Peixoto H, et al. Functional Whole-Genome Analysis Identifies Polo-Like Kinase 2 and Poliovirus Receptor as Essential for Neuronal Differentiation Upstream of the Negative Regulator alphaB-Crystallin. *J Biol Chem* (2009) 284 (46):32053–65. doi: 10.1074/jbc.M109.009324
56. Fiore R, Rajman M, Schwale C, Bicker S, Antoniou A, Bruehl C, et al. MiR-134-Dependent Regulation of Pumilio-2 is Necessary for Homeostatic Synaptic Depression. *EMBO J* (2014) 33(19):2231–46. doi: 10.15252/embj.201487921
57. Seeburg DP, Feliu-Mojer M, Gaiottino J, Pak DT, Sheng M. Critical Role of CDK5 and Polo-Like Kinase 2 in Homeostatic Synaptic Plasticity During Elevated Activity. *Neuron* (2008) 58(4):571–83. doi: 10.1016/j.neuron.2008.03.021

58. Seeburg DP, Sheng M. Activity-Induced Polo-Like Kinase 2 is Required for Homeostatic Plasticity of Hippocampal Neurons During Epileptiform Activity. *J Neurosci* (2008) 28(26):6583–91. doi: 10.1523/JNEUROSCI.1853-08.2008
59. Evers DM, Matta JA, Hoe HS, Zarkowsky D, Lee SH, Isaac JT, et al. Plk2 Attachment to NSF Induces Homeostatic Removal of GluA2 During Chronic Overexcitation. *Nat Neurosci* (2010) 13(10):1199–207. doi: 10.1038/nn.2624
60. Lee KJ, Lee Y, Rozeboom A, Lee JY, Udagawa N, Hoe HS, et al. Requirement for Plk2 in Orchestrated Ras and Rap Signaling, Homeostatic Structural Plasticity, and Memory. *Neuron* (2011) 69(5):957–73. doi: 10.1016/j.neuron.2011.02.004
61. Rozeboom AM, Pak DT. Identification and Functional Characterization of Polo-Like Kinase 2 Autoregulatory Sites. *Neuroscience* (2012) 202:147–57. doi: 10.1016/j.neuroscience.2011.11.003
62. Ang XL, Seeburg DP, Sheng M, Harper JW. Regulation of Postsynaptic RapGAP SPAR by Polo-Like Kinase 2 and the SCFbeta-TRCP Ubiquitin Ligase in Hippocampal Neurons. *J Biol Chem* (2008) 283(43):29424–32. doi: 10.1074/jbc.M802475200
63. Walkup WG, Mastro TL, Schenker LT, Vielmetter J, Hu R, Iancu A, et al. A Model for Regulation by SynGAP-Alpha1 of Binding of Synaptic Proteins to PDZ-Domain 'Slots' in the Postsynaptic Density. *Elife* (2016) 5:e16813. doi: 10.7554/eLife.22495
64. Walkup Sweredoski WGt MJ, Graham RL, Hess S, Kennedy MB. Phosphorylation of Synaptic GTPase-Activating Protein (synGAP) by Polo-Like Kinase (Plk2) Alters the Ratio of its GAP Activity Toward HRas, Rap1 and Rap2 GTPases. *Biochem Biophys Res Commun* (2018) 503(3):1599–604. doi: 10.1016/j.bbrc.2018.07.087
65. Lee Y, Lee JS, Lee KJ, Turner RS, Hoe HS, Pak DTS. Polo-Like Kinase 2 Phosphorylation of Amyloid Precursor Protein Regulates Activity-Dependent Amyloidogenic Processing. *Neuropharmacology* (2017) 117:387–400. doi: 10.1016/j.neuropharm.2017.02.027
66. Schell H, Boden C, Chagas AM, Kahle PJ. Impaired C-Fos and Polo-Like Kinase 2 Induction in the Limbic System of Fear-Conditioned Alpha-Synuclein Transgenic Mice. *PloS One* (2012) 7(11):e50245. doi: 10.1371/journal.pone.0050245
67. Zhu Y, Pak D, Qin Y, McCormack SG, Kim MJ, Baumgart JP, et al. Rap2-JNK Removes Synaptic AMPA Receptors During Depotentiation. *Neuron* (2005) 46(6):905–16. doi: 10.1016/j.neuron.2005.04.037
68. Zhu JJ, Qin Y, Zhao M, Van Aelst L, Malinow R. Ras and Rap Control AMPA Receptor Trafficking During Synaptic Plasticity. *Cell* (2002) 110 (4):443–55. doi: 10.1016/S0092-8674(02)00897-8
69. Lee KJ, Hoe HS, Pak DT. Plk2 Raps Up Ras to Subdue Synapses. *Small GTPases* (2011) 2(3):162–6. doi: 10.4161/sgtp.2.3.16454
70. Weng FJ, Garcia RI, Lutzu S, Alvina K, Zhang Y, Dushko M, et al. Npas4 Is a Critical Regulator of Learning-Induced Plasticity at Mossy Fiber-CA3 Synapses During Contextual Memory Formation. *Neuron* (2018) 97 (5):1137–1152.e5. doi: 10.1016/j.neuron.2018.01.026
71. Sun H, Kosaras B, Klein PM, Jensen FE. Mammalian Target of Rapamycin Complex 1 Activation Negatively Regulates Polo-Like Kinase 2-Mediated Homeostatic Compensation Following Neonatal Seizures. *Proc Natl Acad Sci USA* (2013) 110(13):5199–204. doi: 10.1073/pnas.1208010110
72. Chutabhakdikul N, Surakul P. Prenatal Stress Increased Snk Polo-Like Kinase 2, SCF Beta-TrCP Ubiquitin Ligase and Ubiquitination of SPAR in the Hippocampus of the Offspring at Adulthood. *Int J Dev Neurosci* (2013) 31(7):560–7. doi: 10.1016/j.ijdevneu.2013.06.011
73. Li J, Ma W, Wang PY, Hurley PJ, Bunz F, Hwang PM. Polo-Like Kinase 2 Activates an Antioxidant Pathway to Promote the Survival of Cells With Mitochondrial Dysfunction. *Free Radic Biol Med* (2014) 73:270–7. doi: 10.1016/j.freeradbiomed.2014.05.022
74. Fan Y, Wang J, He N, Feng H. PLK2 Protects Retinal Ganglion Cells From Oxidative Stress by Potentiating Nrf2 Signaling via GSK-3beta. *J Biochem Mol Toxicol* (2021) 35(8):e22815. doi: 10.1002/jbt.22815
75. Matsumoto T, Wang PY, Ma W, Sung HJ, Matoba S, Hwang PM. Polo-Like Kinases Mediate Cell Survival in Mitochondrial Dysfunction. *Proc Natl Acad Sci USA* (2009) 106(34):14542–6. doi: 10.1073/pnas.0904229106
76. Guo C, Zhu J, Wang J, Duan J, Ma S, Yin Y, et al. Neuroprotective Effects of Protocatechuic Aldehyde Through PLK2/p-GSK3beta/Nrf2 Signaling Pathway in Both In Vivo and In Vitro Models of Parkinson's Disease. *Aging (Albany NY)* (2019) 11(21):9424–41. doi: 10.18632/aging.102394
77. Kim JH, Lee JO, Lee SK, Kim N, You GY, Moon JW, et al. Celastrol Suppresses Breast Cancer MCF-7 Cell Viability via the AMP-Activated Protein Kinase (AMPK)-Induced P53-Polo Like Kinase 2 (PLK-2) Pathway. *Cell Signal* (2013) 25(4):805–13. doi: 10.1016/j.cellsig.2012.12.005
78. Zou HH, Yang PP, Huang TL, Zheng XX, Xu GS. PLK2 Plays an Essential Role in High D-Glucose-Induced Apoptosis, ROS Generation and Inflammation in Podocytes. *Sci Rep* (2017) 7(1):4261. doi: 10.1038/s41598-017-00686-8
79. Gao Z, Zhang J, Wu Y. TFAP2A Inhibits microRNA-126 Expression at the Transcriptional Level and Aggravates Ischemic Neuronal Injury. *Biochem Cell Biol* (2021) 99(4):403–13. doi: 10.1139/bcb-2020-0361
80. Suzuki S, Tsutsumi S, Chen Y, Ozeki C, Okabe A, Kawase T, et al. Identification and Characterization of the Binding Sequences and Target Genes of P53 Lacking the 1st Transactivation Domain. *Cancer Sci* (2020) 111 (2):451–66. doi: 10.1111/cas.14279
81. Yamashita Y, Morita S, Hosoi H, Kobata H, Kishimoto S, Ishibashi T, et al. Targeting Adaptive IRE1alpha Signaling and PLK2 in Multiple Myeloma: Possible Anti-Tumor Mechanisms of KIRA8 and Nilotinib. *Int J Mol Sci* (2020) 21(17):6314. doi: 10.3390/ijms21176314
82. Shen T, Li Y, Chen Z, Liang S, Guo Z, Wang P, et al. CHOP Negatively Regulates Polo-Like Kinase 2 Expression via Recruiting C/EBPalpha to the Upstream-Promoter in Human Osteosarcoma Cell Line During ER Stress. *Int J Biochem Cell Biol* (2017) 89:207–15. doi: 10.1016/j.biocel.2017.06.012
83. Mortlock SA, Wei J, Williamson P. T-Cell Activation and Early Gene Response in Dogs. *PloS One* (2015) 10(3):e0121169. doi: 10.1371/journal.pone.0121169
84. Schwarz J, Schmidt S, Will O, Koudelka T, Kohler K, Boss M, et al. Polo-Like Kinase 2, a Novel ADAM17 Signaling Component, Regulates Tumor Necrosis Factor Alpha Ectodomain Shedding. *J Biol Chem* (2014) 289 (5):3080–93. doi: 10.1074/jbc.M113.536847
85. Sueyoshi T, Kawasaki T, Kitai Y, Ori D, Akira S, Kawai T. Hu Antigen R Regulates Antiviral Innate Immune Responses Through the Stabilization of mRNA for Polo-Like Kinase 2. *J Immunol* (2018) 200(11):3814–24. doi: 10.4049/jimmunol.1701282
86. Chevrier N, Mertins P, Artyomov MN, Shalek AK, Iannacone M, Ciaccio MF, et al. Systematic Discovery of TLR Signaling Components Delineates Viral-Sensing Circuits. *Cell* (2011) 147(4):853–67. doi: 10.1016/j.cell.2011.10.022
87. Strebhardt K. Multifaceted Polo-Like Kinases: Drug Targets and Antitargets for Cancer Therapy. *Nat Rev Drug Discovery* (2010) 9(8):643–60. doi: 10.1038/nrd3184
88. Zurnic I, Hutter S, Rzeha U, Stanke N, Reh J, Mullers E, et al. Interactions of Prototype Foamy Virus Capsids With Host Cell Polo-Like Kinases Are Important for Efficient Viral DNA Integration. *PloS Pathog* (2016) 12(8): e1005860. doi: 10.1371/journal.ppat.1005860
89. Quan R, Wei L, Hou L, Wang J, Zhu S, Li Z, et al. Proteome Analysis in a Mammalian Cell Line Reveals That PLK2 is Involved in Avian Metapneumovirus Type C (aMPV/C)-Induced Apoptosis. *Viruses* (2020) 12(4):375. doi: 10.3390/v12040375
90. Benetatos L, Dasoula A, Hatzimichael E, Syed N, Voukelatou M, Dranitsaris G, et al. Polo-Like Kinase 2 (SNK/PLK2) is a Novel Epigenetically Regulated Gene in Acute Myeloid Leukemia and Myelodysplastic Syndromes: Genetic and Epigenetic Interactions. *Ann Hematol* (2011) 90(9):1037–45. doi: 10.1007/s00277-011-1193-4
91. Ramirez-Herrick AM, Mullican SE, Sheehan AM, Conneely OM. Reduced NR4A Gene Dosage Leads to Mixed Myelodysplastic/Myeloproliferative Neoplasms in Mice. *Blood* (2011) 117(9):2681–90. doi: 10.1182/blood-2010-02-267906
92. Hatzimichael E, Dasoula A, Benetatos L, Syed N, Dranitsaris G, Crook T, et al. Study of Specific Genetic and Epigenetic Variables in Multiple Myeloma. *Leuk Lymphoma* (2010) 51(12):2270–4. doi: 10.3109/10428194.2010.528095
93. Smith P, Syed N, Crook T. Epigenetic Inactivation Implies a Tumor Suppressor Function in Hematologic Malignancies for Polo-Like Kinase 2 But Not Polo-Like Kinase 3. *Cell Cycle* (2006) 5(12):1262–4. doi: 10.4161/cc.5.12.2813
94. de Viron E, Knoops L, Connerotte T, Smal C, Michaux L, Saussoy P, et al. Impaired Up-Regulation of Polo-Like Kinase 2 in B-Cell Chronic Lymphocytic Leukaemia Lymphocytes Resistant to Fludarabine and 2-

Chlorodeoxyadenosine: A Potential Marker of Defective Damage Response. *Br J Haematol* (2009) 147(5):641–52. doi: 10.1111/j.1365-2141.2009.07900.x
95. Ebrahimi F, Gopalan V, Smith RA, Lam AK. miR-126 in Human Cancers: Clinical Roles and Current Perspectives. *Exp Mol Pathol* (2014) 96(1):98–107. doi: 10.1016/j.yexmp.2013.12.004
96. Li Z, Lu J, Sun M, Mi S, Zhang H, Luo R, et al. Distinct microRNA Expression Profiles in Acute Myeloid Leukemia With Common Translocations. *Proc Natl Acad Sci USA* (2008) 105(40):15535–40. doi: 10.1073/pnas.0808266105
97. Zhang L, Nguyen LXT, Chen YC, Wu D, Cook GJ, Hoang DH, et al. Targeting miR-126 in Inv(16) Acute Myeloid Leukemia Inhibits Leukemia Development and Leukemia Stem Cell Maintenance. *Nat Commun* (2021) 12(1):6154. doi: 10.1038/s41467-021-26420-7
98. Zeng Y, Li N, Liu W, Zeng M, Cheng J, Huang J. Analyses of Expressions and Prognostic Values of Polo-Like Kinases in non-Small Cell Lung Cancer. *J Cancer Res Clin Oncol* (2020) 146(10):2447–60. doi: 10.1007/s00432-020-03288-6
99. Matthew EM, Hart LS, Astrinidis A, Navaraj A, Dolloff NG, Dicker DT, et al. The P53 Target Plk2 Interacts With TSC Proteins Impacting mTOR Signaling, Tumor Growth and Chemosensitivity Under Hypoxic Conditions. *Cell Cycle* (2009) 8(24):4168–75. doi: 10.4161/cc.8.24.10800
100. Matthew EM, Yang Z, Peri S, Andrake M, Dunbrack R, Ross E, et al. Plk2 Loss Commonly Occurs in Colorectal Carcinomas But Not Adenomas: Relationship to mTOR Signaling. *Neoplasia* (2018) 20(3):244–55. doi: 10.1016/j.neo.2018.01.004
101. Pellegrino R, Calvisi DF, Ladu S, Ehemann V, Staniscia T, Evert M, et al. Oncogenic and Tumor Suppressive Roles of Polo-Like Kinases in Human Hepatocellular Carcinoma. *Hepatology* (2010) 51(3):857–68. doi: 10.1002/hep.23467
102. Tian Y, Fu S, Qiu GB, Xu ZM, Liu N, Zhang XW, et al. MicroRNA-27a Promotes Proliferation and Suppresses Apoptosis by Targeting PLK2 in Laryngeal Carcinoma. *BMC Cancer* (2014) 14:678. doi: 10.1186/1471-2407-14-678
103. Alafate W, Xu D, Wu W, Xiang J, Ma X, Xie W, et al. Loss of PLK2 Induces Acquired Resistance to Temozolomide in GBM via Activation of Notch Signaling. *J Exp Clin Cancer Res* (2020) 39(1):239. doi: 10.1186/s13046-020-01750-4
104. Syed N, Coley HM, Sehouli J, Koensgen D, Mustea A, Szlosarek P, et al. Polo-Like Kinase Plk2 is an Epigenetic Determinant of Chemosensitivity and Clinical Outcomes in Ovarian Cancer. *Cancer Res* (2011) 71(9):3317–27. doi: 10.1158/0008-5472.CAN-10-2048
105. Ju W, Yoo BC, Kim IJ, Kim JW, Kim SC, Lee HP. Identification of Genes With Differential Expression in Chemoresistant Epithelial Ovarian Cancer Using High-Density Oligonucleotide Microarrays. *Oncol Res* (2009) 18(2-3):47–56. doi: 10.3727/096504009789954672
106. Xu JH, Hu SL, Shen GD, Shen G. Tumor Suppressor Genes and Their Underlying Interactions in Paclitaxel Resistance in Cancer Therapy. *Cancer Cell Int* (2016) 16:13. doi: 10.1186/s12935-016-0290-9
107. Lee JH, Kim MS, Yoo NJ, Lee SH. Frameshift Mutation and Loss of Expression of PLK2, a Serine/Threonine Kinase-Encoding Gene, in Colorectal Cancers. *Pathol Res Pract* (2017) 213(8):1019–20. doi: 10.1016/j.prp.2017.06.011
108. Matthew EM, Yen TJ, Dicker DT, Dorsey JF, Yang W, Navaraj A, et al. Replication Stress, Defective S-Phase Checkpoint and Increased Death in Plk2-Deficient Human Cancer Cells. *Cell Cycle* (2007) 6(20):2571–8. doi: 10.4161/cc.6.20.5079
109. Ding Y, Liu H, Zhang C, Bao Z, Yu S. Polo-Like Kinases as Potential Targets and PLK2 as a Novel Biomarker for the Prognosis of Human Glioblastoma. *Aging (Albany NY)* (2022) 14(5):2320–34. doi: 10.18632/aging.203940
110. Gao Y, Kabotyanski EB, Shepherd JH, Villegas E, Acosta D, Hamor C, et al. Tumor Suppressor PLK2 may Serve as a Biomarker in Triple-Negative Breast Cancer for Improved Response to PLK1 Therapeutics. *Cancer Res Commun* (2021) 1(3):178–93. doi: 10.1158/2767-9764.CRC-21-0106
111. Ou B, Zhao J, Guan S, Wangpu X, Zhu C, Zong Y, et al. Plk2 Promotes Tumor Growth and Inhibits Apoptosis by Targeting Fbxw7/Cyclin E in Colorectal Cancer. *Cancer Lett* (2016) 380(2):457–66. doi: 10.1016/j.canlet.2016.07.004
112. Wang CH, Lu TJ, Wang LK, Wu CC, Chen ML, Kuo CY, et al. Tazarotene-Induced Gene 1 Interacts With Polo-Like Kinase 2 and Inhibits Cell Proliferation in HCT116 Colorectal Cancer Cells. *Cell Biol Int* (2021) 45(11):2347–56. doi: 10.1002/cbin.11681
113. Xie Y, Liu Y, Li Q, Chen J. Polo-Like Kinase 2 Promotes Chemoresistance and Predicts Limited Survival Benefit From Adjuvant Chemotherapy in Colorectal Cancer. *Int J Oncol* (2018) 52(5):1401–14. doi: 10.3892/ijo.2018.4328
114. Han T, Lin J, Wang Y, Fan Q, Sun H, Tao Y, et al. Forkhead Box D1 Promotes Proliferation and Suppresses Apoptosis via Regulating Polo-Like Kinase 2 in Colorectal Cancer. *BioMed Pharmacother* (2018) 103:1369–75. doi: 10.1016/j.biopha.2018.04.190
115. Fingas CD, Mertens JC, Razumilava N, Sydor S, Bronk SF, Christensen JD, et al. Polo-Like Kinase 2 is a Mediator of Hedgehog Survival Signaling in Cholangiocarcinoma. *Hepatology* (2013) 58(4):1362–74. doi: 10.1002/hep.26484
116. Valenti F, Fausti F, Biagioni F, Shay T, Fontemaggi G, Domany E, et al. Mutant P53 Oncogenic Functions are Sustained by Plk2 Kinase Through an Autoregulatory Feedback Loop. *Cell Cycle* (2011) 10(24):4330–40. doi: 10.4161/cc.10.24.18682
117. Aubele DL, Hom RK, Adler M, Galemmo RA, Jr. , Bowers S, Truong AP, et al. Selective and Brain-Permeable Polo-Like Kinase-2 (Plk-2) Inhibitors That Reduce Alpha-Synuclein Phosphorylation in Rat Brain. *ChemMedChem* (2013) 8(8):1295–313. doi: 10.1002/cmdc.201300166
118. Fitzgerald K, Bergeron M, Willits C, Bowers S, Aubele DL, Goldbach E, et al. Pharmacological Inhibition of Polo Like Kinase 2 (PLK2) Does Not Cause Chromosomal Damage or Result in the Formation of Micronuclei. *Toxicol Appl Pharmacol* (2013) 269(1):1–7. doi: 10.1016/j.taap.2013.02.012
119. Hu ZB, Liao XH, Xu ZY, Yang X, Dong C, Jin AM, et al. PLK2 Phosphorylates and Inhibits Enriched TAp73 in Human Osteosarcoma Cells. *Cancer Med* (2016) 5(1):74–87. doi: 10.1002/cam4.558
120. Hu Z, Xu Z, Liao X, Yang X, Dong C, Luk K, et al. Polo-Like Kinase 2 Acting as a Promoter in Human Tumor Cells With an Abundance of Tap73. *Onco Targets Ther* (2015) 8:3475–88. doi: 10.2147/OTT.S90302
121. Li W, Zhang X, Xi X, Li Y, Quan H, Liu S, et al. PLK2 Modulation of Enriched TAp73 Affects Osteogenic Differentiation and Prognosis in Human Osteosarcoma. *Cancer Med* (2020) 9(12):4371–85. doi: 10.1002/cam4.3066
122. Szenajch J, Szabelska-Beresewicz A, Swiercz A, Zyprych-Walczak J, Siatkowski I, Goralski M, et al. Transcriptome Remodeling in Gradual Development of Inverse Resistance Between Paclitaxel and Cisplatin in Ovarian Cancer Cells. *Int J Mol Sci* (2020) 21(23):9218. doi: 10.3390/ijms21239218
123. Liu LY, Wang W, Zhao LY, Guo B, Yang J, Zhao XG, et al. Silencing of Polo-Like Kinase 2 Increases Cell Proliferation and Decreases Apoptosis in SGC-7901 Gastric Cancer Cells. *Mol Med Rep* (2015) 11(4):3033–8. doi: 10.3892/mmr.2014.3077
124. Liu LY, Wang W, Zhao LY, Guo B, Yang J, Zhao XG, et al. Mir-126 Inhibits Growth of SGC-7901 Cells by Synergistically Targeting the Oncogenes PI3KR2 and Crk, and the Tumor Suppressor PLK2. *Int J Oncol* (2014) 45(3):1257–65. doi: 10.3892/ijo.2014.2516
125. Sulzer D, Edwards RH. The Physiological Role of Alpha-Synuclein and its Relationship to Parkinson's Disease. *J Neurochem* (2019) 150(5):475–86. doi: 10.1111/jnc.14810
126. Lou H, Montoya SE, Alerte TN, Wang J, Wu J, Peng X, et al. Serine 129 Phosphorylation Reduces the Ability of Alpha-Synuclein to Regulate Tyrosine Hydroxylase and Protein Phosphatase 2A In Vitro and In Vivo. *J Biol Chem* (2010) 285(23):17648–61. doi: 10.1074/jbc.M110.100867
127. Khandelwal PJ, Dumanis SB, Feng LR, Maguire-Zeiss K, Rebeck G, Lashuel HA, et al. Parkinson-Related Parkin Reduces Alpha-Synuclein Phosphorylation in a Gene Transfer Model. *Mol Neurodegener* (2010) 5:47. doi: 10.1186/1750-1326-5-47
128. Lim J, Choi HS, Choi HJ. Estrogen-Related Receptor Gamma Regulates Dopaminergic Neuronal Phenotype by Activating GSK3beta/NFAT Signaling in SH-SY5Y Cells. *J Neurochem* (2015) 133(4):544–57. doi: 10.1111/jnc.13085
129. Kofoed RH, Betzer C, Ferreira N, Jensen PH. Glycogen Synthase Kinase 3 Beta Activity is Essential for Polo-Like Kinase 2- and Leucine-Rich Repeat

Kinase 2-Mediated Regulation of Alpha-Synuclein. *Neurobiol Dis* (2020) 136:104720. doi: 10.1016/j.nbd.2019.104720
130. Khandelwal PJ, Dumanis SB, Herman AM, Rebeck GW, Moussa CE. Wild Type and P301L Mutant Tau Promote Neuro-Inflammation and Alpha-Synuclein Accumulation in Lentiviral Gene Delivery Models. *Mol Cell Neurosci* (2012) 49(1):44–53. doi: 10.1016/j.mcn.2011.09.002
131. Meng Y, Qiao H, Ding J, He Y, Fan H, Li C, et al. Effect of Parkin on Methamphetamine-Induced Alpha-Synuclein Degradation Dysfunction In Vitro and In Vivo. *Brain Behav* (2020) 10(4):e01574. doi: 10.1002/brb3.1574
132. Martinez A, Ramirez J, Osinalde N, Arizmendi JM, Mayor U. Neuronal Proteomic Analysis of the Ubiquitinated Substrates of the Disease-Linked E3 Ligases Parkin and Ube3a. *BioMed Res Int 2018* (2018) p:3180413. doi: 10.1155/2018/3180413
133. Corsa CAS, Pearson GL, Renberg A, Askar MM, Vozheiko T, MacDougald OA, et al. The E3 Ubiquitin Ligase Parkin is Dispensable for Metabolic Homeostasis in Murine Pancreatic Beta Cells and Adipocytes. *J Biol Chem* (2019) 294(18):7296–307. doi: 10.1074/jbc.RA118.006763
134. Hong CT, Chen KY, Wang W, Chiu JY, Wu D, Chao TY, et al. Insulin Resistance Promotes Parkinson's Disease Through Aberrant Expression of Alpha-Synuclein, Mitochondrial Dysfunction, and Deregulation of the Polo-Like Kinase 2 Signaling. *Cells* (2020) 9(3):740. doi: 10.3390/cells9030740
135. Oueslati A, Schneider BL, Aebischer P, Lashuel HA. Polo-Like Kinase 2 Regulates Selective Autophagic Alpha-Synuclein Clearance and Suppresses its Toxicity In Vivo. *Proc Natl Acad Sci USA* (2013) 110(41):E3945–54. doi: 10.1073/pnas.1309991110
136. Kofoed RH, Zheng J, Ferreira N, Lykke-Andersen S, Salvi M, Betzer C, et al. Polo-Like Kinase 2 Modulates Alpha-Synuclein Protein Levels by Regulating its mRNA Production. *Neurobiol Dis* (2017) 106:49–62. doi: 10.1016/j.nbd.2017.06.014
137. Dahmene M, Berard M, Oueslati A. Dissecting the Molecular Pathway Involved in PLK2 Kinase-Mediated Alpha-Synuclein-Selective Autophagic Degradation. *J Biol Chem* (2017) 292(9):3919–28. doi: 10.1074/jbc.M116.759373
138. Looyenga BD, Brundin P. Silencing Synuclein at the Synapse With PLK2. *Proc Natl Acad Sci U.S.A.* (2013) 110(41):16293–4. doi: 10.1073/pnas.1315622110
139. Weston LJ, Stackhouse TL, Spinelli KJ, Boutros SW, Rose EP, Osterberg VR, et al. Genetic Deletion of Polo-Like Kinase 2 Reduces Alpha-Synuclein Serine-129 Phosphorylation in Presynaptic Terminals But Not Lewy Bodies. *J Biol Chem* (2021) 296:100273. doi: 10.1016/j.jbc.2021.100273
140. Wang R, Wang Y, Qu L, Chen B, Jiang H, Song N, et al. Iron-Induced Oxidative Stress Contributes to Alpha-Synuclein Phosphorylation and Up-Regulation via Polo-Like Kinase 2 and Casein Kinase 2. *Neurochem Int* (2019) 125:127–35. doi: 10.1016/j.neuint.2019.02.016
141. Li X, Yang W, Chen M, Liu C, Li J, Yu S. Alpha-Synuclein Oligomerization and Dopaminergic Degeneration Occur Synchronously in the Brain and Colon of MPTP-Intoxicated Parkinsonian Monkeys. *Neurosci Lett* (2020) 716:134640. doi: 10.1016/j.neulet.2019.134640
142. Bi M, Du X, Xiao X, Dai Y, Jiao Q, Chen X, et al. Deficient Immunoproteasome Assembly Drives Gain of Alpha-Synuclein Pathology in Parkinson's Disease. *Redox Biol* (2021) 47:102167. doi: 10.1016/j.redox.2021.102167
143. Inglis KJ, Chereau D, Brigham EF, Chiou SS, Schobel S, Frigon NL, et al. Polo-Like Kinase 2 (PLK2) Phosphorylates Alpha-Synuclein at Serine 129 in Central Nervous System. *J Biol Chem* (2009) 284(5):2598–602. doi: 10.1074/jbc.C800206200
144. Bergeron M, Motter R, Tanaka P, Fauss D, Babcock M, Chiou SS, et al. In Vivo Modulation of Polo-Like Kinases Supports a Key Role for PLK2 in Ser129 Alpha-Synuclein Phosphorylation in Mouse Brain. *Neuroscience* (2014) 256:72–82. doi: 10.1016/j.neuroscience.2013.09.061
145. Mbefo MK, Paleologou KE, Boucharaba A, Oueslati A, Schell H, Fournier M, et al. Phosphorylation of Synucleins by Members of the Polo-Like Kinase Family. *J Biol Chem* (2010) 285(4):2807–22. doi: 10.1074/jbc.M109.081950
146. Samuel F, Flavin WP, Iqbal S, Pacelli C, Sri Renganathan SD, Trudeau LE, et al. Effects of Serine 129 Phosphorylation on Alpha-Synuclein Aggregation, Membrane Association, and Internalization. *J Biol Chem* (2016) 291(9):4374–85. doi: 10.1074/jbc.M115.705095
147. McCormack AL, Mak SK, Di Monte DA. Increased Alpha-Synuclein Phosphorylation and Nitration in the Aging Primate Substantia Nigra. *Cell Death Dis* (2012) 3:e315. doi: 10.1038/cddis.2012.50
148. Landeck N, Hall H, Ardah MT, Majbour NK, El-Agnaf OM, Halliday G, et al. A Novel Multiplex Assay for Simultaneous Quantification of Total and S129 Phosphorylated Human Alpha-Synuclein. *Mol Neurodegener* (2016) 11(1):61. doi: 10.1186/s13024-016-0125-0
149. Chen M, Yang W, Li X, Wang P, Yue F, Yang H, et al. Age- and Brain Region-Dependent Alpha-Synuclein Oligomerization is Attributed to Alterations in Intrinsic Enzymes Regulating Alpha-Synuclein Phosphorylation in Aging Monkey Brains. *Oncotarget* (2016) 7(8):8466–80. doi: 10.18632/oncotarget.6445
150. Wang P, Li X, Yang W, Yu S. Blood Plasma of Patients With Parkinson's Disease Increases Alpha-Synuclein Aggregation and Neurotoxicity. *Parkinsons Dis* (2016) 2016:7596482. doi: 10.1155/2016/7596482
151. Elfarrash S, Jensen NM, Ferreira N, Schmidt SI, Gregersen E, Vestergaard MV, et al. Polo-Like Kinase 2 Inhibition Reduces Serine-129 Phosphorylation of Physiological Nuclear Alpha-Synuclein But Not of the Aggregated Alpha-Synuclein. *PloS One* (2021) 16(10):e0252635. doi: 10.1371/journal.pone.0252635
152. Krishnaswamy VKD, Alugoju P, Periyasamy L. Multifaceted Targeting of Neurodegeneration With Bioactive Molecules of Saffron (Crocus Sativus): An Insilco Evidence-Based Hypothesis. *Med Hypotheses* (2020) 143:109872. doi: 10.1016/j.mehy.2020.109872
153. Greco M, Spinelli CC, De Riccardis L, Buccolieri A, Di Giulio S, Musaro D, et al. Copper Dependent Modulation of Alpha-Synuclein Phosphorylation in Differentiated SHSY5Y Neuroblastoma Cells. *Int J Mol Sci* (2021) 22(4):2038. doi: 10.3390/ijms22042038
154. Ambrosi G, Cerri S, Blandini F. A Further Update on the Role of Excitotoxicity in the Pathogenesis of Parkinson's Disease. *J Neural Transm (Vienna)* (2014) 121(8):849–59. doi: 10.1007/s00702-013-1149-z
155. Johnson KA, Niswender CM, Conn PJ, Xiang Z. Activation of Group II Metabotropic Glutamate Receptors Induces Long-Term Depression of Excitatory Synaptic Transmission in the Substantia Nigra Pars Reticulata. *Neurosci Lett* (2011) 504(2):102–6. doi: 10.1016/j.neulet.2011.09.007
156. Bradley SR, Marino MJ, Wittmann M, Rouse ST, Awad H, Levey AI, et al. Activation of Group II Metabotropic Glutamate Receptors Inhibits Synaptic Excitation of the Substantia Nigra Pars Reticulata. *J Neurosci* (2000) 20(9):3085–94. doi: 10.1523/JNEUROSCI.20-09-03085.2000
157. Tan Y, Xu Y, Cheng C, Zheng C, Zeng W, Wang J, et al. LY354740 Reduces Extracellular Glutamate Concentration, Inhibits Phosphorylation of Fyn/NMDARs, and Expression of PLK2/pS129 Alpha-Synuclein in Mice Treated With Acute or Sub-Acute MPTP. *Front Pharmacol* (2020) 11:183. doi: 10.3389/fphar.2020.00183
158. Inigo-Marco I, Valencia M, Larrea L, Bugallo R, Martinez-Goikoetxea M, Zuriguel I, et al. E46K Alpha-Synuclein Pathological Mutation Causes Cell-Autonomous Toxicity Without Altering Protein Turnover or Aggregation. *Proc Natl Acad Sci USA* (2017) 114(39):E8274–83. doi: 10.1073/pnas.1703420114
159. Wang S, Xu B, Liou LC, Ren Q, Huang S, Luo Y, et al. Alpha-Synuclein Disrupts Stress Signaling by Inhibiting Polo-Like Kinase Cdc5/Plk2. *Proc Natl Acad Sci U.S.A.* (2012) 109(40):16119–24. doi: 10.1073/pnas.1206286109
160. Buck K, Landeck N, Ulusoy A, Majbour NK, El-Agnaf OM, Kirik D. Ser129 Phosphorylation of Endogenous Alpha-Synuclein Induced by Overexpression of Polo-Like Kinases 2 and 3 in Nigral Dopamine Neurons is Not Detrimental to Their Survival and Function. *Neurobiol Dis* (2015) 78:100–14. doi: 10.1016/j.nbd.2015.03.008
161. Distler JHW, Gyorfi AH, Ramanujam M, Whitfield ML, Konigshoff M, Lafyatis R. Shared and Distinct Mechanisms of Fibrosis. *Nat Rev Rheumatol* (2019) 15(12):705–30. doi: 10.1038/s41584-019-0322-7
162. Guo N, Zhang N, Yan L, Lian Z, Wang J, Lv F, et al. Weighted Gene Coexpression Network Analysis in Identification of Key Genes and Networks for Ischemicreperfusion Remodeling Myocardium. *Mol Med Rep* (2018) 18(2):1955–62. doi: 10.3892/mmr.2018.9161
163. Li GY, Lee HY, Shin HS, Kim HY, Lim CH, Lee BH. Identification of Gene Markers for Formaldehyde Exposure in Humans. *Environ Health Perspect* (2007) 115(10):1460–6. doi: 10.1289/ehp.10180
164. Tan LB, Chen KT, Yuan YC, Liao PC, Guo HR. Identification of Urine PLK2 as a Marker of Bladder Tumors by Proteomic Analysis. *World J Urol* (2010) 28(1):117–22. doi: 10.1007/s00345-009-0432-y

165. Gee HE, Buffa FM, Harris AL, Toohey JM, Carroll SL, Cooper CL, et al. MicroRNA-Related DNA Repair/Cell-Cycle Genes Independently Associated With Relapse After Radiation Therapy for Early Breast Cancer. *Int J Radiat Oncol Biol Phys* (2015) 93(5):1104–14. doi: 10.1016/j.ijrobp.2015.08.046
166. Rodriguez-Nogales C, Garbayo E, Martinez-Valbuena I, Sebastian V, Luquin MR, Blanco-Prieto MJ. Development and Characterization of Polo-Like Kinase 2 Loaded Nanoparticles-A Novel Strategy for (Serine-129) Phosphorylation of Alpha-Synuclein. *Int J Pharm* (2016) 514(1):142–9. doi: 10.1016/j.ijpharm.2016.06.044
167. Zhan MM, Yang Y, Luo J, Zhang XX, Xiao X, Li S, et al. Design, Synthesis, and Biological Evaluation of Novel Highly Selective Polo-Like Kinase 2 Inhibitors Based on the Tetrahydropteridin Chemical Scaffold. *Eur J Med Chem* (2018) 143:724–31. doi: 10.1016/j.ejmech.2017.11.058
168. Reddy MV, Akula B, Jatiani S, Vasquez-Del Carpio R, Billa VK, Mallireddigari MR, et al. Discovery of 2-(1H-Indol-5-Ylamino)-6-(2,4-Difluorophenylsulfonyl)-8-Methylpyrido[2,3-D]Pyrimi Din-7(8H)-One (7ao) as a Potent Selective Inhibitor of Polo Like Kinase 2 (PLK2). *Bioorg Med Chem* (2016) 24(4):521–44. doi: 10.1016/j.bmc.2015.11.045
169. Ahmed AF, Wen ZH, Bakheit AH, Basudan OA, Ghabbour HA, Al-Ahmari A, et al. A Major Diplotaxis Harra-Derived Bioflavonoid Glycoside as a Protective Agent Against Chemically Induced Neurotoxicity and Parkinson's Models; In Silico Target Prediction; and Biphasic HPTLC-Based Quantification. *Plants (Basel)* (2022) 11(5):648. doi: 10.3390/plants11050648
170. Bowers S, Truong AP, Ye M, Aubele DL, Sealy JM, Neitz RJ, et al. Design and Synthesis of Highly Selective, Orally Active Polo-Like Kinase-2 (Plk-2) Inhibitors. *Bioorg Med Chem Lett* (2013) 23(9):2743–9. doi: 10.1016/j.bmcl.2013.02.065
171. Lee JS, Lee Y, Andre EA, Lee KJ, Nguyen T, Feng Y, et al. Inhibition of Polo-Like Kinase 2 Ameliorates Pathogenesis in Alzheimer's Disease Model Mice. *PloS One* (2019) 14(7):e0219691. doi: 10.1371/journal.pone.0219691
172. Kristl J, Slanc P, Krasna M, Berlec A, Jeras M, Strukelj B. Calcipotriol Affects Keratinocyte Proliferation by Decreasing Expression of Early Growth Response-1 and Polo-Like Kinase-2. *Pharm Res* (2008) 25(3):521–9. doi: 10.1007/s11095-007-9388-z

Conflict of Interest: The authors declare that the research was conducted in the absence of any commercial or financial relationships that could be construed as a potential conflict of interest.

frontiers | Frontiers in Oncology

REVIEW
published: 19 July 2022
doi: 10.3389/fonc.2022.931995

Resident Immune Cells of the Liver in the Tumor Microenvironment

Yunjie Lu[1†], Shiying Ma[1†], Wei Ding[2†], Pengcheng Sun[1], Qi Zhou[1], Yunfei Duan[1*] and Kurt Sartorius[3,4,5*]*

[1] The Third Affiliated Hospital of Soochow University, Chanozhou, China, [2] Department of General Surgery, Wujin Hospital Affiliated to Jiangsu University, Changzhou, China, [3] Hepatitis Diversity Research Unit, School of Internal Medicine, University of the Witwatersrand, Johannesburg, South Africa, [4] Africa Hepatopancreatobiliary Cancer Consortium (AHPBCC), Mayo Clinic, Jacksonville, FL, United States, [5] University of Kwazulu-Natal Gastrointestinal Cancer Research Unit (UKZN/GICRC), Durban, South Africa

The liver is a central immunomodulator that ensures a homeostatic balance between protection and immunotolerance. A hallmark of hepatocellular carcinoma (HCC) is the deregulation of this tightly controlled immunological network. Immune response in the liver involves a complex interplay between resident innate, innate, and adaptive immune cells. The immune response in the liver is modulated by its continuous exposure to toxic molecules and microorganisms that requires a degree of immune tolerance to protect normal tissue from damage. In HCC pathogenesis, immune cells must balance a dual role that includes the elimination of malignant cells, as well as the repair of damaged liver tissue to maintain homeostasis. Immune response in the innate and adaptive immune systems extends to the cross-talk and interaction involving immune-regulating non-hematopoietic cells, myeloid immune cells, and lymphoid immune cells. In this review, we discuss the different immune responses of resident immune cells in the tumor microenvironment. Current FDA-approved targeted therapies, including immunotherapy options, have produced modest results to date for the treatment of advanced HCC. Although immunotherapy therapy to date has demonstrated its potential efficacy, immune cell pathways need to be better understood. In this review article, we summarize the roles of specific resident immune cell subsets and their cross-talk subversion in HCC pathogenesis, with a view to identifying potential new biomarkers and therapy options.

Keywords: immunology, tumorigenesis, adaptive, innate, cells, liver

OPEN ACCESS

Edited by:
Liangrong Shi,
Central South University, China

Reviewed by:
Yanqing Liu,
Columbia University, United States
Xin Wang,
National Institutes of Health (NIH), United States

***Correspondence:**
Qi Zhou
dr_qzhou@163.com
Yunfei Duan
duanyunfei1980@suda.edu.cn
Kurt Sartorius
kurt.sartorius@wits.ac.za

[†]These authors have contributed equally to this work

Specialty section:
This article was submitted to Molecular and Cellular Oncology, a section of the journal Frontiers in Oncology

Received: *29 April 2022*
Accepted: *13 June 2022*
Published: *19 July 2022*

Citation:
Lu Y, Ma S, Ding W, Sun P, Zhou Q, Duan Y and Sartorius K (2022) Resident Immune Cells of the Liver in the Tumor Microenvironment. Front. Oncol. 12:931995. doi: 10.3389/fonc.2022.931995

INTRODUCTION

The liver is a central player in immune regulation because of its constant exposure to gut-derived pathogens that require its multitude of innate and adaptive immune cells to respond to some pathogens and tolerate others. Immune response in the liver must carefully balance pro-inflammatory cytokines (IL-2/IL-7/IL-12/IL-15/IFN-γ) and anti-inflammatory cytokines (IL-10/IL-13/TGF-β) to coordinate resident and periphery leukocytes like T cells, B cells, macrophages (KCs/monocytes), natural killer (NK) cells, natural killer T (NKT) cells, and hepatic stellate cells (HSCs). Hepatocellular carcinoma (HCC), which accounts for approximately 90% of primary liver cancers, arises almost exclusively in a setting of chronic inflammation, which is a hallmark of HCC pathogenesis. This inflammation causes liver damage, compensatory tissue regeneration, and the

activation of non-parenchymal cells that promote the development of fibrosis/cirrhosis. Over time, these conditions lead to chromosomal instability and the development of the tumor microenvironment (TME) (1).

The TME can be broadly classified into cellular and non-cellular components. The major cellular components include HSCs, fibroblasts, immune, and endothelial cells. These cell types produce the non-cellular components of the tumor stroma, including extracellular matrix (ECM) proteins, proteolytic enzymes, growth factors, and inflammatory cytokines. The non-cellular component of the tumor stroma regulates HCC pathogenesis by influencing cancer signaling pathways in the TME, tumor invasion, and metastasis (2). In these conditions, HCC pathogenesis promotes the constant expression of pro-inflammatory cytokines that outweigh the anti-inflammatory response to drive fibrogenesis resulting in the progressive buildup of fibrotic tissue, cirrhosis, and progression to HCC (3). Simultaneously, T-cell tolerance develops in the presence of a reduction in $CD4^+$ effector T cells and an increase in T reg cells and T-cell exhaustion in the face of upregulated KCs and elevated IL-10/TGF-β (**Table 1**).

Despite the approval of a range of FDA-approved drugs for the treatment of HCC, the results have been disappointing and survival time has only been modestly extended. Innovative developments in immunotherapy, however, have improved the probability of developing a successful treatment for advanced HCC. In this review article, we summarize the roles of specific resident immune cell subsets and their pathways in HCC pathogenesis to outline potential new biomarkers of disease and therapy options.

RESIDENT MYELOID IMMUNE CELLS IN THE LIVER

Macrophages

Macrophages are an umbrella term for a diverse group of phagocytic cells (4). Hepatic macrophages are the first line of defense against pathogens, and this group of non-parenchymal cells consists mainly of resident and non-resident macrophages. Liver-resident macrophages that reside in the space of Disse consist of Kupffer cells (KCs) and monocytes that play a crucial role in chronic liver inflammation and the TME. Macrophages abundantly infiltrate the HCC microenvironment and tumor-associated macrophages (TAMs) promote tumorigenesis by regulating the immune responses to HCC cells and secreting various cytokines (5, 6) that promote ECM development and angiogenesis in tumorigenesis (7). Macrophages include two distinct polarization phenotypes, namely, M1 and M2 macrophages, that are triggered by their response to different microenvironments. M1 macrophages exert a cytotoxic function by releasing IL-1α, IL-1β, IL-12, IL-18, iNOS, and TNF-α, which are induced by LPS, IFN-γ, and GM-CSF. Conversely, M2 macrophages exert anti-inflammatory activities by expressing low levels of IL-12 and high levels of IL-10, arginase 1 and PD-L1, which are induced by IL-4, IL-10, IL-13, M-CSF, and helminth (5).

Monocyte-derived macrophages (MoMϕs) are derived from monocytes that are synthesized from hematopoietic stem cells (HSCs) in the bone marrow and enter the liver *via* the bloodstream (8). MoMϕs can also be classified as Ly-$6C^{high}$ and Ly-$6C^{low}$ monocytes. Ly-$6C^{high}$ monocytes play an essential role in initiating HSC activation through secreting high levels of CCR2 (9) while the accumulation of Ly-$6C^{low}$ monocytes attenuates liver fibrosis (10). Targeting CCR2 expression, therefore, has been demonstrated as a feasible therapeutic intervention (11). Interestingly, $CD14^+CD16^-$ monocytes in humans correlate with $Ly6C^{high}$ monocytes in mice and are associated with $Ly6C^{low}$ monocytes in mice (12).

Glucose homeostasis, which is mainly controlled by the liver, is vital for the energy demand of human organs and is partly mediated by SUV39H1, which makes it a potential target for therapy interventions (13). The importance of modulating glucose homeostasis is emphasized by its role in the promotion of inflammatory cytokines in macrophages (14).

Tumor-activated macrophages (TAMs) are associated with poor prognosis, as are two separate genes in TAM-like signatures, SLC40A1 and GPNMB (15). Therefore, TAMs that target the oncogenic expression of Wnt2b offer an exciting potential therapeutic strategy in HCC immunotherapy (16). In addition, Miz1 is a tumor suppressor that limits the ability of tumor hepatocytes to activate tumor-infiltrating macrophages and drive inflammation. Miz1 expression in HCC is negatively correlated with the phosphorylation of RelA and MTDH, as well as poorer overall survival and higher recurrence rates (17). Targeting the Miz1–MTDH–RelA axis, therefore, may also provide a potential therapeutic strategy for HCC. HOMER3-AS1 also drives HCC progression by regulating the behavior of tumor cells and macrophages, and HOMER3-AS1 may be another promising prognostic and therapeutic target for HCC (18) (**Figure 1**). Finally, TAM-elevated CCL2 levels are associated with reduced survival in HCC patients, thus demonstrating a new potential CCL2-targeted therapy for HCC (19).

Notch blockade impedes the differentiation of moTAMs but upregulates the Wnt/β-catenin signaling pathway to promote KclTAM proliferation and tumor-promoting cytokine production during hepatocarcinogenesis (20). CD74 is an independent predictor of HCC prognosis and $CD74^+$ macrophages are closely associated with immunoreactive TME with $CD8^+$ CTL function.

TABLE 1 | Expression of innate and adaptive immune cells.

Immune cells	Expression in HCC
$CD8^+$ T cells	Dysregulated up/down
$CD4^+$ effector T cells	Dysregulated up/down
Treg cells	Upregulated
B cells	Dysregulated up/down
KCs or monocytes	Upregulated
NKT cells	Downregulated
NK cells	Downregulated
HSCs	Upregulated
DCs	Upregulated
Neutrophils	Upregulated

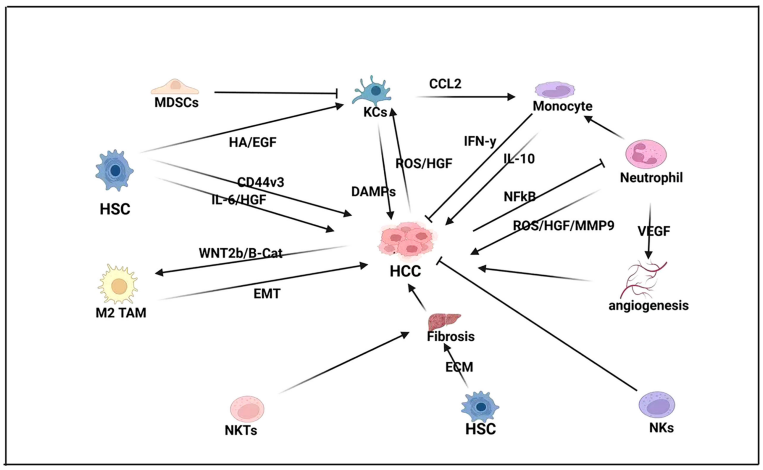

FIGURE 1 | Innate immune response in HCC-BM. In HCC pathogenesis, hepatic stellate cells (HSCs) drive fibrogenesis by promoting extracellular matrix (ECM), as well as directly influencing proliferation by expressing pro-inflammatory cytokines like interleukin-6 (IL-6) and hepatocyte growth factor (HGF). HSCs also express the glycoprotein CD44v3 that promotes cell migration and invasion in HCC. Natural killer T (NKT) cells also promote fibrogenesis while neutrophils express vascular endothelial growth factor (VEGF) to promote angiogenesis and proliferation. Neutrophils also activate monocytes that can both repress HCC by expressing interferon-gamma (IFN-γ) and promote HCC by expressing interleukin-10 (IL-10). Kupffer cells (KCs) also play a crucial role in HCC pathogenesis by promoting monocytes by expressing C-C motive chemokine ligand-2 (CCL2), which acts as a monocyte attracting protein. KCs also express damage-associated molecular pattern molecules (DAMPs) and are activated by HSC. Expression of histamine (HA) and epidermal growth factor (EGF), as well as HCC expression of reactive oxygen species (ROS) and hepatocyte growth factor (HGF). However, KC expression is modulated by myeloid-derived suppressor cells (MDSCs).

Therefore, CD74 can be used as a predictive biomarker and potential therapeutic target for HCC (21).

Kupffer Cells

KCs are tissue macrophages located in the lumen of the hepatic sinusoids. They are important members of the innate and adaptive immune systems. As antigen-presenting cells, KCs bridge the gap between the innate and adaptive immune systems. Following their activation by danger signals, KCs modulate inflammation and recruit immune cells, including large numbers of monocytes to the liver. KCs are a specific type of macrophage, and a combination of KCs and monocytes is involved in inflammation and wound healing by adjusting their phenotypes according to local signals (22). KCs in the liver act as sentinel cells to capture antigens and pathogens to maintain liver tolerance. Recruitment of macrophages is highly bactericidal and is a response to liver damage caused by acute inflammation, playing a key role in rapid infection control. Thus, the KCs that reside in the liver and the macrophages that they recruit are functionally different (23). Their constitutive ability reflects the potential of preserving tolerance of KCs in homeostasis by secreting IL-10, which can be stimulated in the presence of lipopolysaccharides (LPS). Under LPS challenges, IL-10, secreted by KCs plays a critical role in maintaining liver homeostasis (24), which involves a dynamic balance between inflammatory substances initiated by KCs and immune regulatory molecules. If this balance is broken, liver injury rises (25).

SNHG20 induces hepatic KC M2 polarization, through activation of STAT6, to promote the progression of NAFLD to HCC (26). Therefore, silencing SNHG20 expression could delay the progression of NAFLD to HCC. Upregulation of FTX inhibits the conversion of NAFLD to HCC by promoting M1 polarization of KC and provokes another effective target for the treatment of NAFLD-HCC (27). Taking an RNAi-based approach, microRNA-15a/16-1 attenuates immunosuppression by disrupting CCL22-mediated communication between KCs and Tregs, thus representing an additional potential immunotherapy approach for HCC (28).

Dendritic Cells

DCs are antigen-presenting cells that not only participate in the intrinsic immune response but also serve as a bridge between intrinsic and adaptive immunity. DCs recognize and ingest exogenous antigens, present them to immature T cells and induce T-cell activation and proliferation. The unique DC compartment in the liver contains multiple DC subpopulations that secrete type I interferons, regulate NK cell activity, and induce antiviral immune responses (29). DCs also play an essential role in regulating the microenvironment by capturing and presenting antigens to activate effector cells in the immune system. Hepatic DCs also interact with $CD4^+$ T cells during liver injury and tolerogenic DCs in the liver suppress the activation and proliferation of liver effective T cells to reduce the I/R injury (30). It has been demonstrated that a subset of human $CD14^+CTLA\text{-}4^+$ DCs can suppress $CD4^+$ T cells by secreting IL-10 and IDO (indoleamine-2,3- dioxygenase) (31). DC-derived IDO is vital for the function of the immune regulating ability of liver-resident DCs and IFN-γ or low-level LPS is the main upstream activator that enhances the IDO signal (32).

Importantly, IL-6-mediated STAT3 activation is necessary for the DC differentiation of IDO-producing regulatory DCs in the liver. In addition, foreign DNA and HMGB1 immune complexes also activate liver-resident DCs *via* interacting with the receptors of TLR9 and RAGE (33).

Hypoxia-inducible factor 1-α (HIF-1α) transcriptionally upregulates the expression of the ectonucleotidases CD39 and CD73 in HCC cells and induces the production of extracellular adenosine (eADO) that significantly promotes pDC recruitment into tumors *via* the adenosine A1 receptor (ADORA1). High-density tumor-infiltrating pDCs are associated with poor prognosis in HCC patients offering a potential role for targeting pDC recruitment as a potential adjuvant immunotherapy for HCC (34). Intratumor pDCs may promote HCC progression and recurrence through induction of immune tolerance by Treg cells and an inflammatory TME of IL-17$^+$ cells. Targeting anti-immune responses induced by TA-pDCs, therefore, may become an additional new strategy for the clinical treatment of HCC (35). In addition, CD40L co-stimulation could also provide a promising tool for enhancing DC immunotherapy in liver cancer (36).

LIVER LYMPHOID IMMUNE CELL POPULATIONS

T Cells

T cells occupy a central position in the adaptive immune response. Mature T cells are divided into CD4$^+$ T cells and CD8$^+$ T cells, which are mainly involved in the transduction of T-cell activation signals (**Figure 2**). CD4$^+$ T cells and CD8$^+$ T cells are crucial mediators of the intrahepatic antiviral immune response. Liver parenchymal and non-parenchymal cells protect against the tolerogenic environment by suppressing T-cell responses (37, 38). This mediation commonly leads to the balance between immune response and tolerance under steady-state conditions. Liver injury mediated signals, though, may override the tolerance and induce immune effector cellular activation. Upregulation of ICAM-1, VCAM-1, and VAP-1 and other adhesion molecules are crucial factors that induce the activation of T cells (39–42). Interestingly, TGF-β is essential for the survival and development of T-cell subsets and could be reverted by silencing SUV39H1. SUV39H1 inhibits TCR-mediated IL-2 transcription *via* the TGF-β-Smad pathway. Knockdown of SUV39H1 partially blocked TGF-β-mediated IL-2 inhibition; thus, SUV39H1 may become a new target for autoimmune disease therapy (43). SUV39H1-deficient Th2 cells express Th1 characteristic genes, and intervention of SUV39H1 may have a therapeutic effect in Th2 cell-mediated inflammatory diseases (44).

In another study, it was demonstrated that norisoboldine downregulated the glycolytic process of CD4$^+$ T cells under hypoxic conditions, reduced NAD$^+$ and SIRT1 levels, promoted ubiquitin-proteasomal degradation of SUV39H1 protein, and inhibited the enrichment of H3K9me3 in the Foxp3 promoter region of CD4$^+$ T cells, thereby enhancing Treg polarization (45). Since Th1, Th2, and Treg cells are essential for liver immunology, the SUV39H1 network needs to be further investigated.

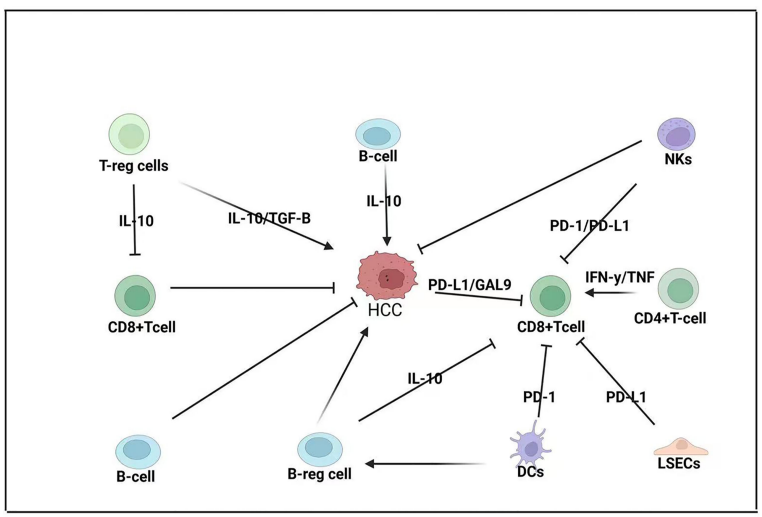

FIGURE 2 | Adaptive immune response in HCC-BM. CD8$^+$ T cells are considered the primary anti-cancer cells in HCC pathogenesis but their function is modulated by both the TME and the innate immune system. CD8$^+$ T cells are modulated by regulatory T cells (T-reg cells) that express interleukin 10 (IL-10); T-reg cells can also promote the expression of transforming growth factor beta (TGF-B), which promotes HCC. Regulatory B cells (B-reg cells) can also directly promote HCC by expressing IL-10 or modulating CD8$^+$ T-cell expression. HCC tumors can express programmed death ligand-1 (PD-L1) and galactin-9 (GAL-9) to repress CD8$^+$ T cells that can also be repressed by liver sinusoidal endothelial cells (LSECs) that can express PD-L1 and dendritic cells (DCs) that express programmed cell death protein 1 (PD-1). Natural killer (NK) cells can repress both CD8$^+$ T cells and HCC pathogenesis.

The relationship between the liver and Treg cells under various pathophysiological conditions is being gradually revealed in recent years. KCs can induce Treg cells *via* the secretion of prostaglandins (PG) E2 and 15d-PGJ2 (46, 47). In another study, pre-treatment of KCs by IFN-γ indicated an upregulation of the enzyme IDO *in vitro* (48). Under pathological conditions, the strong immunosuppressive ability of Treg can control liver inflammation, reduce liver damage, and regulate immune tolerance during liver transplantation. However, the Treg cell's ability to suppress the immune response may also lead to chronic viral hepatitis and speed up the growth of tumors by helping the tumors evade immune response (49).

Natural Killer T Cells

NKT cells are a particular subset of T cells with both T-cell receptors (TCRs) and NK receptors on the cell surface. NKT cells can produce a large number of cytokines and induce the same cytotoxic effect as NK cells. Liver sinusoidal endothelial cells (LSECs) and KCs can secrete CXCL6 that promotes the homing of $CXCR6^+$ NKT cells (50, 51). Liver dendritic cells (DCs) also interact and activate patrolling NKT cells by expressing IL-4 and IFN-γ through IL-12 (52, 53).

The nuclear factor TOX promotes $CD8^+$ T-cell depletion in HCC by regulating the intracellular recycling of PD-1. Downregulation of TOX expression in $CD8^+$ T cells has a synergistic effect with anti-PD-1 treatment. Thus, TOX may be a promising target for reversing T-cell depletion and enhancing anti-tumor immunity (54). Moreover, 4-1BB co-stimulation further enhances T-cell activation after PD-1 blockade, and immunotherapy targeting co-stimulatory receptor 4-1BB, in combination with anti-PD-1 therapy, may be an effective therapeutic strategy (55).

Innate Lymphoid Cells

ILCs are vital in maintaining metabolic balance and act as an anti-infection immune response. The ILC family includes ILC1, which mainly secretes IFN-γ; ILC2, which primarily secretes IL-5, IL-9, and IL-13; and ILC3, which mainly expresses IL-22 and IL-17 (56). In the liver, ILC1 reduces the severity of acute liver injury by regulating Bcl-xL expression by hepatocytes (33) while ILC2 controls liver fibrosis and tissue repair by interacting with macrophages following injury (57, 58). A human experiment study showed that ILC3 promoted fibrosis by expressing IL-17 and IL-22 (59) and that the tumor cytokine microenvironment controls the composition of ILC and the prognosis of HCC. In addition, patients with a high ILC2/ILC1 ratio that express IL-33 in their tumors promote the production of ILC2 and induce an increase in $CD8^+$ T cells and a decrease in regulatory T cells (Treg) in tumors, resulting in improved patient survival. Thus, modulation of the cytokine gradient of ILC may enhance the antitumor immune response in HCC (60). In other studies, ILC3, which lacks the natural cytotoxic trigger receptor (NCR-ILC3), promotes HCC development in response to interleukin 23 (IL-23). Furthermore, NCR-ILC3 initiates IL-17 production in response to IL-23 stimulation and directly suppresses $CD8^+$ T-cell immunity by promoting lymphocyte apoptosis and limiting their proliferation (61). Thus, NCR-ILC3 should also be considered a target for future tumor immunotherapy.

Natural Killer Cells

NK cells are essential liver-resident lymphocytes in the innate immune system. The phenotypes/functions of NK cells in the liver are different from those of peripheral circulation NK cells, containing subsets with tissue-resident characteristics to resist viral infection and tumor immune surveillance. NK cell phenotypes are altered and dysfunctional in the disease environment, indicating that NK cells are essential in mediating the immunology of the liver under steady-state conditions. Liver-resident NK (LR-NK) cells also play a crucial role in liver immune homeostasis maintenance. LR-NK cells co-locate with $CD4^+$ T cells and can significantly suppress T-cell proliferation and function. In contrast, NK cells from the circulation system do not have this ability (62). Recently published data also indicated that liver-resident NK cells suppressed T cells' antiviral ability through controlling PD-1/PD-L1 signaling (63).

Multiple studies have investigated various signaling pathways influencing NK expression. SIRT2, for instance, may enhance the tumor-killing effect of NK cells by activating the ERK1/2 and p38MAPK signaling pathways and is potentially a new therapeutic target for immunotherapy of liver cancer (64). In another study, Glypian-3 (GPC3) was shown to be a suitable target for Chimeric antigen receptor (CAR) therapy in HCC, and therapeutic approaches using GPC3-targeted antibodies or peptide vaccines are safe (65). Patients with high CD96 expression in tumors have a poor clinical prognosis, and the blockade of CD96–CD155 interaction or TGF-β1 restores NK cell antitumor immunity by reversing NK cell depletion (66). Interestingly, the expression of failure-associated checkpoint molecules such as PD-1, CD96, and TIGIT on $CD49a^+$ NK cells within the tumor is upregulated, allowing tumor cells to escape from immune surveillance, and $CD49a^+$ NK cell accumulation in liver tumor tissue is associated with disease progression and poor prognosis (67). In addition, blocking the inhibitory receptors NKG2A, TIGIT, LAG3, or KIR, expressed on NK cells with antibodies, is a potential therapeutic strategy (68). Finally, micro-RNA like miR-561-5p promotes HCC metastasis by inhibiting its target CX_3CL1, thereby blocking NK cell recruitment and infiltration. One study demonstrated that miR-561-5p/CX_3CL1/CX_3CR1^+ components of the NK cell axis are potential immunotherapeutic targets in HCC (69).

B Cells

B cells not only mediate humoral immune responses through antibody production but also present antigens and participate in immune regulation. However, the role of tumor-infiltrating B cells (TIBs) remains controversial. Experimental data using mice deficient for B cells [Igh6(-/-), μMT] and data on mRNA expression in human HCC suggest that T cells prevent initial tumor formation, while B cells critically limit the growth of established tumors (70). In addition, the number of TIBs in HCC

correlates with T cells and tumor-infiltrating T- and B-cell density correlates with high survival rates in HCC (71). The density of TIBs also correlates with the activation of both$CD8^+$ T and $CD56^+$ NK cells intratumorally, which may lead to an enhanced local antitumor immune response (71). The critical role of T-cell and B-cell interactions in cancer progression provides new ideas for immunotherapy. In particular, CD40 is a co-stimulatory molecule expressed on B cells that activates T cells and B cells when linked to CD40 ligands, making CD40 a promising target for immunotherapy (1).

B-cell-mediated IL-10 expression is known to suppress $CD4^+$ T cell proinflammatory cytokine expressions, such as TNF-α, IFN-γ, and IL-17; inhibit $CD8^+$ T-cell cytotoxicity; and promote Treg cell differentiation (72). The increase of IL-10-expressing B cells could contribute to the immune inhibition in the liver microenvironment (73) and TLR-2 and TLR-9 agonists were shown to increase IL-10 production in B cells (74). In addition, the presence of IgA^+ plasma cells expressing PD-L1 and IL-10 in the tumor environment was associated with poor T-cell immunity in human liver cancers (75). Recently, it was found that GABA secreted by B cells promotes the differentiation of monocytes into anti-inflammatory macrophages, which secrete IL-10 and suppress the anti-tumor response of $CD8^+$ T cells (76).

IMMUNE-REGULATING LIVER NON-HEMATOPOIETIC CELLS

Liver Sinusoidal Endothelial Cells

In the liver, up to 50% of the non-parenchymal cells are LSECs. LSECs are interrelated with the apoptosis of activated T cells and affect the function of DCs in several ways. LSECs are located in an ideal anatomical position that can absorb exogenous antigens efficiently and rapidly and their expression eventually promotes immune tolerance to a specific antigen (77). The space of Disse is a narrow space of approximately 0.4 μm between LSECs and hepatocytes, which is in continuity with the sinusoidal lumen. Stellate cells are found in the space of Disse, while KCs and intrahepatic lymphocytes are arranged in the lumen of the hepatic sinusoids. The slow blood flow in the hepatic sinusoids and the unique structure of LSECs facilitate prolonged contact between lymphocytes and antigen-presenting cells and promote lymphocyte extravasation. In addition, hepatocytes and LSECs secrete the chemokine CXCL9 to recruit lymphocytes into the liver (78). Similar to DCs, LSECs are crucial in receptor-mediated endocytosis and/or phagocytosis, antigen processing and presentation (78). Human LSECs express ICAM-1, TNF α and IFN-γ, and induce high expression of MHC-II, CD40, ICAM-1, and VCAM-1. LSECs can also activate the interaction between hepatic sinusoidal endothelial cells and immune cells. Under normal circumstances, hepatic sinusoidal endothelial cells will trigger an anti-inflammatory response after antigen presentation to create a self-balanced environment. KLF2-NO signaling in LSECs can also inhibit tumor progression by inducing CXCL16 overexpression and recruiting NKT cells (79). Finally, the overexpression of PD-L1 by LSECs inhibits CD8+ T-cell activation, leading to a poor prognosis of HCC (77).

Hepatocytes

Hepatocytes, which express a wide array of innate immune receptors, account for 90% of all liver cells. With the immune receptors, they play an irreplaceable role in metabolism, protein production, toxin neutralization, pathogen detection, and the host immune response. Hepatocytes express toll-like receptors (TLRs) that respond to TLR2 and TLR4 ligands (80), as well as act as antigen-presenting cells to naive T cells by physically interacting in an ICAM-1/MHC-dependent pathway (81). Hepatocytes are responsible for the production of most of the acute phase proteins and their complement components that are the first line of defense against pathogens (82).

AXIN1 is a negative regulator of the Wnt/b-linked protein signaling pathway. AXIN1 mutant HCC induces the Notch and YAP pathways, and these pathways also provide new therapeutic targets for AXIN1 mutant HCC (83). Finally, siRNA-mediated transient GPC3 silencing inhibits the invasion and migration of hepatocellular carcinoma cells. Therefore, GPC3 can be investigated as an immunotherapeutic target for HCC (84).

Hepatic Stellate Cells

HSCs exist in the space of Disse and account for 30% of non-parenchymal cells. In normal liver conditions, HSCs are at rest and have a low ability to synthesize collagen and their primary function is to store retinoids. TLR4 and TLR9 are expressed in HSCs (85) and TLR4 directly stimulates HSCs to secrete chemokines (CCL2, CCL3, and CCL4), thus exhibiting pro-inflammatory features. Interestingly, TLR9 signaling enhances collagen production in HSCs but inhibits HSC migration to regulate liver fibrosis. In addition, a series of related transcription factors may be involved in the formation of liver fibrosis through different mechanisms (86, 87). For example, the c-Abl-MRTF-A positive feedback loop contributes to HSC activation and liver fibrosis, and MKL1 interacts with AP-1 and SMAD3 to activate CTGF transcription to promote HSC activation in a non-autonomous fashion (88, 89).

GDF15 is an important mediator in the TME linking HSCs and hepatic tumor cells, to promote the progression of HCC. Therefore, the anti-GDF15 neutralizing antibody may be a novel therapeutic agent for patients with HCC (90). HSC-induced N-methyltransferase (NNMT) promotes HCC cell invasion and tumor metastasis by enhancing the expression of CD44v3, making it a promising prognostic biomarker and therapeutic target for HCC (91). HSCs promote MDSC migration *via* the SDF-1/CXCR4 axis, thereby promoting tumor progression (92). In this regard, the miR-1246-RORα-Wnt/β-catenin axis is a novel pathway for HSCs to promote HCC progression, and thus miR-1246 and RORα may become new therapeutic targets for HCC (93). The Sox9/INHBB axis also promotes the growth and metastasis of HCC tumors *in situ* by activating HSCs in the TME, which may also be a potential target for HCC therapy (94).

CROSS-TALK BETWEEN INNATE AND ADAPTIVE IMMUNE SYSTEMS

In HCC pathogenesis, immune cells in both pathways are both activated and repressed (see **Table 1**). In HCC progression

leading to metastasis, the homeostatic cross-talk between the innate and adaptive immune system is dysregulated in an increasing manner (4). In general, $CD8^+$ T cells are often considered to be the main anti-cancer immune cells (95) and a common feature is the subversion of their priming, which occurs in three ways. This occurs *via* the repression of TCR interaction with MHC class 1 peptides, the absence of co-stimulation of other receptors (CD28), and the repression of cytokine signals such as IL-12 IFN-1 (96).

Immune escape is also facilitated by dysfunction or a reduced number of DCs that facilitate $CD8^+$ T-cell priming (97). In addition, NK interaction with DCs (cDC1) is essential to promote their effectiveness and abundance (98). In the TME, the stimulation of CCL2 often promotes the abundance of monocytes that can act as a barrier to intratumoral penetration of antigen-specific T cells that gather in the surrounding stroma (99). Myeloid-derived suppressor cells (MDSCs) consist of monocytes and neutrophils. In carcinogenesis, a wide range of cancer-induced monocytes repress $CD8^+$ T cells and IFN-γ (100), as well as promote Tregs to promote tumor growth. Interestingly, monocytes can also promote NKs (101). Treg stimulation also occurs *via* TAM-stimulated CCL2 (102), as well as *via* TAM expression of PD-L1/2 to repress TCR/CTLs to promote a strong immunosuppressive effect to illustrate the cross-talk between TAMs and the adaptive immune system (103). In another example of cross-talk, $CD8^+$ T cells can also be repressed by neutrophils in the metastasis stage (104). Treg expression that is promoted by DCs (105) can also repress CTLs and promote NK apoptosis (106, 107). Finally, Breg expression that is promoted by B-cell production of IL-10 (108) can promote $CD4^+$ T-cell stimulation of FOXP3 Tregs (109).

DISCUSSION

Immune response in the liver incorporates a network of lymphocytes to both respond to pathogens and injury, and maintain homeostasis. Dysfunctional inflammatory mechanisms may lead to liver injury, non-resolving hepatitis, and eventually carcinogenesis. The function of hematopoietic progenitor cells may decrease this inflammatory activity and maintain liver homeostasis to protect from tissue damage and reduce infection and metastasis. Many other studies have defined the characteristics, function, and mechanism of several other organ-specific immune cells including skin, lung, and other tissue; however, limited attention has been focused on the liver's residential immune cells. Further studies, using new technologies such as single-cell sequencing and mass spectrometry streaming, may contribute to a more profound understanding of liver-specific immunology to maintain homeostasis, as well as respond to carcinogenesis. The limited efficacy of immunotherapy to date for the treatment of HCC requires the investigation of new immunogenic targets.

AUTHOR CONTRIBUTIONS

All authors listed have made a substantial, direct, and intellectual contribution to the work, and approved it for publication.

FUNDING

This work was supported by the National Natural Science Foundation of China (Grant No. 81971504), Post-Doctoral Special Foundation of China (2020M670065ZX), Post-Doctoral Foundation of Jiangsu Province (Grant No. 2020Z021), Changzhou Social Development Foundation (CE20205038), Changzhou Science and Technology Planning Project (CE20215042), Jiangsu 333 Talent Training Project (2022 3-4-116), Changzhou Health Commission Major Science and Technology Project (ZD201901), Young Talent Development Plan of Changzhou Health Commission (CZQM2020118), the Development Foundation of Affiliated Hospital of Xuzhou Medical University (XYFY2020016), DAAD-K.C. WONG FUNDING (57501535) and the Changzhou Sci&Tech Program (CJ20210013, CJ20220008).

ACKNOWLEDGMENTS

We would like to show sincere appreciation to the reviewers for their many useful comments on the early version of the manuscript.

REFERENCES

1. Ringelhan M, Pfister D, O'Connor T, Pikarsky E, Heikenwalder M. The Immunology of Hepatocellular Carcinoma. *Nat Immunol* (2018) 19(3):222–32. doi: 10.1038/s41590-018-0044-z
2. Yang JD, Nakamura I, Roberts LR. The Tumor Microenvironment in Hepatocellular Carcinoma: Current Status and Therapeutic Targets. *Semin Cancer Biol* (2011) 21(1):35–43. doi: 10.1016/j.semcancer.2010.10.007
3. Lu C, Rong D, Zhang B, Zheng W, Wang X, Chen Z, et al. Current Perspectives on the Immunosuppressive Tumor Microenvironment in Hepatocellular Carcinoma: Challenges and Opportunities. *Mol cancer* (2019) 18(1):1–12. doi: 10.1186/s12943-019-1047-6
4. Garner H, de Visser KE. Immune Crosstalk in Cancer Progression and Metastatic Spread: A Complex Conversation. *Nat Rev Immunol* (2020) 20 (8):483–97. doi: 10.1038/s41577-019-0271-z
5. Tian Z, Hou X, Liu W, Han Z, Wei L. Macrophages and Hepatocellular Carcinoma. *Cell Biosci* (2019) 9(1):1–10. doi: 10.1186/s13578-019-0342-7
6. Koyama Y, Brenner DA. Liver Inflammation and Fibrosis. *J Clin Invest* (2017) 127(1):55–64. doi: 10.1172/JCI88881
7. De Palma M, Biziato D, Petrova TV. Microenvironmental Regulation of Tumour Angiogenesis. *Nat Rev Cancer* (2017) 17(8):457–74. doi: 10.1038/nrc.2017.51
8. Tacke F, Zimmermann HW. Macrophage Heterogeneity in Liver Injury and Fibrosis. *J Hepatol* (2014) 60(5):1090–6. doi: 10.1016/j.jhep.2013.12.025
9. Krenkel O PT, Govaere O, Abdallah AT, Mossanen JC, Kohlhepp M, Liepelt A, et al. Therapeutic Inhibition of Inflammatory Monocyte Recruitment Reduces Steatohepatitis and Liver Fibrosis. *Hepatol* (2018) 67(4):14. doi: 10.1002/hep.29544
10. Yada A IY, Uyama N, Uda Y, Okada T, Fujimoto J. Splenectomy Attenuates Murine Liver Fibrosis With Hypersplenism Stimulating Hepatic Accumulation

of Ly-6C(Lo) Macrophages. *J Hepatol* (2015) 63(4):12. doi: 10.1016/j.jhep.2015.05.010
11. Yao W, Ba Q, Li X, Li H, Zhang S, Yuan Y, et al. A Natural CCR2 Antagonist Relieves Tumor-Associated Macrophage-Mediated Immunosuppression to Produce a Therapeutic Effect for Liver Cancer. *EBioMedicine* (2017) 22:58–67. doi: 10.1016/j.ebiom.2017.07.014
12. França CN IM, Hortêncio MNS, do Amaral JB, Ferreira CES, Tuleta ID, Fonseca FAH. Monocyte Subtypes and the CCR2 Chemokine Receptor in Cardiovascular Disease. *Clin Sci (Lond)* (2017) 131(12):10. doi: 10.1042/CS20170009
13. Han HS, Kang G, Kim JS, Choi BH, Koo SH. Regulation of Glucose Metabolism From a Liver-Centric Perspective. *Exp Mol Med* (2016) 48: e218. doi: 10.1038/emm.2015.122
14. Li MF, Zhang R, Li TT, Chen MY, Li LX, Lu JX, et al. High Glucose Increases the Expression of Inflammatory Cytokine Genes in Macrophages Through H3K9 Methyltransferase Mechanism. *J Interferon Cytokine Res Off J Int Soc Interferon Cytokine Res* (2016) 36(1):48–61. doi: 10.1089/jir.2014.0172
15. Zhang Q, He Y, Luo N, Patel SJ, Han Y, Gao R, et al. Landscape and Dynamics of Single Immune Cells in Hepatocellular Carcinoma. *Cell* (2019) 179(4):829–45.e20. doi: 10.1016/j.cell.2019.10.003
16. Jiang Y, Han Q, Zhao H, Zhang J. Promotion of Epithelial-Mesenchymal Transformation by Hepatocellular Carcinoma-Educated Macrophages Through Wnt2b/β-Catenin/C-Myc Signaling and Reprogramming Glycolysis. *J Exp Clin Cancer Res* (2021) 40(1):13. doi: 10.1186/s13046-020-01808-3
17. Zhang W, Zhangyuan G, Wang F, Jin K, Shen H, Zhang L, et al. The Zinc Finger Protein Miz1 Suppresses Liver Tumorigenesis by Restricting Hepatocyte-Driven Macrophage Activation and Inflammation. *Immunity* (2021) 54(6):1168–85.e8. doi: 10.1016/j.immuni.2021.04.027
18. Pu J, Li W, Wang A, Zhang Y, Qin Z, Xu Z, et al. Long non-Coding RNA HOMER3-AS1 Drives Hepatocellular Carcinoma Progression *via* Modulating the Behaviors of Both Tumor Cells and Macrophages. *Cell Death Dis* (2021) 12(12):1103. doi: 10.1038/s41419-021-04309-z
19. Avila MA, Berasain C. Targeting CCL2/CCR2 in Tumor-Infiltrating Macrophages: A Tool Emerging Out of the Box Against Hepatocellular Carcinoma. *Cell Mol Gastroenterol Hepatol* (2019) 7(2):293–4. doi: 10.1016/j.jcmgh.2018.11.002
20. Ye YC, Zhao JL, Lu YT, Gao CC, Yang Y, Liang SQ, et al. NOTCH Signaling *via* WNT Regulates the Proliferation of Alternative, CCR2-Independent Tumor-Associated Macrophages in Hepatocellular Carcinoma. *Cancer Res* (2019) 79(16):4160–72. doi: 10.1158/0008-5472.CAN-18-1691
21. Xiao N, Li K, Zhu X, Xu B, Liu X, Lei M, et al. CD74(+) Macrophages are Associated With Favorable Prognosis and Immune Contexture in Hepatocellular Carcinoma. *Cancer Immunol Immunother* (2022) 71(1):57–69. doi: 10.1007/s00262-021-02962-z
22. Heymann F, Tacke F. Immunology in the Liver–From Homeostasis to Disease. *Nat Rev Gastroenterol Hepatol* (2016) 13(2):88–110. doi: 10.1038/nrgastro.2015.200
23. Bleriot C, Dupuis T, Jouvion G, Eberl G, Disson O, Lecuit M. Liver-Resident Macrophage Necroptosis Orchestrates Type 1 Microbicidal Inflammation and Type-2-Mediated Tissue Repair During Bacterial Infection. *Immunity*. (2015) 42(1):145–58. doi: 10.1016/j.immuni.2014.12.020
24. Knolle P, Schlaak J, Uhrig A, Kempf P, Meyer zum Buschenfelde KH, Gerken G. Human Kupffer Cells Secrete IL-10 in Response to Lipopolysaccharide (LPS) Challenge. *J Hepatol* (1995) 22(2):226–9. doi: 10.1016/0168-8278(95)80433-1
25. Ji H, Shen X, Gao F, Ke B, Freitas MC, Uchida Y, et al. Programmed Death-1/B7-H1 Negative Costimulation Protects Mouse Liver Against Ischemia and Reperfusion Injury. *Hepatology* (2010) 52(4):1380–9. doi: 10.1002/hep.23843
26. Wang B, Li X, Hu W, Zhou Y, Din Y. Silencing of lncRNA SNHG20 Delays the Progression of Nonalcoholic Fatty Liver Disease to Hepatocellular Carcinoma *via* Regulating Liver Kupffer Cells Polarization. *IUBMB Life* (2019) 71(12):1952–61. doi: 10.1002/iub.2137
27. Wu H, Zhong Z, Wang A, Yuan C, Ning K, Hu H, et al. LncRNA FTX Represses the Progression of non-Alcoholic Fatty Liver Disease to Hepatocellular Carcinoma *via* Regulating the M1/M2 Polarization of Kupffer Cells. *Cancer Cell Int* (2020) 20:266. doi: 10.1186/s12935-020-01354-0
28. Liu N, Chang CW, Steer CJ, Wang XW, Song G. MicroRNA-15a/16-1 Prevents Hepatocellular Carcinoma by Disrupting the Communication Between Kupffer Cells and Regulatory T Cells. *Gastroenterology* (2022) 162(2):575–89. doi: 10.1053/j.gastro.2021.10.015
29. Eckert C, Klein N, Kornek M, Lukacs-Kornek V. The Complex Myeloid Network of the Liver With Diverse Functional Capacity at Steady State and in Inflammation. *Front Immunol* (2015) 6:179. doi: 10.3389/fimmu.2015.00179
30. Funken D I-AH, Uhl B, Lerchenberger M, Rentsch M, Mayr D, Massberg S, et al. *In Situ* Targeting of Dendritic Cells Sets Tolerogenic Environment and Ameliorates CD4(+) T-Cell Response in the Postischemic Liver. *FASEB J* (2017) 31(11):13. doi: 10.1055/s-0037-1605052
31. Han Y CZ, Yang Y, Jiang Z, Gu Y, Liu Y, Lin C, et al. Human CD14+ CTLA-4+ Regulatory Dendritic Cells Suppress T-Cell Response by Cytotoxic T-Lymphocyte Antigen-4-Dependent IL-10 and Indoleamine-2,3-Dioxygenase Production in Hepatocellular Carcinoma. *Hepatology* (2014) 59(2):13. doi: 10.1002/hep.26694
32. Yoshida R, Oku T, Imanishi J, Kishida T, Hayaishi O. Interferon: A Mediator of Indoleamine 2,3-Dioxygenase Induction by Lipopolysaccharide, Poly(I) X Poly(C), and Pokeweed Mitogen in Mouse Lung. *Arch Biochem Biophys* (1986) 249(2):596–604. doi: 10.1016/0003-9861(86)90038-X
33. Tian J, Avalos AM, Mao SY, Chen B, Senthil K, Wu H, et al. Toll-Like Receptor 9-Dependent Activation by DNA-Containing Immune Complexes is Mediated by HMGB1 and RAGE. *Nat Immunol* (2007) 8(5):487–96. doi: 10.1038/ni1457
34. Pang L, Ng KT-P, Liu J, Yeung W-HO, Zhu J, Chiu T-LS, et al. Plasmacytoid Dendritic Cells Recruited by HIF-1α/eADO/ADORA1 Signaling Induce Immunosuppression in Hepatocellular Carcinoma. *Cancer Lett* (2021) 522:80–92. doi: 10.1016/j.canlet.2021.09.022
35. Zhou ZJ, Xin HY, Li J, Hu ZQ, Luo CB, Zhou SL. Intratumoral Plasmacytoid Dendritic Cells as a Poor Prognostic Factor for Hepatocellular Carcinoma Following Curative Resection. *Cancer Immunol Immunother* (2019) 68 (8):1223–33. doi: 10.1007/s00262-019-02355-3
36. Vogt A, Sadeghlar F, Ayub TH, Schneider C, Mohring C, Zhou T, et al. Alpha-Fetoprotein- and CD40Ligand-Expressing Dendritic Cells for Immunotherapy of Hepatocellular Carcinoma. *Cancers (Basel)* (2021) 13 (13) 3375. doi: 10.3390/cancers13133375
37. Wong YC, Tay SS, McCaughan GW, Bowen DG, Bertolino P. Immune Outcomes in the Liver: Is CD8 T Cell Fate Determined by the Environment? *J Hepatol* (2015) 63(4):1005–14. doi: 10.1016/j.jhep.2015.05.033
38. Tedesco D, Grakoui A. Environmental Peer Pressure: CD4(+) T Cell Help in Tolerance and Transplantation. *Liver Transplant Off Publ Am Assoc Study Liver Dis Int Liver Transplant Soc* (2018) 24(1):89–97. doi: 10.1002/lt.24873
39. von Oppen N, Schurich A, Hegenbarth S, Stabenow D, Tolba R, Weiskirchen R, et al. Systemic Antigen Cross-Presented by Liver Sinusoidal Endothelial Cells Induces Liver-Specific CD8 T-Cell Retention and Tolerization. *Hepatology* (2009) 49(5):1664–72. doi: 10.1002/hep.22795
40. Tuncer C, Oo YH, Murphy N, Adams DH, Lalor PF. The Regulation of T-Cell Recruitment to the Human Liver During Acute Liver Failure. *Liver Int* (2013) 33(6):852–63. doi: 10.1111/liv.12182
41. Crispe IN. Hepatic T Cells and Liver Tolerance. *Nat Rev Immunol* (2003) 3 (1):51–62. doi: 10.1038/nri981
42. Schildberg FA, Wojtalla A, Siegmund SV, Endl E, Diehl L, Abdullah Z, et al. Murine Hepatic Stellate Cells Veto CD8 T Cell Activation by a CD54-Dependent Mechanism. *Hepatology* (2011) 54(1):262–72. doi: 10.1002/hep.24352
43. Wakabayashi Y, Tamiya T, Takada I, Fukaya T, Sugiyama Y, Inoue N, et al. Histone 3 Lysine 9 (H3K9) Methyltransferase Recruitment to the Interleukin-2 (IL-2) Promoter Is a Mechanism of Suppression of IL-2 Transcription by the Transforming Growth Factor-Beta-Smad Pathway. *J Biol Chem* (2011) 286(41):35456–65. doi: 10.1074/jbc.M111.236794
44. Allan RS, Zueva E, Cammas F, Schreiber HA, Masson V, Belz GT, et al. An Epigenetic Silencing Pathway Controlling T Helper 2 Cell Lineage Commitment. *Nature* (2012) 487(7406):249–53. doi: 10.1038/nature11173
45. Lv Q, Wang K, Qiao S, Yang L, Xin Y, Dai Y, et al. Norisoboldine, a Natural AhR Agonist, Promotes Treg Differentiation and Attenuates Colitis *via* Targeting Glycolysis and Subsequent NAD(+)/SIRT1/SUV39H1/H3K9me3 Signaling Pathway. *Cell Death Dis* (2018) 9(3):258. doi: 10.1038/s41419-018-0297-3

46. Heymann F, Peusquens J, Ludwig-Portugall I, Kohlhepp M, Ergen C, Niemietz P, et al. Liver Inflammation Abrogates Immunological Tolerance Induced by Kupffer Cells. *Hepatology* (2015) 62(1):279–91. doi: 10.1002/hep.27793
47. You Q, Cheng L, Kedl RM, Ju C. Mechanism of T Cell Tolerance Induction by Murine Hepatic Kupffer Cells. *Hepatology* (2008) 48(3):978–90. doi: 10.1002/hep.22395
48. Yan ML, Wang YD, Tian YF, Lai ZD, Yan LN. Inhibition of Allogeneic T-Cell Response by Kupffer Cells Expressing Indoleamine 2,3-Dioxygenase. *World J Gastroenterol* (2010) 16(5):636–40. doi: 10.3748/wjg.v16.i5.636
49. Zhang H, Jiang Z, Zhang L. Dual Effect of T Helper Cell 17 (Th17) and Regulatory T Cell (Treg) in Liver Pathological Process: From Occurrence to End Stage of Disease. *Int Immunopharmacol* (2019) 69:50–9. doi: 10.1016/j.intimp.2019.01.005
50. Geissmann F, Cameron TO, Sidobre S, Manlongat N, Kronenberg M, Briskin MJ, et al. Intravascular Immune Surveillance by CXCR6+ NKT Cells Patrolling Liver Sinusoids. *PloS Biol* (2005) 3(4):e113. doi: 10.1371/journal.pbio.0030113
51. Wehr A, Baeck C, Heymann F, Niemietz PM, Hammerich L, Martin C, et al. Chemokine Receptor CXCR6-Dependent Hepatic NK T Cell Accumulation Promotes Inflammation and Liver Fibrosis. *J Immunol* (2013) 190(10):5226–36. doi: 10.4049/jimmunol.1202909
52. Trobonjaca Z, Leithäuser F, Möller P, Schirmbeck R, Reimann J. Activating Immunity in the Liver. I. Liver Dendritic Cells (But Not Hepatocytes) are Potent Activators of IFN-Gamma Release by Liver NKT Cells. *J Immunol* (2001) 167(3):1413–22. doi: 10.4049/jimmunol.167.3.1413
53. Schmieg J, Yang G, Franck RW, Van Rooijen N, Tsuji M. Glycolipid Presentation to Natural Killer T Cells Differs in an Organ-Dependent Fashion. *Proc Natl Acad Sci U S A* (2005) 102(4):1127–32. doi: 10.1073/pnas.0408288102
54. Wang X, He Q, Shen H, Xia A, Tian W, Yu W, et al. TOX Promotes the Exhaustion of Antitumor CD8(+) T Cells by Preventing PD1 Degradation in Hepatocellular Carcinoma. *J Hepatol* (2019) 71(4):731–41. doi: 10.1016/j.jhep.2019.05.015
55. Kim H-D, Park S, Jeong S, Lee YJ, Lee H, Kim CG, et al. 4-1bb Delineates Distinct Activation Status of Exhausted Tumor-Infiltrating CD8 T Cells in Hepatocellular Carcinoma. *Hepatology* (2020) 71(3):955–71. doi: 10.1002/hep.30881
56. Peng H, Tian Z. Re-Examining the Origin and Function of Liver-Resident NK Cells. *Trends Immunol* (2015) 36(5):293–9. doi: 10.1016/j.it.2015.03.006
57. Gonzalez-Polo V P-MM, Cervera V, Gambaro S, Yantorno SE, Descalzi V, Tiribelli C, et al. Group 2 Innate Lymphoid Cells Exhibit Progressively Higher Levels of Activation During.*Ann Hepatol* (2019) 18(2) :366–372 doi: 10.1016/j.aohep.2018.12.001
58. Gieseck RL3rd WM, Wynn TA. Type 2 Immunity in Tissue Repair and Fibrosis. *Nat Rev Immunol* (2018) 18(1):15. doi: 10.1038/nri.2017.90
59. Wang S, Li J, Wu S, Cheng L, Shen Y, Ma W, et al. Progression. Tilcanpilf. *Clin Sci (Lond)* (2018) 132(24):18.
60. Heinrich B, Gertz EM, Schäffer AA, Craig A, Ruf B, Subramanyam V, et al. The Tumour Microenvironment Shapes Innate Lymphoid Cells in Patients With Hepatocellular Carcinoma. *Gut* (2021) 71(6):1161–75. doi: 10.1136/gutjnl-2021-325288
61. Liu Y, Song Y, Lin D, Lei L, Mei Y, Jin Z, et al. NCR(-) Group 3 Innate Lymphoid Cells Orchestrate IL-23/IL-17 Axis to Promote Hepatocellular Carcinoma Development. *EBioMedicine* (2019) 41:333–44. doi: 10.1016/j.ebiom.2019.02.050
62. Zhi-Bin Zhao F-TL, Ma H-D, Wang Y-H, Yang W, Long J, Miao Q, et al. Liver-Resident NK Cells Suppress Autoimmune Cholangitis and Limit the Proliferation of CD4 + T Cells. *Cell Mol Immunol* (2019) 17(2):12. doi: 10.1038/s41423-019-0199-z
63. Zhou J PH, Li K, Qu K, Wang B, Wu Y, Ye L, et al. Liver-Resident NK Cells Control Antiviral Activity of Hepatic T Cells *via* the PD-1-PD-L1 Axis. *Immunity* (2019) 50(2):15. doi: 10.1016/j.immuni.2018.12.024
64. Chen M, Xu M, Zhu C, Wang H, Zhao Q, Zhou F. Sirtuin2 Enhances the Tumoricidal Function of Liver Natural Killer Cells in a Mouse Hepatocellular Carcinoma Model. *Cancer Immunol Immunother* (2019) 68(6):961–71. doi: 10.1007/s00262-019-02337-5
65. Yu M, Luo H, Fan M, Wu X, Shi B, Di S, et al. Development of GPC3-Specific Chimeric Antigen Receptor-Engineered Natural Killer Cells for the Treatment of Hepatocellular Carcinoma. *Mol Ther* (2018) 26(2):366–78. doi: 10.1016/j.ymthe.2017.12.012
66. Sun H, Huang Q, Huang M, Wen H, Lin R, Zheng M, et al. Human CD96 Correlates to Natural Killer Cell Exhaustion and Predicts the Prognosis of Human Hepatocellular Carcinoma. *Hepatology* (2019) 70(1):168–83. doi: 10.1002/hep.30347
67. Sun H, Liu L, Huang Q, Liu H, Huang M, Wang J, et al. Accumulation of Tumor-Infiltrating CD49a(+) NK Cells Correlates With Poor Prognosis for Human Hepatocellular Carcinoma. *Cancer Immunol Res* (2019) 7(9):1535–46. doi: 10.1158/2326-6066.CIR-18-0757
68. Jacquelot N, Seillet C, Souza-Fonseca-Guimaraes F, Sacher AG, Belz GT, Ohashi PS. Natural Killer Cells and Type 1 Innate Lymphoid Cells in Hepatocellular Carcinoma: Current Knowledge and Future Perspectives. *Int J Mol Sci* (2021) 22(16) 9044. doi: 10.3390/ijms22169044
69. Chen EB, Zhou ZJ, Xiao K, Zhu GQ, Yang Y, Wang B, et al. The miR-561-5p/CX3CL1 Signaling Axis Regulates Pulmonary Metastasis in Hepatocellular Carcinoma Involving CX3CR1(+) Natural Killer Cells Infiltration. *Theranostics* (2019) 9(16):4779–94. doi: 10.7150/thno.32543
70. Schneider C, Teufel A, Yevsa T, Staib F, Hohmeyer A, Walenda G, et al. Adaptive Immunity Suppresses Formation and Progression of Diethylnitrosamine-Induced Liver Cancer. *Gut* (2012) 61(12):1733–43. doi: 10.1136/gutjnl-2011-301116
71. Garnelo M, Tan A, Her Z, Yeong J, Lim CJ, Chen J, et al. Interaction Between Tumour-Infiltrating B Cells and T Cells Controls the Progression of Hepatocellular Carcinoma. *Gut* (2017) 66(2):342–51. doi: 10.1136/gutjnl-2015-310814
72. Mauri C, Bosma A. Immune Regulatory Function of B Cells. *Annu Rev Immunol* (2012) 30:221–41. doi: 10.1146/annurev-immunol-020711-074934
73. Xue H, Lin F, Tan H, Zhu ZQ, Zhang ZY, Zhao L. Overrepresentation of IL-10-Expressing B Cells Suppresses Cytotoxic CD4+ T Cell Activity in HBV-Induced Hepatocellular Carcinoma. *PloS One* (2016) 11(5):e0154815. doi: 10.1371/journal.pone.0154815
74. Liu J, Zhan W, Kim CJ, Clayton K, Zhao H, Lee E, et al. IL-10-Producing B Cells are Induced Early in HIV-1 Infection and Suppress HIV-1-Specific T Cell Responses. *PloS One* (2014) 9(2):e89236. doi: 10.1371/journal.pone.0089236
75. Shalapour S, Lin XJ, Bastian IN, Brain J, Burt AD, Aksenov AA, et al. Inflammation-Induced IgA+ Cells Dismantle Anti-Liver Cancer Immunity. *Nature.* (2017) 551(7680):340–5. doi: 10.1038/nature24302
76. Zhang B, Vogelzang A, Miyajima M, Sugiura Y, Wu Y, Chamoto K, et al. B Cell-Derived GABA Elicits IL-10(+) Macrophages to Limit Anti-Tumour Immunity. *Nature* (2021) 599(7885):471–6. doi: 10.1038/s41586-021-04082-1
77. Li H. Intercellular Crosstalk of Liver Sinusoidal Endothelial Cells in Liver Fibrosis, Cirrhosis and Hepatocellular Carcinoma. *Dig Liver Dis* (2021) 54(5):598–613. doi: 10.1016/j.dld.2021.07.006
78. Racanelli V, Rehermann B. The Liver as an Immunological Organ. *Hepatology* (2006) 43(2):S54–62. doi: 10.1002/hep.21060
79. Yu Z, Guo J, Liu Y, Wang M, Liu Z, Gao Y, et al. Nano Delivery of Simvastatin Targets Liver Sinusoidal Endothelial Cells to Remodel Tumor Microenvironment for Hepatocellular Carcinoma. *J Nanobiotechnol* (2022) 20(1):9. doi: 10.1186/s12951-021-01205-8
80. Seki E, Brenner DA. Toll-Like Receptors and Adaptor Molecules in Liver Disease: Update. *Hepatology* (2008) 48(1):322–35. doi: 10.1002/hep.22306
81. Warren A, Le Couteur DG, Fraser R, Bowen DG, McCaughan GW, Bertolino P. T Lymphocytes Interact With Hepatocytes Through Fenestrations in Murine Liver Sinusoidal Endothelial Cells. *Hepatology* (2006) 44(5):1182–90. doi: 10.1002/hep.21378
82. Jenne CN, Kubes P. Immune Surveillance by the Liver. *Nat Immunol* (2013) 14(10):996–1006. doi: 10.1038/ni.2691
83. Abitbol S, Dahmani R, Coulouarn C, Ragazzon B, Mlecnik B, Senni N, et al. AXIN Deficiency in Human and Mouse Hepatocytes Induces Hepatocellular Carcinoma in the Absence of β-Catenin Activation. *J Hepatol* (2018) 68(6):1203–13. doi: 10.1016/j.jhep.2017.12.018
84. Montalbano M, Rastellini C, McGuire JT, Prajapati J, Shirafkan A, Vento R, et al. Role of Glypican-3 in the Growth, Migration and Invasion of Primary

Hepatocytes Isolated From Patients With Hepatocellular Carcinoma. *Cell Oncol (Dordr)* (2018) 41(2):169–84. doi: 10.1007/s13402-017-0364-2
85. Watanabe A, Hashmi A, Gomes DA, Town T, Badou A, Flavell RA, et al. Apoptotic Hepatocyte DNA Inhibits Hepatic Stellate Cell Chemotaxis *via* Toll-Like Receptor 9. *Hepatology* (2007) 46(5):1509–18. doi: 10.1002/hep.21867
86. Kisseleva T, Brenner D. Molecular and Cellular Mechanisms of Liver Fibrosis and its Regression. *Nat Rev Gastroenterol Hepatol* (2021) 18 (3):151–66. doi: 10.1038/s41575-020-00372-7
87. Dhar D, Baglieri J, Kisseleva T, Brenner DA. Mechanisms of Liver Fibrosis and its Role in Liver Cancer. *Exp Biol Med (Maywood)* (2020) 245(2):96–108. doi: 10.1177/1535370219898141
88. Lu Y, Lv F, Kong M, Chen X, Duan Y, Chen X, et al. A Cabl-MRTF-A Feedback Loop Contributes to Hepatic Stellate Cell Activation. *Front Cell Dev Biol* (2019) 7. doi: 10.3389/fcell.2019.00243
89. Li Z, Li P, Lu Y, Sun D, Zhang X, Xu Y. A non-Autonomous Role of MKL1 in the Activation of Hepatic Stellate Cells. *Biochim Biophys Acta Gene Regul Mech* (2019) 1862(6):609–18. doi: 10.1016/j.bbagrm.2019.03.001
90. Myojin Y, Hikita H, Sugiyama M, Sasaki Y, Fukumoto K, Sakane S, et al. Hepatic Stellate Cells in Hepatocellular Carcinoma Promote Tumor Growth *Via* Growth Differentiation Factor 15 Production. *Gastroenterology* (2021) 160(5):1741–54 e16. doi: 10.1053/j.gastro.2020.12.015
91. Li J, You S, Zhang S, Hu Q, Wang F, Chi X, et al. Elevated N-Methyltransferase Expression Induced by Hepatic Stellate Cells Contributes to the Metastasis of Hepatocellular Carcinoma *via* Regulation of the CD44v3 Isoform. *Mol Oncol* (2019) 13(9):1993–2009. doi: 10.1002/1878-0261.12544
92. Xu Y, Fang F, Jiao H, Zheng X, Huang L, Yi X, et al. Activated Hepatic Stellate Cells Regulate MDSC Migration Through the SDF-1/CXCR4 Axis in an Orthotopic Mouse Model of Hepatocellular Carcinoma. *Cancer Immunol Immunother* (2019) 68(12):1959–69. doi: 10.1007/s00262-019-02414-9
93. Huang JL, Fu YP, Gan W, Liu G, Zhou PY, Zhou C, et al. Hepatic Stellate Cells Promote the Progression of Hepatocellular Carcinoma Through microRNA-1246-RORalpha-Wnt/beta-Catenin Axis. *Cancer Lett* (2020) 476:140–51. doi: 10.1016/j.canlet.2020.02.012
94. Chen Y, Qian B, Sun X, Kang Z, Huang Z, Ding Z, et al. Sox9/INHBB Axis-Mediated Crosstalk Between the Hepatoma and Hepatic Stellate Cells Promotes the Metastasis of Hepatocellular Carcinoma. *Cancer Lett* (2021) 499:243–54. doi: 10.1016/j.canlet.2020.11.025
95. Chen DS, Mellman I. Oncology Meets Immunology: The Cancer-Immunity Cycle. *Immunity* (2013) 39(1):1–10. doi: 10.1016/j.immuni.2013.07.012
96. Curtsinger JM, Mescher MF. Inflammatory Cytokines as a Third Signal for T Cell Activation. *Curr Opin Immunol* (2010) 22(3):333–40. doi: 10.1016/j.coi.2010.02.013
97. Almand B, Resser JR, Lindman B, Nadaf S, Clark JI, Kwon ED, et al. Clinical Significance of Defective Dendritic Cell Differentiation in Cancer. *Clin Cancer Res* (2000) 6(5):1755–66.
98. Böttcher JP, Bonavita E, Chakravarty P, Blees H, Cabeza-Cabrerizo M, Sammicheli S, et al. NK Cells Stimulate Recruitment of Cdc1 Into the Tumor Microenvironment Promoting Cancer Immune Control. *Cell* (2018) 172 (5):1022–37.e14. doi: 10.1016/j.cell.2018.01.004
99. Molon B, Ugel S, Del Pozzo F, Soldani C, Zilio S, Avella D, et al. Chemokine Nitration Prevents Intratumoral Infiltration of Antigen-Specific T Cells. *J Exp Med* (2011) 208(10):1949–62. doi: 10.1084/jem.20101956
100. Youn J-I, Nagaraj S, Collazo M, Gabrilovich DI. Subsets of Myeloid-Derived Suppressor Cells in Tumor-Bearing Mice. *J Immunol* (2008) 181(8):5791–802. doi: 10.4049/jimmunol.181.8.5791
101. Schlecker E, Stojanovic A, Eisen C, Quack C, Falk CS, Umansky V, et al. Tumor-Infiltrating Monocytic Myeloid-Derived Suppressor Cells Mediate CCR5-Dependent Recruitment of Regulatory T Cells Favoring Tumor Growth. *J Immunol* (2012) 189(12):5602–11. doi: 10.4049/jimmunol.1201018
102. Gomez Perdiguero E, Klapproth K, Schulz C, Busch K, Azzoni E, Crozet L, et al. Tissue-Resident Macrophages Originate From Yolk-Sac-Derived Erythro-Myeloid Progenitors. *Nature.* (2015) 518(7540):547–51. doi: 10.1038/nature13989
103. Daurkin I, Eruslanov E, Stoffs T, Perrin GQ, Algood C, Gilbert SM, et al. Tumor-Associated Macrophages Mediate Immunosuppression in the Renal Cancer Microenvironment by Activating the 15-Lipoxygenase-2 Pathway. *Cancer Res* (2011) 71(20):6400–9. doi: 10.1158/0008-5472.CAN-11-1261
104. Coffelt SB, Kersten K, Doornebal CW, Weiden J, Vrijland K, Hau C-S, et al. IL-17-Producing γδ T Cells and Neutrophils Conspire to Promote Breast Cancer Metastasis. *Nature.* (2015) 522(7556):345–8. doi: 10.1038/nature14282
105. Kenkel JA, Tseng WW, Davidson MG, Tolentino LL, Choi O, Bhattacharya N, et al. An Immunosuppressive Dendritic Cell Subset Accumulates at Secondary Sites and Promotes Metastasis in Pancreatic Cancer. *Cancer Res* (2017) 77(15):4158–70. doi: 10.1158/0008-5472.CAN-16-2212
106. Karavitis J, Hix LM, Shi YH, Schultz RF, Khazaie K, Zhang M. Regulation of COX2 Expression in Mouse Mammary Tumor Cells Controls Bone Metastasis and PGE2-Induction of Regulatory T Cell Migration. (2012). doi: 10.1371/journal.pone.0046342*PLoS One* 7(9) :e46342
107. Allard B, Beavis PA, Darcy PK, Stagg J. Immunosuppressive Activities of Adenosine in Cancer. *Curr Opin Pharmacol* (2016) 29:7–16. doi: 10.1016/j.coph.2016.04.001
108. Sarvaria A, Madrigal JA, Saudemont A. B Cell Regulation in Cancer and Anti-Tumor Immunity. *Cell Mol Immunol* (2017) 14(8):662–74. doi: 10.1038/cmi.2017.35
109. Olkhanud PB, Damdinsuren B, Bodogai M, Gress RE, Sen R, Wejksza K, et al. Tumor-Evoked Regulatory B Cells Promote Breast Cancer Metastasis by Converting Resting CD4+ T Cells to T-Regulatory Cells. *Cancer Res* (2011) 71(10):3505–15. doi: 10.1158/0008-5472.CAN-10-4316

Conflict of Interest: The authors declare that the research was conducted in the absence of any commercial or financial relationships that could be construed as a potential conflict of interest.

frontiers | Frontiers in Oncology

TYPE Original Research
PUBLISHED 28 July 2022
DOI 10.3389/fonc.2022.960066

OPEN ACCESS

EDITED BY
Liangrong Shi,
Xiangya Hospital, Central South University, China

REVIEWED BY
Bibo Ke,
University of California, Los Angeles, United States
Xiao-Kang Li,
National Center for Child Health and Development (NCCHD), Japan

*CORRESPONDENCE
Jian Gu
gujian@njmu.edu.cn
Yue Yu
yuyue@njmu.edu.cn

†These authors have contributed equally to this work and share first authorship

SPECIALTY SECTION
This article was submitted to Molecular and Cellular Oncology, a section of the journal Frontiers in Oncology

RECEIVED 02 June 2022
ACCEPTED 05 July 2022
PUBLISHED 28 July 2022

CITATION
Zhou J, Shao Q, Lu Y, Li Y, Xu Z, Zhou B, Chen Q, Li X, Xu X, Pan Y, Deng Z, Wang Y, Yu Y and Gu J (2022) Monocarboxylate transporter upregulation in induced regulatory T cells promotes resistance to anti-PD-1 therapy in hepatocellular carcinoma patients.
Front. Oncol. 12:960066.
doi: 10.3389/fonc.2022.960066

Monocarboxylate transporter upregulation in induced regulatory T cells promotes resistance to anti-PD-1 therapy in hepatocellular carcinoma patients

Jinren Zhou[1†], Qing Shao[1†], Yunjie Lu[2†], Yu Li[1], Zibo Xu[1], Bo Zhou[3], Qiuyang Chen[1], Xiangyu Li[1], Xiaozhang Xu[1], Yufeng Pan[1,4], Zhenhua Deng[1], Yiming Wang[1], Yue Yu[1*] and Jian Gu[1*]

[1]Liver Transplantation Center, First Affiliated Hospital of Nanjing Medical University, Nanjing, China, [2]Department of Hepatobiliary Surgery, The First People's Hospital of Changzhou, The Third Hospital Affiliated to Soochow University, Changzhou, China, [3]Department of General Surgery, Ningbo Medical Center Lihuili Hospital, Ningbo University, Ningbo, China, [4]School of Medicine, Southeast University, Nanjing, China

Background: Programmed cell death-1 (PD-1) immune checkpoint inhibitors are not effective in treating all patients with hepatocellular carcinoma (HCC), and regulatory T cells (Tregs) may determine the resistance to anti-PD-1 therapy.

Methods: Patients were divided into two groups based on the clinical efficacy of anti-PD-1 therapy. Flow cytometry was used to determine the phenotype of CD4+, CD8+, and Tregs in peripheral blood mononuclear cells (PBMCs). CD4+ CD45RA+T cells were sorted to analyze Treg differentiation and function.

Results: No significant differences were found between resistant and sensitive patients in the percentage of CD4+ T cells and Tregs in PBMCs or the differentiation and function of induced Tregs (iTregs). However, iTregs from resistant patients presented higher monocarboxylate transporter (MCT) expression. Lactate induced more iTregs and improved OXPHOS levels in the resistant group. MCT1 and MCT2 were highly expressed in tumor-infiltrating Tregs, and patients with higher MCT1 expression had worse clinical outcomes. Combinatorial therapy with MCT antibody and anti-PD-1 therapy effectively inhibited tumor growth.

Conclusion: MCT and its downstream lactate signal in Tregs can confer anti-PD-1 resistance and may be a marker of poor prognosis in HCC.

KEYWORDS

hepatocellular carcinoma, monocarboxylate transporter, lactate, regulatory T cells, treatment resistance

Introduction

Hepatocellular carcinoma (HCC) is a common malignancy worldwide (1). Except for surgical resection and liver transplantation, effective anti-tumor drugs are limited, and the prognosis of patients with HCC is relatively poor. Immunotherapy alone or combined with targeted therapy of HCC has received considerable attention in clinical research of HCC (2). However, a significant number of patients remain resistant to immunotherapy. Studying the immune microenvironment in these patients could provide a theoretical basis for the underlying mechanism of resistance and identify potential targets for clinical treatment (3).

Regulatory T cells (Tregs) play an important role in maintaining immunological homeostasis (4). Tregs are divided into two main subsets: thymus-derived natural Tregs (nTregs) and induced Tregs (iTregs). Tregs are present in the tumor microenvironment (TME) and can crosstalk with anti-tumor cells, such as infiltrating lymphocytes, macrophages, and natural killer cells (5). They utilize multiple mechanisms to achieve immunosuppression, including the inhibition of antigen-presenting cell (APC) maturation, inhibitory cytokines secretion, and cytotoxic granzyme and perforin production. Although tTregs can be recruited into tumors to suppress the effective T cells, most tumor-infiltrating Tregs are iTregs, which can be induced by interleukin (IL)-2 and transforming growth factor beta (TGF-β) and express forkhead box P3 (Foxp3) and cytotoxic T-lymphocyte-associated protein 4 (CTLA-4) (6). Tregs suppress anti-tumor immune responses, and their infiltration into tumors affects prognosis. The removal of Treg cells can enhance anti-tumor immunity, but their depletion may also trigger detrimental autoimmune responses (7). The response of Tregs to immune checkpoint inhibition (ICI) differs from that induced by other immune cells (8). A recent study showed that tumor resistance to anti-programmed cell death-1 (anti-PD-1) therapy might be related to an increase in CTLA-4$^+$Tregs (9). Moreover, the targeting of CCR8 to deplete tumor-infiltrating Tregs may elicit antitumor immunity and synergize with anti-PD-1 therapy (10).

The proton-coupled monocarboxylic acid transporter (MCT) catalyzes the transmembrane movement of essential monocarboxylate salts, such as L-lactic acid, ketone bodies, and pyruvate, which are essential in many cellular processes. MCT also catalyzes lactate exchange between tumors and the circulation (11) and has become a target for cancer treatment because of its enhanced expression in various tumors (12). Here, we demonstrated that higher expression of MCT and sensitivity to lactate may upregulate the function of Tregs in the TME, which may explain the poor prognosis of patients with HCC who are resistant to anti-PD-1 therapy. We propose that by evaluating MCT expression and suppressing the MCT signaling, the efficacy of therapeutic strategies can be improved.

Materials and methods

Clinical study and the patients

We selected 10 patients with a clear clinical diagnosis of HCC between January 2020 and December 2021 as research participants. Some patients experienced tumor recurrence and underwent liver resection within <1 year. Patients received four treatments of anti-PD-1 therapy every 3 weeks (camrelizumab, Jiangsu Hengrui Medicine) and 9 weeks of apatinib. Patients with decreased tumor volume were included in the sensitive group; patients with a 25% increase in tumor volume were included in the resistant group. Kaplan–Meier survival curves were used to estimate overall survival (OS) and disease-free survival (DFS). Survival curves were exported using GraphPad Prism software (GraphPad Software, San Diego, CA, USA). The local ethics committee of the First Affiliated Hospital of Nanjing Medical University (Jiangsu Province Hospital) approved this study (2020-SRFA-377).

Specimen collection

Fasting blood samples were collected at 7 a.m. before treatment. Blood samples (10–20 ml) were used to monitor T-cell function and phenotype in peripheral blood mononuclear cells (PBMCs). PBMCs were prepared from heparinized venous blood by Ficoll–Hypaque density gradient centrifugation. To evaluate the proportion of $CD8^+$ T cells and $CD4^+$ T cells, PBMCs were surface stained with CD8 and CD4. PBMCs were stained with CD4, CD25, and CD127, and $CD4^+CD25^+CD127^-$ cells were considered to be Tregs. Naive human T cells were extracted from PBMCs by gating $CD4^+CD45RA^+$ cells (>97% purity). iTregs were activated, induced, and expanded with TGF-β (1ng/ml), IL-2 (100 U/ml), and anti-CD3/CD28 beads (one bead per cell) for 7 days.

Tregs were sorted for the next analysis after tissue lymphocytes were extracted (P5700 kit, Solarbio). In HCC and para-cancerous tissues, we analyzed MCT and lactate expression levels using Western blot (Abcam, Cambridge, UK) and a lactic acid content assay kit (BL868A, Biosharp), respectively.

Animal models and tumor generation

Hepa1-6 tumor cells (5×10^6) were injected into the armpits of C57L/B6 and Rag1 −/− 6–8-week-old mice (purchased from the Model Animal Research Center of Nanjing University, Nanjing, China). After 5 days, 10 nM anti-MCT1/2 (AR-C155858, MCE) and 200 μg anti-PD1 (HY-P9971, MCE) were injected into the axilla of the experimental group every 2 days,

while the control group was injected with saline. Tumor volume was measured using a digital caliper. After four injections, all mice were euthanized, and the tumor tissues were removed.

Flow cytometry

Human-specific monoclonal antibodies, including CD4 (A161A1), CD25 (BC96), Foxp3 (206D), and CD45RA (HI100), were purchased from BioLegend (UK), and CD127 (A019D5) was purchased from BD Pharmingen (USA). Foxp3 (206D) was used for intracellular flow cytometry assays, while the others were used for surface staining. A MACSQuant Analyzer 10 (Miltenyi Biotec, Germany) was used for detection, and results were analyzed using FlowJo software (FlowJo, Ashland, OR, USA).

Western blot analysis

Proteins were collected from harvested cells, and a Pierce bicinchoninic acid assay (Thermo Fisher Scientific, UK) was used to determine their concentrations. The proteins were resolved and transferred onto polyvinylidene fluoride membranes. The following antibodies were used: MCT1, MCT2, LDH, anti-GAPDH, anti-P85 (loading control), and tubulin (Abcam, Cambridge, UK). Data were displayed using the Kodak autoradiography film (Kodak XAR film, USA).

Immunofluorescence staining

MCT1, MCT2, and Foxp3 were identified by immunofluorescence using rabbit anti-human MCT1, anti-human MCT2, and anti-human Foxp3 mAbs (Cell Signaling Technology, Danvers, MA, USA). Images were obtained using an inverted microscope (Olympus, Tokyo, Japan) and analyzed using ImageJ software (National Institutes of Health, Bethesda, MD, USA).

Cell metabolism measurement

An XF96 analyzer (Agilent Technologies, Santa Clara, CA, USA) was used to measure Treg cell metabolism. First, Tregs were inoculated onto CellTak 96-well plates at 2×10^5 cells/well and centrifuged. Different reagents were added to measure the oxygen consumption rate (OCR), including 5 mM oligomycin, 1.5 μM FCCP, 1 μM rotenone, and 1 μM antimycin A.

ELISA

We measured the levels of IL-10, TGF-β, and other cytokines using ELISA kits (BioLegend, UK) according to the manufacturer's instructions.

Statistical analysis

Data were analyzed and visualized using GraphPad Prism 6.0 (GraphPad Software). Count data were analyzed using a paired t-test and linear and nonlinear regression analysis. A log-rank test was used to analyze differences in the Kaplan–Meier survival curves. Statistical significance was set at $p < 0.05$.

Results

Role of Treg phenotype and cytokine expression in the peripheral blood of anti-PD-1-resistant patients

As the efficiency of the targeted and anti-PD-1 therapy is highly dependent on the immune status of the liver, we first determined the phenotype of Tregs, CD4+, and CD8+ T cells in the blood. Flow cytometry showed no difference in the percentages of $CD4^+$ T cells and $CD4^+CD25^+CD127^-$ Tregs (Figure 1A). However, more $CD8^+$ T cells were present in the sensitive group, indicating that the efficacy of co-treatment might be partially determined by $CD8^+$ T cells (Figures 1B, C). We evaluated cytokine expression in the blood serum and found that, for anti-inflammatory cytokines, TGF-β was upregulated in the resistant group, and IL-10 levels were similar between the sensitive and resistant groups (Figure 1D). The expression of inflammatory cytokines, such as TNF-α, interferon-gamma (IFN-γ), IL-1, and IL-6, which act as anti-tumor effectors, did not vary between the sensitive and resistant groups (Figure 1E). Tregs can differentiate into nTregs and iTregs (13) and suppress $CD8^+$ T cells (14, 15). As no differences in nTregs were observed under resting conditions between the sensitive and resistant groups, naive T cells were examined for their ability to differentiate into iTregs.

Naive T cells regulated iTreg induction and function *in vitro*

$CD4^+CD45RA^+$ naive T cells were sorted and differentiated into iTregs (*Section 2.2*). After 6 days, flow cytometry showed similar level of expression for Foxp3 in both groups (Figures 2A, B). We counted the absolute number of Tregs after 3 and 6 days to assess iTregs activity in the sensitive and resistant groups, but no differences were observed between the groups (Figure 2C). Tregs maintain an immunosuppressive environment through the expression of specific cytokines, which is important for the establishment of a tumor-dominant microenvironment. We monitored the expression of IL-10 and TGF-β using ELISA

10.3389/fonc.2022.960066

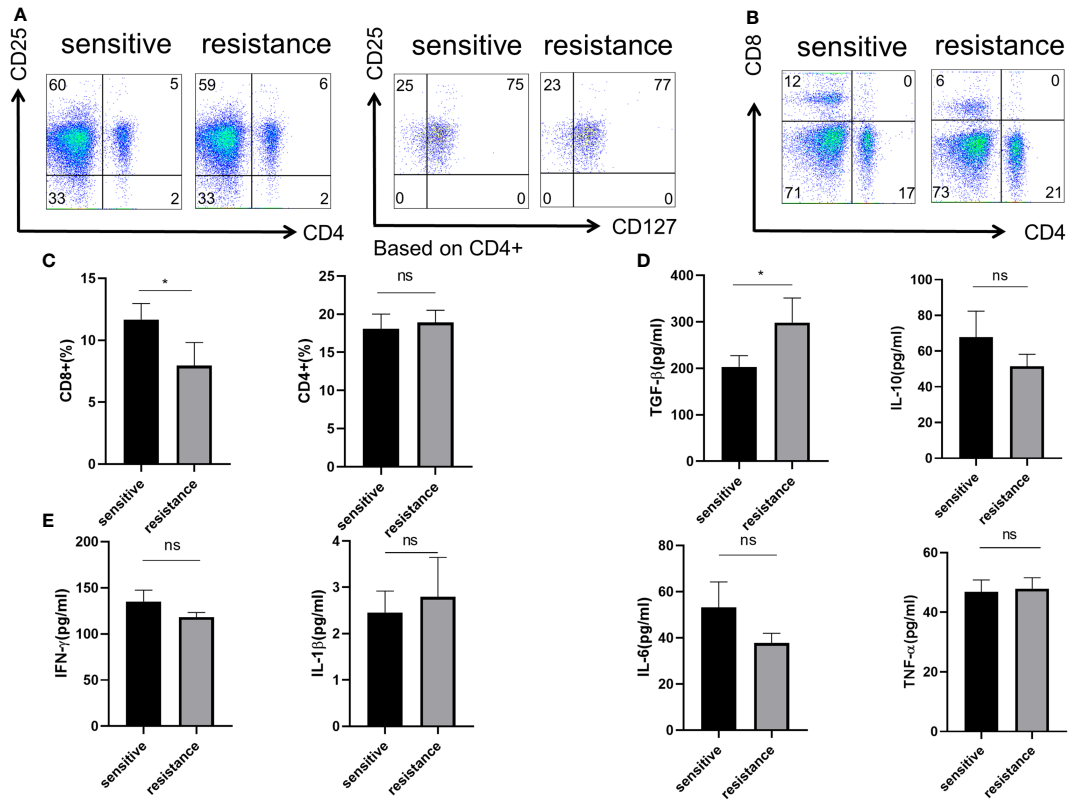

FIGURE 1
Role of Treg phenotype and cytokine expression in the peripheral blood of anti-PD-1-resistant patients. **(A)** Representative flow plot for CD4, CD25, and CD127 expression in the periphery blood of sensitive and resistant patients. **(B)** Representative flow plot for CD4 and CD8 expression in the periphery blood of sensitive and resistant patients. **(C)** The proportion of CD4+ and CD8+ T cells between both groups. The expression of anti-inflammatory cytokines **(D)** and inflammatory cytokines **(E)** from the serum was evaluated through ELISA. The bar shows the mean ± SEM of the levels of indicated proteins (sensitive patients n=4; resistant patients n=4). *p < 0.05. ns, non-significant.

and found no discrepancy in the secretory ability of Tregs between the sensitive and resistant groups (Figures 2D, E).

Induction of iTregs by lactate in the resistance group

Lactate improves the function of iTregs in tumors and is one of the most important mechanisms mediating immunosuppression and tumor immune escape (16, 17). We treated the sensitive and resistant groups with lactate (10 mM) to investigate its effects on iTreg induction. Lactate improved the expression of Foxp3 in the resistant group but not in the sensitive group (Figures 3A, B). In addition, we observed that lactate improved the proliferation of iTregs in the resistant group compared with that in the sensitive group (Figure 3C). As expected, the expression of IL-10 and TGF-β was also upregulated, which corresponded with the above findings (Figure 3D).

Foxp3 was upregulated in the iTregs of the resistant group in an MCT-dependent manner

Lactate acidifies the extracellular space and maintains intracellular pH homeostasis inside the cell through MCT (18). To investigate why iTregs could be induced more effectively by lactate treatment in the resistant group, we examined the expression of MCT1 and MCT2, which are the most important contributors to the regulation of tumor intracellular pH and induction of extracellular acidosis (19). Western blot analysis revealed higher MCT1 and MCT2 expression levels in the resistant group (Figure 4A). Although lactate improved Foxp3 expression, the addition of MCT1 and MCT2 antibodies eliminated this effect and reduced the expression of Foxp3 (Figures 4B, C). Because lactate alters the metabolism of Tregs (16), we evaluated the bioenergetics changes after lactate treatment and found that Tregs in the resistance group

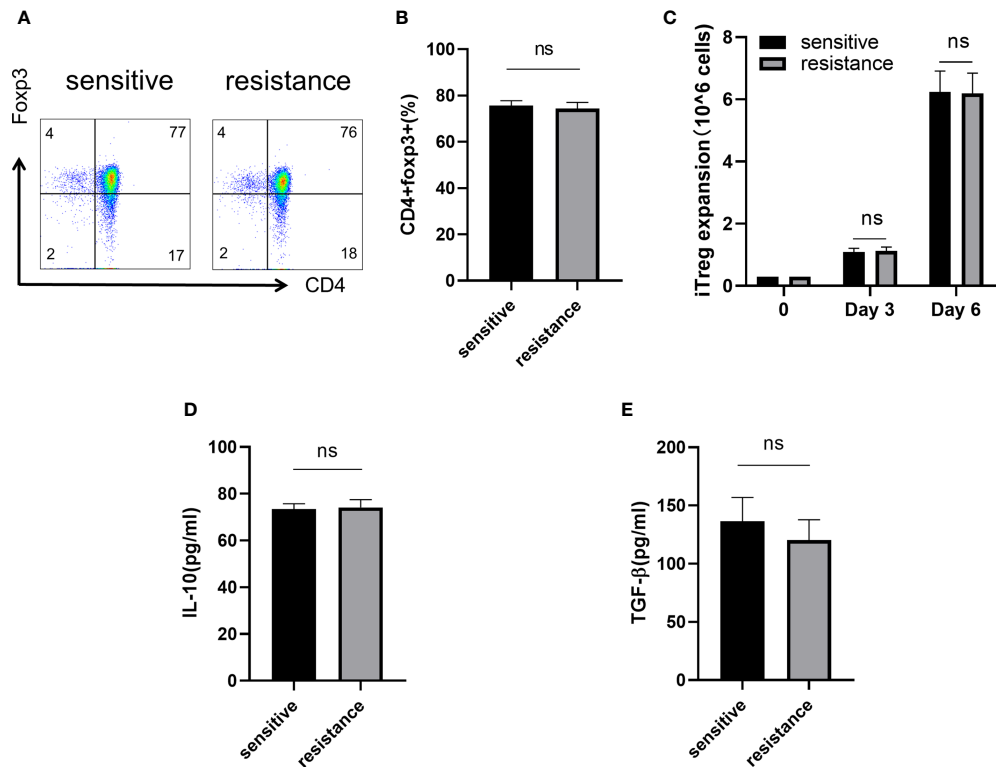

FIGURE 2
Naive T cells regulated iTreg induction and function *in vitro*. Representative flow plot **(A)** and the frequency **(B)** of Foxp3 expression in iTregs of sensitive and resistant patients. The expansion ability of iTregs. **(C)** The expression of anti-inflammatory cytokines including IL-10 **(D)** and TGF-β **(E)** from the serum was evaluated through ELISA. The bar shows the mean ± SEM of the levels of indicated proteins (sensitive patients n=4; resistant patients n=4). ns, non-significant.

exhibited an increased basal OCR and maximal respiratory capacity (evident after exposure to FCCP), indicating increased mitochondrial activity (Figure 4D). Electron microscopy also revealed that mitochondria were fused (Figure 4E) and had greater metabolic capacity in the resistant group (20).

Higher MCT1 and MCT2 expression was observed in tumor-infiltrating Tregs in resistant patients

The *in vitro* expression of LDH, MCT1, and MCT2 was upregulated in the iTregs of the resistant group but not the sensitive group. In resected tumor samples, we observed higher levels of MCT^+ cells by immunofluorescence staining (Figures 5A, B) and Western blot analysis (Figures 5C, D) in resistant than sensitive patients.

MCT1 and MCT2 was a poor prognosis marker of aggressive HCC

As lactate functions in cells in the presence of MCT, we further evaluated the role of lactate or MCT in the prognosis of HCC. We enrolled 43 patients who underwent HCC resection surgery at our center in 2017, who were then divide into high- and low-lactate groups according to Treg lactate content. Although lower-lactate patients had slightly lower OS rates than those with high-lactate patients, no statistically significant differences were observed in the OS and DFS between the groups (Figure 6A). Patients were also grouped according to their MCT1 and MCT2 expression levels in Tregs (Table 1). As expected, patients with higher MCT1 and MCT2 levels had poorer prognosis in terms of OS and DFS rates than those with lower levels (Figure 6B).

Co-treatment of MCT and PD-1 inhibitors reduced tumor growth by downregulating Tregs and upregulating anti-tumor cytokine expression

Lastly, we tested whether co-treatment with MCT inhibitor would promote the curative effects of anti-PD-1 therapy. The tumor volume in mice receiving the co-treatment was significantly smaller than that in mice injected with anti-PD-1 alone (Figure 7A). Hematoxylin and eosin staining revealed the presence of more tumor-infiltrating lymphocytes in mice

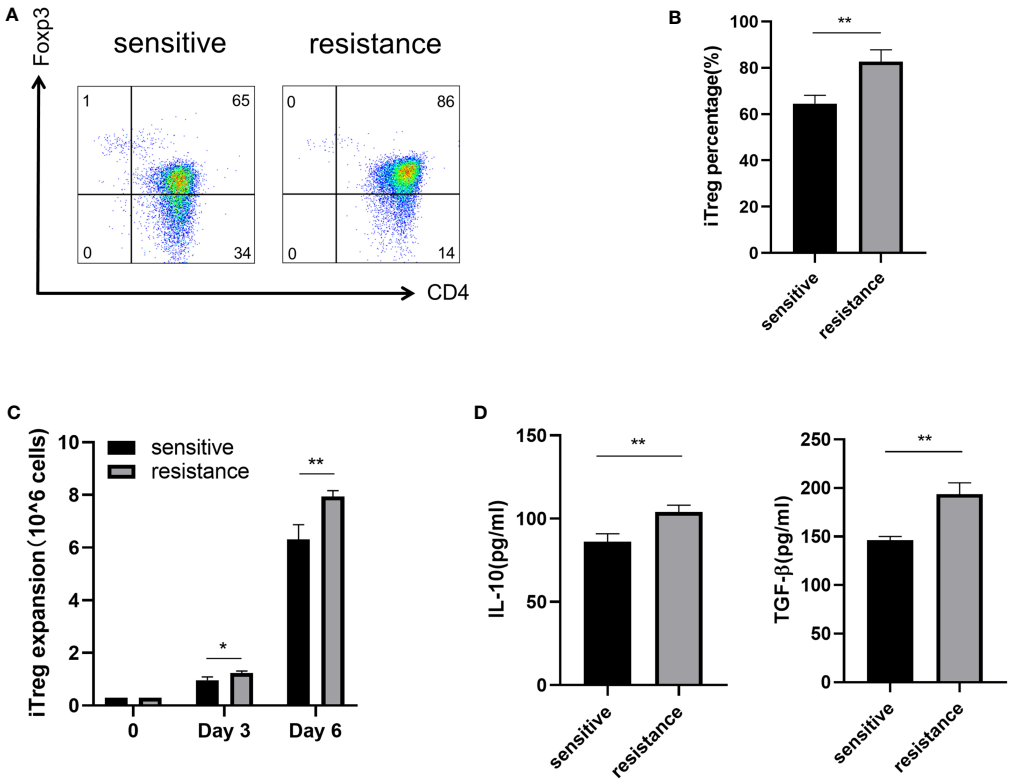

FIGURE 3
Induction of iTregs by lactate in the resistance group. Representative flow plot **(A)** for and the frequency **(B)** of Foxp3 expression in iTregs with the addition of lactate (10 mM) from sensitive and resistant patients. **(C)** The expansion ability of iTregs. **(D)** The expression of anti-inflammatory cytokines including IL-10 and TGF-β from the serum was evaluated through ELISA. The bar shows the mean ± SEM of the levels of indicated proteins. (sensitive patients n=4; resistant patients n=4). *p < 0.05; **p < 0.01.

injected with the MCT inhibitor. Moreover, the proportion of cells undergoing nuclear fragmentation and cell death increased. This indicated that the anti-tumor inflammatory response was much more intensive, thus inhibiting the growth of the tumor (Figure 7B). Western blot analysis confirmed that Foxp3 and TNF-α expression was markedly decreased and increased, respectively, in the co-treated group (Figures 7C, D).

Discussion

HCC is a lethal malignancy that originates from hepatocytes differentiation (21). In China, 466,000 new cases of HCC and 422,000 related deaths occur annually (22). In addition, only 10%–15% of patients meet the criteria for surgical excision due to disease severity (23). The current treatments for primary HCC are diverse and include radical surgical resection, multi-target antitumor drugs, combined chemotherapy, trans-arterial chemoembolization, radiofrequency ablation, and anhydrous alcohol injection (24). Due to heterogeneity between HCC cases and the complexity of immunoregulatory mechanisms in the TME, targeted combined immunotherapy is currently the most efficient clinical cancer treatment, other than surgery.

Among the possible targets for immunotherapies, PD-1/PD-L1—a major immune checkpoint (9, 16)—is widely used in clinical treatments in China. However, anti-PD-1 therapy is sometimes ineffective (25). Single-agent anti-PD-1 therapy using nivolumab achieved an objective response rate (ORR) of 20% (95% confidence interval [CI], 15%–26%) and a disease control rate (DCR) of 64% (95% CI, 58%–71%) (26). The CheckMate-459 trial, a multi-center phase III randomized trial, found that nivolumab was not a suitable alternative to sorafenib (27). Even with targeted combined immunotherapy, ORR and DCR were <50% (28).

In this study, we assessed the underlying mechanisms of resistance to anti-PD-1 therapy according to the generation, activation, and function of iTregs. Our cytometry data did not show a difference in the immune cell phenotypes of PBMCs. The Treg induction rate and suppressive functions were also similar in both sensitive and resistant groups *in vitro*. We hypothesized that the TME determines the different functions of Tregs and the prognosis of anti-PD-1 therapy. Concurrently, in the no-TME

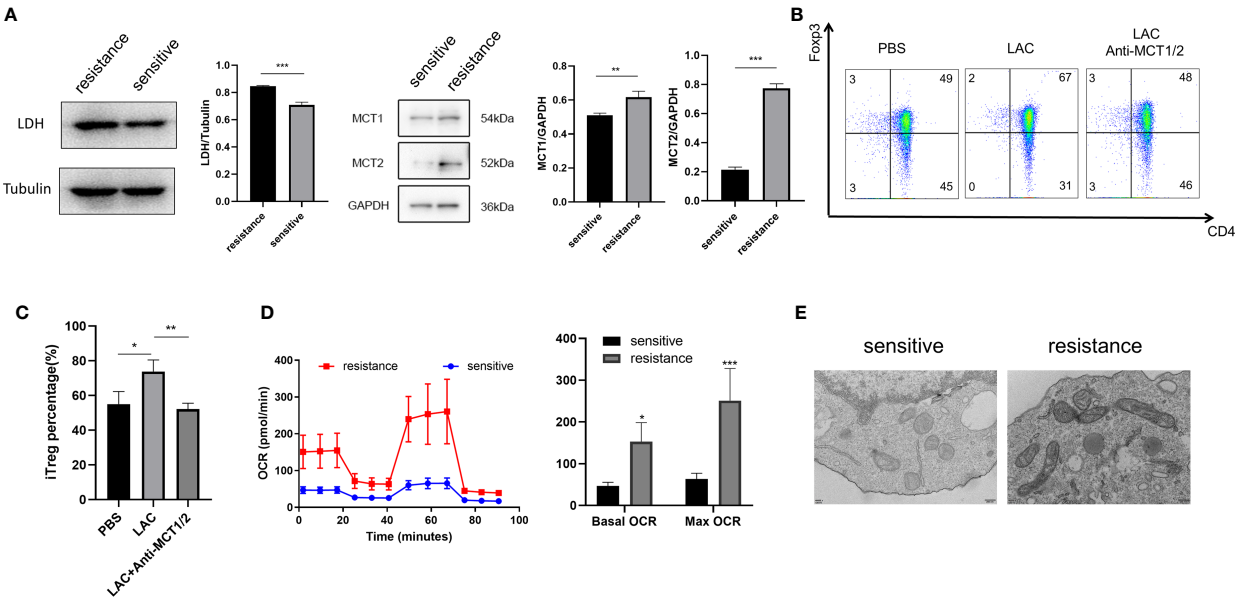

FIGURE 4
Foxp3 was upregulated in the iTregs of the resistant group in an MCT-dependent manner. **(A)** Representative blot plot for expression of LDH, MCT1, and MCT2 in both groups. Representative flow plot **(B)** for and the frequency **(C)** of Foxp3 expression in iTregs with the addition of lactate (10 mM) and inhibitors of MCT1 and MCT2 in resistance patients. **(D)** Oxygen consumption per unit time of two groups. **(E)** Representative plot for mitochondrial morphology observed through electron microscopy. The bar shows the mean ± SEM of the levels of indicated proteins. *p < 0.05; **p < 0.01; ***P<0.001.

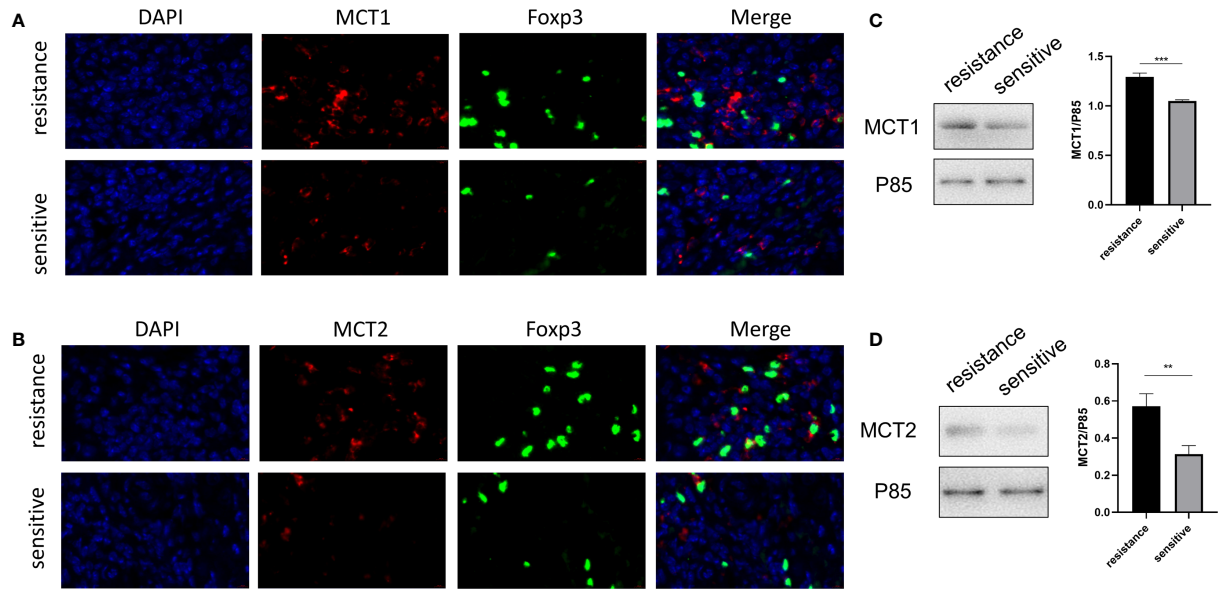

FIGURE 5
Higher MCT1 and MCT2 expression was observed in tumor-infiltrating Tregs in resistant patients. Representative plot for expression of MCT1 and MCT2 in Tregs in resected tumor samples from both groups under the confocal microscopy **(A, B)** and Western blot **(C, D)**. **p < 0.01; ***P<0.001.

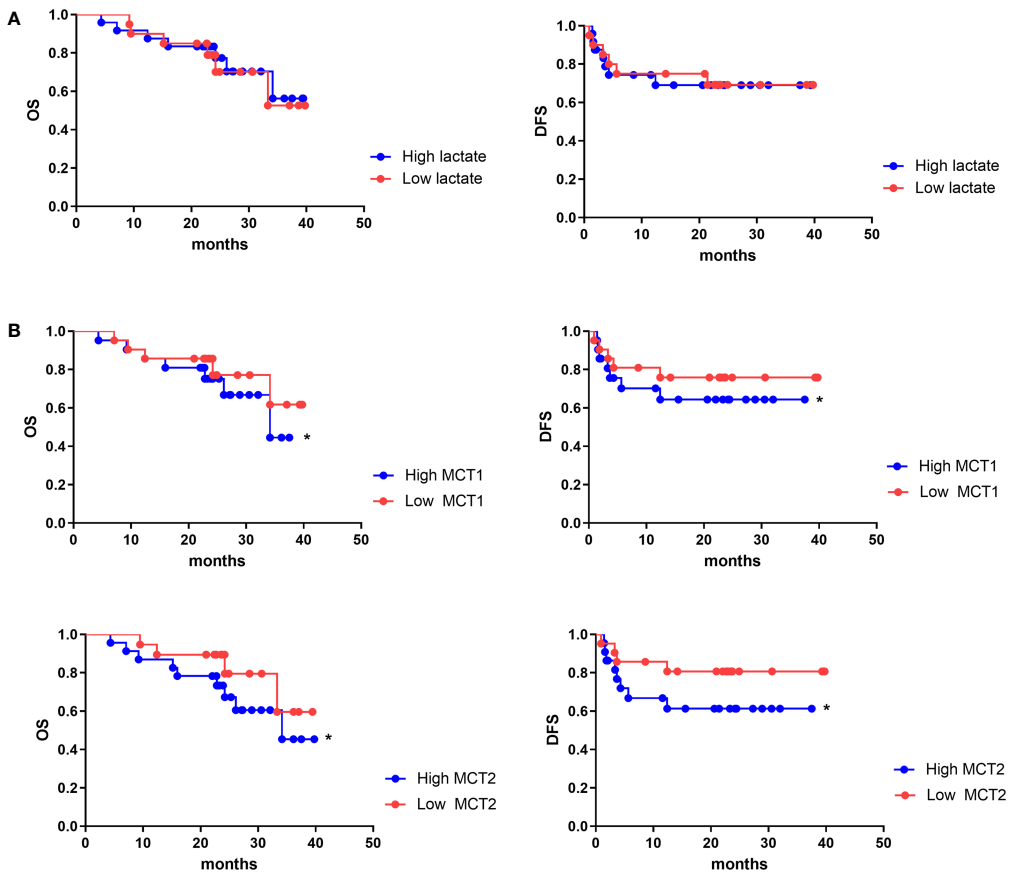

FIGURE 6
MCT1 and MCT2 was a poor prognosis marker of aggressive HCC. Kaplan–Meier survival analyses were conducted to assess the influence of lactate **(A)** and MCT1 and MCT2 **(B)** on overall survival and disease-free survival of HCC. *p < 0.05.

condition, Tregs did not show an obvious difference in function, which may be caused by differences in between the *in vitro* and *in vivo* environments.

A recent study showed that lactate, a metabolite produced by tumors, is critical for regulating the tumor environment, especially the expression of Tregs and macrophages (29). Lactate can regulate the number, induction, inhibitory function, and metabolic mechanisms of Tregs in the TME (17). Tregs acquire higher PD-1 expression than effector T cells in the TME, which is mediated by MCT1. PD-1 blockade activates PD-1-expressing Tregs, which leads to treatment failure (30). Therefore, we investigated whether iTreg induction varied between the two groups. Lactate induced more iTregs in the resistant than in the sensitive group. As MCT can promote lactate transport both inside and outside Tregs, we also evaluated MCT expression in iTregs and resected tumors, which showed that resistant patients had higher MCT expression than sensitive patients. High MCT expression and

TABLE 1 Patient characteristics.

	MCT1 high(n=20)	MCT1 low (n=21)
Gender(male/female, n)	17/3	17/4
Age(years, mean ± SD)	59.30 ± 10.70	57.48 ± 8.87
AFP(ng/ml, mean ± SD)	334.55 ± 453.50	223.00 ± 417.60
tumor size(cm, mean ± SD)	5.31 ± 2.44	6.00 ± 2.42
MVI [n(%)]	10(50.0)	11(52.4)
Liver function(Child score)	5.10 ± 0.30	5.19 ± 0.50

AFP, alpha-fetoprotein; MVI, microvascular invasion.

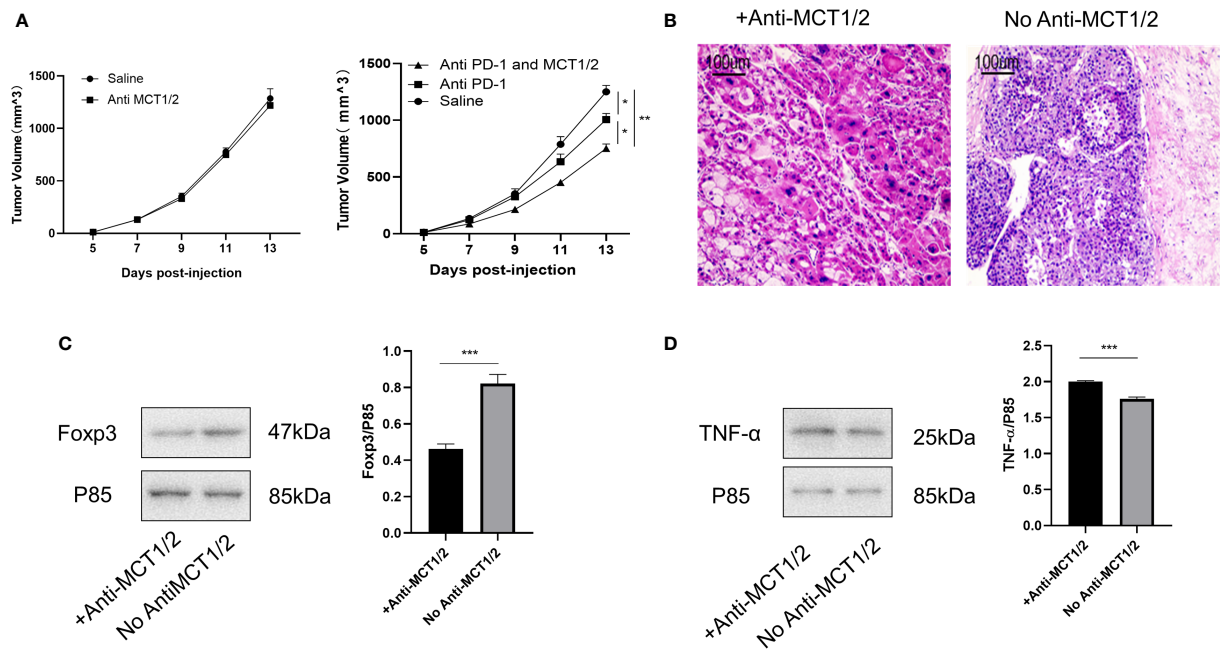

FIGURE 7
Co-treatment of MCT and PD-1 inhibitors reduced tumor growth by downregulating Tregs and upregulating anti-tumor cytokine expression. **(A)** Tumor growth in different groups post-injection (left Rag1$^{-/-}$ mice and right C57L/B6 mice). **(B)** HE staining of tumor from different groups. **(C, D)** Western blot for expression of Foxp3 and TNF-α in different groups. The result is representative of three independent experiments. Data were mean ± SD of three independent experiments (each group, n=3). *p < 0.05; **p < 0.01; ***P<0.001.

sensitivity to lactate can upregulate the function of Tregs in the TME. The blocking of MCT abolished Foxp3 upregulation by lactate in the resistant group. Finally, we demonstrated that co-treatment with an MCT neutralizer and anti-PD-1 was effective in murine subcutaneous tumor models. As MCT expression is important for Treg generation in the TME, further studies should be performed to analyze the underlying mechanism of T cells with both high and low expression.

In conclusion, we have shown that MCT and its downstream lactate signals in Tregs may result in resistance to anti-PD-1 therapy. Therefore, the expression of MCT in the iTregs from PBMCs or resected tumors can be used to predict prognosis before anti-PD-1 therapy. We acknowledged that our findings are based on a relatively small sample size; thus, future studies should consider larger multi-center cohorts. Our study provides insights into the modulation of immunosuppression in HCC and novel targets for the development of intuitive therapeutic strategies.

Data availability statement

The original contributions presented in the study are included in the article/supplementary material. Further inquiries can be directed to the corresponding authors.

Ethics statement

The animal study was reviewed and approved by the Institutional Animal Care and Research Advisory Committee of Nanjing Medical University. Written informed consent was obtained from the individual(s) for the publication of any potentially identifiable images or data included in this article.

Author contributions

JZ, YJ L, YY, and JG designed the experiments. JG and JZ provided the study materials or patients. QS, YL, BZ, ZX, XL, and XX performed the experiments and interpreted the data. QC, YP, ZD, and YW revised the manuscript. All authors read and approved the final manuscript.

Funding

This work was supported by the National Natural Science Foundation of China (81971504), Natural Science Foundation of Jiangsu (BK20201486), Post-Doctoral Special Foundation of China (2020M670065ZX), Post-Doctoral Foundation of Jiangsu Province (2020Z021), Medical and Health Science and Technology Program of Zhejiang Province (2021KY1036), Changzhou Society

Development Funding (CE20205038), and the lifting Project of 2021 Young Scientific and Technological Talents in Changzhou.

Conflict of interest

The authors declare that the research was conducted in the absence of any commercial or financial relationships that could be construed as a potential conflict of interest.

Publisher's note

References

1. Llovet JM, Montal R, Sia D, Finn RS. Molecular therapies and precision medicine for hepatocellular carcinoma. *Nat Rev Clin Oncol* (2018) 15(10):599–616. doi: 10.1038/s41571-018-0073-4

2. Ruf B, Heinrich B, Greten TF. Immunobiology and immunotherapy of HCC: spotlight on innate and innate-like immune cells. *Cell Mol Immunol* (2021) 18 (1):112–27. doi: 10.1038/s41423-020-00572-w

3. Kalbasi A, Ribas A. Tumour-intrinsic resistance to immune checkpoint blockade. *Nat Rev Immunol* (2020) 20(1):25–39. doi: 10.1038/s41577-019-0218-4

4. Wing JB, Tanaka A, Sakaguchi S. Human FOXP3(+) regulatory T cell heterogeneity and function in autoimmunity and cancer. *Immunity* (2019) 50 (2):302–16. doi: 10.1016/j.immuni.2019.01.020

5. Togashi Y, Shitara K, Nishikawa H. Regulatory T cells in cancer immunosuppression - implications for anticancer therapy. *Nat Rev Clin Oncol* (2019) 16(6):356–71. doi: 10.1038/s41571-019-0175-7

6. Pacella I, Piconese S. Immunometabolic checkpoints of treg dynamics: Adaptation to microenvironmental opportunities and challenges. *Front Immunol* (2019) 10:1889. doi: 10.3389/fimmu.2019.01889

7. Tanaka A, Sakaguchi S. Regulatory T cells in cancer immunotherapy. *Cell Res* (2017) 27(1):109–18. doi: 10.1038/cr.2016.151

8. Whiteside TL. FOXP3+ treg as a therapeutic target for promoting anti-tumor immunity. *Expert Opin Ther Targets* (2018) 22(4):353–63. doi: 10.1080/14728222.2018.1451514

9. Kamada T, Togashi Y, Tay C, Ha D, Sasaki A, Nakamura Y, et al. PD-1(+) regulatory T cells amplified by PD-1 blockade promote hyperprogression of cancer. *Proc Natl Acad Sci U.S.A.* (2019) 116(20):9999–10008. doi: 10.1073/pnas.1822001116

10. Van Damme H, Dombrecht B, Kiss M, Roose H, Allen E, Van Overmeire E, et al. Therapeutic depletion of CCR8(+) tumor-infiltrating regulatory T cells elicits antitumor immunity and synergizes with anti-PD-1 therapy. *J Immunother Cancer* (2021) 9(2):e001749. doi: 10.1136/jitc-2020-001749

11. Garcia-Canaveras JC, Chen L, Rabinowitz JD. The tumor metabolic microenvironment: Lessons from lactate. *Cancer Res* (2019) 79(13):3155–62. doi: 10.1158/0008-5472.CAN-18-3726

12. Wang N, Jiang X, Zhang S, Zhu A, Yuan Y, Xu H, et al. Structural basis of human monocarboxylate transporter 1 inhibition by anti-cancer drug candidates. *Cell* (2021) 184(2):370–383 e313. doi: 10.1016/j.cell.2020.11.043

13. Brustle A, Brenner D, Knobbe-Thomsen CB, Cox M, Lang PA, Lang KS, et al. MALT1 is an intrinsic regulator of regulatory T cells. *Cell Death Differ* (2017) 24(7):1214–23. doi: 10.1038/cdd.2015.104

14. Siddiqui I, Schaeuble K, Chennupati V, Fuertes Marraco SA, Calderon-Copete S, Pais Ferreira D, et al. Intratumoral Tcf1(+)PD-1(+)CD8(+) T cells with stem-like properties promote tumor control in response to vaccination and checkpoint blockade immunotherapy. *Immunity* (2019) 50(1):195–211 e110. doi: 10.1016/j.immuni.2018.12.021

15. Kumagai S, Togashi Y, Kamada T, Sugiyama E, Nishinakamura H, Takeuchi Y, et al. The PD-1 expression balance between effector and regulatory T cells predicts the clinical efficacy of PD-1 blockade therapies. *Nat Immunol* (2020) 21 (11):1346–58. doi: 10.1038/s41590-020-0769-3

16. Angelin A, Gil-de-Gomez L, Dahiya S, Jiao J, Guo L, Levine MH, et al. Foxp3 reprograms T cell metabolism to function in low-glucose, high-lactate environments. *Cell Metab* (2017) 25(6):1282–1293 e1287. doi: 10.1016/j.cmet.2016.12.018

17. Gu J, Zhou J, Chen Q, Xu X, Gao J, Li X, et al. Tumor metabolite lactate promotes tumorigenesis by modulating MOESIN lactylation and enhancing TGF-beta signaling in regulatory T cells. *Cell Rep* (2022) 39(12):110986. doi: 10.1016/j.celrep.2022.110986

18. Faubert B, Li KY, Cai L, Hensley CT, Kim J, Zacharias LG, et al. Lactate metabolism in human lung tumors. *Cell* (2017) 171(2):358–371 e359. doi: 10.1016/j.cell.2017.09.019

19. Latif A, Chadwick AL, Kitson SJ, Gregson HJ, Sivalingam VN, Bolton J, et al. Monocarboxylate transporter 1 (MCT1) is an independent prognostic biomarker in endometrial cancer. *BMC Clin Pathol* (2017) 17:27. doi: 10.1186/s12907-017-0067-7

20. Buck MD, O'Sullivan D, Klein Geltink RI, Curtis JD, Chang CH, Sanin DE, et al. Mitochondrial dynamics controls T cell fate through metabolic programming. *Cell* (2016) 166(1):63–76. doi: 10.1016/j.cell.2016.05.035

21. Mody K, Abou-Alfa GK. Systemic therapy for advanced hepatocellular carcinoma in an evolving landscape. *Curr Treat Options Oncol* (2019) 20(2):3. doi: 10.1007/s11864-019-0601-1

22. Torre LA, Bray F, Siegel RL, Ferlay J, Lortet-Tieulent J, Jemal A. Global cancer statistic. *CA Cancer J Clin* (2015) 65(2):87–108. doi: 10.3322/caac.21262

23. Liu W, Li X, Zheng W, Yao R, Zheng J. Preoperative evaluation of the degree of liver fibrosis based on matter-element analysis using serological indicators in patients with hepatocellular carcinoma. *Biosci Trends* (2019) 13(1):70–6. doi: 10.5582/bst.2018.01311

24. Faivre S, Rimassa L, Finn RS. Molecular therapies for HCC: Looking outside the box. *J Hepatol* (2020) 72(2):342–52. doi: 10.1016/j.jhep.2019.09.010

25. Dixon ML, Luo L, Ghosh S, Grimes JM, Leavenworth JD, Leavenworth JW. Remodeling of the tumor microenvironment *via* disrupting Blimp1(+) effector treg activity augments response to anti-PD-1 blockade. *Mol Cancer* (2021) 20(1):150. doi: 10.1186/s12943-021-01450-3

26. El-Khoueiry AB, Sangro B, Yau T, Crocenzi TS, Kudo M, Hsu C, et al. Nivolumab in patients with advanced hepatocellular carcinoma (CheckMate 040): an open-label, non-comparative, phase 1/2 dose escalation and expansion trial. *Lancet* (2017) 389(10088):2492–502. doi: 10.1016/S0140-6736(17)31046-2

27. Yau T, Park JW, Finn RS, Cheng AL, Mathurin P, Edeline J, et al. CheckMate 459: A randomized, multi-center phase III study of nivolumab (NIVO) vs sorafenib (SOR) as first-line (1L) treatment in patients (pts) with advanced hepatocellular carcinoma (aHCC). *Ann Oncol* (2019) 30:v874–5. doi: 10.1093/annonc/mdz394.029

28. D'Alessio A, Rimassa L, Cortellini A, Pinato DJ. PD-1 blockade for hepatocellular carcinoma: Current research and future prospects. *J Hepatocell Carcinoma* (2021) 8:887–97. doi: 10.2147/JHC.S284440

29. Kes MMG, Van den Bossche J, Griffioen AW, Huijbers EJM. Oncometabolites lactate and succinate drive pro-angiogenic macrophage response in tumors. *Biochim Biophys Acta Rev Cancer* (2020) 1874(2):188427. doi: 10.1016/j.bbcan.2020.188427

30. Kumagai S, Koyama S, Itahashi K, Tanegashima T, Lin YT, Togashi Y, et al. Lactic acid promotes PD-1 expression in regulatory T cells in highly glycolytic tumor microenvironments. *Cancer Cell* (2022) 40(2):201–218 e209. doi: 10.1016/j.ccell.2022.01.001

frontiers | Frontiers in Oncology

TYPE Original Research
PUBLISHED 12 August 2022
DOI 10.3389/fonc.2022.985484

OPEN ACCESS

EDITED BY
Liangrong Shi,
Xiangya Hospital, Central South University, China

REVIEWED BY
Yi Wang,
Sichuan Academy of Medical Sciences and Sichuan Provincial People's Hospital, China
Yaru Xu,
University of Texas Southwestern Medical Center, United States

*CORRESPONDENCE
Lianjun Ma
horsejlm@jlu.edu.cn

†These authors have contributed equally to this work

SPECIALTY SECTION
This article was submitted to Molecular and Cellular Oncology, a section of the journal Frontiers in Oncology

RECEIVED 04 July 2022
ACCEPTED 18 July 2022
PUBLISHED 12 August 2022

CITATION
Liu Y, Liu Y, Ye S, Feng H and Ma L (2022) Development and validation of cuproptosis-related gene signature in the prognostic prediction of liver cancer. *Front. Oncol.* 12:985484. doi: 10.3389/fonc.2022.985484

Development and validation of cuproptosis-related gene signature in the prognostic prediction of liver cancer

Yanqing Liu[1,2†], Yang Liu[1†], Shujun Ye[1], Huijin Feng[2] and Lianjun Ma[1*]

[1]Endoscopy Center, China-Japan Union Hospital of Jilin University, Changchun, China, [2]Herbert Irving Comprehensive Cancer Center, Columbia University, New York, NY, United States

Liver cancer is a generic term referring to several cancer types arising from the liver. Every year, liver cancer causes lots of deaths and other burdens to the people all over the world. Though the techniques in the diagnosis and therapy of liver cancer have undergone significant advances, the current status of treating liver cancer is not satisfactory enough. The improvement of techniques for the prognosis of liver cancer patients will be a great supplement for the treatment of liver cancer. Cuproptosis is a newly identified regulatory cell death type, which may have a close connection to liver cancer pathology. Here, we developed a prognostic model for liver cancer based on the cuproptosis-related mRNAs and lncRNAs. This model can not only effectively predict the potential survival of liver cancer patients, but also be applied to evaluate the infiltration of immune cell, tumor mutation burden, and sensitivity to anti-tumor drugs in liver cancer. In addition, this model has been successfully validated in lots of liver cancer patients' data. In summary, we wish this model can become a helpful tool for clinical use in the therapy of liver cancer.

KEYWORDS

liver cancer, cuproptosis, lncRNA, mRNA, prognostic model

Introduction

Liver cancer is one of the major cancer types and among the most malignant liver diseases around the world (1–5). Liver cancer comprises several sub-types, including hepatocellular carcinoma (the most common type of liver cancer), cholangiocarcinoma, hepatoblastoma, and angiosarcoma (1). Liver cancer causes great healthy and economic burdens to the people and the society of both developed and underdeveloped area. According to the estimation of epidemiologists, there were about 905,677 new cases of liver cancer and 830,180 new deaths caused by it (2). In the US, although liver cancer is

not among the top 10 cancer types regarding the estimated new cases in 2022, it may cause more than 30,000 deaths in the same year, which ranks 5th in all the cancer types (6). Albeit the dramatic development in the diagnosis and treatment of liver cancer in the past decades, its mortality increases rapidly, partially due to the change of environment, life style, and dietary habit (1, 7, 8). For scientific and clinical researchers, elucidating the underlying mechanism for the initiation and development of liver cancer is a crucial and long-term task. In the meantime, development of novel prognostic biomarker for liver cancer patients will greatly benefit their treatments (1, 9).

For the somatic cells in mammalian life, the equilibrium between cell death and proliferation is of vital importance. To achieve a concerted life circle, human cells "master" multiple regulated cell death (RCD) modalities (including apoptosis, ferroptosis, necroptosis, and pyroptosis) evolutionally (10). During normal development, these RCDs cooperate with each other to orchestrate a suitable rate of cell turnover in different organs. In addition, these RCDs also function in dealing with various inner or environmental stresses. From a clinical perspective, these RCDs have been demonstrated to be involved with a wide range of disease processes, including organ injury, immune system dysfunction, neurodegenerative disorder, and particularly tumor (10). Identifying novel RCD type will not only deepen our understanding of the human cell, but also create new therapeutic opportunity for lots of diseases, including liver cancer. Cuproptosis is a quite recently discovered RCD mode, which is characterized by unique features different from other RCDs mentioned above (11). Cuproptosis is caused by copper-induced aggregation of lipoylated proteins in TCA cycle. The data in the seminal paper suggested that cuproptosis may participate in the modulation of various diseases, including cancer. Whether cuproptosis is associated with liver cancer has not been investigated. However, it is of evident significance to explore the potential link between liver cancer and cuproptosis (and essential genes underlying it).

Long non-coding RNA (lncRNA) is one of the research hotspots in these years (12). This is a family of RNAs with diverse lengths, localizations, structures, and functions. The dysregulation of lncRNAs have been demonstrated to be involved in the progression of various tumor types, including liver cancer (13). These lncRNAs can not only be therapeutic targets in liver cancer treatment, but may also constitute unique expression profiles to indicate distinct characteristics of liver cancer, including the malignant stage, the sensitivity to therapeutics, and the prognosis of patients (14). Particularly, differential lncRNA expression profiles can be established based on specific cellular processes. Constructing a solid lncRNA signature in the context of a crucial activity in liver cancer cell will be of great use for predicting the development of liver cancer in patients.

In this study, we leveraged our current knowledge about liver cancer, cuproptosis, and lncRNA to construct a novel prognostic model based on cuproptosis-related lncRNAs and mRNAs in liver cancer. This model fits well with diverse pathologic parameters of liver cancer. Moreover, this model has been successfully validated by using a batch of patients' data. We believe that, this model can be beneficial to the prognosis of liver cancer patients.

Materials and methods

Microarray data

We obtained the gene expression profile, survival information and clinical characteristics of liver cancer patients from TCGA database (https://cancergenome.nih.gov/). A total of 424 samples were used in this study, including 374 liver cancer samples and 50 non-tumor tissues. The mRNAs related to cuproptosis obtained from previous literatures are summarized in Table S1 (11, 15–19). Pearson correlation analysis was used to identify cuproptosis-related lncRNAs, and the co-expression networks of lncRNAs-mRNAs were established and visualized with R package "ggalluvial".

Construction of cuproptosis-related prognostic signature for liver cancer

Univariate Cox regression analysis was used to screen cuproptosis-related mRNAs and lncRNAs that were closely associated with survival. Subsequently, mRNAs and lncRNAs with statistically significant difference ($p<0.01$) in univariate Cox regression analysis were selected for multivariate Cox regression analysis to determine the potential optimal cuproptosis-related prognostic genes. Based on the prognostic potential and the regression coefficient, the 9-gene signature was finally developed. Next, risk score is calculated according to the formula: Risk score = (exprgene1 × Coefgene1) + (exprgene2 × Coefgene2) + … + (exprgenen × Coefgenen).

Evaluation of the 9-gene signature including 3 mRNAs and 6 lncRNAs

Median of risk score is used to divide patients into two groups (high and low risk, respectively). Kaplan-Meier survival analysis was performed with "survival" and "survminer" R software packages. ROC curve was performed to calculate the area under the curve (AUC) to evaluate the diagnostic value of the 9-gene signature. Then, C-index curve were used to estimate the model accuracy.

Construction of nomogram

We used the clinical features (including age, gender, grade and stage) to establish nomograms for predicting survival in patients with liver cancer. In addition, to assess the consistency between predicted and actual survival, calibration curves were drawn.

Correlation analysis between distinct groups and clinical characteristics

To further explore the correlation between risk scores and clinical characteristics, the distribution of clinicopathological features in differential groups was displayed by R software package "pheatmap".

Validation of the model in GEO dataset

1. Spearman correlation analysis was used to screened mRNAs correlated with 9 signature genes (coefficients > 0.40, $p < 0.001$).
2. Differential expression analysis was performed to classify mRNAs into gene up-regulated cluster A and down-regulated cluster B.
3. The Gene set variation analysis (GSVA) was employed to calculate enrichment score of cluster A and cluster B. Then, we calculated RS score equivalent to subtraction of the enrichment score of cluster B from the enrichment score of cluster A.
4. After calculating the RS scores in each GEO sample, Kaplan-Meier curve was used to evaluate the difference of OS between high RS score group and low RS score group.

Enrichment functional analysis

We first determined the expression of a set of differentially expressed genes (DEGs) containing mRNAs and lncRNAs between the high-risk group and the low-risk group. The cutoff criteria were FDR < 0.05 and |logFC| > 1. Then go function enrichment analysis and KEGG pathway analysis were performed for DEGs.

Immune-related functional analysis

To explore the relationship between risk scores and infiltration of immune cell, we quantified the abundance of immune cells in the two risk groups using algorithms such as TIMER, CIBERSORT, and others. In addition, the ssGSEA algorithm was applied to assess the immune-related functions in two risk groups. Besides, referring to existing studies, the expression level of immune checkpoint related genes may be correlated to the clinical efficacy of immune checkpoint inhibitor blockade therapy (20). Therefore, the correlation between risk scores and immune checkpoints was also studied.

Relationship between hypoxia-related genes and risk score

Hypoxia can regulate TCA cycle and may involve in cuproptosis initiation (21). Therefore, we studied the correlation between expression of hypoxia related genes and risk score.

Analysis of tumor mutation burden and drug sensitivity

According to the somatic mutation data of each tumor, TMB was calculated as the mutation bases per million bases. The maftools package was used to aggregate and visualize mutation data and evaluate the relationship between risk score and Tumor mutation burden (TMB). Tumor immune dysfunction and Exclusion (TIDE) algorithm was used to predict the immune response. Next, the "pRRophetic" software package of R software was used to evaluate the sensitivity of chemotherapy drugs with the half maximum inhibitory concentration (IC50).

Results

Identification of cuproptosis-related LncRNAs and construction of the 9-gene signature

The flowchart of the research is shown in Figure 1. Firstly, 980 cuproptosis-related lncRNAs were identified from 16,773 lncRNAs based on the filtering criteria of a correlation coefficient <0.4 and $p < 0.001$. The co-expression relationship between cuproptosis-related lncRNAs and cuproptosis-related mRNAs was shown using Sankey diagram (Figure 2A). In the TCGA set, univariate Cox regression analysis was used to screen 249 prognostic genes including mRNAs and lncRNAs associated with cuproptosis from the 999 cuproptosis-related genes. Performing Lasso Cox regression analysis and multivariate Cox regression analysis on the TCGA set, we identified robust 9 cuproptosis-related genes containing 3 mRNAs and 6 lncRNAs. The correlation between 6 screened lncRNAs and cuproptosis-related genes was shown in the correlation heatmap and network diagram (Figures 2B, C). As a

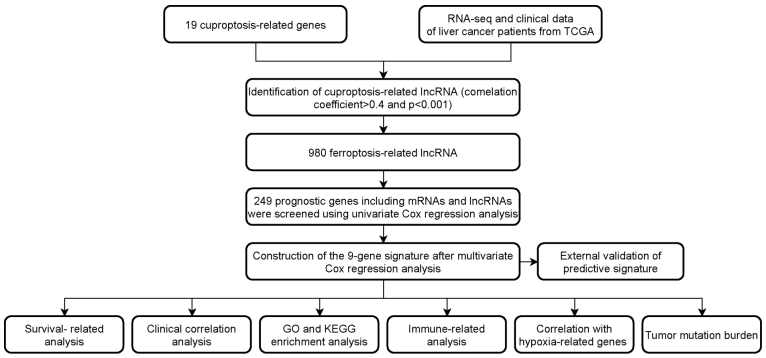

FIGURE 1
Workflow of the study design.

result, the risk score model was constructed as follows: risk score = (-0.1369×ATP7A expression) + (0.0174×DLAT expression) + (-0.0124×GLS expression) + (0.2669×POLH-AS1 expression) + (0.0868×AL117336.2 expression) + (0.3621×MKLN1-AS expression) + (0.2207×AC005479.2 expression) + (0.1527×AL928654.1 expression) + (0.1200×AL031985.3 expression).

Evaluation of the 9-gene signature

Patients in the TCGA cohort were divided into low-risk and high-risk subgroups according to the median risk score. The overall survival rate (OS) of low-risk group was significantly lower than that of high-risk group (Figure 3A). In order to study the prediction accuracy of this 9-gene signature, we conducted a time-dependent ROC analysis (Figures 3B, C). Besides, compared with other variables, the risk score (AUC = 0.791) was a better predictor than other clinical traits, such as age (AUC = 0.506), gender (AUC = 0.507), grade (AUC = 0.477) and stage (AUC = 0.685). The area under the ROC curve (AUC) of OS was 0.791 at 1 year, 0.732 at 2 years and 0.729 at 3 years, indicating the 9-gene signature had a good prognostic prediction efficacy. Next, we constructed a C-Index curve of risk score and clinical traits (age, gender, and stage), and the results showed the consistency of risk score was higher than that of the clinical traits (Figure 3D). In addition, the distribution of patient risk score, survival status and the 9 genes expression profiles were shown in Figures 3E–G.

Construction and validation of the nomogram

A nomograph model including risk score, age, gender, grade, and stage was constructed to predict the 1-, 3- and 5-years OS of liver cancer patients by calculating the nomograph score based on the point scale (Figure 4A). The calibration curve of nomogram showed that there was a good consistency between the predicted results and the observed results (Figure 4B).

The correlation between risk score and different clinicopathological factors

In order to clarify the clinical significance of risk score, the correlation between risk score and major clinicopathological

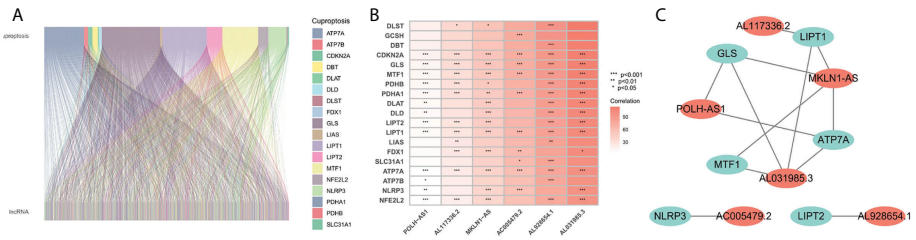

FIGURE 2
Screening of prognosis-related genes. **(A)** Sankey diagram of the associations between between cuproptosis-related lncRNAs and mRNAs. **(B)** The correlation heatmap of 6 screened lncRNAs and cuproptosis-related genes. **(C)** The network diagram of 6 screened lncRNAs and cuproptosis-related genes.

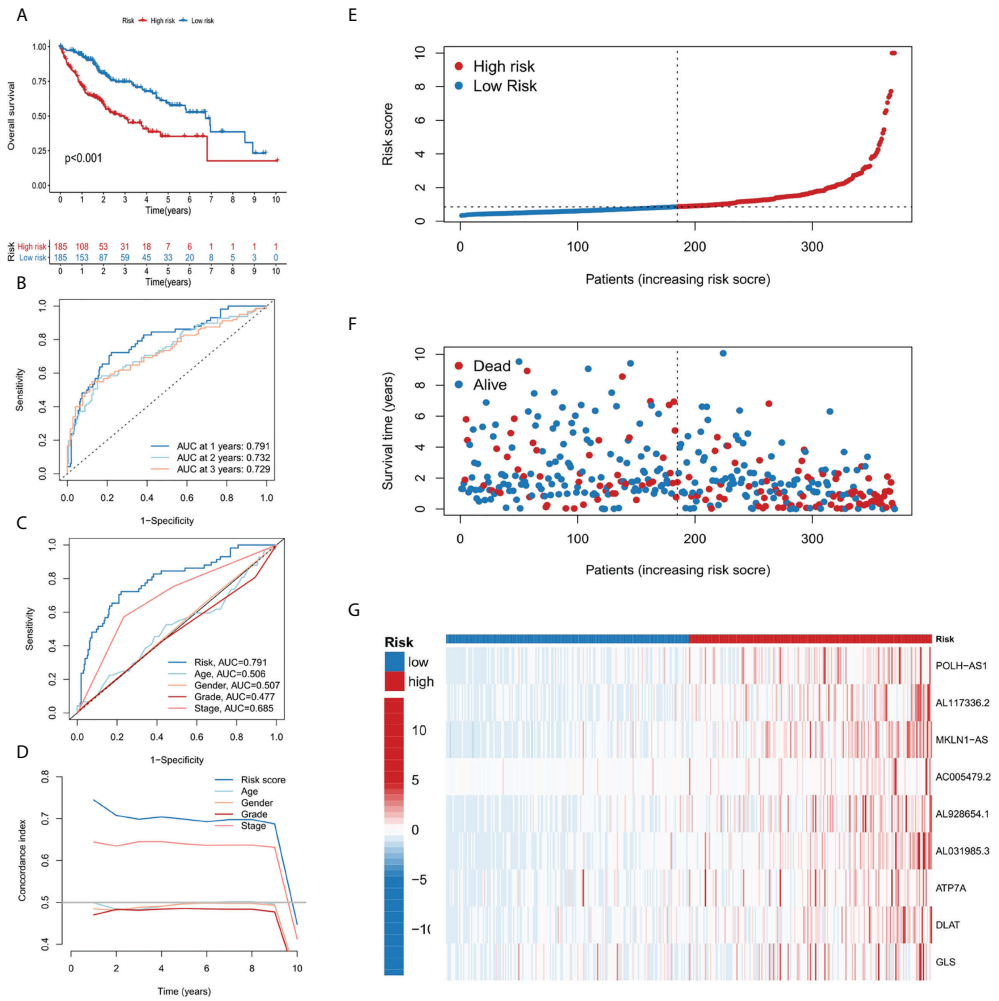

FIGURE 3
Establishment and evaluation of the 9-gene signature. **(A)** Kaplan-Meier survival analysis of liver cancer patients in the high-risk and low-risk groups. **(B)** Time dependent ROC curves of overall survival at 1, 2- and 3- years. **(C)** ROC curves of risk score for clinical features in liver cancer patients. **(D)** The C-index curve analyzes the consistency index of risk score. **(E–G)** The distribution of risk score, survival status, and 9-gene expression profiles for each liver cancer patient.

variables such as gender, age, grade, and pathological stage were analyzed. As showcased in Figure 4C, the clinical grade and T stage of liver cancer patients in the high-risk group was later than that in the low-risk group, suggesting a worse prognosis than the low-risk group.

Validation of cuproptosis-related risk model in GEO dataset

Since there are no corresponding lncRNAs in other data sets, it is difficult to verify the performance of the risk model. Therefore, we calculated the RS scores in TCGA and GSE144269. There was a strongly correlation between risk score and RS score in TCGA dataset (p-value = $1.016 * 10^{-5}$), indicating that the RS score can be used as an alternative scoring model for risk score. The result of Kaplan–Meier (KM) survival analysis showed the 9-gene signature exhibited good prognostic performance (Figure 4D).

Functional enrichment analysis

We performed GO (Figure 4E) and KEGG (Figure 4F) pathway analysis on genes of differentially expressed lncRNAs and mRNAs in two risk groups. In BP (biological processes) category, cell division related activity including nuclear division

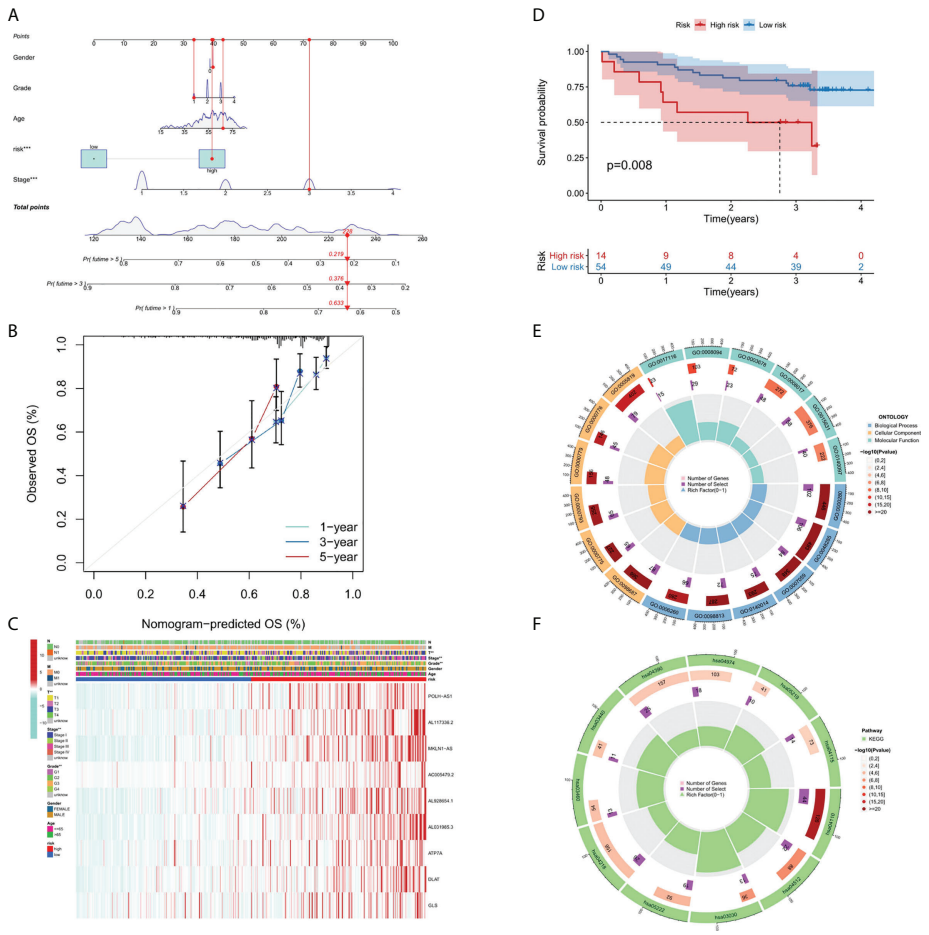

FIGURE 4
Nomogram, calibration curves and functional enrichment analysis. **(A)** Nomograms predicting 1-year, 3-year and 5-year OS for patients with liver cancer. **(B)** Nomogram model calibration curve. **(C)** Heatmap displaying expression profile of the 9 genes and correlation between clinical features and risk score. **(D)** Results of Kaplan-Meier analysis for the different RS score groups in GEO dataset. **(E)** Results of GO enrichment analyses. **(F)** Results of KEGG enrichment analyses.

(GO:0000280), organelle fission (GO:0048285) and chromosome segregation (GO:0007059) were significantly enriched. In CC (cellular components) category, the differentially expressed genes were involved in chromosomal region (GO:0098687), centromeric region (GO:0000775), condensed chromosome (GO:0000793), kinetochore (GO:0000776) and spindle (GO:0005819). In MF (molecular functions) category, DEGs were enriched in enriched in DNA-related activities, such as single-stranded DNA helicase activity (GO:0017116), ATP-dependent activity (GO:0008094) and DNA helicase activity (GO:0003678). KEGG pathway analysis showed that differentially expressed genes were mainly enriched in Cell cycle (hsa04110), DNA replication (hsa03030), and p53 signaling pathway (hsa04115), etc. In summary, the results of the enrichment analysis showed the 9-gene signature was closely associated with cell proliferation.

Immune-related functional analysis

Immune cell infiltration is a crucial component of tumor microenvironment, which is strongly related to tumor behavior and patient prognosis (22, 23). Several algorithms (TIMER, XCELL, QUANTISEQ, MCPCOUNTER, CIBERSORT, CIBERSORT-ABS and EPIC) were used to study the correlation between the infiltration of various immune cells and risk score and the results were shown in Figure 5A. In the ssGSEA, the immune status of low-risk group was relatively higher than that of high-risk group (Figure 5B). In addition, we found that the high risk group showed a higher expression level of immune checkpoint genes, thus indicating a better response to immunotherapy (Figure 5C). In conclusion, these results suggested that the 9-gene signature was related to immune cell infiltration to some extent.

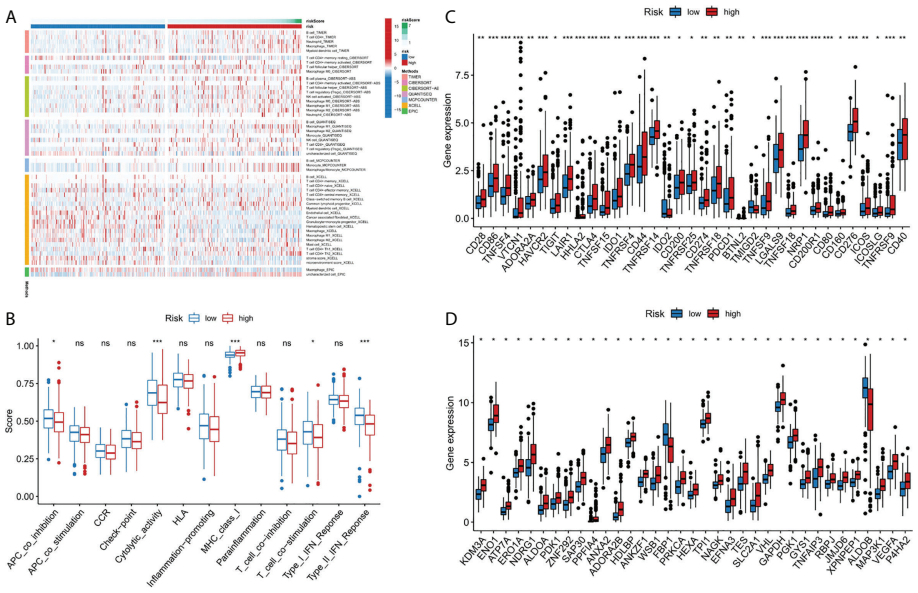

FIGURE 5
Immune-related functional analysis. **(A)** The landscape of immune infiltration in two risk groups for liver cancer patients. **(B)** Boxplot visualizing differentially immune functions. "ns" stands for not significant. **(C)** Comparisons of immune checkpoints between the two risk groups in liver cancer patients. *p < 0.05; **p < 0.01; ***p < 0.001. **(D)** Comparison of the expression of hypoxia-associated genes between the two risk groups in liver cancer patients. *p < 0.001. ns, not significant.

Relationship between hypoxia-related gene and risk score

Since there may be a close relationship between hypoxia and cuproptosis, we studied the expression of hypoxia related genes in the two risk groups. The majority of the hypoxia-related genes, such as LXN, HAS1, AKAP12, and ETS1, were significant upregulated in the high risk group than in the low risk group ($p<10^{-10}$) (Figure 5D). Based on the above results, we considered there were relations between cuproptosis and hypoxia in liver cancer, and specific clinical trials are needed, to further test this hypothesis.

Analysis of tumor mutation burden and drug sensitivity

The somatic mutation data of liver cancer patients were downloaded from the TCGA database and visualized using the "maftools" R software package. The results showed the mutation frequency in high-risk group was higher than that in low-risk group (77.35% vs. 68.89%), and in high risk group, mutation rate of TP53 was dramatically higher than that in low risk group (36% vs 16%) (Figures 6A, B). In addition, we studied the difference of tumor mutation burden between high-risk group and low-risk group, and the result showed the high risk score group had significant higher tumor mutation burden than the low risk group ($p<0.05$) (Figure 6C). As shown in the Figure 6D, the high TMB group had a better prognosis than low TMB group. Then, we further combined risk score and TMB to evaluate the prognosis of liver cancer patients, and we found the overall survival rate of low TMB and low-risk group was the best, and that of high TMB and high-risk group was the worst (Figure 6E). In addition, the sensitivity difference of immunotherapy between high-risk group and low-risk group was further studied based on TIDE algorithm. We found that the TIDE level was higher in the low-risk group than in the high-risk group, indicating that patients in the high-risk group had a lower possibility of immune escape, and better immunotherapy (Figure 6F). Finally, we used the R software package pRRophetic to analyze the half maximum inhibitory concentration (IC50) of some chemotherapeutic drugs commonly in two risk groups. AICAR (Figure 6G) and AMG.706 (Figure 6H) were more effective in the low-risk group, while AG.014699 (Figure 6I) and A.443654 (Figure 6J) were more efficacious in the high-risk group ($p<10^{-11}$).

At last, we attempted to compare our 9-gene signature with other previously published cuproptosis-related prognostic models in liver cancer, but there is rare paper in this field. Our model may initiate research in this field.

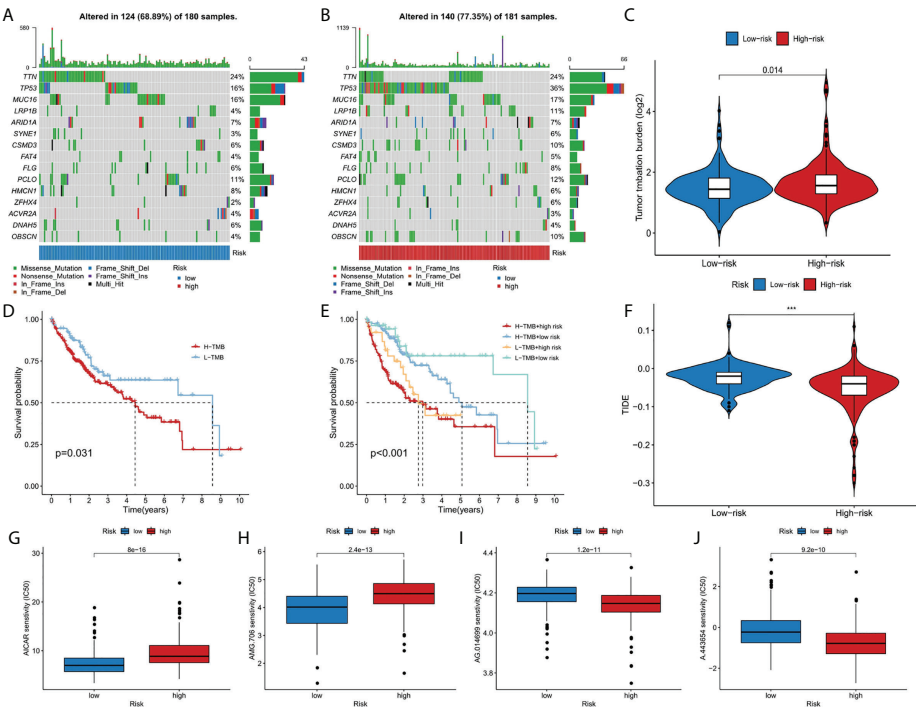

FIGURE 6
The relationship between TMB and the 9-gene signature. **(A, B)** The oncoplots of the mutation genes in liver cancer patients for the high-risk and low-risk groups. **(C)** Higher TMB levels correlated with high-risk group. **(D)** Higher TMB level demonstrated poorer OS. **(E)** Kaplan-Meier curves for patients by both risk score and TMB. **(F)** Higher TIDE levels correlated with low-risk group. **(G-J)** Drug sensitivity analysis. ***p < 0.001.

Discussion

Copper is an essential mineral for human health (24). The fact that dysregulation of copper level will cause damage to the normal cell life has been known for a long time. The discovery of cuproptosis makes an interesting and important explanation for this phenomenon (25). Although the field of cuproptosis is just in its infancy, it is reasonable to speculate that this cell death mode has tight correlation with human diseases, including liver cancer. There are two basic elements for the initiation of cuproptosis: copper and lipoylated protein. About the first element, liver is the central organ for the metabolism of copper (26, 27). For the lipoylated proteins, most of them function in the TCA cycle in the mitochondrion. To avoid cuproptosis, these two elements must be maintained in check. In liver cancer cell, dysregulation of the normal gene regulatory network is a major hallmark, which applies to the essential genes associated with copper metabolism and TCA cycle (28, 29). It will not be surprising that liver cancer cell may be one of the major sites where cuproptosis happens. We believe that in the near future, the regulation and the pathologic relevance of cuproptosis will be revealed in liver cancer. Before that, if we can utilize the key genes in cuproptosis to make a prognostic model for liver cancer patient, this will accelerate the translation of this field to clinical practice, which also applies to other tumor types (30).

Given the severe threat of liver cancer to human society, much more efforts are needed to figure out the etiology and pathogenesis of liver cancer and develop effective therapeutics to treat it. In the meantime, advances in the diagnosis and prognosis techniques for liver cancer are of urgent demand. In this study, we leveraged the lncRNA and mRNA associated with cuproptosis to make a novel prognostic signature for liver cancer. In this model, we incorporated 6 lncRNAs (POLH-AS1, AL117336.2, MKLN1-AS, AC005479.2, AL928654.1, and AL031985.3) and 3 mRNAs (ATP7A, DLAT, and GLS) after a stringent selection process (Figures 1, 2). Our model exhibits an effective application in the prognosis of liver cancer patient (Figures 3, 4). Our model is capable of reflecting several major hallmarks (including the immune cell infiltration and TMB) of liver cancer (Figures 5, 6). This model also satisfactorily passed the validation procedure. The inclusion of the 3 mRNAs is an advantage of our model compared with those only analyze lncRNA. These proteins encoded by the 3 mRNAs are closely related to the induction of cuproptosis. ATP7A is a copper exporter, which is essential for the homeostasis of intracellular copper level (31). Mutation of ATP7A is demonstrated to be associated with Menkes disease, occipital horn syndrome, and X-linked distal spinal muscular atrophy (32). It will be interesting to investigate whether there is liver cancer-related mutation in ATP7A gene and if so, whether

this mutation will affect cuproptosis and liver cancer development. DLAT is an important subunit of the PDH complex and also one of the major substrates for cuproptosis (33). A recent study found that the DLAT level in hepatocellular carcinoma was influenced by blueberry malvidin-3-galactoside and 5-fluorouracil (34). This may establish links between cuproptosis and intestinal microbiota and chemotherapy of liver cancer. GLS, as a mitochondrial glutaminase, which hydrolyzes glutamine to glutamate, has a close relationship with liver cancer progression (35, 36). Huang et al. revealed that GLS along with PDH complex was important in liver cancer metabolism and autophagy, which might be the underlying mechanism for the chemo-resistance of liver cancer cell (37). Whether cuproptosis participates in the regulation of sensitivity to chemotherapy of liver cancer cell needs to be clarified in the future. For these lncRNAs, several of them have been linked with other RCDs like ferroptosis (POLH-AS1, MKLN1-AS, AL928654.1, and AL031985.3) and pyroptosis (MKLN1-AS, AC005479.2, and AL031985.3) in liver cancer (38–41). Their involvement with cuproptosis suggests there may be molecular relevance between those distinct RCDs. In fact, these RCDs do share similar mechanism of initiation (for example, ROS triggers apoptosis and ferroptosis), regulator (like Caspases in apoptosis, pyroptosis, and necroptosis; metal ion in ferroptosis and cuproptosis), and function (for example, apoptosis, ferroptosis, and pyroptosis all modulate immune activity) (10, 11). We wish future researches will shed more light on the link between these different RCDs. Moreover, POLH-AS1, AC005479.2 and AL928654.1 have been found to involve immune response in papillary thyroid cancer and hepatocellular carcinoma, respectively (42–44). Our model not only incorporates these two lncRNAs, but also expand this list of immune-associated lncRNAs in liver cancer to other 4 lncRNAs. AL117336.2 is a novel lncRNA with little study to date. It is worthy to explore its potential role in liver cancer and cuproptosis in the future. As hypoxia can dramatically influence TCA cycle and mitochondrion function, our results may reveal a link between hypoxia and cuproptosis in liver cancer (Figure 5D) (21). Another interesting result about our model is its correlation with TMB in liver cancer, which is related to the sensitivity of liver cancer cell to several chemotherapeutic drugs (Figure 6). A notable point is the mutual exclusiveness or co-occurence of p53 mutation and mutations of other genes. p53 here is of vital pathological relevance, not only because it is among the most important tumor suppressor genes, but also that it is a master regulator of several RCDs, including apoptosis, ferroptosis, and pyroptosis (45–47). p53 also has vital role in regulating TCA cycle (45). It should be one major direction to study whether p53 can regulate cuproptosis or not in liver cancer.

To sum up, we established an effective prognostic signature in liver cancer based on cuproptosis-related lncRNAs and mRNAs. We believe that this work will not only benefit the liver cancer patient in clinical use, but also make useful suggestions for the research field of cuproptosis. We wish in the near future, there will be great advances in researches about cuproptosis in liver cancer, based on which we can validate and improve our model to make it more accurate and efficient.

Data availability statement

The original contributions presented in the study are included in the article/Supplementary Material. Further inquiries can be directed to the corresponding author. The public datasets analyzed in this study can be found in the TCGA (https://portal.gdc.cancer.gov/) and GEO (https://www.ncbi.nlm.nih.gov/geo/) repository.

Author contributions

LM and YQL conceived the project. YL, YQL, and HF analyzed the data. YL, YQL, SY, and HF wrote the manuscript. LM reviewed and revised the manuscript. The authors read and approved the final manuscript. The requirements for authorship have been met. Each author believes that the manuscript represents honest work.

Funding

This work was supported by grants from the Natural Science Foundation of Jilin Province, China [20210101248JC].

Conflict of interest

The authors declare that the research was conducted in the absence of any commercial or financial relationships that could be construed as a potential conflict of interest.

Publisher's note

Supplementary material

The Supplementary Material for this article can be found online at: https://www.frontiersin.org/articles/10.3389/fonc.2022.985484/full#supplementary-material

References

1. Sia D, Villanueva A, Friedman SL, Llovet JM. Liver cancer cell of origin, molecular class, and effects on patient prognosis. *Gastroenterology* (2017) 152 (4):745–61. doi: 10.1053/j.gastro.2016.11.048

2. Sung H, Ferlay J, Siegel RL, Laversanne M, Soerjomataram I, Jemal A, et al. Global cancer statistics 2020: GLOBOCAN estimates of incidence and mortality worldwide for 36 cancers in 185 countries. *Ca-Cancer J Clin* (2021) 71(3):209–49. doi: 10.3322/caac.21660

3. Tasneem AA, Luck NH. Autoimmune hepatitis: Clinical characteristics and predictors of biochemical response to treatment. *J Transl Intern Med* (2020) 8 (2):106–11. doi: 10.2478/jtim-2020-0016

4. Ridola L, Faccioli J, Nardelli S, Gioia S, Riggio O. Hepatic encephalopathy: Diagnosis and management. *J Transl Intern Med* (2020) 8(4):210–9. doi: 10.2478/jtim-2020-0034

5. Benz F, Mohr R, Tacke F, Roderburg C. Pulmonary complications in patients with liver cirrhosis. *J Transl Intern Med* (2020) 8(3):150–8. doi: 10.2478/jtim-2020-0024

6. Siegel RL, Miller KD, Fuchs HE, Jemal A. Cancer statistics, 2022. *Ca-Cancer J Clin* (2022) 72(1):7–33. doi: 10.3322/caac.21708

7. Anwanwan D, Singh SK, Singh S, Saikam V, Singh R. Challenges in liver cancer and possible treatment approaches. *Bba-Rev Cancer* (2020) 1873(1):188314. doi: 10.1016/j.bbcan.2019.188314

8. Belopolsky Y, Khan MQ, Sonnenberg A, Davidson DJ, Fimmel CJ. Ketogenic, hypocaloric diet improves nonalcoholic steatohepatitis. *J Transl Intern Med* (2020) 8(1):26–31. doi: 10.2478/jtim-2020-0005

9. Xu J, Zhang JJ, Wang J. The application of traditional Chinese medicine against the tumor immune escape. *J Transl Intern Med* (2020) 8(4):203–4. doi: 10.2478/jtim-2020-0032

10. Galluzzi L, Vitale I, Aaronson SA, Abrams JM, Adam D, Agostinis P, et al. Molecular mechanisms of cell death: recommendations of the nomenclature committee on cell death 2018. *Cell Death Diff* (2018) 25(3):486–541. doi: 10.1038/s41418-017-0012-4

11. Tsvetkov P, Coy S, Petrova B, Dreishpoon M, Verma A, Abdusamad M, et al. Copper induces cell death by targeting lipoylated TCA cycle proteins. *Science* (2022) 375(6586):1254–61. doi: 10.1126/science.abf0529

12. Geisler S, Coller J. RNA In unexpected places: long non-coding RNA functions in diverse cellular contexts. *Nat Rev Mol Cell Bio* (2013) 14(11):699–712. doi: 10.1038/nrm3679

13. Dickson I. Hepatocellular carcinoma: A role for lncRNA in liver cancer. *Nat Rev Gastroenterol Hepatol* (2016) 13(3):122–3. doi: 10.1038/nrgastro.2016.21

14. Abbastabar M, Sarfi M, Golestani A, Khalili E. lncRNA involvement in hepatocellular carcinoma metastasis and prognosis. *EXCLI J* (2018) 17:900–13. doi: 10.17179/excli2018-1541

15. Ren XY, Li YC, Zhou Y, Hu WY, Yang C, Jing QA, et al. Overcoming the compensatory elevation of NRF2 renders hepatocellular carcinoma cells more vulnerable to disulfiram/copper-induced ferroptosis. *Redox Biol* (2021) 46:102122. doi: 10.1016/j.redox.2021.102122

16. Aubert L, Nandagopal N, Steinhart Z, Lavoie G, Nourreddine S, Berman J, et al. Copper bioavailability is a KRAS-specific vulnerability in colorectal cancer. *Nat Commun* (2020) 11(1):3701. doi: 10.1038/s41467-020-17549-y

17. Polishchuk EV, Merolla A, Lichtmannegger J, Romano A, Indrieri A, Ilyechova EY, et al. Activation of autophagy, observed in liver tissues from patients with Wilson disease and from ATP7B-deficient animals, protects hepatocytes from copper-induced apoptosis. *Gastroenterology* (2019) 156 (4):1173–89.e5. doi: 10.1053/j.gastro.2018.11.032

18. Cobine PA, Brady DC. Cuproptosis: Cellular and molecular mechanisms underlying copper-induced cell death. *Mol Cell* (2022) 82(10):1786–7. doi: 10.1016/j.molcel.2022.05.001

19. Dong JJ, Wang X, Xu CC, Gao ML, Wang SJ, Zhang J, et al. Inhibiting NLRP3 inflammasome activation prevents copper-induced neuropathology in a murine model of wilson's disease. *Cell Death Dis* (2021) 12(1):87. doi: 10.1038/s41419-021-03397-1

20. Goodman A, Patel SP, Kurzrock R. PD-1-PD-L1 immune-checkpoint blockade in b-cell lymphomas. *Nat Rev Clin Oncol* (2017) 14(4):203–20. doi: 10.1038/nrclinonc.2016.168

21. Solaini G, Baracca A, Lenaz G, Sgarbi G. Hypoxia and mitochondrial oxidative metabolism. *Bba-Bioenergetics* (2010) 1797(6-7):1171–7. doi: 10.1016/j.bbabio.2010.02.011

22. Man YG, Stojadinovic A, Mason J, Avital I, Bilchik A, Bruecher B, et al. Tumor-infiltrating immune cells promoting tumor invasion and metastasis: existing theories. *J Cancer* (2013) 4(1):84–95. doi: 10.7150/jca.5482

23. Hanahan D, Coussens LM. Accessories to the crime: functions of cells recruited to the tumor microenvironment. *Cancer Cell* (2012) 21(3):309–22. doi: 10.1016/j.ccr.2012.02.022

24. Bost M, Houdart S, Oberli M, Kalonji E, Huneau JF, Margaritis I. Dietary copper and human health: Current evidence and unresolved issues. *J Trace Elements Med Biol Organ Soc Miner Trace Elements* (2016) 35:107–15. doi: 10.1016/j.jtemb.2016.02.006

25. Gaetke LM, Chow-Johnson HS, Chow CK. Copper: toxicological relevance and mechanisms. *Arch Toxicol* (2014) 88(11):1929–38. doi: 10.1007/s00204-014-1355-y

26. Johncilla M, Mitchell KA. Pathology of the liver in copper overload. *Semin Liver Dis* (2011) 31(3):239–44. doi: 10.1055/s-0031-1286055

27. Doguer C, Ha JH, Collins JF. Intersection of iron and copper metabolism in the mammalian intestine and liver. *Compr Physiol* (2018) 8(4):1433–61. doi: 10.1002/cphy.c170045

28. Ozen C, Yildiz G, Dagcan AT, Cevik D, Ors A, Keles U, et al. Genetics and epigenetics of liver cancer. *New Biotechnol* (2013) 30(4):381–4. doi: 10.1016/j.nbt.2013.01.007

29. Pavlova NN, Thompson CB. The emerging hallmarks of cancer metabolism. *Cell Metab* (2016) 23(1):27–47. doi: 10.1016/j.cmet.2015.12.006

30. Mohamed AA, Omar AAA, El-Awady RR, Hassan SMA, Mohamed W, Eitah S, et al. MiR-155 and MiR-665 role as potential non-invasive biomarkers for hepatocellular carcinoma in Egyptian patients with chronic hepatitis c virus infection. *J Transl Intern Med* (2020) 8(1):32–40. doi: 10.2478/jtim-2020-0006

31. Kaler SG. ATP7A-related copper transport diseases-emerging concepts and future trends. *Nat Rev Neurol* (2011) 7(1):15–29. doi: 10.1038/nrneurol.2010.180

32. Kaler SG, DiStasio AT. ATP7A-related copper transport disorders. In: MP Adam, GM Mirzaa, RA Pagon, SE Wallace, LJH Bean, KW Gripp, editors. *GeneReviews((R))*. Seattle, WA: GeneReviews database (1993).

33. Mathias RA, Greco TM, Oberstein A, Budayeva HG, Chakrabarti R, Rowland EA, et al. Sirtuin 4 is a lipoamidase regulating pyruvate dehydrogenase complex activity. *Cell* (2014) 159(7):1615–25. doi: 10.1016/j.cell.2014.11.046

34. Cheng Z, Lin J, Gao NX, Sun XY, Meng XJ, Liu RH, et al. Blueberry malvidin-3-galactoside modulated gut microbial dysbiosis and microbial TCA cycle KEGG pathway disrupted in a liver cancer model induced by HepG2 cells. *Food Sci Hum Well* (2020) 9(3):245–55. doi: 10.1016/j.fshw.2020.04.006

35. Saha SK, Islam SMR, Abdullah-AL-Wadud M, Islam S, Ali F, Park KS. Multiomics analysis reveals that GLS and GLS2 differentially modulate the clinical outcomes of cancer. *J Clin Med* (2019) 8(3):355. doi: 10.3390/jcm8030355

36. Katt WP. A unique metabolic dependency for liver cancer stem cells. *EBioMedicine* (2019) 39:9–10. doi: 10.1016/j.ebiom.2018.12.026

37. Huang X, Gan GM, Wang XX, Xu T, Xie W. The HGF-MET axis coordinates liver cancer metabolism and autophagy for chemotherapeutic resistance. *Autophagy* (2019) 15(7):1258–79. doi: 10.1080/15548627.2019.1580105

38. Zhang Z, Zhang WW, Wang YF, Wan T, Hu BY, Li CH, et al. Construction and validation of a ferroptosis-related lncRNA signature as a novel biomarker for prognosis, immunotherapy and targeted therapy in hepatocellular carcinoma. *Front Cell Dev Biol* (2022) 10. doi: 10.3389/fcell.2022.792676

39. Wang T, Yang Y, Sun T, Qiu HZ, Wang J, Ding C, et al. The pyroptosis-related long noncoding RNA signature predicts prognosis and indicates immunotherapeutic efficiency in hepatocellular carcinoma. *Front Cell Dev Biol* (2022) 10. doi: 10.3389/fcell.2022.779269

40. Qu GZ, Wang D, Xu WY, Guo W. Comprehensive analysis of the correlation between pyroptosis-related LncRNAs and tumor microenvironment, prognosis, and immune infiltration in hepatocellular carcinoma. *Front Genet* (2022) 13. doi: 10.3389/fgene.2022.867627

41. Lin XX, Yang SJ. A prognostic signature based on the expression profile of the ferroptosis-related long non-coding RNAs in hepatocellular carcinoma. *Adv Clin Exp Med* (2022). doi: 10.17219/acem/149566

42. Fang CK, Liu SL, Feng KL, Huang CY, Zhang Y, Wang JA, et al. Ferroptosis-related lncRNA signature predicts the prognosis and immune microenvironment of hepatocellular carcinoma. *Sci Rep* (2022) 12(1):6642. doi: 10.1038/s41598-022-10508-1

43. Li ZY, Lin WX, Zheng JH, Hong WD, Zou J, Zhang TF, et al. Identification of immune-related lncRNAs to improve the prognosis prediction for patients with papillary thyroid cancer. *Biosci Rep* (2021) 41(2). doi: 10.1042/BSR20204086

44. Li XY, Zhang SQ, Zhang SJ, Kuang WH, Tang CZ. Inflammatory response-related long non-coding RNA signature predicts the prognosis of

hepatocellular carcinoma. *J Oncol* (2022) 2022:9917244. doi: 10.1155/2022/9917244

45. Liu Y, Gu W. The complexity of p53-mediated metabolic regulation in tumor suppression. *Semin Cancer Biol* (2021). doi: 10.1016/j.semcancer.2021.03.010

46. Liu Y, Gu W. p53 in ferroptosis regulation: the new weapon for the old guardian. *Cell Death Diff* (2022) 29(5):895–910. doi: 10.1038/s41418-022-00943-y

47. Liu YQ, Tavana O, Gu W. p53 modifications: exquisite decorations of the powerful guardian. *J Mol Cell Biol* (2019) 11(7):564–77. doi: 10.1093/jmcb/mjz060

frontiers | Frontiers in Oncology

TYPE Original Research
PUBLISHED 31 October 2022
DOI 10.3389/fonc.2022.1016721

OPEN ACCESS

EDITED BY
Adam Yongxin Ye,
Boston Children's Hospital and
Harvard Medical School, United States

REVIEWED BY
David Zhan,
Johns Hopkins Medicine, United States
Huiwu Ouyang,
Cold Spring Harbor Laboratory,
United States
Xiao Hong,
University of California, San Francisco,
United States

*CORRESPONDENCE
Wei Ding
dwdoctor@163.com

†These authors have contributed equally to this work

SPECIALTY SECTION
This article was submitted to Molecular and Cellular Oncology, a section of the journal Frontiers in Oncology

RECEIVED 11 August 2022
ACCEPTED 18 October 2022
PUBLISHED 31 October 2022

CITATION
Jiang P, Xue W, Xi C, Zhuang L, Yuan Z, Liu Z, Sun T, Xu X, Tan Y and Ding W (2022) A new acidic microenvironment related lncRNA signature predicts the prognosis of liver cancer patients.
Front. Oncol. 12:1016721.
doi: 10.3389/fonc.2022.1016721

A new acidic microenvironment related lncRNA signature predicts the prognosis of liver cancer patients

Peng Jiang[1,2†], Wenbo Xue[1,2†], Cheng Xi[1,2†], Lin Zhuang[1,2], Zhiping Yuan[3], Zhilin Liu[4], Tao Sun[5], Xuezhong Xu[1,2], Yulin Tan[1,2] and Wei Ding[1,2,6*]

[1]Department of General Surgery, Wujin Hospital Affiliated with Jiangsu University, Changzhou, China, [2]Department of General Surgery, The Wujin Clinical College of Xuzhou Medical University, Changzhou, China, [3]Department of Gastroenterology, Wujin Hospital Affiliated with Jiangsu University, Changzhou, China, [4]Department of Gastrointestinal Surgery, The Third Affiliated Hospital of Soochow University, Changzhou, China, [5]Department of Hepatopancreatobiliary Surgery, The Third Affiliated Hospital of Soochow University, Changzhou, China, [6]Changzhou Key Laboratory of Molecular Diagnostics and Precision Cancer Medicine, Wujin Hospital Affiliated with Jiangsu University, Changzhou, China

Background: The acidic microenvironment (AME), like hypoxia, inflammation, or immunoreaction, is a hallmark of the tumor microenvironment (TME). This work aimed to develop a prediction signature dependent on AME-associated lncRNAs in order to predict the prognosis of LC individuals.

Methods: We downloaded RNA-seq information and the corresponding clinical and predictive data from The Cancer Genome Atlas (TCGA) dataset and conducted univariate and multivariate Cox regression analyses to identify AME-associated lncRNAs for the construction of a prediction signature The Kaplan-Meier technique was utilized to determine the overall survival (OS) rate of the high (H)-risk and low (L)-risk groups. Using gene set enrichment analysis (GSEA) the functional variations between the H- and L-risk groups were investigated. The association between the prediction signature and immunological state was investigated using single-sample GSEA (ssGSEA). Additionally, the association between the predicted signature and the therapeutic response of LC individuals was evaluated. Lastly, quantitative reverse transcription polymerase chain reaction (qRT-PCR) was performed to verify the risk model.

Results: We generated a signature comprised of seven AME-associated lncRNAs (LINC01116, AC002511.2, LINC00426, ARHGAP31-AS1, LINC01060, TMCC1-AS1, AC012065.1). The H-risk group had a worse prognosis than the L-risk group. The AME-associated lncRNA signature might determine the prognosis of individuals with LC independently. The AME-related lncRNA signature shows a greater predictive effectiveness than clinic-pathological factors, with an area under the receiver operating characteristic (ROC) curve of 0.806%. When participants were categorized based on several clinico-pathological characteristics, the OS of high-risk individuals was shorter

compared to low-risk patients. GSEA demonstrated that the metabolism of different acids and the PPAR signaling pathway are closely associated with low-risk individuals. The prognostic signature was substantially associated with the immunological status of LC individuals, as determined by ssGSEA. High risk individuals were more sensitive to some immunotherapies (including anti-TNFSF4 anti-SIRPA, anti-CD276 and anti-TNFSF15) and some conventional chemotherapy drugs (including lapatinib and paclitaxel). Finally, the expression levels of the seven lncRNAs comprising the signature were tested by qRT-PCR.

Conclusions: A basis for the mechanism of AME-associated lncRNAs in LC is provided by the prediction signature, which also offers clinical therapeutic recommendations for LC individuals.

KEYWORDS

acidic microenvironment, lncRNAs, liver cancer, immune infiltration, drug therapy

Introduction

Globally, liver cancer (LC) accounts for the 4th most prevalent tumor-related death and ranks sixth in terms of cancer morbidity, the incidence of which is on the rise (1, 2). Surgery is currently the most popular type of therapy for LC, although most individuals are already in advanced stages when they're found, and some patients with severe cirrhosis are not suitable candidates for surgical treatment (3). Despite advances in curative LC treatment in recent years, the five-year survival rate (SR) for LC individuals is still low owing to the disease's spread, metastasis, and recurrence rate (4). Therefore, understanding the molecular mechanisms underlying the progression and searching for diagnostic indicators of LC can be crucial for detecting recurrences of LC and identifying novel treatment strategies.

Because tumor cells are typically reprogrammed for glycolysis, which generates lactic acid (LA) even under aerobic conditions, and tumor vasculature is typically dysfunctional, the tumor microenvironment (TME) has an acidic pH, sometimes known as acidic microenvironment (AME) (5). The acidic microenvironment, like hypoxia, inflammation, or immunoreaction, is a hallmark of the TME (6–8). Recent research has demonstrated that AME can promote numerous crucial oncogenic pathways, such as angiogenesis, tissue invasion/metastasis, and medication resistance (9). By promoting autophagy in an acidic environment, FOXO3a prevented the development of human gastric adenocarcinoma cell (10). Acidic microenvironment can increase hepatocellular carcinoma (HCC) cell-derived exosomal miR-21 and miR-10b levels, hence stimulating HCC cell motility and invasion (11).

Long noncoding RNA (lncRNA) was typically described as RNA with a limited ability to for code protein, which was strongly associated with the inactivation of cancer suppressor genes and the activation of oncogenes in HCC (12). lncRNA-PDPK2P increases the progression of HCC *via* the PDK1/AKT/Caspase 3 pathway (13). BCAR4 increases LC development by elevating ANAPC11 expression *via* miR1261 sponging (14). LncRNA NBR2 suppresses carcinogenesis in HCC through controlling autophagy (15). There are currently fewer investigations on lncRNAs associated to acidic microenvironment, and no study has been published on AME-associated lncRNAs in LC. In this investigation, a prediction signature based on AME-associated lncRNAs was constructed and assessed for prognosis, chemotherapeutic response, and tumor immune infiltration in LC individuals. Internal validation was also performed. As a next step, we conducted gene enrichment analysis (GSEA) to investigate possible mechanisms.

Methods

Patients and tissue samples

We gathered gene expression RNAseq and accompanying medical and predictive data for The Cancer Genome Atlas liver cancer (TCGA-LIHC) database from the UCSC Xena website (https://xenabrowser.net/datapages/); data for 424 samples were obtained. A total of 788 AME-related genes (relevance score > 7) were downloaded from GeneCards website (https://www.genecards.org/). 345 patients who met the eligibility requirements of being followed for more than 30 days were

taken part in the investigation. All participants were assigned in a random fashion into two groups: training (n = 173) and testing (n = 172), with a ratio of 1:1. The demographic characteristics of patients in the two groups are shown in Table 1.

From January 2021 to August 2021, 10 human HCC samples were collected at Wujin Hospital Affiliated with Jiangsu University (Changzhou, China). Neither chemotherapy nor radiotherapy had been administered to any of these patients before surgery. The study was approved by the Wujin Hospital Institutional Ethical Review Board (2022-SR-086), and informed consent was obtained from each patient.

Functional enrichment analysis (FEA) of differentially expressed AME-associated genes

As screening criteria for identifying differentially expressed genes (DEGs) related with AME, we applied a false discovery rate< 0.05 and $\log_2$|fold change (FC)| > 1. The "clusterProfiler" software (Ver. 4.4.4) was employed to assess Gene Ontology (GO) and Kyoto Encyclopedia of Genes and Genomes (KEGG) evaluations.

Construction of the prognostic signature for AME-associated lncRNA

Using the "limma" program (Ver. 3.52.2), the association between AME-associated genes and lncRNAs was computed. On the basis of a correlation coefficient $r^2 > 0.5$ and $P< 0.001$, 542 AME-associated lncRNAs with expression values were identified. Firstly, we employed univariate Cox regression (UCR) assessment to identify AME-associated lncRNAs correlated to the prognosis of LC individuals., Next, we used least absolute shrinkage and selection operator (LASSO) regression assessment to exclude high-impact factors, Eventually, the risk score model was developed using multivariate Cox regression (MCR)evaluation. The risk score equation was built as the following:

TABLE 1 The clinical characteristics of patients in different groups.

Variables	Training group(n=173)	Testing group (n=172)	Combined group(n=345)	*P* value(Training vs. Testing)
Age				
≤65	115	104	219	0.247
>65	58	68	126	
Gender				
Male	122	114	236	0.397
Female	51	58	109	
Grade				
I-II	106	109	215	0.856
III-IV	64	61	125	
Unknow	3	2	5	
T stage				
T1-T2	128	127	255	0.841
T3-T4	44	43	87	
TX-Unknow	1	2	3	
N Stage				
N0	122	119	241	0.828
N1	1	2	3	
NX-Unknow	50	51	101	
M stage				
M0	124	122	246	0.217
M1	0	3	3	
MX	49	47	96	
Stage				
I-II	124	117	241	0.125
III-IV	43	40	83	
Unknow	6	15	21	

T, tumor; M, metastasis; N, lymph node.

$$Risk \quad score = \sum_{i=0}^{n} \beta_i * Exp_i$$

In this equation, β is the regression coefficient acquired from the multivariate Cox regression analysis and *Exp* is the expression value of selected AME-associated lncRNAs. Each LC patient received a risk score according to this equation.

Construction of nomogram for overall survival (OS)

On the basis of the risk score and clinicopathological parameters of age, gender, tumor stage (T, N and M), we created a nomogram that predicts one-, three-, and five-year survival in LC individuals. We utilized a calibration curve to determine if the expected SR was in line accordance with the actual SR.

FEA of the AME-associated lncRNA prognostic signature

LC individuals were categorized into high (H)- and low (L)-risk groups on the basis of the median value of their risk scores. Gene enrichment analysis with GSEA was employed to determine which pathways were enriched the most (16). The analysis was conducted using GSEA 4.2.3 (http://www.gsea-msigdb.org/gsea/). We considered nominal $p< 0.05$ and FDR<0.25 to be statistically significance.

Immune infiltration and immune checkpoint analysis of AME-related lncRNA predictive signature

Utilizing "GSVA" package (Version 1.44.2) by single-sample gene set enrichment analysis (ssGSEA), the infiltration scores of 28 immune cells were computed (17). The phenotypic genes of immune cells were downloaded from the TISIDB website (http://cis.hku.hk/TISIDB/). A total of 40 immune checkpoints (Supplementary Table S1) were assessed with the Wilcoxon signed-rank test (WS-RT).

The function of the prognostic signature in predicting medical therapeutic response

The half-maximal inhibitory concentrations (IC50) of well-known chemotherapy agents were computed to evaluate whether the predictive signature predicts the outcome of LC therapy. The WS-RT was performed to evaluate the IC50 values across the H- and L-risk groups.

RNA extraction and quantitative RT-PCR

Total RNA was extracted from the liver tissues using TRIzol™ (Invitrogen, Carlsbad, CA, USA), and 2.0 μg of total RNA were applied to reverse transcription using the PrimeScript™ RT reagent Kit with gDNA Eraser (TaKaRa, Tokyo, Japan). Quantitative PCR was conducted using the TB Green® Premix Ex Taq™ II (TaKaRa, Tokyo, Japan). LncRNAs expression were quantified using the $2^{-\Delta\Delta Ct}$ method and standardized to GAPDH. The primer sequences are listed in Supplementary Table S2.

Statistical analysis

All statistical evaluations were conducted using R (ver 4.2.0) and GraphPad Prism (ver 9.0.1), and all statistical tests were two-tailed, with a p value< 0.05 deemed statistical significance. The Kaplan-Meier (K-M) technique and log-rank test were utilized to evaluate the OS of individuals in the H- and L-risk groups. The "timeROC" (ver. 0.4) program was utilized to plot the ROC curves and compute the area under the curve (AUC) results. Principal component analysis (PCA) was employed to evaluate the distribution of participant with various risk scores.

Results

Enrichment analysis of AME-associated genes

Figure 1 depicts the pipeline of the present investigation. We obtained 222 AME-associated DEGs (Figure 2A). KEGG and GO analyses were performed on DEGs associated with AME. KEGG pathway evaluation demonstrated that AME- associated DEGs were predominantly enriched in lipid and atherosclerosis, bladder cancer, AGE–RAGE signaling pathway in diabetes - related complications, rheumatoid arthritis, glioma, PI3K-Akt signaling pathway, central carbon metabolism in tumor, non-small cell lung cancer, etc. (Figure 2B). In the domain of biological process, GO findings revealed that DEGs were predominantly enriched in reaction to xenobiotic stimulation, response to nutritional concentrations, response to extracellular stimuli, etc. DEGs were predominantly abundant in cytoplasmic vesicle lumen, secretory granule lumen, platelet alpha granule lumen, and other lumens of cellular organelles. In the area of molecular activity, the DEGs were primarily enriched for carboxylic acid binding, monooxygenase activity, signaling receptor activator activity, etc. (Figure 2C).

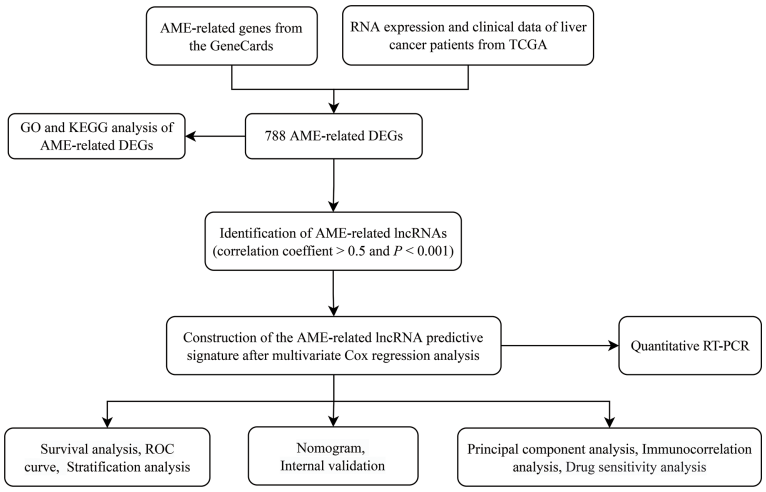

FIGURE 1
The flowchart of our research. TCGA, The Cancer Genome Atlas; DFS, disease-free survival; DEGs, differentially expressed genes; GO, Gene Ontology; KEGG, Kyoto Encyclopedia of Genes and Genomes; lncRNAs, long noncoding RNAs.

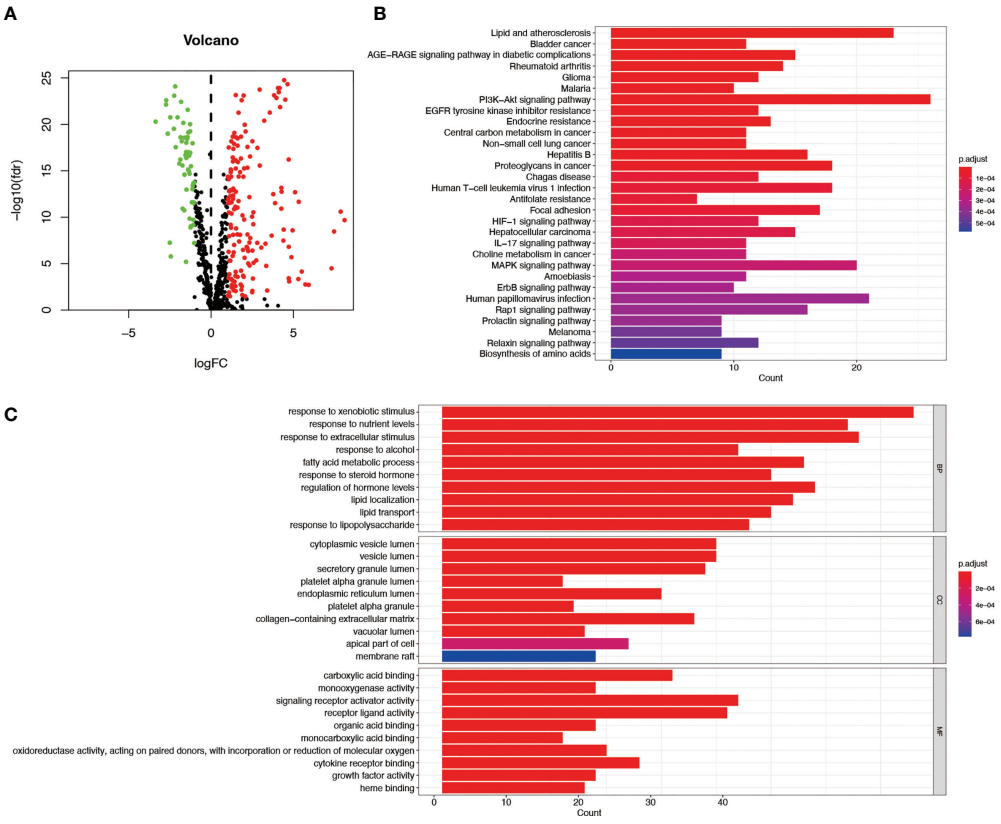

FIGURE 2
GO and KEGG assessments of AME-associated DEGs in tumor and adjacent tissues. **(A)** Volcano plot of 788 AME-associated genes in liver cancer. Red dots show up-regulated genes, while green dots indicate down-regulated genes. **(B)** KEGG assessment of AME-associated DEGs. **(C)** GO evaluation of AME-associated DEGs. FC, fold change; fdr, false discovery rate; BP, biological process; CC, cellular components; MF, molecular function.

Construction of prognostic signature for the AME-associated lncRNA

We found 542 AME-associated lncRNAs (Supplementary Table S3). UCR analysis demonstrated that 136 lncRNAs were correlated with the prognosis of LC individuals (Supplementary Table S4). LASSO analysis screened out 16 high-impact AME-related lncRNAs (Figures 3A, B). MCR analysis showed that a seven AME-related lncRNAs (LINC01116, AC002511.2, LINC00426, ARHGAP31-AS1, LINC01060, TMCC1-AS1, AC012065.1) prognostic signature (ALPS) was identified (Figure 3C). Figure 4A depicts the levels of expression of seven AME-associated lncRNAs in LC individuals. On the basis of Pearson's correlation ($r^2 > 0.5$ and $P< 0.001$), the lncRNA-mRNA co-expression network was created. Figures 4B, C illustrates additional visualizations of the network using Cytoscape and the "ggalluvial" module. ARHGAP31-AS1 was co-expressed with five AME-associated genes (LPAR2, ABCC1, ABCC4, TGFB2 and TFAP2), LINC00426 was co-expressed with five AME-related genes (IDO1, SIGLEC7, CD4, CTLA4 and LTA), LINC01116 was co-expressed with seven AME-associated genes (FABP5, PLAU, IL10, BIRC5, SLC38A5, GJA1 and NES), TMCC1-AS1 was co-expressed with six AME-related genes (G6PD, AKR1C1, PTK2, NPM1, TKT and AKR1). AC002511.2 was co-expressed with MYCN, AC012065.1 was co-expressed with HSPA4, LINC01060 was co-expressed with ABCC1. The score for risk was computed as follows:

$$\begin{aligned}\text{Risk score} = {} & (0.137{\star}\text{EXP}_{\text{LINC01116}}) + (0.175{\star}\text{EXP}_{\text{AC002511.2}}) \\ & + (-0.393{\star}\text{EXP}_{\text{LINC00426}}) \\ & + (0.239{\star}\text{EXP}_{\text{ARHGAP31-AS1}}) \\ & + (0.198{\star}\text{EXP}_{\text{LINC01060}}) + (0.229{\star}\text{EXP}_{\text{TMCC1-AS1}}) \\ & + (0.297{\star}\text{EXP}_{\text{AC012065.1}})\end{aligned}$$

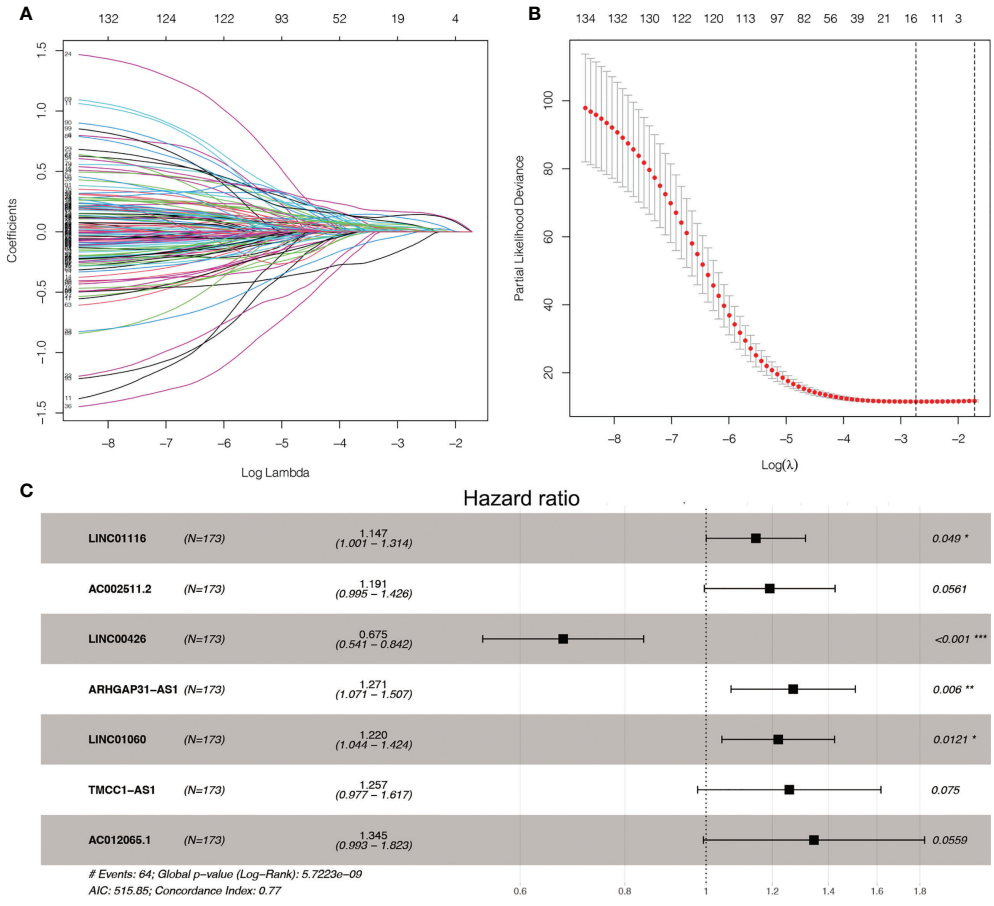

FIGURE 3
LASSO and Cox regression for tuning parameter selection. **(A)** LASSO coefficient profiles of the 136 AME-related lncRNAs. **(B)** Plots of the ten-fold cross-validation error rates. **(C)** Forest map of the seven prognostic lncRNAs by multivariate Cox regression.

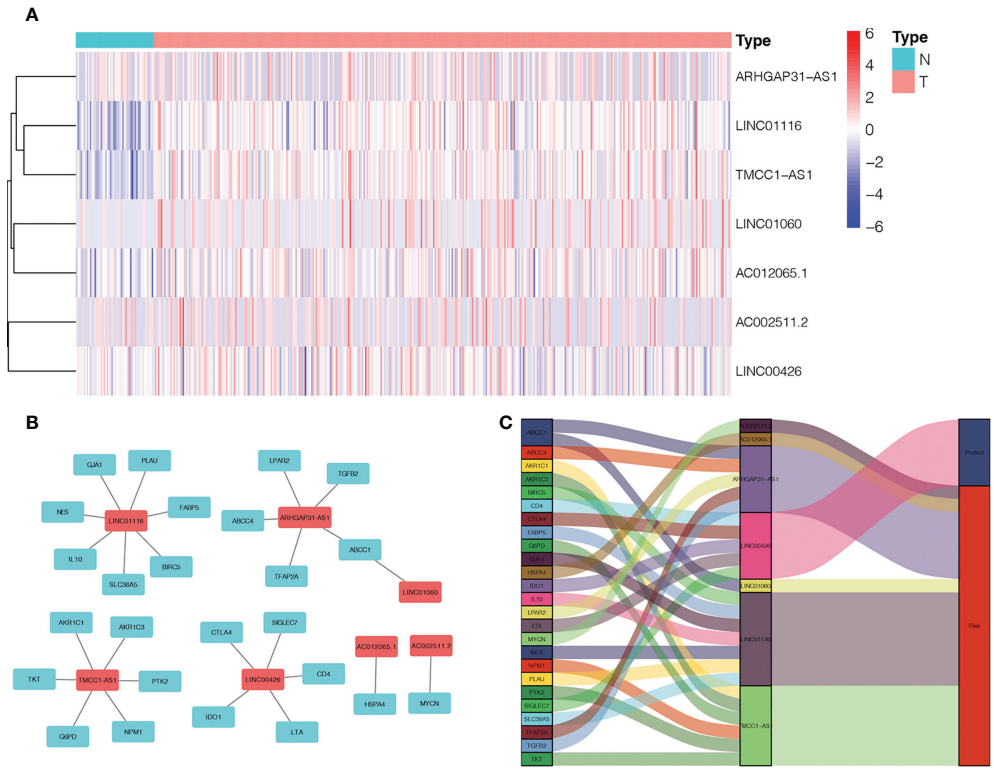

FIGURE 4
Expression levels and lncRNA-mRNA network of seven AME-associated lncRNAs in the predicted signature. **(A)** The expression levels of seven AME-related lncRNAs in liver cancer and normal tissues. **(B)** The co-expression network of prognostic AME-associated lncRNAs. **(C)** Sankey diagram of prognostic AME-based lncRNAs. T, tumor; N, non-tumor.

Association between the ALPS, clinic-pathological features and the prognosis of LC patients

Based on their median risk ratings (0.8587, determined in the training group), the individuals were categorized into 2 groups (H-risk and L-risk) (Figure 5). Figure 6A demonstrates that in the training, testing and combined groups, individuals in the H-risk group showed poorer prognoses, as shown in Figure 6A. Additionally the accuracy of the ALPS in predicting the prognosis of LC in all groups was assessed using ROC curve analysis (Figure 6B). Our outcomes showed that the ALPS could be a reliable marker of LC prognosis.

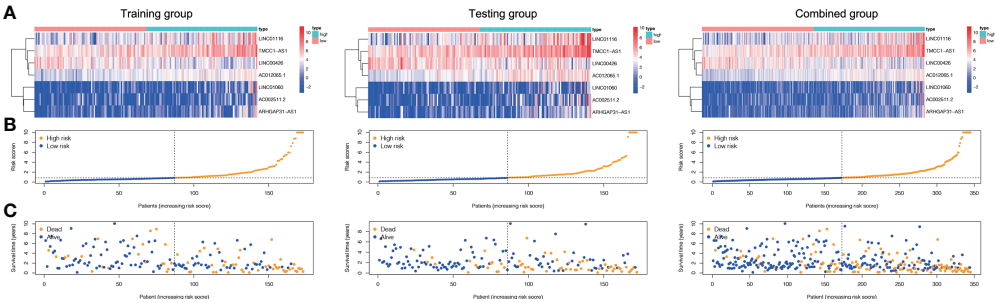

FIGURE 5
Risk score of the three groups. **(A)** Heatmap of the three-gene signature in the training, testing, and combined groups. **(B)** Allocation of individuals with various risk scores in the training, testing, and combined groups. **(C)** Survival status of individuals with various risk scores in the training, testing, and combined groups.

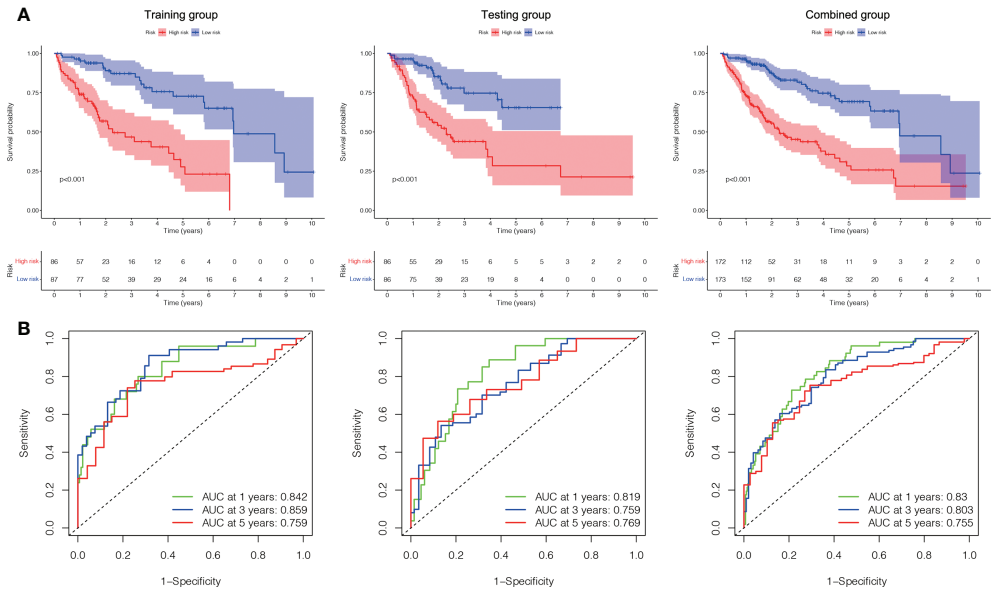

FIGURE 6
Internal validation of the ALPS for OS according to the entire TCGA database. **(A)** Kaplan-Meier survival curve in the training, testing and combined groups. **(B)** ROC curve and AUCs at one-year, three-years and five-years survival in the training, testing and combined groups. ALPS, AME-associated lncRNAs prognostic signature.

A Cox regression analysis was undertaken to evaluate if the predictive signature is an independent prognostic variable for LC individuals. Both T and M stage, as well as risk score, were substantially related to the OS of LC individuals, according to UCR analysis. (Figure 7A). Analysis using MCR revealed that stage and risk score were independent predictors of OS in individuals with LC (Figure 7B). In terms of estimating the prognosis of LC individuals, the AUC of the risk score was 0.806%, that was superior to those of clinicopathological factors (Figure 7C). We evaluated the variation in clinicopathological factors between the H- and L- risk groups and reported that tumor stage ($P< 0.05$), T stage ($P< 0.05$), grade ($P< 0.01$) and state ($P< 0.05$) were substantially different (Figure 7D).

To further estimate the one, three, and five-years prognosis of LC individuals, we developed a nomogram using stage and the risk score (Figure 8A). The calibration curves demonstrated good consistency among actual OS rates and expected survival rates at one-, three- and five-years (Figures 8B).

To examine the correlation between the ALPS and the prognosis of LC individuals categorized by various clinicopathological factors, LC individuals were allocated into groups based on age, sex, and stage (T, N, and M). The OS of individuals in the H- risk group was considerably shorter relative to those of individuals in the L- risk group across all classes (Figure 9). The findings demonstrated that the ALPS could predict the outcome of individuals with LC regardless of their clinicopathological characteristics.

Immune cell infiltration (ICI) and immune checkpoint

To further investigate the association among risk scores and immune cells, we assessed the enrichment scores of ssGSEA for several subgroups of immune cells. The results showed that activated CD8 T cell, effector memeory CD8 T cell, T follicular helper cell, gamma delta T cell, type 1 T helper cell, activated B cell, immature B cell, natural killer cell (NKC), CD56bright NKC, CD56dim NKC, myeloid derived suppressor cell, NK T cell, macrophage, eosinophil, mast cell and Monocyte were substantially different in the H- and L-risk groups (Figure 10A). Then we compared the relation between risk score and the expression of immune checkpoint, the results revealed that the expression of TNFSF4, SIRPA, CD276 and TNFSF15 in the H- risk group were substantially greater (Figure 10B), indicated that high risk individuals have a potential response to the immunotherapy by targeting them.

Correlation between the ALPS and LC therapy

In addition to immuno-therapy, we investigated the relationship between the ALPS and the effectiveness of conventional chemotherapy for LC. In the L-risk group, the IC50s of erlotinib, irinotecan, olaparib and oxaliplatin were

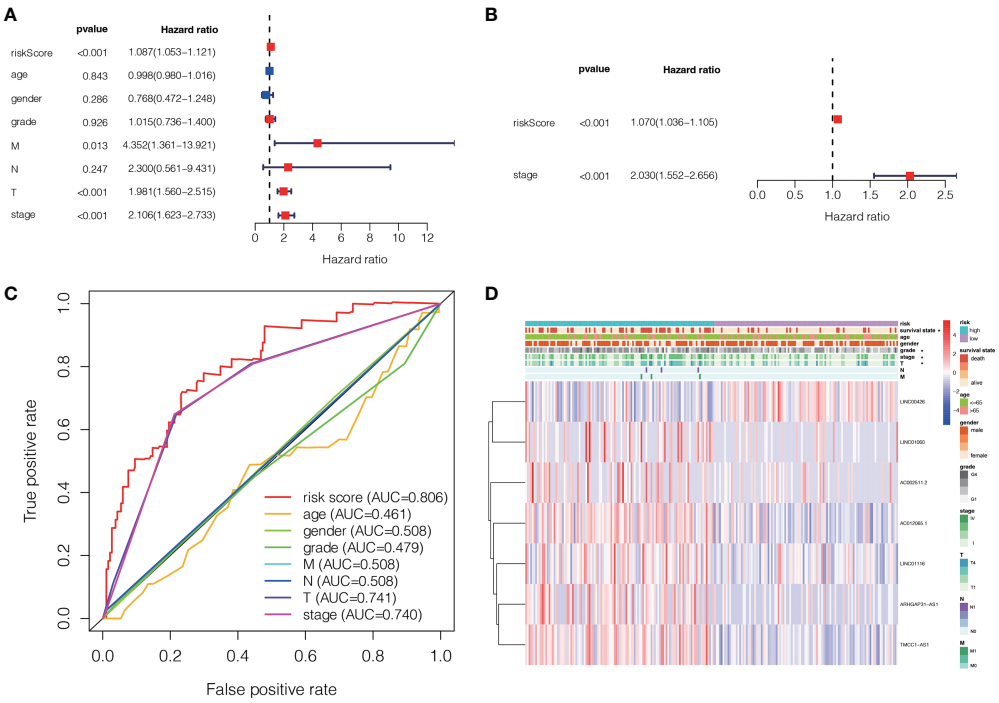

FIGURE 7
The association between the ALPS and the prognosis of liver individuals. **(A)** Forest plot for univariate Cox regression assessment. **(B)** Forest plot for multivariate Cox regression analysis. **(C)** The ROC curve of the risk score and clinio-pathological factors. **(D)** Heatmap of the ALPS and clinical significance in the combined group. T, tumor; N, non-tumor.

shown to be lower, while the IC50s of lapatinib and paclitaxel were shown to be lower in H-risk group (Figure 11). This information was useful for investigating therapeutic alternatives for H- and L- risk groups.

Principal component analysis and GSEA

We visualized the individuals distribution according to the whole genome, AME-correlated gene sets, AME-related lncRNAs, and the ALPS using PCA maps. According to our findings, the ALPS was the best for individuals. Due to the disparate prognoses of individuals in the H- and L- risk groups, we utilized GSEA to investigate potential variation between the both groups (Figures 12A–D). Our outcomes revealed that complement and coagulation cascades, drug metabolism cytochrome p450, fatty acid metabolism, retinol metabolism, linoleic acid metabolism, tryptophan metabolism, glycine serine and threonine metabolism, primary bile acid biosynthesis, PPAR signaling pathway, valine leucine and isoleucine degradation, peroxisome, metabolism of xenobiotics by cytochrome p450, steroid hormone biosynthesis, tyrosine metabolism, histidine metabolism, arachidonic acid metabolism, adipocytokine signaling pathway and aromatase activity were substantially enriched in the low risk group (Figures 12E–H and Table 2), demonstrating that L- risk individuals are tightly correlated to metabolism of different acids and PPAR signaling pathway.

Validation of expression of the ALPS

We evaluated the expression level of the seven AME-related lncRNAs in clinical samples retrieved from HCC patients in our hospital. Interestingly, the qRT-PCR results indicated that the expression of AC012065.1, LINC01116, TMCC1-AS1 and LINC01060, was significantly higher in tumor tissue while expression of AC002511.2, LINC00426 and ARHGAP31-AS1 was similar between tumor and normal tissue (Figures 13A–G). Considering the tight association between our risk model and metabolism and immunity, we believe that the metabolic and immune environment surrounding tumor cells may affect lncRNA expression. According to these results, we speculate that AME-related lncRNAs, especially the four differentially expressed lncRNAs, may play a role in liver cancer regulation.

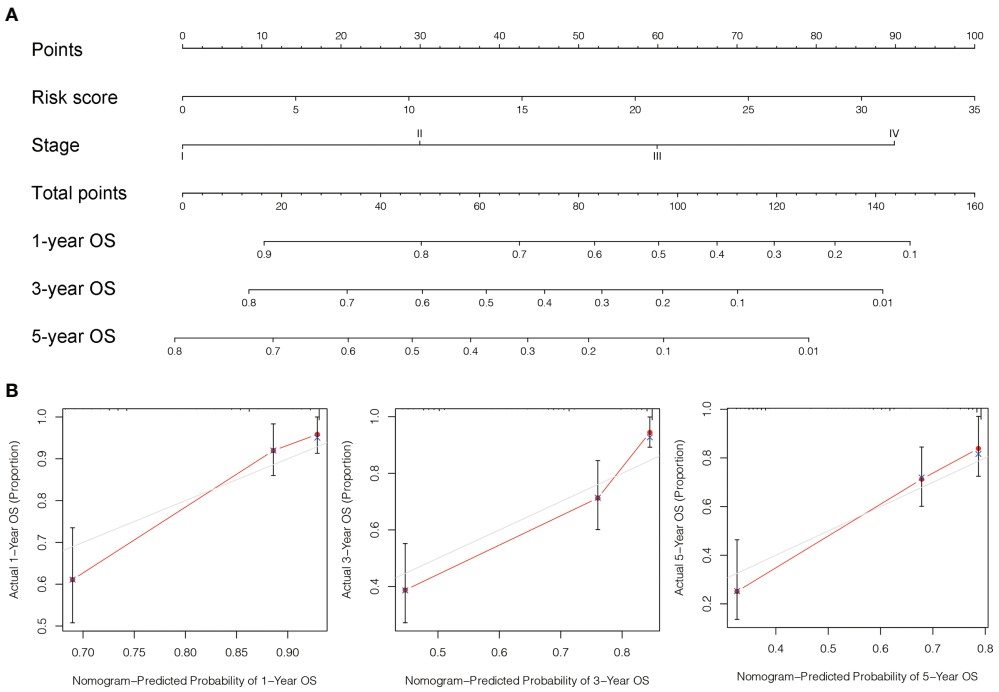

FIGURE 8
Design and validation of the nomogram. **(A)** A nomogram integrating combining clinio-pathological factors and risk score predicts one, three, and five- years OS of liver cancer individuals. **(B)** The calibration curves assess consistency among the actual OS rates and the expected survival rates at one-, three- and five-years.

Discussion

Liver cancer is one of the most prevalent malignant tumors of digestive system, majority of which starting from hepatocytes. The effect of the AME in tumor is complicated. More and more investigations have shown that AME has a vital part in the incidence and development of tumor, yet the present investigation focuses mainly on the contribution of AME in tumor therapy. There is few research on its role in tumor prognosis. In recent years, there have been no studies to predict the prognosis of LC individuals by establishing lncRNA predictive features related to AME.

In the current investigation, we first gathered 788 AME-associated genes and 542 AME-related lncRNAs. KEGG findings revealed that the DEGs were primarily the DEGs were mainly enriched in AGE-RAGE, PI3K-Akt as well as HIF-1 signaling pathway. According to studies, sRAGE and CML-AGE levels are inversely correlated to the development of HCC (18). Wu et al. reported that the oncogenic PI3K/AKT/mTOR pathway was a typical dysregulated pathway in the pathogenesis of HCC (19). Vincent et al. identified that hypoxia drove the stabilization of hypoxia-inducible factors (HIFs) that behave as central regulators to suppress dampen the innate immune system of LC (20). Such findings show that AME-associated genes could regulate the progress of LC *via* the AGE-RAGE and PI3K/AKT/mTOR pathway. Additionally, AME-related genes were also associated with hypoxia. Even so, more studies are needed to validate the function of AME-associated genes in LC.

Numerous research has reported that a strongly extracellular acidic environment can cause double-stranded DNA breaks and clastogenic effects (21). Research in cell culture as well as *in vivo* also supported the notion that acidosis could affect tumor cell epigenetics and RNA processing (22). Thus, it can be seen that AME-associated lncRNAs might have a significant part in LC. We allocated 345 LC participants into three groups: a training, testing, and combined. 136 lncRNAs were identified as being associated with the prediction of LC individuals. LINC01116, AC002511.2, LINC00426, ARHGAP31-AS1, LINC01060, TMCC1-AS1 and AC012065.1 were included in the ALPS built for the training group using LASSO and MCR analysis. In all three groups, individuals with a high-risk score had a shorter OS compared to those with a low-risk score. According to the ROC analysis, the ALPS accurately predicted the prognosis of LC in all three groups. Multivariate Cox analysis showed a significant independent relationship between the ALPS and LC outcome. Lastly, we developed a nomogram to estimate the one-, three-, and five-year survival of individuals with LC. In addition, the calibration curves demonstrated that the nomogram had excellent predictive ability. Of these seven lncRNAs, LINC01116 was tightly associated to immune

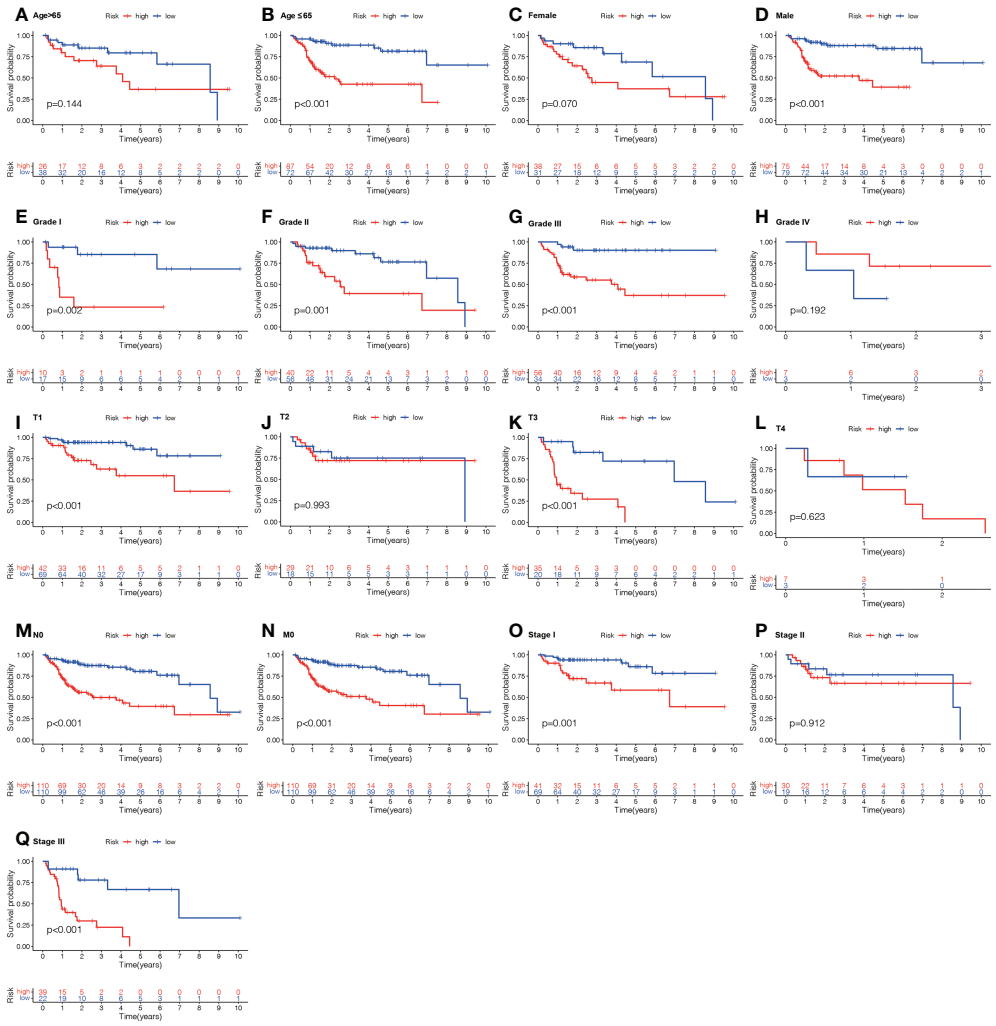

FIGURE 9
Kaplan-Meier survival graphs for high (H)- and low (L)-risk individual subgroups based on various clinic-pathological factors. **(A, B)** Age. **(C, D)** Gender. **(E–H)** Grade. **(I–L)** T stage. **(M)** N stage. **(N)** M stage. **(O–Q)** Stage. T, tumor; N, Node; M, metastasis.

regulation. LINC01116 could stimulate cell proliferation, cell cycle progression, and tumor metastasis in HCC (23). Shi et al. found that LINC01060 prevented pancreatic cancer growth and invasion *in-vitro* and *in-vivo* through modulating vinculin expression (24). Li et al. reported that exosomes containing LINC01060 from hypoxic glioma stem cells increase glioma growth *via* modulating the MZF1/c-Myc/HIF1α axis (25). Study showed that autophagy-related TMCC1-AS1 predicted poor prognosis in LC (26). In addition, the importance of AC002511.2, LINC00426, ARHGAP31-AS1, LINC01060 in LC is seldom documented in the literature; hence, future study will concentrate on these 3 lncRNAs. GSEA revealed that metabolism of different acids and the PPAR signaling pathway are tightly associated with low-risk individuals. The impact of the complement and coagulation cascades signaling pathway in the aetiology of malignancies is yet unknown. Zhang et al. identified that C8B in the complement and coagulation cascades signaling pathway is a survival indicator in HBV-associated HCC individuals (27). Khamis et al. reported that cytochrome P450-2D6 enzyme (CYP2D6) might act as a putative marker in LC health inequalities, with a negative correlation to IL6 proclaimed a complex relation between CYP2D6 and inflammation in the ethnic differences observed in Asian Americans and Caucasian Americans LC individuals (28). Seo et al. indicated that fatty-acid-induced FABP5 overexpression caused HCC development *via* HIF-1-driven reprogramming of lipid metabolism (29). Lai et al. suggested that greater -carotene and retinol levels are correlated with

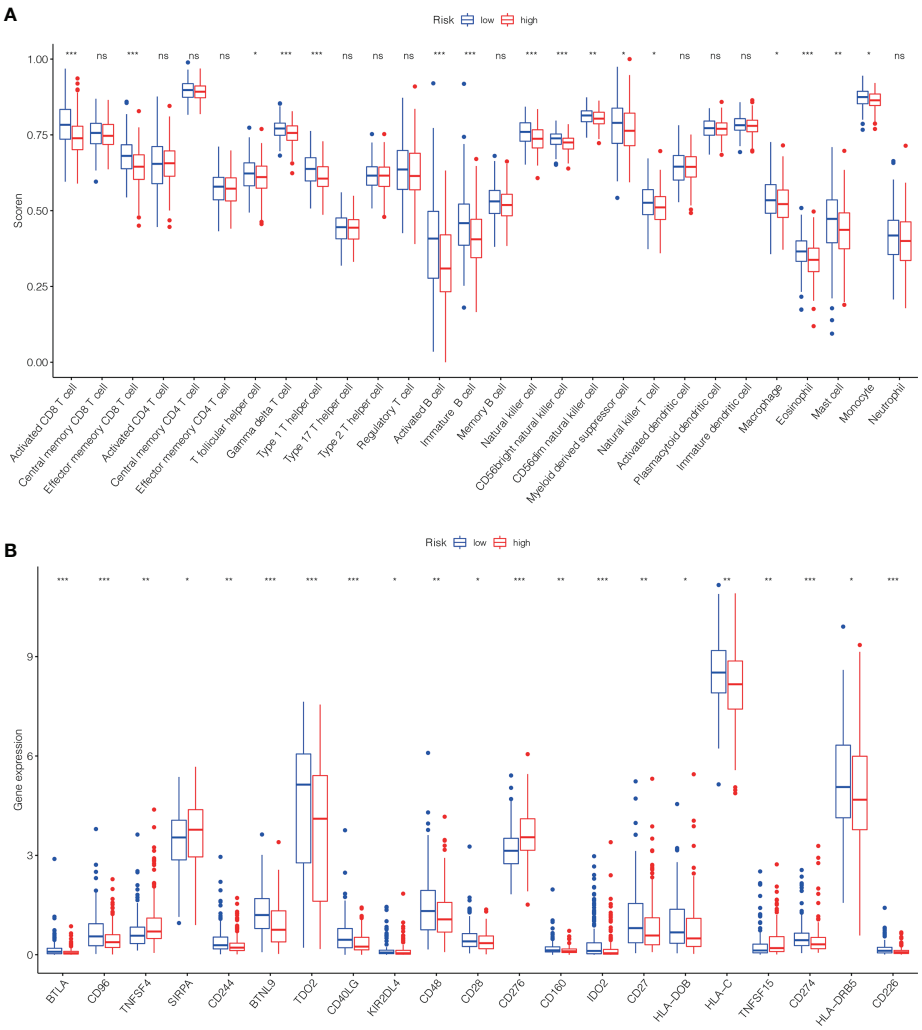

FIGURE 10
The scores of immune infiltrating cells (IIC) and immunological checkpoint in H- and L- risk groups. **(A)** The infiltration levels of 28 immune cells in H- and L- risk groups. **(B)** The expression levels of 21 immune checkpoint in H- and L- risk groups. *$P < 0.05$; **$P < 0.01$; ***$P < 0.001$; ns, no significant.

incidence LC (30). Brown et al. reported that carnitine palmitoyltransferase gene overexpression with linoleic acid promotes CD4+ T cell apoptosis hence promoting the development of HCC (31). Cui et al. concluded that ERRFI1-induced apoptosis rendered HCC cells more sensitive to tryptophan shortage, and ERRFI1 interacted with PDCD2 to cause apoptosis in HCC cells (32). Thomas et al. identified that increased primary bile acids and taurine over glycine-conjugated ratios were highly correlated with HCC risk, while the secondary bile acids over primary bile acids ratios were inversely correlated with HCC risk (33). By decreasing PPAR-mediated glycolysis, simvastatin re-sensitizes HCC cells to sorafenib, according to Feng et al. (34). Therefore, these metabolic changes may account for the good prognosis in the L-risk group.

The acidic microenvironment of tumors also has a significant influence in drug research and development. When tumor cells are not well-nourished in culture, conditions like hypoxia or acidity can affect drug efficacy (35). The acid- dependent drug release avoid premature drug release at physiological pH, allowing for the successful delivery of the largest therapeutic cargo to target tumor cells (which are known to have an acidic internal pH compared to normal cells) (36). Previous studies have shown that multistage delivery nanoparticles (MDNP) are substantially more effective in targeting tumors compared to conventional delivery carriers. This is attributable to the fact that MDNP is capable of evading cellular absorption at neutral pH (as in blood), whereas it successfully penetrates cells at acidic pH (as in cancer tissues) (37). Additionally, therapeutic reversal of tumor acidity using RNAi

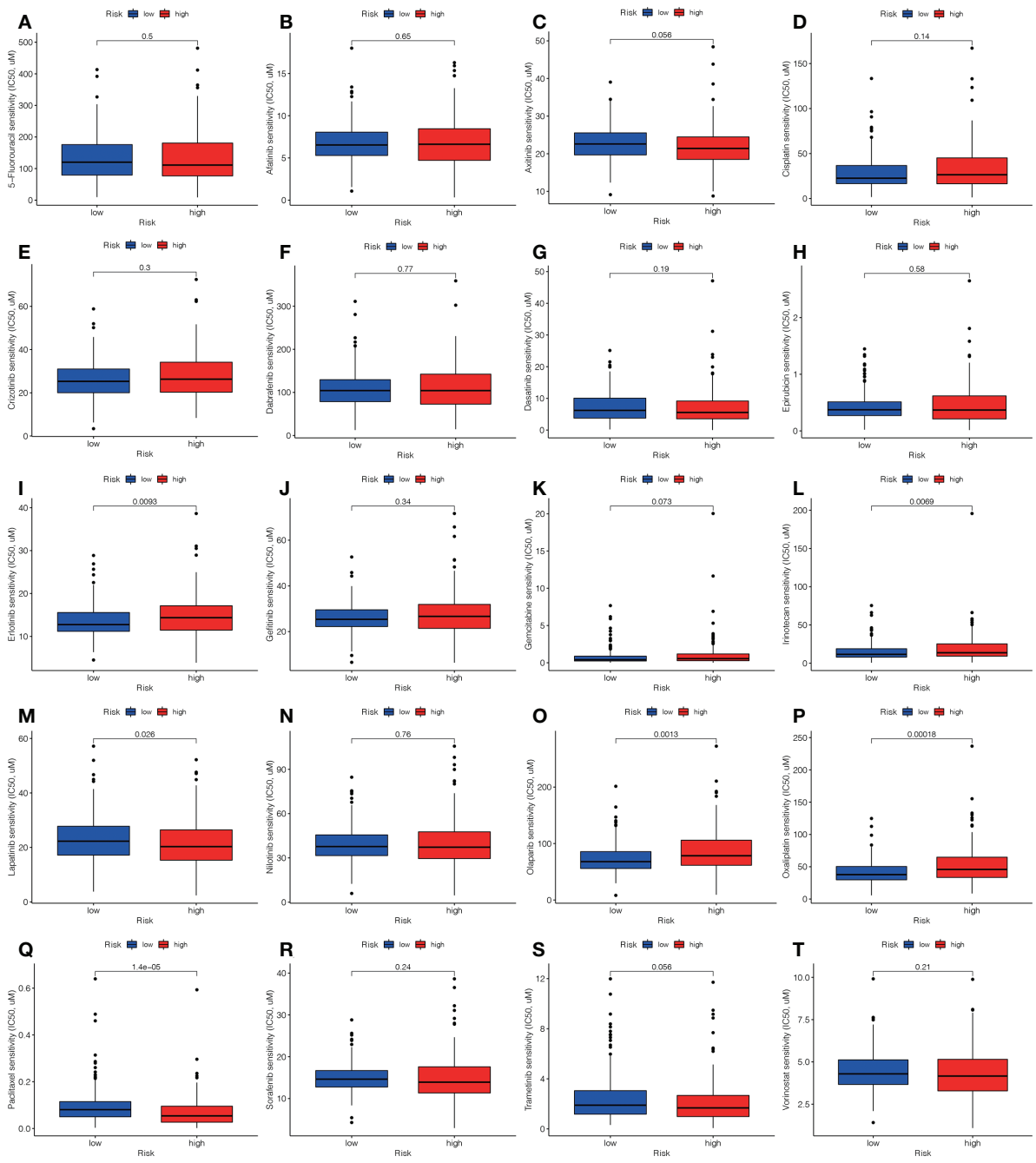

FIGURE 11
Comparison of the treatment medication sensitivity of individuals at high (H)- and low (L)-risk. IC50s of **(A)** 5-fluorouracil, of **(B)** afatinib, of **(C)** axitinib, of **(D)** cisplatin, of **(E)** crizotinib, of **(F)** dabrafenib, of **(G)** dasatinib, of **(H)** epirubicin, of **(I)** erlotinib, of **(J)** gefitinib, of **(K)** gemcitabine, of **(L)** irinotecan, of **(M)** lapatinib, of **(N)** nilotinib, of **(O)** olaparib, of **(P)** oxaliplatin, of **(Q)** paclitaxel, of **(R)** sorafenib, of **(S)** trametinib, of **(T)** vorinostat in H and L risk groups.

nanoparticles can restore the anticancer capabilities of T cells and enhance checkpoint blockade treatment (38). In this research, we found most of the immune cells were higher in the low-risk group. It might indicate that in the low-risk group, more immune cells play an anti-tumor role in the tumor tissue, which makes them have a lower risk and better prognosis. Moreover, our study indicates that high-risk individuals are likely to be susceptible to some immunotherapies (including anti-TNFSF4, anti-SIRPA,

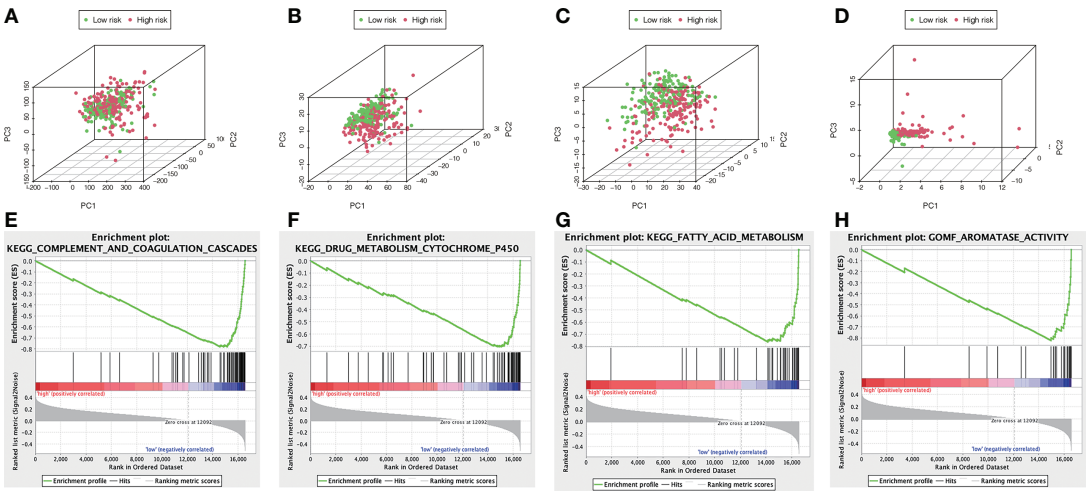

FIGURE 12
The metabolic condition of individuals with high and low risk scores varies. PCA maps depict the allocation of individuals according to the **(A)** whole genes **(B)** AME-associated gene sets; **(C)** AME-associated lncRNAs; and **(D)** the ALPS. GSEA showed significant enrichment of the **(E)** complement and coagulation cascades, **(F)** drug metabolism cytochrome p450, **(G)** fatty acid metabolism, **(H)** aromatase activity.

anti-CD276 and anti-TNFSF15) and some conventional chemotherapy drugs (including lapatinib and paclitaxel). The findings suggest that people at high risk may benefit from the combination of relatively sensitive immuno- and chemo- therapy, which sets the foundation for accurate and personalized LC therapy.

Nevertheless, our research has two drawbacks. Firstly, we utilized only the TCGA dataset information for internal validation, and other databases are still needed for peer approval to determine the relevance of the predicted signature. Secondly, the mechanism of the AME-associated lncRNAs in LC requires further confirmation by experiments.

TABLE 2 The high-risk group enriched gene sets.

Gene set	ES	NES	NOM *p*-val	FDR *q*-val
Complement and coagulation cascades	-0.780	-1.984	0.002	0.129
Drug metabolism cytochrome p450	-0.705	-1.928	0.002	0.114
Fatty acid metabolism	-0.765	-1.877	0.016	0.134
Retinol metabolism	-0.708	-1.863	0.002	0.113
Linoleic acid metabolism	-0.641	-1.848	0.002	0.104
Tryptophan metabolism	-0.675	-1.835	0.002	0.096
Glycine serine and threonine metabolism	-0.766	-1.821	0.008	0.092
Primary bile acid biosynthesis	-0.853	-1.759	0.006	0.126
PPAR signaling pathway	-0.588	-1.741	0.011	0.131
Valine leucine and isoleucine degradation	-0.679	-1.706	0.049	0.151
Peroxisome	-0.567	-1.694	0.046	0.150
Metabolism of xenobiotics by cytochrome p450	-0.598	-1.686	0.039	0.135
Steroid hormone biosynthesis	-0.596	-1.673	0.035	0.136
Tyrosine metabolism	-0.527	-1.637	0.048	0.152
Arachidonic acid metabolism	-0.463	-1.573	0.023	0.179
Adipocytokine signaling pathway	-0.400	-1.512	0.028	0.212
Aromatase activity	-0.824	-1.943	0.004	0.245

ES, enrichment score; NES, normalized enrichment score; NOM, nominal; FDR, false discovery rate; PPAR, peroxisome proliferators-activated receptor.

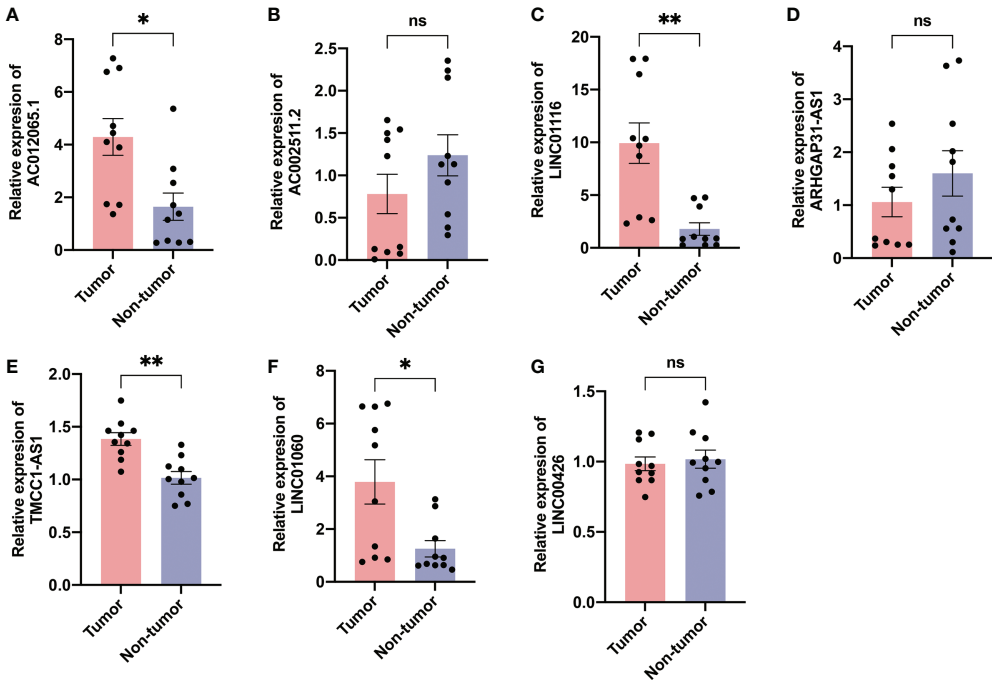

FIGURE 13
Validation of expression of the ALPS in human tissues. Expression analysis of **(A)** AC012065.1, **(B)** AC002511.2, **(C)** LINC01116, **(D)** ARHGAP31-AS1, **(E)** TMCC1-AS1, **(F)** LINC01060 and **(G)** LINC00426 in 10 pairs of liver cancer tissue samples. *$P < 0.05$; **$P < 0.01$; ns, not significant.

Conclusion

In summary, the AME-associated lncRNA signature could independently diagnose the prognosis of LC individuals and establish a foundation for the response to medical therapy, however it will require future experimental confirmation.

Data availability statement

The datasets presented in this study can be found in online repositories. The names of the repository/repositories and accession number(s) can be found in the article/ Supplementary material.

Ethics statement

The studies involving human participants were reviewed and approved by Wujin Hospital Institutional Ethical Review Board. The patients/participants provided their written informed consent to participate in this study.

Author contributions

PJ, WX, CX, and WD: Study design, Data collection, Data analysis, Writing. LZ: Study design, Data collection. ZY: Study design, Data analysis. ZL and TS: biological experiment. WD, XX, and YT: Study design, Data collection, Data analysis, Revision. All authors contributed to the article and approved the submitted version.

Funding

This work was supported by the Changzhou Sci&Tech Program (CJ20210013, CJ20220008), Young Talent Development Plan of Changzhou Health Commission (CZQM2020118, CZQM2021028), the Development Foundation of Affiliated Hospital of Xuzhou Medical University (XYFY2020016), Medical Research Project of Jiangsu Health Commission (No.Z2019027), Changzhou HighLevel Medical Talents Training Project (2022CZBJ105).

Acknowledgments

Thanks for the support of Changzhou High-Level Medical Talents Training Project.

Conflict of interest

The authors declare that the research was conducted in the absence of any commercial or financial relationships that could be construed as a potential conflict of interest.

Publisher's note

All claims expressed in this article are solely those of the authors and do not necessarily represent those of their affiliated organizations, or those of the publisher, the editors and the reviewers. Any product that may be evaluated in this article, or claim that may be made by its manufacturer, is not guaranteed or endorsed by the publisher.

Supplementary material

The Supplementary Material for this article can be found online at: https://www.frontiersin.org/articles/10.3389/fonc.2022.1016721/full#supplementary-material

References

1. Wang Y, Wang J, Li X, Xiong X, Wang J, Zhou Z, et al. N(1)-methyladenosine methylation in trna drives liver tumourigenesis by regulating cholesterol metabolism. *Nat Commun* (2021) 12(1):6314. doi: 10.1038/s41467-021-26718-6

2. Chang C, Rajasekaran M, Qiao Y, Dong H, Wang Y, Xia H, et al. The aberrant upregulation of exon 10-inclusive Srek1 through Srsf10 acts as an oncogenic driver in human hepatocellular carcinoma. *Nat Commun* (2022) 13(1):1363. doi: 10.1038/s41467-022-29016-x

3. Zhang PF, Wei CY, Huang XY, Peng R, Yang X, Lu JC, et al. Circular rna Circtrim33-12 acts as the sponge of microrna-191 to suppress hepatocellular carcinoma progression. *Mol Cancer* (2019) 18(1):105. doi: 10.1186/s12943-019-1031-1

4. Huang JL, Cao SW, Ou QS, Yang B, Zheng SH, Tang J, et al. The long non-coding rna Pttg3p promotes cell growth and metastasis *Via* up-regulating Pttg1 and activating Pi3k/Akt signaling in hepatocellular carcinoma. *Mol Cancer* (2018) 17(1):93. doi: 10.1186/s12943-018-0841-x

5. Helmlinger G, Yuan F, Dellian M, Jain RK. Interstitial ph and Po2 gradients in solid tumors in vivo: High-resolution measurements reveal a lack of correlation. *Nat Med* (1997) 3(2):177–82. doi: 10.1038/nm0297-177

6. Terashima Y, Toda E, Itakura M, Otsuji M, Yoshinaga S, Okumura K, et al. Targeting frount with disulfiram suppresses macrophage accumulation and its tumor-promoting properties. *Nat Commun* (2020) 11(1):609. doi: 10.1038/s41467-020-14338-5

7. Massara M, Bonavita O, Savino B, Caronni N, Mollica Poeta V, Sironi M, et al. Ackr2 in hematopoietic precursors as a checkpoint of neutrophil release and anti-metastatic activity. *Nat Commun* (2018) 9(1):676. doi: 10.1038/s41467-018-03080-8

8. Corbet C, Bastien E, Santiago de Jesus JP, Dierge E, Martherus R, Vander Linden C, et al. Tgfbeta2-induced formation of lipid droplets supports acidosis-driven emt and the metastatic spreading of cancer cells. *Nat Commun* (2020) 11(1):454. doi: 10.1038/s41467-019-14262-3

9. Wang JX, Choi SYC, Niu X, Kang N, Xue H, Killam J, et al. Lactic acid and an acidic tumor microenvironment suppress anticancer immunity. *Int J Mol Sci* (2020) 21(21):8363. doi: 10.3390/ijms21218363

10. Zhang L, Liu L, Zhan S, Chen L, Wang Y, Zhang Y, et al. Arsenic trioxide suppressed migration and angiogenesis by targeting Foxo3a in gastric cancer cells. *Int J Mol Sci* (2018) 19(12):3739. doi: 10.3390/ijms19123739

11. Tian XP, Wang CY, Jin XH, Li M, Wang FW, Huang WJ, et al. Acidic microenvironment up-regulates exosomal mir-21 and mir-10b in early-stage hepatocellular carcinoma to promote cancer cell proliferation and metastasis. *Theranostics* (2019) 9(7):1965–79. doi: 10.7150/thno.30958

12. Wang X, Kang M, Liu C, Lin T, Han X, Jiang X. Current state and progress of research on the role of lncrna in hbv-related liver cancer. *Front Cell Infect Microbiol* (2021) 11:714895. doi: 10.3389/fcimb.2021.714895

13. Pan W, Li W, Zhao J, Huang Z, Zhao J, Chen S, et al. Lncrna-Pdpk2p promotes hepatocellular carcinoma progression through the Pdk1/Akt/Caspase 3 pathway. *Mol Oncol* (2019) 13(10):2246–58. doi: 10.1002/1878-0261.12553

14. Zhang Y, Zhou H. Lncrna Bcar4 promotes liver cancer progression by upregulating Anapc11 expression through sponging Mir1261. *Int J Mol Med* (2020) 46(1):159–66. doi: 10.3892/ijmm.2020.4586

15. Sheng JQ, Wang MR, Fang D, Liu L, Huang WJ, Tian DA, et al. Lncrna Nbr2 inhibits tumorigenesis by regulating autophagy in hepatocellular carcinoma. *BioMed Pharmacother* (2021) 133:111023. doi: 10.1016/j.biopha.2020.111023

16. Subramanian A, Tamayo P, Mootha VK, Mukherjee S, Ebert BL, Gillette MA, et al. Gene set enrichment analysis: A knowledge-based approach for interpreting genome-wide expression profiles. *Proc Natl Acad Sci U.S.A.* (2005) 102(43):15545–50. doi: 10.1073/pnas.0506580102

17. Hanzelmann S, Castelo R, Guinney J. Gsva: Gene set variation analysis for microarray and rna-seq data. *BMC Bioinf* (2013) 14:7. doi: 10.1186/1471-2105-14-7

18. Hollenbach M. The role of glyoxalase-I (Glo-I), advanced glycation endproducts (Ages), and their receptor (Rage) in chronic liver disease and hepatocellular carcinoma (Hcc). *Int J Mol Sci* (2017) 18(11):2466. doi: 10.3390/ijms18112466

19. Wu Y, Zhang Y, Qin X, Geng H, Zuo D, Zhao Q. Pi3k/Akt/Mtor pathway-related long non-coding rnas: Roles and mechanisms in hepatocellular carcinoma. *Pharmacol Res* (2020) 160:105195. doi: 10.1016/j.phrs.2020.105195

20. Yuen VW, Wong CC. Hypoxia-inducible factors and innate immunity in liver cancer. *J Clin Invest* (2020) 130(10):5052–62. doi: 10.1172/JCI137553

21. Boedtkjer E, Pedersen SF. The acidic tumor microenvironment as a driver of cancer. *Annu Rev Physiol* (2020) 82:103–26. doi: 10.1146/annurev-physiol-021119-034627

22. Rohani N, Hao L, Alexis MS, Joughin BA, Krismer K, Moufarrej MN, et al. Acidification of tumor at stromal boundaries drives transcriptome alterations associated with aggressive phenotypes. *Cancer Res* (2019) 79(8):1952–66. doi: 10.1158/0008-5472.CAN-18-1604

23. Tao H, Zhang Y, Yuan T, Li J, Liu J, Xiong Y, et al. Identification of an emt-related lncrna signature and Linc01116 as an immune-related oncogene in hepatocellular carcinoma. *Aging (Albany NY)* (2022) 14(3):1473–91. doi: 10.18632/aging.203888

24. Shi X, Guo X, Li X, Wang M, Qin R. Loss of Linc01060 induces pancreatic cancer progression through vinculin-mediated focal adhesion turnover. *Cancer Lett* (2018) 433:76–85. doi: 10.1016/j.canlet.2018.06.015

25. Li J, Liao T, Liu H, Yuan H, Ouyang T, Wang J, et al. Hypoxic glioma stem cell-derived exosomes containing Linc01060 promote progression of glioma by regulating the Mzf1/C-Myc/Hif1alpha axis. *Cancer Res* (2021) 81(1):114–28. doi: 10.1158/0008-5472.CAN-20-2270

26. Deng X, Bi Q, Chen S, Chen X, Li S, Zhong Z, et al. Identification of a five-Autophagy-Related-Lncrna signature as a novel prognostic biomarker for hepatocellular carcinoma. *Front Mol Biosci* (2020) 7:611626. doi: 10.3389/fmolb.2020.611626

27. Zhang Y, Chen X, Cao Y, Yang Z. C8b in complement and coagulation cascades signaling pathway is a predictor for survival in hbv-related hepatocellular carcinoma patients. *Cancer Manag Res* (2021) 13:3503–15. doi: 10.2147/CMAR.S302917

28. Khamis ZI, Pang X, Cui Z, Sang QA, Zhang J. Cytochrome P450-2d6: A novel biomarker in liver cancer health disparity. *PloS One* (2021) 16(10):e0257072. doi: 10.1371/journal.pone.0257072

29. Seo J, Jeong DW, Park JW, Lee KW, Fukuda J, Chun YS. Fatty-Acid-Induced Fabp5/Hif-1 reprograms lipid metabolism and enhances the proliferation of liver cancer cells. *Commun Biol* (2020) 3(1):638. doi: 10.1038/s42003-020-01367-5

30. Lai GY, Weinstein SJ, Albanes D, Taylor PR, Virtamo J, McGlynn KA, et al. Association of serum alpha-tocopherol, beta-carotene, and retinol with liver cancer incidence and chronic liver disease mortality. *Br J Cancer* (2014) 111(11):2163–71. doi: 10.1038/bjc.2014.365

31. Brown ZJ, Fu Q, Ma C, Kruhlak M, Zhang H, Luo J, et al. Carnitine palmitoyltransferase gene upregulation by linoleic acid induces Cd4(+) T cell apoptosis promoting hcc development. *Cell Death Dis* (2018) 9(6):620. doi: 10.1038/s41419-018-0687-6

32. Cui M, Liu D, Xiong W, Wang Y, Mi J. Errfi1 induces apoptosis of hepatocellular carcinoma cells in response to tryptophan deficiency. *Cell Death Discovery* (2021) 7(1):274. doi: 10.1038/s41420-021-00666-y

33. Thomas CE, Luu HN, Wang R, Xie G, Adams-Haduch J, Jin A, et al. Association between pre-diagnostic serum bile acids and hepatocellular carcinoma: The Singapore Chinese health study. *Cancers (Basel)* (2021) 13(11):2648. doi: 10.3390/cancers13112648

34. Feng J, Dai W, Mao Y, Wu L, Li J, Chen K, et al. Simvastatin re-sensitizes hepatocellular carcinoma cells to sorafenib by inhibiting hif-1alpha/Ppar-Gamma/Pkm2-Mediated glycolysis. *J Exp Clin Cancer Res* (2020) 39(1):24. doi: 10.1186/s13046-020-1528-x

35. Klinghoffer RA, Bahrami SB, Hatton BA, Frazier JP, Moreno-Gonzalez A, Strand AD, et al. A technology platform to assess multiple cancer agents simultaneously within a patient's tumor. *Sci Transl Med* (2015) 7(284):284ra58. doi: 10.1126/scitranslmed.aaa7489

36. Poulose AC, Veeranarayanan S, Mohamed MS, Aburto RR, Mitcham T, Bouchard RR, et al. Multifunctional Cu2-xte nanocubes mediated combination therapy for multi-drug resistant mda Mb 453. *Sci Rep* (2016) 6:35961. doi: 10.1038/srep35961

37. Liu Q, Zhao K, Wang C, Zhang Z, Zheng C, Zhao Y, et al. Multistage delivery nanoparticle facilitates efficient Crispr/Dcas9 activation and tumor growth suppression in vivo. *Adv Sci (Weinh)* (2019) 6(1):1801423. doi: 10.1002/advs.201801423

38. Zhang YX, Zhao YY, Shen J, Sun X, Liu Y, Liu H, et al. Nanoenabled modulation of acidic tumor microenvironment reverses anergy of infiltrating T cells and potentiates anti-Pd-1 therapy. *Nano Lett* (2019) 19(5):2774–83. doi: 10.1021/acs.nanolett.8b04296

Frontiers in Oncology

Advances knowledge of carcinogenesis and tumor progression for better treatment and management

The third most-cited oncology journal, which highlights research in carcinogenesis and tumor progression, bridging the gap between basic research and applications to imrpove diagnosis, therapeutics and management strategies.

Discover the latest Research Topics

See more →

Frontiers

Avenue du Tribunal-Fédéral 34
1005 Lausanne, Switzerland
frontiersin.org

Contact us

+41 (0)21 510 17 00
frontiersin.org/about/contact